Catalytic Methanol Synthesis

Nielsen, Niels Dyreborg

Publication date:
2020

Document Version
Publisher's PDF, also known as Version of record

DTU Chemical Engineering
Department of Chemical and Biochemical Engineering

Catalytic Methanol Synthesis

PhD Thesis

Author:
Niels Dyreborg Nielsen

Supervisors:
Jakob Munkholt Christensen, Technical University of Denmark
Anker Degn Jensen, Technical University of Denmark

THE VELUX FOUNDATIONS
VILLUM FONDEN VELUX FONDEN

Technical University of Denmark
Department of Chemical and Biochemical Engineering CHEC research center
31st October, 2020

Preface

This thesis is part of the PhD project conducted by Niels Dyreborg Nielsen from November 1st 2017 to October 31st 2020 in the research group for Combustion and Harmful Emission Control (CHEC) at the Department of Chemical and Biochemical Engineering (KT) at the Technical University of Denmark (DTU). Associate professor Jakob Munkholt Christensen from KT is the main supervisor, while professor Anker Degn Jensen from KT has the role as co-supervisor. The VILLUM FONDEN V-SUSTAIN grant 9455 to the Villum Center for the Science of Sustainable Fuels and Chemicals is gratefully acknowledged for funding of the project.

I would like to express my deepest gratitude to my main supervisor Jakob Munkholt Christensen, who contributed profoundly to the success of this project. His extensive state-of-the-art knowledge, excellent pedagogical competences, unceasing enthusiasm for science, willingness and readiness to assist upon request at any time, and excellent informative feedback encouraged and guided me in a fruitful direction. His unprecedented work engagement transmitted directly to me and encouraged me to pursue otherwise unachievable scientific endeavours. Another great contributor was co-supervisor Anker Degn Jensen, who applied his comprehensive knowledge to suggest new ideas to pursue and provided valuable constructive feedback thus playing an extremely vital role for the great outcome of the project.

My thanks also go to the KT technicians especially Malene Hessellund Dinesen, Anders Kjersgaard, and Nikolaj Vinterberg Nissen, who all helped with crucial technical support and good laboratory guidance. Without their immense efforts, I could not have accomplished the presented the work. In addition, I would like to thank Jens Henry Poulsen from the KT workshop, who rapidly assisted with vital components for the quenching experiments and set other tasks aside.

Working in an open-minded, engaged, argumentative atmosphere with intelligent and helpful colleagues at CHEC has been a pleasure. I overtook the experimental setup from Steen Riis Christensen, who despite working on his own time-consuming PhD project found time to introduce me to the setup and assist with emerging issues. The effortless start-up with the experimental setup allowed extensive and thorough scientific work to be conducted all attributed to the meticulously guidance by Steen for which I am deeply grateful for. My deepest thanks also go to Adam Paul Karcz, who concurrent with his own PhD was kind enough to assign time for valuable spectroscopy measurements at DTU Nanolab.

Successful scientific work requires inter-disciplinary work and an open mindset towards new ideas. DTU encourages cross-department collaboration, which allowed me to conduct experiments at the Department of Chemistry and collaborate with DTU Nanolab and DTU Physics. At chemistry, I had the pleasure of collaborating with associate professor Susanne Mossin and her PhD student David Nielsen. During the experimental campaigns, I learned from their comprehensive experience and engaged in fruitful discussions. Electron microscopy imaging at DTU Nanolab was performed by senior researcher Thomas Willum Hansen followed by discussions with professor Jacob Birkedal Wagner, who both possess an exhaustive knowledge about electron microscopy and thereby contributed to highly valuable discussions. Finally, I had the privileged to collaborate with PhD student Thomas E. L. Smitshuysen and associate professor Christian D. Damsgaard at DTU Physics on XRD experiments, which was vital to the acceptance of one of our publications. To all collaborators I would like to express my

deepest gratitude for your commitment and hard work and wishes you all the best of luck in the future.

A well-grounded social network ready to discuss both scientific and personal matter is highly important to us as human beings. I am grateful to have worked, travelled, partied, danced, and performed physical exercise among my great colleges at CHEC. These friendships have provided me with many fantastic memories, which I will remember for the rest of my life.

Finally, I would expressed my warm-hearted thanks to my family for their interest and discussions, which contributed with new insights and challenged my dissemination competences. I am for ever extremely grateful for your wholehearted love and support.

Yours sincerely,
Niels Dyreborg Nielsen

Abstract

Limited fossil resources and accelerating climate change necessitates global, sustainable solutions. Renewable energy sources are envisioned to replace fossil fuels but their intermittent production requires efficient storage media and/or immediate use when produced. Liquid chemicals including methanol constitute convenient energy carriers due to their generally high energy density and long term storage stability. Conventional methanol synthesis occurs by converting fossil-derived syngas ($CO_2/CO/H_2$) over a $Cu/ZnO/Al_2O_3$ catalyst but sustainable methanol can be produced from renewably generated H_2 and industrially captured CO_2 to concurrently store renewable energy efficiently and facilitate a greener chemical production. Achieving a sustainable methanol-based global society necessitates a massive expansion in the methanol production capacity which naturally requires improved methanol catalysts provided through a better understanding of the working process and catalyst configuration. Cu is regarded as the active metal but the influence of support, the nature of the active catalytic site(s) and the role of CO and CO_2 are imperfectly understood topics that are addressed in this thesis.

Unsupported Cu catalysts and Raney Cu featuring intrinsic Cu catalytic properties are applied as Cu benchmarking catalysts together with Cu supported catalysts including Cu/SiO_2, Cu/TiO_2, Cu/ZnO, $Cu/ZnO/Al_2O_3$, Cu/Al_2O_3 and Cu/MgO.

CO and CO_2 hydrogenation are two possible pathways to methanol. CO_2 is the primary carbon source for Cu/ZnO-based catalysts based on kinetic and isotope labelling studies but the dominant carbon source to methanol over pure Cu is unclear. Clarification on this matter is established by syngas switching experiments with CO/H_2, $CO/CO_2/H_2$ and CO_2/H_2 at industrially relevant conditions (523 K, 50 bar) over Cu-based catalysts. Results show that CO_2 is the main carbon source on zinc-free Cu-based catalysts. Special supports including basic MgO can exert a bifunctional metal/support synergy effect with high CO hydrogenation activity. Methanol synthesis from CO_2 over Cu is governed by a direct route at low conversion ($\lesssim 0.1$ mol% methanol) and a methanol-assisted autocatalytic pathway (especially for $Cu/ZnO/Al_2O_3$) that accelerates the rate due to the direct CO_2 route by several times. Cu/SiO_2 exhibits similar autocatalytic behaviour but at a substantially lower absolute activity.

Insight into the direct CO_2 route is provided by TPH experiments of formate pre-covered catalysts after formic acid dosage. Hydrogenation of formate evolved methanol and substantiated that formate is a key reaction intermediate for direct CO_2 hydrogenation to methanol. Formate also governs the autocatalytic pathway where methanol and formate react to methyl formate that hydrogenates to methanol.

Estimating the surface coverage of key intermediates is an important parameter for catalytic reactions. A reproducible and quantitative method delivered for the first time experimental estimations of the formate coverage on Cu under industrially relevant conditions ($CO_2/CO/H_2$ = 3/29/68, 523 K, 50 bar). The method involves rapid quenching of the working catalyst and subsequent integration of desorbed CO_2 upon TPD. Applying this method to quantify adsorbate coverages can provide valuable guidance for kinetic modelling studies.

Low and high conversion are scenarios with different optimal CO_x/H_2 compositions. Methanol activity rises with the CO_2 concentration at low conversion with CO being a weakly surface poison. Higher conversion entails greater product concentrations including inhibiting water and (autocatalytically) promoting methanol. Though CO is a mild surface poison it promotes the activity by displacing severely poisoning water by the water-gas shift reaction. The optimal CO_x fraction at high conversion consists of $\sim 10\%$ CO_2 and $\sim 90\%$ CO.

Cu dispersion on supports stabilizes the Cu particles and ensure high Cu surface area but supports also regulate the methanol TOF. Activity measurements at industrially relevant conditions ($CO_2/CO/H_2$, 523 K, 50 bar) of Cu-based catalysts confirm the well-known support effect with the TOF following the order: $Cu/SiO_2 < Cu/Al_2O_3 < Cu/ZnO$-based catalysts. Models proposed in the literature are inadequate to describe the support effect across different Cu supported catalysts. Activity of Cu supported catalysts declines with smaller Cu particles ($\lesssim 5-8$ nm) though interfacial metal-support sites, whose concentration generally increases with smaller Cu particle size, are suggested to feature high activity. Reduced Zn facilitating Cu-Zn surface sites are suggested in the literature to be highly active. Investigating this theory involves methanol synthesis in firstly CO_2/H_2 and secondly $CO_2/CO/H_2$ (at 1 and 20 bar) over mildly reduced $Cu/ZnO/Al_2O_3$ with intact ZnO. Addition of reducing and Cu-Zn site generating CO is detrimental to the TOF and reduced zinc cannot describe the support effect for Cu/ZnO. Clarifying the support effect is of high significance as it heavily influences the methanol TOF and can guide optimization work, which is necessary for the implementation of widespread sustainable methanol production on a global scale.

Support-regulated chemisorption properties of CO on Cu is investigated by IR spectroscopy. The stretching frequency of C-O ($\nu_{\text{C-O}}$) adsorbed on a (catalytic) surface is sensitive to the surface charge. Supports regulated the Cu surface charge with high $\nu_{\text{C-O}}$ on Cu/SiO_2 corresponding to oxidized and electron-deficient Cu ($Cu^{\delta+}$) and ZnO yielding low $\nu_{\text{C-O}}$ resembling electron-rich Cu ($Cu^{\delta-}$). CO adsorption on formate-covered Cu/SiO_2 and Cu/ZnO indicate that the support controls the formate population on Cu with high population for Cu/ZnO and low population for Cu/SiO_2. The support-regulated Cu surface charging is further investigated by IR spectroscopy in inert gas after intermediate and harshly activated ZnO-based samples, which exhibit broad IR transparency loss following the order: $ZnO > Cu/ZnO/Al_2O_3 > Cu/ZnO$. Electrons donated from H_2 and trapped in ZnO can explain the reduced transparency for ZnO, while contact to Cu (Cu/ZnO-based samples) promotes electron flow from ZnO to Cu due to Fermi level alignment and thereby higher transparency for Cu/ZnO. Verification of trapped H_2 in the harshly activated ZnO-based samples is provided by subsequent H_2 desorption in a TPD. In contrast, harshly activated but insulating SiO_2 shows no H_2 desorption in agreement with the model of electron transfer from reducible oxides to Cu.

IR results shows relation between electron-enriched Cu and high TOF for supported Cu catalysts and oppositely low TOF for electron-deficient Cu. Potential mechanisms behind this relation include support-regulated formate population level and formate conversion rate. Applying the quantitative method allows estimates of the working formate coverage ($CO_2/CO/H_2$, 523 K, 50 bar) on Cu/ZnO, Raney Cu and Cu/SiO_2. A similar experiment (cooling in the reaction mixture and then TPD) is performed in the IR cell to disentangle the CO_2 signal and only integrate the (partial) CO_2 profile attributed to Cu-HCOO desorption. Raney Cu and Cu/SiO_2 feature similar formate coverage despite four times lower TOF for Cu/SiO_2 hence the formate population level is not the single determinant for the support effect. TOF and formate coverage values for Cu/ZnO are substantially higher than Raney Cu and Cu/SiO_2 indicating that supports can regulate the formate coverage sustained by Cu. Hydrogenation of formate pre-covered catalysts is rapid for Raney Cu but slow for Cu/SiO_2. Consequently, the detrimental role of SiO_2 relates primarily to an impeded ability to convert formate into methanol.

This work focused mainly on methanol from CO_2 though Cu/MgO features high CO/H_2 activity. CO hydrogenation in CO_2- and water-free atmosphere is interesting for decentralized methanol plants due to more favourable thermodynamics and absence of inhibiting water. Combining a metal and a basic oxide (Cu/MgO) outlines a path towards optimally engineered low temperature methanol catalysts.

This thesis aims at clarifying the support effect in catalytic methanol synthesis as current models are insufficient in explaining the effect. Support-regulated electron transfer is thoroughly investigated and reported to account for the support effect. Acquired knowledge about the role of support can highly promote optimization work, which is a pre-requisite for the potential implementation of sustainable methanol production in the future. Cu/MgO is subjected to a special bifunctional metal-support mechanism yielding high CO/H_2 activity. Provided with sustainable and low-cost syngas with negligible CO_2 concentrations Cu/MgO can work as an active, low temperature methanol catalyst suitable for decentralized plants that use renewable energy to produce sustainable methanol.

Resumé

Begrænsede fossile ressourcer og accelererende klimaforandringer nødvendiggør globale, bære-dygtige løsninger. Vedvarende energikilder forventes at kunne erstatte fossile brændsler, men deres fluktuerende produktion fordrer et effektiv lagringsmedie og/eller umiddelbar anvendelse efter produktion. Flydende kemikalier inklusiv metanol udgør bekvemmelige energibærere pga. deres generelle høje energitæthed og langvarig lagringsstabilitet. Konventionel metanolsyntese foregår ved at omdanne fossilt afledt syngas ($CO_2/CO/H_2$) over en $Cu/ZnO/Al_2O_3$ katalysator, men bæredygtig metanol kan produceres fra vedvarende brint og industrielt indfanget CO_2 for samtidig at opbevare vedvarende energi effektivt og fremme en grønnere kemisk produktion. Realisering af et bæredygtigt metanol-baseret globalt samfund kræver en massiv ekspansion i metanol produktionskapaciteten, som naturligt fordrer forbedrede metanol katalysatorer opnået via en bedre forståelse af den arbejdende proces og katalysatorens konfiguration. Cu anses for at være det aktive metal, men indflydelsen af bæremateriale, karakteren af de aktive katalytiske postion(er) og rollen af CO og CO_2 er ikke fuldkomne forståede emner, som alle bliver adresseret i denne afhandling.

Ikke-understøttet Cu katalysatorer og Raney Cu, som besidder iboende Cu katalytiske egenskaber, anvendes som Cu reference katalysatorer sammen med understøttede Cu katalysatorer inklusiv Cu/SiO_2, Cu/TiO_2, Cu/ZnO, $Cu/ZnO/Al_2O_3$, Cu/Al_2O_3 og Cu/MgO.

CO og CO_2 hydrogenering er to mulige ruter til metanol. CO_2 er den primære karbonkilde for Cu/ZnO-baserede katalysatorer på baggrund af kinetiske og isotop mærkningsstudier, men den primære karbonkilde til metanol over rent Cu er uafklaret. Afklaring af denne sag etableres ved syngas skifteforsøg med CO/H_2, $CO/CO_2/H_2$ og CO_2/H_2 ved industrielt relevante betingelser (523 K, 50 bar) over Cu-baserede katalysatorer. Resultaterne viser, at CO_2 er den primære karbonkilde på zink-fri Cu baserede katalysatorer. Specielle bæremateriale inklusiv basisk MgO kan udvise en bifunktionel metal/bæremateriale synergieffekt med høj CO hydrogeneringsaktivitet. Metanolsyntese fra CO_2 over Cu reguleres af en direkte rute ved lav omdannelse ($\lesssim$ 0.1 mol% metanol) og en metanol-assisteret autokatalytisk vej (specielt udtalt for $Cu/ZnO/Al_2O_3$), som accelererer raten relateret til den direkte CO_2 rute adskillige gange. Cu/SiO_2 udviser lignende autokatalytisk opførsel men ved en substantiel lavere absolut aktivitet.

Indsigt i den direkte CO_2 vej bliver leveret af TPH forsøg af formiattildækkede katalysatorer efter myresyre dosering. Hydrogenering af formiat udviklede metanol og understøttede, at formiat er en nøgle reaktionsintermediate for direkte CO_2 hydrogenering til metanol. Formiat kontrollerer i tillæg den autokatalytiske rute, hvor metanol og formiat reagerer til metylformiat, som hydrogeneres til metanol.

Estimering af overfladedækningsgraden for væsentlige intermediater er en vigtig parameter for katalytiske reaktioner. En reproducerbar og kvantitativ metode leverer for første gang eksperimentelle estimeringer af formiatdækningsgraden på Cu under industrielt relevante betingelser (523 K, 50 bar, $CO_2/CO/H_2 = 3/29/68$). Metoden involverer bratkøling af den arbejdende katalysator og efterfølgende integration af desorberet CO_2 under TPD. Anvendelse af denne metode til kvantificering af adsorbaters dækningsgrader kan levere værdifuld vejledning til kinetiske modelstudier.

Lav og høj omdannelse er scenarier med forskellig optimal CO_x/H_2 kompositioner. Metanolaktiviteten stiger med CO_2 koncentrationen ved lav omdannelse med CO værende et svagt overfladegiftstof. Højere omdannelse indebærer højere produktkoncentrationer inklusiv hæmmende vand og (autokatalytisk) fremmende metanol. Selvom CO er et mildt overfladegiftstof, da promoverer den aktiviteten ved at

fjerne særdeles forgiftende vand via vand-gas skiftereaktionen. Den optimale CO_x fraktion ved høj omdannelse består af $\sim 10\%$ CO_2 og $\sim 90\%$ CO.

Cu dispersion på bærematerialer stabiliserer Cu partikler og sikrer høj Cu overfladeareal, men bærematerialer regulerer også metanol TOF. Aktivitetsmålinger ved industrielt relevante betingelser ($CO_2/CO/H_2$, 523 K, 50 bar) af Cu-baserede katalysatorer bekræfter denne velkendte bærematerialeeffekt med TOF i følgende rækkefølge: $Cu/SiO_2 < Cu/Al_2O_3 < Cu/ZnO$-baserede katalysatorer. Modeller fremlagt i litteraturen er utilstrækkelige i at beskrive bærematerialeeffekten for forskellige understøttede Cu katalysatorer. Aktiviteten af understøttede Cu katalysatorer falder med mindre Cu partikelstørrelse ($\lesssim 5-8$ nm), selvom interface metal-bærematerialе positioner, hvis koncentration generelt øges i takt med mindre Cu partikelstørrelse, foreslås at besidde høj aktivitet. Reduceret Zn faciliterer Cu-Zn overfladepositioner, som i litteraturen foreslås at være særdeles aktive. Undersøgelse af denne teori involverer metanolsyntese i først CO_2/H_2 og dernæst $CO_2/CO/H_2$ (ved 1 og 20 bar) over mildt reduceret $Cu/ZnO/Al_2O_3$ med intakt ZnO. Tilføjelse af reducerende og Cu-Zn position genererende CO er skadelig for TOF'en, hvorfor reduceret zink ikke kan beskrive bæreeffekten for Cu/ZnO. Opklaring af bæreeffekten er af stor betydning, idet den kraftigt påvirker metanol TOF og kan vejlede optimeringsarbejde, hvilket er nødvendigt for at implementere en udbredelse af bæredygtig metanolproduktion på global skala.

Bærematerialе-regulerede kemisorptionsegenskaber af CO på Cu undersøges med IR spektroskopi. Strækningsfrekvensen af C-O ($\nu_{\text{C-O}}$) adsorberet på en (katalytisk) overflade er sensitiv til overfladens ladning. Bærematerialer regulerer Cu overfladens ladning med høj $\nu_{\text{C-O}}$ for Cu/SiO_2 svarende til oxideret og elektronfattig Cu ($Cu^{\delta+}$), mens ZnO giver lav $\nu_{\text{C-O}}$ symboliserende elektronrig Cu ($Cu^{\delta-}$). CO adsorption på formiattildækkede Cu/SiO_2 og Cu/ZnO indikerede, at bærematerialet kontrollerer formiatpopulation på Cu med høj population for Cu/ZnO og lav population for Cu/SiO_2. Den bærematerialе-regulerende Cu overfladeladning undersøges yderligere med IR spektroskopi i inert gas efter mellem og hårdt aktiveret ZnO-baserede prøver, som udviser bredt tab af IR transparens i følgende rækkefølge: $ZnO > Cu/ZnO/Al_2O_3 > Cu/ZnO$. Elektroner doneret fra H_2 og indfanget i ZnO kan forklare den reducerede transparens for ZnO, mens kontakt til Cu (Cu/ZnO-baserede prøver) fremmer elektronflow fra ZnO til Cu som følge af Fermi niveau justering og derved højere transparens for Cu/ZnO. Bekræftelse af indfanget H_2 i hårdt aktiveret ZnO-baserede prøver leveres af efterfølgende H_2 desorption i en TPD. I modsætning hertil udviser hårdt aktiveret men isolerende SiO_2 ingen H_2 desorption i overenstemmelse med modellen omkring elektronoverførsel fra reducerede oxider til Cu.

IR resultater viser relation mellem elektronrig Cu og høj TOF for understøttede Cu katalysa-torer og modsat lav TOF for elektronfattig Cu. Potentielle mekanismer bag denne relation inkluderer bærematerialе-regulerende formiatpopulationsniveau og formiats omdannelsesrate. Anvendelse af den kvantitative metode tillader estimeringer af den arbejdende formiatdæknings-grad ($CO_2/CO/H_2$, 523 K, 50 bar) for Cu/ZnO, Raney Cu og Cu/SiO_2. Et lignende eksperiment (køling i reaktionsgassen og derefter TPD) udføres i IR cellen for at adskille CO_2 signalet og kun integrere den (delvise) CO_2 profil hidhørende fra Cu-HCOO desorption. Raney Cu og Cu/SiO_2 giver sammenlignelige formiatdæknings-grader, selvom TOF er fire gange lavere for Cu/SiO_2, hvorfor formiatpopulationsniveauet ikke er den eneste determinant for bærematerialeeffekten. TOF og formiatdækningsgrads værdier for Cu/ZnO er substantielt højere end Raney Cu og Cu/SiO_2, hvilket indikerer, at bærematerialer kan regulere formiatdækningsgraden understøttet af Cu. Hydrogenering af formiattildækkede katalysatorer er hurtig for Raney Cu men langsom for Cu/SiO_2. I konsekvens heraf relateres den skadelige rolle af Cu/SiO_2 hovedsagligt til en hæmmet evne til at omdanne formiat til metanol.

Dette arbejde fokuserede hovedsagligt på metanol fra CO_2, selvom Cu/MgO udviser høj CO/H_2 aktivitet. CO hydrogenering i CO_2 og vandfri atmosfære er interessant for decentrale metanolanlæg pga. mere favorabel termodynamik og fravær af inhiberende vand. Kombinationen af metal og et basisk oxid (Cu/MgO) skitserer en vej mod optimalt konstruerede lav temperatur metanolkatalysatorer.

Denne afhandling har til formål at udrede bærematerialeeffekten i katalytisk metanolsyntese, idet nuværende modeller er utilstrækkelige i at forklare denne effekt. Bærematerialе-regulerende elektronoverførsel undersøges grundigt og rapporteres til at kunne forklare bærematerialeeffekten. Erhvervet viden omkring rollen af bærematerialet kan være særdeles fremmende for optimeringsarbejde, som er en forudsætning for potentiel implementering af bære-dygtig metanolproduktion i fremti-

den. Cu/MgO er underlagt en speciel bifunktionel metal-bæremateriale mekanisme resulterende i høj CO/H_2 aktivitet. Forudsat at vedvarende og billig syngas med negligerbar CO_2 koncentrationer er tilgængelig, da kan Cu/MgO fungere som en aktiv, lav temperatur metanolkatalysator egnet for decentrale anlæg, der anvender vedvarende energi til at producere bæredygtig metanol.

Publications and Conference Contributions

Published articles in peer-reviewed journals

Niels D. Nielsen, Joachim Thrane, Anker D. Jensen, Jakob M. Christensen, *Bifunctional Synergy in CO Hydrogenation to Methanol with Supported Cu*, Catalysis Letters (2020), 150, 1427-1433
https://doi.org/10.1007/s10562-019-03036-7

Niels D. Nielsen, Anker D. Jensen, Jakob M. Christensen, *Quantification of Formate and Oxygen Coverages on Cu Under Industrial Methanol Synthesis Conditions*, Catalysis Letters (2020), 150, 2447-2456
https://doi.org/10.1007/s10562-020-03162-7

Joachim Thrane, Sebastian Kuld, **Niels D. Nielsen**, Anker D. Jensen, Jens Sehested, Jakob M. Christensen, *Methanol-assisted autocatalysis in catalytic methanol synthesis*, Angewandte Chemie International Edition (2020), 59, 18189-18193
https://doi.org/10.1002/anie.202006921

Niels D. Nielsen, Thomas E. L. Smitshuysen, Christian D. Damsgaard, Anker D. Jensen, Jakob M. Christensen, *Characterization of oxide-supported Cu by infrared measurements on adsorbed CO*, Surface Science (2012), 703, 121725,
https://doi.org/10.1016/j.susc.2020.121725

Submitted articles in peer-reviewed journals

Niels D. Nielsen, Anker D. Jensen, Jakob M. Christensen, *The roles of CO and CO_2 in high pressure methanol synthesis over Cu-based catalysts*, Journal of Catalysis, submitted September, 2020

Articles in preparation for peer reviewed journals

Niels D. Nielsen, Anker D. Jensen, Jakob M. Christensen, *Support-dependent electron transfer to Cu explains the support effect for catalytic methanol synthesis over Cu*, in preparation

Conference contributions

Niels D. Nielsen, Anker D. Jensen, Jakob M. Christensen, *Support Effects in Catalytic Methanol Synthesis*, Presented at North American Catalysis Society Meeting (NAM), 2019, Chicago, United States

Niels D. Nielsen, Anker D. Jensen, Jakob M. Christensen, *Support Effects in Catalytic Methanol Synthesis*, Presented at the 14th European Congress on Catalysis (Europacat), 2019, Aachen, Germany

Other publications

Niels D. Nielsen, Anker D. Jensen, Jakob M. Christensen, *Fremtidens bæredygtige samfund kan baseres på grøn metanol*, Dansk Kemi (2019), 100, 16-19

Nomenclature

Abbreviation	Description
AES	Atomic Emission Spectroscopy
AGA	American Gas Association
ATR	Autothermal Reactor
BASF	Badische Anilin und Soda Fabrik
BFW	Boiler Feed Water
BPR	Back Pressure Regulator
BWR	Boiling Water Reactor
CRI	Chemical Recycling International
DME	Di-methyl-ether
DFT	Density Function Theory
DRIFTS	Diffuse Reflactance Infrared Fourier Transform Spectroscopy
EELS	Electron Energy Loss Spectroscopy
EDX	Energy Dispersive X-ray Spectroscopy
EFTEM	Energy Filtered Transmission Electron Microscopy
ETEM	Environmental Transmission Electron Microscopy
EXAFS	Extended X-ray Adsorption Fine Structure
FBR	Fixed Bed Reactor
FID	Flame Ionization Detector
FTIR	Fourier Transform Infrared
GC	Gas Chromatography
GL	Graphite Like
GLC	Gas-Liquid Chromatography
GLS	Gas-Solid Chromatography
HAADF	High-angle Annular Dark Field
HPLC	High-performance liquid chromatography
HREELS	High-Resolution Electron Energy Loss Spectroscopy
HRTEM	High-Resolution Transmission Electron Microscopy
ICI	Imperical Chemical Industries
IRRAS	Infrared Reflection-Adsorption Spectroscopy
IWI	Incipient Wetness Impregnation
KIE	Kinetic Isotope Effect
LEED	Low Energy Electron Diffraction
MFC	Mass Flow Controller
ML	Monolayer
MOR	Mordenite

Abbreviation	Description
MTPD	Metric Tonne Per Day
MTY	Mass Time Yield
ND	Neutron Diffraction
NMR	Nuclear Magnetic Resonance
NP	Nanoparticle
QMS	Quadrupole Mass Spectroscopy
RAIRS	Reflection Adsorption Infrared Spectroscopy
RFC	Reactive Frontal Chromatography
(R)WGS	(Reverse) Water Gas Shift
SC	Single Crystal
SEM	Secondary Electron Multiplier
SMSI	Strong Metal Support Interaction
STEM	Scanning Transmission Electron Microscopy
STM	Scanning Tunneling Microscopy
TC	Thermocouple
TCD	Thermal Conductivity Detector
TOF	Turnover Frequency
TPD	Temperature Programmed Desorption
TPH	Temperature Programmed Hydrogenation
TPR(S)	Temperature Programmed Reduction (Spectroscopy)
UHV	Ultra High Vacuum
UPS	Ultraviolet Photo-electron Spectroscopy
XPS	X-ray Photo-electron Spectroscopy
XRD	X-ray Diffraction

Symbol	Description	Unit
$\theta_{\text{Cu-HCOO}}$	Formate surface coverage on Cu	[ML]
H	Oxygen vacancy formation enthalpy	[eV]
k_B	Boltzmann's constant	[J/K]
$\text{m}_{\text{cat.}}$	Mass of catalyst	[mg]
m/z	Mass-to-charge ratio	[-]
n_e^-	Charge concentration	[cm^{-3}]
$\nu_{\text{C-O}}$	C-O stretching frequency	[cm^{-1}]
P	Pressure	[bar]
(GH)SV	Gas Hourly Space velocity	[$\text{Nl/kg}_{\text{cat}}$/h] or [$\text{Nml/g}_{\text{cat}}$/h]
T	Temperature	[K]
TOF	Turnover frequency	[CH_3OH molec./Cu surface atom/s]
$[\text{V}_\text{O}^{++}]$	Oxygen vacancy concentration	[cm^{-3}]
$\nu_{\text{OCO,asym}}$	Asymmetric OCO stretching frequency	[cm^{-1}]
$\nu_{\text{OCO,sym}}$	Symmetric OCO stretching frequency	[cm^{-1}]
$\phi(b)$	Schottky barrier height	[eV]
$\phi(t)$	Barier bending height	[eV]

Contents

Chapter 1

Introduction

1 Motivation

Limited oil- and gas resources (projected depletion in 2070 based on 2018 consumption [1]), rising global energy demand and increasing carbon emissions are key global challenges [1, 2]. Future energy and chemical production must therefore be based on renewable sources but how can we store and efficiently exploit intermittent renewable energy on cloudy and/or calm days?

The ideal energy storage medium features effective charge-discharge cycles and high energy density. Moreover, it would be favorable if the medium possess upgrading potential towards higher valuable products. Batteries are challenged by their low energy density, and hydrogen contains a limited energy density. Instead, reacting H_2 with captured CO_2 allow synthesis of the liquid chemical methanol with a high energy density fairly comparable to gasoline as shown in figure 1.

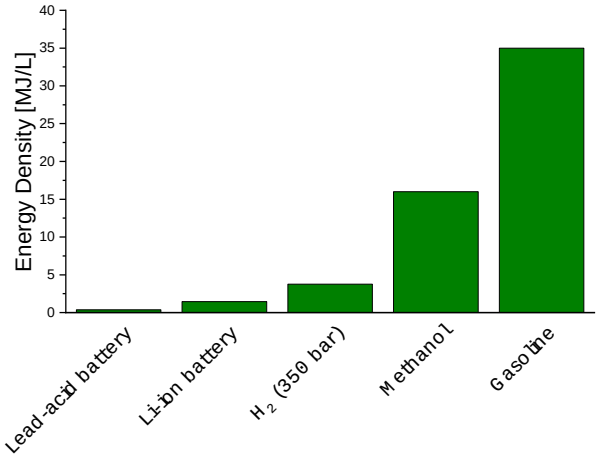

Fig. 1: Energy density of battery technologies and chemicals (lower heating value, LHV, applied) [3].

The concept behind carbon neutral methanol production is depicted in figure 2. Renewable electricity drives the splitting of water into oxygen and hydrogen and the latter reacts with captured CO_2 from industrial sources to produce methanol (see reaction R1).

$$CO_2 + 3\,H_2 \rightleftharpoons CH_3OH + H_2O \qquad \{R1\}$$

Reaction R1 depicts a well-established industrial process (80-90 million tonnes demand in 2018, 6% yearly growth) accelerated over a $Cu/ZnO/Al_2O_3$ catalyst at 50-100 bars of pressure at 473-573 K [4]. The company Carbon Recycling International (CRI) from Iceland proved that this sustainable methanol concept is industrially profitable provided with favourable infrastructural conditions. These conditions include readily access to renewable energy sources (geothermal energy and water power in Iceland) and reasonably high concentrations of easily extractable CO_2 supplied in the CRI case from

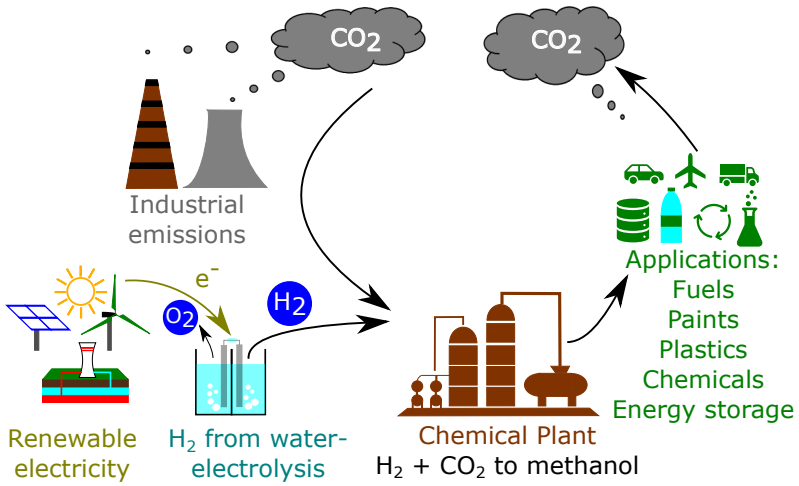

Fig. 2: Concept behind sustainable methanol production based on industrial CO_2 emissions and renewable H_2 produced from water-electrolysis.

the extraction process of geothermal energy due to degassing of volcanic magma [5]. CRI proves that places with low electricity cost and significant CO_2 emissions can produce cost-effective and industrially feasible and sustainable methanol.

Besides the ability of methanol to store renewable electricity efficiently it is a key chemical feedstock for the synthesis of higher valuable products including paints, plastics, chemicals and fuels [4]. Carbon neutral methanol therefore holds the potential to displace fossil fuels as a key chemical commodity and facilitate the transition towards a more sustainable chemical industry. Encapsulation of a "methanol based economy" is depicted in figure 2 and suggested by Noble laureate in chemistry (1994) George A. Olah [6] to address the challenge with limited fossil resources and concurrently presents a way to produce energy and chemicals without detrimental environmental consequences.

Noble laureate in chemistry (1986) Richard E. Smalley examined the challenges connected to the future energy supply and concluded that efficient renewable electricity storage in decentralised facilities is a prerequisite [2]. Local methanol plants based on renewable H_2 from water-electrolysis and captured CO_2 from point sources necessitates milder operation conditions in terms of temperature and pressure compared to the today's industrial process to be economically feasible. However, milder reaction conditions entail adverse effects on the methanol production from a kinetic viewpoint. Consequently, active catalysts operating at mild conditions must be developed based on improved understanding of the catalytic active site, which for $Cu/ZnO/Al_2O_3$ remains a highly debated topic [4].
Cu is regarded as the active metal due to linearity between the methanol rate ($g_{MeOH}/g_{cat}/h$) and the specific Cu surface area (m^2 Cu/g_{cat}) for various supported Cu catalysts [4, 7, 8]. Interestingly, the rate to area ratio (called the turnover frequency, TOF) depends strongly on the support material hence the term support effect [8]. As the support highly regulates the methanol TOF an improved understanding of the effect is of high significance for optimizing conventional methanol catalysts and fundamentally understand the catalytic systems. Mechanistic studies suggest formate (HCOO) on the metal surface as a key reaction intermediate for methanol synthesis [9, 10]. Therefore, it is of high importance to quantify the formate surface coverage on Cu ($\theta_{Cu\text{-}HCOO}$) at working conditions.
Another key feature in methanol synthesis over Cu is the role of CO and CO_2 and the current dispute regarding the main carbon source to methanol over Cu.
This PhD project seeks to establish a mechanism describing the support effect and clarify the roles of CO and CO_2 at various reaction conditions. The proposed support effect mechanism is that support-induced electron flow at the metal-support interface regulates the catalytic properties of the metal. Kinetic studies at conventional conditions coupled with various in situ spectroscopy methods with mainly IR spectroscopy constitute the framework for investigating the proposed mechanism. The acquired knowledge contributes with an improved fundamental understanding of how supports direct catalytic reactions and could be of high industrial value by providing guidelines for future optimization

work of metal-supported catalysts.

2 Project Description

This thesis focuses on metal-support electronic interactions to account for the reported support effect on the methanol rate over supported Cu catalysts. Various supported and unsupported Cu catalysts are synthesized and tested by means of:

- Hydrogen activation followed by Cu surface area estimation using N_2O-Reactive Frontal Chromatography (RFC)
- Kinetic experiments at conventional methanol synthesis conditions ($P = 50$ bar mainly, $T = 523$ K mainly) in syngas (mainly $CO_2/CO/H_2$ or $CO_2/N_2/H_2$ or $CO/Ar/H_2 = 3/29/68$) at mainly low conversion (< 0.3 mol% CH_3OH) conditions unless otherwise stated
- In situ Diffusive Reflectance Infrared Fourier Transform Spectroscopy (DRIFTS) of
  - CO adsorption on oxidized and reduced samples as well as with co-adsorbate formate
  - Formate synthesis in CO_2/H_2 at 373 K, 1 atm and subsequent hydrogenation
  - Methanol synthesis at 10 bar in $CO_2/CO/H_2$ at 523 K with subsequent TPD
  - Formate injection and subsequent temperature programmed hydrogenation (TPH)
  - Methanol injection and subsequent temperature programmed desorption (TPD)
- In situ X-ray Diffraction (XRD) of reduced samples for Cu crystallite size estimations
- Ex situ X-ray Photoelectron Spectroscopy (XPS) to study surface composition and system impurities

Cu supported catalysts (Cu/SiO_2, Cu/TiO_2, Cu/ZnO, $Cu/ZnO/Al_2O_3$, Cu/Al_2O_3 and Cu/MgO) were synthesized by standard precipitation or impregnation methods. All catalysts were activated in hydrogen unless otherwise stated. Experiments were mainly conducted using a high-pressure flow-reactor setup with two separate gas routes; one leading to U-shaped glass lined reactors applicable for high-pressure reactions and another to an Harricks IR cell with accessories to perform cryogenic temperature (atmospheric pressure) and high temperature (high-pressure) experiments. Inlet gas flows for both gas routes through a carbonyl trap consisting of active carbon before entering the reactor/cell containing the samples. Effluent gasses from both gas routes were analysed online by a mass spectrometer and a gas chromatograph while samples placed in the IR cell was investigated by a Nicolet iS50 Fourier Transform IR (FTIR) spectrometer. In situ XRD experiments were conducted in a separate setup.

Chapter 2 provides a literature overview regarding the current scientific understanding of catalytic methanol synthesis. Conventional synthesis methods for methanol catalysts are outlined followed by micro-kinetic models describing the reaction pathway for methanol and the role of reaction conditions on methanol synthesis. Based on this fundamental background the overview focuses on metal-support interactions, the coverage of formate (HCOO) on Cu and the support effect on the methanol activity. Finally, chemisorption methods to quantify the Cu surface area and alternative methanol catalysts are briefly discussed before summarizing the scientific work and models for the active methanol site.

Chapter 3 is a reprint of the submitted and currently editing for review manuscript *The roles of CO and CO_2 in high pressure methanol synthesis over Cu-based catalysts.* It clarifies the main carbon source for methanol over Cu-based catalysts at low and high conversion and highlights the role of CO at these two conversion regimes. Supplementary material is provided in appendix A.
Niels Dyreborg Nielsen performed all presented investigations and did visualization, wrote, edited and reviewed the manuscript , and conducted formal analysis and partly formulated the research objective. Jakob Munkholt Christensen participated with conceptualization, methodology and formal

analysis together with editing and reviewing the manuscript. He also acquired funding for the project, managed and supervised the project.
Anker Degn Jensen supervised, managed the project, acquired funding for the project and reviewed and edited the manuscript.
All authors proofread the article prior to submission.

Chapter 4 is a reprint of the publication entitled *Methanol-Assisted Autocatalysis in Catalytic Methanol Synthesis*. It describes a newly discovered methanol accelerated autocatalytic mechanism present at methanol concentrations above 0.5 mol% for especially the conventional $Cu/ZnO/Al_2O_3$. This breakthrough explains some of the current disputes about higher methanol rates at higher conversion and provides vital understanding valuable for future optimization of conventional methanol synthesis. Supplementary material is provided in appendix B. Niels Dyreborg Nielsen contributed with high-pressure methanol synthesis experiments over $Cu/ZnO/Al_2O_3$ in CO-free and CO-containing atmosphere at low and high conversion and proofread the final manuscript. Joachim Thrane and Sebastian Kuld did formal analysis, methodology, investigation, editing and reviweing manuscript. Anker Degn Jensen and Jens Sehested supervised, performed editing and reviewing of the manuscript and conceptualization. Jakob performed conceptualization, methodology, formal analysis, writing and editing the manuscript. All authors participated in proofreading the article before submission.

Chapter 5 is a reprint of the paper *Quantification of Formate and Oxygen Coverages on Cu Under Industrial Methanol Synthesis Conditions*. It outlines the reproducible quenching method develop to quantify surface coverages of adsorbates present under high-pressure reaction conditions. Supplementary material is provided in appendix C.
Niels Dyreborg Nielsen performed all presented investigations and did visualization, wrote, edited and edited the manuscript, and conducted formal analysis and partly formulated the research objective. Jakob Munkholt Christensen participated with conceptualization, methodology and formal analysis together with editing and reviewing the manuscript. He also acquired funding for the project, managed and supervised the project.
Anker Degn Jensen supervised, managed the project, acquired funding for the project and reviewed and edited the manuscript.
All authors proofread the article prior to submission.

Chapter 6 is a print of the paper *Characterization of oxide-supported Cu by infrared measurements on adsorbed CO*. This shows that support regulates the Cu surface charge observed by C-O stretching frequency changes for Cu supported catalysts. Support-regulated electron transfer is the proposed mechanism for this effect, which highly impacts the population level of adsorbate on surface illustrated by profoundly different formate population levels for Cu/SiO_2 and Cu/ZnO. Supplementary material is provided in appendix D.
Niels Dyreborg Nielsen contributed to the conceptualization and performed all investigations except XRD experiments, performed formal analysis, wrote original manuscript and was responsible for editing and final drafting including visualization.
Thomas Erik Lyck Smitshuysen contributed with XRD investigations and formal analysis on these tests, while Christian Danvad Damsgaard supervised primarily the XRD studies.
Anker Degn Jensen supervised, managed the project and was responsible for funding acquisition and contributed to the writing and editing process.
Jakob Munkholt Christensen participated in the conceptualization and methodology processes, supervised, managed the project and data, acquired funding and participated significantly to the reviewing, editing and visualization process of the final manuscript.
All authors participated in proofreading the article before submission.

Chapter 7 is a reprint of in preparation manuscript *Support-dependent electron transfer to Cu explains the support effect for catalytic methanol synthesis over Cu*. It encapsulates the support effect and suggest a detail description of the highly debated support effect.
Supplementary material is provided in appendix E.
Niels Dyreborg Nielsen performed all presented investigations and did visualization, wrote, edited and reviewed the manuscript , and conducted formal analysis and partly formulated the research objective. Jakob Munkholt Christensen participated with conceptualization, methodology and formal analysis together with editing and reviewing the manuscript. He also acquired funding for the project,

managed and supervised the project.
Anker Degn Jensen supervised, managed the project, acquired funding for the project and reviewed and edited the manuscript.
All authors proofread the article prior to submission.

Chapter 8 is a reprint of the article with the title *Bifunctional Synergy in CO Hydrogenation to Methanol with Supported Cu*. The article concentrates on methanol synthesis at mild conditions from CO and H_2 over MgO supported Cu. Synergy effects between MgO and Cu are found to be of vital importance in understanding methanol synthesis over Cu/MgO. Supplementary material is reprinted in appendix F and provides a general description of the experimental setup used throughout the PhD.
Niels Dyreborg Nielsen contributed with conceptualization, methodology, formal analysis and investigation. This entailed synthesis of unsupported Cu, Raney Cu and supported Cu catalysts and later analyses of measurements involving i) IR spectroscopy and ii) X-ray photoelectron spectroscopy, and iii) syngas switching experiments between CO hydrogenation and CO_2 hydrogenation atmospheres for Cu/MgO, Cu/Al_2O_3, unsupported Cu, and Raney Cu. Niels participated in the editing, reviewing and visualization process of the final manuscript.
Joachim Thrane contributed with conceptualization, investigating and formal analysis. This was evident by with CO chemisorption experiments including subsequent TPD and partly long term stability tests (+10 hours) of Cu and MgO based catalysts in high pressure CO hydrogenation atmosphere. This work is contained in his BSc thesis named *Investigation of Copper Based Catalysts by Chemisorption Methods*. He also participated in the editing and reviewing process.
Anker Degn Jensen supervised, managed the project, acquired funding for the project and reviewed and edited the manuscript.
Jakob Munkholt Christensen contributed with investigation, formal analysis, conceptualization and methodology. Details of his work includes a description of the water inhibition effect, partly long term stability tests (+10 hours) of Cu and MgO based catalysts in high pressure CO hydrogenation atmosphere, and suggested the mechanism based on IR spectroscopy and syngas switching experiments. He wrote, reviewed, visualized and edited the manuscript and acquired funding, supervised and managed the project.
All authors proofread the article prior to submission.

Chapter 9 summarizes the results in a combined conclusion section.

Chapter 10 suggests future work on the basis of the work presented in this thesis.

Appendix G summarizes the preparation parameters for the various catalysts prepared.

Appendix H describes calibration of various instruments applied in the flowreactor setup.

References

[1] D. Spencer. BP Statistical Review of World Energy Statistical Review of World. *The Editor BP Statistical Review of World Energy*, pages 1–69, 2019.

[2] R. E. Smalley. Our Energy Challenge. In James A. Baker III Institute for Public Policy, editor, *Energy and Nanotechnology: Prospects for Solar Energy in the 21st Century*, James A. Baker III Institute for Public Policy, 2005. James A. Baker III Institute for Public Policy.

[3] H. H. Larsen and L. S. Petersen. DTU International Energy Report 2013: Energy storage options for future sustainable energy systems. Technical report, Technical University of Denmark (DTU), 2013.

[4] J. Sehested. Industrial and scientific directions of methanol catalyst development. *Journal of Catalysis*, 371:368–375, 2019. doi: 10.1016/j.jcat.2019.02.002.

[5] M. Kauw, M. J. Benders, and C. Visser. Green methanol from hydrogen and carbon dioxide using geothermal energy and/or hydropower in Iceland or excess renewable electricity in Germany. *Energy*, 90:208–217, 2015. doi: 10.1016/j.energy.2015.06.002.

[6] G. A. Olah, A. Goeppert, and G. K. S. Prakash. Chemical Recycling of Carbon Dioxide to Methanol and Dimethyl Ether: From Greenhouse Gas to Renewable, Environmentally Carbon Neutral Fuels and Synthetic Hydrocarbons. *J. Org. Chem.*, 74(2):487–498, 2009. doi: 10.1021/jo801260f.

[7] C. Baltes, S. Vukojević, and F. Schüth. Correlations between synthesis, precursor, and catalyst structure and activity of a large set of $CuO/ZnO/Al_2O_3$ catalysts for methanol synthesis. *Journal of Catalysis*, 258(2):334–344, 2008. doi: 10.1016/j.jcat.2008.07.004.

[8] M. Kurtz, H. Wilmer, T. Genger, O. Hinrichsen, and M. Muhler. Deactivation of Supported Copper Catalysts for Methanol Synthesis. *Catalysis Letters*, 86(1-3):77 – 80, 2003. doi: 10.1023/A:1022663125977.

[9] S. G. Neophytides, A. J. Marchi, and G. F. Froment. Methanol synthesis by means of diffuse reflectance infrared Fourier transform and temperature-programmed reaction spectroscopy. *Applied Catalysis*, 86:45–64, 1992. doi: 10.1016/0926-860X(92)80041-A.

[10] S. Fujita, M. Usui, H. Ito, and N. Takezawa. Mechanisms of Methanol Synthesis from Carbon Dioxide and from Carbon Monoxide at Atmospheric Pressure over Cu/ZnO. *Journal of Catalysis*, 157(2):403–413, 1995. doi: 10.1006/jcat.1995.1306.

Chapter 2

Literature Review

Decades of research into catalytic methanol synthesis together with its industrial application potential are outlined and thoroughly discussed in this chapter. The preparation procedure for a typical industrial type methanol catalyst is presented before the methanol synthesis reaction scheme and industrial methanol production are discussed.
Modeling of the direct methanol synthesis reaction pathway based on experimental and theoretical studies is evaluated before a possible indirect autocatalytic reaction pathway is presented. Knowledge about the reaction mechanism is applied in the scientific debate including proposed models to account for the well-substantiated Cu-Zn synergy effect on the catalytic activity. Chemisorption methods including N_2O-RFC and H_2-TPD are widely applied to estimate the Cu surface area of supported Cu catalysts hence a thorough evaluation of these methods is included.
Perspective is provided by a short presentation of alternative methanol catalysts for methanol production based on renewable energy sources.

1 Historical Overview

Methanol production based on a syngas mixture of H_2, CO, and CO_2 was for the first time described in 1921 by Patart [1, 2]. This method was a few years later patented by BASF (today a world-leading chemical production company) based on a ZnO/Cr_2O_3 catalyst operating at $T = 573$-633 K, $P = 150-250$ bar [3]. After decades of work into Cu-based catalysts [4] and improved steam reforming pioneered by Imperical Chemical Industries [4, 5] resulting in lower impurity levels of the syngas [6], ICI patented in 1965 a more active ternary $Cu/ZnO/Al_2O_3$ catalyst synthesized by co-precipitation for methanol synthesis [7] operating at milder conditions in comparison to the ZnO/Cr_2O_3 catalyst. The $Cu/ZnO/Al_2O_3$ catalyst has ever since been the preferred catalyst for catalytic methanol synthesis with excellent methanol selectivity ($> 99.8\%$) and good energy conversion (75%) [4, 6] but it is susceptible to inhibtion over time by thermal sintering [4, 8]. Initially, the working conditions ($T = 503$, $P = 50-100$ atm) for stable methanol production involved a mixture of CO and H_2 [9]. However, early radiolabelling studies at high pressure conditions conducted first by Kagan et al. [10] and later by Chinchen et al. [11, 12] and Liu et al. [13] with support from transient kinetic measurements [14] showed that the carbon component in methanol originated from CO_2 rather than CO as previously proposed by Natta [15] and supported by the Klier group [16].
Consequently, the syngas mixture changed in composition to $H_2/CO/CO_2$ with ratios around 80/10/10 [17] supplied by coal gasification or steam reforming of natural gas as the dominant sources [18].

The three components in the $Cu/ZnO/Al_2O_3$ catalyst are suggested to promote methanol synthesis in different ways as described below:

Al_2O_3 acts as a structural promoter by facilitating a high Cu dispersion (defined as the ratio between surface atoms and total number of Cu atoms) [19–21]. It is associated with high thermal stability and

enhanced catalytic activity [22] through modified ZnO reducibility by Al^{3+} incorporation into ZnO [20].

Cu can synthesize methanol from CO_2 and H_2 based on single crystal experiments [23–25] and is regarded as the active metal based on the linear relationship between the methanol activity and the specific Cu surface area [26–28]. Recent studies have attributed the ability of Cu to synthesize methanol to defective Cu step sites and Cu lattice strain [29].

ZnO works as a structural promoter by inhibiting Cu particle sintering [21, 22, 30, 31] as shown by Kasatkin et al. [32] in figure 2.1.1, and it profoundly enhances the activity compared to Cu [33, 34] (known as the Cu-Zn synergy effect) as seen by Fujitani et al. [35] in figure 2.1.2. Moreover, it scavenges poisons (e.g. sulfur and chlorides) and thereby minimizes Cu poisoning [4, 21]. The Cu-Zn synegy effect is suggested to arise from metal-support interactions between Cu and ZnO resulting in partial ZnO_x formation, which is suggested to cover Cu under reducing conditions [29]. Several mechanisms based on both experimental and theoretical work have been proposed to describe these interesting metal-support interactions for highly active Cu/ZnO based catalysts as presented in section 7. However, the nature of the active sites remains a controversial topic, and future research are required to solve this long standing debate.

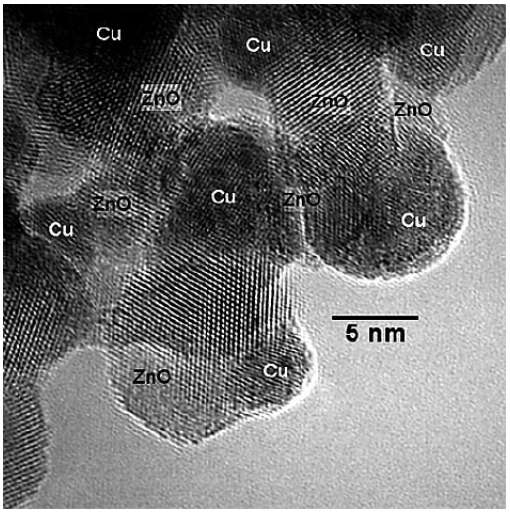

Fig. 2.1.1: High-Resolution Transmission Electron Microscopy (HRTEM) image of a calcined (in air at 603 K) and activated (in H_2 at 523 K) $Cu/ZnO/Al_2O_3$ catalyst with an industrially relevant Cu/Zn/Al molar ratio of 6/3/1. ZnO prevents Cu particles from sintering. Figure is from [32].

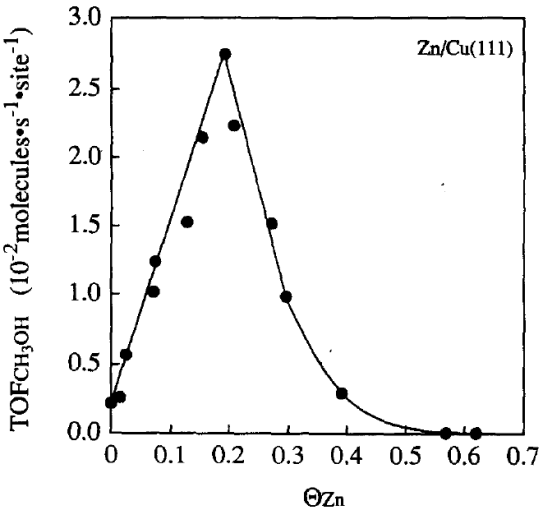

Fig. 2.1.2: Methanol TOF for a Zn/Cu(111) catalyst exposed to $H_2/CO_2 = 3$ at 523 K and 18 atm as function of Zn coverage (Θ_{Zn}), which was determined after methanol synthesis by XPS. Figure is from [35].

2 Conventional Methanol Catalyst Preparation

Conventional methanol catalysts consist of 50-70 mol%, CuO, 20-50 mol% ZnO and 5-20 mol% Al_2O_3. The preparation procedure includes co-precipitation of Cu, Zn, and Al containing nitrates mixed with precipitating agents such as alkali bicarbonate or alkali carbonate. Co-precipitation refers to the phenomenon where otherwise soluble species react and undergo simultaneous precipitation facilitated by the presence of precipitating agents. Alternative precursors with readily accessible metal includes sulfates and chlorides are deselected due to their poisoning effect on the catalyst [4, 27]. Mixing of nitrate metal precursors and the precipitating agents produce hydroxy-carbonate precursors with Cu and Zn on supporting Al_2O_3 at pH $= 6 - 7$ and $T =$ 333-343 K with first aging for 0.5-2 hours ($T =$

333-343 K) and second washing and drying and third calcination at 327-427°C. Catalyst activation by H_2-reduction at 463-503 K represents the final step [22].

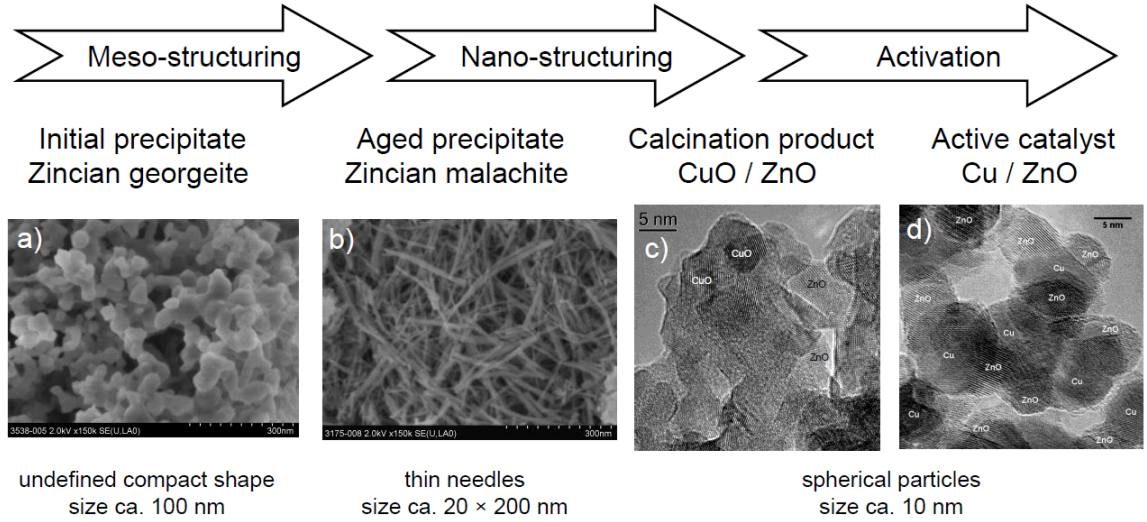

Fig. 2.2.1: Preparation scheme for $Cu/ZnO/Al_2O_3$ from initial catalyst precursor (a) to final activated catalyst (d). This demonstrates catalyst configuration modifications during preparation and activation steps. Figure is from [31].

Zincian malachite ($(Cu,Zn)_2(OH)_2CO_2$) is identified as a vital precursor phase for the conventional $Cu/ZnO/Al_2O_3$ catalyst because of a clear relation between the Zn content in zincian malachite and the Cu surface area [31] as seen in figure 2.2.2. A decreased zincian malachite interplanar distance d($20\bar{1}$) suggests lattice contraction caused by more Zn^{2+} incorporation (substituting Cu^{2+}) into zincian malachite [31]. As evident from figure 2.2.2, a conventional-type catalyst prepared with a Cu:Zn ratio of 70:30 yields close to the highest obtainable Cu surface area.

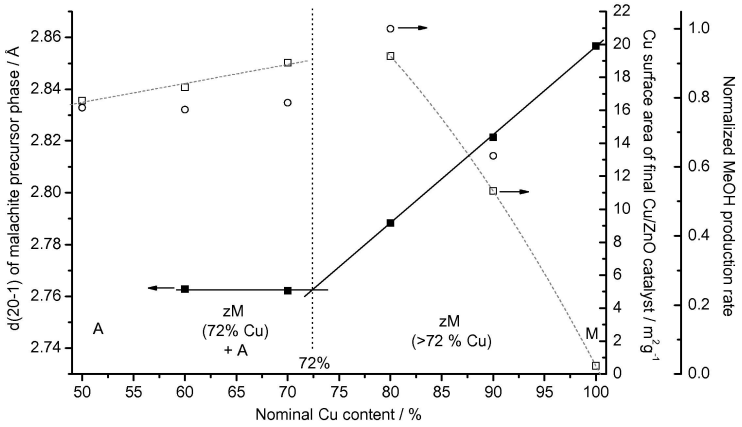

Fig. 2.2.2: The effect of Cu/Zn content on the lattice properties of zincian malachite displays the amount of Zn^{2+} incorporation (solid black squares) into zincian malachite seen by the interplanar distance d($20\bar{1}$) and the specific Cu surface area (open squares). All samples are activated before structural characterization experiments are conducted. Figure is from [31].

Promoters can be added to the $Cu/ZnO/Al_2O_3$ catalyst as exemplified by MgO, which facilitates a higher and more stable catalytic activity [8].

3 Reaction Scheme for Methanol Synthesis

The overall reactions involved in methanol synthesis from syngas are depicted in table 1. The exothermic nature of the presented reactions combined with the stoichiometry ratio between products and reactants entail that methanol synthesis according to thermodynamics is favourable at high-pressure (Le Chatelier's principle) and low temperature. Contrary, reaction kinetics increases exponentially with temperature [36]. Optimal reaction conditions concerning temperature and pressure are therefore partly a trade-off between rapid (kinetics) and high (thermodynamics) methanol production.
Methanol synthesis by-products including dimethylether (DME) and aldehydes are thermodynamically more stable than methanol. Therefore, the methanol catalyst must be (highly) selective towards synthesizing methanol, and the methanol selectivity of typical industrial catalysts exceeds 99.8% [4, 6, 18].

Table 1: Standard heat of formation ($\Delta H^0_{298\mathrm{K}}$) for reactions relevant for methanol production from syngas based on [36].

Reaction name	**Reaction**	**Enthalpy of formation** $\Delta H^0_{298\mathrm{K}}[\mathrm{kJ\,mol^{-1}}]$
CO hydrogenation	$CO + 2\ H_2 \rightleftharpoons CH_3OH$	-91
CO_2 hydrogenation	$CO_2 + 3\ H_2 \rightleftharpoons CH_3OH + H_2O$	-47
Water-gas shift (WGS)	$CO + H_2O \rightleftharpoons H_2 + CO_2$	-41

CO_2 hydrogenation is the main reaction pathway for conventional methanol synthesis [37–39] and higher CO_2 partial pressure should enhance the methanol activity. However, a high CO_2 concentration (assuming constant CO concentration) favours the reverse WGS reaction and results in CO formation and methanol activity inhibiting and co-produced H_2O [40–42] (see WGS in table 1). The CO:CO_2 ratio in the feed gas influences the WGS/RWGS reactions and the oxidation/reduction potential [43, 44] of the feed gas with consequences for the methanol activity [44, 45].

4 Industrial Methanol Synthesis

Industrial methanol production involves careful considerations about the supply and preparation of syngas, choice of catalyst and reactors, method of optimally controlling the reaction temperature etc. Modern methanol plants produce methanol with a selectivity above 99.8% and with an energy efficiency around 75% making it a highly optimized process [4, 6]. The main steps towards producing methanol is depicted in figure 2.4.1 with a starting feedstock of hydrocarbons (derived chiefly from natural gas by steam reforming), which is subsequently reformed (incl. possible purification) to the optimal or desired syngas mixture. Synthesised methanol is collected by distillation [46] to yield different qualities of methanol [4].

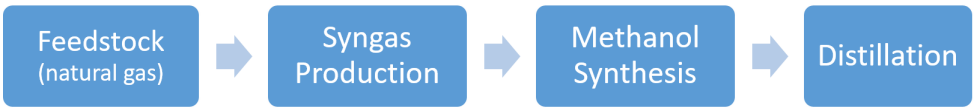

Fig. 2.4.1: General steps for conventional methanol synthesis with inspiration from [46] though coal gasification is another major feedstock for syngas production.

The dominant method for conventional methanol production is steam reforming of natural gas [18] involving reaction R2 [36] at 25-35 bar and up to 1273 K:

$$CH_4 + H_2O \rightleftharpoons CO + 3\,H_2 \qquad \Delta H^0_{298\ \mathrm{K}} = 206\,\mathrm{kJ\,mol^{-1}} \qquad \{\mathrm{R2}\}$$

with WGS/RWGS (see table 1) occurring simultaneously. Regions with insufficient cheap natural gas resources (e.g. China) use coal gasification as the dominant feedstock to prepare syngas [18].

Characteristic properties of the syngas are the module, M, defined in equation 4.1 and the CO/CO_2 ratio [18]. A high CO/CO_2 ratio enhances the reaction rate by displacing inhibiting water, which otherwise accelerates catalyst deactivation [18]. However, CO_2 is required, because it is the primary carbon source to methanol synthesis from CO_2 hydrogenation (see section 1).

$$M \equiv \frac{H_2 - CO_2}{CO + CO_2} = 2 \quad \text{(stoichiometric)} \tag{4.1}$$

Stoichiometric methanol syngas is achieved using a module of 2 (see CO and CO_2 hydrogenation reactions in table 1).

Conventional methanol synthesis is primarily produced based on three designs [4, 18, 21]; tubular boiling water reactors (BWRs) applied by the Lurgi company, quench reactors developed by ICI (now Johnson Matthey), and adiabatic reactors in series used by Topsøe and Kellogg (now Kellogg Brown & Root). Their main differences originate from their method of controlling the reaction heat with associated advantages and limitations [21]. Figure 2.4.2 provides an overview of the designs and the conversion to methanol as function of temperature profiles, which will be discussed in further detail next.

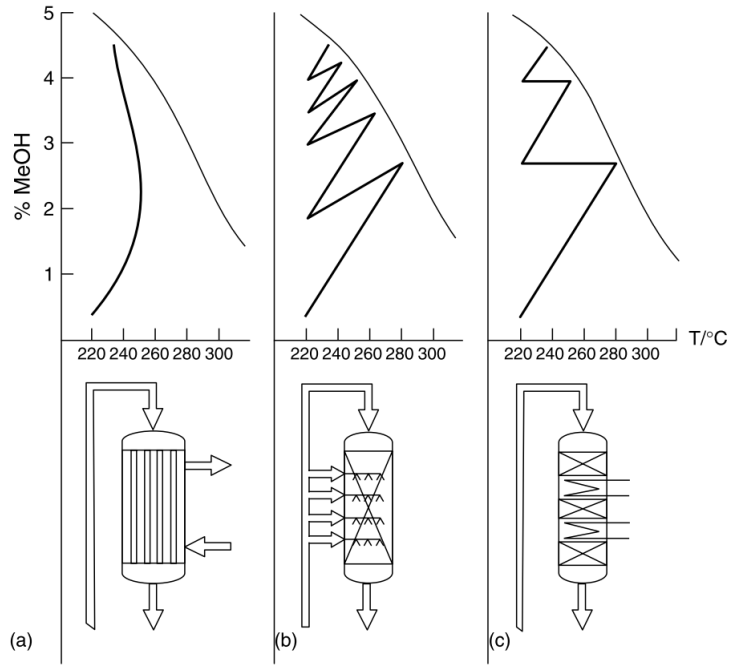

Fig. 2.4.2: Upper panel: Methanol yield (bold lines) and methanol equilibrium (thin lines) as function of temperature associated with lower panel reactors: (a) tubular boiling water reactor (b) series quench reactor and (c) series adiabatic reactor. Figure is from [4].

4.1 Boiling Water Reactor

This design implemented by Lurgi (see figure 2.4.3) consists of catalyst material loaded into vertical reactor tubes immersed into boiling water, which ensures good temperature control and converts 80% of the reaction heat into high-pressure steam applicable for syngas compression and electricity generation [47]. Figure 2.4.3 shows a simplified diagram of the Lurgi process with (1) compression of fresh syngas and subsequent mixing with recycled gas. Reaction heat preheats the mixed syngas in the heat exchanger (2) before the gas enters at the top of the reactor (3). Methanol in the product gas leaving the reactor is condensed in a cooler-condenser (4) and separated (5) before gas recycling (7) with injection of fresh syngas. Part of the recycled gas is purged (6) to avoid built up of inert gas but purging lowers the yield to around 90% because it unavoidably contains syngas [48].
Similar process diagrams including a syngas recycling loop to achieve high conversion ($> 90 - 95\%$ of the make-up gas) exist for the quench and adiabatic reactor designs [21]. This recycle requirement due to unfavourable gas-phase thermodynamics at conventional reaction temperature is one of the most profound disadvantages about conventional methanol synthesis [4]. The isothermal configuration facilitates high thermal efficiency (product energy content divided by reactant energy content), good temperature control, and high selectivity, conversion, and yield. BWRs well-controlled temperature profile and low average operation temperature results in high yields, minimal sintering and consequently high catalyst lifetime (5 years) [4, 18, 21, 48, 49]. However, the complex mechanical design with a tube sheet limits the reactor diameter to approximately 6 m thus restricting the methanol capacity to 1800 ton/day [4, 49]. Parallel BWRs can be installed but this configuration is associated high investment cost making large scale methanol production unsuited with current BWR technologies [18, 21, 49]. Operational conditions are typically 40-100 bar and 493-538 K [8, 21] with a recycling to feed ratio of 3-4 [18, 21].

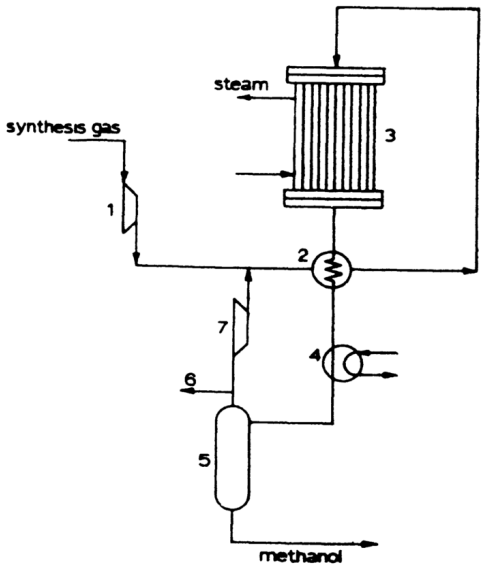

Fig. 2.4.3: Simplified diagram from [48] of the Lurgi process with: 1: Feed gas compressor, 2: Heat exchanger, 3: Lurgi BWR, 4: Methanol condensers, 5: Gas-liquid separator, 6: Purge, 7: Recycle gas compressor.

4.2 Quench Reactor

ICI (now Johnson Matthey) designed a quench reactor consisting of several adiabatic reactors in series embedded within the same shell with internal cooling of the reaction heat supplied by shot cooling with syngas (and partly cooled recycled syngas, see figure 2.4.4) through lozenges in between the beds as shown in figure 2.4.4 [21, 49]. Heat exchangers between the beds are therefore unnecessary resulting

in a simple mechanical design. Its simple and reliable design combined with low cost make it a popular choice and it dominates the market of methanol reactor designs with 61% compared to 27% for the Lurgi design (data based on [50] presented in [6]) and is normally used for methanol production up to around 3000 metric tonnes per day (MTPD) [8]. However, gas dilution by cold (recycled) syngas injected from the sides causes temperature variation across the catalysts beds resulting in low catalyst utilization, which necessitates high catalyst volume and high recycle streams (recycle to feed ratio of 5-7) [4, 8, 21]. Figure 2.4.2 shows the undesired saw-toothed conversion profile as function of temperature implying profound temperature gradients and poor thermal efficiency with increased risk of thermal sintering of the catalyst and lower selectivity [21]. Quench reactors usually operate at 50-100 bar at 493-553 [8, 21].

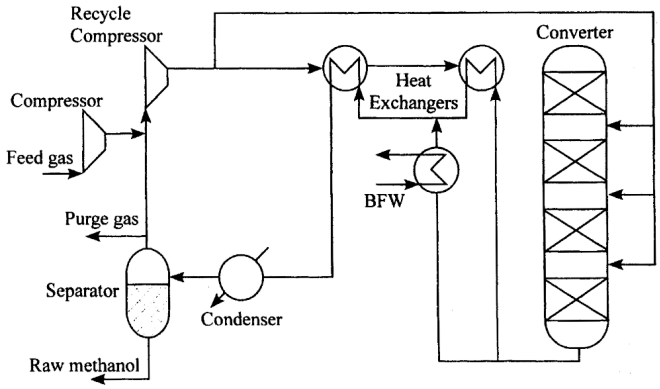

Fig. 2.4.4: Simplified flow diagram for the ICI design with fixed-bed adiabatic reactors and multiple feed gas injection positions to quench the reaction. Figure is from [21].

4.3 Serial Adiabatic Reactor

Though designs by ICI and Lurgi dominate the methanol plant market, the series of adiabatic reactor configuration designed by Topsøe and Kellogg (now Kellogg Brown & Root) is the optimal choice for large capacity methanol plants [4, 21]. Single-line capacities up to 10 000 MTPD can be achieved with this design. They are constructed as spherical reactors with the advantage over cylindrical vessels that they can be constructed with thinner reactor walls yet withstanding the same reaction pressure resulting in lower construction costs. Moreover, the design consists of two perforated spherical shells with catalyst loaded in between, which allows the gas flow to enter from the outside and flow through a relatively thin catalyst bed thus minimizing the pressure drop. This increases the methanol rate compared to cylindrical reactor designs [21, 51]. The advantages of this design are high thermal efficiency, high selectivity and good temperature control, but its relative high cost and complex loading procedures make it most applicable for large capacity plants [4, 21]. Figure 2.4.5 shows a methanol synthesis loop for three adiabatic reactors in series with heat exchanger units placed between each reactor. Optimal reaction conditions are 50 to 100 bar at around 493 K using a recycle ratio of 3 to 5 [4, 21, 48].

4.4 Sustainable Methanol from CO_2 and H_2

Methanol produced from captured CO_2 and renewable H_2 constitutes a potential vital component in realising a methanol economy based on a carbon neutral cycle as envisioned by Noble laureate in Chemistry 1994 George Olah (see section 1). However, CO-free CO_2/H_2 mixtures enhance the risk of substantial inhibiting water concentrations by the RWGS and CO-free conditions is thermodynamic unfavourable for the methanol equilibrium [52, 53]. If restricted to a renewable CO_2/H_2 feedstock, one solution is to initially pass the feedstock through a shift reactor to produce CO and H_2O from CO_2 and H_2 with subsequent water out-condensation resulting in a conventional $CO/CO_2/H_2$ mixture as

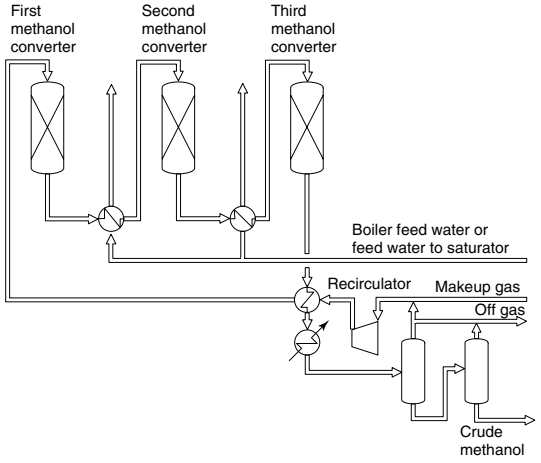

Fig. 2.4.5: Methanol synthesized using a loop of three adiabatic reactors resemble a type of reactor configuration optimal for large capacity methanol plants designed by Topsøe and Kellogg (now Kellogg Brown & Root). Figure is from [4].

illustrated in figure 2.4.6 using the isothermal BWR Lurgi type reactor. Presence of CO favours a higher methanol equilibrium and can scavenge produced and inhibiting water from CO_2 hydrogenation [52].

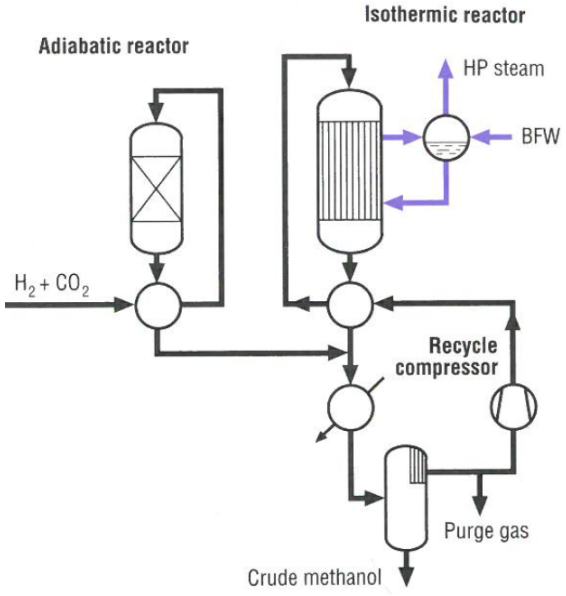

Fig. 2.4.6: Flow scheme for converting a CO_2/H_2 feedstock into methanol using a two reactor (adiabatic and isothermic) system attached with a boiler feed water (BFW) system, which allows utilization of the high-pressure (HP) steam. Figure is from [47].

Alternatively, new catalysts, which converts CO_2 and H_2 directly into methanol while suppressing the RWGS reaction and/or being more water-tolerant, have been proposed [54, 55]. One advantage of a "water-resistant" catalyst is that the shift reactor (adiabatic reactor in figure 2.4.6) can be excluded resulting in economic gain, which must at least outweigh the investment costs associated with developing the "water-resistant" catalyst, before such a "water-resistant" catalyst becomes economically feasible.

Invention of feasible methanol catalysts operating at mild conditions in decentralized areas may pave the way for widespread sustainable methanol production through integration with renewable sources. Low-pressure methanol synthesis is attractive in terms of lower operational and investment costs and supports small decentralized methanol plants but it also lowers the equilibrium methanol conversion. This could be counteracted by lowering the temperature, which in turn decreases the kinetic rate substantially. Therefore, catalysts for methanol synthesis from CO_2 and H_2 must be highly active at low temperature, stable against product inhibition and suppress the endothermic RWGS assisted by lower reaction temperature [52]. Solving these challenges open the possibility for sustainable methanol production at industrial scale.

The Icelandic company CRI demonstrates that renewable methanol production from a CO_2/H_2 feed is economically feasible in areas with inexpensive and available renewable electricity to produce H_2 together with easily accesible CO_2 emissions in high concentrations. CRI uses 5600 metric tonnes of CO_2 to produce 4000 metric tonnes of methanol per year [56]. Their patent issued in 2007 [57] disclosures the overall process, which is a modified version of the two reactor Lurgi design (see figure 2.4.6). H_2 generated from water-electrolysis and captured CO_2 are pressurized and react in a RWGS reactor to produce CO and H_2O. CO is fed to a syngas storage tank containing H_2 and CO_2, which is connected to a methanol reactor, while water is collected in a storage tank. They describe methanol synthesis from different H_2/CO_x syngas mixtures including $CO_2/H_2 = 1/3$ at 50 bar and 498 K over $Cu/ZnO/Al_2O_3$, Cu/ZrO_2 or Cu/Zn/Cr based catalysts with a 20-25% conversion. Temperature control of both the endothermic RWGS and exothermic methanol synthesis reactions is achieved by heat exchange between the two reactors. Excess heat from the methanol synthesis reactor is applied to preheat the cold inlet gas. Their design features an energy-efficiency (electricity to methanol) of 58%, which is slightly higher than the theoretical maximum of 54.1% for a Lurgi design [58]. Therefore, CRI most likely modified the Lurgi design.

Overall, CRI proofs that sustainable methanol from CO_2 and H_2 is economically feasible provided with favourable conditions including abundant, cheap renewable electricity and readily accessible CO_2 in high concentrations and at a low cost preferably with within close proximity to minimize transportation costs. Capital costs for conventional and green methanol production is estimated to be roughly the same [47, 59] whereas the sustainable syngas preparation procedure for green methanol is significantly more expensive compared to natural gas steam reforming [58, 59]. Model scenarios [58] for green methanol production revealed a ten fold higher methanol cost compared to natural gas based methanol and that hydrogen production accounted for around 70-80% of the energy consumption [58, 60] though the actual price increase for green methanol may be location and facility dependent. Improved and cheaper hydrogen production potentially promoted by lower electricity prices is therefore a key challenge for large scale green methanol production. Moreover, electrolysers working efficiently with a variable energy source such as intermittent renewable energy posses an inherent challenge in cheap and renewable hydrogen production from water electrolysis [58]. In comparison, syngas preparation accounts for 50-60% of the total investment cost in conventional methanol plants supplied by natural gas [4, 6, 61]. Expansion in the installed renewable power capacity, initiatives to reduce carbon emissions (e.g. carbon tax) combined with improved CO_2 capturing and electrolysis technologies could expand the locations for economically feasible and commercially interesting sustainable methanol production.

4.5 Catalyst Deactivation

Cu is especially susceptible to poisons including sulphur, chlorine, and iron carbonyls. Sulphur can block the active sites but rarely constitutes a problem for syngas derived from natural gas, whereas desulfurization using a ZnO guard bed may be required for syngas based on coal gasification. Chlorine significantly promotes sintering of Cu and Zn phases but is not normally present in the feedstock. Iron carbonyls may constitute part of the make-up gas in gasification plants but is also generated, when high-pressure and highly reducing syngas contacts the steel-made synthesis loop components including reactor, tubes, heat exchangers etc. Syngas purification and passivation and/or minimizing of carbon-steel tubes in the synthesis loop make catalyst poisoning a minor issue in commercial plants [4, 21].
The major source for deactivation in conventional methanol synthesis is Cu sintering. Tammann's rule

states that thermal sintering of Cu (with a melting point of 1358 K) is minimal if not absent during conventional methanol synthesis operated around 480-580 K [4, 26] as seen in equation 4.2 [4].

$$T_{\text{mobility}} > 0.5\, T_{\text{bulk, melting point}} \tag{4.2}$$

However, above the Hüttig temperature [62] (see equation 4.3 [4]) surface mobility of atoms and molecules becomes significant which promotes sintering [4, 63].

$$T_{\text{Hüttig}} = 0.3\, T_{\text{bulk, melting point}} \tag{4.3}$$

The importance of catalyst sintering for $Cu/ZnO/Al_2O_3$ is evidenced by an activity loss of more than one-third after 1000 h (∼42 days) of operation at commercial conditions [4, 64]. Reduced reaction temperature minimizes the sintering risk, but operational policy generally dictates temperature rise over time to maintain high activity (fast kinetics). Due to the aforementioned thermally promoted sintering, the temperature increase is usually small [21]. Trade-offs between high activity and minimal sintering are considered when deciding on the reaction trajectory. Eventually, the catalyst is replaced after 2-5 years of operation [4, 21, 26, 59].

5 Literacy for methanol synthesis over $Cu/ZnO/Al_2O_3$

Decades of scientific research on catalytic methanol synthesis over Cu-based catalysts have advanced the understanding and resulted in well-established knowledge, which is briefly outlined in this section. Especially the nature of the active sites is subjected to scientific dispute and a comprehensive discussion is allocated for this topic later in section 7.

- Metallic Cu and ZnO were reported as the dominant copper and zinc phases during conventional methanol synthesis conditions based on the following observations:
  - In situ XRD in $CO/CO_2/H_2$ syngas mixture at $T = 493$ K, $P = 30$ bar for a $Cu/ZnO/Al_2O_3$ catalyst found metallic Cu and ZnO [65].
  - IR spectra of CO adsorbed on reduced Cu/ZnO catalysts (reducing gas: $CO/CO_2/H_2$) showed metallic Cu characteristic features [66].
  - XRD investigations after reduction in syngas mixture for a Cu/ZnO catalyst showed ZnO characteristic XRD features [67].
  - In situ neutron diffraction (ND) experiments for a $Cu/ZnO/Al_2O_3$ catalyst at industrially relevant conditions ($CO_2/CO/H_2$ gas, $T = 503$, $P = 60$ bar) showed Cu and ZnO reflections even after 148 h of time-on-stream (TOS) [68].
  - XPS analysis of Cu/ZnO [69] and $Cu/ZnO/Al_2O_3$ [70] catalysts after H_2 reduction at 523 K and 493 K, respectively, identified metallic Cu and ZnO. The surface of a commercial $Cu/ZnO/Al_2O_3$ catalyst after methanol synthesis ($T = 523$ K in $H_2/CO/CO_2 = 73/25/2$, $P = 2$ atm) was reported [71] to consist of metallic Cu and ZnO based on post synthesis XPS analyses.
- The methanol productivity ($g_{MeOH}/g_{cat.}/h$) depends linearly on the specific Cu surface area (m^2 $Cu/g_{cat.}$) for Cu/ZnO-based catalysts in $CO_2/CO/H_2$ gas mixtures based on studies with the following reaction conditions:
  - $T = 473$-493 K, ambient pressure [28]
  - $T = 523$ K, $P = 50$ bar [72]
  - $T = 518$ K, $P = 45$ bar [27]
  - $T = 513$ K, $P = 50$ bar (all areas evaluated by N_2O-RFC).

- Supports profoundly influence the methanol TOF [33, 73, 74] known as the support effect. ZnO and Al_2O_3 supports can promote/stabilize the methanol synthesis activity. Direct relation between methanol production and ZnO coverage after synthesis evaluated by XPS on a zinc deposited Cu(111) catalyst was reported [35] yielding a maximum thirteen fold TOF increase in comparison to zinc-free Cu(111). Al_2O_3 acted as a structural promoter and ensured high methanol activity and long catalyst lifetime [19, 22].

- CO_2 was identified by isotope labelling studies as the main carbon source for methanol synthesis on Cu/ZnO(/Al_2O_3) catalysts [11, 13, 38] at industrially relevant conditions in agreement with mechanistic studies [37] and single crystal studies on Cu(100) [25].

- Formate (HCOO) is the predominant reaction intermediate on the Cu surface and attributed to play a pivotal role for the methanol activity due to:

  - DRIFTS shows HCOO dominance on an ICI catalyst after both methanol synthesis (CO_2/H_2 = 9/91, 473 K, 44 bar) and methanol adsorption (P = 20 mbar, T = 303 K) [75].
  - FTIR study on methanol synthesis (CO_2/H_2 = 1/9, T = 503 K, P = 100 bar) on Cu/SiO_2 revealed predominantly Cu-HCOO surface species [76].
  - Kinetic model coverage calculations show HCOO as the dominant hydrocarbon surface species (0.07 ML) on Cu in a gas composition ($H_2/CO_2/CO/H_2O/CH_3OH$ = 88.65/3.65/1.79/1.35/4.56, T = 506 K, P = 50 bar) corresponding to a 85% approach to equilibrium [77].
  - XPS post-reaction investigations on a zinc deposited Cu(111) catalyst revealed relation between formate coverage and methanol activity (H_2/CO_2, T = 523-563 K, P = 18 bar) [35].
  - In situ IR spectroscopy of Cu/ZnO/Al_2O_3 identified formate and observed direct relation between the absorbance intensity of the formate band and the evolved methanol when exposed to i) CO_2/H_2, P = 10 bar, T = 550 K [78] and ii) at 0 to 3 bars of CO_2 in fixed 7 bars of H_2, T = 523 K [79].
  - Sum-frequency generation study on single and polycrystalline Cu catalysts at 8 bar in CO_2/H_2 = 10/90, T = 573 K reported profound formate coverage of 0.3-0.4 ML [80].
  - TPD measurements on an ICI standard Cu/ZnO/Al_2O_3 catalyst after methanol synthesis (CO_2/H_2 = 1/9, T = 473 K, P = 1 bar) exhibited simultaneous desorption of CO_2 and H_2 at 440 K [81] assigned to formate decomposition in agreement with [82]. Quantitative amounts of CO_2 and H_2 agreed well with the amount of methanol produced [81].
  - DFT calculations on Cu(111) found hydrogenation of adsorbed formate as a key reaction intermediate due to its relative high reaction barrier [37].
  - Kinetic isotope effect (KIE) studies [83] on Cu/ZnO/Al_2O_3 (P = 30 bar, T = 413-523 K in CO_2/X = 1/3 (X being H_2 or D_2) reported formate hydrogenation as the rate determining step.

6 Methanol Synthesis Reaction Pathway

Methanol synthesis by CO_2 hydrogenation involves multiple reaction steps usually described as direct HCOO formation and its conversion to methanol by kinetic models. Hydrogenation of formate to methanol Theoretical and experimental studies on the reaction pathway in conjunction to the rate-limiting step are discussed. Reaction conditions and type of support impact the activity and is therefore considered. An alternative and recently suggested additional methanol-assisted autocatalytic pathway is suggested to profoundly accelerate methanol production of Cu/ZnO-based catalysts at higher conversion ($\gtrsim$0.3 mol% MeOH in the effluent gas) when operated at industrially relevant conditions.

6.1 Direct Hydrogenation Mechanism

A micro-kinetic model for methanol synthesis based on CO_2 hydrogenation was suggested by Askgaard et al. [77]. The model consisted of 13 elementary reaction steps (see table 1) of which eight steps (step 1-8) were designated to the WGS reaction and five steps (step 9-13) assigned to the simplest reaction pathway for methanol synthesis. Three steps were added to allow formation of the by-product formaldehyde. One feature of the model was the incorporation of nearest adsorbate neighbor repulsion, which restricted the saturation surface coverage to one molecule per active surface site defined as two Cu sites whereby complete surface coverage ($\theta = 1$) corresponded to a $c(2 \times 2)$ surface structure. Model simplification was obtained by focusing on the low index planes Cu(100), Cu(110), and Cu(111) as the dominating facets.
Input parameters for the micro-kinetic model were adapted from gas-phase thermodynamics and single crystal (SC) experiments on Cu(100) [23] performed at $P = 2$ bar and $T = 483 - 563$ K with CO_2:H_2 = 1:1. Good agreement for the methanol TOF was found between model-predictions and experimental TOF rates for commercial type $Cu/ZnO/Al_2O_3$ catalysts [84] at $T = 484 - 517$ K, $P = 15 - 50$ bar with different CO:CO_2:H_2 gas compositions, when additional methanol input parameters for Cu(111) were applied as shown in figure 2.6.1.
The good correspondence between model and experimental results supported the application of SC experiments in modeling industrial catalysts and led the authors to suggest that the dominant active Cu facet for methanol synthesis was the Cu(111) facet. Based on comparisons between model-scenarios assuming step 10, 11 or 12 to be the rate-limiting step with SC experiments [23], the authors proposed hydrogenation of H_2COO^* to methoxide and oxide (step 11) to be the rate-limiting step.
Limitations of Aksgaard's micro-kinetic model includes the influence of support (and potential bifunctional mechanisms) and surface structure [21], which to some extent were addressed later by Ovesen et al. [85].

Table 1: Isolated * symbolizes a free surface site, whereas X^* signifies that the molecule/atom X is adsorbed on the surface or in the gaseous (g) state. The kinetic model is adapted from [77].

Step no.	Reaction		
1	$H_2O(g) + *$	$\leftrightharpoons$	H_2O^*
2	$H_2O^* + *$	$\leftrightharpoons$	$OH^* + H^*$
3	$2\ OH^*$	$\leftrightharpoons$	$H_2O^* + O^*$
4	$OH^* + *$	$\leftrightharpoons$	$O^* + H^*$
5	$2\ H^*$	$\leftrightharpoons$	$H_2 + 2\ *$
6	$CO(g) + *$	$\leftrightharpoons$	CO^*
7	$CO^* + O^*$	$\leftrightharpoons$	$CO_2^* + *$
8	CO_2^*	$\leftrightharpoons$	$CO_2(g) + *$
9	$CO_2^* + H^*$	$\leftrightharpoons$	$HCOO^* + *$
10	$HCOO^* + H^*$	$\leftrightharpoons$	$H_2COO^* + *$
11	$H_2COO^* + H^*$	$\leftrightharpoons$	$H_3CO^* + O^*$
12	$H_3CO^* + H^*$	$\leftrightharpoons$	$CH_3OH^* + *$
13	CH_3OH^*	$\leftrightharpoons$	$CH_3OH(g) + *$
14	$H_2COO^* + *$	$\leftrightharpoons$	$HCHO^* + O^*$
15	$HCHO^*$	$\leftrightharpoons$	$HCHO(g) + *$
16	$H_2COO^* + H^*$	$\leftrightharpoons$	$HCHO^* + OH^*$

In contrast to Askgaard's model (based on Cu SC experiments), Fujita et al. [86] reported hydrogenation of HCOO-Zn and/or HCOO-Cu into CH_3O-Zn as rate-limiting step(s) based on combined FTIR, TPD and activity investigations on Cu/ZnO catalysts. FTIR performed during methanol synthesis

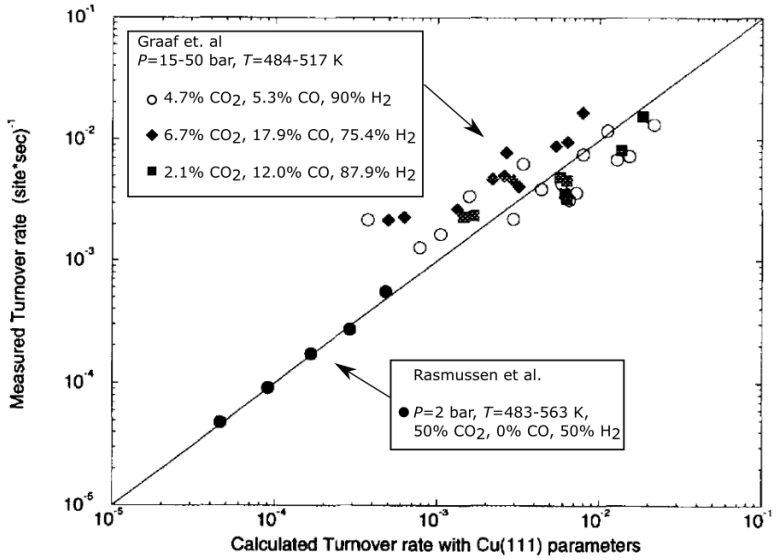

Fig. 2.6.1: Experimental studies conducted by both Rasmussen et al. [23] and Graaf [84] agree well with predictions (line) from a kinetic model suggested by Askgaard et al. [77]. Original figure from [77] was been modified with annotations.

(CO_2/H_2 = 1/9, T = 438 K, 1 atm) demonstrated a rapid initial rise in the amount of HCOO-Cu, whereas the rate of the CH_3O-Zn signal increase was significantly less pronounced upon methanol synthesis as evident from figure 2.6.2. Further investigations of catalysts containing preadsorbed HCOO-Cu and HCOO-Zn showed that decrease in the HCOO-Cu signal was accompanied by an increase in the CH_3O-Zn signal, whereas the HCOO-Zn signal both during methanol synthesis and H_2 treatment remained constant over time as shown in figure 2.6.3. This supported the suggested methanol synthesis route from HCOO-Cu to CH_3O-Zn. Based on the facile formation of HCOO-Cu (rapid initial rise), the relation between HCOO-Cu decrease and CH_3O-Zn increase, relation between CH_3O-Zn formation from HCOO-Cu and partial pressure of H_2, and previously reported fast hydrolysis of CH_3O-Zn into methanol [87], hydrogenation of formate on Cu into methoxy was suggested as the rate-limiting step for methanol synthesis in CO_2/H_2 syngas on Cu/ZnO catalysts. DRIFTS studies by Neophytides et al. [75] on an ICI type $Cu/ZnO/Al_2O_3$ catalyst substantiated that hydrogenation of formate species adsorbed on Cu into methoxy was the rate-limiting step.

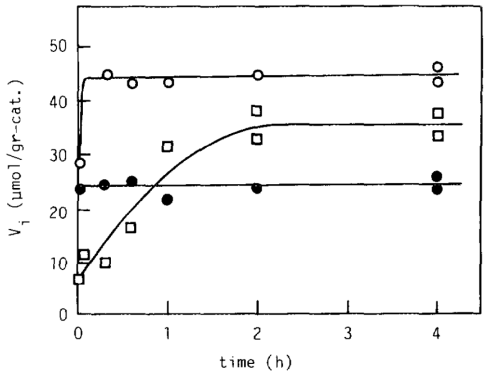

Fig. 2.6.2: Time-evolution in the amounts of HCOO-Cu (○), HCOO-Zn (●), and CH_3O-Zn (□) during CO_2/H_2-reaction for 30 mol% Cu/ZnO catalyst. Figure is form [86].

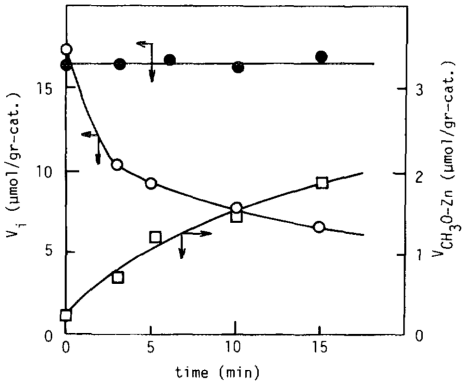

Fig. 2.6.3: Changes in the amounts of HCOO-Cu (○), HCOO-Zn (●), and CH_3O-Zn (□) with time of H_2 pretreatment at 383 K on catalysts containing preadsorbed HCOO-Cu and HCOO-Zn. Figure is from [86].

The origin of the different reported rate-limiting steps may be ascribed to catalyst type, reaction conditions etc. as will be discussed later in section 7.5. Nevertheless, the elementary steps contained in the micro-kinetic model by Askgaard et al. [77] are still regarded as applicable [4, 37].

Changes in the particle morphology in response to the reaction conditions were incorporated into Askgaard's static model by Ovesen et al. [85]. Their revised model included the impact of syngas composition on the interface surface free energy between Cu and ZnO (support), which enabled a description of the dynamic behaviour based on the change in the number of active sites upon applying various syngas mixtures. The profound effect of including the dynamic behaviour was shown by in situ EXAFS studies [88], where syngas oxidation potential variations resulted in particle morphology changes for a Cu/ZnO catalyst system and hence changed the number of active sites. Reversible particle morphology response was observed upon changing the syngas between standard syngas ($CO/CO_2/H_2$) and oxidizing syngas ($H_2O/CO/CO_2/H_2$). Support to a mobile surface under reaction conditions was provided by Spencer [89], who reported the onset temperature for surface mobility (Hüttig temperature equal to $\approx \frac{1}{3}$ of the melting temperature i.e. $\frac{1}{3}T_{\mathrm{m}}$ [4, 89]) for Cu to be ~ 450 K (in agreement with [64]) well below conventional reaction conditions (473-573 K).
Based on this "dynamic" micro-kinetic model, methanol activities for $Cu/ZnO/Al_2O_3$ catalysts using different CO/CO_2 gas mixtures were calculated agreed with experimental studies. Both theoretical and experimental investigations demonstrated that particle morphology dynamics profoundly impacted the catalytic activity.

Work to improve the dynamic model by Ovesen et al. [85] was performed in a comprehensive DFT study by Grabow and Mavrikakis [37]. They established a mean-field micro-kinetic model, which investigated the methanol synthesis and the WGS reaction based on 8 gas and 22 adsorbed species evaluated using 49 elementary steps. The fundamental model assumptions are listed next:

- Mean-field approximation with no adsorbate-adsorbate interactions was justified by assuming the adsorbates to be well-mixed ($T \sim 500$ K for methanol synthesis) on the surface together with negligible diffusion limitations.
- A Cu(111) surface was used to determine kinetic and thermodynamic parameters due to:
  - The most stable Cu facet is Cu(111). [37]
  - TEM imaging showed Cu(111) and Cu(100) surfaces to prevail during methanol synthesis. [90]
  - Reaction rates on polycrystalline Cu with Cu(111) as the major facet and industrial type $Cu/ZnO/Al_2O_3$ catalysts [91] agreed well.
- Surface coverage was limited to 1 ML, and multilayer adsorption was not considered.
- All input parameters were derived from periodic and self-consistent GGA-PW91 DFT calculations conducted on Cu(111) and fitted to experimental activities for $Cu/ZnO/Al_2O_3$ catalysts operating at industrially relevant conditions.

Generally, assumptions about the limiting steps etc. are a prerequisite to estimate input parameters as conducted by Ovesen et al. [85]. However, Grabow and Mavrikakis [37] eliminated this requirement by applying DFT to determine the input parameters. The reaction mechanisms for CO_2 and CO hydrogenations proposed by the DFT calculations are shown in the following (X^* and * are described in table 1):

CO_2 hydrogenation

$$CO_2^* \rightarrow HCOO^* \rightarrow HCOOH^* \rightarrow CH_3O_2^* \rightarrow CH_2O^* \rightarrow CH_3O^* \rightarrow CH_3OH^*$$

CO hydrogenation

$$CO^* \rightarrow HCO^* \rightarrow CH_2O^* \rightarrow CH_3O^* \rightarrow CH_3OH^*$$

On the basis of a micro-kinetic model comprehensively evaluated by DFT, the active methanol site was proposed to consist of a partially oxidized and more open Cu facet including Cu(110), Cu(211) and Cu(100) rather than Cu(111).
Figure 2.6.4 revealed the impact of WGS and CO/CO_2 hydrogenation on the methanol synthesis reaction pathways. Enthalpies and activation energy barriers were obtained after fitting the micro-kinetic model to experimental methanol synthesis results obtained for CO_2 hydrogenation (blue), CO hydrogenation (green) and RWGS reaction (red).
The model performed better in CO_2-rich syngas mixtures because the dominant part of the experimental studies applied for model fitting was performed with CO_2-rich syngas mixtures.
Through comparison between DFT derived binding energies and micro-kinetic model inputs, the authors suggested Cu as the active site for methanol synthesis, though they could not definitively eliminate possible synergy effects between Cu and ZnO.

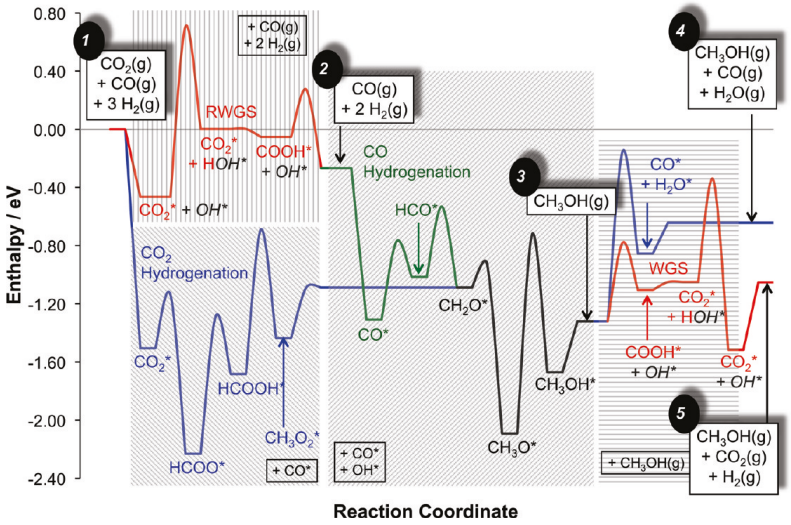

Fig. 2.6.4: Potential energy surface for different methanol synthesis pathways calculated based on the micro-kinetic model, which was fitted to experimental data. Enthalpies are shown w.r.t. to CO_2(g), CO(g) and 3 H_2(g) at $T = 499$ K. The (R)WGS reactions (red) are assumed to involve OH^* species marked in gray italic font. Path for CO_2 hydrogenation: state 1 → blue line → black line → state 3 ending with either i) blue line → state 4 if no WGS or ii) red line → state 5 if incl. WGS. Path for CO hydrogenation: state 2 → green line → black line state 3. Spectator molecules are shown in black boxes with shaded background, and adsorbed H^* has been removed. Figure is from [37].

The influence of zinc on the reaction pathway was studied using DFT by Behrens et al. [29], who examined a flat (defect-free) Cu(111) surface, a stepped Cu(211) surface to incorporate surface defects with and without Zn as illustrated in figure 2.6.5. Increase in the methanol activity was found for the Cu stepped surface compared to the flat Cu surface attributed to stabilization of reaction intermediates on the steps as shown by figure 2.6.6. Activity experiments ($T = 483$ and 523 K, $P = 60$ bar, 59.5% H_2, 8.0% CO_2, 6.0% CO, balanced inert) confirmed the relation between enhanced activity and presence of a stepped surface by a linear increase in the activity as function of the stacking fault probability (identified by the inter-planar spacing ratios d_{111}/d_{200} and d_{222}/d_{400}). Both DFT and catalytic activity measurements reported further activity rise for zinc containing Cu catalysts. Enhanced adsorption strength of reaction intermediates and lowering of reaction barriers between intermediate steps were suggested as explanations for the beneficial role of zinc.

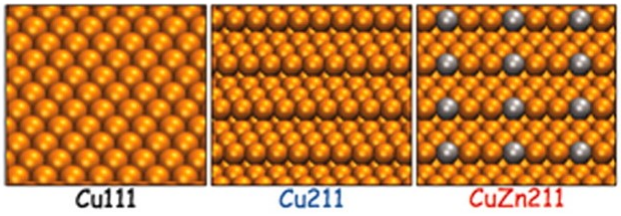

Fig. 2.6.5: Examined surface facets in figure 2.6.6 with one Zn atom replacing one Cu atom in the Cu stepped surface and termed CuZn211. Figure is from [29].

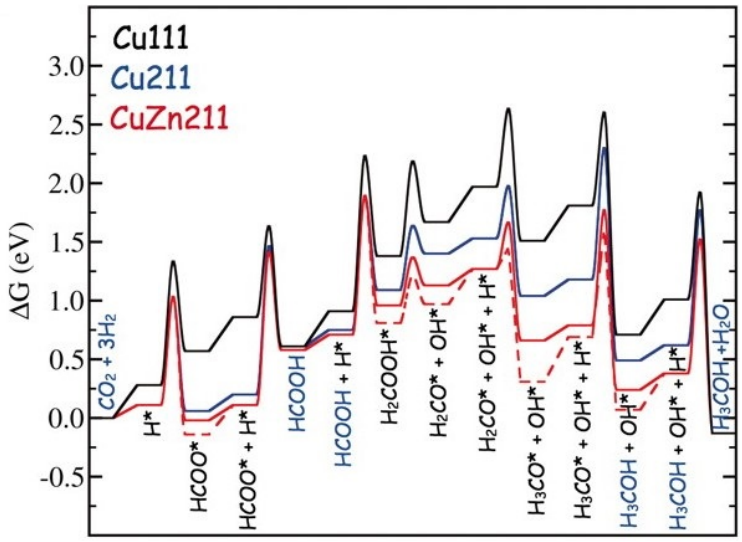

Fig. 2.6.6: DFT calculated energy diagrams for CO_2 hydrogenation at $T = 500$ K, $P_{H_2} = 40$ bar, $P_{CO} = 10$ bar, $P_{CO_2} = 10$ bar, $P_{CH_3OH} = 1$ bar and $P_{H_2O} = 1$ bar on various facets. The energies are relative to gas phase CO_2 and H_2 on clean surfaces ($\Delta G = 0$). The facets are close-packed (black), stepped Cu with three atoms (blue) and surface Zn replacing Cu one to one (red solid) or two Zn atoms to one Cu atom (red dashed). Figure is from [29].

6.2 Indirect Autocatalytic Mechanism

A reaction exhibiting autocatalytic behaviour is characterized by a reaction product acting as catalyst for further product formation resulting in a net activity gain [92]. An autocatalytic mechanism is attractive because it offers an explanation for conflicting reported activity results measured at different conversion levels and syngas composition using various support types. These conflicting studies are briefly discussed, as a further discussion and description of the autocatalytic mechanism is presented in the published paper *Methanol-Assisted Autocatalysis in Catalytic Methanol Synthesis* in chapter 4. Once an equilibrium limited reaction reaches a steady state and equilibrium concentration of reactants and products is achieved. At low conversion or equivalent differential conditions the concentrations of products are not expected to substantially impede the reaction rate. At higher conversion (finite conditions), the product concentrations rise and shifts the equilibrium towards the product size. Consequently, it is expected that the turnover frequency of a simple reaction occurring over a given catalyst at identical reaction conditions (temperature, pressure, feed gas composition) except the conversion level (regulated by e.g. space velocity and catalyst loading) is highest at differential conditions. Inconsistent results with this description points to an imperfectly understood reaction mechanism. Studies reporting higher TOF at finite conditions at certain reaction conditions are discussed next.
Lee et al. [40] exposed a commercial (ICI) $Cu/ZnO/Al_2O_3$ catalyst to both CO- and CO_2-rich $CO/CO_2/H_2$ syngas mixtures under different space velocities to study the influence of space velocity and CO/CO_2 concentration on the methanol activity. In CO-rich syngas with CO_x fractions of 10-30% CO_2 and 70-90% CO, the methanol rate is higher at finite (54×10^3 l/kg/h) conditions compared to more differential (108×10^3 l/kg/h) conditions.

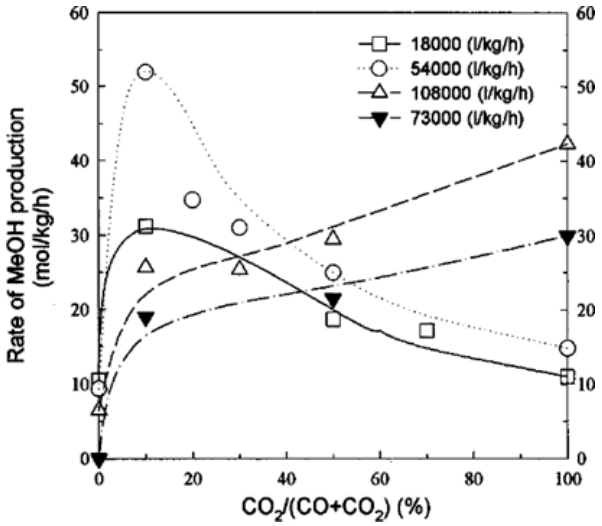

Fig. 2.6.7: Methanol rate at various space velocities (SV) and different feed gas compositions over a commercial ICI $Cu/ZnO/Al_2O_3$ catalyst. All experiments are conducted at $T = 523$ K, $P = 30$ bar with $H_2/CO_x = 4$ except for 73×10^3 l/kg/h with $H_2/CO_x = 8$. Figure is from [40].

Similar observations was reported by Sahibzada et al. [41] as seen in figure 2.6.8 with higher rate at finite conditions in CO-rich syngas mixtures. This methanol activity acceleration at higher conversion that contradicts the normal behaviour of a catalytic reaction especially equilibrium limited reactions creates room for a second potentially autocatalytic mechanism, which becomes important at higher conversion conditions. Further discussion on this matter is provided in chapter 4

7 Metal-Support Interactions

Supported metal catalysts can experience interactions between metal and support with profound consequences for the catalytic properties of the catalyst including the methanol TOF [74, 93–95]. Reported

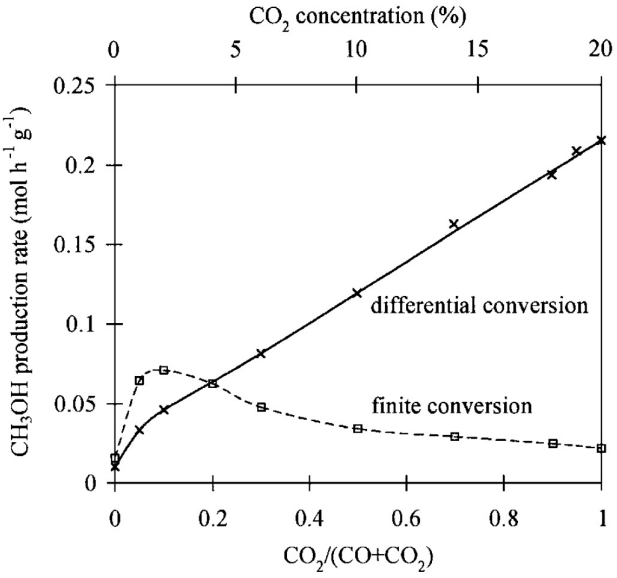

Fig. 2.6.8: Methanol rate from $CO/CO_2/H_2$ ($CO_x/H_2 = 1/4$) feed gas mixtures measured at differential conditions in a tubular reactor and at finite conditions in a internal recycle reactor. Figure is from [41].

metal-support interactions for Cu/ZnO-based catalysts are often abbreviated the Cu-ZnO synergy and is suggested to account for the supremacy of the conventional $Cu/ZnO/Al_2O_3$ catalyst. Several mechanisms have been proposed to explain the Cu-ZnO synergy including:

- Gas-dependent surface morphology
- ZnO induced Cu strain and defects
- ZnO decoration of Cu generation an active Cu-ZnO interface
- Cu-Zn surface alloy formation
- Electron transfer induced by the support

The proposed electron transfer mechanism constitutes a main research objective in this PhD work.

7.1 Gas-dependent Morphology of Cu on ZnO

Changing the gaseous environments over Cu-based catalysts altered the surface morphology of Cu particles with profound implications for the catalytic activity. The suggested gas-dependent Cu surface morphology mechanism is discussed in the following.

Cu/ZnO and Cu/SiO_2 catalysts were investigated by EXAFS in two syngas environments with different oxidation potentials (Dry: 5% CO, 5% CO_2, balanced hydrogen, low oxidation potential, Wet: 3% H_2O, 4.85% CO, 4.85% CO_2, balanced H_2, high oxidation potential) by Clausen et al. [88]. Cu/SiO_2 exhibited no apparent change in the Cu coordination number upon switching from dry to wet syngas mixture whereas Cu/ZnO showed reversible changes in the coordination number, which was attributed to Cu particle shape variations. By applying the Wulff construction [96] the authors explained the dynamic coordination number response to dry/wet syngas exposure with changes in the Cu/ZnO contact surface free energy induced by variation in the oxygen vacancy concentration as a consequence of the different oxidation potentials. The dry/wet syngas caused support wetting/non-wetting phenomena and disc-like/sphere Cu particle shapes.
Absence of changes for Cu/SiO_2 was attributed to the strong Si-O bond making it difficult to generate

oxygen vacancies, which could alter the Cu surface morphology.
Later IR studies by Topsøe and Topsøe [66] supported the increase in oxygen vacancy concentration under reducing atmosphere for Cu/ZnO catalysts and found no reversible variation in the surface structure for Cu/SiO_2 (and Cu/Al_2O_3) in agreement with Clausen et al. [88].

A similar Cu/ZnO catalyst exposed to the same gas mixtures (as Clausen et al. [88]) were investigated by Grunwaldt et al. [67], who in addition measured the methanol production rate. The rate of methanol production responded reversibly as the gas mixture altered between wet and dry gas mixtures as seen in figure 2.7.1 (compare dry gas exp. no. 2, 4 and 6 with wet gas exp. no. 3, 5 and 7) again in support of the work by Clausen et al. [88].

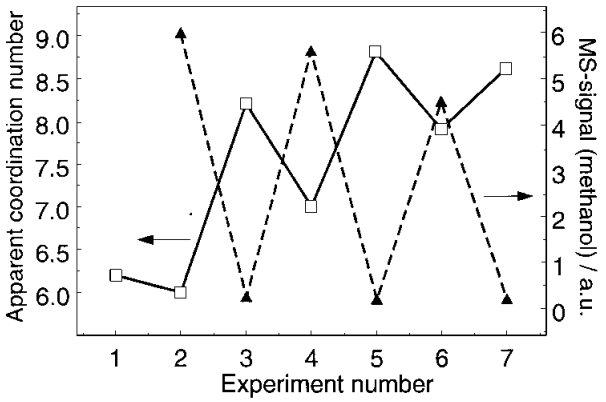

Fig. 2.7.1: EXAFS and MS analyses combined on a Cu/ZnO catalyst (4.5 wt% Cu) demonstrated relation between methanol activity obtained at 493 K (ambient pressure) in dry or wet syngas and variation in the apparent Cu-Cu coordination number in the reducing gas (1), dry syngas (2, 4, 6) and wet syngas (3, 5, 7). Figure is from [67].

The proposed relation between reaction conditions, oxygen vacancies and the resulting Cu particle shapes were modeled as seen in figure 2.7.2 and described in reactions R3 and R4 [85].

$$H_2(g) + Zn{-}O \rightleftharpoons H_2O(g) + Zn{-}V^O \qquad \{R3\}$$

$$CO(g) + Zn{-}O \rightleftharpoons CO_2(g) + Zn{-}V^O \qquad \{R4\}$$

with V^O symbolizing an oxygen vacancy in ZnO formed at the Cu/ZnO interface under reducing conditions. ZnO reduction could facilitate Cu-ZnO_x surface alloy formation as seen in figure 2.7.2c. Oxidizing syngas was associated with spherically shaped Cu particles and high Cu coordination number, whereas reducing syngas flattened the Cu particles and lowered the Cu coordination number.

Dry syngas conditions enhanced the methanol signal attributed to a larger Cu particle surface area. The authors ruled out inhibiting water as a key factor influencing the methanol activity based on a micro-kinetic model [77], which reported that water adsorb weakly on Cu. However, even small amounts of water added to the feed gas has recently shown substantial decrease in the methanol activity (see section 6.2) thus water deficiency under dry syngas conditions may partly explain the larger methanol signal reported by Grunwaldt et al. [67]. The gradual decline in the MS signal with higher (odd) experiment number (figure 2.7.1) was associated with Cu sintering over time [67].
Ovesen et al. [85] applied the knowledge obtained by Clausen et al. [88] and Grunwaldt et al. [67] to construct a dynamic micro-kinetic model (see section 6), which demonstrated good agreement with independent studies in terms of describing the gas-dependent particle morphology and its effect on the catalytic activity.

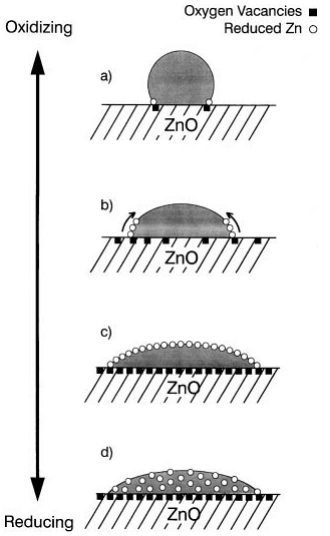

Fig. 2.7.2: Interaction model for Cu particles and ZnO support under various conditions from round-shaped particle (a) over a disk-like Cu particle (b) and formation of a Cu-ZnO_x surface alloy (c) to brass alloy formation (d) involving oxygen vacancies and reduced Zn. Figure is from [67].

Imaging of the gas-dependent surface morphology was obtained by Hansen et al. [90] using in situ TEM as seen in figure 2.7.3. Clearly, reducing gas conditions promoted flat Cu particles, while oxidizing gas mixtures resulted in more spherical Cu particles. The in situ TEM results agreed well with the dynamic model by Ovesen et al. [85] and the interaction model presented in figure 2.7.2.

Studies discussed here evidently suggested gas-dependent surface morphology wetting/non-wetting behaviour of Cu on ZnO, which in turn influenced the methanol activity. However, it can be debated, whether the examined model Cu/ZnO catalysts with small Cu particles dispersed on a "large" ZnO support (and reported gas-dependent surface morphology) are representative for the conventional catalyst with 50-70 atomic % CuO and 20-50 atomic % ZnO (see section 2). Moreover, the exclusion of the detrimental role of water in wet syngas environments seem to contradict other studies (see discussion in section 6.2).

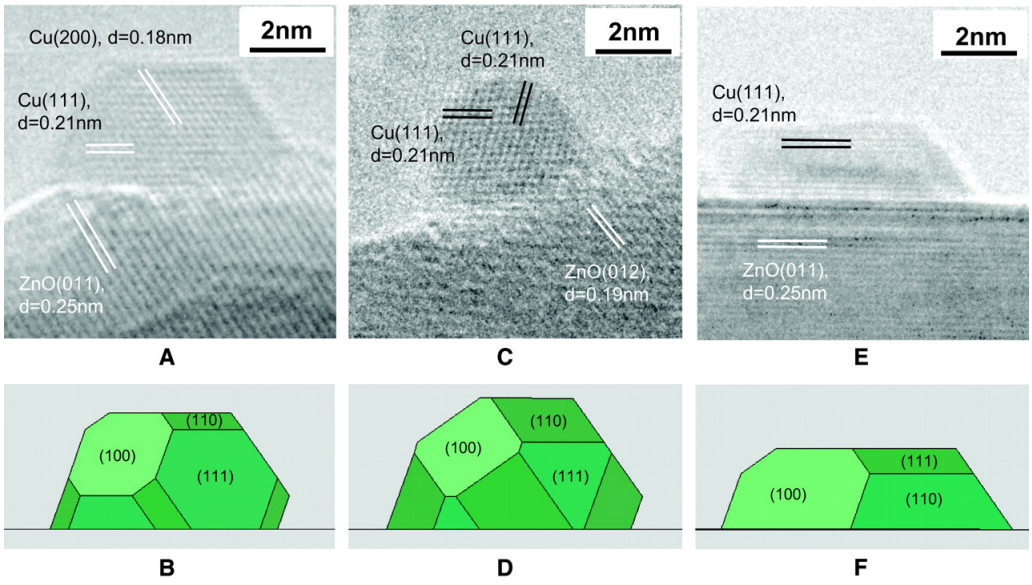

Fig. 2.7.3: In situ TEM imaging obtained at the following conditions: A (reducing): H_2, $T = 493$ K, $P_{tot} = 1.5$ mbar, C (wet, oxidizing): $H_2/H_2O = 3/1$, $P_{tot} = 1.5$ mbar, $T = 493$ K, E (dry, reducing): $H_2/CO = 95/5$, $P_{tot} = 5$ mbar, $T = 493$ K. Images A, C, and E show the equilibrium shapes after 1 h gas exposure. B, D, and F reveal the Wulff constructions determined by surface and interface free energies obtained from A, C and E. Figure is from [90].

7.2 Defective and Strained Cu Lattice Promoted by ZnO

Microstrained and defective Cu induced by ZnO was suggested to facilitate the generation of active Cu edge sites (e.g. steps), which was proposed to account for the Cu-ZnO synergy effect according to the studies presented in this section.
Günter et al. [97] synthesized Cu/ZnO catalysts with different Cu/Zn ratios and applied XRD to examine both the microstructure and the Cu surface area with MS applied to evaluate the activity in $CO/CO_2/H_2 = 10/4/72$ (balanced in He) syngas at $T = 493$ K and atmospheric pressure. The Cu/Zn precursor ratio (shown in figure 2.7.4) regulated the Cu microstrain, which in turn affected the activity (most beneficial for Cu/Zn = 20/80 mol%) as evident in 2.7.5 and explained by:

- ZnO dissolved in Cu facilitated structural Cu defects.
- Incomplete Cu reduction caused oxygen leftover in Cu.
- Epitaxial bonding of Cu on ZnO caused interfacial strain.

Support to the relation between Cu microstrain and catalytic activity was provided by work of Kasatkin et al. [32], who examined an industrial type catalyst at $T = 483$ K in a H_2:CO:CO_2:He (72:10:4:14 molar ratio) syngas mixture at 60 bar. Based on XRD and TEM with EDX measurements the authors reported that both the overall faulting probability ($1.5\alpha + \beta$ in figure 2.7.6c), and the microstrain (Strain in figure 2.7.6b) correlated with the catalytic activity. Lattice imperfections such as planar defects and strain explained the increase in the methanol activity, because the imperfections could facilitate the formation of unique active sites, according to the authors [32].

Behrens et al. [29] underpinned the activity promotion effect attributed to Cu defects and the stacking fault probability as seen in figure 2.7.7 based on methanol synthesis experiments on an unsupported (pure) Cu and five $Cu/ZnO/Al_2O_3$ catalysts. They argued [29] that Cu due to strong metal support interactions (SMSI), which describes suboxide covering supported metal particles mediated by reducing atmosphere [98], was partially covered by ZnO_x, which facilitated the formation of $Zn^{\delta+}$. The Cu-ZnO synergy effect was explained by substitution of partial oxidized zinc species ($Zn^{\delta+}$) into highly active

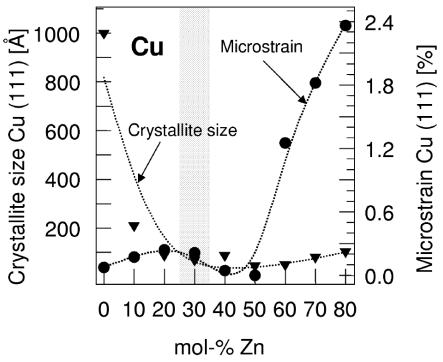

Fig. 2.7.4: Changes Cu crystallite size (triangles) and microstrain (circles) in response to the nominal Zn content (mol%). Figure is from [97].

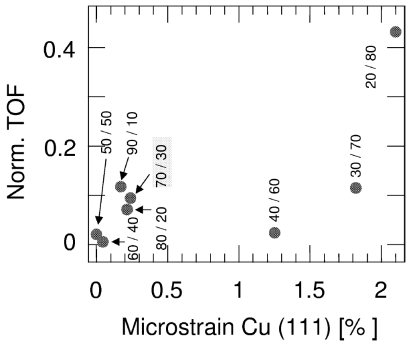

Fig. 2.7.5: Influence of the Cu(111) microstrain (Cu/Zn mol%) on the normalized methanol TOF. Figure is from [97].

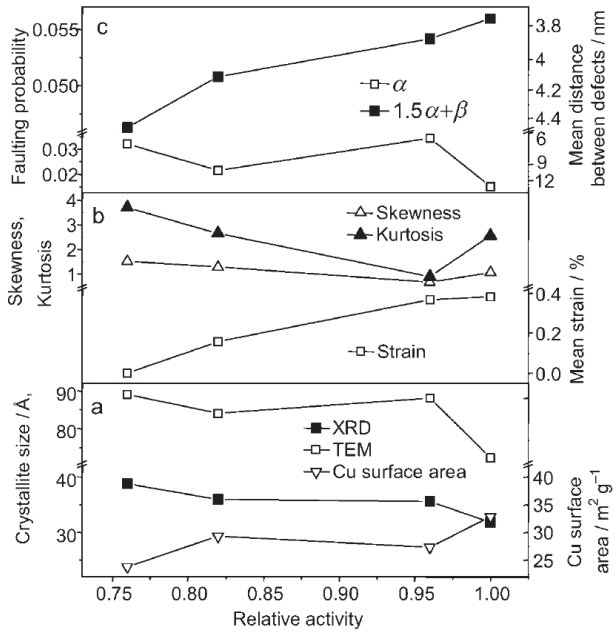

Fig. 2.7.6: Relation between different microstructural properties and the relative methanol activity. Notice, the clear trend between methanol activity and both microstrain fig. b (open squares) and overall faulting probability fig. c (solid squares). Figure is from [32].

Cu step sites resulting in stabilization of reaction intermediates. Gibbs free energy diagrams for the different Cu(Zn) facets shown in figure 2.6.5 demonstrated the following activity order Cu/Zn(211) > Cu(211) > Cu(111) due to variations in reaction intermediate stabilization and reaction barrier energies as illustrated in figure 2.6.6.

Activity measurements concerning CO_2 hydrogenation on zinc-free and zinc-containing catalysts supported the DFT calculations regarding stabilization of CO_2 hydrogenation intermediates in the presence of zinc by reporting a clear beneficial role of zinc on the activity [29].

The active Cu step site mechanism implied methanol rate increase (on top of the rate increase associated with a larger Cu surface area) as the Cu particle size decreased, because smaller Cu particles generally facilitated a higher probability of stacking fault (e.g. steps). However, very small Cu particles (below 8 nm according to Van den Berg et al. [99]) may not be able to accommodate highly active step-edge sites. Accordingly, a non-linear increase in the activity with larger Cu surface area facilitated by moderately small Cu particles (above 8 nm) is expected, if strained and defective Cu (potentially

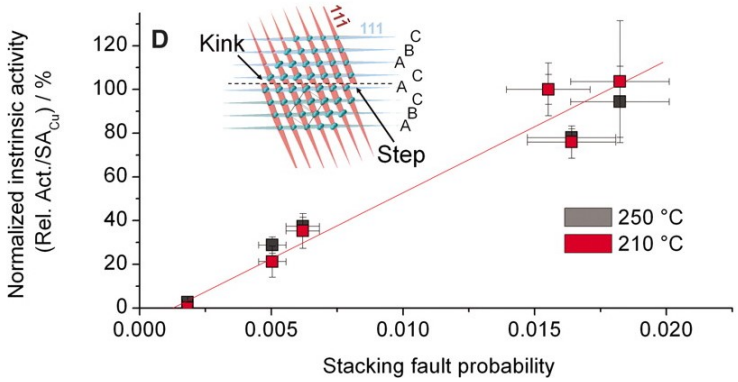

Fig. 2.7.7: Intrinsic activity ($P = 60$ bar, $T = 483$ and 523 K, $H_2/CO_2/CO = 59.5/8/6$ and balanced inert) of Cu catalysts (5-15 nm in size) as function of the Cu stacking fault concentration (determined by shifts in the 111, 200, 222 and 400 diffraction peaks) with the inset figure illustrating how a stacking fault in a (111) surface can facilitate kinks and surface steps. Figure is from [29].

decorated with ZnO_x) constitutes the active site. This model is in conflict with the well-substantiated linear relation (see section 5) between activity and Cu surface area, which is normally based on the N_2O uptake of Cu after catalyst reduction. However, the reduction treatment may partially reduce reducible oxides including ZnO causing an additional N_2O uptake [70, 100, 101]. The potentially biased Cu surface area (discussed later in section 8.1) may conceal the "expected" (if defect sites are the active centres) non-linear relation between the activity and the Cu surface area. Whether the additional N_2O-uptake exactly cancelled out the structure sensitive effect is questionably especially because the linearity between surface area and activity was also reported in studies working with ZnO-free catalysts [33, 102, 103].
Behrens et al. [29] reported that stepped Cu sites covered by $Zn^{\delta+}$ ensured high methanol activity obtained by a highly optimized catalyst preparation procedure. Therefore, for industrial applications only a small fraction of the Cu surface area contributed to the activity by significantly enhancing the TOF, and this catalyst configuration was difficult to obtain for simple model systems, the authors argued.
Whether such highly active Cu steps decorated with $Zn^{\delta+}$ exist at conventional reaction conditions, or the TOF is independent of the Cu particle size (potentially restricted to a specific size range above ~ 8 nm) requires additional work.

Overall, the discussed studies reported a highly active and defective/strained Cu surface induced by ZnO_x to account for the Cu-ZnO synergy effect.

7.3 Promoted Activity by ZnO Decoration of Cu

Interactions between Cu and ZnO were proposed to generate a sintering protective and activity promoting ZnO overlayer on Cu nanoparticles (NPs), which is the subject for discussion in this section. This mechanism builds on the model of a defective and highly active Cu surface but differs by the additional promoting aspects of a protective ZnO overlayer.
Recently, the Cu-ZnO interaction has been attributed to a graphite like (GL) ZnO overlayer on top of Cu NPs by Lunkenbein et al. [104]. After reduction of $Cu/ZnO/Al_2O_3$ in H_2/Ar (20/80) at 523 K, the catalyst was transferred to a glove box and prepared for investigations using scanning transmission electron microscopy (STEM), HRTEM, energy filtered transmission electron microscopy (EFTEM), and electron energy loss spectroscopy (EELS) with the results shown in figure 2.7.8. The analyses revealed a core-shell structure with a Cu core (in figure 2.7.8 Cu is A: identified, B: grey, D: red) surrounded by a ZnO shell (in figure 2.7.8 zinc is A: identified, B: yellow, C: yellow).

The authors highlighted the importance of a defective Cu surface by associating a defective surface Cu with high kinetic stability of the GL ZnO layer, which inhibited Cu NPs sintering. The GL ZnO

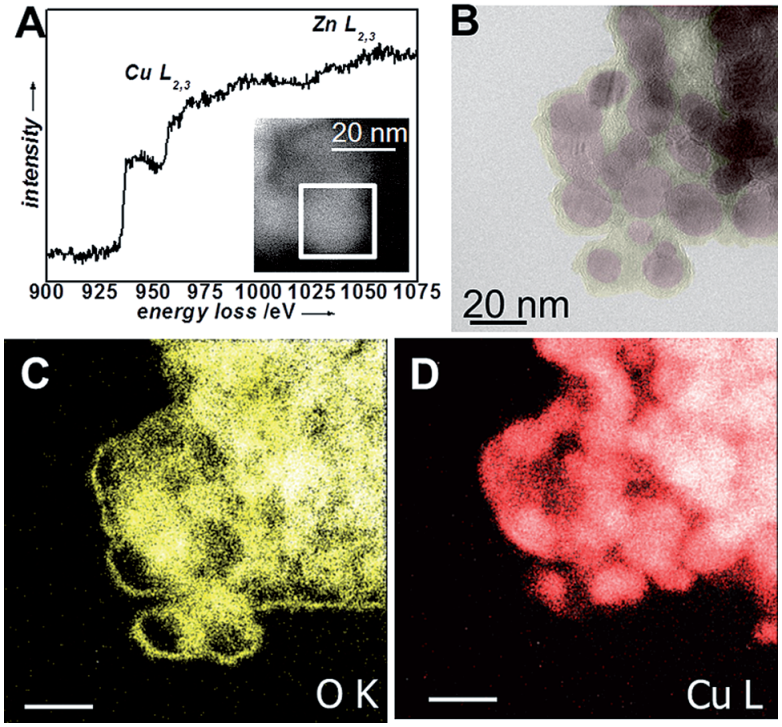

Fig. 2.7.8: A: STEM-EELS spectrum of the Cu/ZnO/Al_2O_3 catalyst shows the Cu $L_{2,3}$ and Zn $L_{2,3}$ EELS features obtained from the single NP and its surrounding environment (see inserted HAADF-STEM image with the 20 nm scale bar). B: TEM image indicated the core-shell structure shown clearer by EFTEM maps for C) the oxygen K edge and D) the copper L edge. Figure is from [104].

overlayer was observed ex situ on a real catalyst making room for future in situ experiments to evaluate the dynamics and stability of this GL ZnO overlayer under working conditions as also recognized by the authors [104].

An active Cu-ZnO interface layer benefiting the methanol rate was suggested by Kattel et al. [105] to explain the substantial methanol production (T = 550 K, P_{CO_2} = 0.5 atm, P_{H_2} = 4.5 atm) increase as 0.4 ML ZnO was vapour-deposited Cu/Zn(000$\bar{1}$) termed ZnO/Cu/Zn(000$\bar{1}$) as seen in figure 2.7.9. Cu/Zn(000$\bar{1}$) consisted of small Cu particles deposited on the ZnO single crystal facet. Figure 2.7.9 shows a volcano-shaped methanol production dependency on the fraction of covered Cu indicating that the combination of Cu and ZnO NPs were key to a high methanol production.
Similar reaction conditions to Kattel et al. [105] were applied by Palomino et al. [106] to investigate the methanol production for ZnO NPs deposited on Cu(111) and Cu(100). Generally, ZnO/Cu(100) featured a doubling in the methanol production w.r.t. ZnO/Cu(111), while the methanol production exhibited a volcano-shaped dependency on the fraction of Cu covered by ZnO as shown in figure 2.7.10.

Overall, the studies highlighted the Cu-ZnO interface accommodated by a thin ZnO layer as important for high methanol activity. Similar to the discussion in section 7.2, the active overlayer mechanism or Cu-ZnO interface is a localized phenomena related to specific step-edge sites. This entails an effect of the particle size on the activity and that special sites and not the entire Cu surface dictate the activity, which seems to contradict the linear relation between the methanol rate and Cu surface area as outlined in section 5.

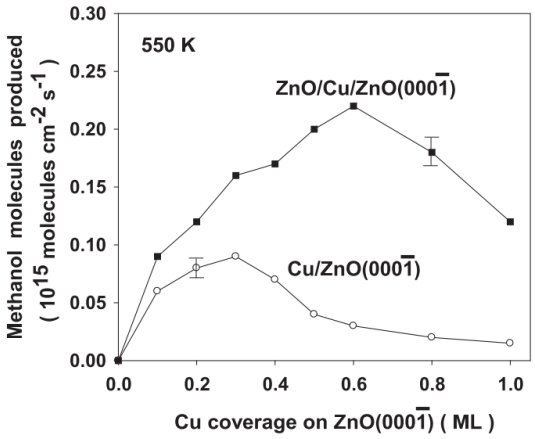

Fig. 2.7.9: Methanol production rates at T = 550 K, P_{CO_2} = 0.5 atm, P_{H_2} = 4.5 atm as function of Cu coverage on the ZnO surface for Cu particles deposited on ZnO(000$\bar{1}$) (open circles) and for ZnO particles vapour-deposited on Cu/ZnO(000$\bar{1}$) (solid squares). Figure is from [105].

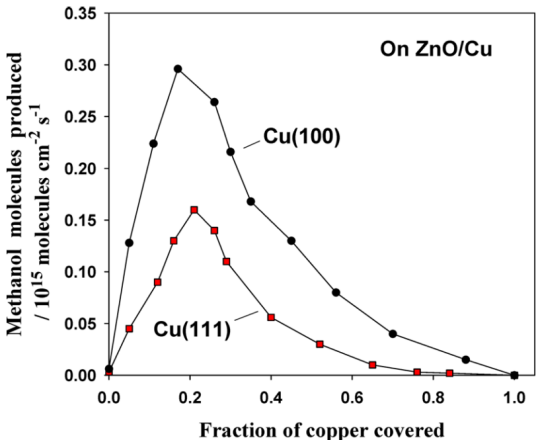

Fig. 2.7.10: Relation between the methanol production for ZnO NPs deposited on Cu SC (Cu(100) and Cu(111)) and the fraction of covered Cu by ZnO under the following reaction conditions: T = 550 K, P_{CO_2} = 0.5 atm, P_{H_2} = 4.5 atm Figure is from [106].

7.4 Cu-Zn Surface Alloy

A Cu-Zn surface alloy facilitated by reducing pretreatment was proposed to describe the Cu-ZnO synergy effect based on the relation between Zn coverage and methanol activity and this model is evaluated in the following.

Fujitani et al. [35] showed relation between activity and surface coverage of formate (HCOO) for Zn/Cu(111) after methanol synthesis (T = 523-563 K, H_2/CO_2 = 3, P = 18 bar) as evident from comparing figures 2.7.11 and 2.1.2. The simultaneous increase in activity and formate coverage until (zinc surface coverage) $\theta_{Zn} \approx 0.19$ was attributed to metallic Zn substituting into the Cu surface thus stabilizing formate species, whereas for $\theta_{Zn} > 0.19$ the ZnO content increased (see figure 2.7.11) causing a decreased activity, according to the authors. These findings are both qualitatively and quantitative similar to the volcano-shaped behaviour observed in figure 2.7.10.

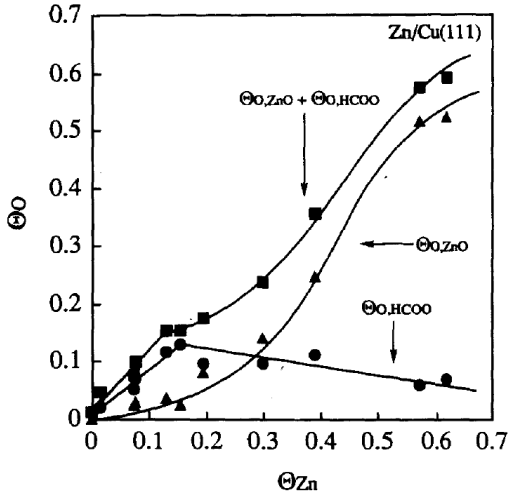

Fig. 2.7.11: Coverage (Θ) of ZnO-oxygen ($\Theta_{O,ZnO}$) and formate-oxygen ($\Theta_{O,HCOO}$) on Zn/Cu(111) with oxygen 1s peaks at binding energies 530.4 eV and ∼532 eV respectively determined by XPS post methanol synthesis. Figure is from [35].

Evidence for Cu-Zn surface alloy formation was provided by Sano et al. [107] based on Ultra High Vacuum Scanning Tunneling Microscopy (UHV-STM) and Low Electron Energy Diffraction - Auger Electron Spectroscopy (LEED-AES) because substituted Zn atoms into a Cu(111) surface caused a surface height increase of ∼ 0.35 Å w.r.t. pure Cu(111). Kinetic analysis by Sano et al. [107] using

STM revealed fast Zn diffusion over the surface towards the step edge, where alloy formation was suggested to initiate by atomic local-exchange due to the high concentration of Zn at the step edge followed by Zn movement inside the terrace as seen in figure 2.7.13.

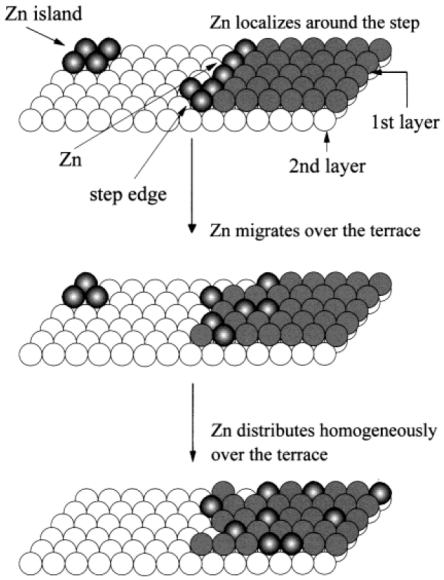

Fig. 2.7.12: Cu-Zn surface alloy formation model. Figure is from [107].

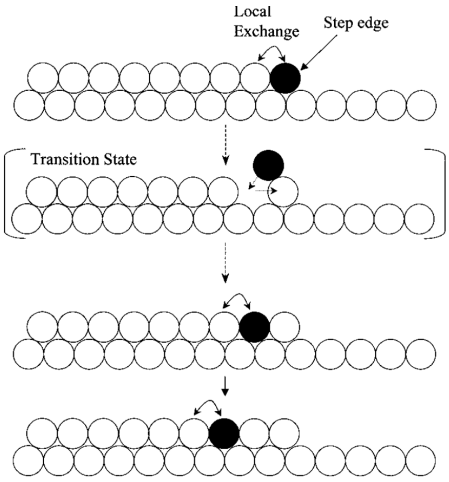

Fig. 2.7.13: Local-exchange model for Zn incorporation (solid black circle, top) at a Cu step with subsequent migration over the terrace. Figure is from [107].

Quantification of Zn in a Cu-Zn surface alloy for $Cu/ZnO/Al_2O_3$ catalysts was performed by Kuld et al. [70], who conducted several pretreatments with variation in the H_2 pressure (0.01-1 bar) while maintaining a fixed temperature ramp of 2 K/min from 300 K to 493 K in a H_2/He atmosphere. After pretreatment, the catalysts were characterised by XPS, H_2-TPD, N_2O-RFC, and H_2-TA with results from the three former methods depicted in figures 2.7.14 and 2.7.15. Increased H_2 pretreatment pressure was assigned with higher metallic Zn concentration due to shifts in the XPS Zn $L_3M_{4.5}M_{4.5}$ Auger peak towards lower binding energies with harsher pretreatment conditions. A geometric model was applied to estimate the Cu surface area using the XPS measurements (see figure 2.7.14), whereas the H_2 signal and N_2O surface uptake were employed to determine the Zn ratio in Cu (see figure 2.7.15). Good support to the surface alloy model was provided by the quantitative correspondence between the Cu surface area (figure 2.7.14) and the Zn ratio in Cu (figure 2.7.15) as functions of H_2 pretreatment pressure despite application of individual characterization methods.

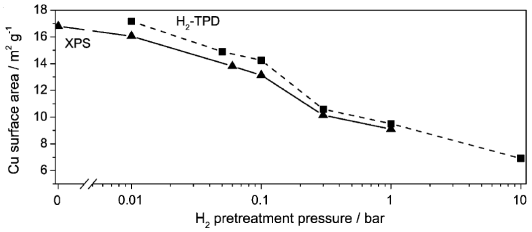

Fig. 2.7.14: XPS and H_2-TPD evaluated Cu surface areas as function of pretreatment H_2 pressure. Figure is from [70].

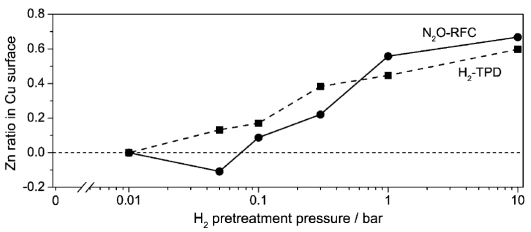

Fig. 2.7.15: Quantification of the Zn ratio in the Cu surface using N_2O-RFC and H_2-TPD methods. Figure is from [70].

Improvements to the quantitative description of the Zn coverage was subsequently provided by Kuld et al. [44], who established a theoretical model based on thermodynamic considerations regarding ZnO reduction to Zn (see reaction R5) and DFT calculations. $Cu/ZnO/Al_2O_3$ catalysts were exposed to different CO/CO_2 ratios (with small amounts of H_2) at 493 K and 553 K followed by Zn coverage

estimations using H_2-TPD and their previous model to quantify the Zn coverage [70] with results shown in figure 2.7.16. The overall good agreement for the Zn coverage estimated experimentally (points) and model-predicted (lines) validated the application of the model under synthesis gas conditions, according to the authors.

$$ZnO(s) + CO(g) \rightleftharpoons Zn + CO_2(g) \qquad \{R5\}$$

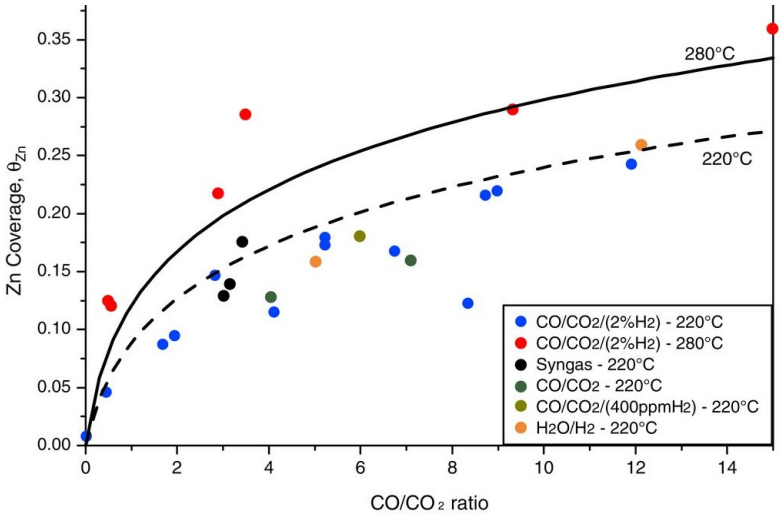

Fig. 2.7.16: Comparison between DFT calculations at 493 K (dashed line) and 553 K (solid line) and H_2-TPD determined θ_{Zn} (circles) as function of the CO/CO_2 ratio. Figure is from [44].

Industrial-type catalysts were exposed to different H_2 pressures (0.01-40 bar) at 493-553 K to yield various θ_{Zn} followed by first methanol synthesis in $CO/CO_2/H_2 = 18/18/64$ at 363-413 K and second θ_{Zn} determination by H_2-TPD based on reduced H_2 desorption caused by Zn atoms directly replacing Cu atoms in the surface. Incorporation of these experimental results into the model demonstrated as seen in figure 2.7.17 a relation between θ_{Zn} and activity, which both were influenced by the ZnO and Cu particle sizes. Peak activity were reported for a pretreatment at 543-553 K in H_2 at 30-40 bar with $\theta_{Zn} \approx 0.47$.
Small ZnO particles were found to be unstable and prefer to surface alloy with Cu thereby increasing θ_{Zn} whereas larger Cu particles supported higher θ_{Zn}, according to the model.

The authors argued that a vital parameter for the methanol activity was θ_{Zn} regulated by the syngas reduction potential (CO/CO_2 ratio, see equation R5), the size of ZnO and Cu particles and/or the H_2 pretreatment conditions.

Overall, the studies presented good support to a promotional Cu-Zn surface alloy model, though further operando studies evaluating the state of zinc at industrially relevant conditions are required to further examine the Cu-Zn surface alloy model and its relevance for the Cu-ZnO synergy effect at conventional conditions.

The quantitative Cu-Zn surface alloy model by Kuld et al. (see figure 2.7.17) suggested the methanol rate to be structure sensitive due to the change in relative TOF as the Cu particle size increased. Contrary, size independent TOF was found by the linear relation between rate and Cu surface area (see section 5). Kuld et al. [44] suggested that the absence of reported size dependent TOF's in previous studies were due the studied Cu particle sizes being $d_{Cu} > 10$ nm, where the Cu particle size effect according to the quantitative model (see figure 2.7.17) was less pronounced in agreement with [19]. Supporting the structure sensitive mechanism are studies by Berg et al. [99] and Karelovic et al. [108] both reporting 3-5 fold increase in the methanol TOF upon increasing the Cu particle size from 2-4 nm to above ~10 nm. Berg et al. [99] presented two models to account for the structure

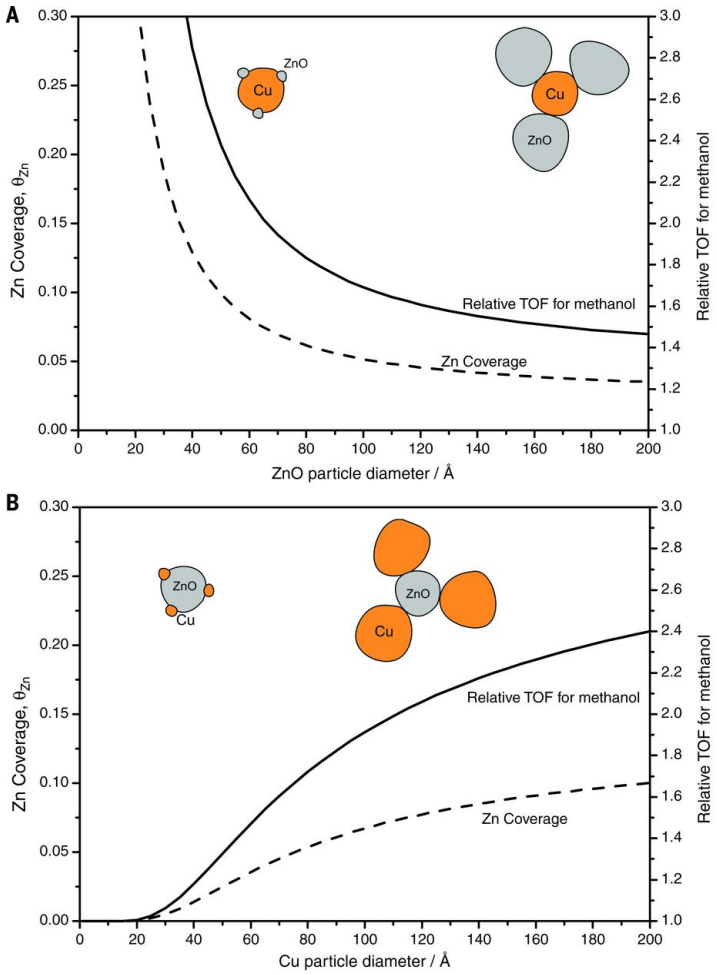

Fig. 2.7.17: Relation between relative methanol TOF, θ_{Zn}, and particle size for ZnO (**A**) and Cu (**B**). Figure is from [44].

sensitivity. One proposed [109] that very small nanoparticles ($\lesssim$ 10 nm) could not accommodate the highly active Cu step sites (B5A, B6 and B5B sites), whose abundance increase with particle size until $\sim$4 nm (B5A, B6) or 8 nm (B5B). Another model suggests that small Cu particles with high fraction of low-coordinated sites below 8 nm [110] strongly adsorb formate and inhibit the activity [99]. Further work is necessary to experimentally investigate the relation between the methanol TOF and the Cu (and ZnO) particle sizes reported in the model by Kuld et al. (see figure 2.7.17).

7.5 Electron Transfer Mechanism

Cu is regarded as the active component for methanol synthesis but the support plays a pivotal role for the catalytic activity. The linearity between activity and Cu surface area strongly indicates that the whole Cu surface is active and entails that the support effect must influence the entire Cu surface. Support effects in methanol synthesis arising from delocalised electronic metal-support interactions are discussed in this section in relation to the formate coverage on Cu and methanol activity.

Charge Transfer Phenomena

Contact between a semiconductor (e.g. oxide) and a metal causes a narrow interface region in the semiconductor, where charges are depleted from. This region is termed the depletion layer or Schottky barrier [111, 112] as shown in figure 2.7.18 for an n-type semiconductor in contact with a metal, where the metal work function is higher than the semiconductor electron affinity [112]. Alignment between the metal Fermi level $E_{\mathrm{F,M}}$ and the semiconductor Fermi level $E_{\mathrm{F,SC}}$ forces electrons to flow from the semiconductor to the metal until the Fermi energy levels (broken lines in figure 2.7.18) align and an equilibrium is established.

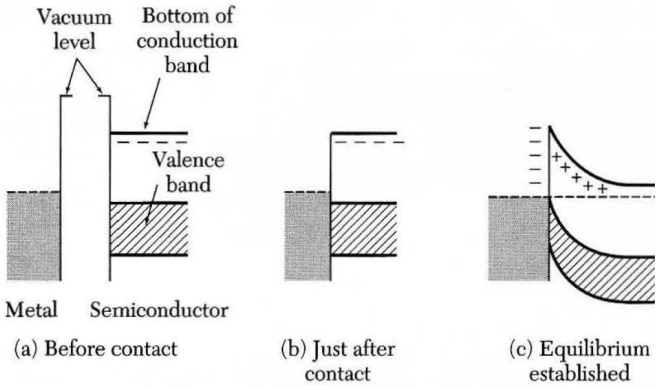

Fig. 2.7.18: Formation of a Schottky (potential energy) barrier $\phi(b)$ and resulting Fermi level (broken line) alignment between a metal and an n-type semiconductor. Figure is from [111].

Several studies on prereduced metal-supported systems report support-dependent properties regarding; catalytic activity [102, 113, 114], CO adsorption [113], H_2 [115] and N_2O uptakes [102], and surface morphology changes [104].
Electron transfer phenomena between metal and semiconducting materials were suggested as possible explanations for these observed metal support interaction effects. Reduction of metal-oxide systems at sufficiently harsh conditions can facilitate charge transfer between support and metal through oxide reduction [69, 115], because reduction of the transition metal oxide surface cations (e.g. $Ti^{4+} \rightarrow Ti^{3+}$ for TiO_2 support) enables the cations to acquire d orbital electrons while removing surface anions. This reduction facilitated mechanism permits physical interaction between reduced cations and the metal and thereby allows electron transfer to the metal with potential implications for the catalytic properties [115].

Indications of a metal-support charge transfer was provided by Chung et al. [116], who investigated $SrTiO_3$ (100) with increasing Pt surface coverage (θ_{Pt}) ranging from 0 to 2 ML. Profound changes in the EELS spectrum combined with a clear increase in the support work function from 4.2 eV at θ_{Pt} = 0 ML to 5.0 eV at θ_{Pt} = 1 ML measured by Ultraviolet Photo-electron Spectroscopy (UPS) was assigned to electron transfer from $SrTiO_3$ to Pt.

Kähler et al. [114] reported similar charge transfer mechanism. Methanol adsorption on pure ZnO NPs and ZnO NPs decorated with Au were investigated by TPD and DRIFTS as seen in figure 2.7.19 for 1.9 wt% Au/ZnO. Adsorption of methanol was performed by exposing the catalyst to 3000 ppm methanol in He at 373 K.

Quantification results of the surface species by TPD (reprinted in table 1) showed a clear decrease in the (desorbed) effluent CO/CO_2 ratio with increased Au loading thus suggesting higher oxygen vacancy concentration and more facile ZnO reduction in presence of Au.
the DRIFTS spectra of Au/ZnO displayed a high absorbance intensity and broad band with growing absorbance during methanol exposure. This enhanced IR absorbance was explained by electron transfer from donor sites (oxygen vacancies) to the conduction band of the semiconductor [117].
Combined DRIFTS and TPD analyses indicated that methanol exposure enhanced the concentration of oxygen vacancies ($[V_O^{++}]$), which previously had been shown to be the dominating intrinsic defect type in Zn-rich ZnO due to its low formation energy relative to other defect types [118, 119].

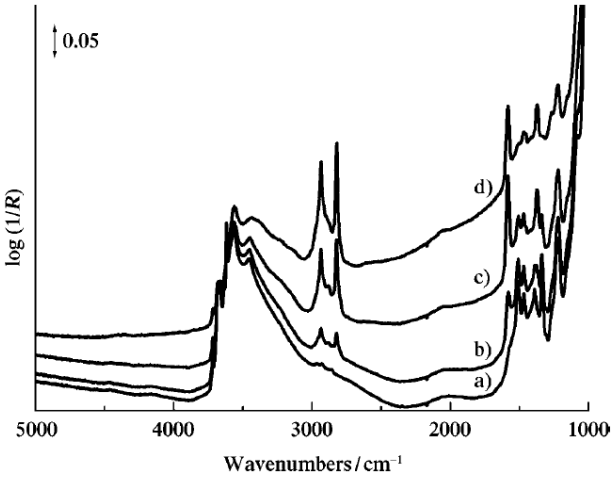

Fig. 2.7.19: DRIFTS (absorbance) spectra for oxygen-pretreated 1.9 wt% Au/ZnO obtained a) prior to methanol exposure at 373 K, b) after methanol exposure for 2 min. c) 3 min. and d) 10 min. displaying a broad band with reduced IR intensity. Figure is from [114].

Table 1: Quantification of desorbed species (normalised to the catalyst loading) during TPD with 3 K min^{-1} as heat rate performed after methanol exposure (3000 ppm methanol in He until methanol surface saturation) at 373 K. Figure is from [114].

Species	n_{des} [µmol g_{cat}^{-1}] ZnO	0.9 wt% Au/ZnO	1.9 wt% Au/ZnO
CH_3OH	7	8	8
H_2	96	121	62
CO	43	29	8
CO_2	6	32	32

The link between higher ZnO reducibility and enhanced generation of oxygen vacancies accounting for electron transfer phenomena was in accordance with a metal-semiconductor (oxide support) junction hypothesis proposed by Frost [120].
Frost argued [120] that the energy required to move electrons to the oxide conduction band played a major role for the formation of oxygen vacancies. Band bending between metal and oxide could facilitate electron movement and cause a decrease in the enthalpy of oxygen vacancy formation by $2\phi(b) = 2(E_{C,SC} - E_{F,M})$ ($\phi(b)$ is the Schottky barrier height) resulting in higher $[V_O^{++}]$ (C, SC designates the conduction band of the semiconductor), which for the Cu/ZnO interface is 0.45 eV [120, 121]. Metals with a high work function (low $E_{F,M}$) in comparison to the semiconductor electron affinity promote a high $[V_O^{++}]$ by lowering the oxygen vacancy formation energy. Enhanced oxide reducibility when contacted with a metal was supported by early studies [3, 122] showing partial to full reduction of ZnO in the presence of Cu during H_2 treatment of CuO/ZnO mixtures at 573 K (close to working conditions), whereas reduction of pure ZnO required higher reduction temperature.
Another important parameter for $[V_O^{++}]$ was the reduction potential (CO/CO_2) of the syngas determined by the equilibrium seen in reaction R6. The H_2-H_2O equilibrium, which also influence $[V_O^{++}]$, was not considered by Frost probably due to the applied reaction conditions and the higher reducible

character of CO compared to H_2.

$$\mathrm{CO(g)} + \frac{1}{2}\,\mathrm{O_2(g)} \rightleftharpoons \mathrm{CO_2(g)} \qquad \{\mathrm{R6}\}$$

$$\mathrm{CO(g)} + {\mathrm{O_{ZnO}}}^{2-} \rightleftharpoons 2\,\mathrm{e^-} + {\mathrm{V_O}}^{++} + \mathrm{CO_2(g)} \qquad \{\mathrm{R7}\}$$

By only considering oxygen vacancies and applying the requirement of charge neutrality ($n_e^- = 2[\mathrm{V_O^{++}}]$) together with reaction R7, the authors established an analytic expression for $[\mathrm{V_O^{++}}]$ as seen in equation 7.1. Here, the partial pressure of oxygen ($p_{\mathrm{O_2}}$) and the work function difference between (semiconducting) oxide and metal $\phi(b) = E_{\mathrm{C,SC}} - E_{\mathrm{F,M}}$ were the dominating variables (assuming both fixed temperature and catalyst system).

$$[\mathrm{V_O^{++}}] \propto \exp\left[\frac{-H\nu - 2\phi(b) + 2\phi(t)}{3k_B T}\right] p_{\mathrm{O_2}}^{-1/6} \tag{7.1}$$

with the band bending height $\phi(t)$, formation energy for vacancies termed $H\nu$, Boltzmann's constant k_B and the temperature T.

$[\mathrm{V_O^{++}}] \propto p_{\mathrm{O_2}}^{-1/6}$ can be rewritten into $[\mathrm{V_O^{++}}] \propto \left(\frac{p_{\mathrm{CO}}}{p_{\mathrm{CO_2}}}\right)^{\frac{1}{3}}$ by applying the CO-CO_2 equilibrium (see reaction R6). Moreover, Frost [120] reported $H\nu > \phi(b) \sim \phi(t)$ for a Cu/ZnO catalyst whereby a temperature increase results in higher $[\mathrm{V_O^{++}}]$ according to equation 7.1.
The surface concentration of $\mathrm{V_O^{++}}$ was calculated based on equation 7.1 and found to be substantial. Methanol synthesis (473 K, 10 bar, $H_2/CO_x \sim 2/1$) over Cu/ThO_2 confirmed the proposed "junction theory" with oxygen vacancies as the active sites and deactivation by CO_2. However, his proposed prevalence of such a mechanism as a unified "junction theory" for methanol synthesis catalysts seems rather speculative. The "junction theory" predictions with oxygen vacancies as the active sites, which are eliminated in presence of CO_2 are in direct conflict with the well-established knowledge with Cu as the active metal and CO_2 as the main carbon source over Cu/ZnO-based catalysts (see section 1 and 5). Regarding Cu as the active component entails that proposed electronic metal-support interactions accounting for the support activity effect must be delocalized on Cu and not confined to specific metal-oxide inter-facial sites.
While the "junction theory" may fail in generally assigning oxygen vacancies as the active sites for methanol catalysts and quantitatively overestimate the charge transfer concentration [123], it may qualitatively capture the electron transfer phenomena occurring between metal and oxide(s).

Interestingly, the temperature and CO/CO_2 ratio trends for $[\mathrm{V_O^{++}}]$ agreed qualitatively with the tendencies for θ_{Zn} reported by Kuld et al. [44], who assigned an enhanced 3 eV downward energy shift for the Zn $L_3M_{4.5}M_{4.5}$ Auger peak upon increased reduction potential (higher H_2 pressure) to a valence change state from Zn^{2+} (ZnO) to Zn^0 (see section 7.4).
Increase in the electrical conductivity of ZnO was previously attributed with a more pronounced 3 eV energy shifted Zn peak [124, 125], and since formation of oxygen vacancies involves generation of electrons (see reaction R7), it is likely that higher $[\mathrm{V_O^{++}}]$ contributed to the 3 eV energy shifted Zn Auger peak. Consequently, the CO/CO_2 ratio and temperature tendencies for θ_{Zn} reported by Kuld et al. may (at least partially) be due to oxygen vacancies as the qualitative agreement between equation 7.1 and figure 2.7.16 indicates.

Charge transfer upon contact between metal and semiconducting oxides is possible but the importance of charge transfer on the catalytic properties may vary depending on the specific catalyst system (metal and oxide), as Frost [120] emphasized. Investigations on real catalysts under operation studied by in situ and surface sensitive characterization techniques may clarify the importance and prevalence of this charge transfer.

Formate Coverage

The reaction pathway for methanol synthesis depends on the reaction conditions [37, 41, 86] and the support influences the methanol TOF [74, 93, 94]. This section is devoted to industrial-type catalysts

exposed to syngas mixtures composed of $CO_2/CO/H_2$ or CO_2/H_2. Under these restrictions hydrogenation of formate (HCOO), dioxymethylene (H_2COO) and methoxy (CH_3O) have been suggested as the rate-limiting steps for CO_2 hydrogenation into methanol. The argumentation for these proposals are outlined in the following.

Nakamura et al. [126] investigated methanol synthesis (H_2/CO_2 = 3/1, T = 523 K, P = 18 atm) on Cu(100), Cu(110), Cu(111), Cu(311) and Zn/Cu(111). After methanol synthesis, XPS analysis revealed a clear correlation between the methanol TOF and the formate coverage with the latter parameter quantified by proposed zinc induced changes in both the O 1s XPS peak at 531.1-531.8 eV as seen in figure 2.7.20 and the C 1s XPS peak at 287.7-289.0 eV (not shown here). Notice, the formate coverage (Θ_{HCOO}) in figure 2.7.21 with maximum $\Theta_{HCOO} \sim 0.05$ ML, which was similar to the micro-kinetic model predicted $\Theta_{HCOO} \sim 0.07$ ML reported by Askgaard et al. [77] at industrially relevant conditions (P = 50 bar, T = 500 K, H_2:CO_2:H_2O:CH_3OH = 88.65:3.65:1.79:1.35:4.56, surface coverage of free sites $\Theta_X \sim 0.52$ ML). A formate coverage on Cu of a few percentage creates amble room for engineering the catalyst towards achieving higher formate coverage to potentially enhance the TOF.

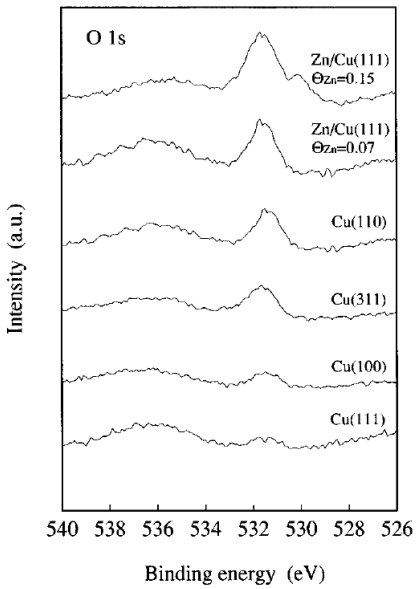

Fig. 2.7.20: Postreaction O 1s XPS spectra of different model catalysts with emerging peak at around 531 eV attributed to increased formate coverage (Θ_{HCOO}). Figure is from [126].

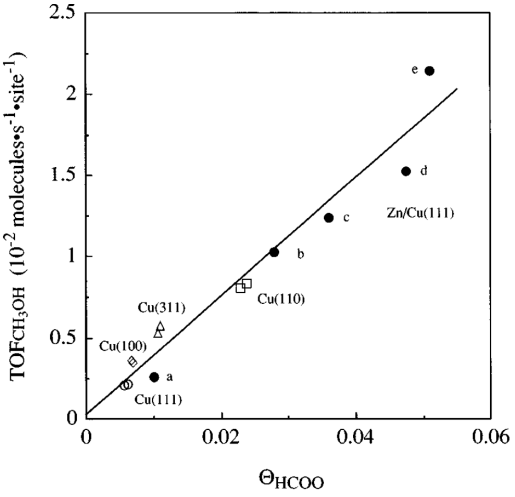

Fig. 2.7.21: Relation between methanol TOF (T = 523 K, P = 18 bar, H_2/CO_2 = 3) and estimated formate coverage (Θ_{HCOO}) based on post methanol reaction surfaces with zinc coverages; a) 0.015, b) 0.073, c) 0.076, d) 0.13) and e) 0.15 for Zn/Cu(111). Figure is from [126].

The clear correlation between formate coverage and methanol activity for Cu based catalysts was supported by Amenomiya and Tagawa [78], who investigated $Cu/ZnO/Al_2O_3$ catalyst in CO_2/H_2 syngas. Methanol synthesis using CO_2/H_2 = 1/4 was performed at 1 and 20 bars of pressure at temperatures up to 550 K. IR experiments were conducted in situ during methanol synthesis with the formate concentration identified by the absorbance of the 1640 cm^{-1} and 1320 cm^{-1} bands.
A clear correlation between the reported HCOO adsorbance bands (1640 cm^{-1} and 1320 cm^{-1}) and the methanol activity as function of the CO_2 partial pressure was found as shown in figure 2.7.22, whereas correlation between the partial pressure of hydrogen and the methanol activity was reported as seen figure 2.7.23. Conclusively, formate hydrogenation was assigned as the rate-limiting step for methanol synthesis.

Another method to investigate the formate coverage was to compare the TPD spectra of the same catalysts pretreated with formate and syngas. Quantified amounts of coincident CO_2 and H_2 desorption were assigned to surface coverage of formate based on TPRS spectra after diluted formic acid-helium dosage of the catalyst by Sakakini et al. [81]. They reported good quantitative agreement between

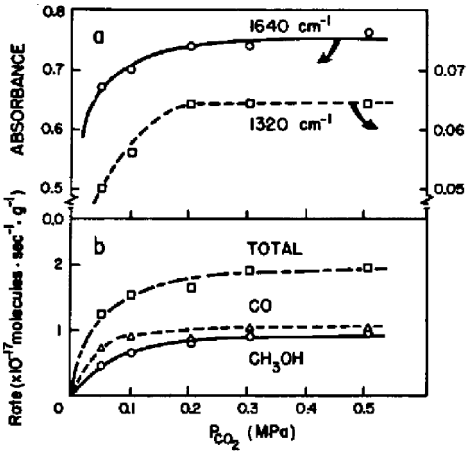

Fig. 2.7.22: Influence of carbon dioxide partial pressure (P_{CO_2}) on the IR bands (formate adsorbed on Cu: $\nu_{OCO,sym}$ = 1320 cm^{-1} and $\nu_{OCO,asym}$ = 1640 cm^{-1}) and methanol rate for 5%CuO-2.2%ZnO-Al_2O_3 at 496 K, constant H_2 pressure of 8 bar and total flow of 50 ml/min. Figure is from [78].

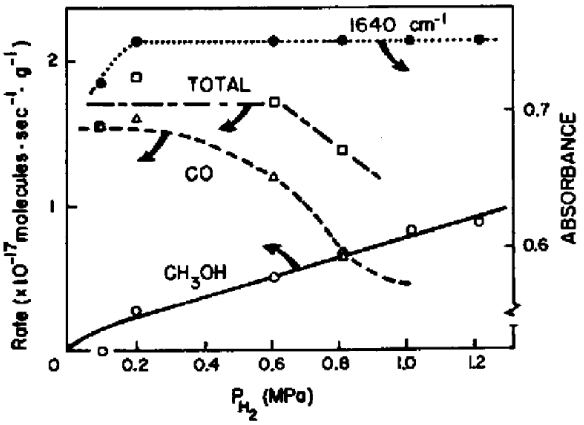

Fig. 2.7.23: Effect of varying the hydrogen partial pressure (P_{H_2}) on the methanol and CO rates, and formate assigned IR band (1640 cm^{-1}) performed on 5%CuO-2.2%ZnO-Al_2O_3 at 496 K, constant CO_2 pressure of 2 bar and a total flow of 50 ml/min. Figure is from [78].

the estimated formate coverage using desorbed CO_2 and H_2 and methanol production during TPH of formate-covered ICI standard (conventional) Cu/ZnO/Al_2O_3 catalyst. With formate being the most stable reaction intermediate and high prevalence formate hydrogenation was assigned to be the rate-limiting step for CO_2 hydrogenation into methanol.

Askgaard et al. [77] constructed a kinetic model of the reaction pathway for methanol synthesis (see section 6). When results from Cu SC ([23]) were inserted into the model, the rate-limiting step was found to be hydrogenation of H_2COO in agreement with combined DFT calculations and experimental investigations of CO_2 hydrogenation on pure and ZnO supported Cu NPs by Yang et al. [127]. Experimental surface sensitive techniques including in situ spectroscopy do not report accumulation or significant H_2COO concentrations on the working catalytic surface as expected, if H_2COO hydrogenation was the rate-limiting step. One could advocate that a small fraction of sites with accompanied minute H_2COO surface coverage dictate the TOF making H_2COO virtually "undetectable". However, this assumes that only special sites (e.g. stepped Cu sites) control the TOF in disagreement with the linearity between rate and Cu surface area.

Based on a comprehensive DFT study, Grabow and Mavrikakis [37] (see section 6) suggested CH_3O hydrogenation as the rate-limiting step in CO_2-rich syngas mixtures for an open Cu surface (e.g. Cu(100), Cu(110), and Cu(211) partially covered by oxygen) due to the energy barriers depicted in figure 2.6.4. Interestingly, the potential energy diagram showed formate as the most stable intermediate, which may explain the identification of formate species in the experimental studies by Nakamura et al. [126], Amenomiya [78], and Sakakini [81]. The clear relation between formate coverage and methanol production in the experimental studies strongly suggested hydrogenation of formate as a key reaction intermediate though not necessarily the rate-limiting step. Figure 2.6.4 supported that hydrogenation of HCOO, H_2COO and CH_3O were all key intermediate steps as evident from the relative large energy barriers for these reaction steps.

Linkage between formate surface coverage and methanol TOF strongly suggests that high formate coverage is a key indicator for a highly active Cu/ZnO-based catalysts but whether this holds for other Cu-based systems requires further work. Despite the strong evidence in favour of formate hydrogenation as the rate-limiting step this statement is disputed among scientists. Moreover, methanol synthesis may be a complex process depending on reactions conditions etc., where a simple rate-limiting step

cannot necessarily encompass its complexity.

Electron-Donating Supports and Methanol Synthesis

A hypothesis, which unifies charge transfer effects and the reported proportionality between formate coverage and methanol TOF for oxide-supported Cu catalysts, is presented and evaluated in this section.
Formate possess electron-withdrawing properties as indicated by a formate-induced change in the C-O stretching frequency of CO (ν_{CO}) adsorbed on Cu, which was shown by Dubois and Zegarski [128] using figure 2.7.24. They studied CO-chemisorption using high-resolution electron energy loss spectroscopy (HREELS) on Cu(100) and observed a change in ν_{CO} from 2090 cm^{-1} for CO adsorbed on pure Cu(100) to 2150 cm^{-1} when CO was co-adsorbed with formate on Cu(100). Previous studies by Sexton [129] showed that HCOOH physically adsorbed on Cu(100) at 100 K transformed to a stable formate layer upon heating with desorption of excess physisorbed HCOOH at 100-300 K. Therefore, the experiment for HCOOH by Dubois and Zegarski [128] was performed at 306 K.

Other studies reported $\nu_{CO} = 2080\text{-}2090\ cm^{-1}$ [130] for Cu(100) in agreement with Dubois and Zegarski [128], whereas a higher $\nu_{CO} = 2120{-}2160\ cm^{-1}$ was found for CO adsorbed on Cu_2O [131]. The higher frequency of ν_{CO} in the presence of surface formate observed by Dubois and Zegarski [128] was explained by formate imposed change to the Cu oxidation state from metallic Cu^0 to more oxidized $Cu^{\delta+}$ character. Similar electron-withdrawing character has been assigned to SiO_2 when used as support for Cu, because characteristic properties for Cu^+ site were identified. Dandekar and Vannice [132] analysed CO adsorption on Cu/SiO_2 by DRIFTS and unambiguously attributed a strong adsorption frequency at 2120 cm^{-1} to CO bonded to Cu^+ sites in agreement with FTIR studies of CO adsorption on Cu/SiO_2 by Topsøe and Topsøe [66]. X-ray adsorption near edge spectroscopy (XANES) measurements by Zhu et al. [133] showed co-existence of similar proportions of Cu^+ and Cu^0 for Cu/SiO_2 prepared catalysts, thus substantiating the proposed electron-withdrawing properties of surface formate.
Stabilization of formate surface species on electron-rich Cu facets could potentially enhance the TOF as the work function and electron-deficiency of Cu facets follows (110) < (100) < (111) with the methanol TOF following the reverse (electron-richness) order (110) > (100) > (111) as seen in figure 2.7.21.

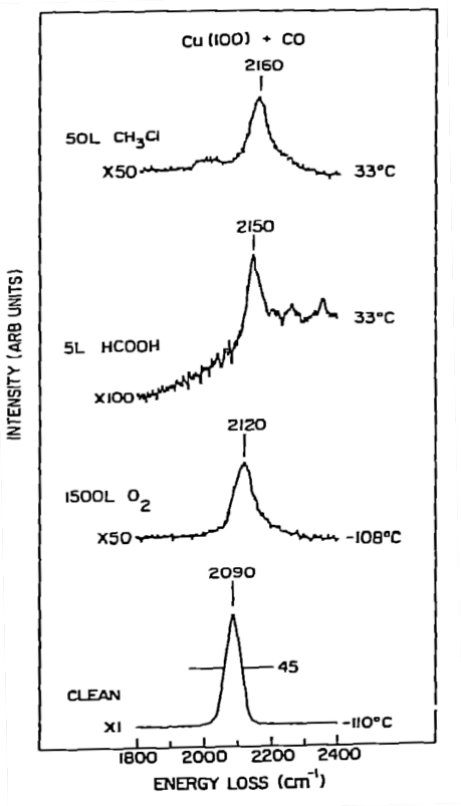

Fig. 2.7.24: HREELS spectra of CO chemisorption performed on a clean Cu(100) facet and with co-adsorbed oxygen, formate and methyl chloride. The expansion scales are relative to the clean Cu(100) surface value. Figure is from [128].

In summary, the combined hypothesis suggested that the support activity effect arise from support-regulated Cu surface charging. This charging impacts the adsorbate population level including the potential key reaction intermediate formate. Consequently, the support highly influences the catalytic properties of Cu supported catalysts. Engineering Cu supported systems to yield maximum TOF may include considerations to the optimal formate coverage as overpopulation of formate may cause surface blockage and impede the TOF. No solid and unified experimental evidence has been provided for the electron transfer model and its role in methanol synthesis. Chapter 7 is based on work in this PhD and contributes with new insight into the electron transfer mechanism.

8 Application of Chemisorption Methods

The Cu dispersion is an important parameter for the methanol activity, and the chemisorption methods H_2-TPD and N_2O-RFC are usually applied to obtain this information. The techniques are based on the interaction between a probing molecule (H_2 or N_2O) and the (Cu) sample surface but to provide estimations on the Cu dispersion the interaction must be highly selective towards Cu to prevent biased results. This and other issues regarding the methods are discussed next.

8.1 N_2O-Reactive Frontal Chromatography

Chinchen et al. [39] presented N_2O-RFC as a convenient and fast technique to determine the Cu surface area of Cu supported catalysts. Diluted N_2O oxidises the pre-reduced Cu surface and this reaction evolves N_2 and a causes a drop in the N_2O signal. Once Cu is completely oxidised the N_2O signal is restored termed N_2O breakthrough and the time required to oxidise Cu is proportional to the Cu surface area, which is estimated based on the applied reaction conditions.
A vital variable in N_2O-RFC experiments conducted on Cu containing catalysts is the temperature, because high temperature facilitates subsurface oxidation, whereas unselective and weak physisorbed N_2O is favoured at low temperature [134]. Both temperature regimes cause an inaccurate N_2O breakthrough and inhibits simple estimation of the Cu surface area from the measured N_2 and N_2O signals. Chinchen et al. [39] suggested 333 K as the optimal temperature with regards to N_2O chemisorbing selectively on Cu. They concluded that quantitative Cu surface area estimations cannot be obtained by N_2O-RFC at $T < 333$ K, whereas bulk oxidation takes place above 363 K. The preferred temperature interval (333-363 K) is supported by Sengupta et al. [135], who observed bulk oxidation already at 343 K.

Previous studies have applied the N_2O-RFC method to determine the Cu surface area of Cu/ZnO-based catalysts under the assumption that N_2O selectively decompose on Cu [134]. However, Fichtl et al. [100] reported recently a substantial bias in the N_2O-RFC measurements of Zn-containing catalysts assigned to additional N_2O uptake on oxophilic $Zn^{\delta+}$. Such oxophilic sites are promoted and regulated by the the reducing atmosphere for reducible oxides. Figure 2.8.1 displays the bias by the deviation for the catalysts containing a "Z" (for Zn) and the (non-biased) solid line.

The Cu surface area evaluated by H_2-TPD and N_2O-RFC for Zn-free Cu catalysts supported on non-reducible oxides demonstrated good correspondence (see figure 2.8.1). It is important to note that the Cu surface areas estimated by H_2-TPD was lower for zinc containing catalysts, whereas the Cu surface area evaluated by N_2O-RFC was fairly unchanged (observe CM1→CMZ1 and CM2→CMZ2 in figure 2.8.1 with C=Cu, M=Mg, Z=Zn).
Reactions for N_2O-decomposition involving Cu in reaction R8 and partially reduced ZnO_x in reaction R9 are well-substantiated [70, 136]. These reactions demonstrated the additional N_2O uptake, when ZnO_x partially substitutes Cu in the surface.

$$N_2O + 2\,Cu \longrightarrow Cu_2O + N_2 \qquad \{R8\}$$

$$N_2O + Zn \longrightarrow ZnO + N_2 \qquad \{R9\}$$

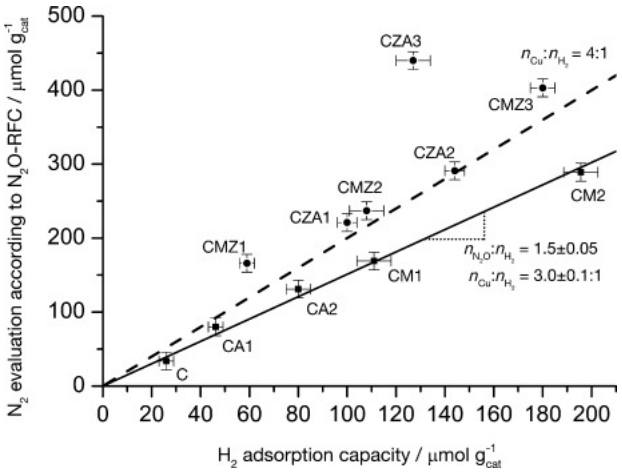

Fig. 2.8.1: Cu surface area determined by H_2-TPD and N_2O-RFC methods with C=Cu, Z=Zn, M=Mg, A=Al. Figure is from [100].

TPD experiments on Cu single crystals [137] revealed that the hydrogen saturation coverage for all the low index Cu planes was one-half (Cu:H = 2:1) corresponding to a Cu:H_2 ratio of 4:1. However, later experimental studies conducted by Fitchl et al. [100] and Chatterjee et al. [136] both reported lower Cu:H_2 ratios with 3.0 by Fichtl et al. [100] based on a single BET measurement of unsupported Cu and 2.8 by Chatterjee et al. [136] obtained from nine different supported Cu catalysts. The exact titration reaction involving H_2-uptake on Cu is disputed, and a generally accepted reaction for dissociate adsorption of hydrogen on Cu has not yet been established.
The lower Cu surface area obtained with the Cu selective H_2-TPD method for zinc-containing catalysts was attributed to a ZnO_x overlayer covering part of the Cu. According to this proposal, presence of zinc should yield lower H_2-uptake due to partial coverage of the Cu surface and higher N_2O-uptake as each oxophilic ZnO_x site decomposes more N_2O in comparison to a Cu site (compare reactions R8 and R9). Other reducible oxides should in theory yield similar trends though the extend of the biased N_2O uptake is oxide-dependent. This non-selective nature of the N_2O-RFC method must be considered when estimating Cu surface areas of Cu supported on reducible oxides based on solely N_2O-RFC. For Zn-free catalysts with non-reducible oxides, the N_2O-RFC method was found to be well applicable in determining the Cu surface area as evident by the position of the Zn-free catalysts in figure 2.8.1 on the straight solid line with a slope corresponding to a N2O:H_2 ratio of 1.5 corresponding to a Cu:N_2O ratio of 2:1 (using the reported Cu:H_2 ratio of 3:1, see figure 2.8.1) as expected for exclusively N_2O decomposition on Cu (see reactions R8 and R9).
Formal Cu oxidation using N_2O produces Cu_2O, whereby the Cu:N_2O ratio is 2:1 according to Fichtl et al. [100], which is in agreement with Chatterjee [136].

The HRTEM image of a Cu/ZnO/MgO catalyst in figure 2.8.2 [100] demonstrated the presence of $Zn^{\delta+}$ sites near Cu atoms, a ZnO_x overlayer and missing surface Cu atoms, according to the authors. These oxygen defect sites were proposed to be adsorption sites for CO_2 and reaction intermediates such as formate.

8.2 H_2-Temperature Programmed Desorption

Cu surface area estimation by H_2-TPD was described by Muhler et al. [138] and includes H_2 adsorption at subambient temperature before heating in inert gas. H_2 desorption from Cu occurs at a characteristic temperature of 300 K and by integrating the amount of desorbed H_2 the Cu surface area can be estimated.

H_2-adsorption on Cu single crystals were reported by Balooch et al. [139] to be an activated process involving energy barriers, which depended on the Cu crystallographic orientation. Activated adsorption diminished the probability for hydrogen readsorption, which potentially could cause broadening

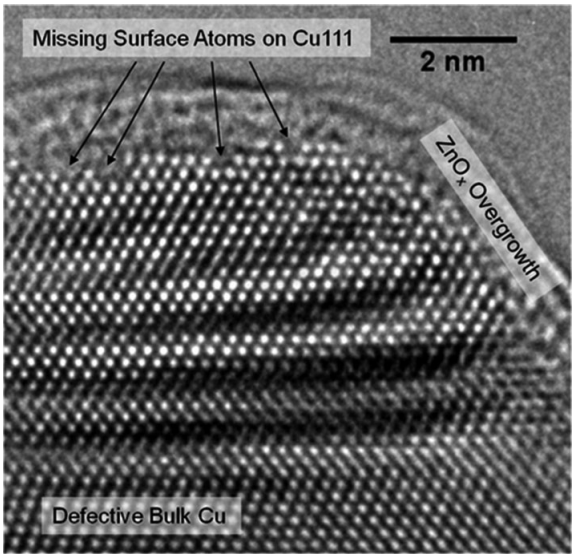

Fig. 2.8.2: HRTEM image of reduced (523 K for 30 min. in 5% H_2/Ar) CMZ1 catalyst (Cu/Mg/Zn = 79/16/5) revealed presence of $Zn^{\delta+}$ sites. Figure is from [100].

and shifts of the H_2-TPD peaks [138]. Moreover, substantial structural surface modifications were prevented by the relative low heat of H_2 adsorption [138].
Therefore, the H_2-TPD method posed a promising method to obtain reproducible and quantifiable Cu surface areas with neglible surface modifications, provided that optimal experimental conditions were applied. Recommendations aiming at obtaining good quantitative Cu surface area experiments using H_2-TPD were proposed by Muhler et al. [138]. They recommended that H_2 adsorption was performed below 300 K with subsequent temperature hold at around 250 K for one to two hours, where they observed no significant hydrogen desorption, before the sample was cooled to $\sim$ 77 K using liquid N_2. The H_2 exposure at $T \leq 300$ K was applied to prevent surface changes including bulk oxide reduction, which has been observed for specifically ZnO containing ternary catalysts, according to Muhler et al. [138]. Moreover, the recommended low H_2 exposure temperature minimized desorption of adsorbed oxygen species on metallic Cu, which Muhler et al. [138] observed to occur already at 300 K. Given the objective of the H_2-TPD method is to quantify the Cu surface area a given conditions removal of surface oxygen at the investigated reaction conditions is undesired.

The integration procedure applied by Muhler et al. [138] consisted of integrating the characteristic H_2 peak around 300 K associated with Cu after subtracting a linear background by drawing a line between two minima on each side of the peak. Reproducible surface areas within 5% were reported by Muhler et al. [138].

The bonding properties of hydrogen to Cu(111) surfaces was investigated using EELS and RAIRS by McCash et al. [140], who proposed hydrogen atoms to bind to the two-fold bridge site on Cu(111). LEED experiments conducted on H_2-saturated Cu(111) demonstrated a transition from a (3x3) LEED pattern at 150 K to a (2x2) LEED pattern at 180 K. These LEED patterns corresponded to (2x1) and (3x1) real surface layer structures corresponding to the classic Cu:H_2 ratio of 4:1 seen in figure 2.8.3 and the 3:1 ratio as suggested for Zn-free catalysts by Fichtl [100] and seen in figure 2.8.4 respectively. Provided with information about the saturation hydrogen coverage, the Cu surface area could be calculated based on integration of desorbed H_2 around 300 K.

Genger et al. [141] showed reproducible surface areas within 3% for a Cu/ZnO/Al_2O_3 catalyst by H_2 dosage at $P = 15$ bar and $T = 240$ K for 1 h, resulting in a saturated hydrogen coverage (Cu:H = 2:1 as in figure 2.8.3) based on TPD experiments on Cu single crystals [137]. Comparison between hydrogen exposure at atmospheric pressure and 15 bar as shown in figure 2.8.5 revealed a relation between decreased peak temperature and enhanced H_2 coverage attributed to a higher initial hydrogen

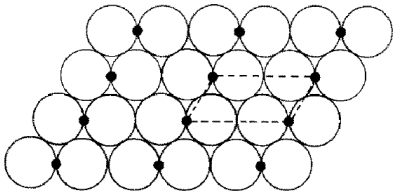

Fig. 2.8.3: Real space (2x1) surface structure with one H atom and two Cu atoms contained in each unit cell (dashed square) equal to Cu:H_2 = 4:1 and a hydrogen surface coverage (θ) of 0.5. Figure is from [140].

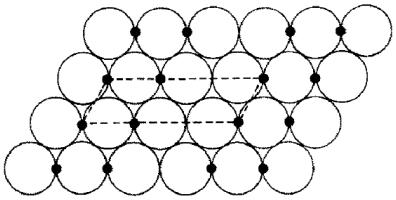

Fig. 2.8.4: Real space (3x1) surface structure with two hydrogen atoms and three Cu atoms in each unit cell yielding a Cu:H_2 ratio of 3:1 and a hydrogen surface coverage (θ) of 0.67. Figure is from [140].

coverage at 15 bar compared to atmospheric pressure. Therefore, the authors proposed H_2 dosing at high pressure. In view of figure 2.8.5 and further experiments, which related an enhanced H_2 dosage to lower peak temperature, the authors interpreted the H_2 desorption as a second order desorption process. Moreover, no significant H_2 re-adsorption was found based on the high symmetry of the TPD peak in figure 2.8.5.

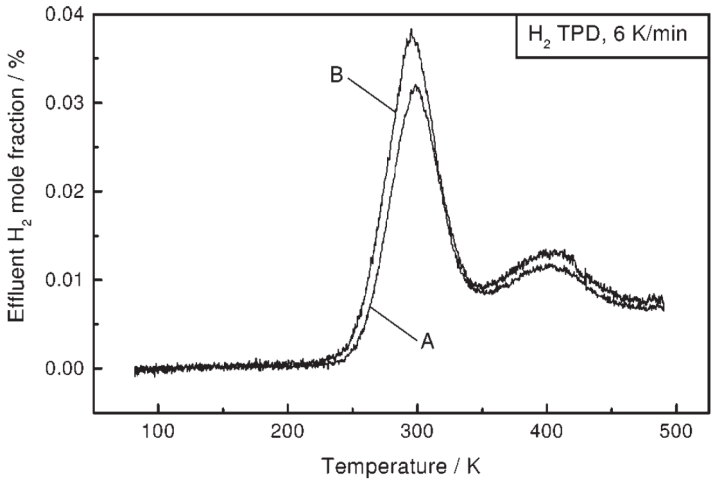

Fig. 2.8.5: Influence of pressure on the H_2 peak performed at A) 1 bar and B) 15 bar. Both profiles are obtained with the following experimental conditions: Flow = 100 Nml min^{-1}, Loading = 200 mg and 6 K/min as heat rate. Figure is from [141].

The actual H_2-TPD experiment was conducted by heating from 78 K with a heat ramp of 6 K/min in 100 Nml/min of He with 200 mg of catalyst (m_{cat}).
Figure 2.8.6 demonstrated that higher heating ramp increased the peak temperature for samples dosed with H_2 at atmospheric pressure. Optimal heating ramp in terms of high symmetric peaks and a large quantifiable signal was according to figure 2.8.6 6 K/min.

DFT calculations conducted by Kuld et. al [70] showed that replacing every third Cu atom by a Zn atom lowers the H_2 adsorption energy by 0.28-0.30 eV and thereby making H_2 adsorption less energetic favourable. Desorption of eventual weakly hydrogen bonded to Zn or Cu with a neighbouring Zn atom occurred at a lower temperature than the main 300 K H_2 peak (from Cu) and did therefore not contribute to the integrated signal centred around 300 K.

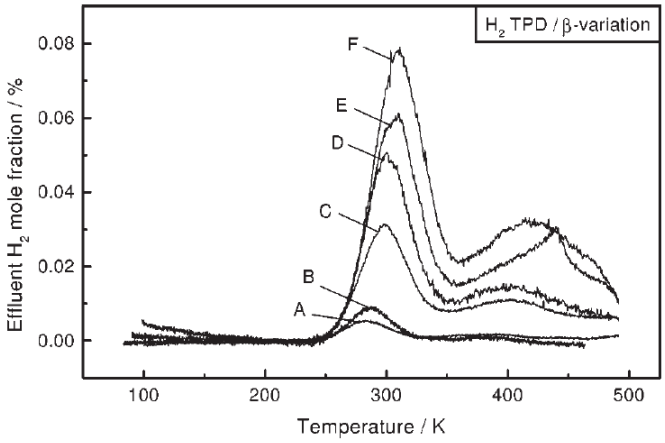

Fig. 2.8.6: H_2-TPD profiles obtained after exposing the catalyst to H_2 at atmospheric pressure with heating ramps of: A) 1 K/min, T_{max} = 283 K, B) 2 K/min, T_{max} = 287 K, C) 6 K/min, T_{max} = 299 K, D) 10 K/min, T_{max} = 302 K, E) 15 K/min, T_{max} = 307 K, F) 20 K/min, T_{max} = 310 K. Figure is from [141].

9 Alternative Methanol Catalysts

The constant pursuit for alternative methanol synthesis catalysts in terms of improved activity, selectivity etc. has lead to the discovery of new, promising catalysts operating at both conventional and milder conditions. Intermittent renewable energy production can advantageously be produced in remote areas but requires efficient storage preferably in close proximity to minimize transportation and energy losses. Liquid methanol constitutes a convenient energy carrier and can be produced from renewable H_2 and captured CO_2. This concept of decentralized methanol plants are attractive but necessitates active methanol catalysts operating at milder conditions. Conventional methanol production is restricted to temperatures above 473 K to achieve profitable reaction rates [26]. Alternative, active catalysts operating at mild conditions are highly desirable and could involve CO hydrogenation due to favorable thermodynamics in CO_2-free syngas [53] and absence of inhibiting water, which is of significant concern at lower temperatures [142, 143]. New catalysts producing methanol from CO_2 must be water-tolerant and simultaneously suppress the ∼100 times (T = 573 K) faster RWGS reaction [127]. Potential low temperature methanol catalysts are discussed before alternative catalysts to $Cu/ZnO/Al_2O_3$ are evaluated.

9.1 Nickel-Gallium

Nickel-Gallium (Ni-Ga) and especially the δ-phase Ni_5Ga_3 was recently studied Studt et al. [144] and found to feature high activity, stability and selectivity for CO_2 hydrogenation at ambient pressure. This catalyst slightly out-competed an industrial-type methanol catalyst in terms of increased suppression of the RWGS activity and increased methanol activity at ambient pressure, where methanol synthesis is less favoured compared to conventional high pressure conditions (see table 1 and section 1).

The authors [144] argued that this observation was due to selective RWGS at Ni-rich sites and methanol synthesis at Ga-rich sites in contrast to $Cu/ZnO/Al_2O_3$, where the same sites are involved in methanol synthesis and RWGS reactions. During operation, Ni sites can get poisoned by CO and C resulting in substantial inhibition of the RWGS activity. Moreover, Studt et al. [144] attributed the enhanced activity to a larger number of active sites for Ni_5Ga_3, because contrary to the $Cu/Zn/Al_2O_3$ catalyst, the Ni-Ga catalyst does not require a promoter such as zinc, hence a higher number of active sites compared to the $Cu/ZnO/Al_2O_3$ catalyst could potentially be achieved.
Later studies by Sharafutdinov et al. [145] outlined the dynamics of Ni_5Ga_3 under reducing conditions and suggested a model for the formation of Ni-Ga NPs. However, the catalyst significantly suffered from cooking. Further optimization on the system in terms of stable methanol production was achieved

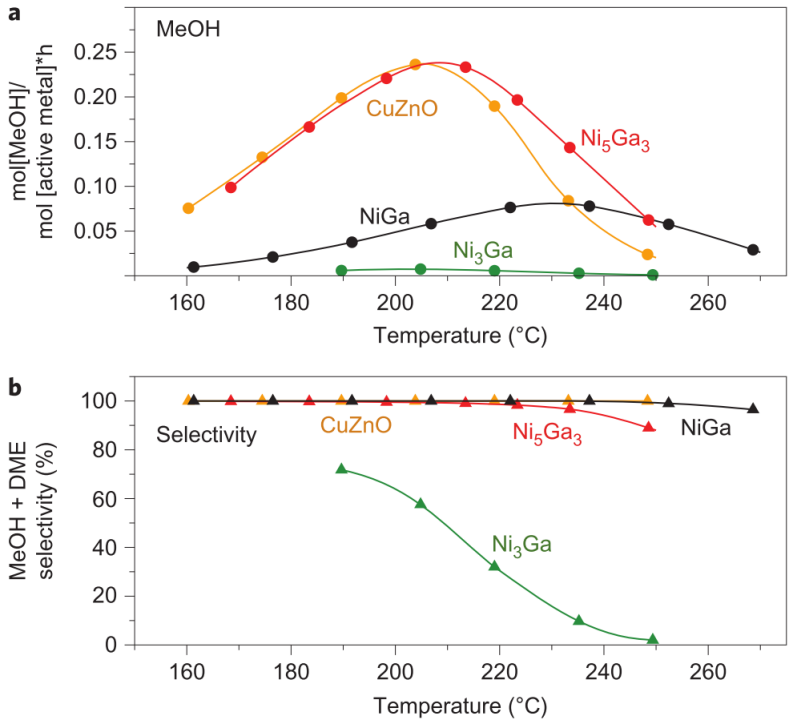

Fig. 2.9.1: a) Methanol yield for a variety of NiGa catalysts benchmarked towards an industrial-type $Cu/ZnO/Al_2O_3$ catalyst and b) CO-free selectivity evaluated at various temperatures. Reaction conditions: $H_2/CO_2 = 3/1$, GHSV: 6000 h^{-1}, 1 atm Figure is from [144].

by a Ni_2FeGa/SiO_2 (Heusler alloy) catalyst with +100 h steady state methanol production (463 K, 1.2 bar, $H_2/CO_2 = 3/1$) after an initial stabilization period of < 10 h. However, a commercially supplied $Cu/ZnO/Al_2O_3/MgO$ catalysts tested at similar conditions outperformed the Ni_2FeGa/SiO_2.

Further work investigating the catalyst under operating conditions in situ could be instructive to elucidate the dynamics of the catalyst during methanol synthesis. Moreover, optimization work to enhance the activity at mild conditions and out-compete conventional benchmarking catalysts is also necessary before feasible industrial-scale methanol production in connection with renewable energy production using Ni-Ga catalysts can be realised.

9.2 Copper-Ceria-Titania

A new interesting copper/ceria catalyst featuring high methanol synthesis activity and its alternative route to methanol is discussed in this section. Almost two orders of magnitude methanol activity enhancement was found by Graciani et al. [146] for Ce containing catalysts. Figure 2.9.2 compares $CeO_x/Cu(111)$ with 20% of a Cu(111) surface covered by ceria and 0.1 ML Cu on a $TiO_2(110)$ surface precovered by 15% ceria and termed $CeO_x/TiO_2(110)$ with Cu nanoparticles on $ZnO(000\bar{1})$ abbreviated $Cu/ZnO(000\bar{1})$ and a Cu(111) surface (benchmarking data are from [127]). Methanol synthesis was performed at elevated temperatures (500-600 K) in a syngas mixture of CO_2 (0.5 atm) and H_2 (4.5 atm). Through IRRAS measurements in CO_2 and CO_2/H_2 environments Graciani et al. [146] argued that $CeO_x/Cu(111)$ activated CO_2 based on the emergence of carboxylate ($CO_2^{\delta-}$) species.

In view of the observation that the carboxylate species were less stable than formate, the authors proposed an alternative reaction mechanism (compared to the conventional pathway in section 6.1) on CeO_x/Cu(111) involving less stable carboxylate species compared to formate. DFT calculations of CO_2 hydrogenation on a CeO_x/Cu(111) catalyst system revealed a potential reaction mechanism with general exothermic nature dominated by reaction steps downhill in energy.
The authors attributed this phenomenon partly to the property of CeO_x NP cations to easily change their oxidation state between +3 and +4 leading to dynamic chemical properties and partly to the special metal-oxide interface composed of Cu and CeO_x NPs.
Further studies by Senanayake et al. [147] supported the work by Graciani et al. [146] and observed significant increase in the methanol activity for CeO_x/Cu(111) (higher than both Cu/ZnO(000$\bar{1}$) and Cu(111)) attributed to the CeO_x-Cu interface. Interestingly, Senanayake et al. [147] reported a clear correlation between the surface concentration of Ce^{3+} and the catalytic activity of CeO_x/Cu(111) based on Ce 3d XPS spectra obtained after activity tests ($P_{CO_2} = 0.5$ atm, $P_{H_2} = 4.5$ atm, $T = 550$ K).

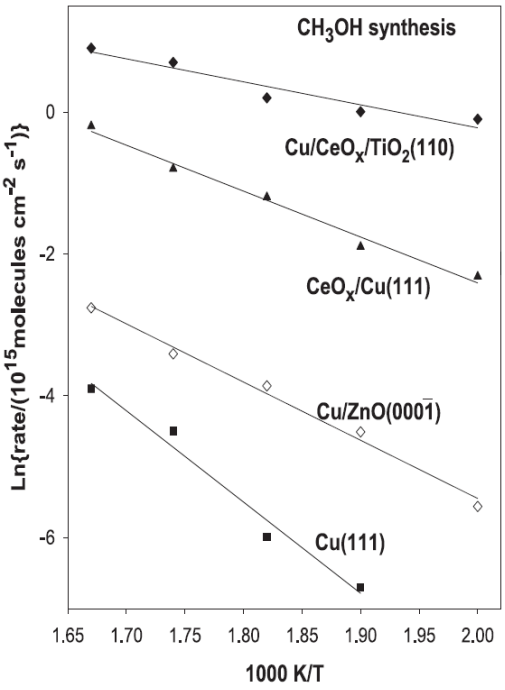

Fig. 2.9.2: Arrhenius plot for methanol synthesis over: Cu(111), 0.2 ML Cu on ZnO(000$\bar{1}$), Cu(111) with 20% surface coverage of ceria, 0.1 ML Cu on TiO_2(110) precovered with 15% ceria. Steady-state methanol rates measured at 600 K, 575 K, 550 K, 525 K, 500 K. Reaction conditions in a batch reactor: 0.5 atm CO_2, 4.5 atm H_2. Figure is from [146].

Supporting this proposal was ambient pressure infrared reflection adsorption spectroscopy (AP-IRRAS) spectra showing a relation between the catalytic activity, concentration of Ce^{3+} sites and generation of $CO_2^{\delta-}$ species, which according to Graciani et al. [146] were vital for the CO_2 conversion to methanol. Calculating the TOF involved estimation of the number of active sites. For the CeO_x containing catalysts, only metal-oxide interface consisting of Cu(111) initially covered by ceria (∼20%) was considered in the TOF calculation, whereas all the Cu atoms in the Cu/ZnO(000$\bar{1}$) were used to estimate the TOF for Cu(111)/ZnO(000$\bar{1}$). The two difference normalization approaches entail a potential bias. Underestimation for Cu/ZnO(000$\bar{1}$) may explain part of the higher activity reported for CeO_x compared to Cu/ZnO(000$\bar{1}$).
Additionally, the CeO_x/Cu(111) and Cu/CeO_x/TiO_2(110) catalyst systems were prepared by vapour deposition using expensive metal evaporators, which may not be economic feasible especially in comparison to abundant and cheap catalyst precursor materials for the conventional methanol catalyst and its simple synthesis procedure.
Further optimized copper/ceria catalysts constitute a promising future conventional methanol catalyst but its suggested new reaction mechanism involving transitions between Ce^{3+} and Ce^{4+} can also provide a pathway for designing active low temperature methanol catalysts .

9.3 Manganese - Cobalt

A hybrid catalyst composed of MnO_x NPs supported on mesoporous Co_3O_4(m-Co_3O_4) by Li et al. [148] exhibited a 10 fold TOF increase (0.18 s^{-1}) at $P = 6$ bar, $T = 523$ K compared to an industrial-

type $Cu/ZnO/Al_2O_3$ operated at industrially relevant conditions (P = 40 bar, T = 523 K [99]). They attributed the high methanol activity and selectivity to a core/shell grain structure consisting of uniformly dispersed metallic cobalt cores shielded by cobalt oxide with contact to manganese oxide. This highlighted the importance of the MnO_x/CoO interface, where manganese NPs facilitate CO_2 reduction to CO species and CoO accounts for the production of methanol.
At higher conversion ($50-60\%$ range), the methanol selectivity increased from 30% ("low conversion": 3-7%) to 45%. The application of this highly active hybrid catalyst under milder conditions made it an attractive catalyst in terms of energy-effectiveness and activity enhancement. Industrial use of this hybrid catalyst requires long-term stability tests, catalyst cost evaluation etc.

9.4 Indium Oxide - Zirconium dioxide

Promising properties in terms of activity, selectivity and stability have been reported for In_2O_3, which exhibited better performance when supported by ZrO_2 in terms of increased amount of active oxygen vacancies and enhanced stability, by Martin et al. [149]. The activity of the catalysts was measured at $T = 473 - 573$ K, $P = 10 - 50$ bar, H_2/CO_2 = 4:1. In the entire temperature range, the methanol selectivity for both In_2O_3 and In_2O_3/ZrO_2 was reported 2-3 times higher than the conventional-type tested catalyst due to the simultaneous RWGS reaction, whereas the maximum STY for In_2O_3/ZrO_2 exceeded the conventional-type catalyst at around $T > 540$ K as shown in figure 2.9.3. Good stable methanol production at T = 573 K is shown in figure 2.9.4 while the conventional catalyst suffered from significant deactivation. The supremacy of In_2O_3/ZrO_2 over $Cu/ZnO/Al_2O_3$ in figure 2.9.4 is biased by the chosen reaction temperature of 573 K, where $Cu/ZnO/Al_2O_3$ yields the lowest STY in the investigated temperature interval (see figure 2.9.3). Still, the long-term stability with high activity for the In_2O_3/ZrO_2 catalyst is interesting.
The active sites were attributed to creation and annihilation of oxygen vacancies based on H_2-TPR features emerging at temperatures below bulk reduction and XPS O 1s features suggesting oxygen atoms next to defect sites.

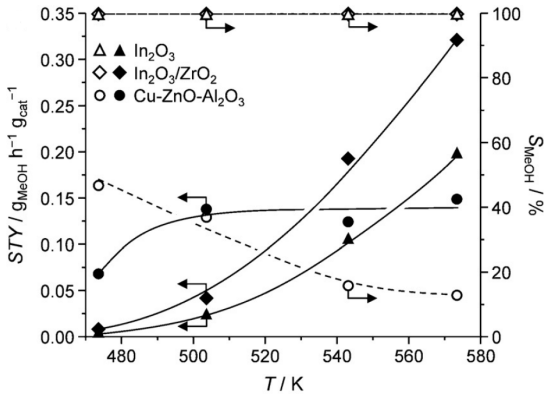

Fig. 2.9.3: Methanol space time yield (STY) and selectivity for bulk In_2O_3, In_2O_3/ZrO_2 (9 wt% In) and $Cu/ZnO/Al_2O_3$ during reaction. Conditions: $P = 50$ bar, $H_2/CO_2 = 4/1$, GHSV = 16 000 h^{-1}. Figure is from [149].

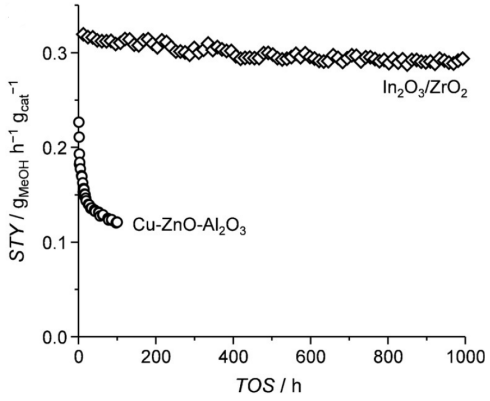

Fig. 2.9.4: Time on stream (TOS) evaluates the time-dependency of the STY over In_2O_3/ZrO_2 (9 wt% In) and $Cu/ZnO/Al_2O_3$. Operational conditions: T = 573 K, P = 50 bar, H_2/CO_2 = 4/1, GSHV = 16 000 h^{-1}. Figure is from [149].

In_2O_3/ZrO_2 constitutes a promising future industrial methanol catalyst in view of its good properties (stability, activity, selectivity) and the fact that In_2O_3 is a simple system with current practical applications (light-emission diodes, thin-film transistors) [150]. However, cost-benefit analysis are required to evaluate the economic feasibility of In_2O_3/ZrO_2 compared to the conventional $Cu/ZnO/Al_2O_3$ catalyst.

Interesting applications lie in engineering metal-oxide interfaces, which support bi-functional properties concerning adsorption and reaction sites. The alternative catalysts have not been applied as industrial catalysts despite promising catalytic properties properly due to reduced long-term stability and/or selectivity, higher cost, testing under non-industrial practical conditions, lower poison tolerance level etc. [4]. Future scientific work on addressing these potential issues are required before alternative methanol catalysts can outperform and replace the conventional $Cu/ZnO/Al_2O_3$ catalyst. Methanol at milder conditions constitute a new, unexplored market with great potential for active, low temperature catalysts.

10 Summary - Active Site Mechanisms

The various mechanisms discussed in section 7 are compared to the well-established literacy (see section 5) to evaluate the credibility of each mechanism.

The oxidation potential of the feed gas was closely related to the methanol activity through generation of oxygen vacancies by the studies in section 7.1. However, the lower methanol signal in wet syngas could as well be ascribed to presence of inhibiting water causing Cu particle sintering instead of gas-dependent Cu particle morphology.
The investigated catalysts consisted of Cu NPs on ZnO support and may not necessarily be representative for the conventional methanol catalyst consisting of mainly Cu and secondly ZnO (see section 2).

Localized Cu steps promoted by ZnO was suggested as the active sites in section 7.2 based on a direct correlation between the methanol activity and the degree of defects/strain found in both theoretical and experimental studies at industrially relevant conditions. ZnO played a pivotal role in section 7.3 as a key paramter for obtaining a high methanol activity. Mechanisms in both sections indicated the methanol synthesis to be structure sensitive, which disagrees with the size independent TOF based on the well-substantiated linear relation between the methanol rate and the specific Cu surface area showed in section 5 with support from Karelovic et al. [19]. They [19] reported the methanol rate to be independent of the Cu particle size for Cu/ZnO catalysts with estimated Cu particle sizes ranging from 8.5 to 37.3 nm. In addition, Berg et al. [99] and Karelovic et al. [108] reported experimental evidence for structure sensitive methanol synthesis for Cu/ZnO and Cu/SiO_2 respectively but only for catalysts with Cu particle size below 8-10 nm. Kuld et al. [44] contributed with a quantitative model, which predicted clear relation between particle sizes (ZnO and Cu) and the methanol activity. However, Kuld et al. [44] supported by Berg et al. [99] and Karelovic et al. [108] argued that larger Cu NPs promoted the methanol synthesis, whereas Behrens et al. [29] and Kasatkin et al. [32] reported a promotional effect for small Cu NPs.
This discrepancy concerning the Cu structure effect on the activity indicates that additional work is required to establish, how the structure of Cu NPs influences the methanol activity including assessment of the Cu particle size dynamics under industrially relevant reaction conditions.

Section 7.4 examined the Cu-Zn surface alloy mechanism. Shifts in the XPS Zn $L_3M_{4.5}M_{4.5}$ Auger peak were related to be regulated by the H_2 pressure during catalyst pretreatment. Good agreement between Zn coverage, formate coverage and methanol synthesis on Cu(111) with increasing amounts of Zn deposited were applied to substantiate the suggested mechanism. However, the mechanism supported the idea of the methanol synthesis being structure sensitive, which as previously discussed disagreed with the linear relation between methanol rate and Cu specific surface area. On the other hand, the Cu-Zn surface alloy model and the quantitative methods using H_2-TPD, N_2O-RFC and XPS described well the observations in figures 2.7.14 and 2.7.15.

Delocalized electronic effects constituted a unified model to explain the both the Cu-ZnO synergy and general support effects based on the well-known metal-semiconductor junction formation as discussed in section 7.5. Support-regulated electron transfer at the metal-oxide interfaces was proposed to alter the Cu surface characteristics hence the catalytic properties. The importance and clear evidence for this proposed model requires future work as provided in chapter 7

Overall, experimental evidence supporting different mechanisms for the active site under conventional methanol synthesis conditions clearly demonstrated the continuous need for in situ surface sensitive techniques (XPS, XAS, IR etc.) to unveil the dynamics and active center of the working Cu/ZnO-based catalysts.

References

[1] M. Patart. French Patent 540 343, 1921.

[2] C. Lormand. Industrial Production of Synthetic Methanol. *Industrial & Engineering Chemistry*, 17(4):430–432, 1925. doi: 10.1021/ie50184a034.

[3] BASF. German Patents 415 686, 441 433, 462 837, 1923.

[4] J. B. Hansen and P. E. H. Nielsen. *Methanol Synthesis*, volume 2. Wiley-VCH Verlag GmbH, 2nd edition edition, 2008. doi: 10.1002/9783527610044.hetcat0148.

[5] C. Murkin and J. Brightling. Eighty years of steam reforming. *Johnson Matthey Technology Review*, 60(4):263–269, 2016. doi: 10.1595/205651316X692923.

[6] G. A. Olah, A. Goeppert, and G. K. Prakash. *Production of Methanol: From Fossil Fuels and Bio-Sources to Chemical Carbon Dioxide Recycling*. John Wiley & Sons, Ltd, 2009. doi: 10.1002/9783527627806.ch12.

[7] P. Davies, F. F. Snowdon, G. W. Bridger, D. O. Hughes, and W. P. Young. Water-gas conversion and catalysts therefor, UK patent 1010871, 1965.

[8] G. Bozzano and F. Manenti. Efficient methanol synthesis: Perspectives, technologies and optimization strategies. *Progress in Energy and Combustion Science*, 56:71–105, 2016. doi: 10.1016/j.pecs.2016.06.001.

[9] H. H. Kung. Methanol Synthesis. *Catalysis Reviews*, 22(2):235–259, 1980. doi: 10.1080/03602458008066535.

[10] Y. B. Kagan, A. Y. Rozovskij, L. G. Liberov, E. V. Slivinskij, G. I. Lin, S. M. Loktev, and A. N. Bashkirov. Study of mechanism of methanol synthesis from carbon monoxide and hydrogen using radioactive carbon isotope C^{14}. *Doklady Akademii Nauk SSSR*, 224(5):1081–1084, 1975.

[11] G. C. Chinchen, P. J. Denny, D. G. Parker, M. S. Spencer, and D. A. Whan. Mechanism of methanol synthesis from $CO_2/CO/H_2$ mixtures over copper/zinc oxide/alumina catalysts: use of ^{14}C-labelled reactants. *Applied Catalysis*, 30(2):333–338, 1987. doi: 10.1016/S0166-9834(00)84123-8.

[12] G. C. Chinchen, K. Mansfield, and M. S. Spencer. The methanol synthesis: How does it work? *Chemtech*, 20:692–699, 1990.

[13] G. Liu, D. Willcox, M. Garland, and H. H. Kung. The role of CO_2 in methanol synthesis on CuZn oxide: An isotope labeling study. *Journal of Catalysis*, 96(1):251–260, 1985. doi: 10.1016/0021-9517(85)90378-1.

[14] M. Muhler, E. Törnqvist, L. P. Nielsen, B. S. Clausen, and H. Topsøe. On the role of adsorbed atomic oxygen and CO_2 in copper based methanol synthesis catalysts. *Catalysis Letters*, 25(1-2):1–10, 1994. doi: 10.1007/BF00815409.

[15] G. Natta. Synthesis of methanol. *Catalysis*, 3:349, 1955.

[16] K. Klier, V. Chatikavanij, R. G. Herman, and G. W. Simmons. Catalytic Synthesis of Methanol from CO/H_2 IV The Effects of Carbon Dioxide. *Journal of Catalysis*, 74:343–360, 1982. doi: 10.1016/0021-9517(82)90040-9.

[17] K. C. Waugh. Methanol synthesis. *Catalysis Letters*, 142(10):1153–1166, 2012. doi: 10.1007/s10562-012-0905-2.

[18] K. Aasberg-Petersen, C. S. Nielsen, I. Dybkjær, and J. Perregaard. Large Scale Methanol Production from Natural Gas. *Haldor Topsoe*, pages 1–14, 2008.

[19] A. Karelovic and P. Ruiz. The role of copper particle size in low pressure methanol synthesis via CO_2 hydrogenation over Cu/ZnO catalysts. *Catal. Sci. Technol.*, 5(2):869–881, 2015. doi: 10.1039/C4CY00848K.

[20] M. Behrens, S. Zander, P. Kurr, N. Jacobsen, J. Senker, G. Koch, T. Ressler, R. W. Fischer, and R. Schlögl. Performance improvement of nanocatalysts by promoter-induced defects in the support material: Methanol synthesis over Cu/ZnO:Al. *Journal of the American Chemical Society*, 135(16):6061–6068, 2013. doi: 10.1021/ja310456f.

[21] C. H. Bartholomew and R. J. Farrauto. *Hydrogen production and synthesis gas reactions.* John Wiley & Sons, 2006. doi: 10.1002/9780471730071.ch6.

[22] M. Behrens and R. Schlögl. How to prepare a good Cu/ZnO catalyst or the role of solid state chemistry for the synthesis of nanostructured catalysts. *Zeitschrift fur Anorganische und Allgemeine Chemie*, 639(15):2683–2695, 2013. doi: 10.1002/zaac.201300356.

[23] P. B. Rasmussen, P. M. Holmblad, T. Askgaard, C. V. Ovesen, P. Stoltze, J. K. Nørskov, and I. Chorkendorff. Methanol synthesis on Cu (100) from a binary gas mixture of CO_2 and H_2. *Catalysis letters*, 26(3-4):373–381, 1994. doi: 10.1007/BF00810611.

[24] I. Nakamura, T. Fujitani, T. Uchijima, and J. Nakamura. A model catalyst for methanol synthesis: Zn-deposited and Zn-free Cu surfaces. *Journal of Vacuum Science & Technology A*, 14 (3):1464–1468, 1996. doi: 10.1063/1.451126.

[25] J. Nerlov and I. Chorkendorff. Methanol synthesis from CO_2, CO, and H_2 over Cu(100) and Ni/Cu(100). *Journal of Catalysis*, 181(2):271–279, 1999. doi: 10.1006/jcat.1998.2301.

[26] J. Sehested. Industrial and scientific directions of methanol catalyst development. *Journal of Catalysis*, 371:368–375, 2019. doi: 10.1016/j.jcat.2019.02.002.

[27] C. Baltes, S. Vukojević, and F. Schüth. Correlations between synthesis, precursor, and catalyst structure and activity of a large set of $CuO/ZnO/Al_2O_3$ catalysts for methanol synthesis. *Journal of Catalysis*, 258(2):334–344, 2008. doi: 10.1016/j.jcat.2008.07.004.

[28] M. Kurtz, N. Bauer, C. Büscher, H. Wilmer, O. Hinrichsen, R. Becker, S. Rabe, K. Merz, M. Driess, R. Fischer, and M. Muhler. New Synthetic Routes to More Active Cu/ZnO Catalysts Used for Methanol Synthesis. *Catalysis Letters*, 92(1):49–52, 2004. doi: 10.1023/B:CATL.0000011085.88267.a6.

[29] M. Behrens, F. Studt, I. Kasatkin, S. Kühl, M. Hävecker, F. Abild-Pedersen, S. Zander, F. Girgsdies, P. Kurr, B. Kniep, M. Tovar, R. W. Fischer, J. K. Nørskov, and R. Schlögl. The Active Site of Methanol Synthesis over $Cu/ZnO/Al_2O_3$ Industrial Catalysts. *Science*, 336:893–898, 2012. doi: 10.1126/science.1219831.

[30] M. S. Spencer. The role of zinc oxide in Cu/ZnO catalysts for methanol synthesis and the water-gas shift reaction. *Topics in Catalysis*, 8(3-4):259–266, 1999. doi: 10.1023/A:1019181715731.

[31] M. Behrens. Meso-and Nanostructuring of Industrial $Cu/ZnO/(Al_2O_3)$ Catalysts. *Journal of Catalysis*, 267:24–29, 2009. doi: 10.1126/science.1219831.

[32] I. Kasatkin, P. Kurr, B. Kniep, A. Trunschke, and R. Schlögl. Role of lattice strain and defects in copper particles on the activity of $Cu/ZnO/Al_2O_3$ catalysts for methanol synthesis. *Angewandte Chemie - International Edition*, 119:7465–7468, 2007. doi: 10.1002/anie.200702600.

[33] R. Burch, S. E. Golunski, and M. S. Spencer. The role of copper and zinc oxide in methanol synthesis catalysts. *Journal of the Chemical Society, Faraday Transactions*, 86(15):2683–2691, 1990. doi: 10.1039/ft9908602683.

[34] J. Nakamura, T. Uchijima, Y. Kanai, and T. Fujitani. The role of ZnO in Cu/ZnO methanol synthesis catalysts. *Catalysis Today*, 28(3):223–230, 1996. doi: 10.1016/0920-5861(95)00240-5.

[35] T. Fujitani, I. Nakamura, and T. Uchijima. The kinetics and mechanism of methanol synthesis by hydrogenation of CO_2 over a Zn-deposited Cu (111) surface. *Surface Science*, 383:285–298, 1997. doi: 10.1016/S0039-6028(97)00192-1.

[36] J. W. Niemantsverdriet and I. Chorkendorff. *Concepts of Modern Catalysis and Kinetics 2nd. edition*. Wiley-VCH, 2007. doi: 10.1002/3527602658.

[37] L. C. Grabow and M. Mavrikakis. Mechanism of Methanol Synthesis on Cu through CO_2 and CO Hydrogenation. *ACS Catalysis*, 1:365–384, 2011. doi: 10.1021/cs200055d.

[38] A. Y. Rozovskii. New data on the mechanism of catalytic reactions with the participation of carbon oxides. *Plenum Publishing Corporation*, 21:78–87, 1980.

[39] G. C. Chinchen, C. M. Hay, H. D. Vandervell, and K. C. Waugh. The measurement of copper surface areas by reactive frontal chromatography. *Journal of Catalysis*, 103(1):79–86, 1987. doi: 10.1016/0021-9517(87)90094-7.

[40] J. S. Lee, S. H. Han, H. G. Kim, K. H. Lee, and Y. G. Kim. Effects of space velocity on methanol synthesis from $CO_2/CO/H_2$ over $Cu/ZnO/Al_2O_3$ catalyst. *Korean Journal of Chemical Engineering*, 17(3):332–336, 2000. doi: 10.1007/BF02699049.

[41] M. Sahibzada, I. S. Metcalfe, and D. Chadwick. Methanol Synthesis from $CO/CO_2/H_2$ over $Cu/ZnO/Al_2O_3$ at Differential and Finite Conversions. *Journal of Catalysis*, 174:111–118, 1998. doi: 10.1006/jcat.1998.1964.

[42] O. Cherifi, S. Monteverdi, M. M. Bettahar, M. Foorissier, and V. Perrichon. Kinetics of CO_2 hydrogenation into methanol on a Cu-Zn-Al oxide catalyst. *Bull. Soc. Chim. Fr.*, pages 405–409, 1985.

[43] P. C. K. Vesborg, I. Chorkendorff, I. Knudsen, O. Balmes, J. Nerlov, A. M. Molenbroek, B. S. Clausen, and S. Helveg. Transient behavior of Cu/ZnO-based methanol synthesis catalysts. *Journal of Catalysis*, 262(1):65–72, 2009. doi: 10.1016/j.jcat.2008.11.028.

[44] S. Kuld, M. Thorhauge, H. Falsig, C. F. Elkjaer, S. Helveg, I. Chorkendorff, and J. Sehested. Quantifying the promotion of Cu catalysts by ZnO for methanol synthesis. *Science*, 352(6288): 969–974, 2016. doi: 10.1126/science.aaf0718.

[45] M. Kurtz, N. Bauer, H. Wilmer, O. Hinrichsen, and M. Muhler. Rational Catalyst Design of Methanol Synthesis Catalysts. *Chemical Engineering & Technology*, 27(11):1146–1150, 2004. doi: 10.1002/ceat.200407032.

[46] P. J. A. Tijm, F. J. Waller, and D. M. Brown. Methanol technology developments for the new millennium. *Applied Catalysis A: General*, 221(1):275–282, 2001. doi: 10.1016/S0926-860X(01) 00805-5.

[47] H. Goehna and P. Koenig. Producing methanol from CO_2. *Chemtech*, 24(6):36–39, 1994.

[48] K. R. Westerterp. New methanol processes. *Energy Efficiency in Process Technology*, 53:1142–1153, 1993. doi: 10.1007/978-94-011-1454-7_101.

[49] R. J. Dry. Possibilities for the development of large-capacity methanol synthesis reactors for synfuel production. *Industrial and Engineering Chemistry Research*, 27(4):616–624, 1988. doi: 10.1021/ie00076a015.

[50] ICI Synetix (now Johnson Matthey). 2006.

[51] F. Hartig and F. J. Keil. Large-Scale Spherical Fixed Bed Reactors: Modeling and Optimization. *Industrial and Engineering Chemistry Research*, 32(3):424–437, 1993. doi: 10.1021/ie00015a005.

[52] M. Behrens. Chemical hydrogen storage by methanol: Challenges for the catalytic methanol synthesis from CO_2. *Recyclable Catalysis*, 2(1):78–86, 2016. doi: 10.1515/recat-2015-0009.

[53] M. Maack, H. Friis-jensen, S. Sckerl, J. H Larsen, and I. Chorkendorff. Methanol synthesis on potassium-modified Cu (100) from CO + H_2 and CO + CO_2 + H_2. *Topics in Catalysis*, 22(3-4): 151–160, 2003. doi: 1022-5528/03/04000151/0.

[54] E. G. Choi, K. H. Song, S. R. An, K. Y. Lee, M. H. Youn, K. T. Park, S. K. Jeong, and H. J. Kim. Cu/ZnO/AlOOH catalyst for methanol synthesis through CO_2 hydrogenation. *Korean Journal of Chemical Engineering*, 35(1):73–81, 2018. doi: 10.1007/s11814-017-0230-y.

[55] H. Bahruji, M. Bowker, G. Hutchings, N. Dimitratos, P. Wells, E. Gibson, W. Jones, C. Brookes, D. Morgan, and G. Lalev. Pd/ZnO catalysts for direct CO_2 hydrogenation to methanol. *Journal of Catalysis*, 343:133–146, 2016. doi: 10.1016/j.jcat.2016.03.017.

[56] C. Hobson and C. Márquez. Renewable Methanol Report. *Methanol Institute*, pages 1–26, 2018.

[57] A. M. Shulenberger, F. R. Jonsson, O. Ingolfsson, and K.-C. Tran. Process for producing liquid fuel from carbon dioxide and water, 2007.

[58] M. Kauw, M. J. Benders, and C. Visser. Green methanol from hydrogen and carbon dioxide using geothermal energy and/or hydropower in Iceland or excess renewable electricity in Germany. *Energy*, 90:208–217, 2015. doi: 10.1016/j.energy.2015.06.002.

[59] A. Álvarez, A. Bansode, A. Urakawa, A. V. Bavykina, T.A. Wezendonk, M. Makkee, J. Gascon, and F. Kapteijn. Challenges in the Greener Production of Formates/Formic Acid, Methanol, and DME by Heterogeneously Catalyzed CO_2 Hydrogenation Processes. *Chemical Reviews*, 117 (14):9804–9838, 2017. doi: 10.1021/acs.chemrev.6b00816.

[60] A. González-Garay, M. S. Frei, A. Al-Qahtani, C. Mondelli, G. Guillén-Gosálbez, and J. Pérez-Ramírez. Plant-to-planet analysis of CO_2-based methanol processes. *Energy & Environmental Science*, 12:3425–3436, 2019. doi: 10.1039/c9ee01673b.

[61] I. Dybkjær and J. B. Hansen. Large-scale production of alternative synthetic fuels from natural gas. *Studies in Surface Science and Catalysis*, 107:99–116, 1997. doi: 10.1016/s0167-2991(97) 80322-9.

[62] G. F. Hüttig. Die theoretischen Grundlagen der Frittungsvorgänge innerhalb von Pulvern. *MetallKunde*, 3:93–99, 1948.

[63] M. Argyle and C. Bartholomew. Heterogeneous Catalyst Deactivation and Regeneration: A Review. *Catalysts*, 5:145–269, 2015. doi: 10.3390/catal5010145.

[64] M. B. Fichtl, Dn Schlereth, N. Jacobsen, I. Kasatkin, J. Schumann, M. Behrens, R. Schlögl, and O. Hinrichsen. Kinetics of deactivation on Cu/ZnO/Al_2O_3 methanol synthesis catalysts. *Applied Catalysis A: General*, 502:262–270, 2015. doi: 10.1016/j.apcata.2015.06.014.

[65] B. S. Clausen, G. Steffensen, B. Fabius, J. Villadsen, R. Feidenhans'l, and H. Topsøe. In situ cell for combined XRD and on-line catalysis tests: Studies of Cu-based water gas shift and methanol catalysts. *Journal of Catalysis*, 132(2):524–535, 1991. doi: 10.1016/0021-9517(91)90168-4.

[66] N.-Y. Topsøe and H. Topsøe. FTIR studies of dynamic surface structural changes in Cu-based methanol synthesis catalysts. *Journal of Molecular Catalysis A: Chemical*, 141:95–105, 1999. doi: 10.1016/s1381-1169(98)00253-2.

[67] J.-D. Grunwaldt, A.M. Molenbroek, N.-Y. Topsøe, H. Topsøe, and B. S. Clausen. In Situ Investigations of Structural Changes in Cu/ZnO Catalysts. *Journal of Catalysis*, 194(2):452–460, 2000. doi: 10.1006/jcat.2000.2930.

[68] T. Lunkenbein, F. Girgsdies, T. Kandemir, N. Thomas, M. Behrens, R. Schlögl, and E. Frei. Bridging the Time Gap: A Copper/Zinc Oxide/Aluminum Oxide Catalyst for Methanol Synthesis Studied under Industrially Relevant Conditions and Time Scales. *Angewandte Chemie - International Edition*, 55(41):12708–12712, 2016. doi: 10.1002/anie.201603368.

[69] Y. Okamoto, K. Fukino, T. Imanaka, and S. Teranishi. Surface Characterization of CuO-ZnO Methanol-Synthesis Catalysts by X-ray Photoelectron Spectrosocpy. 2. Reduced Catalysts. *The Journal of physical chemistry*, 87(19):3747–3754, 1983. doi: 10.1021/j100242a035.

[70] S. Kuld, C. Conradsen, P. G. Moses, I. Chorkendorff, and J. Sehested. Quantification of zinc atoms in a surface alloy on copper in an industrial-type methanol synthesis catalyst. *Angewandte Chemie - International Edition*, 53(23):5941–5945, 2014. doi: 10.1002/anie.201311073.

[71] T. H. Fleisch and R. L. Mieville. Studies on the chemical state of Cu during methanol synthesis. *Journal of Catalysis*, 90(1):165–172, 1984. doi: 10.1016/0021-9517(84)90099-X.

[72] W. X. Pan, R. Cao, D. L. Roberts, and G. L. Griffin. Methanol synthesis activity of Cu/ZnO catalysts. *Journal of Catalysis*, 114(2):440–446, 1988. doi: 10.1016/0021-9517(88)90047-4.

[73] T. Fujitani, M. Saito, Y. Kanai, T. Kakumoto, T. Watanabe, J. Nakamura, and T. Uchijima. The role of metal oxides in promoting a copper catalyst for methanol synthesis. *Catalysis Letters*, 25(3-4):271–276, 1994. doi: 10.1007/BF00816307.

[74] M. Saito, J. Wu, K. Tomoda, I. Takahara, and K. Murata. Effects of ZnO contained in supported Cu-based catalysts on their activities for several reactions. *Catalysis Letters*, 83(1-2):1–4, 2002. doi: 10.1023/A:1020693226903.

[75] S. G. Neophytides, A. J. Marchi, and G. F. Froment. Methanol synthesis by means of diffuse reflectance infrared Fourier transform and temperature-programmed reaction spectroscopy. *Applied Catalysis*, 86:45–64, 1992. doi: 10.1016/0926-860X(92)80041-A.

[76] G. J. Millar, C. H. Rochester, and K. C. Waugh. An in situ high pressure FT-IR study of CO_2/H_2 interactions with model ZnO/SiO_2, Cu/SiO_2 and $Cu/ZnO/SiO_2$ methanol synthesis catalysts. *Catalysis Letters*, 14(3-4):289–295, 1992. doi: 10.1007/BF00769666.

[77] T. S. Askgaard, J. K. Nørskov, C. V. Ovesen, and P. Stoltze. A Kinetic Model of Methanol Synthesis. *Journal of Catalysis*, 156:229–242, 1995. doi: 10.1006/jcat.1995.1250.

[78] Y. Amenomiya and T. Tagawa. Infrared study of methanol synthesis from CO_2 and H_2 on supported copper-zinc oxide catalysts. *Proc. of 8th Int. Congress on Catal*, pages 557–567, 1984.

[79] F. Le Peltier, P. Chaumette, J. Saussey, M. M. Bettahar, and J. C. Lavalley. In situ FT-IR and kinetic study of methanol synthesis from CO_2/H_2 over $ZnAl_2O_4$ and Cu-$ZnAl_2O_4$ catalysts. *Journal of Molecular Catalysis A: Chemical*, 132(1):91–100, 1998. doi: 10.1016/S1381-1169(97)00235-5.

[80] S. Lin, A. Oldfield, and D. Klenerman. In-situ studies of polycrystalline copper during methanol synthesis at high pressure using sum frequency generation at surfaces. *Surface Science*, 464(1):1–7, 2000. doi: 10.1016/S0039-6028(00)00706-8.

[81] B. Sakakini, J. Tabatabaei, M. J. Watson, K. C. Waugh, and F. W. Zemicael. Identification of the intermediate involved in methanol synthesis by gaseous titration. *Faraday Discuss*, 105:369–376, 1996.

[82] M. Bowker, R. A. Hadden, H. Houghton, J. N K Hyland, and K. C. Waugh. The mechanism of methanol synthesis on copper/zinc oxide/alumina catalysts. *Journal of Catalysis*, 109(2):263–273, 1988. doi: 10.1016/0021-9517(88)90209-6.

[83] E. L. Kunkes, F. Studt, F. Abild-Pedersen, R. Schlögl, and M. Behrens. Hydrogenation of CO_2 to methanol and CO on $Cu/ZnO/Al_2O_3$: Is there a common intermediate or not? *Journal of Catalysis*, 328:43–48, 2015. doi: 10.1016/j.jcat.2014.12.016.

[84] G. H. Graaf. *The synthesis of methanol in gas-solid and gas-slurry reactors*. PhD thesis, Groningen, 1988.

[85] C. V. Ovesen, B. S. Clausen, J. Schiøtz, P. Stoltze, H. Topsøe, and J. K. Nørskov. Kinetic Implications of Dynamical Changes in Catalyst Morphology during Methanol Synthesis over Cu/ZnO Catalysts. *Journal of Catalysis*, 168(2):133–142, 1997. doi: 10.1006/jcat.1997.1629.

[86] S. Fujita, M. Usui, H. Ito, and N. Takezawa. Mechanisms of Methanol Synthesis from Carbon Dioxide and from Carbon Monoxide at Atmospheric Pressure over Cu/ZnO. *Journal of Catalysis*, 157(2):403–413, 1995. doi: 10.1006/jcat.1995.1306.

[87] S. I. Fujita, M. Usui, and N. Takezawa. Mechanism of the reverse water gas shift reaction over Cu/ZnO catalyst. *Journal of Catalysis*, 134(1):220–225, 1992. doi: 10.1016/0021-9517(92)90223-5.

[88] B. S. Clausen, J. Schiøtz, L. Gråbæk, C. V. Ovesen, K. W. Jacobsen, J. K. Nørskov, and H. Topsøe. Wetting/ non-wetting phenomena during catalysis: Evidence from in situ on-line EXAFS studies of Cu-based catalysts. *Topics in Catalysis*, 1(3-4):367–376, 1994. doi: 10.1007/BF01492289.

[89] M. S. Spencer. Stable and metastable metal surfaces in heterogeneous catalysis. *Nature*, 323(23):685–687, 1986. doi: 10.1038/324227a0.

[90] P. L. Hansen, J. B. Wagner, S. Helveg, J. R. Rostrup-Nielsen, B. S. Clausen, and H. Topsøe. Atom-Resolved Imaging of Dynamic Shape Changes in Supported Copper Nanocrystals. *Science*, 295(5562):2053–2055, 2002. doi: 10.1126/science.1069325.

[91] J. Yoshihara, S. C. Parker, A. Schafer, and C. T. Campbell. Methanol synthesis and reverse water-gas shift kinetics over clean polycrystalline copper. *Catalysis Letters*, 31(4):313–324, 1995. doi: 10.1007/BF00808595.

[92] J. I. Steinfeld, J. S. Francisco, and W. L. Hase. *Chemical kinetics and dynamics*. Prentice Hall, Upper Saddle Rive, NJ, 2nd edition, 1999.

[93] S. Natesakhawat, J. W. Lekse, J. P. Baltrus, R. Paul, B. H. Howard, X. Deng, and C. Matranga. Active Sites and Structure-activity Relationships of Copper-based Catalysts for Carbon Dioxide Hydrogenation to Methanol. *ACS Catalysis*, 2(8):1667–1676, 2012. doi: 10.1021/cs300008g.

[94] K. H. Lee and J. S. Lee. Effects of catalyst composition on methanol synthesis from CO_2/H_2. *Korean Journal of Chemical Engineering*, 12(4):460–465, 1995. doi: 10.1007/BF02705811.

[95] D. Wang, L. Ma, C.J. Jiang, D.L. Trimm, M.S. Wainwright, and D.H. Kim. The effect of zinc oxide in Raney copper catalysts on methanol synthesis, water gas shift, and methanol steam reforming reaction. *Studies in Surface Science and Catalysis*, 101(16):1379–1387, 1996. doi: 10.1016/S0167-2991(96)80350-8.

[96] G. Wulff. On the question of speed of growth and dissolution of crystal surfaces. *Zeitschrift Fur Krystallographie Und Mineralogie*, 34(5/6):449–530, 1901.

[97] M. M. Günter, T. Ressler, B. Bems, C. Büscher, T. Genger, O. Hinrichsen, M. Muhler, and R. Schlögl. Implication of the microstructure of binary Cu/ZnO catalysts for their catalytic activity in methanol synthesis. *Catalysis Letters*, 71(1-2):37, 2001. doi: 10.1023/A:1016696022840.

[98] S. J. Tauster, S. C. Fung, and R. L. Garten. Strong Metal-Support Interactions. Group 8 Noble Metals Supported on TiO_2. *Journal of the American Chemical Society*, 100(1):170–175, 1978. doi: 10.1021/ja00469a029.

[99] V. D. Berg, Roy, G. Prieto, G. Korpershoek, L. I. Van Der Wal, A. J. Van Bunningen, S. Lægsgaard-Jørgensen, P. E. De Jongh, and K. P. De Jong. Structure sensitivity of Cu and CuZn catalysts relevant to industrial methanol synthesis. *Nature Communications*, 7(13057):1–7, 2016. doi: 10.1038/ncomms13057.

[100] M. B. Fichtl, J. Schumann, I. Kasatkin, N. Jacobsen, M. Behrens, R. Schlögl, M. Muhler, and O. Hinrichsen. Counting of oxygen defects versus metal surface sites in methanol synthesis catalysts by different probe molecules. *Angewandte Chemie - International Edition*, 53(27): 7043–7047, 2014. doi: 10.1002/anie.201400575.

[101] K.-D. Jung, O.-S. Joo, and S.-H. Han. Structural change of Cu/ZnO by reduction of ZnO in Cu/ZnO with methanol. *Catal. Lett.*, 68(1-2):49, 2000. doi: 10.1023/A:1019027302428.

[102] G. J. J. Bartley and R. Burch. Support and morphological effects in the synthesis of methanol over Cu/ZnO, Cu/ZrO_2 and Cu/SiO_2 catalysts. *Applied Catalysis*, 43(1):141–153, 1988. doi: 10.1016/S0166-9834(00)80907-0.

[103] O. S. Joo, K. D. Jung, S. H. Han, and S. J. Uhm. Synergistic Effects between Cu and ZnO in the hydrogenation of their formates. *Journal of Catalysis*, 157(1):259–261, 1995. doi: 10.1006/jcat.1995.1286.

[104] T. Lunkenbein, J. Schumann, M. Behrens, R. Schlögl, and M. G. Willinger. Formation of a ZnO Overlayer in Industrial $Cu/ZnO/Al_2O_3$ Catalysts Induced by Strong Metal-Support Interactions. *Angewandte Chemie - International Edition*, 127:4627–4631, 2015. doi: 10.1002/anie.201411581.

[105] S. Kattel, P. J. Ramírez, J. G. Chen, J.A. Rodriguez, and P. Liu. Active sites for CO_2 hydrogenation to methanol on Cu/ZnO catalysts. *Science*, 355(6331):1296–1299, 2017. doi: 10.1126/science.aal3573.

[106] R. M. Palomino, P J. Ramírez, Z. Liu, R. Hamlyn, I. Waluyo, M. Mahapatra, I. Orozco, A. Hunt, J. P. Simonovis, S. D. Senanayake, and J. A. Rodriguez. Hydrogenation of CO_2 on ZnO/Cu(100) and ZnO/Cu(111) Catalysts: Role of Copper Structure and Metal-Oxide Interface in Methanol Synthesis. *Journal of Physical Chemistry B*, 122(2):794–800, 2018. doi: 10.1021/acs.jpcb.7b06901.

[107] M. Sano, T. Adaniya, T. Fujitani, and J. Nakamura. Formation Process of a Cu-Zn Surface Alloy on Cu (111) Investigated by Scanning Tunneling Microscopy. *J. Phys. Chem*, 106:7627–7633, 2002. doi: 10.1021/jp012810i.

[108] A. Karelovic, G. Galdames, J. C. Medina, C. Yévenes, Y. Barra, and R. Jiménez. Mechanism and structure sensitivity of methanol synthesis from CO_2 over SiO_2-supported Cu nanoparticles. *Journal of Catalysis*, 369:415–426, 2019. doi: 10.1016/j.jcat.2018.11.012.

[109] P. Van Helden, I. M. Ciobica, and R. L.J. Coetzer. The size-dependent site composition of FCC cobalt nanocrystals. *Catalysis Today*, 261:48–59, 2016. doi: 10.1016/j.cattod.2015.07.052.

[110] R. Van Hardeveld and F. Hartog. The statistics of surface atoms and surface sites on metal crystals. *Surf. Sci.*, 15(2):189–230, 1969. doi: 10.1016/0039-6028(69)90148-4.

[111] C. Kittel. *Introduction to Solid State Physics*. John Wiley & Sons, 2005. doi: 10.1119/1.1934457.

[112] L. J. Brillson. The Structure and Properties of Metal-Semiconductor Interfaces. *Surface Science Reports 2*, 123:123–326, 1982. doi: 10.1016/0167-5729(82)90001-2.

[113] H. W. Chen, J. M. White, and J. G. Ekerdt. Electronic effect of supports on copper catalysts. *Journal of Catalysis*, 99(2):293–303, 1986. doi: 10.1016/0021-9517(86)90354-4.

[114] K. Kähler, M. C Holz, M. Rohe, J. Strunk, and M. Muhler. Probing the reactivity of ZnO and Au/ZnO nanoparticles by methanol adsorption: A TPD and DRIFTS study. *ChemPhysChem*, 11(12):2521–2529, 2010. doi: 10.1002/cphc.201000282.

[115] S. J. Tauster. Strong Interactions in Supported-Metal Catalysts. *Science*, 211:1121–1125, 1981. doi: 10.1126/science.211.4487.1121.

[116] Y-W. Chung and W. B. Weissbard. Surface spectroscopy studies of the $SrTiO_3$ (100) surface and the platinum-$SrTiO_2$ (100) interface. *Phys. Rev.*, 20(8):3456–3461, 1979.

[117] F. Boccuzzi, C. Morterra, R. Scala, and A. Zecchina. Infrared Spectrum of Microcrystalline Zinc Oxide Electronic and vibrational contributions under different temperature and environmental conditions. *Chemical society, Faraday Transactions 2*, 77:2059–2066, 1981. doi: 10.1039/F29817702059.

[118] F. A. Selim, M. H. Weber, D. Solodovnikov, and K. G. Lynn. Nature of native defects in ZnO. *Physical Review Letters*, 99(8):1–4, 2007. doi: 10.1103/PhysRevLett.99.085502.

[119] S. B. Zhang, S.-H. Wei, and A. Zunger. Intrinsic n-type versus p-type doping asymmetry and the defect physics of ZnO. *Physical Review B*, 63(7):1–7, 2001. doi: 10.1103/PhysRevB.63.075205.

[120] J. C. Frost. Junction effect interactions in methanol synthesis catalysts. *Nature*, 334:577–580, 1988. doi: 10.1038/332141a0.

[121] C. A. Mead. Metal-semiconductor surface barriers. *Solid-State Electronics*, 9(11-12):1023–1033, 1966. doi: 10.1016/0038-1101(66)90126-2.

[122] W. Rogers. The reduction of mixed oxides. Copper and zinc oxides. *Journal of the American Chemical Society*, 49(6):1432–1435, 1927. doi: 10.1021/ja01405a006.

[123] V. Ponec. On the so-called "junction effects" in methanol synthesis. *Catalysis Letters*, 11(2): 249–250, 1991. doi: 10.1007/BF00764092.

[124] Y. S. Kim and W. P. Tai. Electrical and optical properties of Al-doped ZnO thin films by sol-gel process. *Applied Surface Science*, 253(11):4911–4916, 2007. doi: 10.1016/j.apsusc.2006.10.068.

[125] G. Z. Xing, B. Yao, C. X. Cong, T. Yang, Y. P. Xie, B. H. Li, and D. Z. Shen. Effect of annealing on conductivity behavior of undoped zinc oxide prepared by rf magnetron sputtering. *Journal of Alloys and Compounds*, 457(1-2):36–41, 2008. doi: 10.1016/j.jallcom.2007.03.071.

[126] I. Nakamura, T. Fujitani, T. Uchijima, and J. Nakamura. A model catalyst for methanol synthesis: Zn-deposited and Zn-free Cu surfaces. *Journal of Vacuum Science & Technology*, 14(3): 1464–1468, 1996. doi: 10.1116/1.579970.

[127] Y. Yang, J. Evans, J. A. Rodriguez, M. G. White, and P. Liu. Fundamental studies of methanol synthesis from CO_2 hydrogenation on Cu(111), Cu clusters, and Cu/ZnO(0001). *Physical Chemistry Chemical Physics*, 12(33):9909–9917, 2010. doi: 10.1039/c001484b.

[128] L. Dubois and B. R. Zegarski. The influence of electron-withdrawing on the adsorption of CO on copper. *Chemical Physics Letters*, 120(6):537–541, 1985. doi: 10.1016/0009-2614(85)80550-90.

[129] B. A. Sexton. Observations of formate species on copper(100) surface by high resolution electron energy loss spectroscopy. *Surf. Sci.*, 88:319–330, 1979. doi: 10.1016/0039-6028(79)90078-5.

[130] K. Horn. Infrared Spectrum of CO Chemisorbed on Cu(100). *Surface Science*, 55:701–704, 1976. doi: 10.1063/1.1732824.

[131] D. Scarano, S. Bordiga, C. Lamberti, G. Spoto, G. Ricchiardi, A. Zecchina, and C. O. Arean. FTIR study of the interaction of CO with pure and silica-supported copper(I) oxide. *Applied Surface Science*, 134(411):272–285, 1998. doi: 10.1016/S0169-4332(98)00225-6.

[132] A. Dandekar and M. A. Vannice. Determination of the Dispersion and Surface Oxidation States of Supported Cu Catalysts. *Journal of Catalysis*, 178(2):621–639, 1998. doi: 10.1006/jcat.1998.2190.

[133] Y. Zhu, X. Kong, J. Yin, R. You, B. Zhang, H. Zheng, X. Wen, Y. Zhu, and Y. W. Li. Covalent-bonding to irreducible SiO_2 leads to high-loading and atomically dispersed metal catalysts. *Journal of Catalysis*, 353:315–324, 2017. doi: 10.1016/j.jcat.2017.07.030.

[134] O. Hinrichsen, T. Genger, and M. Muhler. Chemisorption of N_2O and H_2 for the Surface Determination of Copper Catalysts. *Chemical Engineering & Technology*, 23(11):956–959, 2000. doi: 10.1002/1521-4125(200011)23:11⟨956::AID-CEAT956⟩3.0.CO;2-L.

[135] G. Sengupta, D. K. Gupta, M. L. Kundu, and S. P. Sen. Effect of Reduction Conditions upon Metal Area in CuO-ZnO Catalyst. *Journal of Catalysis*, 67:223–225, 1981.

[136] R. Chatterjee, S. Kuld, R. V. D. Berg, A. Chen, and W. Shen. Mapping Support Interactions in Copper Catalysts. *Topics in Catalysis*, 62(7-11):649–659, 2019. doi: 10.1007/s11244-019-01150-9.

[137] G. Anger, A. Winkler, and K. D. Rendulic. Adsorption and desorption kinetics in the systems H_2/Cu(111), H_2/Cu(110) and H_2/Cu(100). *Surface Science*, 220(1):1–17, 1989. doi: 10.1016/0039-6028(89)90459-7.

[138] M. Muhler, L. P. Nielsen, E. Törnqvist, B. S. Clausen, and H. Topsøe. Temperature-programmed desorption of H_2 as a tool to determine metal surface areas of Cu catalysts. *Catalysis letters*, 14 (3):241–249, 1992. doi: 10.1007/BF00769661.

[139] M. Balooch, M. J. Cardillo, D. R. Miller, and R. E. Stickney. Molecular beam study of the apparent activation barrier associated with adsorption and desorption of hydrogen on copper. *Surface Science*, 46:358–392, 1974.

[140] E. M. Mccash, S. F. Parker, and M. A. Chesters. The adsorption of atomic hydrogen on Cu(111) investigated by reflection-adsorption infrared spectroscopy, electron energy losss spectroscopy and low energy electron diffraction. *Surface Science*, 215:363–377, 1989.

[141] T. Genger, O. Hinrichsen, and M. Muhler. The temperature-programmed desorption of hydrogen from copper surfaces. *Catalysis Letters*, 59:137–141, 1999. doi: 10.1023/A:1019076722708.

[142] J. Słoczyński, R. Grabowski, J. Janas, and J. Skrzypek. Adsorption model of methanol synthesis reactants on CuO-ZnO-Al_2O_3 catalyst-I. Adsorption on the catalyst. *Chemical Engineering Science*, 46(10):2599–2610, 1991. doi: 10.1016/0009-2509(91)80053-2.

[143] J. Słoczyński, R. Grabowski, and J. Janas. Adsorption Model of Methanol Synthesis Reactants on CuO-ZnO-Al_2O_3 Catalyst - II Adsorption on the individual components of the catalyst. *Chemical Engineering Science*, 46(10):2611–2623, 1991. doi: 10.1016/0009-2509(91)80054-3.

[144] F. Studt, I. Sharafutdinov, F. Abild-Pedersen, Christian F. Elkjær, J. S. Hummelshøj, S. Dahl, I. Chorkendorff, and J. K. Nørskov. Discovery of a Ni-Ga catalyst for carbon dioxide reduction to methanol. *Nature Chemistry*, 6(4):320–324, 2014. doi: 10.1038/nchem.1873.

[145] I. Sharafutdinov, C. F. Elkjær, H. W. P. De Carvalho, D. Gardini, G. L. Chiarello, C. D. Damsgaard, J. B. Wagner, J. D. Grunwaldt, S. Dahl, and I. Chorkendorff. Intermetallic compounds of Ni and Ga as catalysts for the synthesis of methanol. *Journal of Catalysis*, 320(1):77–88, 2014. doi: 10.1016/j.jcat.2014.09.025.

[146] J. Graciani, K. Mudiyanselage, F. Xu, A. E. Baber, and J. Evans. Highly active copper-ceria and copper-ceria-titania catalysts for methanol synthesis from CO_2. *Science*, 345(6196):546–550, 2014. doi: 10.1126/science.1253057.

[147] S. D. Senanayake, P. J. Ramírez, I. Waluyo, S. Kundu, K. Mudiyanselage, Z. Liu, Z. Liu, S. Axnanda, D. J. Stacchiola, J. Evans, and J. A. Rodriguez. Hydrogenation of CO_2 to Methanol on CeO_x/Cu(111) and ZnO/Cu(111) Catalysts: Role of the Metal-Oxide Interface and Importance of Ce^{3+} Sites. *Journal of Physical Chemistry C*, 120(3):1778–1784, 2016. doi: 10.1021/acs.jpcc.5b12012.

[148] C.-S. Li, G. Melaet, W. T. Ralston, K. An, C. Brooks, Y. Ye, Y.-S. Liu, J. Zhu, J. Guo, S. Alayoglu, and G. A. Somorjai. High-performance hybrid oxide catalyst of manganese and cobalt for low-pressure methanol synthesis. *Nature Communications*, 6(6538):1–5, 2015. doi: 10.1038/ncomms7538.

[149] O. Martin, A. J. Martín, C. Mondelli, S. Mitchell, T. F. Segawa, R. Hauert, C. Drouilly, D. Curulla-Ferré, and J. Pérez-Ramírez. Indium oxide as a superior catalyst for methanol synthesis by CO_2 hydrogenation. *Angewandte Chemie - International Edition*, 55(21):6261–6265, 2016. doi: 10.1002/anie.201600943.

[150] A. Kumar and C. Zhou. The race to replace tin-doped indium oxide: Which material will win? *American Chemical Society*, 4(1):11–14, 2010. doi: 10.1021/nn901903b0.

Chapter 3

The roles of CO and CO_2 in high pressure methanol synthesis over Cu-based catalysts

Authors: Niels D. Nielsen[1], Anker D. Jensen[1], Jakob M. Christensen[1]
[1]*Department of Chemical and Biochemical Engineering, Technical University of Denmark, Søltofts Plads Building 229, 2800 Kgs. Lyngby, Denmark*

*__Correspondence to:__ jmc@kt.dtu.dk

DOI:
Not applicable

Journal specifications:
Journal of Catalysis

Status:
Submitted version has returned. Revised version is currently in progress and the latest revised version is reprinted here.

Abstract

The roles of CO and CO_2 in Cu-catalyzed methanol synthesis from syngas were evaluated in experiments with gas switching between CO/H_2 and CO_2/H_2 feeds and between a $CO_2/CO/H_2$ feed and a corresponding CO-free CO_2/inert/H_2 feed. Switching between $CO/Ar/H_2$ (3/29/68) and $CO_2/N2/H_2$ (3/29/68) for Cu/Al_2O_3 showed that the rate of methanol synthesis on Cu is more than an order of magnitude higher from CO_2 compared to CO. Experiments switching between $CO_2/CO/H_2$ and CO_2/inert/H_2 showed that at low conversion conditions with negligible product formation, CO is purely inhibiting for Raney Cu and for a range of supported (on SiO_2, TiO_2, Al_2O_3 and ZnO) Cu-catalysts including the industrial $Cu/ZnO/Al_2O_3$ catalyst. Given the generality across Cu-based samples the mechanism of this inhibition is most likely competitive adsorption on the Cu surface. However, as conversion is increased by lowering the gas space velocity there is a sharp transition from an inhibiting to a beneficial role of CO relative to a CO-free feed. With increasing conversion more water is formed, and as water is a far stronger inhibitor to Cu-based catalysts than CO, the beneficial effect

of CO arises from the removal of water from the gas atmosphere, through the water-gas shift reaction. At low conversion the methanol synthesis rate is thus highest for a CO-free feed that minimizes CO inhibition, whereas the rate at high conversion is optimal with a CO-rich syngas that minimizes water inhibition. Hence, CO has a beneficial role at commercial, high conversion conditions. The ZnO support exerts a strong, beneficial support effect at low conversion conditions, where the strong reductant CO has a purely negative effect. This could suggest that reduced Zn-sites (oxygen vacancies in ZnO or Cu-Zn surface alloy sites), whose concentration are expected to depend on the reductive potential of the atmosphere, are not critical to the support effect from ZnO. At both industrial conditions (523 K, 50 bar), mild conditions (448 K, atm. pressure) and in a nominally oxidizing gas (498 K, 20 bar with $CO_2 > H_2$) the addition of CO to the feed was detrimental to the activity of $Cu/ZnO/Al_2O_3$ at low conversion conditions. This supports that CO plays no beneficial role by facilitating ZnO-reduction and possibly that Zn alloyed into the Cu surface is unimportant for catalytic activity.

Graphic Abstract

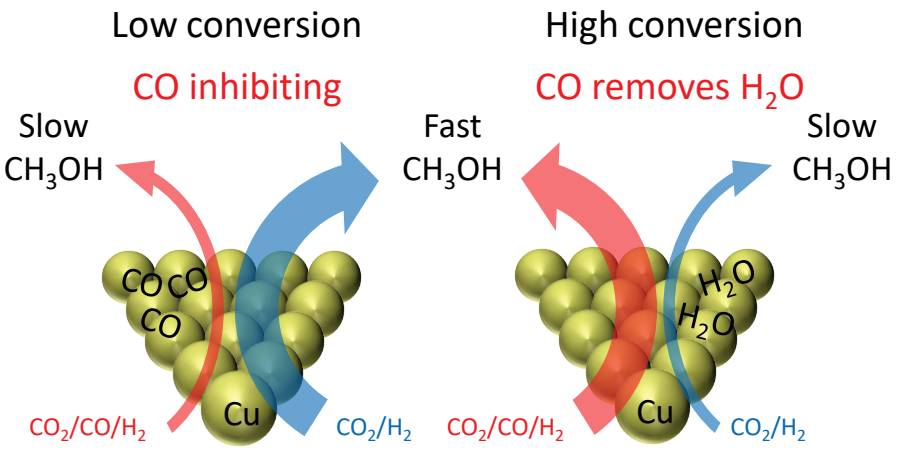

Keywords: Methanol synthesis · Copper catalyst · Metal-support interaction · Reaction mechanisms · CO and CO_2 hydrogenation

1 Introduction

Conventional methanol synthesis proceeds from syngas, a $CO_2/CO/H_2$ mixture, over a $Cu/ZnO/Al_2O_3$ catalyst operating at 473-573 K and 50-100 bar [1–3]. Hydrogenation of CO (R1) and CO_2 (R2) constitute two potential reaction pathways for methanol synthesis on supported Cu catalysts, which raises the question, whether CO or CO_2 is the dominant carbon source for methanol.

$$CO + 2\,H_2 \rightleftharpoons CH_3OH \qquad \{R1\}$$

$$CO_2 + 3\,H_2 \rightleftharpoons CH_3OH + H_2O \qquad \{R2\}$$

For certain Cu-based catalysts, such as Cu/MgO, R1 is faster than R2. However, this is not related to the intrinsic properties of Cu but is instead the result of a Cu-MgO synergy that strongly accelerates R1 [4]. Some theoretical models [5–7] have predicted that R1 should be faster than R2 on pure Cu surfaces, but experimental studies of both single crystals [8] and polycrystalline Cu [4, 9] have shown that the pathway from CO_22 (R2) is 1-2 orders of magnitude faster than the pathway from CO (R1). This is in agreement with prior isotope labeling studies [10, 11] on industrial Cu/ZnO-based catalysts that unambiguously established CO_2 as the primary carbon source for such catalyst systems.
Whereas the role of CO_2 as the primary reactant for Cu and industrial Cu/ZnO-catalysts is relatively unambiguous, the role of CO in the syngas feed for the industrial process is less clear. Some studies

[5, 12–15] observe that the methanol synthesis over $Cu/ZnO/Al_2O_3$ is faster in CO_2/H_2 than in $CO/CO_2/H_2$, and correspondingly kinetic studies [16] have observed a negative reaction order in CO. By contrast other studies [13, 17–19] observe a faster methanol formation from a CO-rich $CO/CO_2/H_2$ mixture. As methanol synthesis from sustainably generated H_2 and locally available CO_2 point sources is envisioned to become an important energy storage solution in a sustainable future society [20], it is important to clarify the exact role of CO in the current industrial process from syngas. There are several potential roles of the CO that need to be unraveled. One of these roles is in removal of water through the water-gas shift (WGS) reaction (R3), as water is observed [16, 21, 22] to be a strong kinetic inhibitor of the methanol synthesis. However, this role will be limited to higher conversions, where significant water concentrations build up.

$$CO + H_2O \rightleftharpoons CO_2 + H_2 \qquad \{R3\}$$

It has also been proposed that the strong promoting support effect of ZnO in the industrial $Cu/ZnO/Al_2O_3$ catalyst is due to the creation of strongly reduced Zn-sites featuring high activity, such as oxygen vacancies in the ZnO phase [23] or Cu-Zn surface alloy sites [24, 25] in the metal surface. With CO being the most reducing component in the syngas [26–28] the CO concentration should regulate the concentration of such sites [23, 25] and hence the activity, if these reduced Zn-sites are the primary active centers. Thirdly, CO may govern the oxygen coverage on the Cu surface. Ambient pressure X-ray Photoelectron Spectroscopy (XPS) studies [29, 30] have shown that oxygen can deposit on the Cu surface in CO_2 or H_2/CO_2 atmospheres, but the oxygen coverage is found to be low on the Cu surface in CO-rich syngas [22], which suggests that CO may play a role in removing oxygen from the Cu surface. Here we investigate the roles of CO and CO_2 in Cu-catalyzed methanol synthesis using Raney Cu and a variety of supported Cu catalysts. This work is based on methanol synthesis experiments switching between CO/H_2 and CO_2/H_2 feeds and by switching between a $CO/CO_2/H_2$ feed and a corresponding CO-free $N_2/CO_2/H_2$ feed.

2 Experimental

Gas flows are reported at normal conditions by "N" and referring to a temperature of 273.15 K and a pressure of 1 atmosphere (e.g. Nml/min).

2.1 Catalysts

The catalysts were synthesized from Cu(II) nitrate hemi(pentahydrate) (98.6%, Alfa Aesar) using co-precipitation ($Cu/ZnO/Al_2O_3$ with 56 wt% Cu, Cu/ZnO with 10 wt% Cu and Cu/Al_2O_3 with 67 wt% Cu), incipient wetness impregnation (Cu/SiO_2 with 36 wt% Cu) or deposition precipitation (Cu/TiO_2(20) with 20 wt% Cu and Cu/TiO_2(60) with 60 wt% Cu). Raney Cu (98.9 wt% Cu, 0.81 wt% Al, 0.1 wt% Fe, 0.05 wt% Ni) from Strem Chemicals was received as an aqueous slurry and was predried in air at room temperature before use. The preparation of the co-precipitated samples is described elsewhere [31]. For the deposition-precipitation the TiO_2 support material (anatase nanopowder, 21 nm particle size from Sigma Aldrich) was dispersed in 500 mL of H_2O before the precipitation. The Cu was then added by dripping aqueous solutions of Cu(II) nitrate and Na_2CO_3 (Sigma Aldrich, $\geq$ 99.8%) into this TiO_2-containing slurry at 338 K and a pH of 6.5 followed by 1 h ageing at 338 K with unrestricted pH (same procedure as in co-precipitations). After precipitation the samples were washed in demineralized H_2O and dried at 313 K overnight. Cu/SiO_2 was prepared by incipient wetness impregnation of crushed and sieve fractionated (150-300 µm) silica (Saint Gobain, SS61138) with an aqueous solution of Cu(II) nitrate hemi(pentahydrate). All catalyst precursors were calcined in 1 NL/min air flow with a 2 K/min ramp to 573 K, which was maintained for 3 hours. Further characterization of some of these samples using various techniques can be found elsewhere [4, 22, 31].

2.2 Catalyst pre-reduction/activation

All catalysts were pre-reduced in a 60 Nml/min flow of 5% H_2/N_2 (Air Liquide Denmark) using a heating ramp of 1 K/min and a holding period of 1-4 hours at 448 K before further heating with 1 K/min to 523 K for 2 hours. At both temperatures, water generation terminated as verified by the MS within the allocated holding times. For Cu/Al_2O_3 the standard reduction was followed by an additional step using 50 Nml/min of 100% H_2 (Air Liquide Denmark) at 523 K for 1 h. After reduction all samples were flushed with He at the final reduction temperature. In selected cases the pre-reduction of the $Cu/ZnO/Al_2O_3$ sample was stopped after the holding period at 448 K and then flushed with He at 448 K in order to probe the effect of CO in the reaction gas after a milder pre-reduction treatment.

2.3 Cu surface area measurement

N_2O-reactive frontal chromatography (RFC) [32, 33] was applied to evaluate the Cu surface area at 333 K using a 19 Nml/min flow of 1% N_2O/He on pre-reduced catalysts. This was done in an Autosorb iQ_2 setup according to the procedure described elsewhere [4]. The Cu surface area was determined using a Cu:O = 2:1 stoichiometry and a Cu surface atom density of $1.47 \cdot 10^{19}$ surface Cu atoms/(m^2 Cu) [33, 34]. Previous studies [21] using the same setup has shown a standard deviation of 6%. For ZnO-supported Cu it is known that ZnO-reduction can distort the Cu area measured by N_2O-RFC. To ensure that the surface area measurements were not impacted by ZnO-reduction the $Cu/ZnO(/Al_2O_3)$ samples were subjected to N_2O-RFC after varying pre-reduction conditions. The sample was either subjected to the standard pre-reduction in 5% H_2 with holding at 448 K and 523 K, to a milder reduction that was terminated after the holding period at 448 K or to a harsher reduction where the standard procedure was followed by exposure to 100% H_2 at 523 K until the water evolution stopped. The results from these 3 pre-reduction tests are shown in Fig. S1a and S1b with substantial N_2O uptake increase when replacing 5% H_2 with 100% H_2 at 523. This substantiates that the standard reduction method with 5% H_2 at 448 K and 523 K should be used prior to N_2-RFC to quantify the Cu surface area of $Cu/ZnO(/Al_2O_3)$ samples. For Cu/Al_2O_3, similar tests (Fig. S1c) showed a profound increase in the Cu surface area from reducing in 5% H_2 at 448 K to 523 K, whereas subsequently change to 100% H_2 at 523 K was within uncertainty the same. Due to the irreducible nature of alumina [1, 34] the increased Cu surface area was attributed to Cu reduction. For this reason it was concluded that 100% H_2 is necessary for obtain complete Cu reduction in Cu/Al_2O_3, and the standard pre-reduction with 5% H_2 used for the other samples was therefore always augmented by a 100% H_2 treatment at 523 K for measurements on Cu/Al_2O_3.

2.4 Catalytic tests

Methanol synthesis experiments were conducted in a high-pressure flow reactor setup with catalysts placed in glass lined, U-shaped, stainless steel reactors and product analysis by a Hiden HPR-20 EGA MS and a Thermo Fisher Trace 1300 GC equipped with one channel . composed of a TG5 column guiding the gas to an FID detector and one channel composed of an OV-1 column followed by a Shincarbon column guiding the gas to a TCD detector equipped with one channel . composed of a TG5 column guiding the gas to an FID detector and one channel composed of an OV-1 column followed by a Shincarbon column guiding the gas to a TCD detector. The setup and calibration procedures are described in detail elsewhere [4].

Syngas switching experiments

After catalyst pre-reduction the reactor was pressurized in He to 50 bar at 523 K before switching to one of three syngas mixtures ($CO_2/CO/H_2$ = 3/29/68, CO/inert/H_2 = 3/29/68 or CO_2/inert/H_2 = 3/29/68 mol%) dosed from pure H_2 (99.9999%), pure He (99.9999%), and pre-mixed 9.50% CO/Ar, 9.00% CO_2/N_2 and 9.00% CO_2/CO all from Air Liquide Denmark. Time resolved monitoring of the methanol synthesis activity was based on mass spectrometry (MS) measurements (m/z = 31), while

reported activities were based on the methanol production quantified by online gas chromatography (GC). After obtaining a steady state or quasi-steady state in one gas mixture the feed was switched to another mixture. Catalyst loadings in the reactor were adapted for each catalyst to yield low conversion reaction conditions (here <0.3 mol% methanol in the effluent gas).

Impact of CO at varying conversion levels

Methanol synthesis was conducted over Cu/Al_2O_3 and $Cu/ZnO/Al_2O_3$ at 523 K and 50 bar at varying conversion levels in the presence ($CO_2/CO/H_2$ = 3/29/68) and absence of CO ($CO_2/N_2/H_2$ = 3/29/68). The feed flow and catalyst loading were adjusted to regulate the conversion level. Reported effluent water concentrations for the CO-free feed were based on an oxygen balance assuming that only methanol synthesis (R2) and WGS (R3) occur, whereby the H_2O production is equal to the sum of the produced CH_3OH and CO, which are quantified by the calibrated GC.

Mild syngas switching experiment over $Cu/ZnO/Al_2O_3$

$Cu/ZnO/Al_2O_3$ was mildly reduced in 60 Nml/min of 5% H_2/N_2 by heating with 1 K/min to 448 K for 1 h to activate Cu but prevent any ZnO reduction. Next, a syngas experiment at 448 K and atmospheric pressure was conducted by starting with $CO_2/N_2/H_2$ (3/29/68) and monitoring the 5 catalytic activity. Once activity had stabilized the feed was switched to $CO_2/CO/H_2$ (3/29/68) at a constant gas flow of 280 Nml/min.

Methanol synthesis in oxidizing atmosphere over $Cu/ZnO/Al_2O_3$

$Cu/ZnO/Al_2O_3$ was mildly reduced in 60 Nml/min of 5% H_2/N_2 by heating with 1 K/min to 448 K to activate Cu but prevent ZnO reduction, which according to [35] initiates above 0.05 bar H_2 at 493 K. Next, the catalyst was flushed with He and heated to 498 K, where it was pressurized to 20 bar in He before switching to CO_2/H_2/He (40/30/30) and monitoring the catalytic activity. The feed was then replaced by a feed of $CO_2/H_2/CO$ (40/30/30) with the same flow rate at 498 K and 20 bar of pressure.

2.5 Equilibrium calculations

Equilibrium constants for the WGS and methanol formation obtained from Graaf and Winkelman [35] were applied to calculate the approach to equilibrium with the assumption of ideality in the gas phase.

3 Results and Discussion

3.1 Sample properties

Nielsen et al. [31] have previously reported Cu surface areas for some of the presently applied samples. Here the Cu surface areas of all the presently applied samples are summarized in Table 1. It is well-established that partial ZnO reduction can distort the Cu surface area measured from the N_2O uptake in Cu/ZnO systems. To ensure that the obtained Cu surface areas were free of this effect, the Cu surface area of the $Cu/ZnO(/Al_2O_3)$ samples was measured after varying pre-reduction treatments to identify the onset of ZnO reduction. Here the standard pre-reduction in 5% H_2 with holding at 448 K and 523 K was compared to a milder pre-reduction terminated after the holding period at 448 K or to a harsher pre-reduction with exposure to 100% H_2 at 523 K after the standard pre-reduction. The results from these experiments are shown in Fig. S1 in the Supporting Information. It is concluded from the results of Kuld et al. [36] that no ZnO reduction will take place with the pre-reduction in 5% H_2 at 448 K, and Fig. S1 shows that with 5% H_2 pre-reduction the Cu area is the same (within

the known uncertainty) after reduction at both 448 K and 523 K. From this it is concluded that ZnO-reduction is negligible in the present standard reduction program using 5% H_2, and consequently the Cu areas in Table 1 should also be accurate for the Cu/ZnO(/Al_2O_3) samples.

Table 1: Results from N_2O-RFC in this study and recent studies by Nielsen et al. [31]. Estimated relative error is 6% based on five repeated measurements on Cu/SiO_2 in the same setup [21].

Sample	**Cu area [m^2/g_{cat}]**	**Ref.**
Cu/SiO_2	1.40	This work
Cu/Al_2O_3	7.16	This work
Cu/TiO_2(60)	1.82	This work
Raney Cu	5.18	[31]
Cu/ZnO	4.90	[31]
Cu/ZnO/Al_2O_3	20.25	[31]
Cu/TiO_2(20)	1.19	[31]

3.2 The carbon source in methanol synthesis over Cu

Theoretical models [5–7] have predicted that the rate of methanol formation on pure Cu should be far higher from CO than from CO_2. However experimental studies [4, 8, 9] unanimously show the opposite – that the rate is far higher from CO_2. A proposed [5] explanation for this contradiction has been that stable CO_2-derived intermediates may obscure the fast pathway from CO identified by theoretical studies. To test this Cu-rich Cu/Al_2O_3 was used, as it features good thermal stability and has previously [4] been shown to qualitatively reflect the behavior of unsupported Cu. Cu/Al_2O_3 was subjected to experiments with gas switching between CO/H_2 and CO_2/H_2 feeds to evaluate, if the reaction rate in CO/H_2 is affected by prior exposure to CO_2/H_2. If very stable CO_2-derived intermediates affect the pathway from CO the order of the gas mixtures should be of great importance. Fig. 1a shows the result of this switching experiment starting from CO_2/H_2, whereas Fig. 1b shows the result when starting in CO/H_2. Fig. 1 illustrates that the rate of methanol synthesis from CO_2 is more than an order of magnitude faster than the rate from CO regardless of the order of the gas mixtures. These results show that even in the absence of CO_2-derived intermediates occupying the surface, the route from CO is still far inferior to the route from CO_2. The results help to substantiate that CO_2 is the primary carbon source in methanol synthesis over Cu. Our previous work [4] and additional tests for the Cu/TiO_2 catalysts (see Supporting Information Fig. S2) show that this conclusion applies to all the Cu-based catalysts investigated here. Here we thus focus on materials that share the intrinsic properties of Cu, where the rate from CO_2 is far higher and where CO_2 consequently is the primary reactant for methanol synthesis. It may be added that the alternative synergistic pathway for CO-hydrogenation, which is particularly strong in materials such as Cu/MgO, most likely relies on basic support sites in the vicinity of the metal particle, and consequently this pathway is strongly inhibited by the acidic gas CO_2 [4].

3.3 The role of CO in methanol synthesis from syngas

Since CO_2 is the primary reactant for methanol synthesis on the investigated catalysts it is relevant to elucidate the role of CO in a ternary CO/CO_2/H_2 atmosphere. To do this both Raney Cu and supported Cu catalysts were allowed to stabilize in a CO_2/CO/H_2 feed, and the CO in the feed was then replaced with an identical concentration of N_2, while all other conditions were maintained. In these experiments flows and catalyst loadings were adjusted to preserve low conversion conditions (< 0.3 mol% CH_3OH produced) with negligible product formation to avoid that effects caused by the products impact the conclusions substantially. Fig. 2 shows the development in methanol productivity during such an experiment for Cu/TiO_2(20) and illustrates that the methanol production actually increases, once CO is removed from the feed. Fig. 3 summarizes the stabilized productivity levels with and

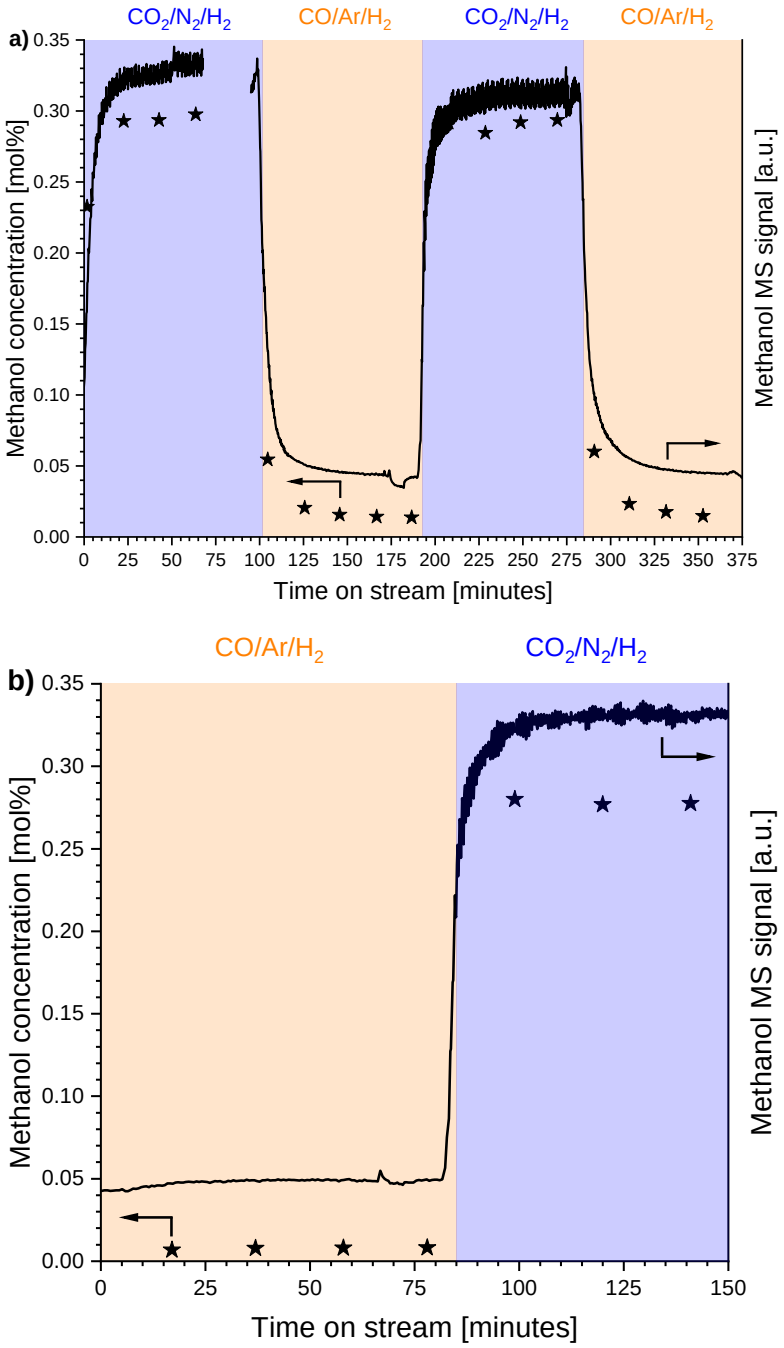

Fig. 1: The methanol production (stars) over Cu/Al_2O_3 as function of time on stream when switching between CO_2/H_2 and CO/H_2 feeds (both balanced with inert gas) starting from a) CO_2/H_2 and b) CO/H_2. The MS signal (solid line) for methanol (m/z = 31) is also shown to better illustrate the transient development. Flow measurement required bypass of the MS resulting in a data gap in the MS signal in a). Reaction conditions: T = 523 K, P = 50 bar, feed flow = 275 ± 3 Nml/min, CO_x/inert/H_2 = 3/29/68, Cu/Al_2O_3 loading = 180.2 mg in a) 148.4 mg in b). Fig. 1b is reproduced with permission from Nielsen et al. [4].

without CO for all samples. To facilitate comparison the stabilized level in $CO_2/N_2/H_2$ is assigned as a relative productivity of 1.00 for each sample, and the final productivity in $CO_2/CO/H_2$ prior to the shift to $CO_2/N_2/H_2$ is shown relative to this level. The figure clearly illustrates that at these low

conversion conditions all samples exhibit a faster rate in $CO_2/N_2/H_2$. Hence, CO is an inhibitor for all the investigated Cu-catalysts. This qualitative generality suggests that the inhibiting effect of CO comes from an interaction with the metallic Cu surface, which is the only common feature of these samples. It follows from this argument that if all the catalysts are impacted by CO interacting with the Cu surface then the reaction must also be located on the Cu surface for all the samples. While there have been previous reports [16, 37] of CO-inhibition for Cu/ZnO-systems the generality of this effect has not previously been identified. From repeated cycling of thermally stable systems, such as $Cu/TiO_2(60)$, it is evident that the effect of CO is fully reversible over the time scale of a few minutes (see Fig. S3). This suggests that the effect of CO is on the kinetics of the surface reactions. The most likely cause for the inhibiting effect of CO is competitive adsorption. The CO adsorbed on the Cu surface is only converted to methanol with a very low rate (Fig. 1), and blockage of the surface with adsorbed CO will inhibit the rate by preventing the much faster pathway from CO_2. However, there could be a secondary inhibiting effect of CO. There are indications from ambient pressure XPS studies [29] that oxygen deposits on the Cu surface in H_2/CO_2 atmospheres, and it has been proposed [9] that this oxygen exerts a promotional role on the methanol synthesis. In a previous study [22] we found that that the oxygen coverage on Cu was insignificant (below our detection limit of 0.04 ML) in a CO-rich syngas. The CO may therefore also inhibit the methanol formation by scavenging away oxygen from the metal surface.

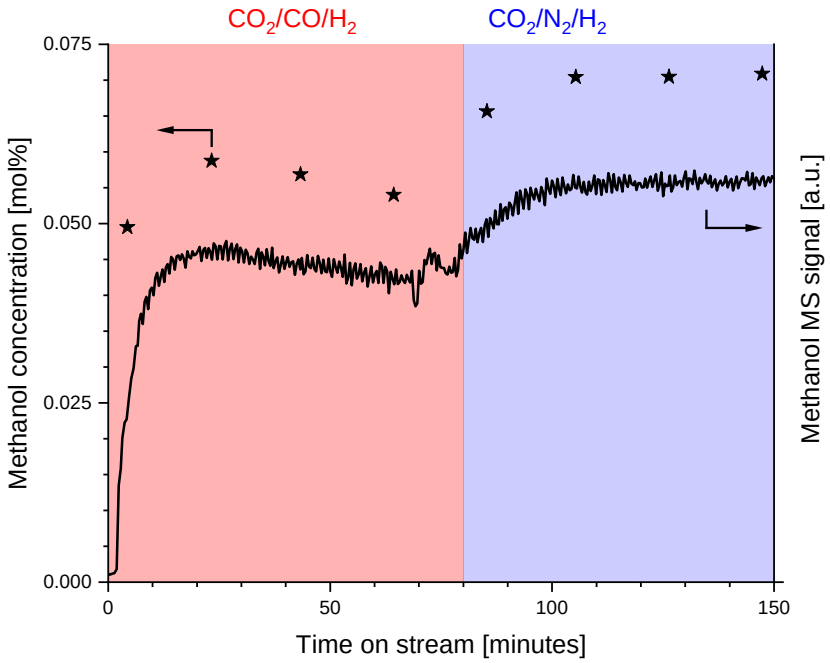

Fig. 2: The methanol concentration (stars) as a function time on stream for $Cu/TiO_2(20)$, when switching from a $CO_2/CO/H_2$ feed to a $CO_2/N_2/H_2$ feed. The MS signal (solid line) for methanol ($m/z = 31$) is also included. Reaction Conditions: T = 523 K, P = 50 bar, feed flow = 280 ± 5 Nml/min, $CO_2/X/H_2$ = 3/29/68 with X = CO or N_2, $Cu/TiO_2(20)$ loading = 261.5 mg. Here the final measurement in each gas is used to construct Fig. 3.

Fig. 3 shows that stronger CO inhibition generally occurs in the experiments with the lowest conversions and hence the lowest product concentration in the effluent. This indicates that the impact of CO is dependent on the conversion level. It is well known that the water produced in the methanol synthesis reaction (R1) is strongly inhibiting to Cu-catalyzed methanol synthesis. Thrane et al. [21] found that adding 1500 ppmv H_2O to the syngas feed caused the methanol synthesis rate over $Cu/ZnO/Al_2O_3$ to drop by 60-70% when operating in the 493-523 K range at 41 bar. Sahibzada et al. [15] also found that such a catalyst lost 90% of its methanol synthesis activity, when 2 vol% H_2O was added to the feed at 523 K and 50 bar of pressure. The occurrence of water inhibition for Cu-catalysts is not support

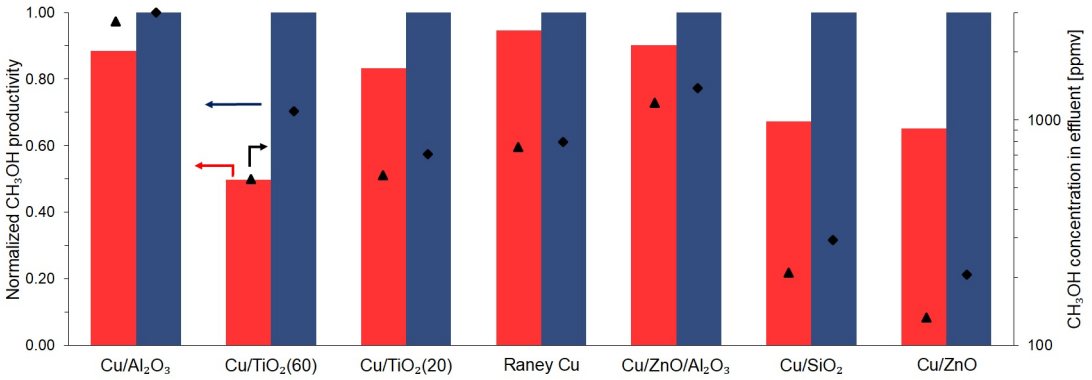

Fig. 3: The normalized methanol productivity (left vertical axis) in $CO/CO_2/H_2$ (red bars) and $CO_2/N_2/H_2$ (blue bars) for Raney Cu and various supported Cu-samples. Each catalyst is allowed to stabilize in $CO/CO_2/H_2$ before replacing CO with an identical concentration of N_2 as illustrated in Fig. 2. The black data points (triangle and diamond) show the effluent methanol concentration in each experiment on the right vertical axis. Reaction conditions: T = 523 K, P = 50 bar, $CO_2/X/H_2$ = 3/29/68 with X = CO or N_2). Space velocity was varied (between $3.1{\cdot}10^4$ and $145{\cdot}10^4$ $Nml/g_{cat}/h$) to ensure low conversion conditions with maximally 0.3 mol% methanol in the effluent.

specific, as Yang et al. [38] found that adding 0.2 mol% H_2O to the feed caused Cu/SiO_2 to lose approximately 40% of its methanol synthesis activity at 413 K 413 K and 6 bar. Hence, the water inhibition is general for Cu catalysts, although the available data do not rule out that the strength of the effect could be support dependent. Saito et al. [37] also conducted direct comparisons of inhibition from CO and H_2O for $Cu/ZnO/ZrO_2$ and found that H_2O is a far stronger inhibitor than CO. Hence, at higher conversion CO can exert a relative positive effect by displacing a worse inhibitor, water, through the WGS reaction (R3). To investigate the water scavenging effect at higher conversion, switching experiments between $CO_2/CO/H_2$ and $CO_2/N_2/H_2$ were conducted for Cu/Al_2O_3 and $Cu/ZnO/Al_2O_3$ at varying conversion levels. The conversion was varied by adjusting the catalyst loading and feed flow to change the space velocity/residence time. Fig. 4 shows the results from such experiments with Cu/Al_2O_3, where the gas switch is conducted at different space velocities. Fig. 4a shows that at the highest space velocity (lowest conversion and water concentration) there is a slight negative effect of CO. Fig. 4b shows that for lower space velocities, where conversion and water concentration are higher, there is oppositely a significant positive effect of CO relative to a CO-free gas. Here it is important to emphasize that both CO and H_2O are inhibitors, and the highest productivity occurs with high space velocity and no CO in the feed (Fig. 4a), whereby the total presence of the inhibitors is minimized. The benefit of CO is a relative benefit due to the exchange of a stronger inhibitor (H_2O) with a weaker one (CO).

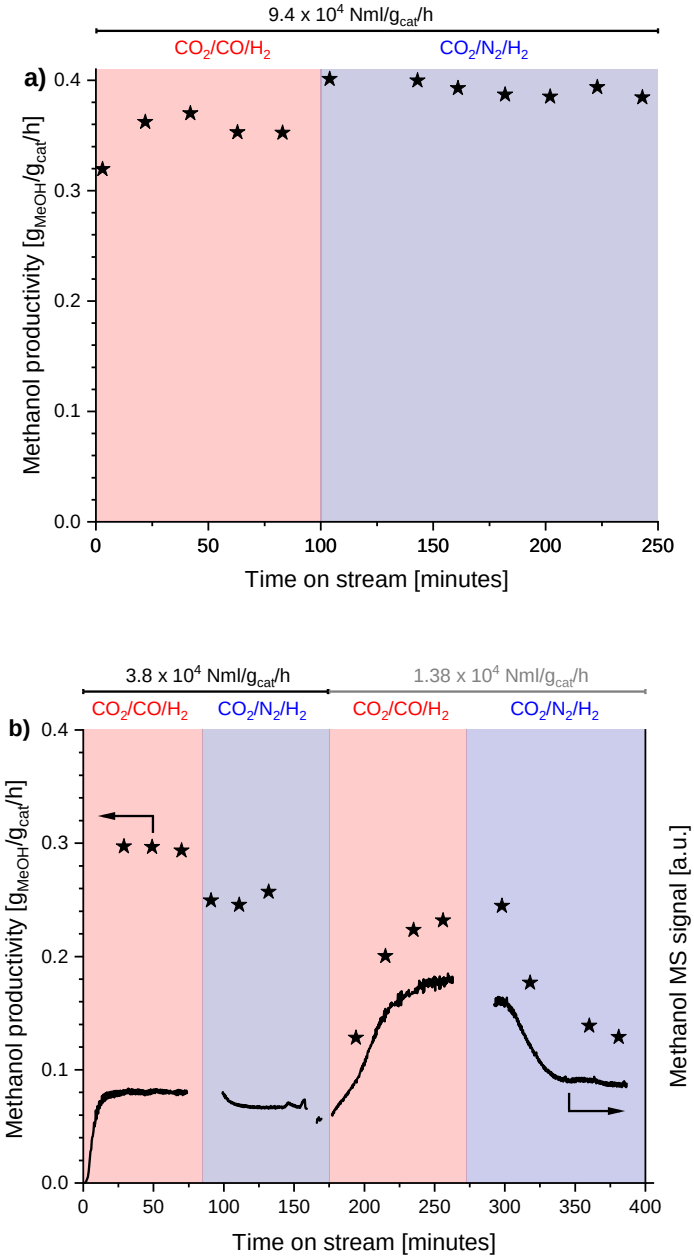

Fig. 4: The methanol production rate as a function of time on stream with Cu/Al_2O_3 and a gas space velocity of a) $(9.42 \pm 0.07)\cdot10^4$ $Nml/g_{cat}/h$ and b) both $(3.80 \pm 0.06)\cdot10^4$ $Nml/g_{cat}/h$ and $(1.38 \pm 0.04)\cdot10^4$ $Nml/g_{cat}/h$. In b) the methanol MS signal (m/z = 31) is also shown to illustrate that the product concentration is higher for the lower space velocity. Gaps in the methanol MS signal are due to bypass for flow measurements at the start and end of each feed flow. Reaction conditions: T = 523 K, P = 50 bar, $CO_2/X/H_2$ = 3/29/68 with X = CO or N_2, Cu/Al_2O_3 loading = 178.6 mg in a) and 433.7 mg in b).

Fig. 5 shows the ratio between the rates with and without CO as a function of the water concentration in the effluent for the CO-free feed. The water concentration is estimated from an oxygen balance as the sum of the production of methanol and CO assuming that only reactions R1 and R3 occur. Since negligible formation of DME or other products were detected by the GC, this is expected to be a good assumption.

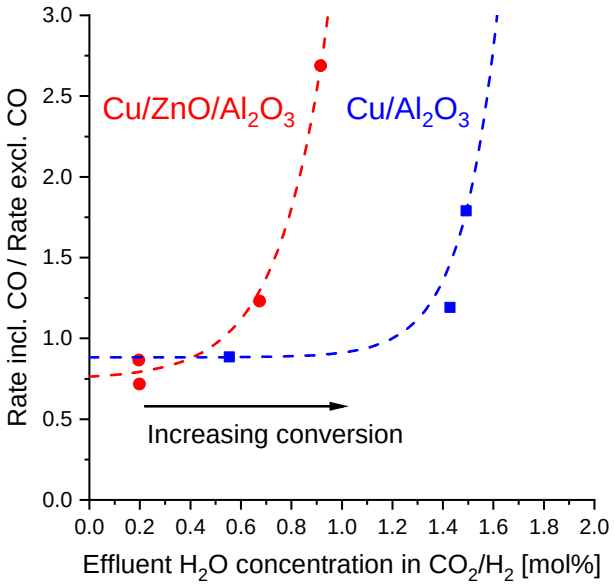

Fig. 5: The ratio between the methanol formation rates in $CO_2/CO/H_2$ and $CO_2/N_2/H_2$ as a function of the estimated effluent concentration of water in the $CO_2/N_2/H_2$ atmosphere for Cu/Al_2O_3 and $Cu/ZnO/Al_2O_3$. Reaction conditions: T = 523 K, P = 50 bar, GHSV = (2.4-14.5)·10^5 Nml/g_{cat}/h for $Cu/ZnO/Al_2O_3$ and (1.4-94.1)·10^4 Nml/g_{cat}/h for Cu/Al_2O_3.

Fig. 5 shows that at low conversion conditions the H_2O formation is low, and CO only impacts the activity in a negative way for both $Cu/ZnO/Al_2O_3$ and Cu/Al_2O_3. By increasing the conversion level the H_2O formation rises, and for both $Cu/ZnO/Al_2O_3$ and Cu/Al_2O_3 there is a sharp transition, where CO becomes beneficial compared to a CO-free gas. As described above this benefit can be attributed to the role of CO as a scavenger of water. The transition to a positive effect of CO occurs at a lower water concentration for $Cu/ZnO/Al_2O_3$. This can be rationalized from the known support effect of ZnO upon the heat of adsorption of water on the catalyst. In the limit of zero water coverage the heat of adsorption of water on $Cu/ZnO/Al_2O_3$ is 65 kJ/mol [39], whereas the heat of adsorption on pure Cu is around 45 kJ/mol [40–42].

It would be consistent with the stronger bonding of water on $Cu/ZnO/Al_2O_3$ that the inhibiting effect of water, and hence the need for water removal by reaction with CO, becomes important at a lower water concentration for $Cu/ZnO/Al_2O_3$. However, the beneficial effect of CO also emerges for Cu/Al_2O_3 although at a higher water concentration. This is in agreement with the results of Yang et al. [38] showing that water inhibition is also important for ZnO-free supports.

For the experiments in Fig. 5 with a CO-free feed, where the water content can be accurately estimated through the oxygen balance, the approach to equilibrium for WGS and methanol synthesis were evaluated, and the results are summarized in Table S1 in the supporting information. The highest approach to equilibrium among these tests were 59.1% for WGS and 20.8% for methanol synthesis. Hence, both reactions are in the kinetically controlled regime although with the faster WGS closer to an equilibration.

3.4 Optimal CO/CO_2 ratio for methanol synthesis over Cu/ZnO-based catalysts

As the hydrogenation of CO_2 provides a faster pathway (Fig. 1) the concentration of CO_2 in the syngas feed is obviously important. Fig 6 summarizes the literature [43–45] on the effect of the CO_2 partial pressure in the feed, when only the CO_2 concentration is varied. Fig. 6 shows that the methanol synthesis is approximately 1^{st} order in CO_2 to around 1 bar of pressure and then becomes 0^{th} order in CO_2 for higher partial pressures. IR studies [43, 45] suggest that the stagnation occurs because the concentration of formate intermediates on the Cu saturates.

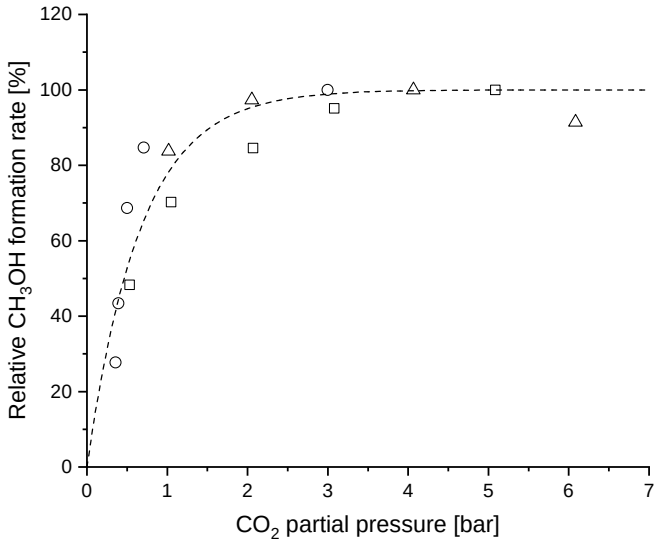

Fig. 6: The relative methanol production rate of Cu/ZnO-based catalysts as a function of the CO_2 partial pressure in the feed. Data (in the 496-523 K range) from: Amenomiya and Tagawa [45] (□), Le Peltier et al. [43] (◯), and Nomura et al. [44] (△). The data are normalized by setting the highest productivity in each study to 100%.

Studies that instead vary the CO/CO_2 ratio in the CO_x part of the syngas have yielded seemingly contradictory observations, as optimal activity has been reported for both CO-free and CO-rich atmospheres. The observation of a transition from a detrimental to a beneficial effect of CO on the activity when varying the conversion level (Figs. 4 and 5) can help to rationalize these observations. At low conversion the inhibiting effect of CO means that the CO concentration should be as low as possible, but at high conversion a high concentration of CO is needed to remove water. Fig. 7 summarizes literature results for $Cu/ZnO(/Al_2O_3)$ catalysts by showing the normalized methanol productivity as a function of the fraction of CO_2 in the CO_x part of syngas feed with a fixed CO_x/H_2 ratio. These results are obtained at industrially relevant high pressure conditions. The literature results are separated into low conversion condition with negligible product formation (Fig. 7a) and high conversion conditions with non-negligible product formation (Fig. 7b).

Fig. 7a shows that at low conversion conditions the methanol formation rate rises strongly until CO_2 constitutes 10-20% of the CO_x whereafter the increase continues albeit less profoundly until CO_2 is the only CO_x component. The sharper initial rise in Fig. 7a until 10-20% CO_2 in the CO_x can be attributed to the regime, where the reaction is 1^{st} order in CO_2 (see Fig. 6) and where CO_2 thus brings an advantage of its own. Above this level additional CO_2 may not bring strong beneficial effects of its own, since the reaction becomes 0^{th} order in CO_2. However, as CO is inhibiting it is nevertheless still beneficial to replace CO with CO_2, and maximal activity occurs in a completely CO–free gas.

An analysis of the product concentrations in the experiments in Fig. 7a shows that this low conversion behavior occurs for methanol effluent concentrations below ca. 1 mol% (see Table S1). Fig. 7b shows that at high conversion conditions with higher product concentrations the methanol production is optimal for a syngas with a CO_x fraction of ca. 10% CO_2 and 90% CO. At high conversion it is beneficial to include sufficient CO_2 to reach the 1-2 bar CO_2 partial pressure that saturates the beneficial effect of CO_2. However, once this CO_2-concentration is reached, the CO_2 offers no additional benefit, and it is instead preferable that the remaining part of the CO_x is CO in order to optimize the removal of water by the shift reaction. The optimal CO_x composition is thus a CO-rich mixture at higher conversions. The composition dependencies in Fig. 7 can thus be described in terms of the beneficial effect of CO_2 (Nielsen et al. [4] and Figs. 1 and 6), the inhibiting effect of CO (Fig. 3), and the inhibiting effect of water (e.g. Thrane et al. [21] and Yang et al. [38]) that all are general among Cu catalysts. This implies that it is the kinetics of the surface reactions on Cu and not support-dependent effects that cause the dependencies on the CO_x composition. However, Fig. 5 clearly shows that the transition between the two regimes in Fig. 7 will depend upon the support, and any support-dependencies in the formate coverage could also cause factors such as the location of the optimum in Fig. 7b to vary with the support.

An analysis of the product concentrations in the experiments in Fig. 7b show that this low conversion behavior occurs for methanol effluent concentrations above ca. 3 mol% (see Table S1). Hence the transition between the behaviors of Fig. 7a and Fig. 7b occurs in the range of 1-2 mol% methanol in the effluent.
It should be added that at high conversion with significant methanol concentrations, the water scavenging effect of CO operates in parallel to a methanol-assisted autocatalytic mechanism, whereby methanol facilities the generation of additional methanol [21]. For catalysts such as $Cu/ZnO/Al_2O_3$ the combined effect of the autocatalytic acceleration and the water scavenging means that the absolute rate increases with increasing conversion for CO-rich feeds [21]. The alcohol-assisted mechanism that causes the autocatalytic effect does not seem to require CO [46–48]. The increase in absolute activity of $Cu/ZnO/Al_2O_3$ with increasing conversion in the presence of CO is therefore not likely the result of CO participating directly in the autocatalytic pathway, but rather the result of CO removing water and thus providing optimal conditions for the autocatalytic pathway.

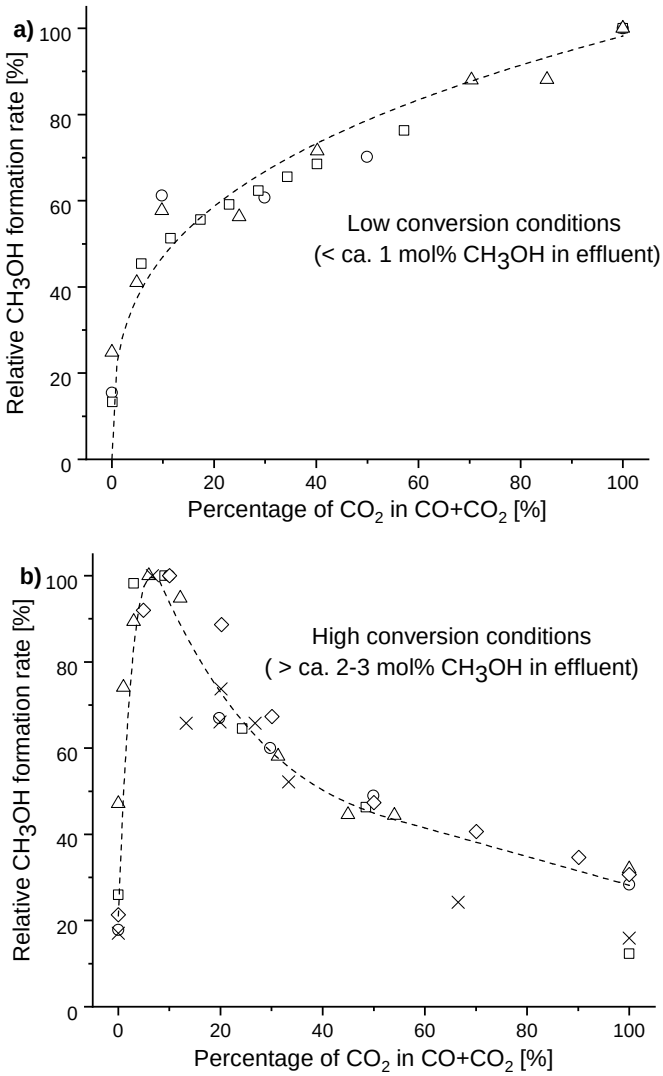

Fig. 7: The relative methanol synthesis activity for $Cu/ZnO(/Al_2O_3)$ catalysts as a function of the CO_2 fraction in the CO_x part of the syngas for: a) low conversion conditions with negligible product concentrations and b) high conversion conditions with non-negligible product concentrations. Here the CO_x composition is varied at a fixed CO_x/H_2 ratio and all studies are normalized to the highest activity achieved in the study. Data in a) from: Studt et al. [5] (□), Chanchlani et al. [12] (△) and Lee et al. [13] (◯). Data in b) from: Martin and Perez-Ramirez [17] (△), Barbier et al. [18] (□), Sahibzada et al. [15] (◇), Lee et al. [13] (◯) and Klier et al. [19] (×). The exact data used from the literature studies are specified in Tables S2 and S3 in the Supporting Information.

3.5 Role of CO-induced rise in reductive potential for Cu/ZnO-catalysts

It is well established that ZnO exerts a strong support effect on the Cu-catalyzed methanol synthesis [21, 49–53], although the exact mechanism by which this support effect operates remains imperfectly understood. One proposal is that reduced Zn-sites, such as oxygen vacancies in the ZnO [23] or Zn alloyed into the metallic surface [25, 36, 54–57], are sites of particularly high activity. The reductive potential of the syngas, which is governed by especially the CO/CO_2 ratio, will have a major impact on the concentration of such reduced Zn-sites [23, 25], which should be reflected in a major impact on the catalytic activity. Fig. 8 shows the turnover frequency (TOF) in methanol synthesis per Cu surface atom for Raney Cu and $Cu/ZnO/Al_2O_3$ at the low conversion conditions of Fig. 3 both with and without CO in the feed.

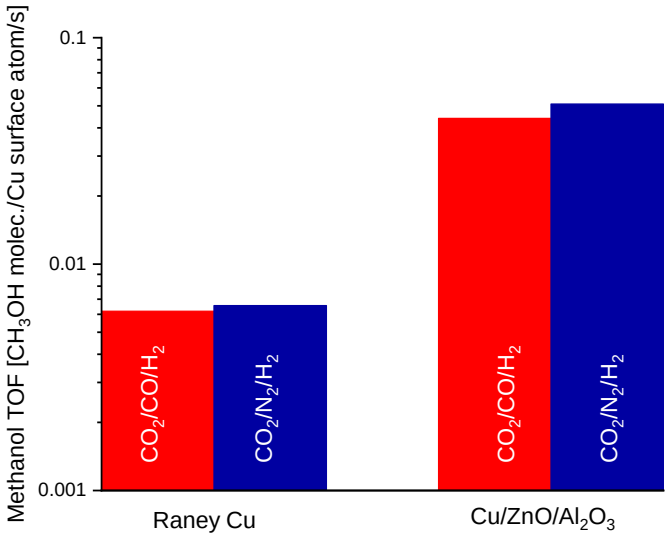

Fig. 8: The turnover frequency for methanol synthesis (per Cu surface atom) for Raney Cu and $Cu/ZnO/Al_2O_3$ in both $CO_2/N_2/H_2$ (red) and $CO_2/CO/H_2$ (blue). These results are at low conversion conditions (see effluent concentrations in Fig. 3). Reaction conditions: T = 523 K, P = 50 bar, $CO_2/X/H_2$ = 3/29/68 with X being CO or N_2, GHSV = (8.3-8.4)·10^4 Nml/g_{cat}/h (Raney Cu) and (1.4-1.5)·10^6 Nml/g_{cat}/h ($Cu/ZnO/Al_2O_3$).

We have previously [22] confirmed that the Raney Cu sample is a good quantitative approximation to the intrinsic properties of Cu, and Fig. 8 shows that at these low conversion conditions the TOF for $Cu/ZnO/Al_2O_3$ is 7-8 times higher than the TOF for Raney Cu. Fig. 8 illustrates that at these conditions a strong support effect is present, but the most reducing component in the gas, CO, nevertheless has a negative effect on the performance of the $Cu/ZnO/Al_2O_3$ system. This could suggest that reduced Zn-sites, whose concentration rise with increasing CO/CO_2 ratio [23, 25], are not critically important for the catalytic activity. However, it cannot be fully excluded that the high hydrogen pressure at the conditions of Fig. 8 is sufficient to saturate the concentration of such reduced Zn-sites. Switching experiments were therefore conducted at two sets of model conditions, where the presence of CO should be essential for the creation of reduced Zn-sites, such as Cu-Zn surface alloy sites. $Cu/ZnO/Al_2O_3$ was subjected to mild (5% H_2 at 448 K) pre-reduction to ensure minimal reduction of the ZnO component. The methanol synthesis activity was then investigated at 448 K and atmospheric pressure starting from a less reducing $CO_2/N_2/H_2$ mixture and then switched to a more reducing $CO_2/CO/H_2$ gas mixture. The N_2 and CO concentrations were identical to ensure that all other parameters remained constant. Fig. 9 shows the methanol formation during the switching experiment and illustrates that also at these conditions CO exerts an exclusively negative effect and causes a 34% drop in the methanol formation rate. Equilibrium methanol concentrations at 448 K

and atmospheric pressure for $CO_2/CO/H_2$ and $CO_2/N_2/H_2$ are calculated to 9136 ppm and 201 ppm, respectively. As the experimentally observed concentrations are well below these levels the presented results are not expected to be influenced by equilibrium constraints. The negative role of CO at these conditions is in good agreement with the results of Cherifi et al. [16], who studied the reaction kinetics with a similar catalyst and conditions and also observed an exclusively negative effect of CO.

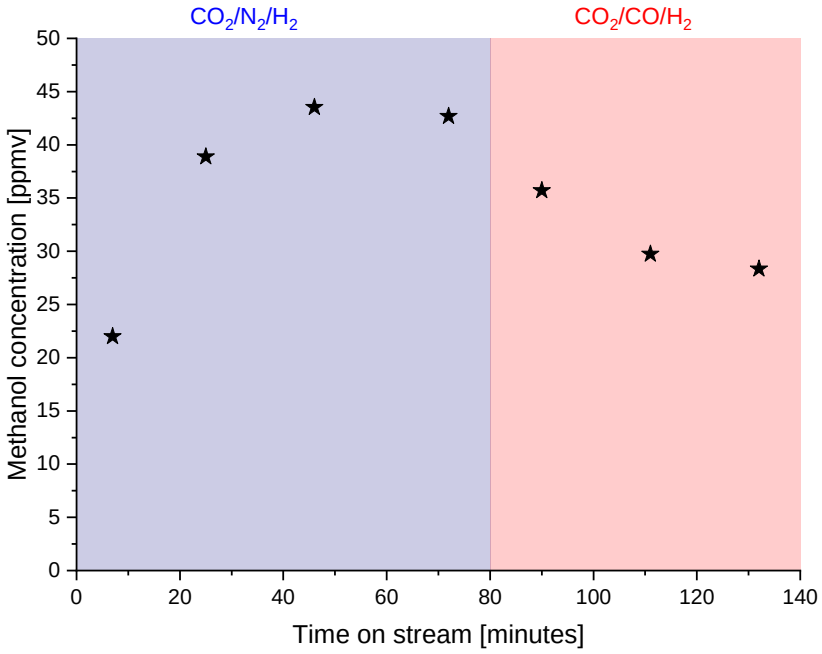

Fig. 9: The methanol production as a function of time on stream when mildly pre-reduced (5% H_2/N_2 at 448 K) $Cu/ZnO/Al_2O_3$ is exposed to first $CO_2/N_2/H_2$ followed by replacement of the N_2 with CO. Reaction conditions: T = 448 K, atmospheric pressure, feed flow = 281 ± 4 Nml/min, $CO_2/X/H_2$ = 3/29/68 with X = N_2 or CO, $Cu/ZnO/Al_2O_3$ loading = 25.3 mg.

In a second model study $Cu/ZnO/Al_2O_3$ was mildly (5% H_2 at 448 K) pre-reduced before being heated in He to 498 K and pressurized to 20 bar. The sample was then subjected to a $CO_2/He/H_2$ (40/30/30) feed i.e. a nominally oxidizing gas ($CO_2 > H_2$). The methanol formation was allowed to stabilize before the He was replaced with CO, which changed the atmosphere to a nominally reducing gas ($CO+H_2 > CO_2$). Fig. 10 shows the methanol formation during the stabilization and gas switch and illustrates that CO is also inhibiting at these conditions, as the activity drops by 40-50% upon introduction of CO. The equilibrium methanol concentrations at these conditions are 3.62 mol% with CO in the feed and 3659 ppm without CO in the feed, and as the experimental concentrations are fare blow these levels the results in Fig. 10 are clearly in the kinetically controlled regime.
These results clearly illustrate that CO plays no beneficial role in facilitating the reduction of $Cu/ZnO/Al_2O_3$. Additionally, the fact that CO has a negative effect at these model conditions, where the reductive power of CO should be critical to the formation of reduced Zn-sites, suggests that e.g. Cu-Zn surface alloy sites are not the source of the beneficial support effect from ZnO. These results showing that a CO-induced rise in the reductive potential to be detrimental for the catalytic activity are in conceptual agreement with the results of Frei et al. [58], who observed that raising the reductive potential during pre-reduction through increasing temperature was detrimental for a $Cu/ZnO/Al_2O_3$ catalyst in terms of TOF and activation energy.

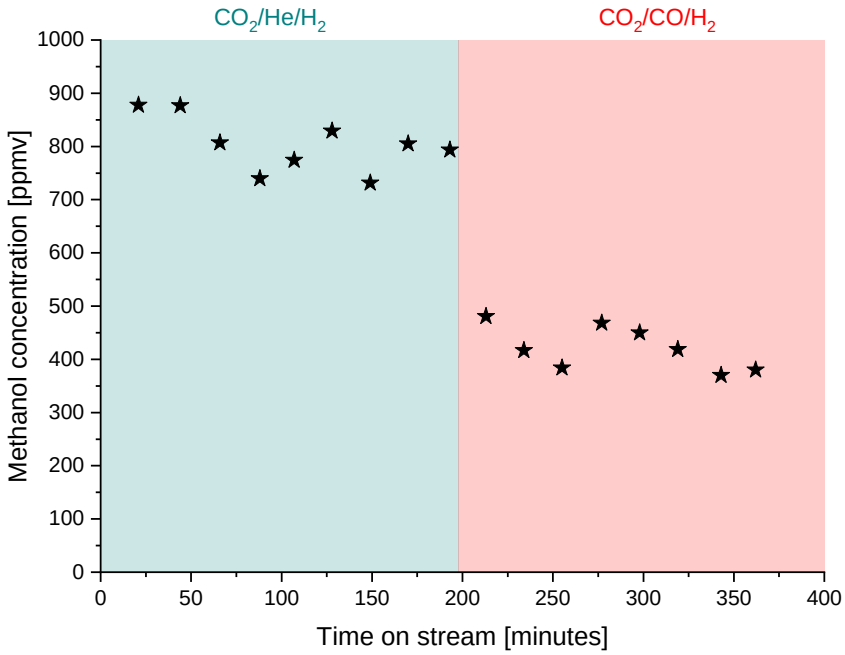

Fig. 10: The methanol concentration as a function of time on stream when mildly pre-reduced (5% HH_2/NH_2 at 448 K) $Cu/ZnO/AlH_2OH_e$ is exposed to first a formally oxidizing $COH_2/He/HH_2$ atmosphere followed by replacement of He with CO to create a formally reducing atmosphere. Reaction conditions: T = 498 K, P = 20 bar, feed flow = 280 ± 3 Nml/min, $X/H_2/CO_2$ = 30/30/40, GHSV = $1.23{\cdot}10^6$ $Nml/g_{cat}/h$.

4 Conclusion

Catalytic methanol synthesis is currently a major industrial process operating from $CO/CO_2/H_2$ with a Cu-based catalyst. However, future uses of the process could involve the conversion of CO_2/H_2 feeds from sustainably derived hydrogen and CO_2 captured at locally available point sources. It is therefore relevant to evaluate the roles of CO and CO_2 for the Cu-catalyzed reaction. Here we have conducted switching experiments between feeds with and without CO over Cu based catalysts to elucidate the roles of CO and CO_2 at varying conversion levels. Switching between CO/H_2 and CO_2/H_2 feeds for Cu/Al_2O_3 clearly showed that the methanol synthesis rate from CO_2 is more than an order of magnitude faster than the rate from CO, which helps to substantiate that CO_2 is the immediate carbon source for methanol on Cu. Low conversion experiments switching between $CO/CO_2/H_2$ and $N_2/CO_2/H_2$ feeds, where the presence or absence of CO is the only change, showed that CO is inhibiting to Raney Cu and to Cu supported on Al_2O_3, SiO_2, TiO_2, ZnO and ZnO/Al_2O_3. Competitive adsorption on the Cu surface could explain the observations, although the removal of promotional oxygen species from the Cu surface by CO cannot be fully excluded as a reason for the inhibiting effect of CO. At higher conversion the presence of CO was found to be beneficial compared to conditions without CO in the feed. This can be explained by the ability of CO to remove a worse inhibitor, water, through the WGS reaction. As a result the optimal feed is a CO-free gas at low conversion, but at higher conversion a CO-rich syngas that efficiently removes produced water is preferable. Comparisons of $Cu/ZnO/Al_2O_3$ and Raney Cu showed that a strong, beneficial support effect from ZnO was present at low conversion conditions, where the effect of CO is observed to be purely detrimental for both samples. One proposed mechanism for the ZnO-support effect has been that reduced Zn species are alloyed into the metal surface, and the CO concentration has previously been found to be important for the creation of the reduced Zn-species. The fact that the support effect is strong at conditions where

the carbon monoxide-induced rise in the reductive potential of the atmosphere was detrimental for the activity is a clear indication that such reduced Zn-species are not critical to the support effect from ZnO. In a further experiment $Cu/ZnO/Al_2O_3$ was at high space velocity (low conversion) exposed to a $H_2/He/CO_2$ gas mixture with an excess of CO_2 compared to H_2 i.e. a nominally oxidizing atmosphere. Once activity had stabilized, the He was replaced with an equal concentration of CO, which changed the atmosphere into a nominally reducing gas. Again the effect of CO was purely inhibiting. The fact that CO is also detrimental at such oxidizing conditions is a further indication that reduced Zn-sites may not be involved in creating the beneficial synergy between Cu and ZnO.

Acknowledgements

This work was supported by a research grant (9455) from VILLUM FONDEN. We thank Saint Gobain for providing the SiO_2 support.

References

[1] J. B. Hansen and P. E. H. Nielsen. *Methanol Synthesis*, volume 2. Wiley-VCH Verlag GmbH, 2nd edition edition, 2008. doi: 10.1002/9783527610044.hetcat0148.

[2] J. Sehested. Industrial and scientific directions of methanol catalyst development. *Journal of Catalysis*, 371:368–375, 2019. doi: 10.1016/j.jcat.2019.02.002.

[3] H. H. Kung. *Methanol production and use*. CRC Press, 1994. doi: 10.5860/choice.32-3898.

[4] N. D. Nielsen, J. Thrane, A. D. Jensen, and J. M. Christensen. Bifunctional Synergy in CO Hydrogenation to Methanol with Supported Cu. *Catalysis Letters*, 150:1427–1433, 2020. doi: 10.1007/s10562-019-03036-7.

[5] F. Studt, M. Behrens, R. Schlögl, E. L. Kunkes, N. Thomas, S. Zander, A. Tarasov, J. Schumann, E. Frei, J. B. Varley, F. Abild-Pedersen, and J. K. Nørskov. The Mechanism of CO and CO_2 Hydrogenation to Methanol over Cu-Based Catalysts. *ChemCatChem*, 7(7):1105–1111, 2015. doi: 10.1002/cctc.201500123.

[6] W. Janse Van Rensburg, J. A. Van Den Berg, M. A. Petersen, M. S. Datt, and P. Van Helden. On the Kinetic Interpretation of DFT-Derived Energy Profiles: Cu-Catalyzed Methanol Synthesis. *Catalysis Letters*, 145(2):559–568, 2015. doi: 10.1007/s10562-014-1407-1.

[7] M. S. Tameh, A. K. Dearden, and C. Huang. Accuracy of Density Functional Theory for Predicting Kinetics of Methanol Synthesis from CO and CO_2 Hydrogenation on Copper. *Journal of Physical Chemistry C*, 122(31):17942–17953, 2018. doi: 10.1021/acs.jpcc.8b06498.

[8] J. Nerlov and I. Chorkendorff. Methanol synthesis from CO_2, CO, and H_2 over Cu(100) and Ni/Cu(100). *Journal of Catalysis*, 181(2):271–279, 1999. doi: 10.1006/jcat.1998.2301.

[9] G. C. Chinchen, M. S. Spencer, K. C. Waugh, and D. A. Whan. Promotion of methanol synthesis and the water-gas shift reactions by adsorbed oxygen on supported copper catalysts. *Journal of the Chemical Society, Faraday Transactions 1*, 83(7):2193–2212, 1987. doi: 10.1039/f19878302193.

[10] Y. B. Kagan, A. Y. Rozovskij, L. G. Liberov, E. V. Slivinskij, G. I. Lin, S. M. Loktev, and A. N. Bashkirov. Study of mechanism of methanol synthesis from carbon monoxide and hydrogen using radioactive carbon isotope C^{14}. *Doklady Akademii Nauk SSSR*, 224(5):1081–1084, 1975.

[11] G. C. Chinchen, P. J. Denny, D. G. Parker, M. S. Spencer, and D. A. Whan. Mechanism of methanol synthesis from $CO_2/CO/H_2$ mixtures over copper/zinc oxide/alumina catalysts: use of ^{14}C-labelled reactants. *Applied Catalysis*, 30(2):333–338, 1987. doi: 10.1016/S0166-9834(00)84123-8.

[12] K. G. Chanchlani, R. R. Hudgins, and P. L. Silveston. Methanol synthesis from H_2, CO, and CO_2 over Cu/ZnO catalysts. *Journal of Catalysis*, 136(1):59–75, 1992. doi: 10.1016/0021-9517(92)90106-R.

[13] J. S. Lee, S. H. Han, H. G. Kim, K. H. Lee, and Y. G. Kim. Effects of space velocity on methanol synthesis from $CO_2/CO/H_2$ over $Cu/ZnO/Al_2O_3$ catalyst. *Korean Journal of Chemical Engineering*, 17(3):332–336, 2000. doi: 10.1007/BF02699049.

[14] S. Zander, E. L. Kunkes, M. E. Schuster, J. Schumann, G. Weinberg, D. Teschner, N. Jacobsen, R. Schlögl, and M. Behrens. The role of the oxide component in the development of copper composite catalysts for methanol synthesis. *Angewandte Chemie - International Edition*, 52(25):6536–6540, 2013. doi: 10.1002/anie.201301419.

[15] M. Sahibzada, I. S. Metcalfe, and D. Chadwick. Methanol Synthesis from $CO/CO_2/H_2$ over $Cu/ZnO/Al_2O_3$ at Differential and Finite Conversions. *Journal of Catalysis*, 174:111–118, 1998. doi: 10.1006/jcat.1998.1964.

[16] O. Cherefi, S. Monteverdi, M. M. Bettahar, M. Forissier, and V. Perrichon. Kinetics of CO_2 hydrogenation into methanol on a Cu-Zn-Al oxide catalyst. *Bull. Soc. Chim. Fr.*, pages 405–409, 1985.

[17] O. Martin and J. Pérez-Ramírez. New and revisited insights into the promotion of methanol synthesis catalysts by CO_2. *Catalysis Science and Technology*, 3(12):3343–3352, 2013. doi: 10.1039/c3cy00573a.

[18] J. Barbier, J. Fortin, P. Courty, and P. Chaumette. Rôle du dioxyde de carbone lors de la synthèse du méthanol sur catalyseurs à base de cuivre. *Bulletin de la Société chimque de france*, 6:925–929, 1987.

[19] K. Klier, V. Chatikavanij, R. G. Herman, and G. W. Simmons. Catalytic Synthesis of Methanol from CO/H_2 IV The Effects of Carbon Dioxide. *Journal of Catalysis*, 74:343–360, 1982. doi: 10.1016/0021-9517(82)90040-9.

[20] G. A. Olah, A. Goeppert, and G. K. S. Prakash. Chemical Recycling of Carbon Dioxide to Methanol and Dimethyl Ether: From Greenhouse Gas to Renewable, Environmentally Carbon Neutral Fuels and Synthetic Hydrocarbons. *J. Org. Chem.*, 74(2):487–498, 2009. doi: 10.1021/jo801260f.

[21] J. Thrane, S. Kuld, N. D. Nielsen, A. D. Jensen, J. Sehested, and J. M. Christensen. Methanol-assisted autocatalysis in catalytic methanol synthesis. *Angewandte Chemie - International Edition*, 59:18189–18193, 2020. doi: 10.1002/anie.202006921.

[22] N. D. Nielsen, A. D. Jensen, and J. M. Christensen. Quantification of Formate and Oxygen Coverages on Cu Under Industrial Methanol Synthesis Conditions. *Catalysis Letters*, 150(9):2447–2456, 2020. doi: 10.1007/s10562-020-03162-7.

[23] J. C. Frost. Junction effect interactions in methanol synthesis catalysts. *Nature*, 334:577–580, 1988. doi: 10.1038/332141a0.

[24] J. Nakamura, I. Nakamura, T. Uchijima, T. Watanabe, and T. Fujitani. Model Studies of Methanol Synthesis on Copper Catalysts. *Stud. Surf. Sci. Cat.*, 101:1389–1399, 1996. doi: 10.1016/s0167-2991(96)80351-x.

[25] S. Kuld, M. Thorhauge, H. Falsig, C. F. Elkjaer, S. Helveg, I. Chorkendorff, and J. Sehested. Quantifying the promotion of Cu catalysts by ZnO for methanol synthesis. *Science*, 352(6288):969–974, 2016. doi: 10.1126/science.aaf0718.

[26] P. C. K. Vesborg, I. Chorkendorff, I. Knudsen, O. Balmes, J. Nerlov, A. M. Molenbroek, B. S. Clausen, and S. Helveg. Transient behavior of Cu/ZnO-based methanol synthesis catalysts. *Journal of Catalysis*, 262(1):65–72, 2009. doi: 10.1016/j.jcat.2008.11.028.

[27] C. V. Ovesen, B. S. Clausen, J. Schiøtz, P. Stoltze, H. Topsøe, and J. K. Nørskov. Kinetic Implications of Dynamical Changes in Catalyst Morphology during Methanol Synthesis over Cu/ZnO Catalysts. *Journal of Catalysis*, 168(2):133–142, 1997. doi: 10.1006/jcat.1997.1629.

[28] K.-D. Jung, O.-S. Joo, and S.-H. Han. Structural change of Cu/ZnO by reduction of ZnO in Cu/ZnO with methanol. *Catal. Lett.*, 68(1-2):49, 2000. doi: 10.1023/A:1019027302428.

[29] Y. Ren, K. Yuan, X. Zhou, H. Sun, K. Wu, S. L. Bernasek, W. Chen, and G. Q. Xu. Catalytic Intermediates of CO_2 Hydrogenation on Cu(111) Probed by In Operando Near-Ambient Pressure Technique. *Chemistry - A European Journal*, 24(60):16097–16103, 2018. doi: 10.1002/chem.201802931.

[30] B. Eren, R. S. Weatherup, N. Liakakos, G. A. Somorjai, and M. Salmeron. Dissociative Carbon Dioxide Adsorption and Morphological Changes on Cu(100) and Cu(111) at Ambient Pressures. *Journal of the American Chemical Society*, 138(26):8207–8211, 2016. doi: 10.1021/jacs.6b04039.

[31] N. D. Nielsen, T. E. L. Smitshuysen, C. D. Damsgaard, A. D. Jensen, and J. M. Christensen. Characterization of oxide-supported Cu by infrared measurements on adsorbed CO. *Surface Science*, 703:121725, 2021. doi: 10.1016/j.susc.2020.121725.

[32] G. C. Chinchen, C. M. Hay, H. D. Vandervell, and K. C. Waugh. The measurement of copper surface areas by reactive frontal chromatography. *Journal of Catalysis*, 103(1):79–86, 1987. doi: 10.1016/0021-9517(87)90094-7.

[33] O. Hinrichsen, T. Genger, and M. Muhler. Chemisorption of N_2O and H_2 for the Surface Determination of Copper Catalysts. *Chemical Engineering & Technology*, 23(11):956–959, 2000. doi: 10.1002/1521-4125(200011)23:11⟨956::AID-CEAT956⟩3.0.CO;2-L.

[34] R. Chatterjee, S. Kuld, R. V. D. Berg, A. Chen, and W. Shen. Mapping Support Interactions in Copper Catalysts. *Topics in Catalysis*, 62(7-11):649–659, 2019. doi: 10.1007/s11244-019-01150-9.

[35] G. H. Graaf and J. G.M. Winkelman. Chemical Equilibria in Methanol Synthesis Including the Water-Gas Shift Reaction: A Critical Reassessment. *Industrial and Engineering Chemistry Research*, 55(20):5854–5864, 2016. doi: 10.1021/acs.iecr.6b00815.

[36] S. Kuld, C. Conradsen, P. G. Moses, I. Chorkendorff, and J. Sehested. Quantification of zinc atoms in a surface alloy on copper in an industrial-type methanol synthesis catalyst. *Angewandte Chemie - International Edition*, 53(23):5941–5945, 2014. doi: 10.1002/anie.201311073.

[37] M. Saito, T. Fujitani, M. Takeuchi, and T. Watanabe. Development of copper/zinc oxide-based multicomponent catalysts for methanol synthesis from carbon dioxide and hydrogen. *Applied Catalysis A: General*, 138(2):311–318, 1996. doi: 10.1016/0926-860X(95)00305-3.

[38] Y. Yang, C. A. Mims, D. H. Mei, C. H. F. Peden, and C. T. Campbell. Mechanistic studies of methanol synthesis over Cu from $CO/CO_2/H_2/H_2O$ mixtures: The source of C in methanol and the role of water. *Journal of Catalysis*, 298:10–17, 2013. doi: 10.1016/j.jcat.2012.10.028.

[39] J. Słoczyński, R. Grabowski, J. Janas, and J. Skrzypek. Adsorption model of methanol synthesis reactants on CuO-ZnO-Al_2O_3 catalyst-I. Adsorption on the catalyst. *Chemical Engineering Science*, 46(10):2599–2610, 1991. doi: 10.1016/0009-2509(91)80053-2.

[40] J. Słoczyński, R. Grabowski, and J. Janas. Adsorption Model of Methanol Synthesis Reactants on CuO-ZnO-Al_2O_3 Catalyst - II Adsorption on the individual components of the catalyst. *Chemical Engineering Science*, 46(10):2611–2623, 1991. doi: 10.1016/0009-2509(91)80054-3.

[41] E. Colbourn, R. A. Hadden, H. D. Vandervell, K. C. Waugh, and G. Webb. Adsorption of water on polycrystalline copper: relevance to the water gas shift reaction. *Journal of Catalysis*, 130(2): 514–527, 1991. doi: 10.1016/0021-9517(91)90132-N.

[42] J. Nakamura, J. M. Campbell, and C. T. Campbell. Kinetics and mechanism of the water-gas shift reaction catalysed by the clean and Cs-promoted Cu(110) surface: A comparison with Cu(111). *Journal of the Chemical Society, Faraday Transactions*, 86(15):2725–2734, 1990. doi: 10.1039/FT9908602725.

[43] F. Le Peltier, P. Chaumette, J. Saussey, M. M. Bettahar, and J. C. Lavalley. In situ FT-IR and kinetic study of methanol synthesis from CO_2/H_2 over $ZnAl_2O_4$ and Cu-$ZnAl_2O_4$ catalysts. *Journal of Molecular Catalysis A: Chemical*, 132(1):91–100, 1998. doi: 10.1016/S1381-1169(97)00235-5.

[44] N. Nomura, T. Tagawa, and S. Goto. Titania supported copper catalysts for methanol synthesis from carbon dioxide. *Reaction Kinetics and Catalysis Letters*, 63(1):9–13, 1998. doi: 10.1007/BF02475423.

[45] Y. Amenomiya and T. Tagawa. Infrared study of methanol synthesis from CO_2 and H_2 on supported copper-zinc oxide catalysts. *Proc. of 8th Int. Congress on Catal*, pages 557–567, 1984.

[46] L. Fan, Y. Sakaiya, and K. Fujimoto. Low-temperature methanol synthesis from carbon dioxide and hydrogen via formic ester. *Applied Catalysis A: General*, 180(1-2):13–15, 1999. doi: 10.1016/S0926-860X(98)00345-7.

[47] N. Tsubaki, M. Ito, and K. Fujimoto. A new method of low-temperature methanol synthesis. *Journal of Catalysis*, 197(1):224–227, 2001. doi: 10.1006/jcat.2000.3077.

[48] P. Reubroycharoen, T. Yamagami, T. Vitidsant, Y. Yoneyama, M. Ito, and N. Tsubaki. Continuous low-temperature methanol synthesis from syngas using alcohol promoters. *Energy and Fuels*, 17(4):817–821, 2003. doi: 10.1021/ef020240v.

[49] M. Behrens, F. Studt, I. Kasatkin, S. Kühl, M. Hävecker, F. Abild-Pedersen, S. Zander, F. Girgsdies, P. Kurr, B. Kniep, M. Tovar, R. W. Fischer, J. K. Nørskov, and R. Schlögl. The Active Site of Methanol Synthesis over $Cu/ZnO/Al_2O_3$ Industrial Catalysts. *Science*, 336:893–898, 2012. doi: 10.1126/science.1219831.

[50] M. Kurtz, N. Bauer, H. Wilmer, O. Hinrichsen, and M. Muhler. Rational Catalyst Design of Methanol Synthesis Catalysts. *Chemical Engineering & Technology*, 27(11):1146–1150, 2004. doi: 10.1002/ceat.200407032.

[51] T. Fujitani, M. Saito, Y. Kanai, T. Kakumoto, T. Watanabe, J. Nakamura, and T. Uchijima. The role of metal oxides in promoting a copper catalyst for methanol synthesis. *Catalysis Letters*, 25 (3-4):271–276, 1994. doi: 10.1007/BF00816307.

[52] K. Murata M. Saito. Development of high performance Cu/ZnO-based catalysts for methanol synthesis and the water-gas shift reaction. *Catal. Surveys Asia*, 8(4):285–294, 2004. doi: 10.1007/s10563-004-9119-y.

[53] R. Burch, S. E. Golunski, and M. S. Spencer. The role of copper and zinc oxide in methanol synthesis catalysts. *Journal of the Chemical Society, Faraday Transactions*, 86(15):2683–2691, 1990. doi: 10.1039/ft9908602683.

[54] T. Fujitani, I. Nakamura, and T. Uchijima. The kinetics and mechanism of methanol synthesis by hydrogenation of CO_2 over a Zn-deposited Cu (111) surface. *Surface Science*, 383:285–298, 1997. doi: 10.1016/S0039-6028(97)00192-1.

[55] Y. Kanai, T. Watanabe, T. Fujitani, M. Saito, J. Nakaumra, and T. Uchijima. Evidence for the migration of ZnO_x in a Cu/ZnO methanol synthesis catalyst. *Catalysis Letters*, 27:67–78, 1994. doi: 10.1007/BF00806979.

[56] M. Sano, T. Adaniya, T. Fujitani, and J. Nakamura. Oxidation of a Zn-deposited Cu(111) surface studied by XPS and STM. *Surface Science*, 514(1-3):261–266, 2002. doi: 10.1016/S0039-6028(02)01639-4.

[57] M. Sano, T. Adaniya, T. Fujitani, and J. Nakamura. Formation Process of a Cu-Zn Surface Alloy on Cu (111) Investigated by Scanning Tunneling Microscopy. *J. Phys. Chem*, 106:7627–7633, 2002. doi: 10.1021/jp012810i.

[58] E. Frei, A. Gaur, H. Lichtenberg, L. Zwiener, M. Scherzer, F. Girgsdies, T. Lunkenbein, and R. Schlögl. Cu-Zn Alloy Formation as Unfavored State for Efficient Methanol Catalysts. *ChemCatChem*, 12:4029–4033, 2020. doi: 10.1002/cctc.202000777.

Chapter 4

Methanol-Assisted Autocatalysis in Catalytic Methanol Synthesis

Authors: Joachim Thrane[a], Sebastian Kuld[b] Niels D. Nielsen[a], Anker D. Jensen[a], Jens Sehested[b], Jakob M. Christensen[a]

[a] *Department of Chemical and Biochemical Engineering, Technical University of Denmark, Søltofts Plads Building 229, 2800 Kgs. Lyngby (Denmark)*
[b] *Haldor Topsøe A/S, Nymøllevej 55, 2800 Kgs. Lyngby (Denmark)*
*__Correspondence to:__ jmc@kt.dtu.dk

DOI:
https://doi.org/10.1002/anie.202006921

Journal specifications:
Angewandte Chemie International Edition, 2020, Volume 59, 18189-18193

Date Accepted/Published:
29 June 2020 / 13 August 2020

Abstract

Catalytic methanol synthesis is one of the major processes in the chemical industry and may grow in importance, as methanol produced from CO_2 and sustainably derived $H_2$are envisioned to play an important role as energy carriers in a future low-CO_2-emission society. However, despite the widespread use, the reaction mechanism and the nature of the active sites are not fully understood. Here we report that methanol synthesis at commercially applied conditions using the industrial $Cu/ZnO/Al_2O_3$ catalyst is dominated by a methanol-assisted autocatalytic reaction mechanism. We propose that the presence of methanol enables the hydrogenation of surface formate via methyl formate. Autocatalytic acceleration of the reaction is also observed for Cu supported on SiO_2 although with low absolute activity, but not for Cu/Al_2O_3 catalysts. The results illustrate an important example of autocatalysis in heterogeneous catalysis and pave the way for further understanding, improvements and process optimization of industrial methanol synthesis.

Graphic Abstract

Keywords: Autocatalysis · Methanol · CO_2 hydrogenation · Copper · Reaction mechanisms

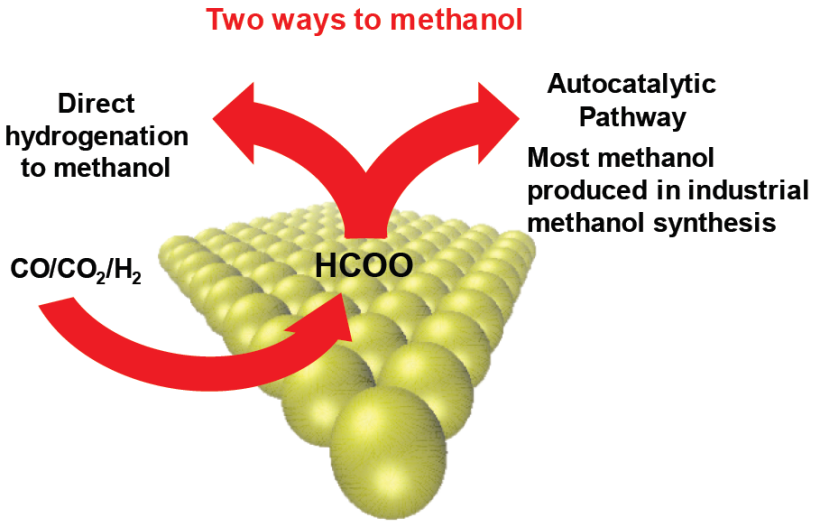

1 Introduction

Heterogeneous catalysis is vital to modern chemical industry. Understanding the nature of the active sites, reaction mechanisms and the origin of metal-support/promoter interactions is therefore not only fundamentally important, but also significant due to the substantial economic impact of improvements to large-scale industrial processes relying on catalysis. Methanol is a major bulk chemical with a production exceeding 70 million tons/year and is produced from syngas ($CO/CO_2/H_2$) over a $Cu/ZnO/Al_2O_3$ catalyst [1]. Methanol synthesis can proceed over Cu surfaces, but the reaction rate is strongly enhanced by the presence of zinc in the catalyst [2–5]. However, the exact nature of the active sites and the beneficial support effect from ZnO in the industrial catalyst are still debated issues. By contrast, there seems to be a more widespread agreement concerning the general reaction mechanism for methanol synthesis over Cu catalysts. Most theoretical and experimental studies advocate that methanol is made directly from carbon dioxide (CO_2) and hydrogen (H_2) via formation of surface formate and its subsequent hydrogenation to methanol, and this mechanism explains most reported data in the literature. Yet, such a mechanism is not able to explain some of the most remarkable observations, where methanol synthesis rates under certain conditions are accelerated with increasing conversion [6, 7]. This acceleration is highly unexpected, as the methanol synthesis has a relatively unfavourable equilibrium and experiences a strong kinetic inhibition from the accompanying water product [7–10]. Here, we demonstrate that the origin of this obvious inconsistency between theoretical understanding and experimental data is a previously unknown, methanol-assisted, autocatalytic reaction pathway. Our data confirm that this reaction pathway is responsible for most of the turnovers to methanol under industrial conditions, and we conclude that the autocatalytic mechanism most likely is via a methyl formate intermediate.

2 Results and Discussion

A series of Cu catalysts supported on ZnO/Al_2O_3, ZnO, Al_2O_3 and SiO_2 were prepared, and the active Cu areas of the catalysts were determined through the oxygen uptake (using $O{:}Cu_{surf.} = 1{:}2$ and $1.47{\cdot}10^{19}$ Cu atoms/m^2) [11] from 1 mol% N_2O/He at 333 K after reduction in 5 vol% H_2/N_2 at atmospheric pressure and 523 K. Cu/Al_2O_3 required that the 5% H_2/N_2 treatment was followed by a 100% H_2 treatment at 523 K to obtain complete Cu reduction. The catalytic activity of pre-reduced catalysts was measured in a flow reactor at 523 K and 50 bar in syngas ($CO/CO_2/H_2 = 29.6/2.8/67.6$ mol%), and for each catalyst, the space velocity (SV) was varied by 1-3 orders of magnitude to vary the level of conversion. Turnover frequencies (TOF: methanol formation rate per Cu surface atom) at the different conversion levels were determined from the Cu surface areas and the methanol production rates, and Fig. 1 shows the TOF as a function of the methanol concentration at the exit of the reactor.

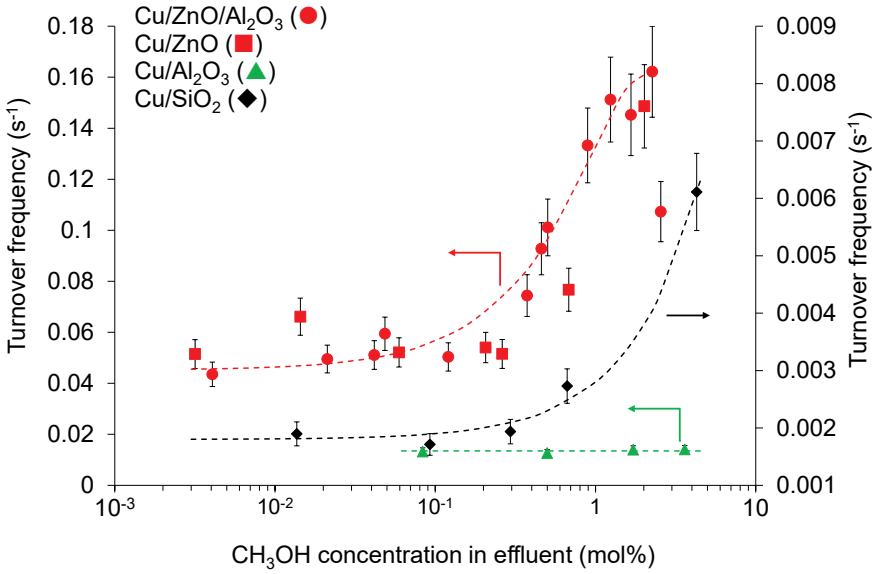

Fig. 1: The dependence of the TOF upon the CH_3OH concentration in the reactor effluent when varying the space velocity. Note the different scaling of the Cu/SiO_2 data. Dashed lines given as guides to the eye. Experimental conditions: 50 bar, 523 K, $H_2/CO/CO_2$ = 67.6/29.6/2.8 mol%, $3{\cdot}10^3 - 4.3 \cdot 10^7$ NL (kg h)$^{-1}$. See Fig. S1 for a definition of the TOF and a comparison in terms of space velocity. The equilibrium concentration of CH_3OH at these conditions is 23 mol% based on data from Graaf and Winkelman [12].

This figure depicts, how the Cu catalysts respond to the changing product concentrations, when the SV is varied. Under differential conditions (below approximately 0.1 mol% methanol produced), the TOF reaches a stable plateau for each catalyst type. Here methanol formation through a mechanism directly from the reactants must dominate. At these conditions there is a notable support effect on the TOF, and the activity order of the supports ($ZnO/Al_2O_3 \cong ZnO > Al_2O_3 > SiO_2$) is in good agreement with the observations in several previous studies [2–4]. Within the uncertainty the same TOF is seen for $Cu/ZnO/Al_2O_3$ and Cu/ZnO at identical conversion levels in Fig. 1, and these two systems are therefore treated collectively in the remaining text. The TOF values are determined from the Cu surface areas obtained from N_2O titrations, and there are uncertainties in methods for determination of metal area, as illustrated by the systematic and carrier-dependent differences between areas from N_2O and H_2 titrations [11]. However, with the applied pre-reduction, the magnitude of these differences [11] is expected to be considerably smaller than the differences between the TOF values of the different catalyst systems, and the uncertainties on the area should therefore not affect the conclusions. Consequently, this issue is not discussed further in the following.
Remarkable changes in TOF are observed in Fig. 1 when the product concentrations are increased by lowering of the SV to achieve finite conversion. Lowering the SV causes the TOF-values for the $ZnO(/Al_2O_3)$ and SiO_2 containing catalysts to increase more than three-fold. Such an increase with rising product concentration is indicative of a significant autocatalytic effect, whereby the product assists the formation of additional product. The magnitude of the acceleration means that the autocatalytic pathway is at least several times faster than the direct pathway, and as a result the substantial majority of turnovers in the industrial process must arise from the autocatalytic pathway. This autocatalytic behaviour is clearly support-dependent. The Cu/SiO_2 catalyst has a low absolute activity but shows an autocatalytic behaviour like that of $Cu/ZnO(/Al_2O_3)$, while reaction rates for Cu/Al_2O_3 are independent of SV (see also Supporting Information Fig. S1d). The heat generated in the exothermic reaction increases with conversion/product concentration regardless of the support, but here no significant temperature rise was observed, and the fact that TOF for Cu/Al_2O_3 did not grow with conversion shows that the acceleration is not due to a temperature rise. As CO_2 is the primary reac-

tant in methanol synthesis over pure Cu and Cu/ZnO(/Al_2O_3) [9, 13, 14] it is important to evaluate, if changes in CO_2 concentration can arise from the variations in conversion. CO_2 is consumed via methanol synthesis (R1), but partly restored by the water-gas shift reaction (R_2).

$$CO_2 + 3\,H_2 \rightleftharpoons CH_3OH + H_2O \qquad \{R1\}$$

$$CO + H_2O \rightleftharpoons H_2 + CO_2 \qquad \{R2\}$$

The activity peak for Cu/ZnO(/Al_2O_3) in Fig. 1 (+ 372%) occurs at 2 mol% methanol in the effluent. If R2 is equilibrated at these conditions there will be a 2.5% net conversion of the CO_2. However, the volume contraction due to the loss of molecules in R1 was measured to be 4% at these conditions, and this leads to a corresponding rise in the CO_2 concentration. The consumption of CO_2 and the concentration rise due to volume contraction thus nearly balance out, and the concentration of CO_2 is therefore essentially unaffected by the reaction (see Fig. S2). Consequently reaction-induced changes in CO_2 concentration cannot affect the experimental results. As diffusion limitations were ruled out by experiments and calculations (see Supporting Information), it can be ruled out that a local concentration rise within the catalyst pores should affect this conclusion.

The increase in reaction rate in Fig. 1 must therefore arise from the emergence of a faster pathway at higher conversions, and at least two parallel reaction pathways in methanol synthesis are needed to explain the results: a direct conversion of the reactants dominating at differential conditions and a faster autocatalytic route involving a reaction product dominant at higher conversions. At the lower SV, where the autocatalytic pathway prevails, the TOF for Cu/ZnO was observed to remain constant across an 8-fold variation in Cu surface area, which corresponds to a linear correlation between absolute activity and Cu surface area (Fig. S3). This would imply that the rate limiting step in the autocatalytic pathway occurs on the metal surface, but there is clearly also an either direct or indirect involvement of the support that is of great importance for the absolute activity. In the industrial process the syngas feed already contains some methanol due to recirculation of unconverted reactants, and the methanol concentration rises to significant percentages through the reactor [15]. Under such conditions, the faster autocatalytic pathway will be responsible for the vast majority of the turnovers and thus dominate the industrial process.

This conclusion raises the question of, which reaction product that causes such an effect. As the highly selective methanol synthesis produces only two major products, namely CH_3OH and H_2O, these two products represent the most likely candidates. Additional experiments were therefore conducted with the Cu/ZnO/Al_2O_3 catalyst (Cu:Zn:Al = 6:3:1, 20 $m^2_{Cu}\ g^{-1}_{cat.}$) to identify the source and possible mechanism of the autocatalytic effect. The methanol synthesis activity was measured for the Cu/ZnO/Al_2O_3 catalyst at differential conditions (SV = $1.6{\cdot}10^6$ NL $(kg\ h)^{-1}$) far from equilibrium (< 1000 ppm CH_3OH produced) with low levels of water added to the syngas feed, and the results are shown in Fig. 2.

The data in Fig. 2 illustrate that even minute amounts of water lower the activity substantially, which strongly indicates that water is not the source of the autocatalytic effect. Competitive adsorption of water or its dissociation products is a likely explanation for this kinetic inhibition, as water adsorption isotherm measurements [16, 17] on Cu/ZnO/Al_2O_3 suggest a high coverage on the Cu surface at temperatures and H_2O partial pressures similar to those where major water inhibition is observed in Fig. 2. The increase in TOF with rising product concentrations in Fig. 1 is even more remarkable when considering the strong inhibition caused by the co-produced water.

The effect of adding the second major product, methanol, to the syngas feed is illustrated in Fig. 3. Two independent methanol co-feeding experiments were performed in two very different setups (described in detail in the Supporting Information), and the results are depicted as Figs. 3a and 3b, respectively. Remarkably, the net rate of methanol formation increases considerably, when methanol is co-fed with the syngas feed, and on this basis we deduce that methanol is the source of the autocatalytic acceleration in methanol synthesis. Liquid phase alcohols were previously found [18–20] to accelerate the Cu-catalysed hydrogenation of CO_2 to methanol at low temperatures ($\leq$ 443 K) well below the industrial operating window. However, the data in Fig. 3 imply that methanol synthesis at commercial conditions is dominated by methanol mediated autocatalysis.

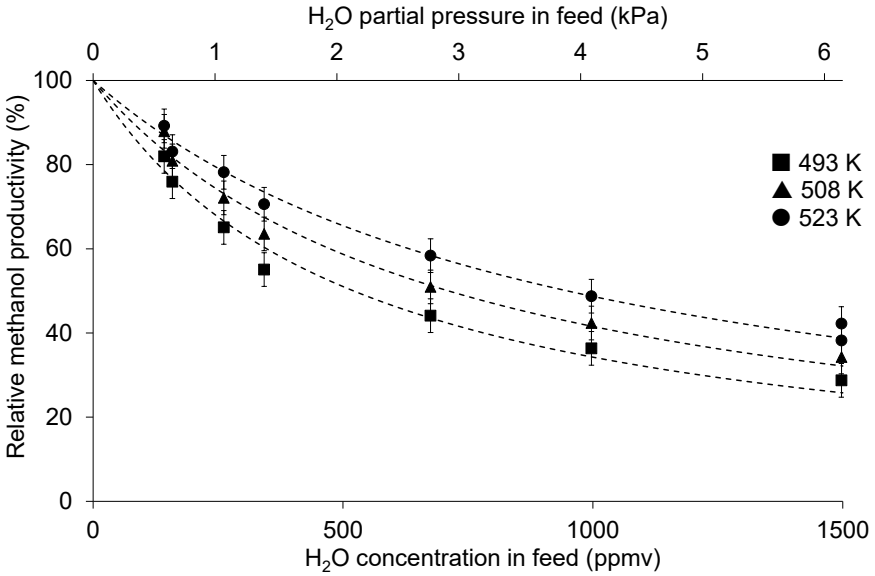

Fig. 2: The relative methanol production as a function of the water content added to the syngas feed. Experimental conditions: Catalyst: $Cu/ZnO/Al_2O_3$, $P = 41$ bar, $H_2/CO/CO_2 = 67.6/29.6/2.8$ mol%, $1.6{\cdot}10^6$ NL (kg h)$^{-1}$. Dashed lines given as guides to the eye. See Supporting Information for a definition of the error bars.

The net increase in reaction rate with increasing conversion seen in a $CO/CO_2/H_2$ feed (Fig. 1) does not occur in CO_2/H_2 gas mixtures as illustrated in Fig. S6. This can be rationalized through the opposite effects of the two reaction products. If CO is present, most of the produced water will be removed by R2, and the beneficial effect of methanol will dominate over the adverse effect of water. In a CO-free atmosphere, water is produced by both the methanol synthesis and the reverse water-gas shift reaction, and the greater concentration of inhibiting water causes the rate to decline with increasing conversion. However, from a CO_2/H_2 feed, only a moderate loss in activity of 6% was observed for a $Cu/ZnO/Al_2O_3$ catalyst at a methanol effluent concentration of 0.4 mol% (see Fig. S6). At these conditions, an oxygen balance suggested that 0.68 mol% water was co-produced, if only R1 and R2 occur. Considering the inhibition expected from such a water concentration (see Fig. 2), the autocatalytic acceleration seems to partly compensate for the negative effect of water and thus also play a major role in a CO_2/H_2 atmosphere. Hence, the net rate of the reaction is determined by the balance between acceleration from the autocatalytic pathway and inhibition from produced water, which will depend on the reaction conditions such as the composition of the syngas.
We show here for the first time that methanol formation over the industrially applied $Cu/ZnO/Al_2O_3$ catalysts is dominated by an autocatalytic pathway that involves methanol. At high SV the formed methanol is almost exclusively from CO_2 with the industrial $Cu/ZnO/Al_2O_3$ catalyst [9, 13, 14]. This is most likely also the case at lower SV, where the rate from a CO_2-containing gas (> 5 g_{MeOH} $g_{cat.}^{-1}$ h^{-1} in Fig. S1c) is also far higher than in a CO/H_2 feed (0.4 g_{MeOH} $g_{cat.}^{-1}$ h^{-1} at comparable conditions [9]). The autocatalytic pathway at lower SV must therefore be expected to proceed from CO_2. At higher conversion with greater water formation more methanol is formed by the $CO \rightarrow CO_2 \rightarrow CH_3OH$ sequence of R2 followed by R1, but the constancy in CO_2 concentration across the reactor (Fig. S2) suggests that R2 is fast, and consequently R1 is solely rate limiting in methanol synthesis. Adsorbed formate is present on the metal surface at methanol synthesis conditions, [14, 21, 22] which suggests that the autocatalytic pathway could involve CO_2-derived formate. Fig. 4a shows that CD_3OOCH was formed at low temperature, when $Cu/ZnO/Al_2O_3$ with pre-adsorbed HCOO (from exposure to $HCOOH/N_2$ at 303 K) was subjected to temperature programmed reaction (TPR) in a flow of CD_3OD in He. This illustrates that methyl formate can be formed from reaction between methanol and surface formate. A role of molecularly adsorbed formic acid cannot be fully excluded here, but previous IR studies [23, 24] also demonstrate that the ester is easily formed by

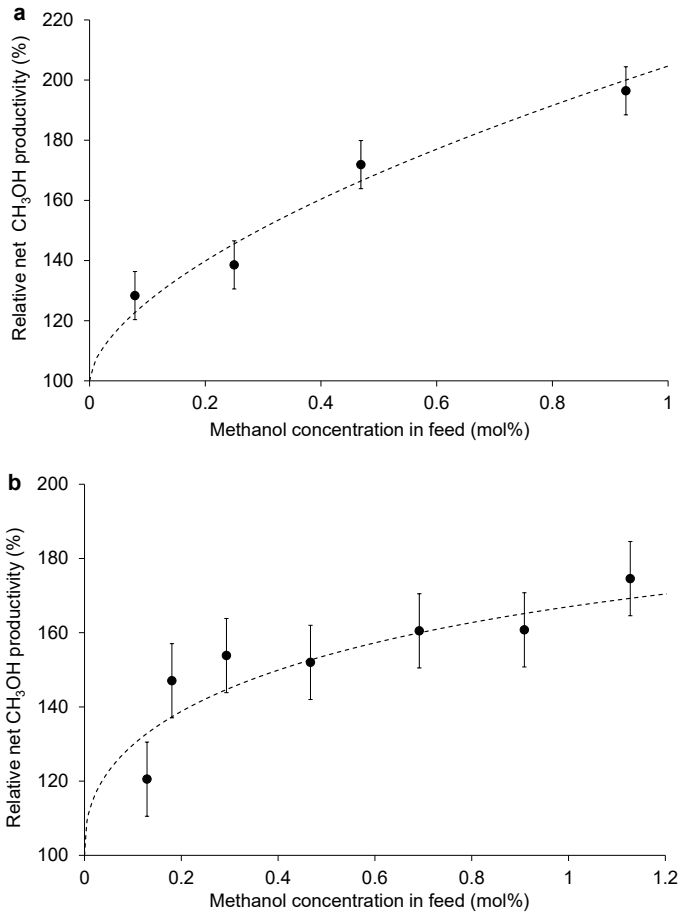

Fig. 3: **(a)** Relative net productivity of methanol as a function of the methanol concentration in the syngas feed at 50 bar. **(b)** Relative net productivity of methanol as a function of the methanol concentration in the syngas feed at 41 bar. Other experimental conditions: Catalyst: $Cu/ZnO/Al_2O_3$, T = 523 K, syngas before MeOH addition: $H_2/CO/CO_2$ = 67.6/29.6/2.8 mol%, $1.6{\cdot}10^6$ NL (kg h)$^{-1}$. Additional data in Figs. S4 and S5. See Supporting Information for a definition of the error bars.

reaction of an alcohol with adsorbed formate at typical methanol synthesis temperatures. A probable pathway for the autocatalytic process is therefore via formation of the methyl formate ester from methanol and surface formate (reaction (3), subsequently denoted R3) followed by hydrogenation of the ester (reaction (4), denoted R4). However, methyl formate may also be decarbonylated to methanol and CO (reaction (5), denoted R5) [25].

$$CH_3OH + HCOO \rightleftharpoons CH_3OOCH + OH \qquad \{R3\}$$

$$CH_3OOCH + 2\,H_2 \rightleftharpoons 2\,CH_3OH \qquad \{R4\}$$

$$CH_3OOCH \rightleftharpoons CH_3OH + CO \qquad \{R5\}$$

Reaction R3 followed by reaction R4 results in a net gain of methanol, whereas the combination of R3 and R5 yields no net gain. Effective autocatalysis via methyl formate therefore relies on the rates of R3 and R4 being faster than direct CO_2 hydrogenation and on a high selectivity to hydrogenation (R4) relative to decarbonylation (R5) in the conversion of methyl formate. Fig. 4b shows the results, when $Cu/ZnO/Al_2O_3$ pre-covered with surface formate (from HCOOH) was subjected to a TPR in a flow of either CH_3OH/He or H_2. Fig. 4b illustrates that the onset of methyl formate formation

in a CH_3OH/He gas occurs at a lower temperature than methanol formation in H_2. Re-adsorption phenomena can delay the appearance of a product in a TPH, but the lower onset temperature does indicate that R3 is considerably faster than direct hydrogenation of HCOO, and there are good indications in the literature that this is also the case for both R4 and R5. Fakley and co-workers [26] used the data from Monti et al. [25] to calculate that R4 should be of ample rate on Cu to account for an acceleration of the methanol synthesis.

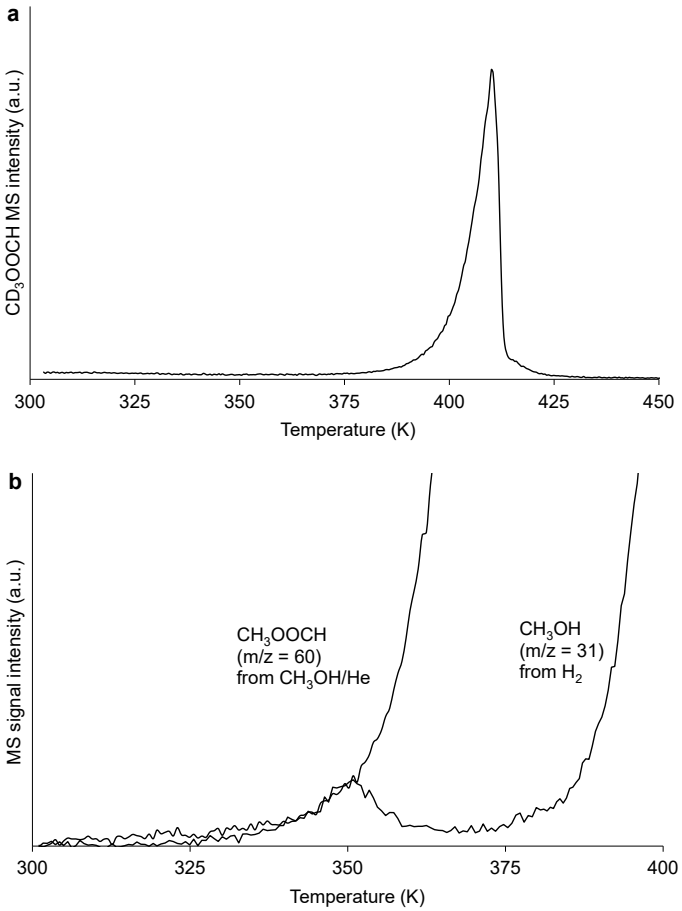

Fig. 4: **(a)** The formation of methyl formate (CD_3OOCH, m/z = 63) as a function of temperature during TPR when HCOO-covered $Cu/ZnO/Al_2O_3$ was heated (1 K min^{-1}) at 1 atm in a 19 NmL min^1 flow of 4.1 mol% CD_3OD in He, 0.5 g cat. See Fig. S7 for details on peak shape. **(b)** Comparison of the onset of methyl formate formation during TPR in 5.5 mol% CH_3OH in He and the onset of methanol formation during TPR in 100% H_2 when formate covered $Cu/ZnO/Al_2O_3$ was subjected to TPR at 1 atm. Ramp: 1 K min^{-1}, Flow: 40 NmL min^{-1}, 0.5 g cat.

Santiago et al. [27] co-fed methyl formate with the synthesis gas, and their results showed that methyl formate was rapidly converted over $Cu/ZnO(/Al_2O_3)$ and Cu/Al_2O_3 catalysts at 473 K and 65 bar. We infer from their data that the additional production of methanol due to methyl formate co-feeding was almost twice as high for $Cu/ZnO/Al_2O_3$ compared to Cu/Al_2O_3, which suggests a preference for R4 on $Cu/ZnO/Al_2O_3$ and a preference for R5 on Cu/Al_2O_3. A preference for R5 on Cu/Al_2O_3 is further supported by the results of Lam et al. [23], who observed decarbonylation of methyl formate over Cu/Al_2O_3 and found that R5 is catalysed by the Al_2O_3 support. By contrast, Cu/ZnO-systems [28] and Cu/SiO_2-systems [25] preserve a high selectivity to R4 versus R5 also at high temperatures, possibly because these supports are less likely to catalyse R5. A pathway via methyl formate would thus explain the observed support dependence in Fig. 1: a net acceleration with increasing conversion for the $Cu/ZnO(/Al_2O_3)$ and Cu/SiO_2 systems, where R4 dominates, whereas R5 dominates for Cu/Al_2O_3 and interrupts the autocatalytic pathway. As previously discussed, the net rate is governed

by the competition between the autocatalytic acceleration and the water inhibition. Consequently, the conversion independent TOF of Cu/Al_2O_3 in Fig. 1 does not rule out that the autocatalytic pathway proceeds to some extent for Cu/Al_2O_3 and partly compensates for inhibiting effects of water, but the efficacy of the autocatalytic pathway is clearly lower for Cu/Al_2O_3 than for the $Cu/ZnO(/Al_2O_3)$ and Cu/SiO_2 systems.

A consequence of the support dependence in the autocatalytic pathway is that conclusions regarding the difference in TOF between $Cu/ZnO(/Al_2O_3)$ and Cu/Al_2O_3 are highly dependent on the conditions. Fig. 1 shows that the ratio between their TOF values increases from a factor of three at differential conditions to more than an order of magnitude at higher conversion. Such variations illustrate the complexity that can emerge in catalytic reactions due to the existence of multiple, parallel reaction pathways with varying dependence on conditions and catalyst composition. This new and more complex picture of the reaction routes over Cu based methanol synthesis catalysts can possibly help to reconcile some apparent disparities between previous conclusions in the literature. Such complexity arising from the existence of multiple reaction pathways should be a general consideration for catalytic processes, since methanol synthesis may not be the only reaction, where multiple, parallel pathways coexist.

3 Conclusion

The discovery of a previously unknown autocatalytic mechanism dominating methanol synthesis at commercial reaction conditions with the industrial catalyst satisfactorily explains the so far unexplained observations. [6, 7] of increasing methanol synthesis rates with increasing conversion. This novel understanding represents a paradigm shift in the mechanistic interpretation of methanol synthesis and shows that important new discoveries can be made even for well-studied and widely applied catalyst systems. Finally, this breakthrough paves the way for further understanding, improvements and process optimization of industrial methanol synthesis.

Acknowledgements

This work was supported by a research grant (9455) from VILLUM FONDEN. We thank Saint Gobain for providing the SiO_2 support.

References

[1] J. Sehested. Industrial and scientific directions of methanol catalyst development. *Journal of Catalysis*, 371:368–375, 2019. doi: 10.1016/j.jcat.2019.02.002.

[2] T. Fujitani, M. Saito, Y. Kanai, T. Kakumoto, T. Watanabe, J. Nakamura, and T. Uchijima. The role of metal oxides in promoting a copper catalyst for methanol synthesis. *Catalysis Letters*, 25 (3-4):271–276, 1994. doi: 10.1007/BF00816307.

[3] K. Murata M. Saito. Development of high performance Cu/ZnO-based catalysts for methanol synthesis and the water-gas shift reaction. *Catal. Surveys Asia*, 8(4):285–294, 2004. doi: 10.1007/s10563-004-9119-y.

[4] R. Burch, S. E. Golunski, and M. S. Spencer. The role of copper and zinc oxide in methanol synthesis catalysts. *Journal of the Chemical Society, Faraday Transactions*, 86(15):2683–2691, 1990. doi: 10.1039/ft9908602683.

[5] I. Nakamura, T. Fujitani, T. Uchijima, and J. Nakamura. A model catalyst for methanol synthesis: Zn-deposited and Zn-free Cu surfaces. *Journal of Vacuum Science & Technology*, 14(3):1464–1468, 1996. doi: 10.1116/1.579970.

[6] J. S. Lee, S. H. Han, H. G. Kim, K. H. Lee, and Y. G. Kim. Effects of space velocity on methanol synthesis from $CO_2/CO/H_2$ over $Cu/ZnO/Al_2O_3$ catalyst. *Korean Journal of Chemical Engineering*, 17(3):332–336, 2000. doi: 10.1007/BF02699049.

[7] M. Sahibzada, I. S. Metcalfe, and D. Chadwick. Methanol Synthesis from $CO/CO_2/H_2$ over $Cu/ZnO/Al_2O_3$ at Differential and Finite Conversions. *Journal of Catalysis*, 174:111–118, 1998. doi: 10.1006/jcat.1998.1964.

[8] O. Cherifi, S. Monteverdi, M. M. Bettahar, M. Foorissier, and V. Perrichon. Kinetics of CO_2 hydrogenation into methanol on a Cu-Zn-Al oxide catalyst. *Bull. Soc. Chim. Fr.*, pages 405–409, 1985.

[9] N. D. Nielsen, J. Thrane, A. D. Jensen, and J. M. Christensen. Bifunctional Synergy in CO Hydrogenation to Methanol with Supported Cu. *Catalysis Letters*, 150:1427–1433, 2020. doi: 10.1007/s10562-019-03036-7.

[10] Y. Yang, C. A. Mims, D. H. Mei, C. H. F. Peden, and C. T. Campbell. Mechanistic studies of methanol synthesis over Cu from $CO/CO_2/H_2/H_2O$ mixtures: The source of C in methanol and the role of water. *Journal of Catalysis*, 298:10–17, 2013. doi: 10.1016/j.jcat.2012.10.028.

[11] R. Chatterjee, S. Kuld, R. V. D. Berg, A. Chen, and W. Shen. Mapping Support Interactions in Copper Catalysts. *Topics in Catalysis*, 62(7-11):649–659, 2019. doi: 10.1007/s11244-019-01150-9.

[12] G. H. Graaf and J. G.M. Winkelman. Chemical Equilibria in Methanol Synthesis Including the Water-Gas Shift Reaction: A Critical Reassessment. *Industrial and Engineering Chemistry Research*, 55(20):5854–5864, 2016. doi: 10.1021/acs.iecr.6b00815.

[13] G. C. Chinchen, P. J. Denny, D. G. Parker, M. S. Spencer, and D. A. Whan. Mechanism of methanol synthesis from $CO_2/CO/H_2$ mixtures over copper/zinc oxide/alumina catalysts: use of ^{14}C-labelled reactants. *Applied Catalysis*, 30(2):333–338, 1987. doi: 10.1016/S0166-9834(00)84123-8.

[14] N. D. Nielsen, A. D. Jensen, and J. M. Christensen. Quantification of Formate and Oxygen Coverages on Cu Under Industrial Methanol Synthesis Conditions. *Catalysis Letters*, 150(9):2447–2456, 2020. doi: 10.1007/s10562-020-03162-7.

[15] H. H. Kung. *Methanol production and use*. CRC Press, 1994. doi: 10.5860/choice.32-3898.

[16] J. Słoczyński, R. Grabowski, J. Janas, and J. Skrzypek. Adsorption model of methanol synthesis reactants on CuO-ZnO-Al_2O_3 catalyst-I. Adsorption on the catalyst. *Chemical Engineering Science*, 46(10):2599–2610, 1991. doi: 10.1016/0009-2509(91)80053-2.

[17] A. V. Tarasov, F. Seitz, R. Schlögl, and E. Frei. In Situ Quantification of Reaction Adsorbates in Low-Temperature Methanol Synthesis on a High-Performance Cu/ZnO:Al Catalyst. *ACS Catalysis*, 9:5537–5544, 2019. doi: 10.1021/acscatal.9b01241.

[18] L. Fan, Y. Sakaiya, and K. Fujimoto. Low-temperature methanol synthesis from carbon dioxide and hydrogen via formic ester. *Applied Catalysis A: General*, 180(1-2):13–15, 1999. doi: 10.1016/S0926-860X(98)00345-7.

[19] N. Tsubaki, M. Ito, and K. Fujimoto. A new method of low-temperature methanol synthesis. *Journal of Catalysis*, 197(1):224–227, 2001. doi: 10.1006/jcat.2000.3077.

[20] P. Reubroycharoen, T. Yamagami, T. Vitidsant, Y. Yoneyama, M. Ito, and N. Tsubaki. Continuous low-temperature methanol synthesis from syngas using alcohol promoters. *Energy and Fuels*, 17(4):817–821, 2003. doi: 10.1021/ef020240v.

[21] S. Lin, A. Oldfield, and D. Klenerman. In-situ studies of polycrystalline copper during methanol synthesis at high pressure using sum frequency generation at surfaces. *Surface Science*, 464(1):1–7, 2000. doi: 10.1016/S0039-6028(00)00706-8.

[22] F. Le Peltier, P. Chaumette, J. Saussey, M. M. Bettahar, and J. C. Lavalley. In situ FT-IR and kinetic study of methanol synthesis from CO_2/H_2 over $ZnAl_2O_4$ and Cu-$ZnAl_2O_4$ catalysts. *Journal of Molecular Catalysis A: Chemical*, 132(1):91–100, 1998. doi: 10.1016/S1381-1169(97)00235-5.

[23] E. Lam, J. José Corral-Pérez, K. Larmier, G. Noh, P. Wolf, A. Comas-Vives, A. Urakawa, and C. Copéret. CO_2 Hydrogenation on Cu/Al_2O_3: Role of the Metal/Support Interface in Driving Activity and Selectivity of a Bifunctional Catalyst. *Angewandte Chemie - International Edition*, 58(39):13989–13996, 2019. doi: 10.1002/anie.201908060.

[24] R. Yang, Y. Zhang, and N. Tsubaki. Rideal-type reaction of formate species with alcohol: A key step in new low-temperature methanol synthesis method. *Catalysis Communications*, 8(11):1829–1833, 2007. doi: 10.1016/j.catcom.2007.02.025.

[25] D. M. Monti, M. S. Walnwrlght, D. L. Trlmm, and N. W. Cant. Kinetics of the Vapor-Phase Hydrogenolysis of Methyl Formate Over Copper on Silica Catalysts. *Industrial and Engineering Chemistry Product Research and Development*, 24(3):397–401, 1985. doi: 10.1021/i300019a012.

[26] M. E. Fakley, H. R. Jennings, and M. S. Spencer. Mechanism of Methanol Synthesis from Carbon Monoxide and Hydrogen on Copper Catalysts. *Journal of Catalysis*, 118:483–486, 1989. doi: 10.1016/0021-9517(89)90334-5.

[27] M. Santiago, K. Barbera, C. Ferreira, D. Curulla-Ferré, P. Kolb, and Pérez-Ramírez J. Byproduct co-feeding reveals insights into the role of zinc on methanol synthesis catalysts. *Catalysis Communications*, 21:63–67, 2012. doi: 10.1016/j.catcom.2012.01.031.

[28] G. Braca, A. M. R. Galletti, N. J. Laniyonu, G. Sbrana, E. Micheli, M. Di Girolamo, and M. Marchionna. Hydrogenolysis of Methyl Formate by H_2/CO Mixtures with $CuO/ZnO/Al_2O_3$ Based Methanol Synthesis Catalysts. *Industrial and Engineering Chemistry Research*, 34(7):2358–2363, 1995. doi: 10.1021/ie00046a018.

Chapter 5

Quantification of Formate and Oxygen Coverages on Cu Under Industrial Methanol Synthesis Conditions

Authors: Niels D. Nielsen[1], Anker D. Jensen[1], Jakob M. Christensen[1]
[1]*Department of Chemical and Biochemical Engineering, Technical University of Denmark, Søltofts Plads Building 229, 2800 Kgs. Lyngby, Denmark*
*__Correspondence to:__ jmc@kt.dtu.dk

DOI:
https://doi.org/10.1007/s10562-020-03162-7

Journal specifications:
Catalysis Letters, 2020, Volume 150, 2447-2456

Date Accepted/Published:
23 February 2020 / 6 March 2020

Abstract

A method for quantifying the surface coverage of adsorbate species for reactions at high pressure and high temperature is presented. Methanol was synthesized from $CO_2/CO/H_2$ (3/29/68) at 523 K and 50 bar on Raney Cu, which yielded a turnover frequency (TOF) per Cu surface atom of $(6.22 \pm 1.04) \times 10^{-3}$ s^{-1}. Rapid quenching by submerging the catalytic reactor in ice water during operation allowed the formate surface coverage on Cu ($\theta_{\text{Cu-HCOO}}$) at reaction conditions to be determined in a subsequent temperature programmed desorption experiment. This yielded $\theta_{\text{Cu-HCOO}} = 0.071 \pm 0.012$ ML and a corresponding TOF per adsorbed HCOO of 0.088 ± 0.021 s^{-1}. CO_2 was essentially observed to be the exclusive source of methanol formation over Raney Cu, as the CO in the syngas could be replaced by N_2 without impact on the methanol formation rate. Based on this observation and the considerable support in the literature for a CO_2-pathway via surface formate on Cu the TOF per surface formate species should represent the true rate of the catalytic cycle in Cu-catalyzed methanol synthesis. Temperature programmed hydrogenation of Raney Cu and unsupported Cu after quenching during high-pressure operation did not indicate a presence of oxygen species (O or OH) on the working Cu surface.

Graphic Abstract

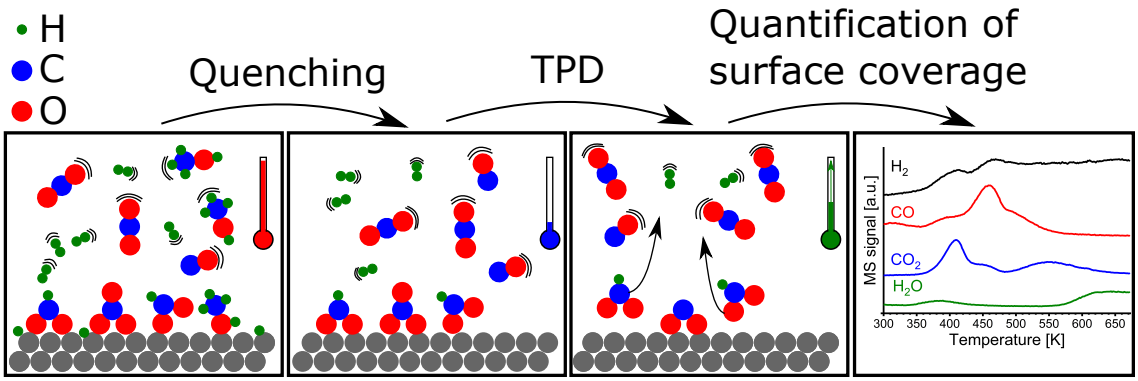

Keywords: Methanol synthesis · Quenching · Copper · Surface coverage quantification

1 Introduction

The surface coverage of adsorbate species under reaction conditions is an important parameter for catalytic reactions. This also applies for the Cu-catalyzed hydrogenation of CO_2 to methanol. Methanol synthesis from CO_2 is a major industrial process from coal or natural gas derived syngas ($CO/CO_2/H_2$) and could have applications for storage of renewable energy in the form of methanol [1]. In methanol synthesis formate (HCOO) is an important adsorbate to quantify on the metallic Cu surface. Formate is an important reaction intermediate as indicated by the correspondence between disappearance of formate on Cu and the appearance of methoxide/methanol [2] and by the similar response of methanol production and formate IR bands to variations in the CO_2 pressure [3, 4]. In situ infrared spectroscopy [3] and sum frequency generation [5] studies on supported and unsupported Cu have unambiguously identified HCOO on the copper surface under methanol synthesis conditions, but no quantification of $\theta_{\text{Cu-HCOO}}$ was provided. Gravimetric analyses [6] show that the industrial $Cu/ZnO/Al_2O_3$ catalyst is highly covered by surface adsorbates in a syngas atmosphere at high pressure, but this technique cannot distinguish between adsorbates on the metal and oxide components of the catalyst. Experimental approaches to quantification of $\theta_{\text{Cu-HCOO}}$ include X-ray photoelectron spectroscopy (XPS) post methanol synthesis (523 K, 18 bar) on Cu single crystals yielding $\theta_{\text{Cu-HCOO}} \cong 0.005$–$0.024$ ML [7] and temperature programmed desorption (TPD) after methanol synthesis (1 atm, 438 K) on Cu/ZnO catalysts resulting in $\theta_{\text{Cu-HCOO}} = 0.083$ ML [2]. However, these studies provide no details regarding the post reaction cooling procedure, which ideally should be infinitely fast to quench the working state of the catalyst. Micro-kinetic models [8–13] based on Cu surface science data or DFT calculations report formate coverages in the entire range from sub-percentage levels to full coverage under industrial methanol synthesis conditions and thus offer no unified estimate of $\theta_{\text{Cu-HCOO}}$. Quantitative estimates of the formate coverage on Cu at industrially relevant conditions (T = 523 K, P = 50 bar [14] are therefore necessary to improve the fundamental understanding of the Cu-catalyzed methanol synthesis and guide kinetic modelling studies.

This study presents a quantitative method for determination of $\theta_{\text{Cu-HCOO}}$ on Cu during methanol synthesis by integrating the desorbed amount of CO_2 in a TPD experiment after rapid quenching of the working catalyst by submerging the reactor in a cooling medium. Coverages are reported as the number of adsorbates relative to the total number of Cu surface atoms. For adsorbates such as HCOO that tend to adopt a bidentate configuration with bonding to two copper atoms full coverage should thus correspond to 0.5 ML. Raney Cu was used to approximate the intrinsic properties of Cu because it was observed to have superior thermal stability compared to unsupported Cu, and studies on Raney Cu thus improve the reliability of the analyses. Comparisons of the TOF for CO_2 hydrogenation for Raney Cu to measurements on unsupported Cu and to single crystal values from the literature are used to support that Raney Cu is a reasonable model for the intrinsic properties of Cu.

2 Experimental

2.1 Catalysts

Raney Cu from Strem Chemicals (The producer reports: 98.9 wt% Cu, 0.81 wt% Al, 0.1 wt% Fe, 0.05 wt% Ni) was received as an aqueous slurry, from which small portions were pre-dried in air at room temperature in a fume hood before loading it into the reactor. This method proved more convenient and no difference in catalytic activity was observed between loading in a wet or dried state. Unsupported Cu was obtained from pure CuO. The CuO used to produce unsupported Cu for activity tests was prepared by precipitation from the nitrate and calcination to CuO in flowing air as described in detail elsewhere [15]. The CuO used to generate unsupported Cu for the TPH experiment searching for adsorbed oxygen on the working copper surface was CuO nanopowder (< 50 nm) from Sigma Aldrich.

2.2 Experimental Setup

Methanol synthesis experiments and subsequent TPD or temperature programmed hydrogenation (TPH) experiments to quantify adsorbate coverages were conducted in a high pressure flow reactor setup described in more detail elsewhere [15]. In brief, the catalyst was placed in a U-tube reactor (SGE Analytical Science borosilicate glass lined steel). The U-tube reactor was placed within an Entech tubular oven that can be opened rapidly to access the reactor. Thereby the U-tube reactor containing the catalyst can be cooled rapidly by raising a liquid (ice water, boiling water or liquid N_2) filled dewar to submerge the U-tube in the cooling liquid. The effluent from the reactor during catalytic reaction and temperature programmed experiments was analyzed using a Thermo Fisher Trace 1300 GC and a Hiden HPR-20 EGA mass spectrometer.

2.3 Activation of Catalyst by H_2 Reduction

Raney Cu is partly oxidized during storage or during the pre-drying of the sample. Thus before any use, Raney Cu was reduced in situ in 5% H_2/N_2 by ramping with 1 K/min to first 448 K and secondly to 523 K with a 2 h dwell time at both temperatures. A similar activation procedure was initially employed for unsupported Cu, but water evolution terminated at the 448 K step indicating complete reduction already at 448 K. Because unsupported Cu was less thermally stable and fully reduced already at 448 K all results reported for unsupported Cu were obtained with pre-reduction at 448 K (1 K/min, 2 h holding time).

2.4 Surface Area Measurement

The specific Cu surface area was evaluated based on the N_2O Reactive Frontal Chromatography (RFC) method [16]. The pre-reduced/activated catalyst was exposed to 19 Nml/min of 1% N_2O/ He at 333 K and ambient pressure. The N_2O consumption was converted into a Cu surface area assuming a Cu:O stoichiometry of 2:1 [17] and an average Cu surface atom density of 1.47 $\times 10^{19}$ atoms/(m^2 Cu) [18] based on the arithmetic mean of the low index Cu facets (Cu(111), Cu(100) and Cu(110)). N_2O-RFC was conducted both in a Quantachrome IQ_2 setup and in the high pressure setup also applied for the quenching and methanol activity experiments. The Raney Cu sample contained residual Al in the form of Al_2O_3. Because of the low surface free energies of oxides compared to metals [19] the oxide components in Raney Cu may represent a larger concentration on the surface. The extent of the Al_2O_3 covered surface was determined from the difference between a BET measurement of the total surface area and an N_2O-RFC measurement of the metallic Cu surface area. A Quantachrome NOVAtouch Gas sorption analyzer was applied to perform the BET analysis. Pre-dried Raney Cu was reduced ex-situ (see Sect. 3.2) with fixed temperature for 4 h (due to use of a larger amount of sample) at 448 K and 2 h at 523 K (ramp 1 K/min) before He flush and cooling to room temperature. The ex-situ activated Raney Cu was then loaded into the NOVAtouch analyzer and vacuum degassed with 10 K/min heating to 423 K and holding for 16 h. Degassed Raney Cu was weighed before performing a standard 6-point BET surface area measurement.

2.5 Measurement of Catalytic Activity and Activation Energy

After catalyst pre-reduction the reactor was pressurized to 50 bar in He (99.999%) and the catalyst was then subjected to the reaction gas, which was mixed from pure H_2 (99.999%) and pre-mixed 9.00 mol% CO_2 in CO or 9.00 mol% CO_2 in N_2 (all gasses from Air Liquide Denmark). The methanol concentration in the effluent was measured by gas chromatography, and the effluent flow was measured by a soap film flowmeter. For determining the activation energy pre-reduced Raney Cu was cooled to 423 K and pressurized in He before feeding with 280 Nml/min of $CO_2/CO/H_2$ (3/29/68). The reaction temperature was raised in steps of 20 K from 423 to 523 K each time with a fixed temperature for 1–2 h to reach a stable methanol effluent concentration, which was quantified by online gas chromatography.

2.6 Procedure to Estimate the Surface Coverage of Formate on Cu

Figure 1 illustrates the experimental procedure for quantifying $\theta_{\text{Cu-HCOO}}$. After pre-reduction of Raney Cu, the reactor was at 523 K pressurized in He to 50 bar before feeding 280 Nml/min of $CO_2/CO/H_2 = 3/29/68$ at constant temperature and pressure. All measurements were conducted at differential conditions with a maximum of 0.10 mol% methanol in the effluent gas stream. Once the methanol signal (evaluated by the MS using $m/z = 31$) reached its peak level, the methanol production was quantified by a GC measurement, before the catalyst was rapidly cooled in the reaction gas by different cooling methods described below. At room temperature or below, the syngas pressure was released, and the reactor was thoroughly purged with He before conducting a TPD in flowing He with a 2 K/min heating ramp.

Fig. 1: Block diagram of the protocol for quantifying the surface adsorbate coverage at reaction conditions on Raney Cu

Figure 2 shows the cooling profile measured by two thermocouples (TCs) – one placed inside the reactor tube at the top of the catalyst bed (red) and one on the external surface of the reactor tube at the bottom of the catalyst bed (blue). The cooling was set to start at $t = 0$ in Fig. 2 by swiftly opening the oven and moving a dewar filled with the cooling liquid (ice water was used in Fig. 2) vertically upwards to cool the U-shaped reactor (see Fig. 2), and after a few seconds both TCs were at (or below) room temperature. The cooling profile experienced by the catalyst bed is an average of the temperature profiles measured by the two TCs, and this average is plotted as T_{ave} in Fig. 2. In the case of cooling with boiling water, the dewar was removed after cooling to 383 K and further cooling was due to ambient air circulation around the U-shaped reactor. Cooling by static air occurred by opening the oven and allowing the reactor to cool by the ambient room temperature air. Two additional repetition experiments confirmed the reproducibility of quenching profiles with ice water (see supplementary information Fig. S1). After cooling to room temperature or below, the pressure was released, and the syngas was thoroughly flushed out with He before removing the dewar with the cooling liquid (except for boiling water where the dewar was removed at 383 K) under continuous He flush and allowing the reactor to heat naturally to room temperature, if the temperature during He purging was below room temperature. Starting from room temperature, a TPD was carried out with 2 K/min heating to 673 K in a He flow. The He flow was calibrated for each experiment using a soap film bubble flow meter and was within the interval from 42 to 45 Nml/min. A Hiden EGA mass spectrometer continuously measured desorbing CO_2 ($m/z = 44$), CO ($m/z = 28$), H_2O ($m/z = 18$) and H_2 ($m/z = 2$). The CO_2 MS signal was calibrated using a certified 500 ppm CO_2 in He gas mixture from Air Liquide Denmark. This allowed determination of $\theta_{\text{Cu-HCOO}}$ from integration of the calibrated CO_2 signal. Desorbed H_2 could in principle also be used to quantify $\theta_{\text{Cu-HCOO}}$, since HCOO on Cu decomposes to CO_2 and H_2, but the hydrogen desorption was observed to be very complex with multiple peaks - most likely from decomposition of species on both the metal and Al_2O_3 parts of the surface yielding H_2. It was therefore concluded that it was too complex to quantify $\theta_{\text{Cu-HCOO}}$ based on desorbed H_2.

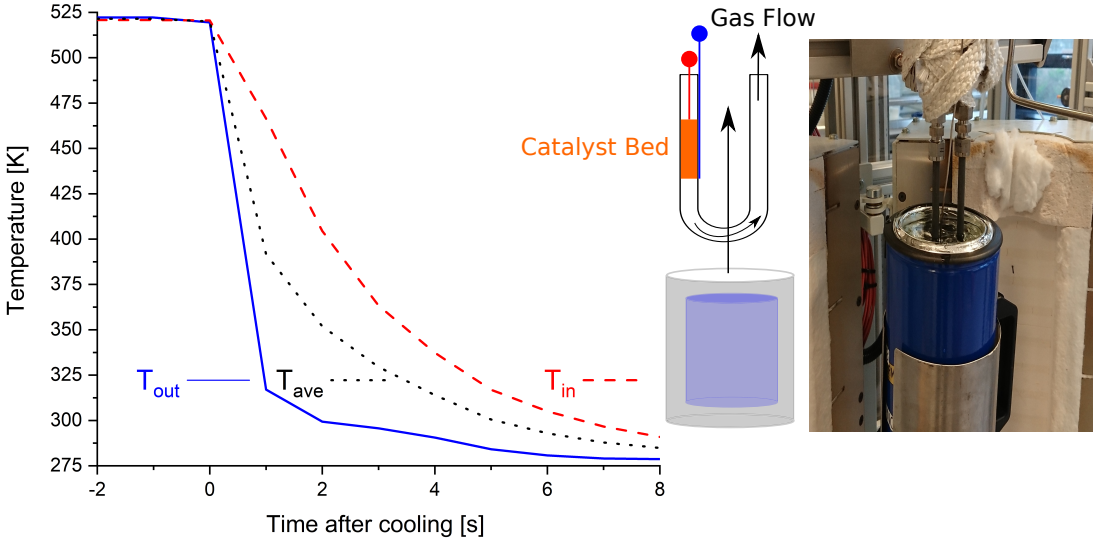

Fig. 2: Left: Cooling of the catalyst in the reaction mixture started at t = 0, while two thermocouples (TCs) positioned inside at the top (red, dashed) of the catalyst bed (orange) and outside at the bottom of the catalyst bed (blue, solid) monitored the cooling process. Right: Schematic view of cooling process by raising the filled dewar to sub-merge and cool the U-tube including positions of the thermocouples (red and blue). Far right: Image of the U-tube submerged in ice water

2.7 Evaluation of the Coverage of Adsorbed Oxygen by Temperature Programmed Hydrogenation

Two TPH experiments were designed to evaluate the coverage of adsorbed oxygen species (O or OH) on the Cu surface under reaction conditions. Both TPHs were performed in 60 Nml/min flow of 5% H_2/N_2 with 2 K/min heating ramp from 300 to 673 K. In one experiment prereduced Cu was oxidized by 1 mol% N_2O in He at 333 K, which yields half a monolayer of oxygen on Cu as verified by studies [16, 17] benchmarking N_2O-RFC against BET surface area measurements. Next, the half monolayer of oxygen was hydrogenated in a TPH and formed H_2O was quantified to calibrate the H_2O (m/z = 18) MS signal by equating the integral H_2O signal to 0.5 ML of O. In a second experiment the working catalyst was quenched using ice water (see Sect. 2.5) and then subjected to a TPH instead of TPD. The oxygen coverage on the working catalyst was estimated from integration of the H_2O MS signal acquired during TPH of the quenched catalyst. A blank TPH experiment with quartz wool but without catalyst (but similar to the procedure for the second experiment) showed no gas desorption thus verifying that products formed in the TPH/TPD experiments were associated with the catalyst.

2.8 X-Ray Photo-Electron Spectroscopy on Raney Cu and Unsupported CuO

XPS analyses were performed on Raney Cu and unsupported CuO to qualitatively assess the surface composition of Raney Cu. The XPS source was a monochromatic and micro-focused Al K-Alpha source (1486.6 eV) with a 180° double focusing hemispherical analyzer and a 128-channel detector from Thermo Scientific with an optimal base pressure of 6×10^{-9} mbar. XPS experiments were performed with a chamber pressure of 4×10^{-8} mbar and analysed using the Avantage software. Survey spectra were acquired for fresh unsupported CuO, predried Raney Cu and predried and then reduced Raney Cu. Survey spectra were recorded for all three samples and extra spectra were recorded to detect Al in Raney Cu.

3 Results and Discussion

3.1 Surface composition of Raney Cu

In agreement with previous XPS studies [20] on Raney Cu ex situ XPS measurements (see supplementary material Figs. S14–S17) on the pre-reduced Raney Cu sample showed that there were two peaks in the 70–80 eV range, namely a Cu3p peak at ca. 78 eV and an Al2p peak at 75 eV (see Fig. S16). The binding energy of the Al2p peak suggests that the Al was in an oxidized Al_2O_3 form [20–23]. This shows that the surface of Raney Cu is partly covered by Al_2O_3. N_2O-RFC yielded a Cu metal area of 5.18 m^2/g for Raney Cu, whereas the BET area of the pre-reduced catalyst, which includes both the metallic Cu surface and the Al_2O_3 covered surface, yielded 13.94 m^2/g. Consequently, the Al_2O_3 covered the major part of the surface (by difference between BET and N_2O- RFC around 8.8 m^2/g) despite Al constituting less than 1 wt% of Raney Cu.

3.2 Benchmarking Against the Intrinsic Properties of Cu

The present work seeks to evaluate the intrinsic properties of Cu at a realistic methanol synthesis temperature of 523 K, and Raney Cu was used because it has a reasonable thermal stability at these conditions. However, as discussed above the Raney Cu sample also had an extensive oxide surface and thus sites such as the Cu/oxide interface that are not present in pure Cu. To evaluate, if Raney Cu is a reasonable approximation of the intrinsic properties of Cu concerning methanol synthesis, the rate of CO_2 hydrogenation to methanol was compared to unsupported Cu (0.494 m^2 Cu/g_{cat}). Both Raney Cu and unsupported Cu were tested at 498 K in CO_2/ $N_2/H_2 = 3/29/68$ at 50 bar of pressure and showed very similar TOFs of 3.65×10^{-3} s^{-1} and 2.78×10^{-3} s^{-1}, respectively (Table 1). The evaluation was performed at 498 K rather than 523 K, as measurements of unsupported Cu were unreliable at 523 K, where it transited from powder to a massive pellet. Rapid activity loss for unsupported Cu at 523 K is also known in the literature [24]. Unsupported Cu is prone to sintering due to a low Hüttig temperature (408 K) above which surface mobility becomes significant [25], and copper particles are known to agglomerate above 473 K [26]. Given the propensity of unsupported Cu towards sintering the TOF agreement within ca. 25% between unsupported and Raney Cu is taken as evidence that Raney Cu is a good approximation of the intrinsic properties of Cu. By assuming a linear hydrogen pressure dependence, as also employed by others [11], and utilizing reported activation energies under the assumption of an Arrhenius-type temperature dependence, previously reported [27, 28] TOF-values for CO_2 hydrogenation on Cu(111) and polycrystalline Cu were extrapolated to the present conditions (498 K, $p_{H_2} = 34$ bar). Table 1 compares these extrapolated TOF-values [27, 28] to the ones for Raney Cu and unsupported Cu obtained in this study, and the results generally show a good agreement. Based on the correspondence in TOF between Raney Cu and both unsupported Cu and previous single crystal studies it is concluded that Raney Cu is a reasonably good approximation to the intrinsic properties of copper. The methanol synthesis rate in $CO/CO_2/H_2$ was measured at 50 bar and temperatures ranging from 423 to 523 K to determine the activation energy for the methanol synthesis on Raney Cu. Figure 3 shows an Arrhenius plot determined from these measurements, which yields an apparent activation energy of 55.3 kJ/mol. Previous measurements [15] in the same setup on unsupported Cu at 50 bar and a CO_2/H_2 feed suggest an activation energy of 60 kJ/mol for unsupported Cu, which within the uncertainty also indicates a reasonable agreement between Raney Cu and unsupported Cu in terms of the activation energy.

3.3 Formate Quantification by a TPD Method

Raney Cu was allowed to reach steady state in $CO_2/CO/H_2$ at 50 bar and 523 K. At that point the activity was measured by gas chromatography, and the catalyst was rapidly quenched by submerging the U-tube reactor in ice water. The ice water cooling yielded reproducible and rapid cooling profiles (see Fig. S1). The quenched sample was then subjected to a TPD, and Fig. 4 shows the evolution of CO, CO_2, H_2 and H_2O during the TPD. The reproducibility of the obtained TPD profiles was verified by three repeated experiments (see also Figs. S2 and S3). Figure 5 shows the CO_2 desorption deconvoluted into three Gaussian peaks termed α, β, and γ.

Table 1: TOF values for Raney Cu and unsuported Cu at 498 K, 50 bar, $CO_2/N_2/H_2$ = 3/29/68 and TOF-values from single crystal studies extrapolated to the conditions of this study (T = 498 K, p_{H_2} = 34 bar using their reported activation energies

Catalyst	T [K]	p_{H_2} [bar]	E_{act} reported [kJ/mol]	TOF reported [s^{-1}]	TOF extrapolated [s^{-1}]	References
Cu(111)	523	13.5	73.6	2.06×10^{-3}	2.07×10^{-3}	[27]
Polycrystal. Cu	510	4.67	77	1.2×10^{-3}	5.7×10^{-3}	[28]
Unsupported Cu	498	34		2.78×10^{-3}	2.78×10^{-3}	This study
Raney Cu	498	34	55.3	3.65×10^{-3}	3.65×10^{-3}	This study

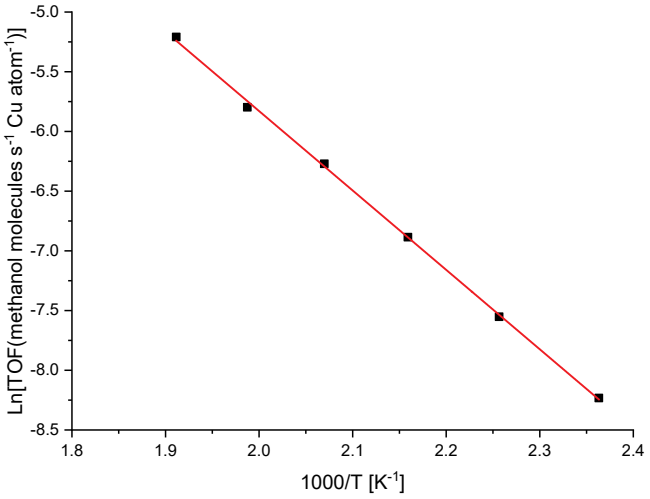

Fig. 3: Arrhenius plot for methanol synthesis over Raney Cu exposed to reaction conditions (50 bar, $CO_2/CO/H_2$ = 3/29/68, GHSV = 6.7 $\times 10^4$ $Nml/g_{cat}/h$).

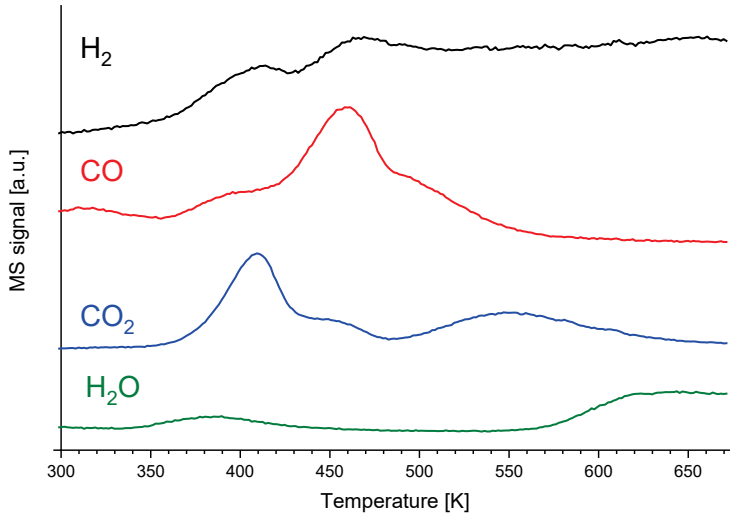

Fig. 4: Measured gas profiles during the TPD with 2 K/min as heating ramp after methanol synthesis at 523 K, 50 bar pressure in $CO_2/CO/H_2$ = 3/29/68 and subsequent quenching. MS signals are vertically off-set on the linear y-axis for clarity.

The main CO_2 desorption (the β-peak) occurred at 410 K. In a Redhead analysis [29, 30] with the commonly applied prefactor of 10^{13} s^{-1} this temperature corresponds to an activation energy for desorption of 122 kJ/mol, which is consistent with formate desorption from Cu [31–34]. Fujita et al. [2] also observed that the CO_2 TPD peak corresponding to the β-peak in Fig. 5 scaled with the Cu surface area for a range of formate covered Cu/ZnO samples. This further supports that the CO_2 β-peak arises from a species on the Cu surface. Although the hydrogen desorption was too diffuse to be used in quantification, the CO_2 β-peak also coincided with a shoulder in the H_2 desorption, which is consistent with formate on Cu yielding desorption of both CO_2 and H_2.

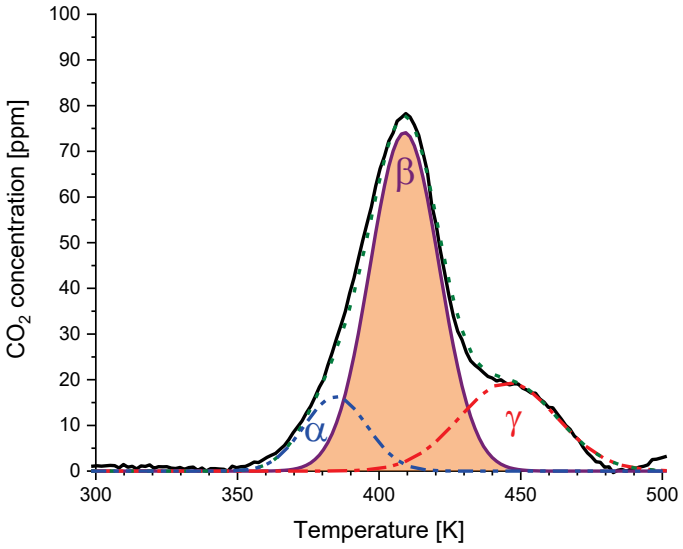

Fig. 5: Peak fitting to the measured black solid CO_2 desorption line using three Gaussian peaks (α, β and γ), which sum up to the dotted green profile. HCOO was quantified by the integrated area (orange) under the CO_2 β-peak. Heat ramp: 2 K/min. He flow: 42.5 Nml/min.

On this basis the CO_2 β-peak was unambiguously assigned to formate on Cu. The β-peak was therefore used to determine $\theta_{\text{Cu-HCOO}}$, and the orange area in Fig. 5 marks the area integrated to calculate the formate coverage. The main CO desorption peak at 464 K was assigned to methoxide on the Al_2O_3 part of the surface. The main argument for this assignment is that Tamm et al. [35] observed concurrent desorption of CO and H_2 and to a lesser extent CO_2 at a similar temperature during TPD after methanol adsorption on γ-Al_2O_3. The CO_2 γ-peak coincided with the CO desorption at 464 K and was therefore most likely also related to desorption from the oxide surface similar to the one observed by Tamm et al. [35]. Desorption above 550 K must originate from highly stable adsorbed species most likely on the oxide and therefore not likely to influence the methanol synthesis reaction at 523 K. It was reported that formate on Al_2O_3 may desorb as CO and H_2O [36] at higher temperatures, and Cu might also facilitate water–gas shift [37, 38] of these species to CO_2 and H_2. The higher temperature desorption was therefore assigned to the oxide surface. As discussed in Sect. 3.1 the oxide surface presents a major fraction of the total surface area, which supports that species on the oxide contributes significantly to desorbed gas species during post reaction TPD. The lower temperature desorption below approximately 383 K was attributed to chemisorbed H_2O and reactants on the sample. This includes the small, low temperature α-CO_2 peak in Fig. 5. As the α-peak is centered at ca. 370 K, where CO_2 chemisorbed on Al_2O_3 is reported [39] to desorb, the α-peak is attributed to chemisorbed CO_2 on the alumina part of the surface and not included in the formate quantification. However, given the small size of the α-peak this does not change the conclusions markedly.

3.4 Evaluation of Cooling Methods

We have previously [15] compared the rates of methanol formation from CO and CO_2 on Cu with the same Cu-based materials investigated here, and found that the rate from CO_2 is approximately an order of magnitude faster than the rate from CO. Additionally, an experiment was performed, where the CO in the syngas was exchanged with N_2, and this had essentially no influence on the methanol formation rate (see Fig. S12). Consequently, there should be little uncertainty in attributing the entire methanol production to the pathway from CO_2. There is considerable experimental data to support that the pathway from CO_2 is via formate [2–4], and the formation and hydrogenation of formate can be expressed in a simplified manner by reactions R1 and R2 (with HCOO* denoting adsorbed formate and * denoting an active site) [8, 40]:

$$CO_2 + \frac{1}{2}H_2 + {}^\star \rightleftharpoons HCOO^\star \qquad \{R1\}$$

$$HCOO^\star \xrightarrow{\text{Hyd.}} CH_3OH + {}^\star \qquad \{R2\}$$

To provide the true working coverage of the catalyst the quenching must therefore be rapid enough to avoid that neither R1 nor R2 change the coverage during cooling. To evaluate this the quenching rate was varied using different cooling media, and the measured formate coverage was compared after cooling with ice water, boiling water, liquid N_2, and static air. Table 2 summarizes the measured TOF and $\theta_{\text{Cu-HCOO}}$ in 3 tests quenching the reaction in ice water, and Fig. 6 illustrates the relation between the measured formate surface coverage and the time it took to reach 383 K during quenching with the various cooling media (showing that ice water was most efficient). Table 2 shows that the TOF at 523 K is (6.22 ± 1.04) $\times 10^{-3}$ s^{-1}. Extrapolation of previously measured [40] rates for R1 on Cu to 523 K suggests that R1 should be 1–2 orders of magnitude faster than the TOF. Consequently, R1 should be quasi equilibrated under reaction conditions, and R2 is the rate limiting step in the reaction.

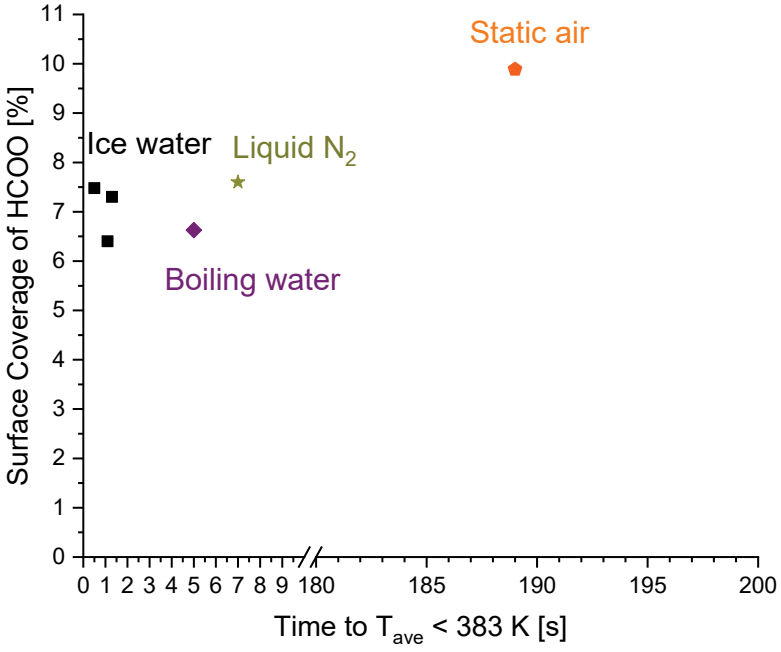

Fig. 6: Formate surface coverage as function of the time it takes the average temperature of the two thermocouples to reach 383 K using different cooling methods.

Adsorption reactions are by necessity exothermic to compensate for the loss of entropy, and this is also the case for R1 [40]. This means that during cooling the reverse reaction of R1 will stop before

Table 2: Experimental parameters for each experiment with methanol synthesis over Raney Cu at 523 K, 50 bar in $CO_2/N_2/H_2$ = 3/29/68 followed by quenching and TPD

	Cooling method	Ave. time to 383 K [s]	m_{cat} [mg_{cat}]	TOF [CH_3OH molec. (Cu surface atom)$^{-1}$ s^{-1}]	θ_{HCOO} [ML]
Test 1	Ice water	1.1	258.43	5.63×10^{-3}	0.0640
Test 2	Ice water	0.5	254.36	6.46×10^{-3}	0.0748
Test 3	Ice water	1.4	259.54	6.59×10^{-3}	0.0730
Average		1		$(6.22 \pm 1.04) \times 10^{-3}$	0.071 ± 0.012

Uncertainties correspond to two standard deviations and the specific Cu surface areas of Raney Cu was 5.18 m^2/g_{cat}

the forward reaction. Consequently, if the cooling is too slow, R1 will raise the HCOO coverage during cooling. Previous measurements [40] suggest that at 383 K the forward rate of R1 is 0.0013 formate molecules/Cu surface atom/second, which means that it would take several hundred seconds to cover the surface with formate. This is so slow compared to the cooling that R1 can be regarded as terminated at 383 K. Figure 6 therefore evaluates the measured coverage as a function of time required to reach 383 K with various cooling methods. Figure 6 shows that water based cooling methods yield a measured coverage that within uncertainty is independent of cooling rate, and this is taken as evidence that the cooling speed has reached the point, where the quenching is sufficiently fast to avoid that R1 modifies the coverage during cooling. Using liquid N_2 as a cooling medium gives a slightly slower cooling. This is rationalized from a poor heat transfer in the gas film created when N_2 boils around the hot reactor tube. However, the coverage obtained with the slower liquid N_2 cooling seems, within the uncertainty, to be identical to the coverage obtained with ice water cooling. By contrast, cooling in static air is considerably slower, and Fig. 6 shows that this slower cooling does result in an increased coverage as expected from the exothermic nature of R1. Table 2 shows that quenching using ice water, which is concluded to be fast enough to avoid being influenced by R1 yields $\theta_{Cu\text{-}HCOO} = 0.071 \pm 0.012$ ML (two standard deviations) and a corresponding TOF per adsorbed HCOO of $(6.22 \pm 1.04) \times 10^{-3}$ $s^{-1}/(0.071 \pm 0.012$ ML) = 0.088 ± 0.021 s^{-1}. This suggests that each surface formate species on average is converted to methanol every $1/(0.088\ s^{-1}) \cong 11.4$ s at 523 K. This represents the time it would take R2 to remove all formate on the surface, if no new formate is generated. As quenching to below 383 K occurred rapidly compared to this lifetime, which increases exponentially with decreasing temperature, the reported formate coverage after ice water quenching was not significantly affected by R2. Since the quenching using ice water was concluded to be sufficiently fast to avoid major alterations of the coverage by both R1 and R2 during quenching the three ice water quenching tests (see Figs. 2, 6, and S1) were used to obtain the best estimate of the formate coverage on the working Cu surface, which as summarized in Table 2 is $\theta_{Cu\text{-}HCOO} = 0.071$ ML. Among existing micro-kinetic models the best agreement is with the model by Askgaard et al. [8] using Cu surface science data and the model by Grabow and Mavrikakis [9] using DFT calculations on Cu(111) both suggesting HCOO coverages of several percent at conditions similar to those used in the present study. With the strong indications of a mechanism via formate [2–4], and assuming that all the detected formate on Cu participates in the reaction, the determined TOF per adsorbed HCOO of 0.088 ± 0.021 s^{-1} should represent the best estimate of the true rate of the catalytic cycle for methanol synthesis on Cu at industrially relevant conditions.

3.5 Oxygen Coverage on Cu During Methanol Synthesis

Previous studies [14, 33, 41, 42], which during methanol synthesis have flushed the reactor with inert gas before cooling and then quantified the free Cu surface with N_2O-RFC, have observed the existence of oxygen species on the Cu surface of the working catalyst. However, the existence of adsorbed oxygen has caused debate [43–46], as it is surprising that any noteworthy oxygen buildup should occur in a reducing gas mixture at high pressure. Nevertheless, recent in situ ambient pressure XPS

studies [47] also observed oxygen on the Cu surface during CO_2 hydrogenation and thus call for further quantification of the oxygen coverage on Cu under industrially relevant methanol synthesis conditions. Quantification of the oxygen coverage on the working Cu surface was based on the evolution of H_2O during two TPH experiments on Raney Cu pre-covered by either (1) 0.5 ML of oxygen after oxidation by 1 mol% N_2O at 333 K or (2) reaction intermediates after quenching during methanol synthesis. Figure 7 displays H_2O formation profiles after the N_2O oxidation (post N_2O) and the methanol synthesis and ice water quenching (post quenching). A minor water evolution was observed during TPH of the quenched sample, but such water evolution also occurred in TPH of a freshly reduced sample (see Fig. S13). The water evolution was therefore attributed to water impurities in the TPH feed that adsorb on the sample prior to the start of the TPH and then desorb in the initial stages of the TPH instead of being due to reduction of oxygen species on the Cu surface. Consequently, the oxygen coverage on the working Cu surface was concluded to be below the detection limit of our TPH method.

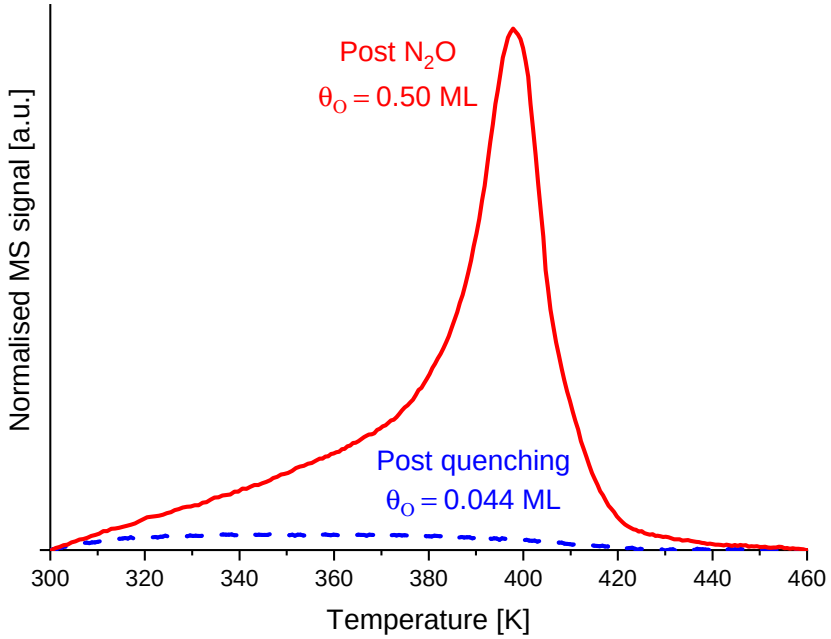

Fig. 7: The H_2O signal in TPH as a function of temperature with Raney Cu after quenching during methanol synthesis at 523 K, 50 bar of pressure in $CO_2/CO/H_2$ = 3/29/68 (post quenching) or after N_2O-RFC on pre-reduced Raney Cu (post N_2O). TPH conditions are 2 K/min in 60 Nml/min of 5% H_2/N_2. Both signals are individually and linearly baseline corrected using the specific data points at T = 300 K and T = 460 K for each experiment.

4 Conclusion

A reproducible and quantitative method for estimating the surface coverage of adsorbate species under high temperature and high-pressure reactions conditions was outlined. Ice water provided the fastest cooling rate and fixated the surface coverages obtained at reaction conditions. Activity measurements in $CO_2/CO/H_2$ at 523 K and 50 bar of pressure yielded a TOF per Cu surface atom of (6.22 ± 1.04) $\times 10^{-3}$ s^{-1} for Raney Cu (all uncertainties are here two std. deviations). Based on the quenching method with ice water, the surface coverage of formate was determined to be $\theta_{Cu\text{-}HCOO}$ = 0.071 ± 0.012 ML for Raney Cu yielding a corresponding TOF per adsorbed HCOO of 0.088 ± 0.021 s^{-1}. Given the strong indications that the methanol synthesis proceeds via formate this TOF per adsorbed HCOO should represent the best estimate of the true rate of the catalytic cycle. Such estimations are vital for improving the understanding of kinetic reactions and guide kinetic modelling studies. Comparisons of Raney Cu to unsupported Cu and reports from single crystal studies suggested that Raney Cu, at least in terms of methanol synthesis activity and CO_2 hydrogenation properties, was a good approximation to pure Cu. TPH of the Raney Cu surface post methanol synthesis suggested that the oxygen coverage on the working Cu surface was below the detection limit of our TPH method.

Acknowledgements

This work was supported by the Villum Foundation Center for Science of Sustainable Fuels and Chemicals, Villum Foundation V-SUSTAIN Grant 9455.

Errata

"$CO_2/N_2/H_2$" in the table caption of table 2 should correctly be "$CO_2/CO/H_2$". Fig. S7 and S8 were identical in the original published paper. The correct fig. S7 is inserted in this thesis work in the supplementary part for this paper. Original figure captions for Figs. S7 and S8 are correct.

References

[1] J. Sehested. Industrial and scientific directions of methanol catalyst development. *Journal of Catalysis*, 371:368–375, 2019. doi: 10.1016/j.jcat.2019.02.002.

[2] S. Fujita, M. Usui, H. Ito, and N. Takezawa. Mechanisms of Methanol Synthesis from Carbon Dioxide and from Carbon Monoxide at Atmospheric Pressure over Cu/ZnO. *Journal of Catalysis*, 157(2):403–413, 1995. doi: 10.1006/jcat.1995.1306.

[3] Y. Amenomiya and T. Tagawa. Infrared study of methanol synthesis from CO_2 and H_2 on supported copper-zinc oxide catalysts. *Proc. of 8th Int. Congress on Catal*, pages 557–567, 1984.

[4] F. Le Peltier, P. Chaumette, J. Saussey, M. M. Bettahar, and J. C. Lavalley. In situ FT-IR and kinetic study of methanol synthesis from CO_2/H_2 over $ZnAl_2O_4$ and Cu-$ZnAl_2O_4$ catalysts. *Journal of Molecular Catalysis A: Chemical*, 132(1):91–100, 1998. doi: 10.1016/S1381-1169(97)00235-5.

[5] S. Lin, A. Oldfield, and D. Klenerman. In-situ studies of polycrystalline copper during methanol synthesis at high pressure using sum frequency generation at surfaces. *Surface Science*, 464(1):1–7, 2000. doi: 10.1016/S0039-6028(00)00706-8.

[6] A. V. Tarasov, F. Seitz, R. Schlögl, and E. Frei. In Situ Quantification of Reaction Adsorbates in Low-Temperature Methanol Synthesis on a High-Performance Cu/ZnO:Al Catalyst. *ACS Catalysis*, 9:5537–5544, 2019. doi: 10.1021/acscatal.9b01241.

[7] I. Nakamura, T. Fujitani, T. Uchijima, and J. Nakamura. A model catalyst for methanol synthesis: Zn-deposited and Zn-free Cu surfaces. *Journal of Vacuum Science & Technology*, 14(3):1464–1468, 1996. doi: 10.1116/1.579970.

[8] T. S. Askgaard, J. K. Nørskov, C. V. Ovesen, and P. Stoltze. A Kinetic Model of Methanol Synthesis. *Journal of Catalysis*, 156:229–242, 1995. doi: 10.1006/jcat.1995.1250.

[9] L. C. Grabow and M. Mavrikakis. Mechanism of Methanol Synthesis on Cu through CO_2 and CO Hydrogenation. *ACS Catalysis*, 1:365–384, 2011. doi: 10.1021/cs200055d.

[10] W. Janse Van Rensburg, J. A. Van Den Berg, M. A. Petersen, M. S. Datt, and P. Van Helden. On the Kinetic Interpretation of DFT-Derived Energy Profiles: Cu-Catalyzed Methanol Synthesis. *Catalysis Letters*, 145(2):559–568, 2015. doi: 10.1007/s10562-014-1407-1.

[11] F. Studt, M. Behrens, R. Schlögl, E. L. Kunkes, N. Thomas, S. Zander, A. Tarasov, J. Schumann, E. Frei, J. B. Varley, F. Abild-Pedersen, and J. K. Nørskov. The Mechanism of CO and CO_2 Hydrogenation to Methanol over Cu-Based Catalysts. *ChemCatChem*, 7(7):1105–1111, 2015. doi: 10.1002/cctc.201500123.

[12] M. S. Tameh, A. K. Dearden, and C. Huang. Accuracy of Density Functional Theory for Predicting Kinetics of Methanol Synthesis from CO and CO_2 Hydrogenation on Copper. *Journal of Physical Chemistry C*, 122(31):17942–17953, 2018. doi: 10.1021/acs.jpcc.8b06498.

[13] I. Chorkendorff, P. A. Taylor, and P. B. Rasmussen. Synthesis and hydrogenation of formate on Cu(100) at high pressures. *Journal of Vacuum Science & Technology A*, 10(4):2277–2281, 1992. doi: 10.1116/1.577930.

[14] G. C. Chinchen, K. C. Waugh, and D. A. Whan. The activity and state of the copper surface in methanol synthesis catalysts. *Applied Catalysis*, 25(C):101–107, 1986. doi: 10.1016/S0166-9834(00)81226-9.

[15] N. D. Nielsen, J. Thrane, A. D. Jensen, and J. M. Christensen. Bifunctional Synergy in CO Hydrogenation to Methanol with Supported Cu. *Catalysis Letters*, 150:1427–1433, 2020. doi: 10.1007/s10562-019-03036-7.

[16] G. C. Chinchen, C. M. Hay, H. D. Vandervell, and K. C. Waugh. The measurement of copper surface areas by reactive frontal chromatography. *Journal of Catalysis*, 103(1):79–86, 1987. doi: 10.1016/0021-9517(87)90094-7.

[17] R. Chatterjee, S. Kuld, R. V. D. Berg, A. Chen, and W. Shen. Mapping Support Interactions in Copper Catalysts. *Topics in Catalysis*, 62(7-11):649–659, 2019. doi: 10.1007/s11244-019-01150-9.

[18] O. Hinrichsen, T. Genger, and M. Muhler. Chemisorption of N_2O and H_2 for the Surface Determination of Copper Catalysts. *Chemical Engineering & Technology*, 23(11):956–959, 2000. doi: 10.1002/1521-4125(200011)23:11⟨956::AID-CEAT956⟩3.0.CO;2-L.

[19] S. H. Overbury, P. A. Bertrand, and G. A. Somorjai. The Surface Composition of Binary Systems. Prediction of Surface Phase Diagrams of Solid Solutions. *Chemical Reviews*, 75(5):547–560, 1975. doi: 10.1021/cr60297a001.

[20] J. Laine, G. Ceballos, F. Severino, G. Castro, and C. Rojas. Structure and activity of a Raney copper film catalyst. *Catalysis Letters*, 10(1-2):11–17, 1991. doi: 10.1007/BF00764731.

[21] H. Li, A. Belkind, F. Jansen, and Z. Orban. An in situ XPS study of oxygen plasma cleaning of aluminum surfaces. *Surface and Coatings Technology*, 92(3):171–177, 1997. doi: 10.1016/S0257-8972(97)00079-0.

[22] E. Paparazzo. XPS and Auger Spectroscopy on mixtures of the oxides SiO_2, Al_2O_3, Fe_2O_3, and Cr_2O_3. *Journal of Electron Spectroscopy and Related Phenomena*, 43:97–112, 1987. doi: 10.1016/0368-2048(87)80022-1.

[23] J. A. Rotole and P. M. A. Sherwood. Gamma-Alumina (γ-Al_2O_3) by XPS. *Surface Science Spectra*, 5(1):18–24, 1998. doi: 10.1116/1.1247852.

[24] W. X. Pan, R. Cao, D. L. Roberts, and G. L. Griffin. Methanol synthesis activity of Cu/ZnO catalysts. *Journal of Catalysis*, 114(2):440–446, 1988. doi: 10.1016/0021-9517(88)90047-4.

[25] M. Argyle and C. Bartholomew. Heterogeneous Catalyst Deactivation and Regeneration: A Review. *Catalysts*, 5:145–269, 2015. doi: 10.3390/catal5010145.

[26] G. C. Chinchen, K. Mansfield, and M. S. Spencer. The methanol synthesis: How does it work? *Chemtech*, 20:692–699, 1990.

[27] I. Nakamura, T. Fujitani, T. Uchijima, and J. Nakamura. A model catalyst for methanol synthesis: Zn-deposited and Zn-free Cu surfaces. *Journal of Vacuum Science & Technology A*, 14(3):1464–1468, 1996. doi: 10.1063/1.451126.

[28] J. Yoshihara, S. C. Parker, A. Schafer, and C. T. Campbell. Methanol synthesis and reverse water-gas shift kinetics over clean polycrystalline copper. *Catalysis Letters*, 31(4):313–324, 1995. doi: 10.1007/BF00808595.

[29] P. A. Redhead. Chemisorption on polycrystalline tungsten. *Transaction of the Faraday Society*, 57:641–656, 1961. doi: 10.1039/TF9615700641.

[30] J. W. Niemantsverdriet and I. Chorkendorff. *Concepts of Modern Catalysis and Kinetics 2nd. edition*. Wiley-VCH, 2007. doi: 10.1002/3527602658.

[31] E. Iglesia and M. Boudart. Decomposition of formic acid on copper, nickel, and copper-nickel alloys. II. Catalytic and temperature-programmed decomposition of formic acid on Cu/SiO_2, Cu/Al_2O_3, and Cu powder. *Journal of Catalysis*, 81(1):214–223, 1983. doi: 10.1016/0021-9517(83)90159-8.

[32] M. Bowker. Chemisorption and industrial catalytic processes. *Vacuum*, 33(10-12):669–685, 1983. doi: 10.1016/0042-207X(83)90591-2.

[33] M. Bowker, R. A. Hadden, H. Houghton, J. N K Hyland, and K. C. Waugh. The mechanism of methanol synthesis on copper/zinc oxide/alumina catalysts. *Journal of Catalysis*, 109(2):263–273, 1988. doi: 10.1016/0021-9517(88)90209-6.

[34] Y. Yao and F. Zaera. Adsorption and thermal chemistry of formic acid on clean and oxygen-predosed Cu(110) single-crystal surfaces revisited. *Surface Science*, 646:37–44, 2016. doi: 10.1016/j.susc.2015.06.007.

[35] S. Tamm, H. H. Ingelsten, M. Skoglundh, and A. E. C. Palmqvist. Mechanistic aspects of the selective catalytic reduction of no_x by dimethyl ether and methanol over γ-al_2o_3. *Journal of Catalysis*, 276(2):402–411, 2010. doi: 10.1016/j.jcat.2010.10.004.

[36] Y. Amenomiya. Active Sites of Solid Acidic Catalysts III Infrared Study of the Water Gas Conversion Reaction on Alumina. 57:64–71, 1979. doi: 10.1016/0021-9517(79)90043-5.

[37] C. V. Ovesen, B. S. Clausen, B. S. Hammershøi, G. Steffensen, T. Askgaard, I. Chorkendorff, J. K. Nørskov, P. B. Rasmussen, P. Stoltze, and P. Taylor. A microkinetic analysis of the water-gas shift reaction under industrial conditions. *Journal of Catalysis*, 158(1):170–180, 1996. doi: 10.1006/jcat.1996.0016.

[38] Z. Zhang, S. S. Wang, R. Song, T. Cao, L. Luo, X. Chen, Y. Gao, J. Lu, W. X. Li, and W. Huang. The most active Cu facet for low-Temperature water gas shift reaction. *Nature Communications*, 8(1):488, 2017. doi: 10.1038/s41467-017-00620-6.

[39] P. Berteau, S. Ceckiewicz, and B. Delmon. Role of the acid-base properties of aluminas, modified γ-alumina, and silica-alumina in 1-butanol dehydration. *Applied Catalysis*, 31:361–383, 1987. doi: 10.1016/S0166-9834(00)80702-2.

[40] P. A. Taylor, P. B. Rasmussen, C. V. Ovesen, P. Stoltze, and I. Chorkendorff. Formate synthesis on Cu(100). *Surface Science*, 261(1-3):191–206, 1992. doi: 10.1016/0039-6028(92)90231-T.

[41] G. C. Chinchen and K. C. Waugh. The chemical state of copper during methanol synthesis. *Journal of Catalysis*, 97(1):280–283, 1986. doi: 10.1016/0021-9517(86)90063-1.

[42] G. C. Chinchen, M. S. Spencer, K. C. Waugh, and D. A. Whan. Promotion of methanol synthesis and the water-gas shift reactions by adsorbed oxygen on supported copper catalysts. *Journal of the Chemical Society, Faraday Transactions 1*, 83(7):2193–2212, 1987. doi: 10.1039/f19878302193.

[43] C. T. Campbell. Comments on: The activity and state of the copper surface in methanol synthesis. *Applied Catalysis1*, 32:367–369, 1987. doi: 10.1016/S0166-9834(00)80641-7.

[44] G. C. Chinchen, M. S. Spencer, K. C. Waugh, and D. A. Whan. Reply to "comments on the activity and state of the copper surface in methanol synthesis catalysts [1]". *Applied Catalysis*, 32:371–372, 1987. doi: 10.1016/S0166-9834(00)80642-9.

[45] J. Nakamura, J. A. Rodriguez, and C. T. Campbell. Does CO_2 dissociatively adsorb on Cu surfaces? *Journal of Physics: Condensed Matter*, 1(SB):149–160, 1989. doi: 10.1088/0953-8984/1/SB/026.

[46] M. Muhler, E. Törnqvist, L. P. Nielsen, B. S. Clausen, and H. Topsøe. On the role of adsorbed atomic oxygen and CO_2 in copper based methanol synthesis catalysts. *Catalysis Letters*, 25(1-2):1–10, 1994. doi: 10.1007/BF00815409.

[47] Y. Ren, K. Yuan, X. Zhou, H. Sun, K. Wu, S. L. Bernasek, W. Chen, and G. Q. Xu. Catalytic Intermediates of CO_2 Hydrogenation on Cu(111) Probed by In Operando Near-Ambient Pressure Technique. *Chemistry - A European Journal*, 24(60):16097–16103, 2018. doi: 10.1002/chem.201802931.

Chapter 6

Characterization of oxide-supported Cu by infrared measurements on adsorbed CO

Authors: Niels D. Nielsen[1], Thomas E. L. Smitshuysen[2], Christian D. Damsgaard[2,3], Anker D. Jensen[1], Jakob M. Christensen[1*]
[1]*Department of Chemical and Biochemical Engineering, Technical University of Denmark, Søltofts Plads Building 229, 2800 Kgs. Lyngby, Denmark*
[2]*Department of Physics, Technical University of Denmark*
Fysikvej, Building 311, 2800 Kgs. Lyngby, Denmark
[3]*National Centre fro Nano Fabrication and Characterization, Technical University of Denmark*
Fysikvej, Building 307, 2800 Kgs. Lyngby, Denmark
[*]**Correspondence to:** jmc@kt.dtu.dk

DOI:
https://doi.org/10.1016/j.susc.2020.121725

Journal specifications:
Surface Science, 2021, Volume 703, 121725

Date Accepted/Published:
27 August 2020 / 4 September 2020

Abstract

Infrared spectroscopy on CO chemisorbed on Raney Cu and materials with Cu dispersed as nanoparticles on oxide supports was used to evaluate support effects on the Cu surface properties. The C-O frequency ($\nu_{\text{C-O}}$) is sensitive to the charge on the adsorption site with $\nu_{\text{C-O}}$ being high on Cu^{+}, intermediate on Cu^{0}, and low on Cu^{-}, whereby this method can probe the charging state of the Cu surface. The Raney Cu reference demonstrates the complex analysis of the IR band intensity, which can be susceptible to dipole coupling. This means that the most intense IR bands may be higher frequency bands strengthened by such coupling effects rather than the bands arising from the most abundant sites. The $\nu_{\text{C-O}}$ of the major band attributable to CO adsorbed on the metallic surface follows the order: Cu/SiO_2 > Raney Cu > Cu/Al_2O_3 > Cu/TiO_2. Given the charge-frequency relationship these support-dependent frequency shifts are attributed to changes in the charging of the Cu surface caused by support effects. The Cu surface is more electron deficient for Cu/SiO_2 and electron enriched for Cu/TiO_2. For the $Cu/ZnO(/Al_2O_3)$ samples, which are important as industrial methanol synthesis catalysts, band assignments are complicated by a low $\nu_{\text{C-O}}$ on Cu^{+} sites connected to the ZnO matrix. However, $Cu/ZnO(/Al_2O_3)$ has a spectral feature at 2065-68 cm^{-1}, which is a lower frequency than

observed in the Cu single crystal studies in the literature and thus indicative of a negative charging of the Cu surface in such systems. Experiments with co-adsorption of CO and electron-withdrawing formate on Cu/ZnO and Cu/SiO_2 show that $\nu_{C\text{-}O}$ in the adsorbed CO shifts upwards with increasing HCOO coverage. This illustrates that the surface charge is donated to the electron-withdrawing formate adsorbate, and as a result co-adsorbed CO experiences a more charge depleted Cu surface that yields higher $\nu_{C\text{-}O}$. The support-dependent surface charging may thus affect the interaction with adsorbates on the metal surface and thereby impact the catalytic properties of the Cu surface. Dilution of the samples in KBr, which has been used in many studies in the literature, had pronounced effects on the spectra. The presence of KBr leads to an increase in $\nu_{C\text{-}O}$ indicative of an electron depleted surface attributed to transfer of electron-withdrawing bromine species from KBr to the sample.

Graphic Abstract

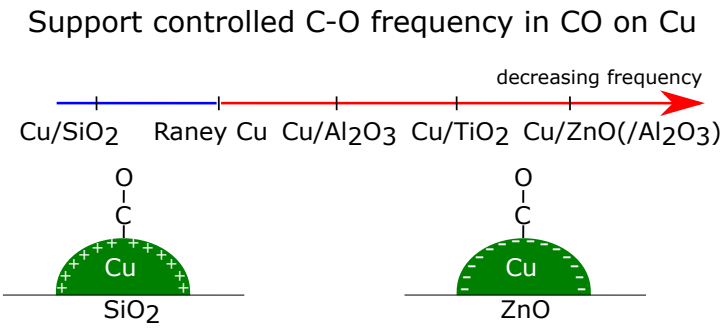

Keywords: Copper catalyst · support effects · CO adsorption · infrared dipole coupling · surface charging

1 Introduction

Materials with copper dispersed as nanoparticles on oxide supports are of great practical importance as catalysts for reactions such as methanol synthesis and the water-gas shift reaction. In these two reactions catalytic activity only emerges once the copper is reduced to the metallic state [1, 2], and catalytic activity scales linearly with the Cu surface area [3–8], which strongly indicates that the reaction occurs on the metallic surface. However, the support used to disperse the Cu has a major impact on the catalytic activity and may cause order of magnitude changes to the rate of the reaction on the Cu surface [9–13]. It is therefore important to investigate, how the properties of the Cu surface depend on the underlying support. Infrared spectroscopy of CO adsorbed on the surface as a probe molecule is a valuable technique because of the high sensitivity of the C-O stretching frequency ($\nu_{C\text{-}O}$) to the nature of the adsorption site. Focusing on the dominant on-top bonding of CO, the most important factor for the C-O frequency on Cu is the charge on the adsorption site. This is illustrated by Fig. 1, which shows how high C-O frequencies correspond to more positively charged adsorption sites, while progressively lower C-O frequencies are characteristic of zero-valent and negatively charged Cu sites.

The charge on the Cu site depends on the surroundings. CO adsorbed on fully developed Cu^+ sites is associated with frequencies above ca. 2105-2110 cm^{-1}, but Davydov [20] observed that Cu cations linked to a basic oxide (MgO or ZnO) appeared to be $Cu^{\delta+}$ sites with a limited positive charge and gave $\nu_{C\text{-}O} < 2100$ cm^{-1} in the adsorbed CO. This can be rationalized from the Lewis definition of a base as an electron donor that thus limits the positive charge on the Cu cation. On the metallic surface the morphology is also important. According to the theory of Smoluchowski [21] the electronic cloud at the metal surface smoothens out, which means that charge flows from protrusions, such as step atoms to the lower lying facets. As a result the step atoms become positively charged $Cu^{\delta+}$. This positive charge on protrusions explains, why stepped Cu single crystal surfaces exhibit the highest C-O

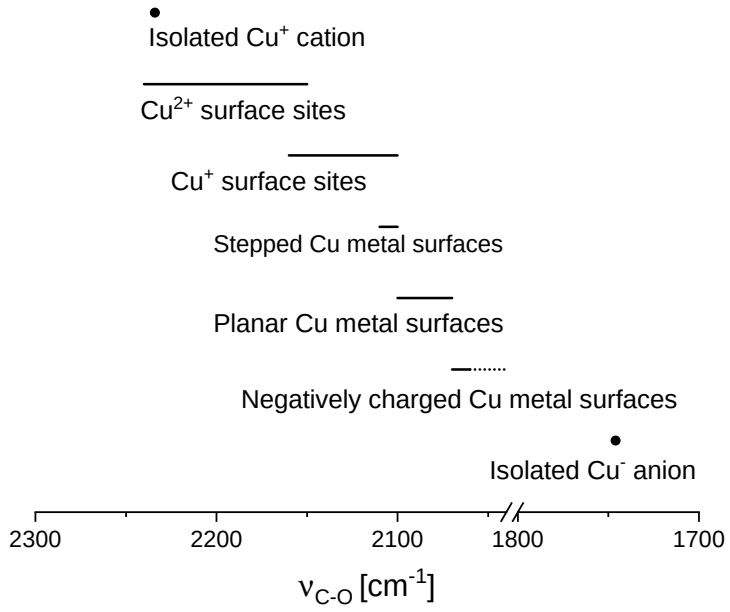

Fig. 1: C-O stretching frequencies ($\nu_{\text{C-O}}$) for CO adsorbed on Cu surfaces or on isolated Cu ions (in frozen Ne) based on reports in the literature [14–19]. The values are for the predominant linear, on-top bonding of CO.

frequencies among metallic surfaces - near the transition to fully developed Cu^+ sites (Fig. 1). The same partial charging applies for other protrusions in nanoparticles, such as edges and corners [22, 23]. On the low-index, planar Cu surfaces the frequency is generally found in the 2070-2100 cm^{-1} range [16]. The highest frequencies occur on the Cu (110) surface that also has protruding rows of atoms. If the metal surface is negatively charged, the C-O stretches shift to lower frequencies. By theoretical calculations Head-Gordon and Tully [17] observed that the C-O frequency in CO adsorbed on a Cu^{14} cluster was lowered by 127 cm^{-1}, when the cluster was negatively charged corresponding to an electric field of -0.5 V/Å.

The relationship between surface charging state and frequency can be rationalized through the Blyholder model [24]. The metal-CO bond is dominated by donation from the 5σ orbital of CO to the metal surface and back donation from the metal surface to the $2\pi^\star$ orbitals of CO. Both the 5σ and $2\pi^\star$ orbitals are anti-bonding with respect to the internal C-O bond [25]. Hence, more positively charged sites will receive more donation from the 5σ orbital and back donate less to the $2\pi^\star$ orbitals, which results in strengthening of the C-O bond and a higher stretching frequency (due to greater removal from a CO anti-bonding orbital). More negatively charged sites will oppositely receive less 5σ donation and back donate more leading to a lower C-O frequency (due to greater donation to a CO anti-bonding orbital).

Although providing valuable information, there are also important factors to consider in the interpretation of the IR spectra of adsorbed CO. Possibly the most important effect is dipole coupling. The vibrations of the adsorbed molecules are coupled by the electrostatic fields from their radiation induced dipoles [26]. Hollins [27] found that if the surface contains two different sites giving C-O frequencies in close proximity, the higher frequency is subjected to constructive interference resulting in enhanced absorbance intensity, whereas the lower frequency experiences destructive interference and weakens. As an example Hollins and co-workers [26, 27] showed that if the surface contains just a few percent of high C-O frequency sites, such as the $Cu^{\delta+}$ atoms at steps, the positive interference from dipole coupling causes these high C-O frequency sites to dominate the recorded IR spectrum completely. The CO on the planar facets, which has a lower CO frequency and therefore receives destructive interference, will only be seen as a minor shoulder in the spectrum despite constituting the majority of the adsorption sites. For complex supported samples with a variety of facets the main

spectral features from CO on the metallic surface must therefore be expected to represent adsorption at the higher frequency sites at surface protrusions (e.g. steps or the protruding rows in (110) facets). Experimentally it is observed [28] that the strengthening of the high frequency band induced by dipole coupling increases with adsorbate coverage as more adsorbates contribute to the interference phenomena. A second important factor to consider is the preferential bonding. In the case of copper, positively charged Cu^+ sites bind CO stronger than metallic Cu sites, which can be attributed to the greater donation from the 5σ orbital of CO to the Cu^+ site [29]. It must therefore be expected that the positively charged Cu sites are occupied first upon exposure to CO and are the last to be vacated upon desorption.
There have been previous comparative studies [30, 31] of support effects on Cu, but these studies have proposed explanations that varied from adsorption dominantly on the metallic surface to full oxide decoration of the Cu particles, and the available studies thus offer no unified conclusions. Consequently it is still highly necessary to examine the issue of support effects in Cu-based materials. Additionally, a significant part of the published literature using infrared spectroscopy has used samples diluted in KBr. However, the presence of KBr has been reported [32, 33] to induce significant chemical modifications to the investigated sample and its properties. It is therefore also relevant to assess the effect of KBr to evaluate the validity of the results in the literature.
Here we conduct FTIR investigations of CO adsorbed on Cu dispersed on a variety of supports (SiO_2, Al_2O_3, $ZnO(/Al_2O_3)$ and TiO_2) using high surface area samples representative of catalytic materials. The main aim is to identify the primary IR band from CO adsorbed on the metallic Cu surface of each sample and to detect the presence of any support effects. Low temperature measurements are used to obtain spectra of CO on Raney Cu to assess the intrinsic properties of Cu for comparison to the supported samples. Experiments with co-adsorption of formate and CO were used to gain further insight into the Cu surface properties. Furthermore, experiments with controlled addition of KBr were conducted to evaluate the effect of dilution by KBr used in much of the previous IR work in the literature.

2 Materials and Methods

2.1 Materials

Flows are reported with reference to normal (N) conditions equal to 273.15 K and 1 atm. of pressure. All supported Cu samples were prepared from the nitrate ($Cu(NO_3)_2{\cdot}3H_2O \geq 98.6\%$ from Alfa Aesar). Cu/ ZnO, $Cu/ZnO/Al_2O_3$ and Cu/Al_2O_3 samples were synthesized by coprecipitation methods with metal nitrate precursors (using Zn $(NO_3)_2{\cdot}6H_2O \geq 98\%$, $Al(NO_3)_3{\cdot}9H_2O \geq 98\%$ from Sigma Aldrich) and a precipitating agent (Na_2CO_3, $\geq 99.8\%$ from Sigma Aldrich). Precipitation conditions were adapted from the optimal conditions reported by Baltes and co-workers [4]. The precipitation was conducted by dripping nitrate solution and precipitation agent into a stirred beaker initially containing 500 mL of demineralized water as a temperature buffer. The precipitation was conducted at pH = 6.5 and T = 338 K until the nitrate solution was consumed and the precipitate was then aged at this temperature for 1 hour with unrestricted pH. Cu/TiO_2 was prepared by deposition-precipitation using similar synthesis parameters, but with TiO_2 anatase powder (nanopowder, 21 nm particle size from Sigma Aldrich) added to the initial 500 mL of water. The aged precipitates for Cu/ZnO (10 wt% Cu), $Cu/ZnO/Al_2O_3$ (63.0 wt% Cu, 32.5 wt% Zn, 4.5 wt% Al), Cu/Al_2O_3 (20 wt% Cu), and Cu/TiO_2 (20 wt% Cu) were filtered and thoroughly washed using demineralized water followed by overnight drying at 313 K before calcination. Dried samples were loaded into alumina crucibles and calcined in a tubular furnace using an air flow of 1 NL/min, while ramping the temperature by 2 K/min (1 K/min for Cu/Al_2O_3) to the calcination temperature of 573 K (603 K for Cu/Al_2O_3) which was held for three hours before cooling. After calcination the samples were pressed, crushed and sieved to 150-300 µm. Cu/SiO_2 (10 wt% Cu) was prepared by impregnation using crushed and sieved (150-300 µm) SiO_2 carrier particles (SS61138, 250 m^2/g, from Saint Gobain) with the Cu nitrate precursor before drying overnight at 313 K and calcination by the same procedure as for the other samples.
Raney Cu (98.9 wt% Cu, 0.81 wt% Al, 0.1 wt% Fe, 0.05 wt% Ni) was purchased as an aqueous solution from Strem Chemicals and was pre-dried in air at room temperature in a fume hood to obtain a dry state before loading. Further characterization of this sample is reported elsewhere [34].

FTIR grade KBr was purchased from Sigma Aldrich and sieve fractionated to 150-300 µm before use.

2.2 Methods

Generally the samples were pre-reduced/activated in situ by hydrogen at atmospheric pressure prior to measurements on reduced samples. The samples were heated (1 K/min) in 5% H_2/N_2 to first 448 K and secondly to 523 K with holding times of generally 30-180 min at both temperatures until no further water evolution could be detected. For Cu/Al_2O_3 the standard procedure was followed by a subsequent treatment in 100% H_2 at 523 K until no further water evolution could be detected.
The exposed Cu surface areas of the pre-reduced samples were measured by the N_2O Reactive Frontal Chromatography (RFC) method [35] using a Quantachrome IQ_2 setup. After pre-reduction the samples were subsequently cooled in He to 333 K and here exposed to a 19 Nml/ min flow of 1% N_2O/He to determine the Cu surface area from the oxygen uptake. The Cu surface area calculations were based on the N_2O consumption, using a Cu:O stoichiometry of 2:1 [36] and an average Cu surface atom density of $1.47 \cdot 10^{19}$ atoms/(m^2 Cu) [37].
In situ XRD was performed using an X'Pert Pro diffractometer from Malvern Panalytical with a CuKα anode and an installed XRK 900 in situ cell from Anton Paar and applied to determine the Cu crystallite size based on the Scherrer method. In situ XRD also verified complete Cu reduction with the applied activation method (Fig. S1-S6). The effluent gas was analyzed by a Pfeiffer quadrupole mass spectrometer. Prior to analyses samples were activated by the same hydrogen concentrations as outlined previously by mixing 99.9999% He and 99.9999% H_2 from Air Liquide Denmark. The Cu crystallite size was estimated from the Scherrer equation [38] using a Scherrer constant of 0.9 [39, 40] and correction for an instrumental broadening of maximally 0.1°. The Inorganic Crystal Structure Database [41] with the collection code written in parentheses is applied to identify observed XRD peaks. XRD patterns featured a growing baseline with increasing 2θ especially for the samples with high Cu weight percentage due to fluorescence from the sample matching the CuKα anode.
Infrared spectroscopy experiments were conducted with a domed reactor cell and Praying Mantis Diffuse Reflectance Infrared Fourier Transform Spectroscopy (DRIFTS) unit from Harrick Scientific Products using a Nicolet iS50 FTIR spectrometer with a liquid N_2 cooled MCT detector. Measured spectra were an average of 76 scans with a resolution of 4 cm^{-1}. In a standard experiment the Cu samples were loaded and compacted in the sample cup of the reactor cell before experiments. Gasses ($\geq$ 99.999% He with $<$ 2 ppm O_2, 9.50% CO/Ar with $<$3 ppm O_2, H_2, 5.01% H_2/N_2 with $<$ 2 ppm O_2, 9.00% CO_2/N_2 with $<$ 3 ppm O_2, $\geq$ 99.999% H_2 with $<$ 2 ppm O_2, $\geq$99.999% N_2 with $<$ 2 ppm O_2) were obtained from Air Liquide Denmark and dosed via Brooks SLA5850 mass flow controllers. The gas passes through an active carbon filter immediately before entering the reactor cell. The effluent gas from the reactor cell was analyzed by a Hiden HPR-20 EGA mass spectrometer (MS).
All measurements were conducted at atmospheric pressure starting with the hydrogen activation procedure outlined above. For CO adsorption experiments, the activated samples were cooled in He to the CO adsorption temperature, where a background spectrum was recorded in He prior to CO exposure. The samples were then exposed to 0.4 mbar CO balanced in inert gas and analyzed as spectra (in Kubelka-Munk units) using the aforementioned background. The typical measurement temperature of 276 K was achieved from adjusting the temperature of the thermostatic bath supplying the cooling water circulating through the IR cell.
Low-temperature measurements were used for Raney Cu. These measurements were conducted using a CHC-CHA-3 reaction chamber (Harrick Scientific Products) that includes a liquid N_2 container connected through a cold finger to the low temperature reaction chamber. Pre-reduced Raney Cu was held in an N_2 atmosphere at room temperature before cooling to a temperature of 152-153 K. At this temperature a background spectrum was recorded in flowing N_2 before exposure to 0.4 mbar CO. Subsequently the cell was purged with N_2 and absorbance spectra of the adsorbed CO were recorded using the background measured at the same temperature in N_2 prior to CO exposure.
To aid the distinction between contributions from metallic and oxidized sites, measurements were conducted on oxidized samples (to eliminate the metallic contributions) and after a harsher reduction in CO to help eliminate oxide contributions. Two types of measurements on oxidized samples were conducted. In one type of measurement the CuO/SiO_2 and CuO/TiO_2 oxide precursors were instead of pre-reduction only outgassed in flowing He at 373 K until no further water evolution could be

detected and then cooled in He to 276 K. Here adsorption of 0.4-100 mbar CO in stepwise increasing CO concentration was conducted. For the other type of measurement on oxidized samples Raney Cu, Cu/Al_2O_3, $Cu/ZnO/Al_2O_3$, and Cu/SiO_2 were activated by the normal pre-reduction and then re-oxidized at room temperature by exposure to a flow of 9% CO_2/N_2. After flushing of the cell with He at room temperature, the CO adsorption was then conducted with 0.4-100 mbar CO in stepwise increasing concentration at 276 K (152-153 K for Raney Cu).
For tests with a harsher reductive treatment of Cu/SiO_2 and $Cu/ZnO/Al_2O_3$ the samples were pre-reduced by the normal treatment, then exposed to a 50 NmL/min flow of 100% H_2 at 523 K for 1 hour. Finally the flow was switched to 79 Nml/min of 9.5 % CO (balanced in Ar) and heated with 5 K/min to 573 K and kept constant for 30 minutes before thorough He purge at 573 K to remove residual and adsorbed CO and cooling in He to 276 K where adsorption of 0.4 mbar CO was conducted.
For experiments with deposition of formate on Cu/ZnO or Cu/SiO_2, the pre-reduced sample was flushed and cooled in He to 373 K (atmospheric pressure), where it was exposed to $CO_2/N_2/H_2$ (3/29/68) flow until stable IR signals before cooling to 276 K in the syngas mixture. A background spectrum was recorded in He at 276 K and used for recording spectra (in Kubelka-Munk units) during a subsequent exposure to 0.4 mbar CO. After CO adsorption, the sample was thoroughly flushed with He at 276 K before performing a TPD in 45 Nml/min He with a heating ramp of 10 K/min to 323 K before further heating by 2 K/min to a final temperature of 393 K with a dwell time of 5 min. During cooling from the final TPD temperature, a 10 min dwell step at 353 K in a 150 Nml/min He flow was included to prevent re-adsorption of desorbed adsorbates. The higher He flow was maintained during further cooling to 276 K, where a new background spectrum was collected for the subsequent CO adsorption exposure. The combined TPD and CO adsorption cycle was repeated with increased final TPD temperature in steps of 20 K (413 K, 433 K and 453 K).
To evaluate the effects of sample dilution with KBr, which has been used for many similar studies in the literature, measurements were conducted with the Cu-based samples physically mixed with KBr. The KBr-sample mixture was then subjected to the same pre-reduction and measurement protocols used in the standard experiments and analyzed by IR measurements on chemisorbed CO.

3 Results and Discussion

3.1 Sample Properties

The results from structural characterization of the samples are summarized in Table 1. Details of the post reduction XRD patterns are shown in the supplementary material Figs. S1-S7. The constant angle (2θ) of the XRD reflections from Cu for all the samples (see Fig. S7b) suggests that bulk alloying of Cu and support components do not occur for any of the samples with the applied reduction methods. Precipitated samples (Cu/Al_2O_3, $Cu/ZnO/Al_2O_3$, Cu/ZnO, Cu/TiO_2) have a smaller crystallite size than the Cu diameter determined from the Cu surface area. This suggests that the samples are polycrystalline with larger particles composed of smaller crystallites. However, an extent of decoration of the metal particles (i.e. an "iceberg" configuration) by the support can also contribute to an overestimation of the Cu particle size relative to the XRD crystallite size estimates. Oppositely, Cu/SiO_2 prepared by impregnation exhibits a larger crystallite size than the size determined from the surface area. This has also been observed previously [42] for Cu/SiO_2 prepared by impregnation. The impregnation method must have resulted in larger crystallites that dominate the XRD measurement over a majority of smaller particles that dominate the Cu area. For Raney Cu the size estimates from XRD and chemisorption are similar, indicating that the sample consists of relatively homogeneous 40-50 nm Cu crystals. Previous characterization [34] has shown that around 30-40% of the surface of these crystals is free metallic surface, whereas the rest is covered with a thin Al_2O_3 film.
It is known that the TOF for methanol synthesis over Cu based samples (and hence expectedly the surface properties) is generally size independent for Cu particles larger than ca. 5 nm [12, 43, 44]. Xu and Goodman [45] also found that the IR spectrum of CO adsorbed on a Cu/ SiO_2 model system became relatively size-independent above ca. 3.5 nm in diameter (below 30% Cu dispersion). The surface properties should therefore be relatively constant for particle sizes above the limit of 3.5-5 nm. As the crystallite sizes are close to or above this limit (Table 1), and as the area-derived particle sizes are well above this limit, it is unlikely that the present comparisons across supports are affected by

Table 1: Results from structural characterization of the reduced samples by N_2O-RFC and in situ XRD.

Sample	**Nominal Cu content** [wt%]	**Cu surface area** [$m^2/Cu/g_{cat}$]	**Cu crystallite size from XRD** [nm] [a)]	**Cu diameter from Cu surface area** [nm]
Cu/SiO_2	10	3.99	67.3	16.8
Raney Cu	98.9	5.18	40.7	47.5 [b)]
Cu/Al_2O_3	20	4.80	2.9	28.0
Cu/TiO_2	20	1.19	65.7	112.9
Cu/ZnO	10	4.90	3.9	13.7
$Cu/ZnO/Al_2O_3$	63	20.25	4.7	20.9

a) Determined based on the Cu {111} diffraction peak at 43.1° (ICSD cc. 64699) after activation.
b) Determined from the combination of the free Cu area and the Al_2O_3 covered surface area determined by Nielsen et al. [34].

differences in particle size.

3.2 Raney Cu

A previous study [34] with the same Raney Cu sample evaluated the catalytic properties and showed that Raney Cu featured the intrinsic properties of Cu. Consequently, CO adsorption on Raney Cu should be representative of the intrinsic properties of Cu in the absence of notable support effects. Spectroscopic measurements on metal-rich Cu samples are complicated by the high reflectance of the metal [16], which is the most likely reason, why only weak signals were obtained in the present DRIFTS experiments on Raney Cu. The measurements were therefore conducted at low temperature, where adsorbed CO can be preserved for some time after purging the cell of gaseous CO. This allows a clearer identification of the band from adsorbed CO.
Fig. 2a shows the IR spectrum of pre-reduced Raney Cu during CO adsorption at 153 K and after a subsequent 3 min N_2 purge until only minor traces of gaseous CO could be detected. The IR band at 2094 cm^{-1}, which is preserved during removal of gaseous CO, is attributed to adsorbed CO on metallic Cu. Comparison to single crystal studies [16, 46] suggests that this spectrum is dominated by the contribution from the (110) facets. Previous [47–49] Wulff-construction modeling on Cu has yielded a distribution of 5-7% (110), 25-30% (100), and 60- 70% (111) for the Cu surface. The catalytic properties of the Raney Cu sample are also relatively similar to those of a Cu(111) single crystal surface [34], which supports that this equilibrium distribution is representative for the present Raney Cu sample. It could thus seem contradictory that the least abundant facet dominates the spectrum in Fig. 2a, but this can be rationalized from the dipole coupling effects mentioned in the introduction. Single crystal studies [16, 46] show that the C-O frequency decreases in the order (110) > (100) > (111). As the interference phenomena from dipole coupling strongly favor the higher C-O frequency sites, the contribution from higher frequency (110) sites dominates the spectrum despite representing a minority of the surface sites. The strong effects of dipole coupling seen for the Raney Cu reference suggests that polycrystalline Cu samples generally must be expected to be dominated by the higher frequency contributions, such as Cu(110), despite the limited concentration of such sites.
Fig. 2b shows the IR spectrum of the adsorbed CO on Raney Cu that had been first pre-reduced and then re-oxidized by 9% CO_2/N_2 at room temperature. Fig. 2b illustrates that this yields a C-O band at 2107 cm^{-1} in the frequency range indicative of CO on oxidized Cu^+ sites (Fig. 1). The fact that the 2094 cm^{-1} band seen for the reduced sample is replaced with a higher frequency band by the oxidative treatment helps to verify that the 2094 cm^{-1} band is due to CO adsorption on metallic Cu.

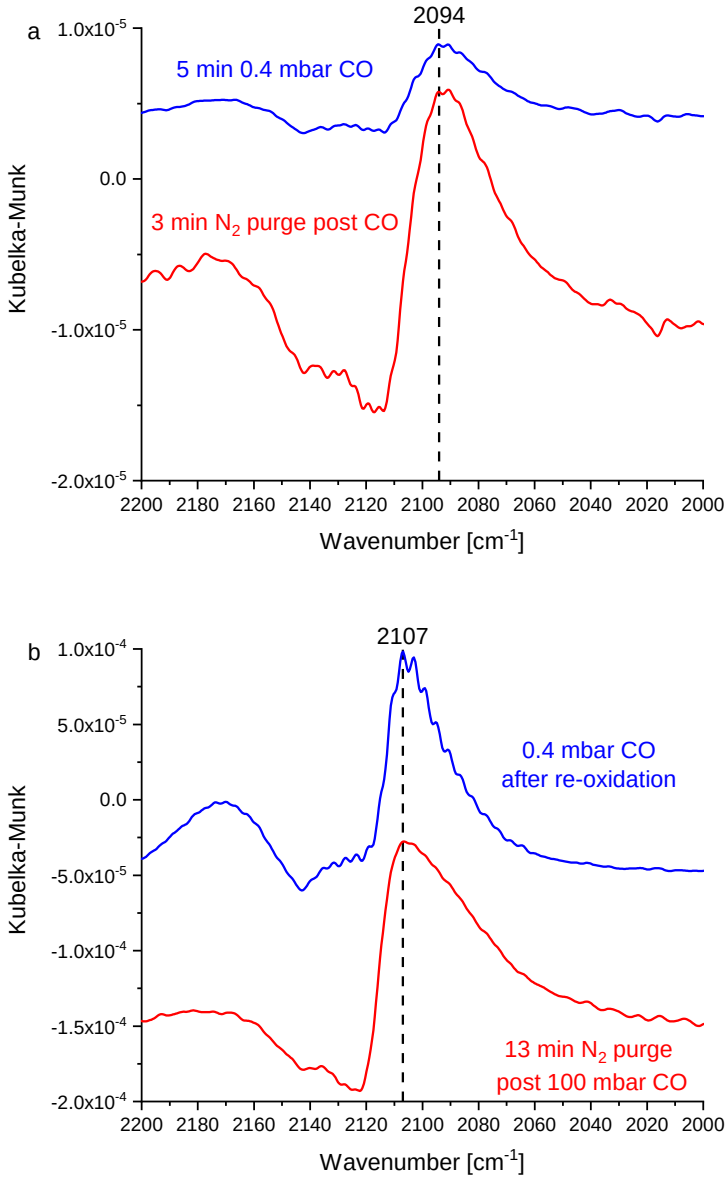

Fig. 2: a) IR spectra of pre-reduced Raney Cu in the presence of 0.4 mbar CO (blue) and after subsequent N_2 purge (red) both at 153 K. b) IR spectra of pre-reduced and then re-oxidized (by 9% CO_2/N_2 at room temperature) Raney Cu in 0.4 mbar CO at 152 K and during N_2 purge at 152 K post stepwise increase in CO pressure from 0.4 mbar to 100 mbar CO.

3.3 Cu/Al_2O_3

Fig. 3a shows the IR spectrum for CO adsorbed at 276 K on prereduced Cu/Al_2O_3 with a main band located at 2089 cm^{-1} attributed to CO on the metallic surface on the basis of a comparison to Fig. 1. Fig. 3b shows the IR spectrum for CO adsorbed at 276 K on pre-reduced and then re-oxidized (9% CO_2/N_2 at room temperature) Cu/Al_2O_3, which shows a main band at 2109 cm^{-1} indicative of CO on relatively welldeveloped Cu^+ sites (Fig. 1). Since the 2089 cm^{-1} band seen for reduced Cu/Al_2O_3 is significantly displaced by the oxidative treatment (Fig. 3), and because D'Alnoncourt et al. [50] observed that more severe reduction of Cu/Al_2O_3 did not change this band substantially, the 2089 cm^{-1} band is attributed to the metallic Cu surface. If the partially oxidized sample is exposed to increasing CO pressures the band also seems to shift down towards the metallic state (Fig. S8). Table 2 compares the presently achieved C-O frequency to values reported for reduced Cu/Al_2O_3 in the literature. Generally the results agree within a few cm^{-1}, which would suggest that measured C-O frequencies are reproducible to the extent that even small variations are significant.

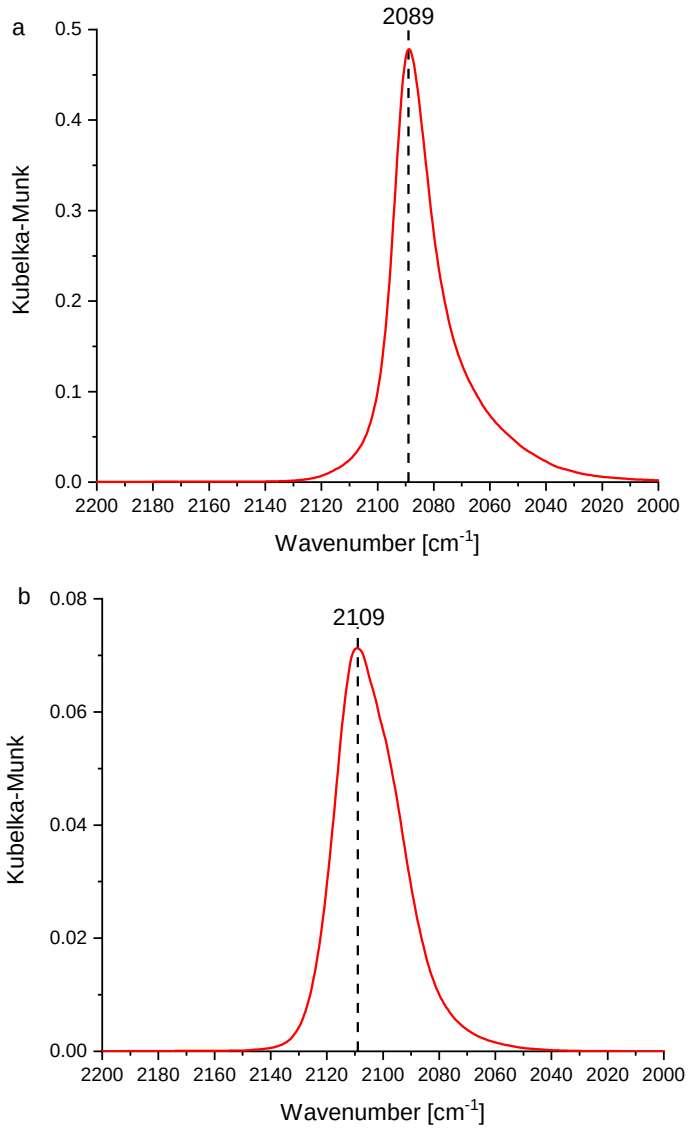

Fig. 3: a) IR spectrum of pre-reduced Cu/Al_2O_3 in 0.4 mbar CO at 276 K. b) IR spectrum of prereduced and then re-oxidized (in 9% CO_2/N_2) Cu/Al_2O_3 in 0.4 mbar CO at 276 K.

Table 2: Measured $\nu_{C\text{-}O}$ for CO adsorption on reduced Cu/Al_2O_3 in this study and comparison to studies in the literature. None of the studies from the literature mention any sample dilution by KBr.

Study	**Reference**	**Cu content [wt%]**	**$\nu_{C\text{-}O}$ on metallic Cu [cm^{-1}]**
Topsøe and Topsøe	[30]	2.5	2094
D'Alnoncourt et al.	[50]	20	2090
Padley et al.	[51]	5	2094
Dulaurent et al.	[52]	4.7	2092
This work		20	2089

3.4 Cu/TiO_2

Arakawa et al. [53] investigated methanol synthesis catalyzed by Cu/TiO_2 and concluded that the turnover frequency per exposed metallic Cu atom was high. TiO_2 is thus an example of a support that can exert a clear support effect on Cu that in methanol synthesis causes a high turnover frequency. Fig. 4 shows IR spectra as a function of time when pre-reduced Cu/TiO_2 is exposed to 0.4 mbar CO at 276 K. This clearly illustrates the existence of two IR bands at 2070 cm^{-1} and 2104 cm^{-1}. These bands are attributed to CO adsorbed on Cu sites, since adsorption on TiO_2 yields higher C-O frequencies [54]. Fig. 5a shows that the 2070 cm^{-1} band is displaced more rapidly than the 2104 cm^{-1} band when the IR cell is flushed with He at 276 K after CO adsorption. Given that CO is bound more strongly to Cu^+ sites [29] this could indicate that the higher frequency 2104 cm^{-1} band is due to more strongly bound CO on $Cu^{\delta+}$ sites at $Cu^{\delta+}$-O-Ti linkages to the support, whereas the lower frequency 2070 cm^{-1} band is due to more weakly bound CO on the metallic surface. This assignment is strongly supported by Fig. 5b, which shows the spectrum of CO adsorbed on the air calcined, CuO/TiO_2 oxide precursor and illustrates that the high-frequency band is very prominent for the oxidized state of the sample. Oppositely, the low-frequency band is absent in the oxidized sample. Consequently, the 2104-2106 cm^{-1} high-frequency band is attributed to CO on $Cu^{\delta+}$-O sites linked to the TiO_2 oxide matrix, whereas the 2070 cm^{-1} band is attributed to CO on the metal surface.

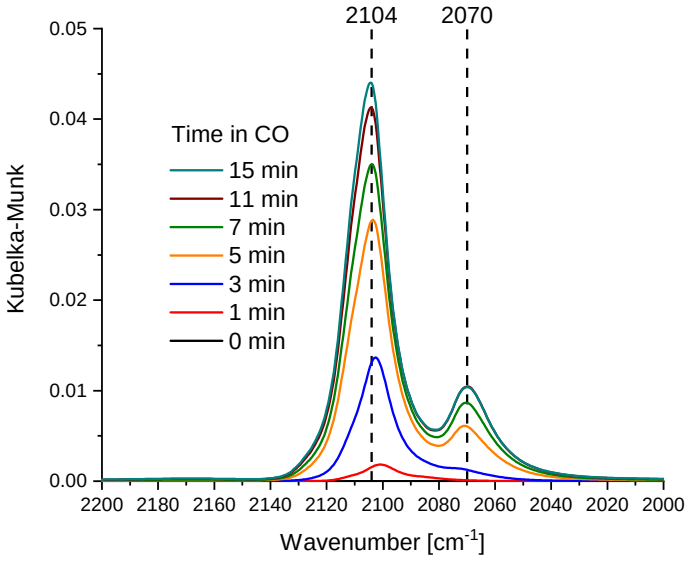

Fig. 4: IR spectra of pre-reduced Cu/TiO_2 as a function of time during exposure to 0.4 mbar CO at 276 K.

The significantly lower C-O frequency on the metal surface of Cu/ TiO_2 compared to the Raney Cu reference suggests that the Cu surface in Cu/TiO_2 is significantly modified by the support. Dipole

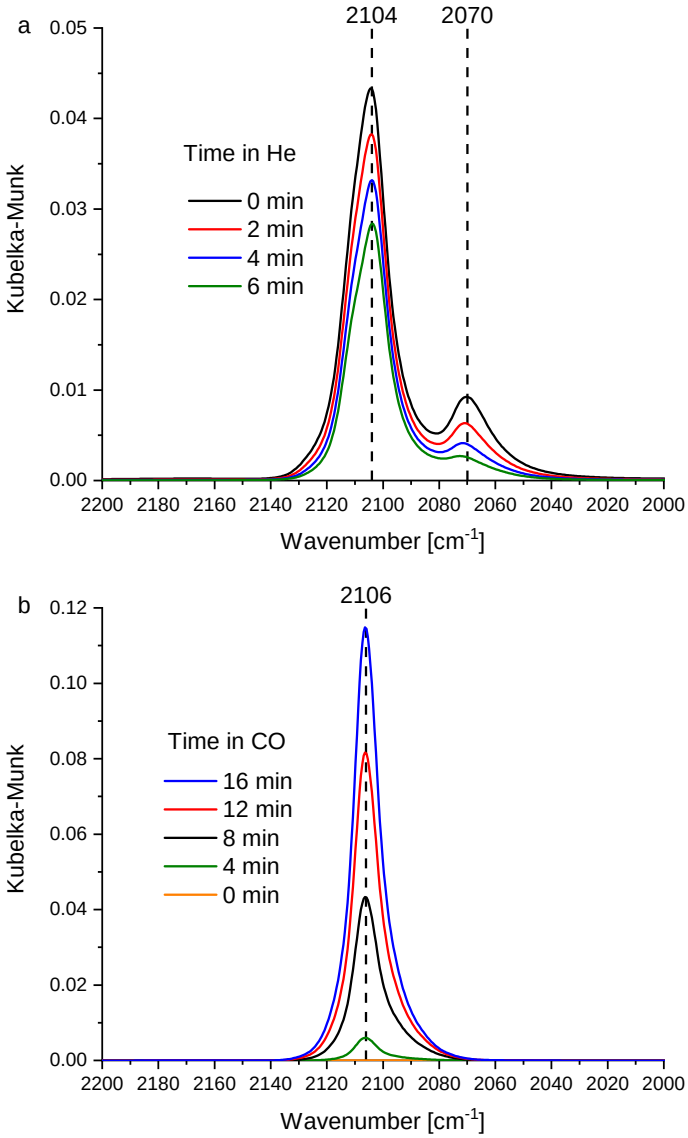

Fig. 5: a) IR spectra of pre-reduced Cu/TiO_2 as a function of time during He flush after exposure to 0.4 mbar CO at 276 K. b) IR spectra of fresh, air calcined CuO/TiO_2 as a function of time during exposure to 0.4 mbar CO at 276 K. Fig. S4 shows that the oxidized sample contains a mixture of CuO and Cu_2O phases.

coupling makes it likely (see section 3.2) that the main contribution from the metallic surface (2070 cm^{-1} for Cu/TiO_2) arises from the sites such as the (110) facet that yield considerably higher frequencies on unperturbed single crystal surfaces [16, 46]. Considering the charge-frequency relationship in Fig. 1 the low frequency on Cu/TiO_2 indicates a negative charging of the Cu surface. At the interface between a metal and an n-type semiconductor such as TiO_2 there will be a charge transfer from the semiconductor to the metal [55–57]. In the classical limit, charge transferred to a conductor, such as the copper metal, is distributed across the surface, and DFT calculations suggest that this behavior of charge distribution across the surface is emerging already in very small metal clusters [58]. Such charge transfer effects can rationalize the negative charging of the Cu surface on the n-type semiconductor supports including TiO_2.

3.5 Cu/SiO_2

Fig. 6 shows time-resolved spectra during CO adsorption at 276 K on pre-reduced Cu/SiO_2 dominated by a central 2100 cm^{-1} band with two shoulders at approximately 2072 cm^{-1} and 2125 cm^{-1}. The present spectra are similar to those of lower Cu-dispersion (< 30%) Cu/SiO_2 model systems in UHV experiments [45], which suggests that the current measurements are free of experimental artifacts such as gas phase impurities. The multiple IR bands for the reduced Cu/SiO_2 sample raises the question of which bands that arise from the metallic surface. Fig. 7a shows the spectrum of CO adsorbed on the freshly calcined CuO/SiO_2 oxide precursor, where the high-frequency band (2127 cm^{-1}) is clearly present. Fig. 7b shows comparisons between CO adsorbed on pre-reduced Cu/SiO_2 and on pre-reduced and then re-oxidized (by 9% CO_2/N_2 at room temperature) Cu/SiO_2. The figure reveals that oxidative treatment strengthens the high-frequency band and eliminates the two lower frequency bands. These results clearly show that the band at 2125-2127 cm^{-1} is from oxidized Cu^+ sites. In the reduced sample the remnant of such species are most likely the Cu^+-O-Si linkages at the metal/oxide interface. Oppositely, the two lower frequency bands are attributed to CO adsorption on the metallic surface. The 2100 cm^{-1} band is thus the main band from the metallic surface, which from analogy to the Raney Cu results is expected to be the higher C-O frequency facets, particularly Cu(110), that are strengthened by dipole coupling. The shoulder towards lower frequency is most likely from the more densely packed facets that are disfavored by the dipole coupling, but nevertheless slightly visible due to the good resolution achieved in spectra for Cu/SiO_2. During flushing of the cell with He the bands from adsorbed CO disappear with similar rates (Fig. S9). There are thus no clear differences in binding strength to aid the band assignment.
The main CO band attributable to the metallic surface of Cu/SiO_2 is thus shifted upwards by 6 cm^{-1} compared to Raney Cu and is between the frequencies observed on reduced and oxidized Raney Cu (see Fig. 2). Considering the discussion in section 3.3 this shift is most likely of sufficient magnitude to represent a significant difference. From the charging-frequency relationship in Fig. 1 the higher frequency on Cu/ SiO_2 indicates that the surface of Cu particles on silica is electron depleted. The most likely reason for this depletion is that the Cu^+-O-Si linkages observable in the spectrum are so electron-withdrawing that the whole Cu surface becomes slightly electron deficient.

3.6 Cu/ZnO based samples

$Cu/ZnO/Al_2O_3$ is the industrial catalyst for methanol synthesis, and it is well-substantiated that ZnO exerts a strong beneficial support effect [9–13]. Cu/ZnO based catalysts with or without alumina have been observed [13] to exhibit similar turnover frequencies for methanol synthesis and are discussed together in this section. Fig. 8a shows the IR spectrum of Cu/ZnO in presence of 0.4 mbar CO at 276 K, whereas Fig. 8b displays the spectrum of $Cu/ZnO/Al_2O_3$ in 0.4 mbar CO at 276 K. In good agreement with previous studies [30, 50, 59] the Cu/ZnO ($/Al_2O_3$) samples show two IR absorption bands centered at 2093-2094 cm^{-1} and at 2065-68 cm^{-1} with the lower frequency band being more clear in Cu/ZnO. Any contribution from CO adsorbed on ZnO is excluded, as this occurs around 2190 cm^{-1} [60, 61]. Fig. S10 shows the development in the spectrum of adsorbed CO at various stages during the reduction of $Cu/ZnO/Al_2O_3$ and illustrates that a band at 2100 cm^{-1} on the initial oxidized state is replaced by the spectrum characteristic of the reduced sample at 448 K.
As touched upon in the introduction band assignments can be particularly difficult on basic oxides,

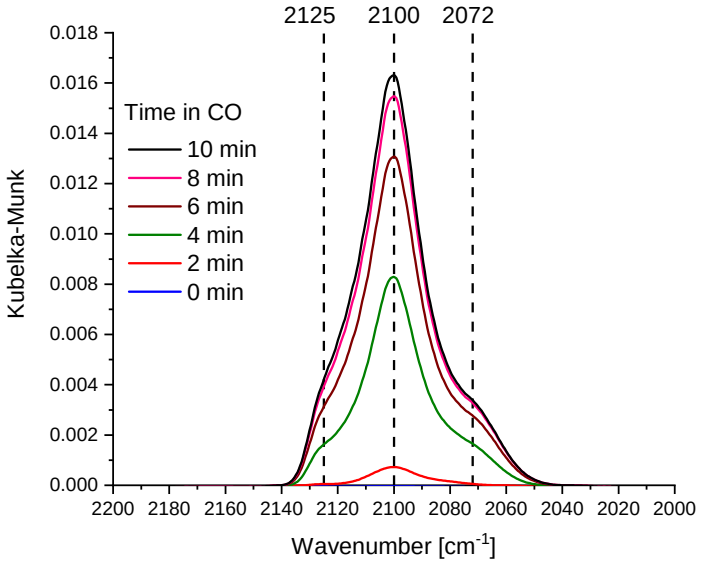

Fig. 6: IR spectra of pre-reduced Cu/SiO_2 as a function of time during exposure to 0.4 mbar CO at 276 K after normal pre-reduction (5% H_2 at 523 K).

where $Cu^{\delta+}$ sites from Cu-O linkages to the support may yield C-O frequencies similar to the $Cu^{\delta+}$ sites seen at protrusions in an unperturbed metallic surface. Previous studies [31, 62] on $Cu/ZnO(/Al_2O_3)$ samples report that the high frequency band can be eliminated by harsher reduction in CO-containing gas. This could indicate that the high-frequency band arises from an oxidized species. However, we were unable to reproduce this elimination of the 2093-2094 cm^{-1} band by harsher reduction (Fig. 9a), although the reason for this discrepancy is not completely clear. Fig. 9b shows IR spectra at various CO pressures and during subsequent flushing in He for a $Cu/ZnO/Al_2O_3$ sample that has been pre-reduced and then reoxidized (9% CO_2 at room temperature). Fig. 9b illustrates that the oxidized sample exhibits a broad band around 2100 cm^{-1}. The fact that the major band is at relatively similar frequencies for both the reduced and oxidized sample (compare Figs. 9a and 9b) could indicate that this band arises from oxidized sites, such as Cu-O-Zn linkages to the support. Additionally, the high frequency band is relatively more stable when the gaseous CO is flushed away with He (Figs. 9b and S11), whereas the shoulder at 2065-2068 cm^{-1} is displaced more easily (Fig. S11). This could also suggest that the lower frequency shoulder represents the more weakly bound CO on the metallic surface, whereas the high-frequency represents stronger bonding on oxidized sites.

Based on these observations it is most likely that the 2093-2094 cm^{-1} main band is part of the reduced particles, since it cannot be modified by hasher reduction (Fig. 9a). However, given the similarity to the main band on an oxidized sample (Fig. 9b) it is also likely that the 2093-2094 cm^{-1} band represents a partially oxidized site, namely the $Cu^{\delta+}$-O-Zn sites at the periphery of the metal particle. The 2065-68 cm^{-1} band is assigned to the CO adsorbed on the interior metallic surface. Chemisorption techniques [63] suggest that there are relatively few Cu-O-Zn sites compared to metallic Cu0 sites in reduced Cu/ZnO ($/Al_2O_3$). If the 2093-2094 cm^{-1} band is due to $Cu^{\delta+}$-O-Zn sites its high intensity must therefore arise from dipole coupling.

Both Cu/SiO_2 and $Cu/ZnO(/Al_2O_3)$ show some similarities in the CO spectra with a main peak in the 2090-2100 cm^{-1} range and a shoulder towards lower frequency. However, as outlined above different band assignments are applied for the two systems with the most intense band assigned to the metallic surface for Cu/SiO_2 and to a site linked to the oxide matrix for $Cu/ZnO(/Al_2O_3)$. The main argument for this interpretive difference comes from the supporting studies of oxidized samples, where oxidized Cu sites for $Cu/ZnO(/Al_2O_3)$ appears to be at a considerably lower frequency (ca. 2100 cm^{-1} in Fig. 9b) than the oxidized Cu sites for Cu/SiO_2 (2125-2127 cm^{-1} in Fig. 7). However, the complex analysis induced by dipole coupling, where the most intense IR bands may arise from the most coupling-favored high-frequency sites rather than from the most physically abundant sites must be remembered in these interpretations. Cu single crystal studies [16, 46] have not shown frequencies

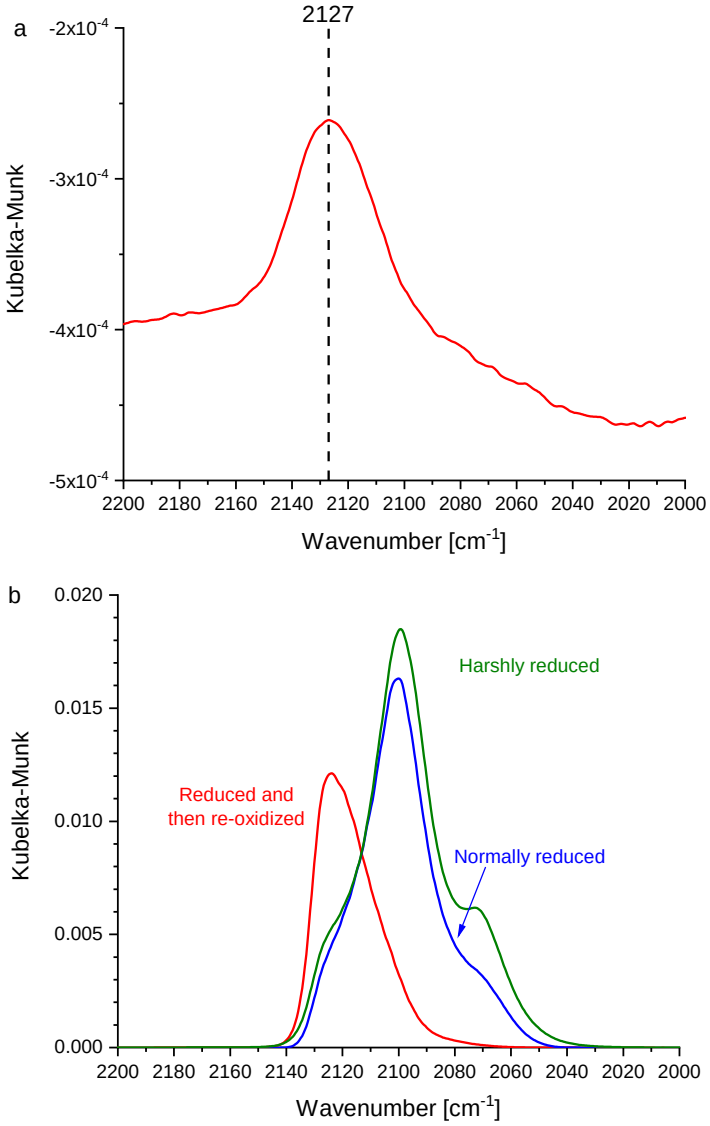

Fig. 7: a) IR spectrum of freshly calcined CuO/SiO_2 after pre-adsorption of 0.4 mbar CO at 276 K followed by 16 min He purge at 276 K. b) IR spectra during exposure to 0.4 mbar CO at 276 K for normally pre-reduced (blue), harshly pre-reduced by 9.5% CO at 573 K (green) and normally prereduced and then re-oxidized (9% CO_2/N_2 at room temperature, red) Cu/SiO_2.

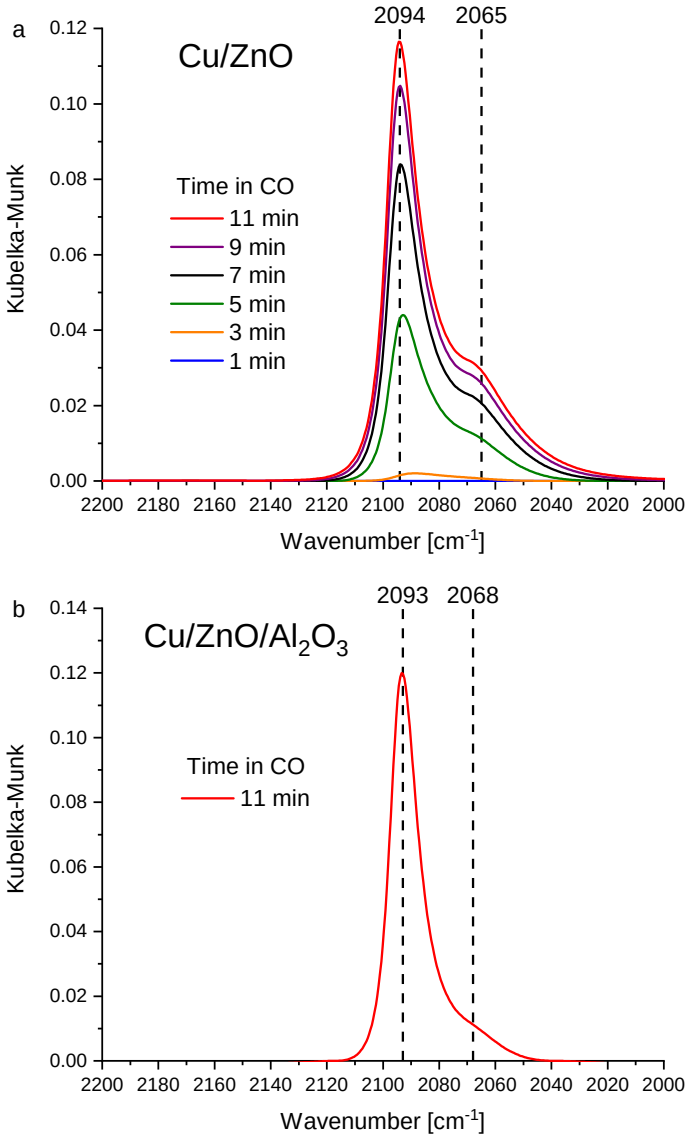

Fig. 8: IR spectra of pre-reduced a) Cu/ZnO in 0.4 mbar CO at 276 K and b) $Cu/ZnO/Al_2O_3$ in 0.4 mbar CO at 276 K.

below 2070 cm^{-1}, so the observation of a lower frequency feature for Cu/ZnO (/Al_2O_3) indicates a negative charging of the metallic surface (see Fig. 1). This would also be consistent with the observation of a low frequency feature for Cu/TiO_2 (see section 3.4) given that both TiO_2 and ZnO are n-type semiconductors. Additionally, Behm and coworkers [64] inferred from the C-O frequency in CO adsorbed on Au/ZnO that the surface of gold dispersed on ZnO is negatively charged. Prior XPS analyses [65, 66] of Cu/ZnO are also consistent with a negative charging of the Cu surface. The conclusion of a negative charging on the Cu surface of Cu/ZnO(/Al_2O_3) is therefore supported by other techniques/systems.

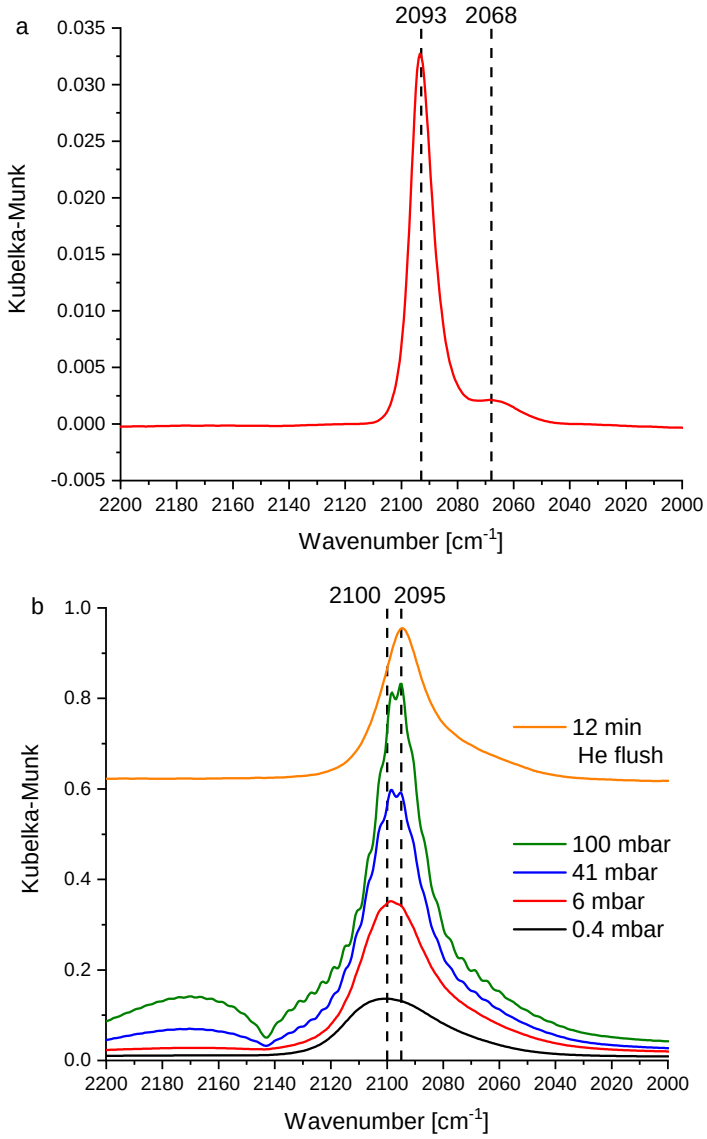

Fig. 9: a) IR spectrum of Cu/ZnO/Al_2O_3 in 0.4 mbar CO at 276 K after harsh pre-reduction with 30 minutes in 9.5% CO/Ar at 573 K after the normal pre-reduction. b) IR spectra of pre-reduced and then re-oxidized (by 9% CO_2/N_2 at room temperature) Cu/ZnO/Al_2O_3 in 0.4 mbar to 100 mbar CO and during subsequent He flush at constant 276 K. Spectra are offset for clarity.

3.7 Effect of formate decoration of the metal surface

The main band for Cu/SiO_2 (2100 cm^{-1}) is between bands seen on the reduced and oxidized states of the Raney Cu reference, which could suggest a charge depletion of the metal surface in Cu/SiO_2.

Oppositely the n-type semiconductor supports ZnO and TiO_2 yield low-frequency features that may indicate an increased negative charge in the Cu surface. It is therefore relevant to validate, if the observed bands indeed are due to adsorption on copper sites. This was examined in experiments involving formate deposition on copper. It is known from single crystal studies [67] that a sufficiently high coverage of formate can partially or completely exclude the CO adsorption on copper, and that pre-adsorbed formate on Cu can be removed by TPD to 450 K [34], whereas desorption of formate on ZnO occurs at higher temperatures [68–70] Cu surface of a HCOO covered sample can thus be selectively exposed by heating to temperatures up to 450 K, where only the formate on Cu desorbs.
Formate was adsorbed on pre-reduced Cu/ZnO and Cu/SiO_2 by $CO_2/N_2/H_2$ (3/29/68) exposure (373 K, 1 atm.). Fig. 10 shows the IR spectra in He at 276 K for the two samples after the CO_2/H_2 treatment. Fig. 10a shows that the exposure of Cu/ZnO to CO_2/H_2 resulted in distinct HCOO features on both Cu [71–73] ($\nu_{OCO,sym}$ = 1352 cm^{-1}, $\nu_{OCO,asym}$ = 1602 cm^{-1} and $\nu_{H\text{-}C}$ = 2852 cm^{-1}) and ZnO [72, 74] (2882 cm^{-1}, 1580 cm^{-1}) as well as CH_3O-ZnO [72] (2931 cm^{-1}) and zinc related bicarbonate species [74] (1305 cm^{-1}). For Cu/ZnO the C-H features are clearer in the raw absorbance spectrum in Fig. S12, which also shows a broad IR absorbance across the entire spectrum attributable to light absorption from intraband excitations of free charge carriers in the ZnO conduction band [75–77]. Fig. 10b shows that the exposure of Cu/SiO_2 to CO_2/H_2 resulted in Cu-HCOO ($\nu_{OCO,sym}$ = 1352 cm^{-1}) and features at 2934 cm^{-1} and 2852 cm^{-1} that may arise from either Cu-HCOO or CH_3O-SiO_2 [78–80].
After decoration of the Cu surface with HCOO (Fig. 10) the spectrum of adsorbed CO on the maximally HCOO covered sample was measured in 0.4 mbar CO at 276 K with the result displayed in Fig. 11. A series of TPD sequences were then conducted. Here the sample was heated in He to progressively higher temperatures to desorb increasing amounts of the adsorbed formate. The gradual desorption of formate during the TPD runs was verified by the progressive disappearance of the Cu-HCOO IR features (Figs. S13 and S14) and by the concurrent detection of H_2 and CO_2 in the effluent during the TPDs (Figs. S15 and S16). After each TPD sequence the sample was cooled and subjected to 0.4 mbar CO adsorption at 276 K, where the IR spectrum for CO adsorption was recorded. Fig. 11 summarizes the CO spectra at 276 K recorded between the TPD sequences for both Cu/ZnO and Cu/SiO_2.
The first conclusion to be drawn from Fig. 11 is that the observed IR bands are due to CO adsorption on copper sites, as they can be displaced by HCOO blockage of the Cu surface and fully restored by TPD to 453 K, which is known [34] to desorb all formate from Cu. The formate species associated with zinc are essentially preserved during the TPD (Fig. S13 and S14), and as such sites thus remain blocked during the experiment in Fig. 11a, it can be ruled out that the observed CO bands are associated with zinc-species. The differences between these two identically treated samples also provide important insight into the support effect upon the Cu surface. Cu/ZnO facilitates a relatively high formate coverage on Cu resulting in a completely physically filled Cu surface as evident from the nearly complete absence of CO uptake for Cu/ZnO after H_2/CO_2 treatment ("Post CO_2/H_2" in Fig. 11a). Oppositely Cu/SiO_2 (Fig. 11b) shows a clear CO band already at the maximal HCOO coverage after CO_2/H_2 treatment. It is also a striking difference that Cu-HCOO on Cu/ZnO exhibits an asymmetric OCO stretch at 1602 cm^{-1} (Fig. 10a), which is completely absent in Cu/SiO_2 (Fig. 10b). This asymmetry could be due to the higher formate coverage on the Cu surface of Cu/ZnO that causes the formate molecules to tilt to accommodate neighbors in close proximity as observed in single crystal studies [67, 81].
Several techniques [49, 82–85] have shown that adsorbed formate is an electron-withdrawing species. With the highest coverage of electron-withdrawing formate Cu/ZnO features two main bands from adsorbed CO at 2098 cm^{-1} and 2127 cm^{-1} (Fig. 11a and more clearly in Fig. S17). As the HCOO coverage gradually decreases by the TPD treatments these CO bands progressively shift to 2068 cm^{-1} and 2098 cm^{-1}, close to the positions for a freshly reduced sample (Fig. 8a). Similar gradual frequency shifts are seen as formate desorb from Cu/SiO_2. Weak van der Waals interactions between adsorbed HCOO and CO are ruled out as an explanation for these frequency shifts. This is because there are no matching changes in the C-H and OCO regions of the spectrum to indicate distortion of the formate by the CO adsorption (Figs. S18-S20). Consequently, the frequency changes in adsorbed CO with the amount of co-adsorbed formate must reflect that the charging state of Cu surface sites not occupied by formate is modified by the amount of electron- withdrawing adsorbates.

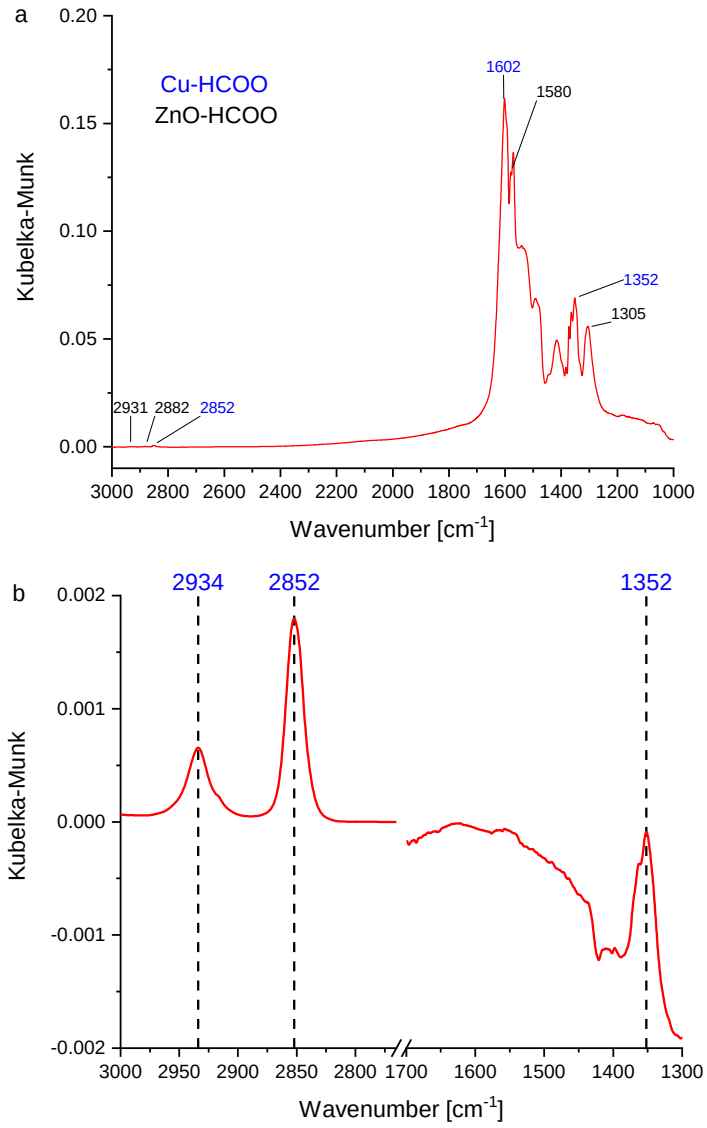

Fig. 10: a) IR spectrum of Cu/ZnO in He at 276 K HCOO bands after $CO_2/N_2/H_2$ (3/29/68) exposure at 373 K, atmospheric pressure. Cu and ZnO related species are marked in blue and black, respectively. See Fig. S12 for a clearer view of the bands above 2700 cm^{-1}. b) IR spectrum of prereduced, and HCOO covered Cu/SiO_2 in He at 276 K with Cu-HCOO bands after $CO_2/N_2/H_2$ (3/29/68) exposure at 373 K, atmospheric pressure.

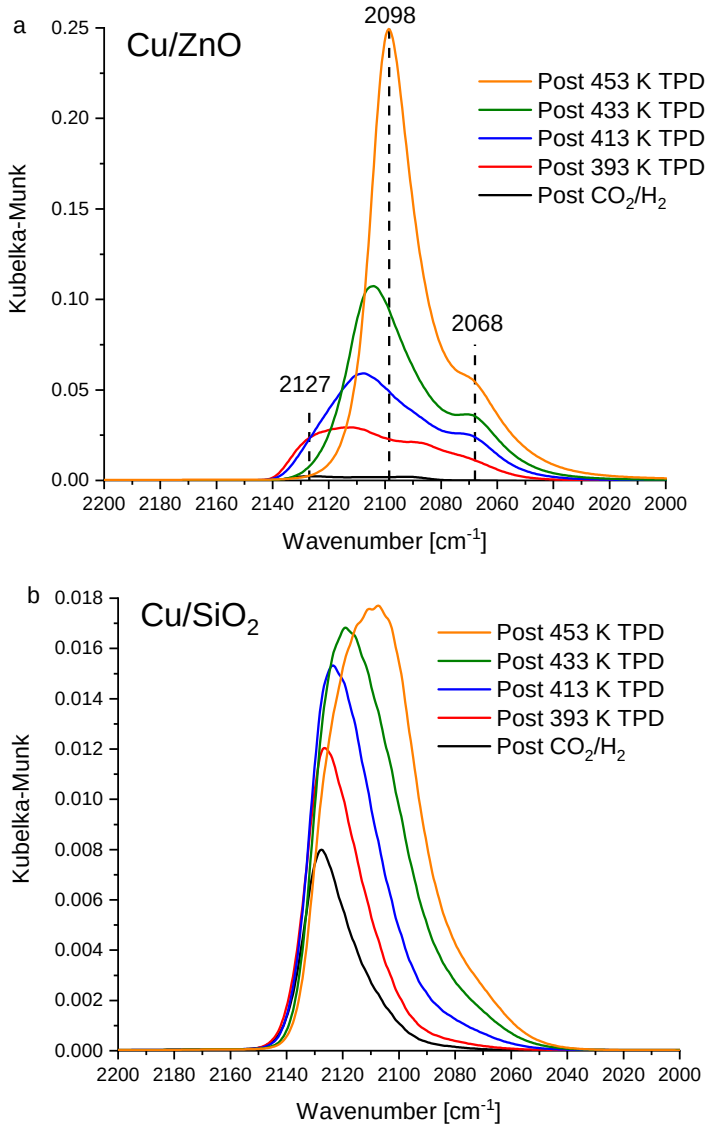

Fig. 11: IR spectra in 0.4 mbar CO at 276 K for a) Cu/ZnO and b) Cu/SiO_2. The measurements are conducted after formate decoration of the samples by CO_2/H_2 treatment and after consecutive TPDs in He to increasingly higher temperatures. Each background is the partly HCOO-covered sample prior to each CO adsorption. The HCOO covered state in Fig. 10 is thus the background for the "Post CO_2/H_2" spectrum here. See Fig. S17 for a detailed view of the very weak "Post CO_2/H_2" spectrum for Cu/ZnO.

These observations suggest that the Cu surface of Cu/ZnO is able to donate charge to the adsorbed formate to the extent that it ensures a complete physical filling of the Cu surface. By contrast the Cu surface of Cu/SiO_2 is only able to support a formate coverage until the point where the remaining Cu surface becomes charge depleted to a degree (evident from a high C-O frequency in the co-adsorbed CO in Fig. 11b) that it is unable to sustain additional formate. This suggests that adsorbates such as formate are able to accomodate the surface charge in the metal-adsorbate bonding. It would be consistent with a support induced negative charging of the metal surface in Cu/ZnO that the metal surface is able to donate more charge to the adsorbates resulting in a higher formate coverage.
The role of surface charging in governing the interaction with electron-withdrawing adsorbates is potentially important for the catalytic properties, as some of the important Cu-catalyzed reactions involve electron-withdrawing adsorbates. This includes formate in the synthesis of methanol [34, 70, 86] and adsorbed oxygen in the water-gas shift reaction [87–89].

3.8 CO stretching frequencies on supported Cu

Table 3 summarizes the C-O frequency for the main band attributed to the metallic Cu surface and to oxidized $Cu^{\delta+}$ sites for each sample and shows a clear variation in the C-O frequency with the choice of support. For the ZnO-free supports the values for the metallic surface in Table 3 represent the most intense band that is not also present in the oxidized sample. For the ZnO-containing samples the interpretation is more difficult and we have tentatively assigned the lower-frequency feature as the major feature from the metallic surface.

Table 3: Measured $\nu_{\text{C-O}}$ associated with metallic Cu on various pre-reduced Cu samples during CO adsorption at 276 K (Raney Cu at 153 K).

Sample	**$\nu_{\text{C-O}}$ for the primary band attributed to the metallic surface** [cm^{-1}]	**$\nu_{\text{C-O}}$ for $Cu^{\delta+}$** [cm^{-1}]
Cu/SiO_2	2100	2125-2127
Raney Cu	2094	2107
Cu/Al_2O_3	2089	2109
Cu/TiO_2	2070	2104-2106
$Cu/ZnO(/Al_2O_3)$	2065-2068*	2093-2100

* Band assignments are challenging as discussed in section 3.6. Here it is assumed that the 2093-2094 cm^{-1} band is from Cu-O linkages to the support and not due to sites on the interior metallic surface.

The previously discussed consistency among the reported C-O stretches for Cu/Al_2O_3 (Table 2) underlines that even small change to the C-O stretch are potentially significant. Figs. 4, 6, and 8 show that the rising intensities (and hence rising CO coverage) as a function of time during CO dosage indicate no substantial shifts in frequencies. This suggests that the coverage dependence of the frequencies is too weak to distort a comparison across the various samples. As discussed in section 3.1 the samples also have Cu crystallite/particle sizes that are close to or above the size where the Cu surface properties become size insensitive. Furthermore there is no correlation between frequencies and XRD crystallite size or area derived particle size as illustrated in Fig. S21 in the supporting information. Structure sensitivity can therefore not account for the changes in the C-O stretches across the samples. Hence the frequency shifts in Table 3 must arise from support effects.
It has been common to interpret the support dependence of the C-O frequency in terms of a preferential faceting by comparison to the most similar single crystal results. By such an interpretation Cu/Al_2O_3 ($\nu_{\text{C-O}}$ = 2089 cm^{-1}) should be dominated by Cu(100) facets, as a Cu(100) single crystal gave $\nu_{\text{C-O}}$ = 2088 cm^{-1} at a very similar CO pressure [90]. Cu/SiO_2 ($\nu_{\text{C-O}}$ = 2100 cm^{-1}) should be dominated by Cu(311) facets considering the observation [16] of $\nu_{\text{C-O}}$ = 2093-2104 cm^{-1} on a Cu(311) single crystal. However, such an interpretation is unlikely to be correct for two reasons. Firstly, a preferential faceting is inconsistent with the catalytic properties for a reaction such as methanol synthesis. If Cu/SiO_2 was dominated by (311) facets and Cu/Al_2O_3 was dominated by (100) facets, then single crystal studies

[91] suggest that the (311) facets, and thereby Cu/SiO_2, should be considerably more active. In fact it is oppositely Cu/Al_2O_3 that is an order of magnitude more active than Cu/SiO_2 at industrially relevant conditions [13, 92]. The interpretation in terms of preferential faceting based on $\nu_{C\text{-}O}$ thus yields an incorrect prediction of the catalytic properties.
Secondly, this interpretation neglects the importance of dipole coupling. The measurements on Raney Cu (Fig. 2) show a spectrum that appears to be dominated by the Cu(110) facet [16, 46] although Wulff construction modeling [47–49] suggests this to be the minor facet (5-8%) in comparison to Cu(100) with 25-30%, and Cu(111) with 60-70%. Because the interference phenomena from dipole coupling favor the higher frequencies it only takes a small percentage of higher frequency sites, such as the (110) facets, to dominate the spectrum. Even if the surface of a polycrystalline particle is dominated by lower frequency (100) or (111) facets it is still the minority of higher frequency (110) sites that tend to dominate the IR spectrum. For supported nanoparticles it is therefore always most likely that the major band arises from higher frequency sites, such as edges, corners, steps and the (110) facet with its rows of protrusions (or possibly Cu-O linkages to the support if present), regardless of the support. Similar coupling-favored sites are therefore likely to dominate the spectrum on all the supports, and the frequency shifts in adsorbed CO compared to the Raney Cu reference should thus reflect the support dependent modifications of these sites.
Given the relationship between charge on the surface sites and the C-O frequency (Fig. 1) it would seem likely that the variations in Table 3 reflect a gradual shift in the charging of the metal surface, from more positively charged in Cu/SiO_2 to more negatively charged in Cu/TiO_2 and $Cu/ZnO(/Al_2O_3)$. The charge transfer from the n-type semiconductors to the metal, which could cause this charging is discussed in section 3.4. An insulator like Al_2O_3 may still have for example oxygen vacancies in the surface that can act as electron donor centers for charge transfer to supported metals as seen [93] for Au on MgO. Oppositely, the difference between Cu/SiO_2 (2100 cm^{-1}) and Raney Cu (2094 cm^{-1}) will mostly reflect a positive charging of the metallic Cu surface in Cu/SiO_2 as discussed in section 3.5.
The observed differences in the abilities of the Cu surface of Cu/ZnO and Cu/SiO_2 towards formate uptake (Figs. 10 and 11) would also be consistent with changes in surface charging that impacts the ability to donate charge to adsorbates. It is likely that this support-dependent surface charging plays a role in regulating the interaction with the adsorbate population, which in turn may be of importance for the catalytic properties of the supported metal particles.

3.9 Effect of KBr dilution

The measurements presented in this study have been without KBr dilution. In the past literature dealing with similar IR measurements on CO adsorbed as a probe molecule it has been a common practice to use samples either physically mixed or pelletized together with KBr. However, there have been observations [32] of chemical modifications caused KBr, and it is therefore important to evaluate, if any such effects are present for CO probe molecule studies on in situ reduced samples.
Fig. 12a shows normalized IR spectra of CO adsorbed on pre-reduced, undiluted Cu/Al_2O_3 and on a physical mixture of KBr and Cu/ Al_2O_3 that has been given the same pre-treatment. The figure illustrates that there are two major effects of KBr. Firstly, the KBr-diluted experiment shows a broad shoulder IR band centered around 2120 cm^{-1} indicative of CO adsorption on fully developed Cu^+ sites. This band is absent for the undiluted experiment. Secondly, the main IR band attributed to CO on the metallic Cu surface (see Section 3.3) is slightly shifted from 2089 cm^{-1} in the undiluted experiment to 2095 cm^{-1} in the diluted experiment. Such frequency shifts in the main frequency for CO on metallic Cu are relatively general for KBr dilution of the presently employed samples as illustrated in Table 4.
The same effects are seen in Fig. 12b, which shows IR spectra of CO adsorption on pre-reduced Cu/SiO_2 with varying degrees of KBr dilution. This figure clearly illustrates that the amount of fully developed Cu^+ sites increases with increasing amount of KBr.
Transfer of potassium species to the Cu-sample is ruled out as the explanation, because this should cause a downshift in the C-O frequency [73, 94], opposite to the actual observations. Instead the effects are proposed to arise from transfer of bromine to the Cu-sample, as shifts to higher C-O frequency have previously been observed [85], when co-adsorbing a halogen (Cl from methyl chloride) with CO on Cu. The transfer of presumably low levels of Br to the sample could for example occur from hydrolysis of

Table 4: Frequencies attributed to CO on the metallic surface of supported Cu samples with and without KBr dilution.

Sample	**KBr dilution** [wt%]	**Metallic C-O frequency** [cm^{-1}]
Cu/SiO_2	50	2109
Cu/SiO_2	0	2100
Raney Cu	50	2105
Raney Cu	0	2094
Cu/Al_2O_3	45	2095
Cu/Al_2O_3	0	2089
Cu/TiO_2	10	2075
Cu/TiO_2	0	2070
Cu/ZnO	10	2068 ± 3
Cu/ZnO	0	2065 ± 3

KBr with the water formed in the prereduction as illustrated by reactions R1 and R2:

$$KBr + H_2O \longrightarrow KOH + HBr \qquad \{R1\}$$

$$HBr + Cu \longrightarrow \frac{1}{2} H_2 + Br^- - Cu^+ \qquad \{R2\}$$

The electronic effect from an electronegative adsorbate such as a halogen will be strongest immediately at the metal atom where it is adsorbed [95], and the fully developed Cu^+ sites emerging in measurements on KBr diluted samples are most likely these Br^--Cu^+ sites. However, the shift towards higher frequency for the main IR band assigned to the metallic surface could indicate that the entire Cu surface becomes more electron deficient due to the presence of the strongly electronegative adsorbates. This observation of both stronger local effects and weaker wider ranging effects could be of significance for catalytic properties of metal catalysts, which are often strongly affected by electronegative adsorbates (sulfur, halogens etc.) [96–100].
The shift in the main C-O frequency on the metallic surface is of a moderate size, and on this basis many qualitative conclusions in the literature based on KBr-diluted samples may still be valid although absolute values will be incorrect. However, the present results illustrate that the effects of dilution can be important – as an example Fig. 12b shows that KBr dilution can lead to very misleading conclusions about the distribution between metallic and oxidized sites in a sample. It is therefore advisable to regard previous studies employing KBr dilution with some caution.

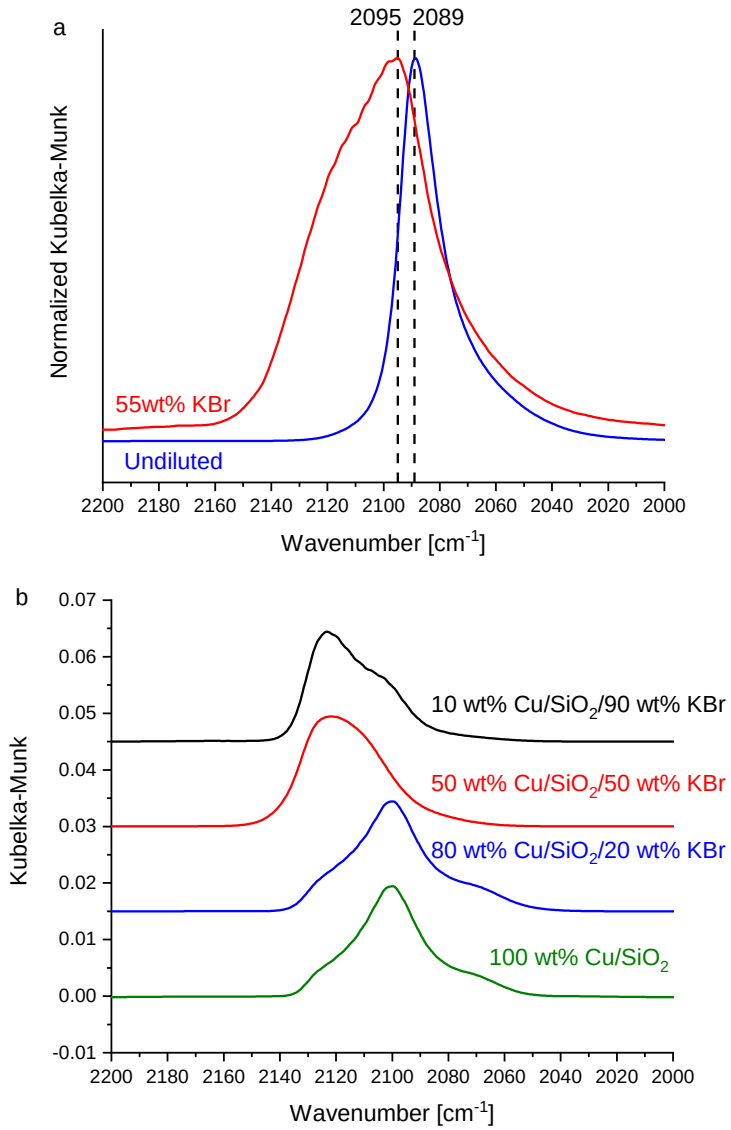

Fig. 12: IR spectra in 0.4 mbar CO at 276 K for a) Cu/ZnO and b) Cu/SiO_2. The measurements are conducted after formate decoration of the samples by CO_2/H_2 treatment and after consecutive TPDs in He to increasingly higher temperatures. Each background is the partly HCOO-covered sample prior to each CO adsorption. The HCOO covered state in Fig. 10 is thus the background for the "Post CO_2/H_2" spectrum here. See Fig. S17 for a detailed view of the very weak "Post CO_2/H_2" spectrum for Cu/ZnO.

4 Conclusion

Support effects on the Cu surface properties were investigated for Raney Cu and materials with Cu dispersed as nanoparticles on oxide supports using infrared spectroscopy on chemisorbed CO. Since the C-O frequency ($\nu_{\text{C-O}}$) is sensitive to the charge on the adsorption site ($\nu_{\text{C-O}}$ higher on Cu^+, intermediate on Cu^0 and lower on Cu^-) this method can provide information about the charging state of the Cu surface. Raney Cu was used as a reference for the intrinsic properties of Cu and illustrates the challenges caused by dipole coupling. The spectrum of CO on Raney Cu is fully dominated by the contribution from CO on the (110) facets despite this being expectedly the least abundant facet on the surface. As the dipole coupling favors the higher frequency sites such as the (110) facet, the most intense spectral features arise from the most coupling-favored sites and not from the most abundant types of sites.
The most intense CO band that was present in the reduced sample, but absent in the oxidized state of the sample was taken as the main contribution from the metallic Cu surface. The frequency for this main contribution from the metallic site varies in the following order for the investigated samples: Cu/SiO_2 > Raney Cu > Cu/Al_2O_3 > Cu/TiO_2. Given the charge-frequency relation this implies that the Cu surface of Cu/SiO_2 is more electron depleted, whereas the Cu surface is electron enriched for Cu/TiO_2. These charging effects were attributed to support dependent tendencies to donate or withdraw electrons from the Cu surface. Adsorbed CO on $Cu^{\delta+}$ sites linked to basic oxides, such as ZnO, may have low frequencies, which makes spectral interpretation even more difficult. For $Cu/ZnO(/Al_2O_3)$ systems that are important as industrial catalysts it is thus difficult to obtain an unambiguous assignment of the CO bands. However, the band that we tentatively assign to the interior of the Cu surface is lower in frequency (2065-2068 cm^{-1}) than observed on Cu single crystals, which may also indicate an electron enrichment of the Cu surface. Experiments with co-adsorption of HCOO and CO suggested that electron-withdrawing adsorbates can accommodate the surface charge in the metal-adsorbate bonding. This conclusion is based on an increased $\nu_{\text{C-O}}$ in CO co-adsorbed with formate, which indicates that CO experiences a more electron-depleted surface because formate attracts the surface charge. A CO_2/H_2 treatment to adsorb formate on Cu/ZnO largely prevented subsequent CO adsorption on copper sites, whereas identically treated Cu/SiO_2 maintained a significant fraction of its intrinsic CO adsorption. This indicates that the Cu surface of Cu/ZnO interacts more strongly with formate adsorbates, which here resulted in a greater filling of the Cu surface. This would be in reasonable agreement with a support-induced electron enrichment of the Cu surface that impacts the ability to donate charge to adsorbates. Consequently, the support dependent electron donation or withdrawal may help to regulate the interaction with adsorbates on the Cu surface and hence the catalytic properties. The effect of sample dilution by KBr, which has been employed in many studies in the literature, was also investigated. It is observed that KBr has a substantial impact on the spectra of the in situ reduced samples. The presence of KBr leads to a growth in the number of fully developed Cu^+ sites and a general electron depletion of the surface (deduced from an increased $\nu_{\text{C-O}}$ for the most intense CO band). These effects were attributed to Br^- transferred to the Cu surface yielding Br^--Cu^+ at the immediate adsorption site and a wider ranging electron depleting effect.

Acknowledgements

This work was supported by the Villum Foundation Center for Science of Sustainable Fuels and Chemicals, Villum Foundation V-SUSTAIN Grant 9455.

References

[1] B. S. Clausen, G. Steffensen, B. Fabius, J. Villadsen, R. Feidenhans'l, and H. Topsøe. In situ cell for combined XRD and on-line catalysis tests: Studies of Cu-based water gas shift and methanol catalysts. *Journal of Catalysis*, 132(2):524–535, 1991. doi: 10.1016/0021-9517(91)90168-4.

[2] V. Kleymenov, J. Sa, J. Abu-Dahrieh, D. Rooney, J. A. Van Bokhoven, E. Troussard, J. Szlachetko, O. V. Safonova, and M. Nachtegaal. Structure of the methanol synthesis catalyst determined by in situ HERFD XAS and EXAFS. *Catalysis Science and Technology*, 2(2):373–378, 2012. doi: 10.1039/c1cy00277e.

[3] J. L. Robbins, E. Iglesia, C. P. Kelkar, and B. DeRites. Methanol synthesis over Cu/SiO_2 catalysts. *Catalysis Letters*, 10(1-2):1–10, 1991. doi: 10.1007/BF00764730.

[4] C. Baltes, S. Vukojević, and F. Schüth. Correlations between synthesis, precursor, and catalyst structure and activity of a large set of $CuO/ZnO/Al_2O_3$ catalysts for methanol synthesis. *Journal of Catalysis*, 258(2):334–344, 2008. doi: 10.1016/j.jcat.2008.07.004.

[5] R. W. Joyner, R. Burch, S. E. Golunski, and M. S. Spencer. 'Good' correlations in methanol synthesis catalysis, a comment on a letter by burch, golunski and spencer. *Catalysis Letters*, 6 (1):151–156, 1990. doi: 10.1007/BF00764064.

[6] M. J. L. Ginés, N. Amadeo, M. Laborde, and C. R. Apesteguía. Activity and structure-sensitivity of the water-gas shift reaction over Cu–Zn–Al mixed oxide catalysts. *Applied Catalysis A, General*, 131(2):283–296, 1995. doi: 10.1016/0926-860X(95)00146-8.

[7] F. S. Stone and D. Waller. Cu-ZnO and $Cu\text{-}ZnO/Al_2O_3$ catalysts for the reverse water-gas shift reaction. The effect of the Cu/Zn ratio on precursor characteristics and on the activity of the derived catalysts. *Topics in Catalysis*, 22(3-4):305–318, 2003. doi: 10.1023/A:1023592407825.

[8] R. A. Hadden, P. J. Lambert, and C. Ranson. Relationship between the copper surface area and the activity of $CuO/ZnO/Al_2O_3$ water-gas shift catalysts. *Applied Catalysis A, General*, 122(1): L1–L4, 1995. doi: 10.1016/0926-860X(94)00263-0.

[9] T. Fujitani, M. Saito, Y. Kanai, T. Kakumoto, T. Watanabe, J. Nakamura, and T. Uchijima. The role of metal oxides in promoting a copper catalyst for methanol synthesis. *Catalysis Letters*, 25(3-4):271–276, 1994. doi: 10.1007/BF00816307.

[10] P. Chaumette, J. Barbier, and J Fortin. Carbonates, a key for selecting methanol synthesis catalysts. *Proc 9th Int Congr Catal*, pages 585–593, 1988.

[11] K. Murata M. Saito. Development of high performance Cu/ZnO-based catalysts for methanol synthesis and the water-gas shift reaction. *Catal. Surveys Asia*, 8(4):285–294, 2004. doi: 10.1007/s10563-004-9119-y.

[12] V. D. Berg, Roy, G. Prieto, G. Korpershoek, L. I. Van Der Wal, A. J. Van Bunningen, S. Lægsgaard-Jørgensen, P. E. De Jongh, and K. P. De Jong. Structure sensitivity of Cu and CuZn catalysts relevant to industrial methanol synthesis. *Nature Communications*, 7(13057): 1–7, 2016. doi: 10.1038/ncomms13057.

[13] J. Thrane, S. Kuld, N. D. Nielsen, A. D. Jensen, J. Sehested, and J. M. Christensen. Methanol-assisted autocatalysis in catalytic methanol synthesis. *Angewandte Chemie - International Edition*, 59:18189–18193, 2020. doi: 10.1002/anie.202006921.

[14] K. Hadjiivanov, T. Venkov, and H. Knözinger. FTIR spectroscopic study of CO adsorption on Cu/SiO_2: Formation of new types of copper carbonyls. *Catalysis Letters*, 75(1-2):55–59, 2001. doi: 10.1023/A:1016759123842.

[15] K. I. Hadjiivanov, M. M. Kantcheva, and D. G. Klissurski. IR study of CO adsorption on Cu-ZSM-5 and CuO/SiO_2 catalysts: σ and π components of the Cu^+-CO bond. *Journal of the Chemical Society Faraday Transactions*, 92(22):4595–4600, 1996. doi: 10.1039/FT9969204595.

[16] P. Hollins and J. Pritchard. Infrared studies of chemisorbed layers on single crystals. *Progress in Surface Science*, 19(4):275–350, 1985. doi: 10.1016/0079-6816(85)90015-2.

[17] M. Head-Gordon and J. C. Tully. Electric field effects on chemisorption and vibrational relaxation of CO on Cu(100). *Chemical Physics*, 175(1):37–51, 1993. doi: 10.1016/0301-0104(93)80227-Z.

[18] J. Dong, L. Miao, and M. Zhou. Infrared spectra and density functional calculations of the $Cu(CO)^{+}_{1-4}$,$Cu(CO)_{1-3}$, and $Cu(CO)^{-}_{1-3}$ in solid neon. *Chemical Physics Letters*, 355(1-2):31–36, 2002. doi: 10.1016/S0009-2614(02)00145-8.

[19] G. Busca. FT-IR study of the surface of copper oxide. *Journal of Molecular Catalysis*, 43(2): 225–236, 1987. doi: 10.1016/0304-5102(87)87010-4.

[20] A. A. Davydov. Study of the state of transitions-metal cations on catalyst surfaces by the IR spectroscopy of adsorbed test molecules (CO, NO). VI. State of copper in CuO. Influence of Supports on the state of copper. *Kinetics and Catalysis*, 26(1):157–167 (135–144 in Engl. transl.), 1985.

[21] R. Smoluchowski. Anisotropy of the electronic work function of metals. *Physical Review*, 60(9): 661–674, 1941. doi: 10.1103/PhysRev.60.661.

[22] C. J. Fall, N. Binggeli, and A. Baldereschi. Work Functions at Facet Edges. *Physical Review Letters*, 88(15):156802, 2002. doi: 10.1103/PhysRevLett.88.156802.

[23] L. Gao, J. Souto-Casares, J. R. Chelikowsky, and A. A. Demkov. Orientation dependence of the work function for metal nanocrystals. *Journal of Chemical Physics*, 147:214301, 2017. doi: 10.1063/1.4991725.

[24] George Blyholder. Molecular Orbital View of Chemisorbed Carbon Monoxide. *The Journal of Physical Chemistry*, 68(10):2772–2777, 1964. doi: 10.1021/j100792a006.

[25] R. A. Van Santen and N. Matthew. *Molecular Heterogeneous Catalysis: A Conceptual and Computational Approach*. Wiley-VCH, 2006. doi: 10.1002/9783527610846.

[26] V. M. Browne, S. G. Fox, and P. Hollins. Coupling effects in infrared spectra from supported metal catalyts. *Materials Chemistry and Physics*, 29(1-4):235–244, 1991. doi: 10.1016/0254-0584(91)90019-Q.

[27] P. Hollins. Effects of dipolar coupling on the intensity of infrared absorption bands from supported metal catalysts. *Spectrochimica Acta - Part A Molecular Spectroscopy*, 43(12):1539–1542, 1987. doi: 10.1016/S0584-8539(87)80044-2.

[28] X. Xu, S. M. Vesecky, and D. W. Goodman. Infrared Reflection-Absorption Spectroscopy and STM Studies of Model Silica-Supported Copper Catalysts. *Science*, 258(5083):788–790, 1992. doi: 10.1126/science.258.5083.788.

[29] D. F. Cox and K. H. Schulz. Interaction of CO with Cu^{+} cations: CO adsorption on $Cu_2O(100)$. *Surface Science*, 249(1-3):138–148, 1991. doi: 10.1016/0039-6028(91)90839-K.

[30] N.-Y. Topsøe and H. Topsøe. FTIR studies of dynamic surface structural changes in Cu-based methanol synthesis catalysts. *Journal of Molecular Catalysis A: Chemical*, 141:95–105, 1999. doi: 10.1016/s1381-1169(98)00253-2.

[31] J. Schumann, J. Kröhnert, E. Frei, R. Schlögl, and A. Trunschke. IR-Spectroscopic Study on the Interface of Cu-Based Methanol Synthesis Catalysts: Evidence for the Formation of a ZnO Overlayer. *Topics in Catalysis*, 60(19-20):1735–1743, 2017. doi: 10.1007/s11244-017-0850-9.

[32] J. Couble, P. Gravejat, F. Gaillard, and D. Bianchi. Quantitative analysis of infrared spectra of adsorbed species using transmission and diffuse reflectance modes case study: Heats of adsorption of CO on TiO_2 and CuO/Al_2O_3. *Applied Catalysis A: General*, 371(1-2):99–107, 2009. doi: 10.1016/j.apcata.2009.09.036.

[33] F. C. Meunier. Pitfalls and benefits of in situ and operando diffuse reflectance FT-IR spectroscopy (DRIFTS) applied to catalytic reactions. *React. Chem. Eng.*, 1(2):134–141, 2016. doi: 10.1039/C5RE00018A.

[34] N. D. Nielsen, A. D. Jensen, and J. M. Christensen. Quantification of Formate and Oxygen Coverages on Cu Under Industrial Methanol Synthesis Conditions. *Catalysis Letters*, 150(9): 2447–2456, 2020. doi: 10.1007/s10562-020-03162-7.

[35] G. C. Chinchen, C. M. Hay, H. D. Vandervell, and K. C. Waugh. The measurement of copper surface areas by reactive frontal chromatography. *Journal of Catalysis*, 103(1):79–86, 1987. doi: 10.1016/0021-9517(87)90094-7.

[36] R. Chatterjee, S. Kuld, R. V. D. Berg, A. Chen, and W. Shen. Mapping Support Interactions in Copper Catalysts. *Topics in Catalysis*, 62(7-11):649–659, 2019. doi: 10.1007/s11244-019-01150-9.

[37] O. Hinrichsen, T. Genger, and M. Muhler. Chemisorption of N_2O and H_2 for the Surface Determination of Copper Catalysts. *Chemical Engineering & Technology*, 23(11):956–959, 2000. doi: 10.1002/1521-4125(200011)23:11⟨956::AID-CEAT956⟩3.0.CO;2-L.

[38] P. Scherrer. Bestimmung der Grösse und der inneren Struktur von Kolloidteilchen mittels Röntgenstrahlen. *Nachr. Ges. Wiss. Gött.*, 26:98–100, 1918.

[39] B. D. Cullity. *Element of X-ray Diffraction*. Addison-Wesley, 2nd edition, 1978.

[40] H. P. Klug and L. E. Alexander. *X-Ray Diffraction Procedures: For Polycrystalline and Amorphous Materials*. Wiley, 2nd editio edition, 1974.

[41] A. Belkly, M. Helderman, V. L. Karen, and P. Ulkch. New developments in the Inorganic Crystal Structure Database (ICSD): Accessibility in support of materials research and design. *Acta Crystallographica Section B: Structural Science*, 58(3 PART 1):364–369, 2002. doi: 10.1107/S0108768102006948.

[42] Q. Wu, L. D. L. Duchstein, G. L. Chiarello, J. M. Christensen, C. D. Damsgaard, C. F. Elkjær, J. B. Wagner, B. Temel, J. D. Grunwaldt, and A. D. Jensen. In situ observation of Cu-Ni alloy nanoparticle formation by X-ray diffraction, X-ray absorption spectroscopy, and transmission electron microscopy: Influence of Cu/Ni ratio. *ChemCatChem*, 6(1):301–310, 2014. doi: 10.1002/cctc.201300628.

[43] A. Karelovic and P. Ruiz. The role of copper particle size in low pressure methanol synthesis via CO_2 hydrogenation over Cu/ZnO catalysts. *Catal. Sci. Technol.*, 5(2):869–881, 2015. doi: 10.1039/C4CY00848K.

[44] A. Karelovic, G. Galdames, J. C. Medina, C. Yévenes, Y. Barra, and R. Jiménez. Mechanism and structure sensitivity of methanol synthesis from CO_2 over SiO_2-supported Cu nanoparticles. *Journal of Catalysis*, 369:415–426, 2019. doi: 10.1016/j.jcat.2018.11.012.

[45] X. Xu and D. W. Goodman. Structural and chemisorptive properties of model catalysts: Copper supported on SiO_2 thin films. *Journal of Physical Chemistry*, 97(3):683–689, 1993. doi: 10.1021/j100105a025.

[46] J. Pritchard, T. Catterick, and R. K. Gupta. Infrared spectroscopy of chemisorbed carbon monoxide on copper. *Surface Science*, 53(1):1–20, 1975. doi: 10.1016/0039-6028(75)90113-2.

[47] J. J. F. Scholten and J. A. Konvalinka. Reaction of nitrous oxide with a nickel surface. *Transaction of the Faraday Society*, 65:2465–2473, 1969. doi: 10.1016/S0166-9834(00)82418-5.

[48] B. E. Sundquist. A direct determination of the anisotropy of the surface free energy of solid gold, silver, copper, nickel, and alpha and gamma iron. *Acta Metallurgica*, 12(1):67–86, 1964. doi: 10.1016/0001-6160(64)90055-0.

[49] C. V. Ovesen, B. S. Clausen, J. Schiøtz, P. Stoltze, H. Topsøe, and J. K. Nørskov. Kinetic Implications of Dynamical Changes in Catalyst Morphology during Methanol Synthesis over Cu/ZnO Catalysts. *Journal of Catalysis*, 168(2):133–142, 1997. doi: 10.1006/jcat.1997.1629.

[50] R. N. D'Alnoncourt, X. Xia, J. Strunk, E. Löffler, O. Hinrichsen, and M. Muhler. The influence of strongly reducing conditions on strong metal-support interactions in Cu/ZnO catalysts used for methanol synthesis. *Physical Chemistry Chemical Physics*, 8(13):1525–1538, 2006. doi: 10.1039/b515487a.

[51] M. B. Padley, C. H. Rochester, G. J. Hutchings, and F. King. FTIR Spectroscopic Study of Thiophene, SO_2, and CO Adsorption on Cu/Al_2O_3 Catalysts. *Journal of Catalysis*, 148:438–452, 1994. doi: 10.1006/jcat.1994.1230.

[52] O. Dulaurent, X. Courtois, C. Perrichon, and D. Bianchi. Heats of adsorption of CO on a Cu/Al_2O_3 catalyst using FTIR spectroscopy at high temperatures and under adsorption equilibrium conditions. *Journal of Physical Chemistry B*, 104(25):6001–6011, 2000. doi: 10.1021/jp9943629.

[53] H. Arakawa, K. Sayama, K. Okabe, and A. Murakami. Promoting effect of TiO_2 addition to CuO-ZnO catalyst on methanol synthesis by catalytic hydrogenation of CO_2. *Studies in Surface Science and Catalysis*, 77:389–392, 1993. doi: 10.1016/S0167-2991(08)63218-8.

[54] K. Hadjiivanov, J. Lamotte, and J. C. Lavalley. FTIR study of low-temperature CO adsorption on pure and ammonia-precovered TiO_2 (anatase). *Langmuir*, 13(13):3374–3381, 1997. doi: 10.1021/la962104m.

[55] J. C. Frost. Junction effect interactions in methanol synthesis catalysts. *Nature*, 334:577–580, 1988. doi: 10.1038/332141a0.

[56] M. W. Allen and S. M. Durbin. Influence of oxygen vacancies on Schottky contacts to ZnO. *Applied Physics Letters*, 92(12):1–4, 2008. doi: 10.1063/1.2894568.

[57] F. Boccuzzi, G. Ghiotti, and A. Chiorino. Metal-semiconductor interaction: Effect of H_2 chemisorption on the IR transparency of the Cu/ZnO system. *Surface Science Letters*, 183 (1-2):285–289, 1987. doi: 10.1016/0167-2584(87)90133-2.

[58] T. Binninger, T. J. Schmidt, and D. Kramer. Capacitive electronic metal-support interactions: Outer surface charging of supported catalyst particles. *Physical Review B*, 96(16):165405, 2017. doi: 10.1103/PhysRevB.96.165405.

[59] G. Ghiotti, F. Boccuzzi, and A. Chiorino. The Operation of the "Metal-Surface Selection Rule" on the Vibrational Spectra of Species Adsorbed on Supported Copper Particles. *Surface Science*, 178:553–564, 1986. doi: 10.1016/0039-6028(86)90332-8.

[60] J. Saussey, J.C. Lavalley, J. Lamotte, and T. Rais. I.R. Spectroscopic Evidence of Formyl Species formed by CO and H_2, Co-adsorption on ZnO and Cu-ZnO. *J. Chem. Soc. Chem. Commun.*, 5: 278–279, 1982. doi: 10.14825/kaseki.40.0_51_1.

[61] F. Boccuzzi, E. Garrone, A. Zecchina, A. Bossi, and M. Camia. Infrared study of ZnO surface properties. II. H_2-CO interaction at room temperature. *Journal of Catalysis*, 51(2):160–168, 1978. doi: 10.1016/0021-9517(78)90289-0.

[62] F. Boccuzzi, G. Ghiotti, and A. Chiorino. CO adsorption on small particles of Cu dispersed on microcrystalline ZnO. *Surface Science*, 156:933–942, 1985. doi: 10.1016/0039-6028(85)90269-9.

[63] N. D. Nielsen, J. Thrane, A. D. Jensen, and J. M. Christensen. Bifunctional Synergy in CO Hydrogenation to Methanol with Supported Cu. *Catalysis Letters*, 150:1427–1433, 2020. doi: 10.1007/s10562-019-03036-7.

[64] A. M. Abdel-Mageed, A. Klyushin, A. Rezvani, A. Knop-Gericke, R. Schlögl, and R. J. Behm. Negative Charging of Au Nanoparticles during Methanol Synthesis from CO_2/H_2 on a Au/ZnO Catalyst: Insights from Operando IR and Near-Ambient-Pressure XPS and XAS Measurements. *Angewandte Chemie - International Edition*, 12613:10325–10329, 2019. doi: 10.1002/anie.201900150.

[65] B. E. Goodby and J. E. Pemberton. XPS Characterization of a commercial $Cu/ZnO/Al_2O_3$ catalyst: Effects of oxidation, reduction, and the steam reformation of methanol. *Applied Spectroscopy*, 42(5):754–760, 1988. doi: 10.1366/0003702884429148.

[66] Y. Okamoto, K. Fukino, T. Imanaka, and S. Teranishi. Surface Characterization of CuO-ZnO Methanol-Synthesis Catalysts by X-ray Photoelectron Spectrosocpy. 2. Reduced Catalysts. *The Journal of physical chemistry*, 87(19):3747–3754, 1983. doi: 10.1021/j100242a035.

[67] L. H. Dubois, B. R. Zegarski, and R. G. Nuzzo. Spontaneous Organization of Carboxylic Acid Monolayer Films in Ultrahigh Vacuum. Kinetic Constraints to Assembly via Gas-Phase Adsorption. *Langmuir*, 2(4):412–417, 1986. doi: 10.1021/la00070a006.

[68] M. Bowker, H. Houghton, and K. C. Waugh. Mechanism and kinetics of methanol synthesis on zinc oxide. *Journal of the Chemical Society, Faraday Transactions 1: Physical Chemistry in Condensed Phases*, 77(12):3023–3036, 1981. doi: 10.1039/F19817703023.

[69] K. Kähler, M. C Holz, M. Rohe, J. Strunk, and M. Muhler. Probing the reactivity of ZnO and Au/ZnO nanoparticles by methanol adsorption: A TPD and DRIFTS study. *ChemPhysChem*, 11(12):2521–2529, 2010. doi: 10.1002/cphc.201000282.

[70] S. Fujita, M. Usui, H. Ito, and N. Takezawa. Mechanisms of Methanol Synthesis from Carbon Dioxide and from Carbon Monoxide at Atmospheric Pressure over Cu/ZnO. *Journal of Catalysis*, 157(2):403–413, 1995. doi: 10.1006/jcat.1995.1306.

[71] K. K. Bando, K. Sayama, H. Kusama, K. Okabe, and H. Arakawa. In-situ FT-IR study on CO_2 hydrogenation over Cu catalysts supported on SiO_2, Al_2O_3, and TiO_2. *Applied Catalysis*, 165 (1-2):391–409, 1997. doi: 10.1016/S0926-860X(97)00221-4.

[72] S. Fujita, M. Usui, E. Ohara, and N. Takezawa. Methanol synthesis from carbon dioxide at atmospheric pressure over Cu/ZnO catalyst. Role of methoxide species formed on ZnO support. *Catalysis Letters*, 13(4):349–358, 1992. doi: 10.1007/BF00765037.

[73] D. B. Clarke and A. T. Bell. An Infrared Study of Methanol Synthesis from CO_2 on Clean and Potassium-Promoted Cu/SiO_2, *Journal of Catalysis*, 154314–328, 1995. doi: 10.1006/jcat.1995.1173.

[74] F. Boccuzzi, A. Chiorino, S. Tsubota, and M. Haruta. FTIR Study of Carbon Monoxide Oxidation and Scrambling at Room Temperature over Gold Supported on ZnO and TiO_2. *The Journal of Physical Chemistry*, 100(9):3625–3631, 2002. doi: 10.1021/jp952259n.

[75] M. Shim and P. Guyot-Sionnest. Organic-capped ZnO nanocrystals: Synthesis and n-type character. *Journal of the American Chemical Society*, 123(47):11651–11654, 2001. doi: 10.1021/ja0163321.

[76] D. A. Panayotov, S. P. Burrows, and J. R. Morris. Infrared spectroscopic studies of conduction band and trapped electrons in UV-photoexcited, H-Atom n-doped, and thermally reduced TiO_2. *Journal of Physical Chemistry C*, 116(7):4535–4544, 2012. doi: 10.1021/jp2053103.

[77] F. Boccuzzi, C. Morterra, R. Scala, and A. Zecchina. Infrared Spectrum of Microcrystalline Zinc Oxide Electronic and vibrational contributions under different temperature and environmental conditions. *Chemical society, Faraday Transactions 2*, 77:2059–2066, 1981. doi: 10.1039/F29817702059.

[78] B. A. Morrow. Infra-red studies of reactions on oxide surfaces. Part 2.-Methanol on silica. *Journal of the Chemical Society, Faraday Transactions 1: Physical Chemistry in Condensed Phases*, 70: 1527–1545, 1974. doi: 10.1039/F19747001527.

[79] I. A. Fisher and A.T. Bell. In Situ Infrared Study of Methanol Synthesis from H_2/CO over Cu/SiO_2 and Cu/ZrO_2/SiO_2. *Journal of Catalysis*, 178:153–173, 1998. doi: 10.1006/jcat.1998.2134.

[80] L. D. White and C. P. Tripp. A low-frequency infrared study of the reaction of methoxymethylsilanes with silica. *Journal of Colloid and Interface Science*, 224(2):417–424, 2000. doi: 10.1006/jcis.1999.6709.

[81] L. Dubois, T. H. Ellis, B. R. Zegarski, and S. D. Kevan. New insights into the kinetics of formic acid decomposition on copper surfaces. *Surface Science*, 172:385–397, 1986. doi: 10.1016/0039-6028(86)90763-6.

[82] E. T. Krastev, D. E. Kuhl, and R. G. Tobin. Multiple mechanisms for adsorbate-induced resistivity: Oxygen and formate on Cu(100). *Surface Science*, 387:L1051–L1056, 1997. doi: 10.1016/S0039-6028(97)00439-1.

[83] A. Chutia, I. P. Silverwood, M. R. Farrow, D. O. Scanlon, P. P. Wells, M. Bowker, S. F. Parker, and C. F. A. Catlow. Adsorption of formate species on Cu(h,k,l) low index surfaces. *Surface Science*, 653:45–54, 2016. doi: 10.1016/j.susc.2016.05.002.

[84] M. Bowker and R. J. Madix. XPS, UPS and thermal desorption studies of the reactions of formaldehyde and formic acid with the Cu(110) surface. *Surface Science*, 102:542–565, 1981. doi: 10.1016/0039-6028(81)90045-5.

[85] L. Dubois and B. R. Zegarski. The influence of electron-withdrawing on the adsorption of CO on copper. *Chemical Physics Letters*, 120(6):537–541, 1985. doi: 10.1016/0009-2614(85)80550-90.

[86] Y. Amenomiya and T. Tagawa. Infrared study of methanol synthesis from CO_2 and H_2 on supported copper-zinc oxide catalysts. *Proc. of 8th Int. Congress on Catal*, pages 557–567, 1984.

[87] J. Nakamura, J. M. Campbell, and C. T. Campbell. Kinetics and mechanism of the water-gas shift reaction catalysed by the clean and Cs-promoted Cu(110) surface: A comparison with Cu(111). *Journal of the Chemical Society, Faraday Transactions*, 86(15):2725–2734, 1990. doi: 10.1039/FT9908602725.

[88] S. I. Fujita, M. Usui, and N. Takezawa. Mechanism of the reverse water gas shift reaction over Cu/ZnO catalyst. *Journal of Catalysis*, 134(1):220–225, 1992. doi: 10.1016/0021-9517(92)90223-5.

[89] C. V. Ovesen, P. Stoltze, J. K. Nørskov, and C. T. Campbell. A kinetic model of the water gas shift reaction. *Journal of Catalysis*, 134(2):445–468, 1992. doi: 10.1016/0021-9517(92)90334-E.

[90] C. M. Truong, J. A. Rodriguez, and D. W. Goodman. CO adsorption isotherms on Cu(100) at elevated pressures and temperatures using infrared reflection absorption spectroscopy. *Surface Science Letters*, 271(3):L385–L391, 1992. doi: 10.1016/0039-6028(92)90896-E.

[91] I. Nakamura, T. Fujitani, T. Uchijima, and J. Nakamura. A model catalyst for methanol synthesis: Zn-deposited and Zn-free Cu surfaces. *Journal of Vacuum Science & Technology*, 14(3): 1464–1468, 1996. doi: 10.1116/1.579970.

[92] M. Saito, J. Wu, K. Tomoda, I. Takahara, and K. Murata. Effects of ZnO contained in supported Cu-based catalysts on their activities for several reactions. *Catalysis Letters*, 83(1-2):1–4, 2002. doi: 10.1023/A:1020693226903.

[93] B. Yoon, H. Häkkinen, U. Landman, A. S. Wörz, J. M. Antonietti, S. Abbet, K. Judai, and U. Heiz. Charging effects on bonding and catalyzed oxidation of CO on Au_8 clusters on MgO. *Science*, 307(5708):403–407, 2005. doi: 10.1126/science.1104168.

[94] L. H. Dubois, B. R. Zegarski, and H. S. Luftman. Summary Abstract: Multiple CO bonding states on potassium-dosed Cu(100). *Journal of Vacuum Science & Technology A: Vacuum, Surfaces, and Films*, 5(4):455–457, 1987. doi: 10.1116/1.574688.

[95] J. K. Nørskov and S Holloway. Microscopic Model for the Poisoning and Promotion of Adsorption Rates by Electronegative and Electropositive Atoms. *Surface Science*, 137:65–78, 1984. doi: 10.1016/0039-6028(84)90676-9.

[96] J. C. J. Bart and R. P. A. Sneeden. Copper-zinc oxide-alumina methanol catalysts revisited. *Catalysis Today*, 2(1):1–124, 1987. doi: 10.1016/0920-5861(87)80001-9.

[97] J. B. Hansen and P. E. H. Nielsen. *Methanol Synthesis*, volume 2. Wiley-VCH Verlag GmbH, 2nd edition edition, 2008. doi: 10.1002/9783527610044.hetcat0148.

[98] D. E. Peebles, D. W. Goodman, and J. M. White. Methanation of carbon dioxide on Ni(100) and the effects of surface modifiers. *Journal of Physical Chemistry*, 87(22):4378–4387, 1983. doi: 10.1021/j100245a014.

[99] D. W. Goodman and M. Kiskinova. Chemisorption and reactivity studies of H_2 and CO on sulfided Ni(100). *Surface Science*, 105:L265–L270, 1981. doi: 10.1016/0039-6028(81)90001-7.

[100] M. Kiskinova and D. W. Goodman. Modification of chemisorption properties by electronegative adatoms: H_2 and CO on chlorided, sulfided, and phosphided Ni(100). *Surface Science*, 108(1): 64–76, 1981. doi: 10.1016/0039-6028(81)90358-7.

Chapter 7

Support-dependent electron transfer to Cu explains the support effect for catalytic methanol synthesis over Cu

Authors: Niels D. Nielsen[1], Anker D. Jensen[1], Jakob M. Christensen[1]
[1]*Department of Chemical and Biochemical Engineering, Technical University of Denmark, Søltofts Plads Building 229, 2800 Kgs. Lyngby, Denmark*
*__Correspondence to:__ jmc@kt.dtu.dk

Status:
In preparation

Abstract

Understanding the role of support on metal-catalyzed reactions is central to the optimization of catalytic materials. This support effect is especially important for the catalytic conversion of syngas to methanol as SiO_2 highly impedes the rate in contrast to the strong activity promoting role of ZnO. In-situ IR spectroscopy and kinetic analysis of supported and unsupported Cu catalysts are applied to investigate a proposed support-regulated electron transfer mechanism to account for the support effect. Photo-ionization of free conducting electrons in oxide structures causes IR absorbance. Reduced ZnO-based samples contained H_2, which due to its electron-donating properties can facilitate free electrons in reducible oxides. Free electrons can be photo-ionized by IR and lead to high IR absorbance. Contact between ZnO and Cu promotes electron transfer to Cu to align the Fermi levels of the two materials. Consequently, the IR absorbance declines and follows the order: $Cu/ZnO < Cu/ZnO/Al_2O_3 < ZnO$. Unlike activity beneficial ZnO, detrimental and insulating SiO_2 does not contain H_2 or absorb IR. Support-regulated electron transfer constitutes a mechanism that jointly explains the support effect on the TOF and involves the entire Cu surface.

Keywords: Copper catalyst · Support effects · Formate · Methanol synthesis · IR-MS

1 Introduction

Methanol synthesis is achieved by syngas ($CO_2/CO/H_2$) conversion over a $Cu/ZnO/Al_2O_3$ (CZnA) catalyst operating at 473-573 K and 50-100 bar at a large industrial scale (∼85 Mtons/year in 2018

[1]). The renewed interest of methanol relates to its dual use as a convenient sustainable fuel and efficient liquid energy carrier of renewable energy [1–3]. Achieving a sustainable methanol society as envisioned by Noble laureate George A. Olah [4] necessitates comprehensive optimization work, where an understanding of the metal-support interactions is central. For methanol synthesis from CO_2-containing feeds over Cu supported catalysts the productivity generally scales linearly with the total metallic Cu surface area as reported for SiO_2 [5–7] (except for a substantially lower activity in very small nanoparticles [8, 9]) and ZnO-based catalysts [10–13], which strongly suggests that the reaction is distributed on the metallic surface. Accordingly, a proposed support effect mechanism must impact the entire metal surface.

2 Results and Discussion

Fig. 1a shows the turnover frequency (TOF, here rate per Cu surface atom) at high temperature and pressure characteristic of industrial operation for Raney Cu (which is a good representation of the intrinsic properties of Cu) [14] and for Cu supported on SiO_2 and ZnO($/Al_2O_3$). The figure illustrates the importance of the support, as ZnO exerts a strong beneficial effect, whereas SiO_2 exerts a significant detrimental effect. Extended data Fig. E3 verifies the detrimental effect of SiO_2 by confirming that the present Cu/SiO_2 sample is characteristic of such materials in the literature and by showing a direct comparison between Cu/SiO_2 and systems such as unsupported Cu and Raney Cu that illustrate the intrinsic properties of Cu.

Samples including pure supports (ZnO and SiO_2) and Cu-based catalysts (Cu/ZnO($/Al_2O_3$) and Cu/SiO_2) were treated with hydrogen up to 523 K before flushing with this temperature. Trapped hydrogen gets incorporated into the ZnO bulk [15], whereas hydrogen on the surfaces of ZnO [15] and Cu [16] desorb below the flushing temperature (523 K). Pre-treating ZnO with hydrogen creates strong absorbance across the entire mid-IR range as shown by the raw spectra in extended data E1 and by the average absorbance (650-4000 cm^{-1}) in Fig. 1b. This absorbance increases with the severity of the hydrogen treatment which can be attributed to intraband transitions among free electrons in the ZnO conduction band (Fig. 1c), that enable the absorbance of a continuum of IR frequencies [17–19]. Absorbed hydrogen in the ZnO bulk acts as an electron donor, and the free charge carriers in the conduction band arise from thermal excitation of electrons in these hydrogen donor-levels (Fig. 1c). Remarkably, Fig 1b shows that the Cu/ZnO($/Al_2O_3$) systems exhibit lower degree of IR absorbance after the hydrogen treatment, even though a temperature programmed desorption (TPD) of the hydrogen pre-treated samples shows that the amount of hydrogen in the ZnO bulk (the desorption peak at 573 K) is substantially higher for the Cu/ZnO($/Al_2O_3$) systems (Fig. 1d) possibly due to hydrogen spillover from Cu. The lower absorbance for Cu/ZnO($/Al_2O_3$) systems despite their greater concentration of ZnO bulk hydrogen to serve as electron donors is rationalized by electrons being transferred to the Cu metal instead of residing in ZnO conduction band (Fig. 1c). These results illustrate that charge is transferred from a beneficial support (ZnO) to the Cu metal. This observation of electron donation can help to rationalise the experimental indications [20–23] of an electron-enriched metal surface of particles dispersed on ZnO. In the classical limit, charge transferred to a conductor will be distributed across the external surface and as theoretical calculations [24] show this behaviour emerges already in very small clusters. Thus the $>$ 5 nm metal particles in industrial catalysts should be reasonably represented by the classical limit [25]. Hence, this electron donation offers a mechanism whereby the support impacts the metal surface in its entirety as indicated by simultaneous dispersion independence ($>$ ca. 5 nm) and support dependence of the catalytic properties in Cu-catalysed methanol synthesis. The IR measurements in Fig. 1b do not suggest any charge donating effect from insulating SiO_2. By contrast prior IR measurements [20] suggest an electron-deficient Cu surface on Cu/SiO_2 attributable to the electron-withdrawing effect of Cu-O-Si linkages to the support. Hence, there is a correlation between the methanol synthesis activity and the support induced charge enrichment/depletion of the Cu surface.

It is also evident from prior IR spectroscopy studies [20] that the charge in the Cu surface is donated to the electron-withdrawing formate adsorbates on Cu, whose conversion are the expected rate limiting step in methanol synthesis [26–28]. A charge enriched Cu surface (as on a ZnO support) may thus have a positive effect on the methanol synthesis by either raising the population of electron-withdrawing

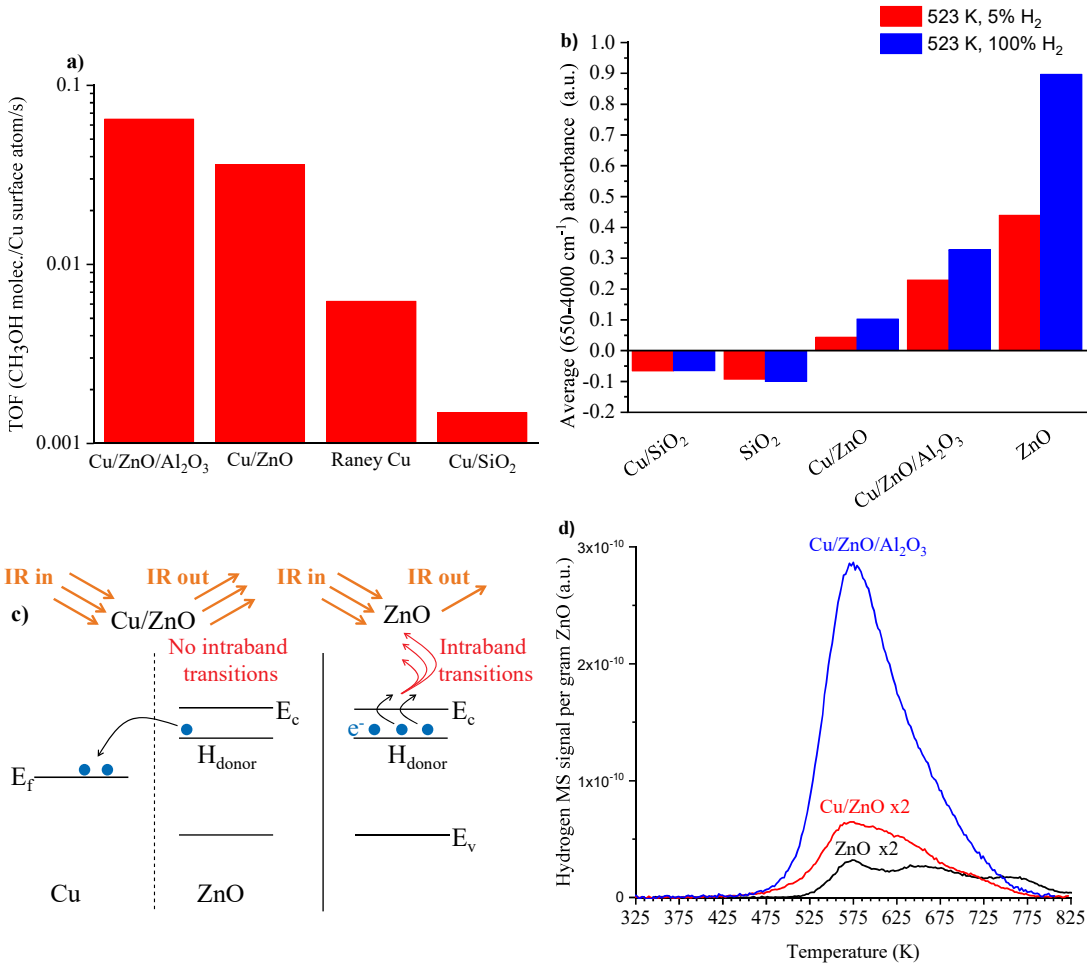

Fig. 1| Mechanism behind the support effect. a Turnover frequencies for methanol synthesis over Raney Cu, which is a good approximation to the intrinsic properties of Cu [14] and over Cu supported on ZnO and SiO_2-based supports ($CO_2/CO/H_2$ = 3/29/68, T = 523 K, P = 50 bar) **b** Average mid-IR (650-4000 cm^{-1}) absorbance of catalysts and supports in He at 298 K after treatments in H_2 containing gas at 523 K, 1 atm. The background is the same sample in He after pre-reduction in 5% H_2 at 448 K, 1 atm. Raw spectra in Extended data Fig. E1. **c** Energy diagram illustrating the intraband transitions leading to mid-IR absorption in H-containing ZnO in the right panel and the electronic transitions from ZnO to Cu that diminishes this absorbance in Cu/ZnO systems shown in the left panel. **d** H_2 evolution during temperature programmed desorption in flowing He (45 NmL/min, 2 K/min heating) for ZnO-based samples pretreated with 1 atm H_2 at 523 K followed by flushing in He at 523 K. Raw data in Extended data Fig. E2.

formate intermediates or by raising the filling of the π-orbitals in formate that are antibonding for the formate C-O bond that needs to be ruptured in the rate limiting conversion to methanol. For formate adsorbed on Cu these antibonding orbitals are located slightly above the Fermi level and receive only marginal filling [29, 30] as also evident from formate's near exclusive tendency to desorb as CO_2 without rupture of the C-O bonds in temperature programmed desorption. Hence, any increased filling of these orbitals from a more charge enriched surface would benefit the methanol formation. A charge depleted Cu surface (as on a SiO_2 support) will oppositely have a detrimental impact on these properties. Extended data Fig. E4 shows an analysis of the formate coverage on Cu for supported catalysts at the conditions of Fig. 1a established using the quenching method presented elsewhere [14]. Although the results show a moderately increased formate coverage on Cu for Cu/ZnO compared to Raney Cu, which can account for a smaller part of the beneficial support effect, the coverages on Raney

Cu and Cu/SiO_2 are very similar despite a major difference in turnover frequency. Consequently, the regulation of the formate population size on the Cu surface is not the primary impact of the support on the catalytic activity.

Fig. 2 shows the methanol formation during temperature programmed hydrogenation of formate deposited from HCOOH on pre-reduced Cu-samples. As also observed by others [31] Cu/SiO_2 is nearly unable to convert formate into methanol in agreement with the low rate of the steady state reaction (Fig. 1a). By contrast the ability to hydrogenate formate into methanol is considerably greater for Raney Cu and especially for $Cu/ZnO/Al_2O_3$ in agreement with the order of the steady state reaction rates. Hence, Fig. 2 shows that the major impact of the support effect is on the ability to perform the rate limiting formate hydrogenation, which correlates directly to the charge enrichment/depletion state of the Cu surface as expected from the changes to the occupancy of the antibonding orbitals in formate.

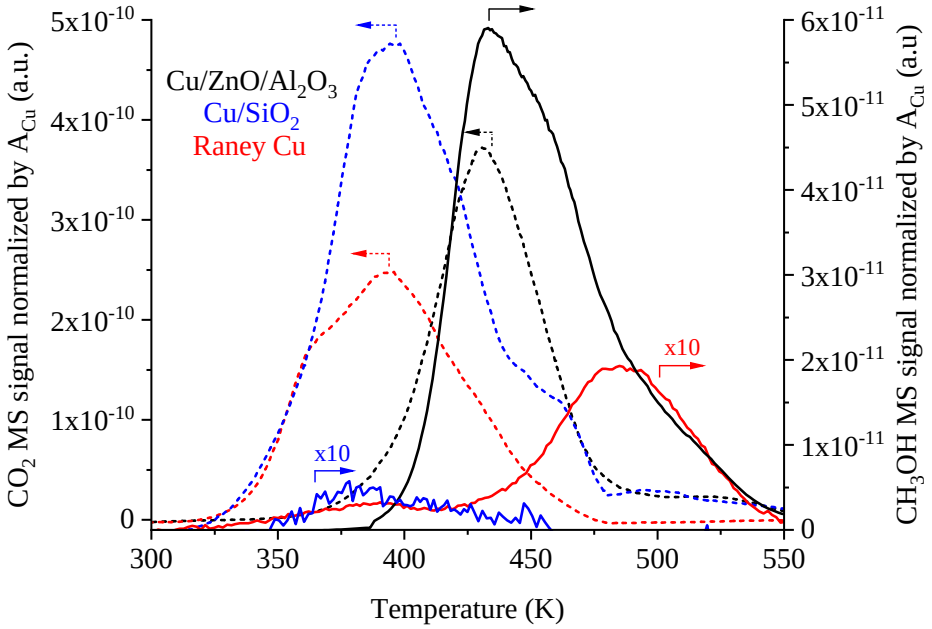

Fig. 2| Support dependence in the ability to hydrogenate HCOO into methanol. The MS signals for CO_2 (m/z = 44, left y-axis marked by dashed lines) and CH_3OH (m/z = 31, right y-axis marked by solid lines) during temperature programmed hydrogenation (2 K/min ramp in 50 Nml/min H_2) for Raney Cu, $Cu/ZnO/Al_2O_3$, and Cu/SiO_2. The signals are normalized to the Cu surface area and blank test corrected. The formate is adsorbed by injecting 1 µl of liquid HCOOH into a He stream passing over the pre-reduced sample at 313 K. Extended data Fig. E5 verifies that the non-appearance of methanol for Cu/SiO_2 is not due to re-adsorption effects.

3 Conclusion

In conclusion, the presented results strongly suggest that electron transfer between Cu and support regulates the conversion of formate to methanol, which readily accounts for the observed variation in TOF for Cu supported catalysts. Improved understanding of the support effect provides tools to optimize metal-support catalysts further and can promote sustainable methanol production.

Acknowledgements

This work was supported by a research grant (9455) from VILLUM FONDEN. We thank Saint Gobain for providing the SiO_2 support.

References

[1] J. Sehested. Industrial and scientific directions of methanol catalyst development. *Journal of Catalysis*, 371:368–375, 2019. doi: 10.1016/j.jcat.2019.02.002.

[2] G. A. Olah, A. Goeppert, and G. K. S. Prakash. Chemical Recycling of Carbon Dioxide to Methanol and Dimethyl Ether: From Greenhouse Gas to Renewable, Environmentally Carbon Neutral Fuels and Synthetic Hydrocarbons. *J. Org. Chem.*, 74(2):487–498, 2009. doi: 10.1021/jo801260f.

[3] M. Kauw, M. J. Benders, and C. Visser. Green methanol from hydrogen and carbon dioxide using geothermal energy and/or hydropower in Iceland or excess renewable electricity in Germany. *Energy*, 90:208–217, 2015. doi: 10.1016/j.energy.2015.06.002.

[4] G. A. Olah and G. K. S. Prakash. *Beyond Oil and Gas: The Methanol Economy*. Wiley, Weinheim, 2006. doi: 10.1002/9783527627806.

[5] J. L. Robbins, E. Iglesia, C. P. Kelkar, and B. DeRites. Methanol synthesis over Cu/SiO_2 catalysts. *Catalysis Letters*, 10(1-2):1–10, 1991. doi: 10.1007/BF00764730.

[6] R. Burch, S. E. Golunski, and M. S. Spencer. The role of copper and zinc oxide in methanol synthesis catalysts. *Journal of the Chemical Society, Faraday Transactions*, 86(15):2683–2691, 1990. doi: 10.1039/ft9908602683.

[7] G. J. J. Bartley and R. Burch. Support and morphological effects in the synthesis of methanol over Cu/ZnO, Cu/ZrO_2 and Cu/SiO_2 catalysts. *Applied Catalysis*, 43(1):141–153, 1988. doi: 10.1016/S0166-9834(00)80907-0.

[8] V. D. Berg, Roy, G. Prieto, G. Korpershoek, L. I. Van Der Wal, A. J. Van Bunningen, S. Lægsgaard-Jørgensen, P. E. De Jongh, and K. P. De Jong. Structure sensitivity of Cu and CuZn catalysts relevant to industrial methanol synthesis. *Nature Communications*, 7(13057):1–7, 2016. doi: 10.1038/ncomms13057.

[9] A. Karelovic, G. Galdames, J. C. Medina, C. Yévenes, Y. Barra, and R. Jiménez. Mechanism and structure sensitivity of methanol synthesis from CO_2 over SiO_2-supported Cu nanoparticles. *Journal of Catalysis*, 369:415–426, 2019. doi: 10.1016/j.jcat.2018.11.012.

[10] G. C. Chinchen, K. C. Waugh, and D. A. Whan. The activity and state of the copper surface in methanol synthesis catalysts. *Applied Catalysis*, 25(C):101–107, 1986. doi: 10.1016/S0166-9834(00)81226-9.

[11] C. Baltes, S. Vukojević, and F. Schüth. Correlations between synthesis, precursor, and catalyst structure and activity of a large set of $CuO/ZnO/Al_2O_3$ catalysts for methanol synthesis. *Journal of Catalysis*, 258(2):334–344, 2008. doi: 10.1016/j.jcat.2008.07.004.

[12] W. X. Pan, R. Cao, D. L. Roberts, and G. L. Griffin. Methanol synthesis activity of Cu/ZnO catalysts. *Journal of Catalysis*, 114(2):440–446, 1988. doi: 10.1016/0021-9517(88)90047-4.

[13] M. Kurtz, N. Bauer, H. Wilmer, O. Hinrichsen, and M. Muhler. Rational Catalyst Design of Methanol Synthesis Catalysts. *Chemical Engineering & Technology*, 27(11):1146–1150, 2004. doi: 10.1002/ceat.200407032.

[14] N. D. Nielsen, A. D. Jensen, and J. M. Christensen. Quantification of Formate and Oxygen Coverages on Cu Under Industrial Methanol Synthesis Conditions. *Catalysis Letters*, 150(9):2447–2456, 2020. doi: 10.1007/s10562-020-03162-7.

[15] W. H. Doh, P. C. Roy, and C. M. Kim. Interaction of hydrogen with ZnO: Surface adsorption versus bulk diffusion. *Langmuir*, 26(21):16278–16281, 2010. doi: 10.1021/la101369r.

[16] R. Chatterjee, S. Kuld, R. V. D. Berg, A. Chen, and W. Shen. Mapping Support Interactions in Copper Catalysts. *Topics in Catalysis*, 62(7-11):649–659, 2019. doi: 10.1007/s11244-019-01150-9.

[17] F. Boccuzzi, C. Morterra, R. Scala, and A. Zecchina. Infrared Spectrum of Microcrystalline Zinc Oxide Electronic and vibrational contributions under different temperature and environmental conditions. *Chemical society, Faraday Transactions 2*, 77:2059–2066, 1981. doi: 10.1039/F29817702059.

[18] M. Shim and P. Guyot-Sionnest. Organic-capped ZnO nanocrystals: Synthesis and n-type character. *Journal of the American Chemical Society*, 123(47):11651–11654, 2001. doi: 10.1021/ja0163321.

[19] D. A. Panayotov, S. P. Burrows, and J. R. Morris. Infrared spectroscopic studies of conduction band and trapped electrons in UV-photoexcited, H-Atom n-doped, and thermally reduced TiO_2. *Journal of Physical Chemistry C*, 116(7):4535–4544, 2012. doi: 10.1021/jp2053103.

[20] N. D. Nielsen, T. E. L. Smitshuysen, C. D. Damsgaard, A. D. Jensen, and J. M. Christensen. Characterization of oxide-supported Cu by infrared measurements on adsorbed CO. *Surface Science*, 703:121725, 2021. doi: 10.1016/j.susc.2020.121725.

[21] A. M. Abdel-Mageed, A. Klyushin, A. Rezvani, A. Knop-Gericke, R. Schlögl, and R. J. Behm. Negative Charging of Au Nanoparticles during Methanol Synthesis from CO_2/H_2 on a Au/ZnO Catalyst: Insights from Operando IR and Near-Ambient-Pressure XPS and XAS Measurements. *Angewandte Chemie - International Edition*, 12613:10325–10329, 2019. doi: 10.1002/anie.201900150.

[22] B. E. Goodby and J. E. Pemberton. XPS Characterization of a commercial $Cu/ZnO/Al_2O_3$ catalyst: Effects of oxidation, reduction, and the steam reformation of methanol. *Applied Spectroscopy*, 42(5):754–760, 1988. doi: 10.1366/0003702884429148.

[23] Y. Okamoto, K. Fukino, T. Imanaka, and S. Teranishi. Surface Characterization of CuO-ZnO Methanol-Synthesis Catalysts by X-ray Photoelectron Spectrosocpy. 2. Reduced Catalysts. *The Journal of physical chemistry*, 87(19):3747–3754, 1983. doi: 10.1021/j100242a035.

[24] T. Binninger, T. J. Schmidt, and D. Kramer. Capacitive electronic metal-support interactions: Outer surface charging of supported catalyst particles. *Physical Review B*, 96(16):165405, 2017. doi: 10.1103/PhysRevB.96.165405.

[25] S. Kuld, M. Thorhauge, H. Falsig, C. F. Elkjaer, S. Helveg, I. Chorkendorff, and J. Sehested. Quantifying the promotion of Cu catalysts by ZnO for methanol synthesis. *Science*, 352(6288): 969–974, 2016. doi: 10.1126/science.aaf0718.

[26] F. Le Peltier, P. Chaumette, J. Saussey, M. M. Bettahar, and J. C. Lavalley. In situ FT-IR and kinetic study of methanol synthesis from CO_2/H_2 over $ZnAl_2O_4$ and Cu-$ZnAl_2O_4$ catalysts. *Journal of Molecular Catalysis A: Chemical*, 132(1):91–100, 1998. doi: 10.1016/S1381-1169(97)00235-5.

[27] S. Fujita, M. Usui, H. Ito, and N. Takezawa. Mechanisms of Methanol Synthesis from Carbon Dioxide and from Carbon Monoxide at Atmospheric Pressure over Cu/ZnO. *Journal of Catalysis*, 157(2):403–413, 1995. doi: 10.1006/jcat.1995.1306.

[28] Y. Amenomiya and T. Tagawa. Infrared study of methanol synthesis from CO_2 and H_2 on supported copper-zinc oxide catalysts. *Proc. of 8th Int. Congress on Catal*, pages 557–567, 1984.

[29] D. W. Bullett and W. G. Dawson. Electronic structure of chemisorbed formate layers on copper surfaces. *Progress in Surface Science*, 25(1-4):275–284, 1987. doi: 10.1016/S0079-6816(87)80018-7.

[30] O. Karis, J. Hasselström, N. Wassdahl, M. Weinelt, A. Nilsson, M. Nyberg, L. G.M. Pettersson, J. Stöhr, and M. G. Samant. The bonding of simple carboxylic acids on Cu(110). *Journal of Chemical Physics*, 112(18):8146–8155, 2000. doi: 10.1063/1.481415.

[31] Y. Yang, C. A. Mims, R. S. Disselkamp, C. H.F. Peden, and C. T. Campbell. Simultaneous MS-IR studies of surface formate reactivity under methanol synthesis conditions on Cu/SiO_2. *Topics in Catalysis*, 52(10):1440–1447, 2009. doi: 10.1007/s11244-009-9320-3.

Chapter 8

Bifunctional Synergy in CO Hydrogenation to Methanol with Supported Cu

Authors: Niels D. Nielsen[1], Joachim Thrane[1], Anker D. Jensen[1], Jakob M. Christensen[1*]

[1] *Department of Chemical and Biochemical Engineering, Technical University of Denmark, Søltofts Plads Building 229, 2800 Kgs. Lyngby, Denmark*

[*] **Correspondence to:** jmc@kt.dtu.dk

DOI:
https://doi.org/10.1016/10.1007/s10562-019-03036-7

Journal specifications:
Catalysis Letters, 2020, Volume 150, 1427-1433

Date Accepted/Published:
31 October 2019 / 14 November 2019

Abstract

Future energy storage could be distributed at local plants and involve production of methanol from reaction of sustainably derived hydrogen with CO or CO_2 from locally available carbon sources. Such decentralized production would benefit from milder operating conditions than found in the current large-scale industrial process. We propose that a route via CO hydrogenation deserves consideration for this purpose, as it will be free of water, which is unavoidable from CO_2-containing gas and strongly inhibiting to the methanol synthesis at lower temperatures. On pure Cu the rate of methanol synthesis from CO is an order of magnitude lower than the rate from CO_2, but active CO hydrogenation catalysts can emerge from a bifunctional mechanism in catalysts that combine copper with a basic oxide. Mechanistic studies are consistent with the bifunctional Cu/support synergy arising from a mechanism, where basic oxide sites activate CO as formates at the metal/oxide interface followed by metal assisted hydrogenation of the interfacial formates. Active catalysts for CO hydrogenation are strongly inhibited by CO_2, which forms carbonates that block the basic oxide sites and thereby prevent the synergistic pathway from CO.

Graphic Abstract

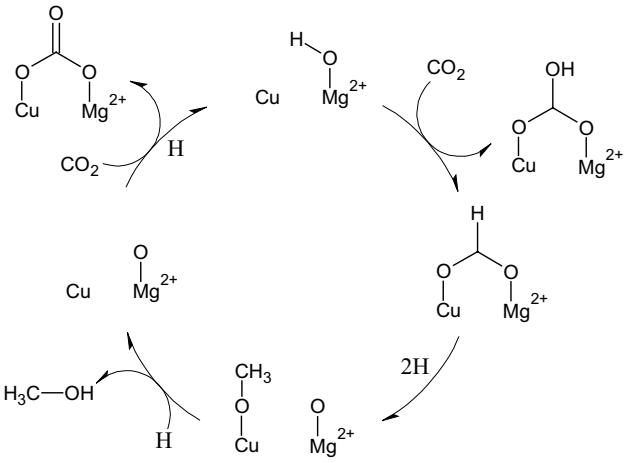

Keywords: Methanol · CO and CO_2 hydrogenation · Support effects · Copper Catalyst · Bifunctional mechanism

1 Introduction

Methanol synthesis from syngas ($CO/CO_2/H_2$) at 500–600 K and 5–10 MPa over $Cu/ZnO/Al_2O_3$ catalysts is a major industrial process [1]. However, future uses of the reaction to store renewable energy in the form of methanol [2] could involve a decentralized production of methanol, where milder reaction conditions would be especially beneficial. While there is a major research focus on CO_2 hydrogenation [1, 3–5], the synthesis of methanol from CO/H_2 should not be neglected in the search for improved low-temperature systems. An advantage of the route from CO/H_2 is that the atmosphere will be free of water, which is unavoidable from CO_2-containing gas and strongly inhibiting to the methanol synthesis — especially at lower temperatures [6–9]. At lower temperatures (<473 K) a few kPa of water partial pressure is sufficient to eliminate the majority of the activity for Cu-based methanol synthesis catalysts [6, 7]. As H_2O adsorption isotherms on Cu [10] or $Cu/ZnO/Al_2O_3$ [10–12] also suggest that a high coverage is reached at H_2O pressures of a few kPa the inhibition can largely be attributed to competitive adsorption (illustrated in supplementary information, Figs. S1 & S2). This is likely to be one of the factors that confine the industrial process to higher (>500 K) temperatures. Consequently, from CO_2 it could be difficult to reach a high yield with a high reaction rate at lower temperatures due to inhibition from the co-produced water. Future energy storage could involve synthesis of methanol from sustainably derived hydrogen and CO_2 from locally available point sources. The inhibition by water means that it is difficult to achieve a high methanol yield directly from a CO_2/H_2 feed, but there are process concepts [13, 14] where the CO_2/H_2 feed is first partially shifted to $CO/CO_2/H_2$ (and formed water is removed) and then converted to methanol. This allows methanol synthesis with the conventional catalyst, as the CO in the syngas can help to remove water formed during methanol synthesis by the shift reaction. However, these concepts are still limited to the harsher synthesis conditions (500–600 K, 5–10 MPa) of the current industrial process. When seeking a process for synthesis of methanol at milder conditions it is worth considering a process, where the CO_2 is fully converted to CO (e.g. by water–gas shift or electrolysis) followed by methanol synthesis from CO/H_2. The pathway from CO/H_2 will both have a more favorable equilibrium [15] and as water is not formed from CO/H_2 the reaction will be free of water inhibition. Both of these factors could lead to improved low-temperature performance, and some Cu-based catalysts are able to achieve considerable methanol synthesis rates from CO/H_2 at lower temperatures [16, 17].

These considerations imply that it is of potential importance to elucidate the active sites and mechanism for CO hydrogenation on Cu-based catalysts. Additionally, the CO hydrogenation can offer fundamental insights into support effects, as single crystal studies [15, 18] suggest that Cu itself has little or no activity for CO hydrogenation, whereas supported Cu catalysts can exhibit catalytic activity with a strong support effect [19]. Here we seek to elucidate the reaction mechanism and the

support effect.

2 Methods

Here Cu/MgO (20 wt%), Cu/ZnO/Al_2O_3 (56 wt%), Cu/Al_2O_3 (50 wt%), unsupported Cu and Cu/C (15 wt%) were all prepared by precipitation methods (nominal Cu loading in parentheses). Cu-MOR was prepared by ion-exchanging Cu into mordenite, and Cu/SiO_2 (20 wt%) and MgO/C were prepared by incipient wetness impregnation. Raney Cu was acquired from Strem Chemicals. Catalytic tests were conducted using two different high-pressure setups. One of these is described elsewhere [20] and the other is described in detail in the supporting information. CO chemisorption, temperature programmed reactions (TPR) on model systems and Cu surface area measurements by N_2O uptake with the reactive frontal chromatography method [21] were performed with a Quantachrome Autosorb iQ_2 setup. Combined TPR and diffuse reflectance infrared Fourier transform spectroscopy (DRIFTS) was conducted in a Harrick Scientific domed reaction chamber and Praying Mantis DRIFTS unit. This was done with a Nicolet iS50 FTIR Spectrometer with a liquid-N_2 cooled MCT detector. X-ray photoelectron spectroscopy (XPS) analyses were performed with a monochromatic and micro-focused Al K-Alpha source equipped with a 180° double focusing hemispherical analyzer with a Thermo Scientific 128-channel detector. Further experimental details are provided in the supporting information.

3 Results and Discussion

Figure 1 illustrates that in high pressure methanol synthesis the CO hydrogenation is around an order of magnitude slower than CO_2 hydrogenation for unsupported Cu, Raney Cu and Cu-rich Cu/Al_2O_3. These samples are all expected to approximate the intrinsic properties of Cu. This is in good agreement with the negligible CO hydrogenation rate observed in Cu single crystal studies performed at low pressure [15, 18]. Ex situ XPS analyses on the fresh and spent unsupported Cu showed that the surface only contained Cu (and O due to the ex situ analysis) and showed that no Ni or Fe deposition from carbonyls occurred (see supplementary information).

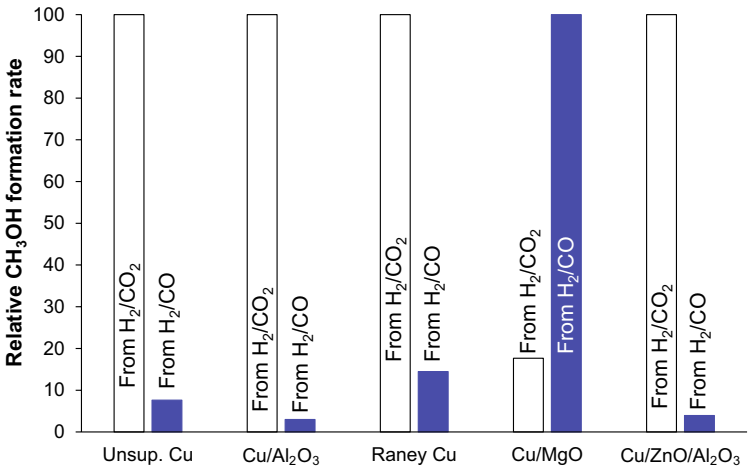

Fig. 1: The relative methanol production rates from CO/H_2 (blue) and CO_2/H_2 (white) over unsupported Cu, Cu-rich (50 wt% Cu) Cu/Al_2O_3, Raney Cu as well as Cu/ZnO/Al_2O_3 and Cu/MgO. The methanol production in the most reactive atmosphere is assigned as 100 for each sample. Reaction conditions: 5 MPa, H_2CO_x/inert = 68/3/29, and 523 K (498 K for unsupported Cu due to poor thermal stability). Details on absolute productivity levels are provided in supporting information Figs. S3-S7.

For Cu-catalyzed methanol synthesis by CO_2 hydrogenation there is a strong support effect [22, 23], but there is generally also a linear correlation between activity and metallic Cu surface area [24–26],

which indicates that the reaction occurs on the metallic surface. However, this (Fig. S8 and other studies [24, 27] observe no such correlation for CO hydrogenation in good agreement with the limited ability of the metallic Cu surface to form methanol from CO (Fig. 1). Some theoretically hypothesized mechanisms [28–30] suggest a faster pathway from CO compared to CO_2 on Cu, but both high pressure (Fig. 1) and low pressure [15, 18] studies contradict this view, and this emphasizes the continued need for theoretical studies of methanol synthesis reactions. Figure 1 also illustrates the role of the support in achieving CO hydrogenation activity. The industry-type catalyst $Cu/ZnO/Al_2O_3$ shows the same preference for CO_2 as Cu itself. However, the relative rates of the CO and CO_2 pathways are completely inverted for Cu on an MgO support. At the conditions of Fig. 1 the TOF (relative to the number of Cu surface atoms) in CO_2/H_2 is at a relatively similar level of 0.014 s^{-1} for Cu/MgO, 0.022 s^{-1} for Cu/Al_2O_3 and 0.0078 s^{-1} for Raney Cu. So it seems clear that the great preference for the CO-pathway on Cu/MgO is due to a much faster CO-pathway rather than due to an inhibition of the CO_2-pathway. Figure 2 shows that this CO hydrogenation activity in Cu/MgO emerges from a Cu/oxide synergy. Co-precipitated Cu/MgO is of high activity for CO hydrogenation, and whereas Cu/C and MgO/C are of negligible activity, MgO/Cu/C prepared by impregnating $Mg(HCOO)_2$ onto the essentially inactive Cu/C catalyst shows a clear improvement in activity. This illustrates that the activity emerging in the Cu/MgO combination is the result of a synergy between two components (Cu and MgO) of low individual activity for CO hydrogenation.

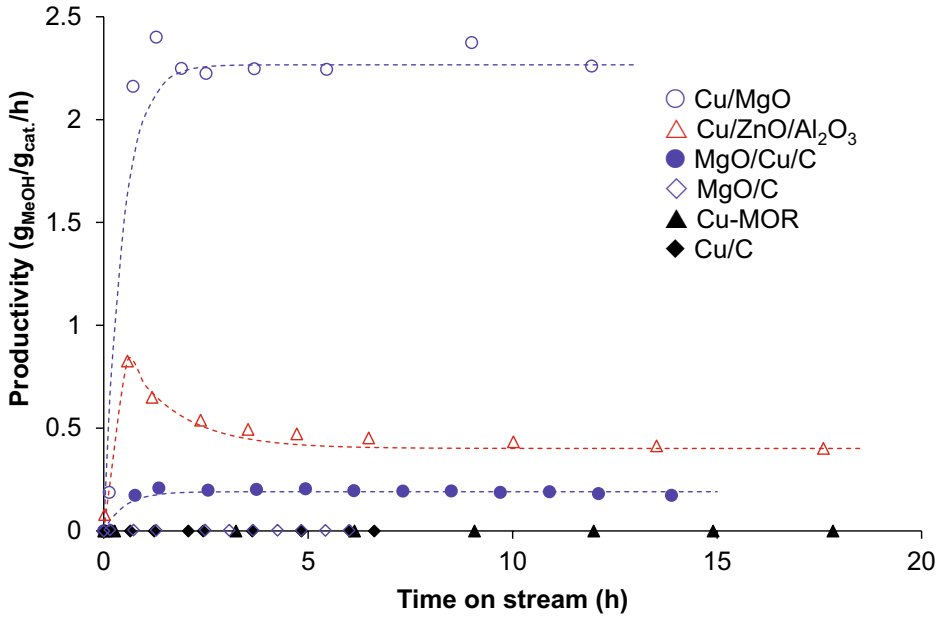

Fig. 2: Methanol synthesis rate in CO hydrogenation as a function of time on stream for various supported Cu catalysts. Reaction conditions: T = 523 K, P = 5 MPa, flow = 300 NmL/min, 0.5 g cat., H_2/CO = 67/33.

Previous studies [31–33] have established a correlation between Cu^+-type surface sites and methanol synthesis activity from CO/H_2. On metallic Cu, CO desorbs at subambient temperatures, and stable chemisorption at ambient temperature is only achieved on Cu^+-type sites, where CO is more strongly bound [34, 35]. CO chemisorption at 303 K and subsequent TPD shows that with the exception of Cu/C all the catalysts investigated in Fig. 2 have Cu^+-type sites ascribed to bridging "$Cu^{\delta+}$–O-support" sites at the metal/oxide interface (Table S1 and Fig. S9). The CO chemisorption capacities of Cu/MgO (143 µmol/$g_{cat.}$) and MgO/Cu/C (25 µmol/$g_{cat.}$) suggest that a major reason for the difference in activity between the two Cu–MgO systems (Fig. 2) is the number of these interfacial $Cu^{\delta+}$–O–Mg sites, which indicates that a key to making active CO hydrogenation catalysts is to maximize the number of interfacial sites. However, a material such as Cu/SiO_2 has a relatively high $Cu^{\delta+}/CuO$ ratio in the surface (Table S1), but only a modest activity (Fig. S7), and an ion-exchanged Cu-mordenite sample (Cu-MOR) prepared specifically as a Cu^+ model system is completely without

activity (Fig. 2) despite a large number of the CO adsorption sites attributable to Cu^+ species (Table S1 and Fig. S9). Consequently, Cu^+ sites are most likely not an exclusive requirement for activity. It is therefore not only the extent of the metal/oxide interface that is important, but also the nature of the interfacial sites. The importance of the sites at the metal/oxide interface most likely arises, as it is here that the two elements of a bi-functional mechanism come together. The argument for the existence of a bifunctional mechanism comes from the results in Fig. 3. Figure 3a shows that Cu/MgO exposed to CO/H_2 at 523 K exhibits infrared bands characteristic of formate (1340, 1625, 2847 and 2925 cm^{-1}) [36] and methoxide (1086, 2600 and 2810 cm^{-1}) [37] on the MgO. The formation of formate (HCOO) by reaction of CO with basic OH species is a well established reaction on oxide surfaces [38, 39], and the oxide can thereby activate CO as formate.

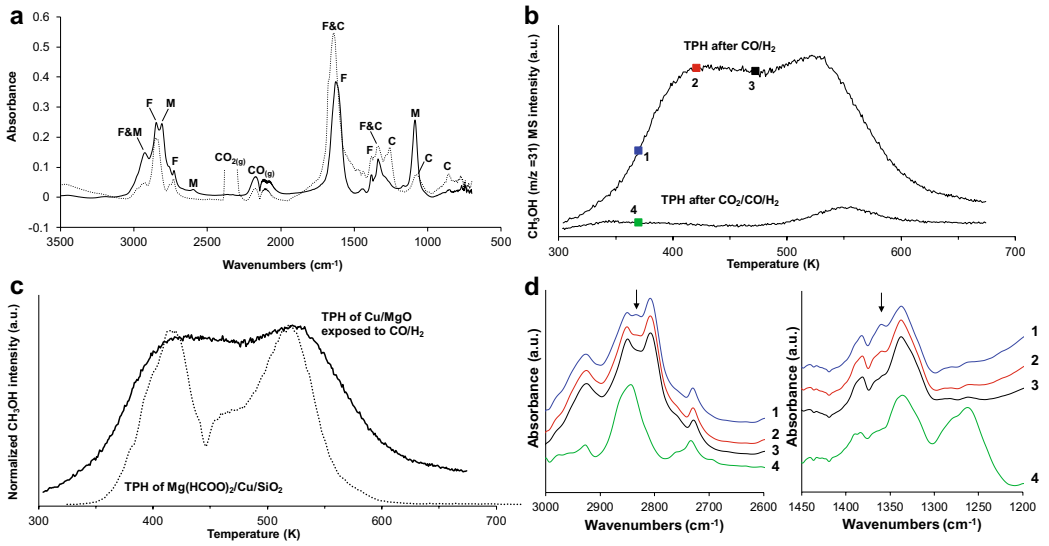

Fig. 3: **a** FTIR spectra of Cu/MgO at 523 K and atmospheric pressure in flowing CO/H_2 (full line) or $CO_2/CO/H_2$ (dotted line) with indications of formate (F), methoxide (M) and carbonate/bicarbonate (C). Conditions: CO/H_2/inert = 3/68/29, $CO_2/CO/H_2$/inert = 1.5/1.5/68/29. **b** Methanol (m/z = 31) MS intensity as a function of temperature during TPH of the Cu/MgO catalyst after the exposure to CO/H_2 or $CO_2/CO/H_2$ at 523 K and atm. pressure (and cooling in this gas). Numbers indicate the positions of the spectra in (**d**). Conditions: 2 K/min, 50 NmL/min H_2 flow, 10 mg catalyst. **c** Normalized methanol (m/z = 31) MS intensity as a function of temperature comparing CO/H_2 treated Cu/MgO to $Mg(HCOO)_2{\cdot}2H_2O$ impregnated to 5 wt% Mg on pre-reduced and passivated 20 wt% Cu/SiO_2. Ramp in both cases: 2 K/min, 50 NmL/min H_2 and 10 mg catalyst for Cu/MgO, 30 NmL/min H_2 and 0.5 g catalyst for $Mg(HCOO)_2/Cu/SiO_2$. **d** FTIR spectra at points 1–4 along the TPH experiments in (**b**). The arrows mark 1360 cm^{-1} and 2834 cm^{-1}.

We propose that the facile CO hydrogenation on materials such as Cu/MgO proceeds via formate (HCOO) created from insertion of CO into a basic OH group from the oxide as illustrated in Fig. 4. This mechanism will take place at the interface between metal and oxide.

There are several arguments for a mechanism via formate. Figure 3b shows that temperature programmed hydrogenation (TPH) of the surface species on Cu/MgO after exposure to CO/H_2 leads to methanol production in two peaks centered at 423 K and 523 K. Figure 3c shows that a model system, where magnesium formate was impregnated onto pre-reduced (and passivated) Cu/SiO_2 and then subjected to TPH, produced methanol at the same two temperatures. This would be consistent with the methanol-forming intermediates from CO/H_2 being formate species. Figure 3b and d shows that the 423 K methanol formation peak coincides with the disappearance of a species with IR bands (1360 cm^{-1} and 2834 cm^{-1}) typical [40, 41] of H–C and symmetric O–C–O stretches in bidentate formate. This suggests that such a formate is the origin of the most facile methanol formation at 423 K. Efficient CO hydrogenation catalysts such as Cu/MgO (Fig. 2) and Cu/CeO_2 [16, 17] include oxides that efficiently produce formate from CO+OH reactions (see Fig. 3a for MgO and Li et al. [42]

for CeO_2). A reliance on basic OH groups explains why the supports/promoters providing higher CO hydrogenation activity, such as MgO and ZnO (Fig. 2), alkali oxides [43] and rare earth oxides [16, 17] all are of a basic character [44, 45]. Additionally, previous $C^{16}O/C^{18}O$ isotope labeling studies [46] with Na_2O–Pd/SiO_2 have shown than in such systems combining a metal with a basic oxide the C–O bond in methanol is scrambled compared to the CO reactant. This is consistent with a mechanism via the two-oxygen formate intermediate, where either oxygen can end in the product molecule.

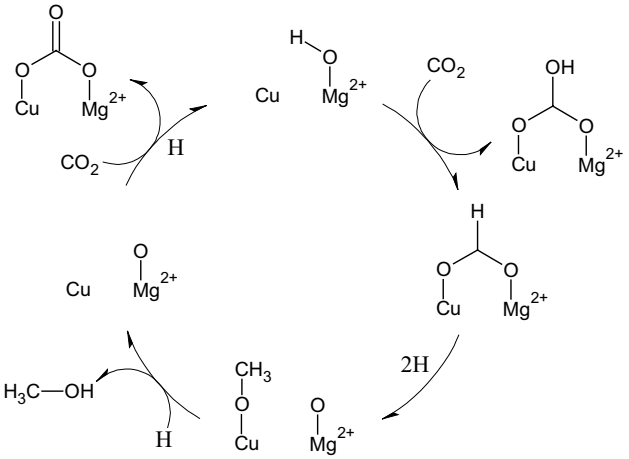

Fig. 4: The proposed oxide assisted mechanism for methanol syn-thesis via formate and methoxide. Here X can represent both Cu or Mg with X = Cu implying a bridging formate across the Cu/oxide interface. The scheme also illustrates the deactivating effect of CO_2. Although illustrated for MgO other oxides with basic sites should perform similarly.

An alternative pathway via the mono-oxygenated inter-mediates formyl (HCO), formaldehyde (H_2CO) and meth-oxide (CH_3O) is the basis of several [4, 28–30] proposed mechanisms for CO hydrogenation. For unsupported Cu such a mechanism seems like the only option, since there is no oxide support to facilitate the creation of a two-oxygen species. That unsupported Cu does have a low, but non-zero formation of methanol from CO (Fig. 1) suggests that such a direct mechanism exists. However, for an efficient CO hydrogenation catalyst like Cu/MgO it is formate-type IR bands (assigned to interfacial species) that correlate to methanol formation in Fig. 3d, whereas a characteristic IR band of formyl (2660–2680 cm^{-1}) [47] was absent in the methanol forming situations in Fig. 3d. While the present results therefore offer support to the intermediate role of interfacial formate species there is nothing to suggest an important role of formyl for an active catalyst such as Cu/MgO. The Cu/MgO catalyst exposed to CO/H_2 produces methanol in two peaks during TPH (Fig. 3b). Figure 3d suggests that the 423 K methanol formation coincides with a species having IR bands characteristic of formate (1360 cm^{-1} and 2834 cm^{-1}). These bands are different from those of formate entirely on MgO [36], but Fig. 3d shows that this species is formed from CO implying a role of surface OH from the oxide. Figure 3d also shows that this species is not formed from $CO_2/CO/H_2$. This counts against it being formate entirely on the metallic surface, where it is well established that formate is produced from CO_2 to H_2 [48]. Consequently, the species forming methanol at 423 K, which does not appear to be entirely on either metal or oxide, is attributed to formate at the metal/oxide interface, possibly a bridging formate across the interface. This species is assigned as the primary reaction intermediate, as it can form methanol at a relatively lower temperature. A pathway to methanol via interfacial formates is supported by studies [49–51] of Cu on ZrO_2. The higher temperature (523 K) methanol formation coincides with the general disappearance of formates and methoxides entirely on the MgO (Figs. S10 and S11) and is thus assigned to the less facile conversion of such species entirely on the oxide.
Contrary to the behavior of Cu itself (Fig. 1) both this (Fig. S12) and other studies [19, 29, 52] observe that catalysts with a high activity from CO/H_2, such as Cu/MgO, are strongly inhibited by CO_2. The inhibition is largely reversible upon removal of CO_2 (Fig. S6). Figure 3a shows that when Cu/MgO is exposed to $CO_2/CO/H_2$ IR bands characteristic of carbonates and bicarbonates appear. An experiment, where Cu/MgO was exposed to CO_2 alone to produce carbonates (Fig. S13),

clearly illustrates that carbonates contribute to the bands at 858, 1078, 1340 and 1630 cm^{-1} in good agreement with the literature [53, 54]. The band at 1254 cm^{-1} occurring in $CO_2/CO/H_2$ is most likely carbonate in a particular configuration bridging two metal atoms/ions [54], but this species is only formed by $CO_2/CO/H_2$ and not by CO_2 alone (Fig. S13) — possibly because it is a bicarbonate species. The Cu/MgO catalyst exposed to $CO_2/CO/H_2$ produces considerably less methanol in the subsequent TPH, which suggests that inhibition is due to a blocking effect of the carbonates that displaces the methanol forming intermediates. Most importantly, the absence of the 423 K methanol formation (Fig. 3b) and the 1360 and 2834 cm^{-1} IR bands (Fig. 3d) shows that the more reactive species assigned as interfacial formates are completely displaced in conjunction with the carbonate formation. This can explain the inhibiting effect of CO_2. In the presence of CO_2 the basic oxide sites that are necessary for the bifunctional synergy are blocked as inactive carbonates (as indicated in Fig. 4), and the formation of the mechanistically important interfacial formates relying on basic OH groups is prevented. The inhibiting effect of CO_2 on a bifunctional pathway from CO might not be limited to the highly basic oxide supports such as MgO. It is possible that such a CO-pathway is also inhibited on less basic oxides, when CO_2 is present. It only appears to be the bifunctional pathway from CO that is inhibited by CO_2. In the presence of CO_2 the methanol formation rate suggests that Cu metal surface produces methanol from the CO_2 with its expected rate (Table S2).

Whereas formate species at the metal/oxide interface are assigned as the key intermediates in the CO hydrogenation the formate and methoxide species entirely on the MgO are only expected to play a limited role in the methanol synthesis, perhaps that of complete spectators. Firstly, these species are only converted at higher temperatures during TPH (Figs. S10 and S11). Secondly, the IR bands of formate on MgO are not strongly affected by the presence of CO_2 (Fig. 3a), which affects productivity significantly. The interfacial formates are more reactive, but also less stable and more easily displaced by carbonates (Fig. 3d), whereas the majority of formates entirely on the MgO are more stable and less reactive and therefore not displaced by carbonates (Fig. 3a.). Consequently, the methanol formation is assigned to formate species specifically at the metal/oxide interface that are displaced by carbonates in the presence of CO_2. It is thus likely that formate is both a spectator on the oxide surface further away from the metal particles and an actual intermediate on interfacial sites. The IR bands of methoxide on MgO drop significantly in the presence of CO_2 (Fig. 3a.). This is most likely because water is produced from the CO_2-containing gas. The removal of methoxide on an oxide by hydrolysis with water is far more facile than hydrogenation [55]. The methoxide on MgO is most likely formed, when produced methanol is re-adsorbed on the oxide, and the combination of the slower methanol production in the presence of CO_2 and the faster removal of methoxide by hydrolysis can explain the lower methoxide coverage in the CO_2-containing gas. While it cannot be fully excluded that methoxide on the MgO can play a mechanistically important role under some conditions its disappearance in the presence of CO_2 may just result from the presence of water that hydrolyzes the methoxide species.

The present results clearly show that the CO hydrogenation to methanol relies on a metal/oxide synergy and suggest that one pathway to methanol is the activation of CO as formate by the oxide followed by a metal-assisted hydrogenation of formate into methanol. The presence of CO_2 interrupts the bifunctional synergy, as the necessary basic oxide sites are blocked as carbonates. Although developed here with Cu/MgO the present mechanistic conclusions are expected to be valid also for other catalyst systems. As an example another system with high activity from CO/H_2 is Cu/CeO_2 [16, 17], where the oxide is also able to activate CO as formate [42], and where the presence of CO_2 also inhibits the methanol synthesis and leads to carbonate formation [52, 56]. Similarly, Pd-based catalysts for CO hydrogenation generally exhibit the same support and promoter effect where basic oxides are beneficial [19, 46].

4 Conclusion

In conclusion, we propose that it is worth considering methanol synthesis from CO/H_2 in the search for methanol synthesis at milder conditions. The pathway from CO/H_2 has a more favorable equilibrium and is free of co-produced water, which is strongly inhibiting to methanol synthesis at lower temperatures. Both factors could be advantageous for low temperature operation. The present results show that active CO hydrogenation catalysts such as Cu/MgO emerge from a synergy between metal

and oxide, which is attributed to a bifunctional mechanism focused at the metal/support interface. The mechanistic investigations are consistent with interfacial formates, produced by reaction of CO with basic OH groups from the oxide surface, as the important reaction intermediates. Active CO hydrogenation catalysts are strongly inhibited by CO_2 and the results suggest that this occurs because CO_2 forms carbonates at the basic oxide and thereby blocks the oxide sites that enable the bifunctional pathway. The results suggest that the key to making active CO hydrogenation catalysts is to engineer system that maximize the number of interfacial sites, where Cu and basic oxide sites come together while ensuring the absence of species such as CO_2 that can block the oxide sites. The combination of optimally engineered catalysts and the water free conditions of CO hydrogenation could lead to improved low temperature performance in methanol synthesis and pave the way for remote and small scale methanol-based energy storage facilities.

Acknowledgements

The Villum Foundation V-SUSTAIN grant 9455 to the Villum Center for the Science of Sustainable Fuels and Chemicals is gratefully acknowledged for funding. We thank Saint Gobain for providing the SiO_2 support.

Errata

50 wt% Cu for Cu/Al_2O_3 should correctly be 67 wt% Cu and concerns the Methods section, caption for Fig. 1 (in the main text). Moreover, this correction concerns Table S3 and Fig. S4 in the supplementary information.

References

[1] M. Behrens. Coprecipitation: An excellent tool for the synthesis of supported metal catalysts - From the understanding of the well known recipes to new materials. *Catalysis Today*, 246:46–54, 2015. doi: 10.1016/j.cattod.2014.07.050.

[2] G. A. Olah and G. K. S. Prakash. *Beyond Oil and Gas: The Methanol Economy*. Wiley, Weinheim, 2006.

[3] F. Studt, I. Sharafutdinov, F. Abild-Pedersen, Christian F. Elkjær, J. S. Hummelshøj, S. Dahl, I. Chorkendorff, and J. K. Nørskov. Discovery of a Ni-Ga catalyst for carbon dioxide reduction to methanol. *Nature Chemistry*, 6(4):320–324, 2014. doi: 10.1038/nchem.1873.

[4] J. Graciani, K. Mudiyanselage, F. Xu, A. E. Baber, and J. Evans. Highly active copper-ceria and copper-ceria-titania catalysts for methanol synthesis from CO_2. *Science*, 345(6196):546–550, 2014. doi: 10.1126/science.1253057.

[5] O. Martin, A. J. Martín, C. Mondelli, S. Mitchell, T. F. Segawa, R. Hauert, C. Drouilly, D. Curulla-Ferré, and J. Pérez-Ramírez. Indium oxide as a superior catalyst for methanol synthesis by CO_2 hydrogenation. *Angewandte Chemie - International Edition*, 55(21):6261–6265, 2016. doi: 10.1002/anie.201600943.

[6] R. Bardet and J. Thivolle-Cazat. Hydrocondensation of carbon oxides, at atmospheric pressure on Cu-ZnO-Al_2O_3 catalysts. Influence of water on the formation of methanol. *Compt. Rend. Acad. Sci. Paris*, 299:423–425, 1984.

[7] O. Cherefi, S. Monteverdi, M. M. Bettahar, M. Forissier, and V. Perrichon. Kinetics of CO_2 hydrogenation into methanol on a Cu-Zn-Al oxide catalyst. *Bull. Soc. Chim. Fr.*, pages 405–409, 1985.

[8] M. Sahibzada, I. S. Metcalfe, and D. Chadwick. Methanol Synthesis from $CO/CO_2/H_2$ over $Cu/ZnO/Al_2O_3$ at Differential and Finite Conversions. *Journal of Catalysis*, 174:111–118, 1998. doi: 10.1006/jcat.1998.1964.

[9] M. Saito, T. Fujitani, M. Takeuchi, and T. Watanabe. Development of copper/zinc oxide-based multicomponent catalysts for methanol synthesis from carbon dioxide and hydrogen. *Applied Catalysis A: General*, 138(2):311–318, 1996. doi: 10.1016/0926-860X(95)00305-3.

[10] J. Słoczyński, R. Grabowski, and J. Janas. Adsorption Model of Methanol Synthesis Reactants on CuO-ZnO-Al_2O_3 Catalyst - II Adsorption on the individual components of the catalyst. *Chemical Engineering Science*, 46(10):2611–2623, 1991. doi: 10.1016/0009-2509(91)80054-3.

[11] J. Słoczyński, R. Grabowski, J. Janas, and J. Skrzypek. Adsorption model of methanol synthesis reactants on CuO-ZnO-Al_2O_3 catalyst-I. Adsorption on the catalyst. *Chemical Engineering Science*, 46(10):2599–2610, 1991. doi: 10.1016/0009-2509(91)80053-2.

[12] A. V. Tarasov, F. Seitz, R. Schlögl, and E. Frei. In Situ Quantification of Reaction Adsorbates in Low-Temperature Methanol Synthesis on a High-Performance Cu/ZnO:Al Catalyst. *ACS Catalysis*, 9:5537–5544, 2019. doi: 10.1021/acscatal.9b01241.

[13] H. Goehna and P. Koenig. Producing methanol from CO_2. *Chemtech*, 24(6):36–39, 1994.

[14] O.-S. Joo, K. D Jung, I. Moon, A. Y. Rozovskii, G. I. Lin, S. H. Han, and S. J. Uhm. Carbon dioxide hydrogenation to form methanol via a reverse-water-gas- shift reaction (the CAMERE process). *Industrial and Engineering Chemistry Research*, 38(5):1808–1812, 1999. doi: 10.1021/ie9806848.

[15] M. Maack, H. Friis-jensen, S. Sckerl, J. H Larsen, and I. Chorkendorff. Methanol synthesis on potassium-modified Cu (100) from CO + H_2 and CO + CO_2 + H_2. *Topics in Catalysis*, 22(3-4): 151–160, 2003. doi: 1022-5528/03/04000151/0.

[16] G. Owen, C. M. Hawkes, D. Lloyd, J. R. Jennings, R. M. Lambert, and R. M. Nix. Methanol synthesis catalysts from intermetallic precursors: Binary lanthanide-copper catalysts. *Applied Catalysis*, 33(2):405–430, 1987. doi: 10.1016/S0166-9834(00)83071-7.

[17] W. J. Shen, Y. Ichihashi, and Y. Matsumura. Low temperature methanol synthesis from carbon monoxide and hydrogen over ceria supported copper catalyst. *Applied Catalysis A: General*, 282 (1-2):221–226, 2005. doi: 10.1016/j.apcata.2004.12.046.

[18] J. Nerlov and I. Chorkendorff. Promotion through gas phase induced surface segregation: Methanol synthesis from CO, CO_2 and H_2 over Ni/Cu(100). *Catalysis Letters*, 54(4):171–176, 1998. doi: 10.1023/A:1019033517855.

[19] S. Fujita, M. Usui, T. Hanada, and N. Takezawa. Methanol synthesis from CO_2-H_2 and from CO-H_2 under atmospheric pressure over Pd and Cu catalysts. *React. Kinet. Catal. Lett.*, 56(1): 15–19, 1995. doi: 10.1007/BF02066946.

[20] J. M. Christensen, P. M. Mortensen, R. Trane, P. A. Jensen, and A. D. Jensen. Effects of H_2S and process conditions in the synthesis of mixed alcohols from syngas over alkali promoted cobalt-molybdenum sulfide. *Applied Catalysis A: General*, 366(1):29–43, 2009. doi: 10.1016/j.apcata.2009.06.034.

[21] G. C. Chinchen, C. M. Hay, H. D. Vandervell, and K. C. Waugh. The measurement of copper surface areas by reactive frontal chromatography. *Journal of Catalysis*, 103(1):79–86, 1987. doi: 10.1016/0021-9517(87)90094-7.

[22] T. Fujitani, M. Saito, Y. Kanai, T. Kakumoto, T. Watanabe, J. Nakamura, and T. Uchijima. The role of metal oxides in promoting a copper catalyst for methanol synthesis. *Catalysis Letters*, 25 (3-4):271–276, 1994. doi: 10.1007/BF00816307.

[23] P. Chaumette, J. Barbier, and J Fortin. Carbonates, a key for selecting methanol synthesis catalysts. *Proc 9th Int Congr Catal*, pages 585–593, 1988.

[24] J. L. Robbins, E. Iglesia, C. P. Kelkar, and B. DeRites. Methanol synthesis over Cu/SiO_2 catalysts. *Catalysis Letters*, 10(1-2):1–10, 1991. doi: 10.1007/BF00764730.

[25] C. Baltes, S. Vukojević, and F. Schüth. Correlations between synthesis, precursor, and catalyst structure and activity of a large set of CuO/ZnO/Al_2O_3 catalysts for methanol synthesis. *Journal of Catalysis*, 258(2):334–344, 2008. doi: 10.1016/j.jcat.2008.07.004.

[26] R. W. Joyner, R. Burch, S. E. Golunski, and M. S. Spencer. 'Good' correlations in methanol synthesis catalysis, a comment on a letter by burch, golunski and spencer. *Catalysis Letters*, 6 (1):151–156, 1990. doi: 10.1007/BF00764064.

[27] W. R. A. M. Robinson and J. C. Mol. Characterization and catalytic activity of copper/alumina methanol synthesis catalysts. *Applied Catalysis*, 44(C):165–177, 1988. doi: 10.1016/S0166-9834(00)80051-2.

[28] W. Janse Van Rensburg, J. A. Van Den Berg, M. A. Petersen, M. S. Datt, and P. Van Helden. On the Kinetic Interpretation of DFT-Derived Energy Profiles: Cu-Catalyzed Methanol Synthesis. *Catalysis Letters*, 145(2):559–568, 2015. doi: 10.1007/s10562-014-1407-1.

[29] F. Studt, M. Behrens, R. Schlögl, E. L. Kunkes, N. Thomas, S. Zander, A. Tarasov, J. Schumann, E. Frei, J. B. Varley, F. Abild-Pedersen, and J. K. Nørskov. The Mechanism of CO and CO_2 Hydrogenation to Methanol over Cu-Based Catalysts. *ChemCatChem*, 7(7):1105–1111, 2015. doi: 10.1002/cctc.201500123.

[30] M. Behrens, F. Studt, I. Kasatkin, S. Kühl, M. Hävecker, F. Abild-Pedersen, S. Zander, F. Girgsdies, P. Kurr, B. Kniep, M. Tovar, R. W. Fischer, J. K. Nørskov, and R. Schlögl. The Active Site of Methanol Synthesis over Cu/ZnO/Al_2O_3 Industrial Catalysts. *Science*, 336:893–898, 2012. doi: 10.1126/science.1219831.

[31] J. R. Monnier, M. J. Hanrahan, and G. Apai. A study of the catalytically active copper species in the synthesis of methanol over Cu-Cr oxide. *Journal of Catalysis*, 92(1):119–126, 1985. doi: 10.1016/0021-9517(85)90241-6.

[32] G. R. Sheffer and T. S. King. Differences in the promotional effect of the group IA elements on unsupported copper catalysts for carbon monoxide hydrogenation. *Journal of Catalysis*, 116(2): 488–497, 1989. doi: 10.1016/0021-9517(89)90115-2.

[33] P. J. Chu, B. C. Gerstein, G. R. Sheffer, and T. S. King. NMR studies of ^{65}Cu and ^{133}Cs in alkali-metal-promoted copper catalysts. *Journal of Catalysis*, 115(1):194–204, 1989. doi: 10.1016/0021-9517(89)90018-3.

[34] D. F. Cox and K. H. Schulz. Interaction of CO with Cu^+ cations: CO adsorption on $Cu_2O(100)$. *Surface Science*, 249(1-3):138–148, 1991. doi: 10.1016/0039-6028(91)90839-K.

[35] A. Dandekar and M. A. Vannice. Determination of the Dispersion and Surface Oxidation States of Supported Cu Catalysts. *Journal of Catalysis*, 178(2):621–639, 1998. doi: 10.1006/jcat.1998.2190.

[36] G. Busca. FT-IR study of the surface of copper oxide. *Journal of Molecular Catalysis*, 43(2): 225–236, 1987. doi: 10.1016/0304-5102(87)87010-4.

[37] J. Kondo, Y. Sakata, K.-I. Maruya, K. Tamaru, and T. Onishi. Infrared studies of methanol adsorbed on magnesium oxide. *Applied Surface Science*, 28:475–478, 1987. doi: 10.1016/0169-4332(87)90143-7.

[38] T. Shido and Y. Iwasawa. Reactant-promoted reaction mechanism for water-gas shift reaction on ZnO, as the genesis of surface catalysis. *Journal of Catalysis*, 129(2):343–355, 1991. doi: 10.1016/0021-9517(91)90040-B.

[39] P. G. Gopal, R. L. Schneider, and K. L. Watters. Evidence for production of surface formate upon direct reaction of CO with alumina and magnesia. *Journal of Catalysis*, 105(2):366–372, 1987. doi: 10.1016/0021-9517(87)90066-2.

[40] A. Chutia, I. P. Silverwood, M. R. Farrow, D. O. Scanlon, P. P. Wells, M. Bowker, S. F. Parker, and C. F. A. Catlow. Adsorption of formate species on Cu(h,k,l) low index surfaces. *Surface Science*, 653:45–54, 2016. doi: 10.1016/j.susc.2016.05.002.

[41] L. Dubois, T. H. Ellis, B. R. Zegarski, and S. D. Kevan. New insights into the kinetics of formic acid decomposition on copper surfaces. *Surface Science*, 172:385–397, 1986. doi: 10.1016/0039-6028(86)90763-6.

[42] C. Li, Y. Sakata, T. Arai, K. Domen, K.-I. Maruya, and T. Onishi. Adsorption of carbon monoxide and carbon dioxide on cerium oxide studied by Fourier-transform infrared spectroscopy. Part 2.—Formation of formate species on partially reduced CeO_2 at room temperature. *J. Chem. Soc. Faraday Trans.*, 1(85):1451–1461, 1989. doi: 10.1039/F198985014510.

[43] R. G Herman. Classical and Non-Classical Routes for Alcohol Synthesis - New Trends in Coactivation. *Studies in Surface Science and Catalysis*, 64(7):265–349, 1991. doi: 10.1016/S0167-2991(08)60949-0.

[44] D. Martin and D. Duprez. Mobility of surface species on oxides. 1. isotopic exchange of $^{18}O_2$ with ^{16}O of SiO_2, Al_2O_3, ZrO_2, MgO, CeO_2, and CeO_2-Al_2O_3. activation by noble metals. correlation with oxide basicity. *Journal of Physical Chemistry*, 100(22):9429–9438, 1996. doi: 10.1021/jp9531568.

[45] A. Auroux and A. Gervasini. Microcalorimetric study of the acidity and basicity of metal oxide surfaces. *Journal of Physical Chemistry*, 94(16):6371–6379, 1990. doi: 10.1021/j100379a041.

[46] Y. Kikuzono, S. Kagami, S. Naito, T. Onishi, and K. Tamaru. Selective hydrogenation of carbon monoxide on palladium catalysts. *Faraday Discussions of the Chemical Society*, 72:135–143, 1981. doi: 10.1039/DC9817200135.

[47] J. Saussey, J.C. Lavalley, J. Lamotte, and T. Rais. I.R. Spectroscopic Evidence of Formyl Species formed by CO and H_2, Co-adsorption on ZnO and Cu-ZnO. *J. Chem. Soc. Chem. Commun.*, 5: 278–279, 1982. doi: 10.14825/kaseki.40.0_51_1.

[48] P. A. Taylor, P. B. Rasmussen, C. V. Ovesen, P. Stoltze, and I. Chorkendorff. Formate synthesis on Cu(100). *Surface Science*, 261(1-3):191–206, 1992. doi: 10.1016/0039-6028(92)90231-T.

[49] I. A. Fisher and A.T. Bell. In Situ Infrared Study of Methanol Synthesis from H_2/CO over Cu/SiO_2 and Cu/ZrO_2/SiO_2. *Journal of Catalysis*, 178:153–173, 1998. doi: 10.1006/jcat.1998.2134.

[50] K. Larmier, W. C. Liao, S. Tada, E. Lam, R. Verel, A. Bansode, A. Urakawa, A. Comas-Vives, and C. Copéret. CO_2-to-Methanol Hydrogenation on Zirconia-Supported Copper Nanoparticles: Reaction Intermediates and the Role of the Metal–Support Interface. *Angewandte Chemie - International Edition*, 56(9):2318–2323, 2017. doi: 10.1002/anie.201610166.

[51] E. Lam, K. Larmier, P. Wolf, S. Tada, O. V. Safonova, and C. Copéret. Isolated Zr Surface Sites on Silica Promote Hydrogenation of CO_2 to CH_3OH in Supported Cu Catalysts. *Journal of the American Chemical Society*, 140(33):10530–10535, 2018. doi: 10.1021/jacs.8b05595.

[52] J. R. Jennings, R. M. Lambert, R. M. Nix, G. Owen, and D. G. Parker. Novel methanol synthesis catalysts derived from intermetallic precursors: CO_2 poisoning and molecular mechanism of the synthesis reaction. *Applied Catalysis*, 50(1):157–170, 1989. doi: 10.1016/S0166-9834(00)80833-7.

[53] D. Cornu, H. Guesmi, J. M. Krafft, and H. Lauron-Pernot. Lewis acido-basic interactions between CO_2 and MgO surface: DFT and DRIFT approaches. *Journal of Physical Chemistry C*, 116(11): 6645–6654, 2012. doi: 10.1021/jp211171t.

[54] G. Busca and V. Lorenzelli. Infrared spectroscopic identification of species arising from reactive adsorption of carbon oxides on metal oxide surfaces. *Materials Chemistry*, 7:89–126, 1982. doi: 10.1016/0390-6035(82)90059-1.

[55] S. Fujita, H. Ito, and N. Takezawa. Methanol Synthesis from CO_2 and H_2 over a ZnO Catalyst. Effect of Pretreatment with CO-H_2 upon the Reaction. *Bull. Chem. Soc. Jpn*, 66(10), 1993. doi: 10.1246/bcsj.66.30940.

[56] L. Lin, S. Yao, Z. Liu, F. Zhang, N. Li, D. Vovchok, A. Martínez-Arias, R. Castaneda, J. Lin, S. D. Senanayake, D. Su, D. Ma, and J. A. Rodriguez. In Situ Characterization of Cu/CeO_2 Nanocatalysts for CO_2 Hydrogenation: Morphological Effects of Nanostructured Ceria on the Catalytic Activity. *Journal of Physical Chemistry C*, 122(24):12934–12943, 2018. doi: 10.1021/acs.jpcc.8b03596.

Chapter 9

Conclusions

Sustainable alternatives to scarce fossil resources must be developed to mitigate climate change and reduce pollution. Renewable generated energy can replace fossil fuels in the energy sector but feasible substitution of fossil fuels in the transportation and chemical sectors and efficient storage of renewable energy remain unsolved challenges. Liquid chemicals including methanol feature high energy densities and long term stability with methanol also being a key chemical feedstock and applicable as a transportation fuel. $Cu/ZnO/Al_2O_3$ synthesizes fossil-derived syngas ($CO/CO_2/H_2$) to industrial methanol. An alternative route involves reacting H_2 from water-splitting powered by renewable energy with industrially captured CO_2 to synthesise sustainable methanol that conveniently stores excess renewable energy. Realizing a methanol based society requires massive methanol capacity expansion and this calls for upgraded methanol catalysts to minimize cost. Such optimization work necessitates fundamental insight into the reaction, which is imperfectly understood. Cu constitutes the active metal but the mechanism governing the profound support effect on activity, the reaction mechanism and role of reaction conditions are subject to debate and constitute the primary areas of this thesis.
Establishing the reaction mechanism includes identifying the main carbon source to methanol among the candidates CO and CO_2. Comprehensive scientific evidence shows that CO_2 is the main carbon source for Cu/ZnO-based catalysts but the dominant source over pure Cu is disputed. Syngas switching experiments in CO/H_2, CO_2/H_2 and $CO_2/CO/H_2$ at working conditions (523 K, 50 bar) are designed to determine the prevalent carbon source over pure Cu. Methanol synthesis over ZnO-free Cu supported catalysts occurs primarily through CO_2 though Cu interacting with special supports such as the basic MgO can feature bifunctional metal-support synergy effects resulting in high CO hydrogenation activity. Direct CO_2 hydrogenation to methanol prevails at low conversion but an autocatalytic reaction promoted by methanol-assisted methyl-formate hydrogenation results in a net rate gain that could explain the observed accelerated rate with higher conversion. This indirect mechanism is especially pronounced for the conventional $Cu/ZnO/Al_2O_3$ catalyst though Cu/SiO_2 also benefits from an autocatalytic pathway but yielding orders of magnitude lower activity.
Concerning the direct CO_2 route to methanol, the role of formate as a key reaction intermediate is substantiated by methanol production during TPH of formate pre-covered catalysts dosed with formic acid. The efficacy of the autocatalytic mechanism is also closely related to the formate population level as the indirect route occurs by reacting methanol and formate to methyl formate that subsequently hydrogenates to methanol.
Estimating the surface coverage of reaction intermediates is of high importance in calculating catalytic rate expressions. Quantitative estimates of the surface coverage of the working ($CO_2/CO/H_2$, 523 K, 50 bar) catalysts is for the first time obtainable by applying a newly developed and reproducible method. At working conditions, the catalyst is rapidly quenched in the syngas and subsequently heated (TPD) and the evolved CO_2 at temperatures characteristic of Cu-HCOO desorption is integrated to determine the formate population level. Quantitative estimates of adsorbate coverages can be compiled to a bench-marking catalogue highly applicable for improving kinetic modelling studies.
Operating at different conversion regimes entails changes to the ideal CO_x/H_2 composition. Higher CO_2 partial pressure promotes the methanol activity at low conversion while CO acts as a weak but unambiguous surface inhibitor. Shifting to higher conversion regimes enhances the concentrations

of methanol with potential for an autocatalytic pathway and strongly surface inhibiting water. CO effectively scavenges water and acts beneficial and maintains high activity yielding ~ 10% CO_2 and ~ 90% CO as the optimal CO_x fraction at high conversion.
Supports provide structural support for dispersed Cu particles and facilitate high Cu surface area but also profoundly impact the methanol TOF. Kinetic studies (CO_2/CO/H_2, 523 K, 50 bar) of Cu supported catalysts show the following TOF order: Cu/SiO_2 < Cu/Al_2O_3 < Cu/ZnO-based catalysts in agreement with literature studies. Numerous mechanisms have been proposed but they are insufficient in describing a mechanism governing the support effect. Activity of Cu particles is generally size-independent but decreases for particles below 5-8 nm, which conflicts with suggested active interfacial metal-support sites whose concentrations rise with smaller particles. Interfacial Cu-Zn surface sites promoted by Zn incorporating into the Cu surface facilitated by reducing atmosphere is proposed as active centers. This mechanism is investigated by exposing mildly reduced Cu/ZnO/Al_2O_3 to prevent ZnO reduction to firstly a relative oxidizing (CO_2/H_2) and secondly to a reducing (CO_2/CO/H_2) gas composition. Addition of reducing CO is detrimental to the activity at both 1 and 20 bar and signifies that Cu-Zn surface sites are not of high importance for the Cu/ZnO synergy effect. Unraveling the mechanism of the support effect is critical to explain its order of magnitude regulation of the TOF and can provide tools for developing highly active catalysts producing sustainable methanol even at mild reaction conditions.
IR spectroscopy of chemisorbed CO, which is sensitive to the adsorbate site including its charge, shows that $\nu_{C\text{-}O}$ is regulated by the support. Cu/SiO_2 features a $\nu_{C\text{-}O}$ corresponding to oxidized Cu ($Cu^{\delta+}$) with reduced electron concentration while $\nu_{C\text{-}O}$ on Cu/ZnO is low owing to electron-rich Cu ($Cu^{\delta-}$). Co-adsorption of electron-withdrawing formate on Cu/ZnO and Cu/SiO_2 modifies the CO spectra and indicates that electron-rich Cu can sustain a higher formate population level than electron-deficient. Further insight into the implications of support-regulated Cu surface charging is provided by IR spectra in inert gas after intermediate and harsh reductive treatment of ZnO-based samples, which all feature IR transparency loss following the order: Cu/ZnO < Cu/ZnO/Al_2O_3 < ZnO. H_2 desorption upon TPD of all harshly ZnO-based samples verifies the presence of trapped H_2 and its associated donated electrons in the ZnO-based samples. Photo-ionization of conducting band electrons constitute a mechanism producing high IR absorbance for ZnO. Contact to Cu (Cu/ZnO) promotes electron transfer to Cu to align the Fermi levels of Cu and ZnO resulting in low IR absorbance for Cu/ZnO. Alumina (Cu/ZnO/Al_2O_3) dispersion reduced the Cu-ZnO perimeter and impedes the electron flow yielding medium absorbance level. Comparable studies on non-reducible and insulating SiO_2 show absence of trapped H_2 and no absorbance loss in accordance with the ability of reducible oxides to sustain electron that can transfer to a metal upon contact.
Comparing the IR results of supports yielding $Cu^{\delta+}$ and $Cu^{\delta-}$ with the kinetic studies demonstrates that high TOF is associated with $Cu^{\delta-}$ and oppositely $Cu^{\delta+}$ yields low TOF. Support-regulated formate coverage and formate conversion rate can potentially account for the support effect on activity. Formate coverage estimates during industrially relevant methanol synthesis (CO_2/CO/H_2, 523 K, 50 bar) of Cu/SiO_2, Raney Cu and Cu/ZnO are based on the reproducible quantitative method. IR spectroscopy is employed to specify the adsorbate desorption temperatures (especially Cu-HCOO) during TPD on post reaction (methanol synthesis) and cooled catalysts. Applying the identified desorption temperatures provides guidance to solely integrate desorbed CO_2 related to Cu-HCOO desorption. The formate coverages are 0.060 ML (Cu/SiO_2), 0.071 ML (Raney Cu) and 0.267 ML (Cu/ZnO) while the TOF values are $1.48{\cdot}10^{-3}$ s^{-1} (Cu/SiO_2), $6.22{\cdot}10^{-3}$ s^{-1} (Raney Cu) and $3.61{\cdot}10^{-2}$ s^{-1} (Cu/ZnO). On this basis, the ~ 4 fold TOF increase for Raney Cu compared to Cu/SiO_2 cannot exclusively be explained by impeded formate coverage on Cu/SiO_2. Instead TPH of formate-covered Raney Cu and Cu/SiO_2 shows facile hydrogenation to methanol on Raney Cu but slow on Cu/SiO_2 thus the detrimental effect of SiO_2 is mainly attributed to impeded formate conversion. However, supports may regulate the formate population level on Cu as evident for Cu/ZnO in comparison to Raney Cu. Kinetic studies show that supports are able to regulate the formate conversion rate (Cu/SiO_2) and the formate coverage (Cu/ZnO) with potential consequences for the activity.
Industrial methanol synthesis over Cu/ZnO/Al_2O_3 is based on CO_2 hydrogenation and this pathway permeates the dominate part of this work but Cu/MgO yields high CO hydrogenation activity. Methanol synthesis from CO hydrogenation in absence of CO_2 and inhibiting water is thermodynamic favorable for decentralized methanol plants integrated with renewable energy production and operated

at milder conditions. Cu dispersion on basic supports yields high CO/H_2 activity (Cu/MgO) and provides guidance for optimally designed low temperature methanol catalysts.
This thesis contributes with new insight into the strong support effect governing catalytic methanol synthesis as current models are inadequate in accounting for the role of support. Comprehensive analysis of Cu supported catalysts showed that electron transfer regulated by the support can account for the role of support. Acquired knowledge provides a framework for optimizing methanol catalysts, which is paramount for instituting sustainable methanol synthesis on a global scale. High CO hydrogenation rate over Cu/MgO owing to a bifunctional metal-support synergy effect made Cu/MgO an intriguing candidate as a low temperature methanol catalyst. Such catalysts can facilitate a prevalence of methanol plants working in synergy with renewable energy production to conveniently store renewable energy in the form of sustainable methanol.

Chapter 10

Future work

Catalytic methanol synthesis over $Cu/ZnO/Al_2O_3$ based on fossil-derived syngas is a well-known industrial process. Yet, the catalytic active sites, the critical reaction mechanism(s) and the profound influence of support on the activity are imperfectly understood.

Support-regulated electron transfer with supports modifying the catalytic properties through changes to the Cu surface charge is proposed to account for the support effect. Substantial charging identified by IR transparency loss on reduced ZnO disappeared upon contact to Cu and low $\nu_{C\text{-}O}$ on Cu/ZnO indirectly shows that Cu is electron-enriched by ZnO. Observations of the Cu chemical state with electron donating and withdrawing supports can provide further evidence for the suggested electron transfer model. Surface sensitive in situ XPS and XAS can provide information on the surface charging state and potential dynamic chemical shifts of Cu associated with charge transfer imposed by the support. In situ XPS experiments are usually restricted to ultra high vacuum or low pressure conditions leaving a substantial pressure gap to the high-pressure conventional methanol synthesis conditions. However, synchrotron capabilities offer high energy X-ray beams capable of penetrating gaseous environments and enable ambient pressure in situ XPS experiments, which are critical to study the suggested electron-donating properties of H_2 on Cu occurring at ambient conditions. IR spectroscopy of CO on Cu reveals that support regulates the charging state of Cu. Application of synchrotron XPS allows studying chemical shifts of Cu on detrimental (e.g. SiO_2) and beneficial (e.g. ZnO) supports in reducing atmosphere (H_2 and CO) in comparison to published work in this thesis thus providing insight into charge transfer phenomena. This includes the possible support effect on the binding strength of adsorbates on the Cu surface and the influence of electron-withdrawing (HCOO) and donating (H_2) adsorbates on the Cu properties. Doping of semiconducting oxides with e.g. Al, Ga, In, Se to engineer the electronic enrichment of the oxides could be of high significance in proving/disproving the electron transfer mechanism. Moreover, the dynamics of the working catalyst in syngas mixtures including chemical shifts of Cu induced by surface adsorbates can provide valuable information about metal-support interactions. Measuring the charging state of supported metal particles and the influence of adsorbate species on the metallic surface could become a powerful technique in characterizing and understanding metal-supported systems.
Cu/ZnO-based catalysts yield high methanol activity attributed to a Cu-ZnO synergy effect explained by mechanisms including gas-dependent surface morphology, strain in Cu induced by the support, ZnO_x layer/species partly covering Cu metal sites or Zn atom incorporation into the Cu surface. Recent studies have strongly advocated for a Cu-Zn surface alloy with highly active Cu-Zn surface sites. Obtained results on mildly reduced $Cu/ZnO/Al_2O_3$ to prevent ZnO reduction before exposing it to reducing atmosphere (CO) to facilitate Cu-Zn site formation in accordance with the surface alloy model proponents do not show activity enhancement upon contact with CO as predicted by the Cu-Zn surface alloy model. Though CO should be able to at least partially reduce ZnO under the applied conditions it would be instructive and informative to perform in situ analysis of the catalyst state after mild reduction as well as during methanol synthesis in different feed gas compositions. X-ray spectroscopy techniques including XPS and XAS applied in situ and/or ex situ especially if performed using synchrotron facilities constitute promising techniques to perform such experiments.

Cu/MgO exhibits high CO hydrogenation activity with great potential to become a highly active methanol catalyst working at milder conditions in water-free atmosphere. Such conditions are favourable due to higher methanol equilibrium in CO_2-free atmosphere, improved stability in absence of inhibiting water and reduced costs by removing expensive compression steps. Such conditions would highly benefit decentralized methanol production close to available carbon sources where feed gas impurities including sulphur from alternative carbon sources (biomass, captured CO_2, geothermal etc.) could pose a potential risk unless a sulphur/impurity tolerant synthesis route is established assisted by a poison tolerant catalyst. Provided with captured CO_2 and renewable generated H_2 the RWGS reaction including water distillation provides a method to produce the CO/H_2 feed gas. Cu/MgO features promising properties and indicates that maximizing the number of metal-support interfacial sites is key to achieving a high activity but the system is far from fully optimized. Activity improvements could be achieved by optimizing the synthesis procedure (maximize the number of crucial Cu-MgO interfacial sites), investigating the influence of promoters and exploring the optimal reaction conditions including pressure, temperature, flow and CO to H_2 ratio etc. Moreover, in situ experiments using advanced synchrotron facilities to study the dynamics of the working catalytic surface could provide mechanistic insight and guide optimization work.

The presented quantitative method to determine the surface coverage of adsorbate species has the potential to be of high interest for other catalytic reactions under high-pressure working conditions including guidance for kinetic modelling studies with experimentally determined kinetic parameters. Additional experiments of the formate coverage on Cu-based catalysts at various pressures (ambient to industrially relevant 50-100 bar) in different syngas mixtures provides knowledge about the influence of pressure, support, gas mixture etc. on the formate coverage. Results from such an experimental campaign could advantageously be applied in mechanistic modelling work to improve the mechanistic understanding of the process and shed further light on the support effect.

Establishing the reaction mechanism for methanol synthesis is paramount for fundamentally understanding the process. Formate hydrogenation is reported to be the rate limiting step in CO_2 hydrogenation to methanol over Cu/ZnO-based samples based on spectroscopy, kinetic and modelling studies. Accordingly, the Langmuir-Hinselwoord (L-H) mechanism (one H atom reacts with formate) describes well the formate hydrogenation process yielding a hydrogen reaction order of 1 in agreement with mechanistic model predictions. Contrary, several experimental studies including single crystal studies report higher hydrogen reaction order of 1.5 and above. This suggests a Eley-Rideal (E-R) mechanism where undissociated H_2 directly hydrogenates formate to methanol. Clarifying this dispute may involve mechanistic D_2/H_2 experiments with HCOO pre-covered Cu/ZnO-based catalysts. Analyses of desorbed gas species during TPH of HCOO pre-covered Cu/ZnO-based catalysts using Nuclear Magnetic Resonance (NMR) allow quantification of the products CH_2DO_x, CH_3O_x and CHD_2O_x. If the L-H mechanism prevails all three product species are equally probable assuming the D_2 and H_2 dissociation steps are equally facile and that the formation rate of DH from D_2 and H_2 is relatively low, which both must be clarified beforehand. However, if the E-R mechanism dominates then product species with intact D_2 or H_2 on HCOO (CH_3O_x and CHD_2O_x) dominate the NMR spectrum. A complimentary mechanistic experiment involves integrating the evolved methanol during a TPH performed in various H_2 concentrations of HCOO pre-covered Cu/ZnO-based catalysts. The resulting relationship between evolved methanol and H_2 partial pressure shows the prevalent mechanism with 1 for an E-R mechanism and 1/2 for a L-H mechanism.

Despite decades of research in catalytic methanol synthesis many aspects regarding active centers, reaction mechanism, role of promoters and support remain unsolved. Work presented in this thesis contributes to the understanding of the support effect but future work is necessary to clarify this effect in greater detail. The complex task of investigating the working state of the catalyst at realistic conditions could be solved by technological improvements of in situ techniques including especially electron microscopy with (sub)atomic resolution of the working catalyst configuration and X-ray adsorption/emission spectroscopy ideally conducted at synchrotron facilities to achieve high brilliance and allow in situ studies of specimens in greater detail in gaseous environments. In situ observations of the reaction at realistic or semi-realistic conditions has a great potential in unravelling the challenging scientific questions.

Appendices

Appendix A

Supplementary information for *The roles of CO and CO_2 in high pressure methanol synthesis over Cu-based catalysts* in chapter 3

Authors: Niels D. Nielsen[1], Anker D. Jensen[1], Jakob M. Christensen[1]
[1] *Department of Chemical and Biochemical Engineering, Technical University of Denmark, Søltofts Plads Building 229, 2800 Kgs. Lyngby, Denmark*
*__Correspondence to:__ jmc@kt.dtu.dk

DOI:
Not applicable

Journal specifications:
Journal of Catalysis

Status:
Submitted version has returned. Revised version is currently in progress and the latest revised version is reprinted here.

S1 Supplementary Material

S1 Evaluation of possible ZnO reduction and determination of reduction protocol for Cu/Al_2O_3

The onset of ZnO reduction for $Cu/ZnO(/Al_2O_3)$ samples was evaluated by measurements of the Cu area from the N_2O uptake. Here the standard pre-reduction in 5% H_2 with holding periods at 448 K and 523 K was compared to a milder variant terminated after the holding period at 448 K or a harsher variant where the normal pre-reduction was followed by exposure to 100% H_2 at 523 K (until H_2O formation stops) after the normal pre-reduction program. Fig. S1a and b show the Cu areas based on the N_2O uptakes after the different pre-reductions for the ZnO-based catalysts. Within the known 6% relative uncertainty, the Cu surface areas after 5% H_2 reductions at 448 K and 523 K are identical, but harsher reduction in 100% H_2 most likely results in partial ZnO reduction as indicated by the statistically significant increase in the apparent Cu surface area – similar to observations elsewhere [1–3]. Fig. S1c shows the Cu surface areas after reducing in different atmospheres. Alumina is generally regarded as an irreducible oxide [4, 5] and the increased Cu surface area from 448 K to 523 K in 5% H_2 is assigned to incomplete Cu reduction at 448 K. Switching from 5% to 100% H_2 at 523 K does within the uncertainty not change the Cu surface area. However to ensure complete Cu reduction the reduction protocol for Cu/Al_2O_3 includes reduction at 5% H_2 (448 K and 523 K) and 100% H_2 (523 K).

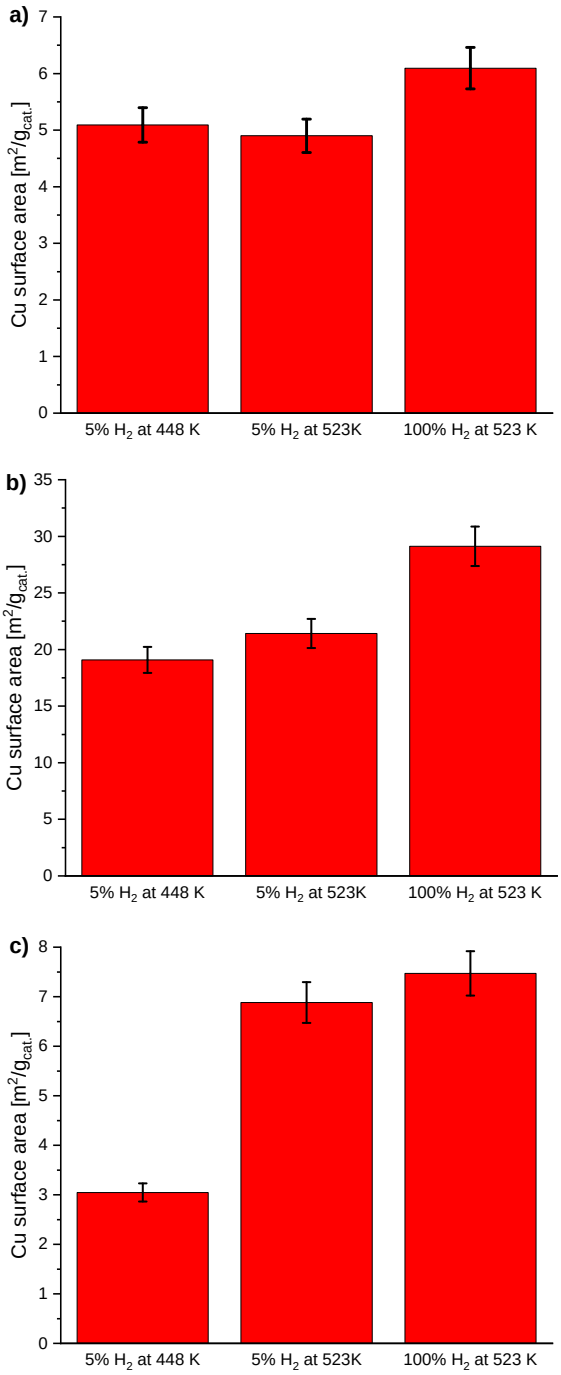

Fig. S1: Cu surface area determined by N_2O-RFC after reduction at the indicated hydrogen pre-treatments for a) Cu/ZnO, b) Cu/ZnO/Al_2O_3, and c) Cu/Al_2O_3. Uncertainty bars correspond to ± one standard deviation as reported by Thrane et al. [6] when using the identical Autosorb iQ_2 setup.

S2 Methanol synthesis with and without CO over Cu/TiO_2 catalysts

Comparisons between the rates of methanol synthesis from CO or CO_2 for the presently applied catalyst samples have been reported by Nielsen et al. [7] and showed that the route from CO_2 is considerably faster than the route from CO. Such a comparison has not previously been made for Cu/TiO_2. For this reason Fig. S2 shows comparison of the TOF per Cu surface atom for Cu/TiO_2 in methanol synthesis from CO_2 or CO. The figure shows that the CO_2-route is favored on Cu/TiO_2, as it is also the case on all the other samples.

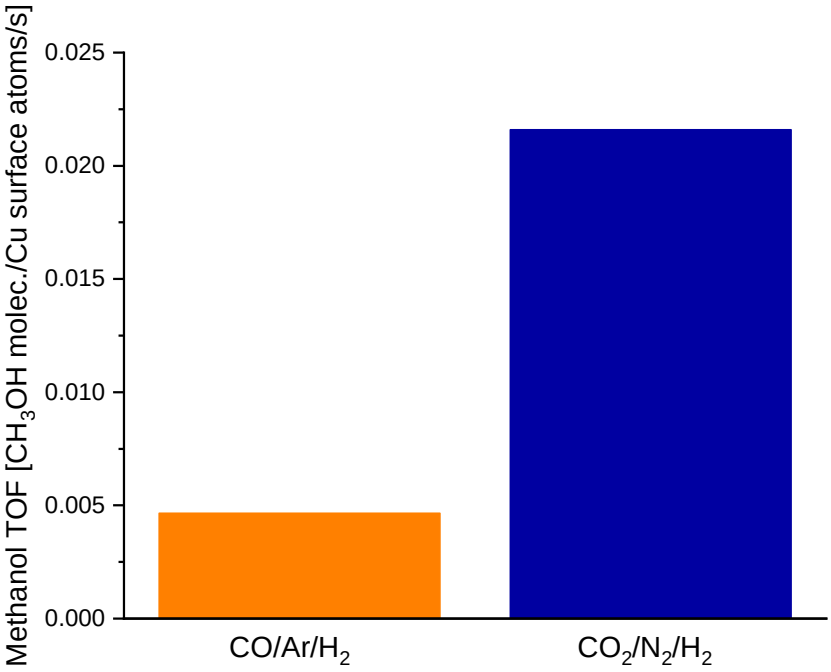

Fig. S2: The turnover frequency for methanol formation (per Cu surface atom) for $Cu/TiO_2(20)$ during methanol synthesis from CO or CO_2. Reaction conditions: T = 523 K, P = 50 bar, feed flow = 280 ± 4 Nml/min, $X/Y/H_2$ = 3/29/68 with X being either CO or CO_2 and Y being Ar or N_2, $Cu/TiO_2(20)$ loading = 261.5 mg.

Fig. S3 shows the MS signal for methanol as a function of time on stream for $Cu/TiO_2(60)$ during cycling between $CO_2/N_2/H_2$ and $CO_2/CO/H_2$ feeds. The periods without measurement are due to bypass of the analyzer during measurements of the gas flow rate. Fig. S3 shows that the effect of CO is reversible within a few minutes.

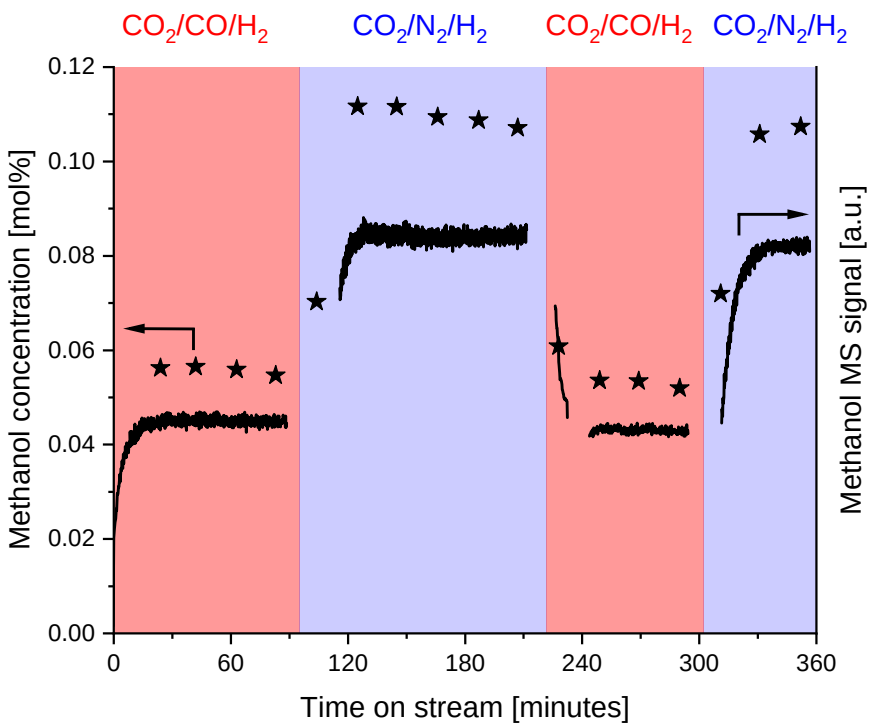

Fig. S3: The MS signal for methanol (m/z = 31) as a function of time on stream during repeated switching between $CO_2/N_2/H_2$ and $CO_2/CO/H_2$ feeds. Reaction conditions: T = 523 K, P = 50 bar, feed flow = 280 ± 4 Nml/min, $CO_2/X/H_2$ = 3/29/68 with X being CO or N_2, Cu/TiO_2(60) loading = 253.4 mg. Bypass of the MS when measuring the gas flow rate results in the gaps in the MS signal.

S3 Equilibrium calculations for experiments at higher conversion

Fig. 5 in the main text evaluates the productivity as a function of the conversion level varied through the space velocity both with and without CO in the feed. For experiments without CO in the feed it is possible to determine the water concentration in the effluent from an oxygen balance and it is therefore possible to determine the approach to equilibrium for both methanol synthesis and water-gas shift. Table S1 summarizes the approach to equilibrium for these experiments and illustrates that WGS is closer to equilibrium than methanol synthesis although none of the reactions are fully equilibrated at these conditions.

Table S1: Experimental data for methanol synthesis ($CO_2/N_2/H_2$ = 3/29/68, 523 K, 50 bar) over Cu/Al_2O_3 and $Cu/ZnO/Al_2O_3$ and the approach to equilibrium for WGS and methanol synthesis in these experiments.

Catalyst	**GHSV** [**Nml/g$_{cat}$/h**]	**Inlet concentrations**		**Product concentrations**			**Approach to equilibrium**	
		y_{CO_2} [%]	**y_{H_2}** [%]	**y_{CO}** [%]	**y_{CH_3OH}** [%]	**y_{H_2O}** [%]	**WGS** [%]	**MeOH synth** [%]
Cu/Al_2O_3	$9.4{\cdot}10^4$	0.03	0.68	0.255	0.299	0.555	6.10	3.71
Cu/Al_2O_3	$3.7{\cdot}10^4$	0.03	0.68	0.961	0.467	1.43	59.1	14.9
Cu/Al_2O_3	$1.5{\cdot}10^4$	0.03	0.68	0.870	0.623	1.49	55.9	20.8
$Cu/ZnO/Al_2O_3$	$1.5{\cdot}10^6$	0.03	0.68	0.078	0.120	0.198	0.664	0.533
$Cu/ZnO/Al_2O_3$	$1.5{\cdot}10^6$	0.03	0.68	0.058	0.138	0.196	0.490	0.607
$Cu/ZnO/Al_2O_3$	$4.9{\cdot}10^5$	0.03	0.68	0.29	0.385	0.675	8.43	5.79
$Cu/ZnO/Al_2O_3$	$2.4{\cdot}10^5$	0.03	0.68	0.34	0.576	0.916	13.4	11.8

S4 Reaction conditions for literature studies

Fig. 7 in the main text summarizes the effect of the CO/CO_2 ratio from a variety of studies in the literature. Some of these studies provide results at various reaction conditions. Tables S1 and S2 summarize the conditions, which are used to obtain the data in Fig. 7 and Table S4 shows the calculated methanol concentrations based on the reported methanol productivities.

Table S2: Parameter specifications for methanol synthesis at differential industrially relevant reaction conditions.

Catalyst	**Temperature [K]**	**Pressure [bar]**	**H_2 conc.** [%]	**Reference**
$Cu/ZnO/Al_2O_3$	503	30	59 (inert: 27)	Studt et al. [8]
Cu/ZnO	498	28.6	83	Chanchlani et al. [9]
$Cu/ZnO/Al_2O_3$	523	30	80	Lee et al. [10]

Table S3: Parameter specifications for methanol synthesis at industrially relevant reaction conditions at high conversion.

Catalyst	**Temperature [K]**	**Pressure [bar]**	**H_2 conc.** [%]	**Reference**
$Cu/ZnO/Al_2O_3$	513	50	75.5	Martin et al. [11]
$Cu/ZnO/Al_2O_3$	488	35-70	67	Barbier et al. [12]
$Cu/ZnO/Al_2O_3$	523	50	80	Sahibzada et al. [13]
$Cu/ZnO/Al_2O_3$	523	30	80	Lee et al. [10]
Cu/ZnO	508	75	70	Klier et al. [14]

Table S4: Methanol concentration calculations based on studies in Fig. 7a and b in the main text.

MeOH Productivity	**Space velocity**	**CO_x conversion**	**Cu dispersion**	**Feed gas composition**	**MeOH conc. [%]**	**Reference**
300 µmol MeOH/ g_{cat}/min	1.82 Nl/ g_{cat}/min*				0.370	Studt et al. [8]
		< 1%		$H_2/CO/CO_2$ = 70/23/7	<0.3	Chanchlani et al. [9]
40 mole MeOH/ kg_{cat}/h	108000 l/ kg_{cat}/h				0.830	Lee et al. [10]
70 g MeOH/ mol Cu/h	7.5 g gas/ g_{cat}/h		8.817 mmol Cu/gcat	$N_2/H_2/CO_2/CO$ = 28/63/7.6/1.4	3.30	Martin et al.
28.5 mmol MeOH/ g_{cat}/h	6.67 Nl/ g_{cat}/h				9.58	Barbier et al. [12]
70 mmol MeOH/ g_{cat}/h	1.67 mol/ g_{cat}/h				4.19	Sahibzada et al. [13]
30 mol MeOH/ kg_{cat}/h	18000 l/ kg_{cat}/h				3.74	Lee et al. [10]
		33.5%		H_2/CO_x = 70/30	10.05	Klier et al. [14]

*Studt et al. [8] reported catalysts loadings of 50-60 mg thus 55 mg was used in the calculations.

References

[1] S. Kuld, C. Conradsen, P. G. Moses, I. Chorkendorff, and J. Sehested. Quantification of zinc atoms in a surface alloy on copper in an industrial-type methanol synthesis catalyst. *Angewandte Chemie - International Edition*, 53(23):5941–5945, 2014. doi: 10.1002/anie.201311073.

[2] D. S. King and R. M. Nix. Thermal stability and reducibility of ZnO and Cu/ZnO catalysts. *Journal of Catalysis*, 160(1):76–83, 1996. doi: 10.1006/jcat.1996.0125.

[3] M. B. Fichtl, J. Schumann, I. Kasatkin, N. Jacobsen, M. Behrens, R. Schlögl, M. Muhler, and O. Hinrichsen. Counting of oxygen defects versus metal surface sites in methanol synthesis catalysts by different probe molecules. *Angewandte Chemie - International Edition*, 53(27):7043–7047, 2014. doi: 10.1002/anie.201400575.

[4] J. B. Hansen and P. E. H. Nielsen. *Methanol Synthesis*, volume 2. Wiley-VCH Verlag GmbH, 2nd edition, 2008. doi: 10.1002/9783527610044.hetcat0148.

[5] R. Chatterjee, S. Kuld, R. V. D. Berg, A. Chen, and W. Shen. Mapping Support Interactions in Copper Catalysts. *Topics in Catalysis*, 62(7-11):649–659, 2019. doi: 10.1007/s11244-019-01150-9.

[6] J. Thrane, S. Kuld, N. D. Nielsen, A. D. Jensen, J. Sehested, and J. M. Christensen. Methanol-assisted autocatalysis in catalytic methanol synthesis. *Angewandte Chemie - International Edition*, 59:18189–18193, 2020. doi: 10.1002/anie.202006921.

[7] N. D. Nielsen, J. Thrane, A. D. Jensen, and J. M. Christensen. Bifunctional Synergy in CO Hydrogenation to Methanol with Supported Cu. *Catalysis Letters*, 150:1427–1433, 2020. doi: 10.1007/s10562-019-03036-7.

[8] F. Studt, M. Behrens, R. Schlögl, E. L. Kunkes, N. Thomas, S. Zander, A. Tarasov, J. Schumann, E. Frei, J. B. Varley, F. Abild-Pedersen, and J. K. Nørskov. The Mechanism of CO and CO_2 Hydrogenation to Methanol over Cu-Based Catalysts. *ChemCatChem*, 7(7):1105–1111, 2015. doi: 10.1002/cctc.201500123.

[9] K. G. Chanchlani, R. R. Hudgins, and P. L. Silveston. Methanol synthesis from H_2, CO, and CO_2 over Cu/ZnO catalysts. *Journal of Catalysis*, 136(1):59–75, 1992. doi: 10.1016/0021-9517(92)90106-R.

[10] J. S. Lee, S. H. Han, H. G. Kim, K. H. Lee, and Y. G. Kim. Effects of space velocity on methanol synthesis from CO_2/CO/H_2 over Cu/ZnO/Al_2O_3 catalyst. *Korean Journal of Chemical Engineering*, 17(3):332–336, 2000. doi: 10.1007/BF02699049.

[11] O. Martin and J. Pérez-Ramírez. New and revisited insights into the promotion of methanol synthesis catalysts by CO_2. *Catalysis Science and Technology*, 3(12):3343–3352, 2013. doi: 10.1039/c3cy00573a.

[12] J. Barbier, J. Fortin, P. Courty, and P. Chaumette. Rôle du dioxyde de carbone lors de la synthèse du méthanol sur catalyseurs à base de cuivre. *Bulletin de la Société chimque de france*, 6:925–929, 1987.

[13] M. Sahibzada, I. S. Metcalfe, and D. Chadwick. Methanol Synthesis from CO/CO_2/H_2 over Cu/ZnO/Al_2O_3 at Differential and Finite Conversions. *Journal of Catalysis*, 174:111–118, 1998. doi: 10.1006/jcat.1998.1964.

[14] K. Klier, V. Chatikavanij, R. G. Herman, and G. W. Simmons. Catalytic Synthesis of Methanol from CO/H_2 IV The Effects of Carbon Dioxide. *Journal of Catalysis*, 74:343–360, 1982. doi: 10.1016/0021-9517(82)90040-9.

Appendix B

Supplementary information for *Methanol-Assisted Autocatalysis in Catalytic Methanol Synthesis* in chapter 4

Authors: Joachim Thrane[a], Sebastian Kuld[b] Niels D. Nielsen[a], Anker D. Jensen[a], Jens Sehested[b], Jakob M. Christensen[a]

[a] *Department of Chemical and Biochemical Engineering, Technical University of Denmark, Søltofts Plads Building 229, 2800 Kgs. Lyngby (Denmark)*
[b] *Haldor Topsøe A/S, Nymøllevej 55, 2800 Kgs. Lyngby (Denmark)*
*__Correspondence to:__ jmc@kt.dtu.dk

DOI:
https://doi.org/10.1002/anie.202006921

Journal specifications:
Angewandte Chemie International Edition, 2020, Volume 59, 18189-18193

Date Accepted/Published:
29 June 2020 / 13 August 2020

S1 Supplementary Material

Methods

In the present work a normal liter (NL) is a liter of gas at 1 atm and 273.15 K. The mass of catalyst in presentation of productivity and Cu area is that of the oxide precursor. Cu/ZnO (3 & 20 wt% Cu), $Cu/ZnO/Al_2O_3$ (Cu:Zn:Al = 60:30:10 & 55:27:18 molar basis) and Cu/Al_2O_3 (20 wt% Cu) samples were prepared by co-precipitation from the nitrates ($Cu(NO_3)_2{\cdot}3H_2O$ ≥99%, $Zn(NO_3)_2{\cdot}6H_2O$ ≥98%, $Al(NO_3)_3 \cdot 9H_2O$ ≥98% from Sigma Aldrich) at 338 K and pH = 6.5 using Na_2CO_3 (Sigma Aldrich, ≥99.8%) as the precipitation agent. The precipitation was followed by ageing for 1 h with unrestricted pH, and then filtration and washing with deionized water. The precipitate was dried overnight at 313 K and then approximately 10 g was calcined at 603 K (1 K/min) in 1 L/min of flowing dry air. 20 wt% Cu/SiO_2 was prepared by incipient wetness impregnation of Saint Gobain SiO_2 (SS61138, 250 m^2/g) with an aqueous solution of copper nitrate. The sample was then dried overnight at 313 K and approximately 5 g was calcined at 583 K (1 K/min) in 1 L/min of flowing dry air. All samples were crushed and sieved to a size range of 150-300 µm. The Cu surface area of the samples was determined from the N_2O uptake (so-called reactive frontal chromatography) using a Quantachrome Autosorb iQ_2 setup. Here a catalyst sample in a quartz cell was heated in a 19 NmL/min flow of 5 mol% H_2 in N_2 at 2 K/min to 523 K and kept at this temperature for 2 h, flushed 20 min in He and cooled to 333 K. Cu/Al_2O_3 was further reduced for 2 h in pure H_2 at 523 K as this was found to be necessary for complete reduction. After pre-reduction the reduced sites were then titrated by the reactive frontal chromatography method [1] using a 19 NmL/min flow of 1 mol% N_2O in He and the effluent gasses were analyzed by a Hiden Analytical QGA mass spectrometer. The N_2O uptake was obtained assuming full conversion between the mid-points of the N_2 front. An O:Cu = 1:2 stoichiometry and a Cu surface site density of $1.47{\cdot}10^{19}$ Cu atoms/m^2 was used [2]. Sample masses were varied to have at least several minutes between the N_2/N_2O fronts to lower uncertainty. The standard deviation on the N_2O uptake from 5 repeated measurements of Cu/SiO_2 was 6%. At higher hydrogen pressure over reduction can distort the N_2O measurement for Cu on reducible supports such as ZnO [2, 3]. With pre-reduction in dilute H_2 as applied here it was previously observed [2] that N_2O RFC and H_2 chemisorption gave relatively similar Cu area estimates for Cu/ZnO-based samples, and based on that triangulation with two methods a reasonable estimate of the Cu surface area is expected for the presently applied reduction in dilute H_2.

The tests of catalytic activity in Figs. 1, 3a and S1-S4 were conducted using a setup described in detail elsewhere [4]. A catalyst sample (varying mass) was installed in an 8 mm i.d. quartz reactor tube between wads of quartz wool. No dilutant was added to the catalyst in order to avoid by-pass effects. The catalyst was first pre-reduced by heating in a 108 NmL/min flow of 5 mol% H_2 in N_2 to 523 K (2 K/min) and held at this temperature for 1 h (holding time had no discernible effect between 1, 4 and 13 h). The reactor was then flushed and pressurized in N_2. A flow (from pure 99.999% H_2 and premixed 8.56 mol% CO_2 in CO all from AGA) of $H_2/CO/CO_2$ = 67.6/29.6/2.8 (molar basis) was then initiated and the composition of the reactor effluent was measured using a Hiden Analytical QGA mass spectrometer and an Agilent 6890N GC-TCD/FID having one channel with a Porapak N + 13X Molsieve column and one channel with a PoraplotQ column. The analysis equipment was calibrated using either certified gas mixtures from AGA or using gas mixtures prepared by injecting a known volume of a liquid component into a known volume of nitrogen in a Tedlar bag. For Cu/ZnO based catalysts, which are deactivating systems, only the initial activities were used in Fig. 1 (see Fig. S1a). For Cu/SiO_2 and Cu/Al_2O_3, which are stable over time, the flow was varied and typically two points for Fig. 1 were obtained using the same catalyst charge. Cu/Al_2O_3 also produces DME from methanol dehydration, which is included as two methanol molecules in the reported methanol productivity. The standard deviation from repeated measurements at differential conditions was 9%, which represents a known uncertainty in the measurements. From the known uncertainties in N_2O uptake and productivity the known uncertainty in TOF calculations is therefore 11%. Error bars are used to indicate this known uncertainty in Fig. 1. Bulk heat effects were ruled out by the absence of measured temperature increase and the non-generality of the increasing rate with increasing conversion. Significant temperature gradients (> 0.5 K) in the laminar boundary layer around the particles were ruled out using the heat transfer coefficient (950 W/($m^2{\cdot}$K)) calculated [5] from the Ranz-Marshall

correlation [6]. Axial dispersion effects for the syngas reactants were ruled out using the Mears criterion [7] (in the worst case bed length/particle size = 18 compared to a requirement of at least 9 from the Mears criterion). Transport limitations were ruled out by comparison to the Mears [7] and Weisz-Prater [8] criteria, by near identical results for Cu/ZnO in two different particle sizes (150-300 μm and < 150μm), and by comparison to the particle size where diffusion limitations can be observed experimentally [9].

For the experiment in Fig. 3a methanol (Sigma Aldrich, ≥99.9%) was added to the syngas feed using a Gilson 305 HPLC pump and the dosed amounts were determined from a blank run without catalyst. Feeding CH_3OH/N_2 over $Cu/ZnO/Al_2O_3$ at 523 K resulted in some decomposition of methanol into $CO/CO_2/H_2$ (reverse reaction of methanol synthesis) – ca. 6% methanol conversion when feeding 0.45 mol% CH_3OH in N_2 at the conditions of Fig. 3a. Since this is also likely to occur and lower the apparent net methanol production during co-feeding of methanol with syngas, the increase in net methanol production during the presented methanol co-feeding experiments may represent a conservative estimate.

The experiment in Fig. S6 was performed in a high-pressure reactor described elsewhere [10] using a U-tube reactor (SGE Analytical Science glass lined tubes 1/4" o.d., 4 mm i.d.). Product analysis was made with a Thermo Fisher Trace 1300 GC fitted with one channel composed of a TG5 column leading to an FID detector and one channel composed of an OV-1 column followed by a Shincarbon column leading to a TCD detector. The fact that both Figs. 1 and S6 using two different reactors show an increase in TOF with increasing conversion in $CO/CO_2/H_2$ verifies that the conclusion is not reactor-dependent.

The experimental setup used for investigating the impact of water and methanol addition (Figs. 2, 3b and S5) consists of a gas delivery system, a U-shaped reactor and a calibrated quadrupole mass spectrometer (Balzers GAM 445), as previously described by Kuld et al. [11]. Gases of high purity were used: He (99.9999%), H_2 (99.9999%), H_2/He (1% H_2, 99.9995%), CO_2 (99.9995%) and CO (99.997%). 10 mg of $Cu/ZnO/Al_2O_3$ catalyst (Cu:Zn:Al = 60:30:10, 20 m^2 $Cu/g_{cat.}$) in the sieve fraction 150-300 μm was mixed with sintered inert calcium aluminate in a 1:10 ratio on volume basis. The catalyst was loaded into a glass lined U-shaped stainless steel reactor with an inner diameter of 4 mm resulting in a bed height of 24-25 mm. The catalyst was initially activated in a flow of 1% H_2/He by raising the temperature from room temperature to 448 K by 1 K/min. After 2 hours at 448 K the gas mixture was changed to pure H_2 and the temperature was raised from 448 K to 513 K for 30 min. At 513 K the gas composition was changed to synthesis gas $H_2/CO/CO_2$ = 67.6/29.6/2.8 mol% at a space velocity of $1.6{\cdot}10^6$ NL/kg/h and the reactor was pressurized to 41 bar and the temperature was increased to 523 K. Water in the range [0-1500 ppmv] and methanol in the range of [0-1.1 mol%] was added to the gas stream by bubbling the synthesis gas through water or methanol. The water/methanol concentration was controlled by adjusting the temperature of the saturator by means of a water bath. The methanol synthesis was measured at three different temperatures: 523 K, 508 K and 493 K before the experiment was terminated. The catalyst sample was replaced between each experimental condition i.e. each water or methanol addition. The known uncertainty for all co-feeding experiments was taken as the greatest deviation from the average among two experimental series at identical conditions at 523 K and is marked by the error bars.

The temperature programmed reactions in Figs. 4 and S7 were obtained using a Quantachrome Autosorb iQ_2 setup with the reactor effluent analyzed by a Hiden Analytical QGA mass spectrometer. Here 0.5 g of $Cu/ZnO/Al_2O_3$ (Cu:Zn:Al = 60:30:10 molar ratio, 20 m^2 Cu/g) was pre-reduced as described for the Cu area measurements, flushed with He, cooled to 303 K and covered with HCOO by 1 h treatment in a 20 NmL/min flow of 2.3 mol% $HCOOH/N_2$ produced by bubbling N_2 through HCOOH (≥98% Sigma Aldrich). The HCOOH treated catalyst was flushed in He for 30 min and then heated at a rate of 1 K/min in either a 19 NmL/min flow of 4.1 mol% CD_3OD/He (produced by bubbling He through CD_3OD ≥99.8 %D Sigma Aldrich), a 40 NmL/min flow of 5.5 mol% CH_3OH/He or a 40 NmL/min flow of H_2. Identical blank runs were made without HCOOH treatment to verify that observed products did arise from surface formate.

Supporting Data

Fig. S1a illustrates that the general behavior of Cu/ZnO-based systems under syngas conditions. The loss of activity is attributed to sintering and loss of Cu surface area [12, 13] rather than a loss of TOF. For the experiment in Fig. S1a the peak activity level (8.18 $g_{MeOH}/g_{cat.}/h$), which occurs as soon as the syngas has fully flushed through the system, is used together with the Cu area of the freshly reduced catalyst (20 m^2 Cu/gcat.) to calculate the TOF. The productivity of this catalyst at differential conditions is 2.45 $g_{MeOH}/g_{cat.}/h$ (see Fig. S1c). For Cu on Al_2O_3 or SiO_2 the rate reaches a steady state, which is used together with the Cu area of the freshly reduced catalyst to calculate the TOF value. Fig. S1b shows, for selected measurements, the TOF as a function of space velocity (SV). The increase in TOF with decreasing SV is observed at different space velocities for different catalysts depending on the absolute activity and is thus not a direct function of SV. Comparing catalytic materials at a set of fixed conditions rather than at a fixed production level can therefore lead to incorrect conclusions. A comparison at fixed conditions could result in the situation where the samples of larger Cu area have entered the autocatalytic regime and appear relatively more active, whereas samples of smaller Cu area are in the differential regime and appear less active. This would for example occur if comparing $Cu/ZnO/Al_2O_3$ (20 $m^2_{Cu}/g_{cat.}$) and Cu/ZnO (9.1 $m^2_{Cu}/g_{cat.}$) at an SV of $4{\cdot}10^5$ NL/kg/h, where the higher area sample has reached its maximal autocatalytic acceleration, whereas the lower area sample is still in the fully differential limit. Fig. S1c shows the results for $Cu/ZnO/Al_2O_3$ (Cu:Zn:Al = 6:3:1, 20 $m^2_{Cu}/g_{cat.}$) from Fig. 1 in the main text in terms of methanol productivity rather than as a turnover frequency. Fig. S1d shows the results from Fig. 1 in the main text focusing only on Cu/Al_2O_3 and Cu/SiO_2 to better show the concentration-independent TOF of Cu/Al_2O_3.

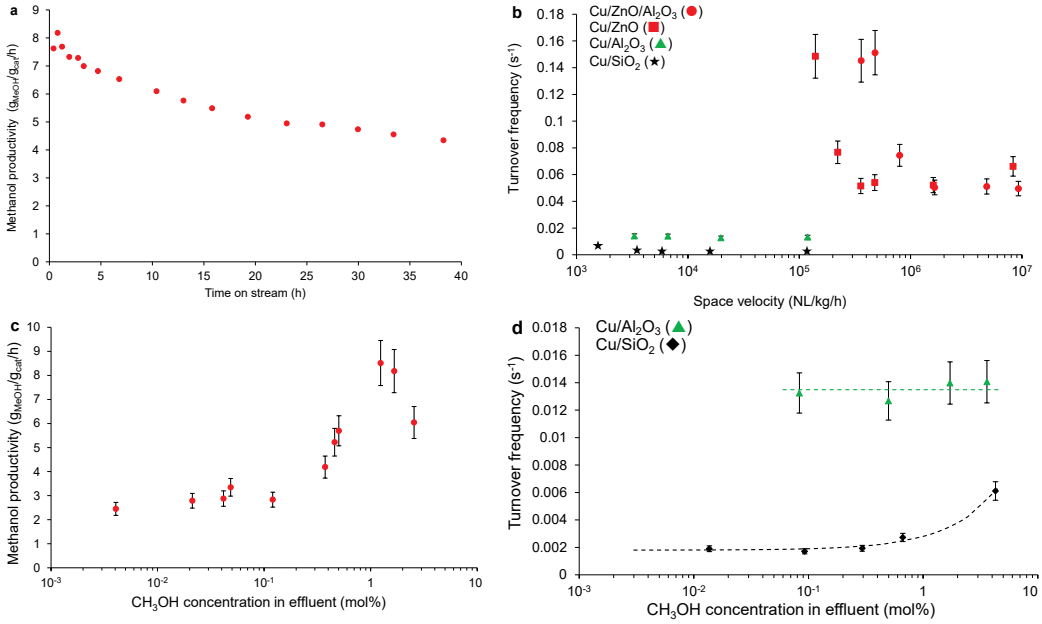

Fig. S1: **(a)** Methanol productivity as a function of time on stream for $Cu/ZnO/Al_2O_3$ (Cu:Zn:Al = 6:3:1). For such deactivating systems the productivity is taken as the initial activity from which productivity begins to decline. In this case the productivity is 8.18 $g_{MeOH}/g_{cat.}/h$. Experimental conditions: 50 bar, 523 K, $H_2/CO/CO_2$ = 67.6/29.6/2.8 mol%, SV: 3.6·105 NL/kg/h (0.1 g cat. & 600 NmL/min). **(b)** Turnover frequency as a function of space velocity for selected measurements. Experimental conditions: 50 bar, 523 K, $H_2/CO/CO_2$ = 67.6/29.6/2.8 mol%. **(c)** The methanol productivity for $Cu/ZnO/Al_2O_3$ (Cu:Zn:Al = 6:3:1, 20 $m^2_{Cu}/g_{cat.}$) as a function of the methanol concentration in the reactor effluent. The highest productivity achieved was 8.52 $g_{MeOH}/g_{cat.}/h$. Experimental conditions: 50 bar, 523 K, $H_2/CO/CO_2$ = 67.6/29.6/2.8 mol%. **(d)** The TOF as a function of methanol effluent concentration for the two lower-activity samples Cu/Al_2O_3 and Cu/SiO_2 illustrating the concentration-independent TOF of Cu/Al_2O_3.

Fig. S2 shows the effluent concentration of CO_2 during the first hours on stream for the experiment in Fig. S1a compared to the inlet concentration. The figure illustrates that essentially no change to the CO_2-concentration occurs as a result of the reaction, and since these experimental conditions are close to the optimal autocatalytic productivity in Fig. 1 in the main text we can fully exclude changes in CO_2 concentration as the reason for the increased productivity at higher conversion levels. The fact that the CO_2 concentration remains constant is also a clear indication that the rate of the water-gas shift reaction is far higher than the rate of CO_2 hydrogenation into methanol.

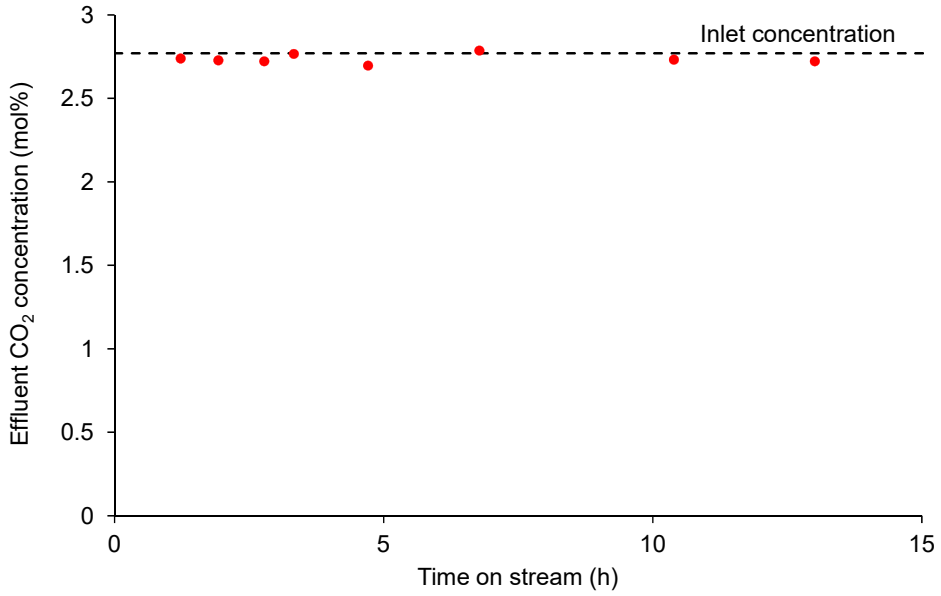

Fig. S2: The CO_2 effluent concentration measured by gas chromatography during the first 10 h on stream for the experiment in Fig. S1a compared to the inlet concentration. The results illustrate that the CO_2 consumption by the reaction and the concentration increase from the volume contraction balance out. Consequently, changes in CO_2 concentration are unimportant for the strong activity increase observed at these conditions.

Fig. S3 shows productivities either at the differential plateau-level or at the optimal finite conversion levels as functions of the Cu surface area. Fig. S3 shows that an 8-fold increase in Cu area for Cu/ZnO is associated with a corresponding increase in productivity under the finite conditions where the autocatalytic pathway prevails.
The experiment with co-feeding of methanol was conducted at varying conditions as shown in Figs. S4 and S5. Fig. S4 shows that as expected the relative increase in methanol productivity is higher at a higher space velocity, where the intrinsic methanol production is lower. Fig S5 shows that the effect of methanol co-feeding is relatively independent up to a feed concentration of ca. 0.5 mol%. Above 508 K this remains so at higher concentrations, but at 493 K the net productivity goes down at higher co-feeding concentrations. This decline at 493 K can have two reasons. At low temperatures methanol could possibly cause inhibition due to competitive adsorption. Alternatively, the intrinsic productivity is also lower at the lower temperature and any uncertainty due to decomposition of the methanol co-fed with the syngas will have a bigger impact at a lower productivity level.
Fig. S6 shows the TOF as a function of effluent methanol concentration for $Cu/ZnO/Al_2O_3$ in both $CO/CO_2/H_2$ and CO_2/H_2. A rise in TOF does not occur in CO_2/H_2 – most likely due to the greater water concentration in the absence of CO. It should however be emphasized that the TOF is preserved in CO_2/H_2 up to an effluent methanol concentration of 0.4 mol%. Under those conditions the effluent water concentration due to methanol synthesis and reverse water gas shift was estimated to be 0.68 mol% from an oxygen balance. Fig. 2 in the main text illustrates that such water levels would have caused major loss of activity, if the autocatalytic acceleration had not been there to compensate for the water inhibition. The autocatalytic mechanism is thus strongly present for $Cu/ZnO/Al_2O_3$ in a CO_2/H_2 feed, but the rise in TOF is prevented by the larger water production.

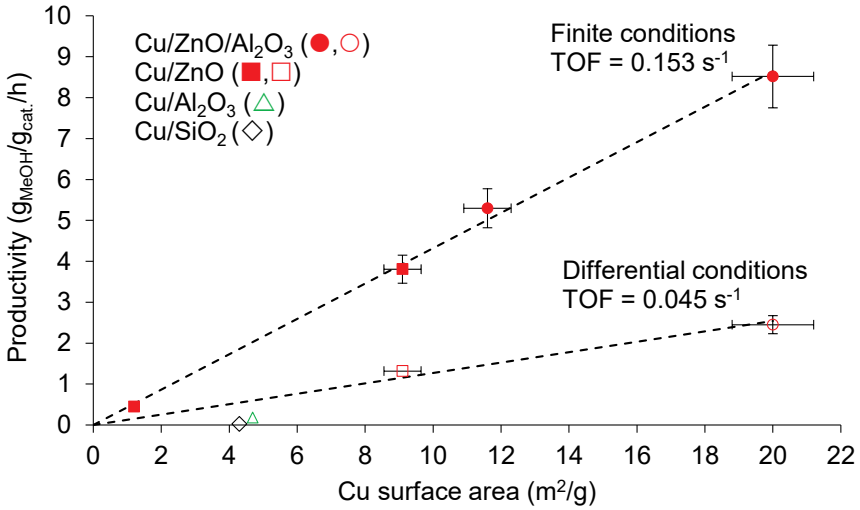

Fig. S3: Dependence of methanol productivity on Cu surface area for differential (open points) and optimal finite (filled points) conditions along with lines of constant TOF indicated. Experimental conditions: 50 bar, 523 K, $H_2/CO/CO_2$ = 67.6/29.6/2.8 mol%, SV: $3{\cdot}10^3$-$4.3{\cdot}10^7$ NL/kg/h. See Fig. S1 for a definition of the TOF and a comparison in terms of space velocity.

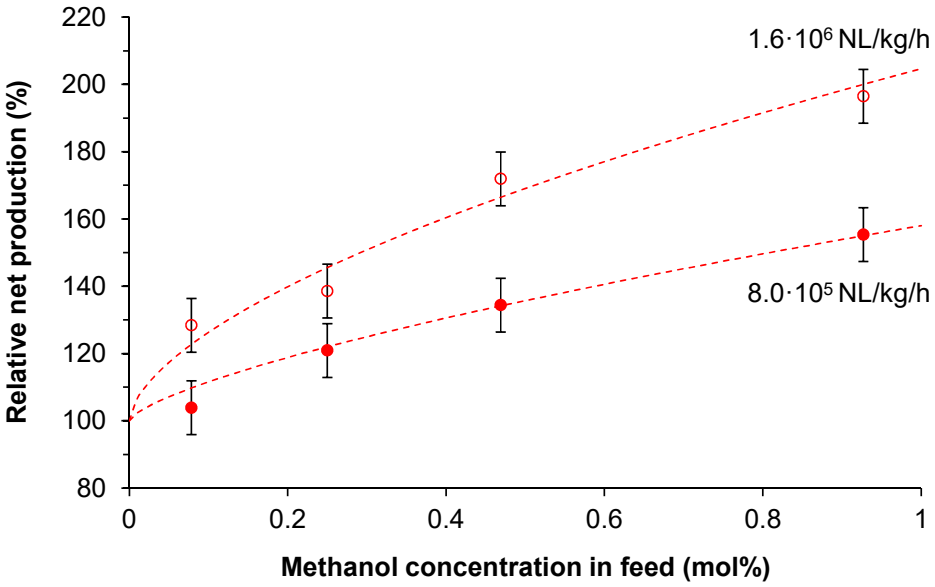

Fig. S4: The relative net methanol production as a function of the methanol concentration in the feed at two different space velocities. Conditions: 50 bar, 523 K, syngas before CH_3OH-addition: $H_2/CO/CO_2$ = 67.6/29.6/2.8 mol%.

When surface formate is reacted with CH_3OH to form methyl formate the resulting TPR peak has a characteristic shape with a very sharp decline (Fig. 4a). Under these atmospheric pressure conditions methanol decomposition is thermodynamically favored and a major onset of methanol decomposition sets in once approximately half the surface formate layer has been converted (judging from the CO_2 peak due to formate decomposition). Fig. S7 shows that once the methanol decomposition sets in (notice the sharp drop in the CD_3OD effluent concentration) the ester formation essentially stops and this creates the steep decline in ester formation. Beyond this temperature any adsorbed methanol will be more likely to decompose rather than react with formate to produce the ester and consequently the ester formation cannot be monitored by the low-pressure TPR technique.

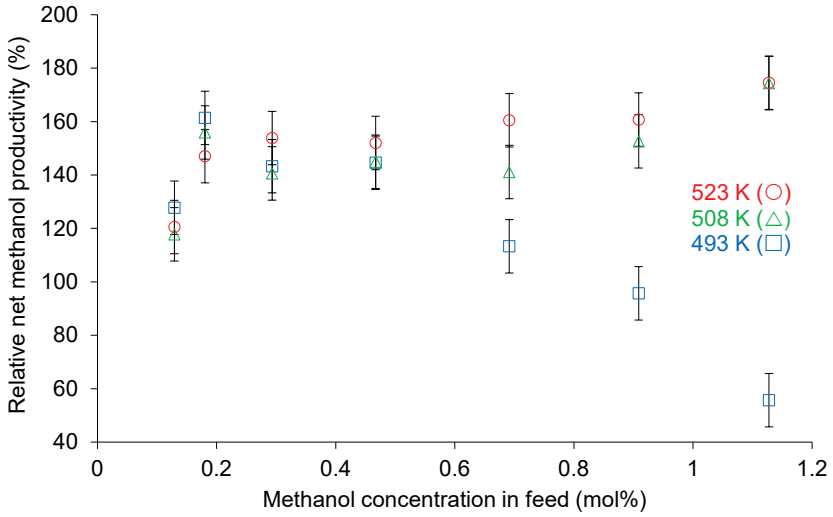

Fig. S5: The relative net methanol production as a function of the methanol concentration in the feed at three different temperatures. Note that both 508 K and 523 K show a continuously increasing trend whereas a net decline in productivity is seen for larger feed concentrations at 493 K. Conditions: 50 bar, SV: $1.6{\cdot}10^6$ NL/kg/h, syngas before CH_3OH-addition: $H_2/CO/CO_2$ = 67.6/29.6/2.8 mol%.

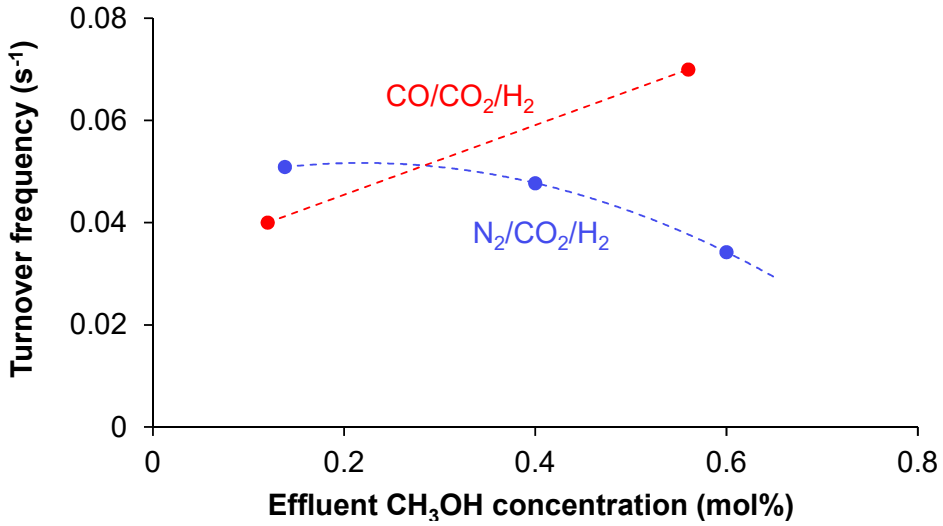

Fig. S6: The turnover frequency for methanol synthesis as a function of the effluent CH_3OH concentration in both $CO/CO_2/H_2$ and $N_2/CO_2/H_2$. Conditions: 50 bar, 523 K SV: $2.4{\cdot}10^5$-$1.6{\cdot}10^6$ NL/kg/h, $H_2/CO/CO_2$ = 68/29/3 mol% or $H_2/N_2/CO_2$ = 68/29/3 mol%.

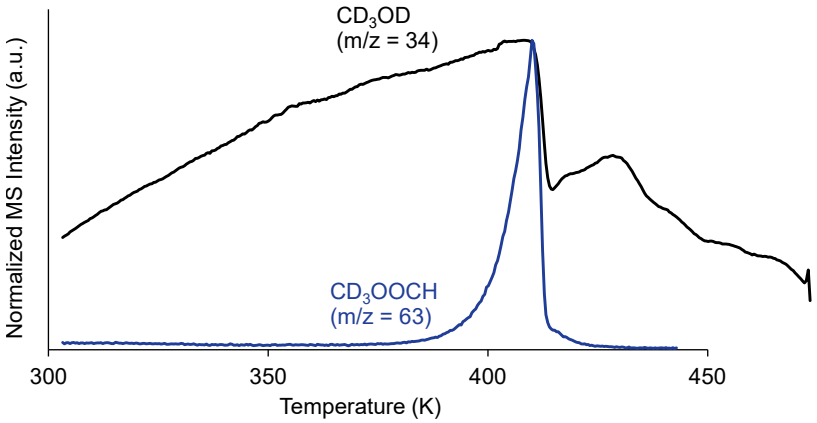

Fig. S7: Normalized MS signals for CD_3OD and CD_3OOCH when $Cu/ZnO/Al_2O_3$ with pre-adsorbed HCOO is subjected to TPR (1 K/min) at 1 atm in a 19 NmL/min flow of 4.1 mol% CD_3OD in He, 0.5 g cat. Part of the data can be seen in Fig. 4a in the main text.

References

[1] G. C. Chinchen, C. M. Hay, H. D. Vandervell, and K. C. Waugh. The measurement of copper surface areas by reactive frontal chromatography. *Journal of Catalysis*, 103(1):79–86, 1987. doi: 10.1016/0021-9517(87)90094-7.

[2] R. Chatterjee, S. Kuld, R. V. D. Berg, A. Chen, and W. Shen. Mapping Support Interactions in Copper Catalysts. *Topics in Catalysis*, 62(7-11):649–659, 2019. doi: 10.1007/s11244-019-01150-9.

[3] S. Kuld, C. Conradsen, P. G. Moses, I. Chorkendorff, and J. Sehested. Quantification of zinc atoms in a surface alloy on copper in an industrial-type methanol synthesis catalyst. *Angewandte Chemie - International Edition*, 53(23):5941–5945, 2014. doi: 10.1002/anie.201311073.

[4] J. M. Christensen, P. M. Mortensen, R. Trane, P. A. Jensen, and A. D. Jensen. Effects of H_2S and process conditions in the synthesis of mixed alcohols from syngas over alkali promoted cobalt-molybdenum sulfide. *Applied Catalysis A: General*, 366(1):29–43, 2009. doi: 10.1016/j.apcata.2009.06.034.

[5] E. N. Lightfoot, W. E. Stewart, and R. B. Bird. *Transport Phenomena*. John Wiley & Sons, USA, 2002. doi: 10.1115/1.1424298.

[6] W. Ranz. Evaporation from drops. *Chem. Eng. Prog.*, 48:141–146, 1952.

[7] D. E. Mears. Tests for Transport Limitations in Experimental Catalytic Reactors. *Industrial and Engineering Chemistry Process Design and Development*, 10(4):541–547, 1971. doi: 10.1021/i260040a020.

[8] P. B. Weisz and C. D. Prater. Interpretation of Measurements in Experimental Catalysis. *Adv. Catal. Related Subj.*, 6(C):143–196, 1954. doi: 10.1016/S0360-0564(08)60390-9.

[9] W. Seyfert and G. Luft. Untersuchungen zur Methanol-Synthese im Mitteldruckbereich. *Chem. Ing. Tech*, 57(5):482–483, 1985. doi: 10.1002/cite.330570526.

[10] N. D. Nielsen, J. Thrane, A. D. Jensen, and J. M. Christensen. Bifunctional Synergy in CO Hydrogenation to Methanol with Supported Cu. *Catalysis Letters*, 150:1427–1433, 2020. doi: 10.1007/s10562-019-03036-7.

[11] S. Kuld, M. Thorhauge, H. Falsig, C. F. Elkjaer, S. Helveg, I. Chorkendorff, and J. Sehested. Quantifying the promotion of Cu catalysts by ZnO for methanol synthesis. *Science*, 352(6288):969–974, 2016. doi: 10.1126/science.aaf0718.

[12] M. Kurtz, H. Wilmer, T. Genger, O. Hinrichsen, and M. Muhler. Deactivation of Supported Copper Catalysts for Methanol Synthesis. *Catalysis Letters*, 86(1-3):77 – 80, 2003. doi: 10.1023/A:1022663125977.

[13] J. T. Sun, I. S. Metcalfe, and M. Sahibzada. Deactivation of $Cu/ZnO/Al_2O_3$ methanol synthesis catalyst by sintering. *Industrial and Engineering Chemistry Research*, 38(10):3868–3872, 1999. doi: 10.1021/ie990078s.

Appendix C

Supplementary information for *Quantification of Formate and Oxygen Coverages on Cu Under Industrial Methanol Synthesis Conditions* in chapter 5

Authors: Niels D. Nielsen[1], Anker D. Jensen[1], Jakob M. Christensen[1]
[1] *Department of Chemical and Biochemical Engineering, Technical University of Denmark, Søltofts Plads Building 229, 2800 Kgs. Lyngby, Denmark*
*__Correspondence to:__ jmc@kt.dtu.dk

DOI:
https://doi.org/10.1007/s10562-020-03162-7

Journal specifications:
Catalysis Letters, 2020, Volume 150, 2447-2456

Date Accepted/Published:
23 February 2020 / 6 March 2020

S1 Supplementary Material

Investigating the reproducibility of the quenching procedure

Additional tests (Test 2 and 3) with Raney Cu were performed to investigate the reproducibility of the cooling profiles upon quenching and they are compared to data from test 1, which was shown in the main article, in Fig. S1.

Cooling profiles during cooling

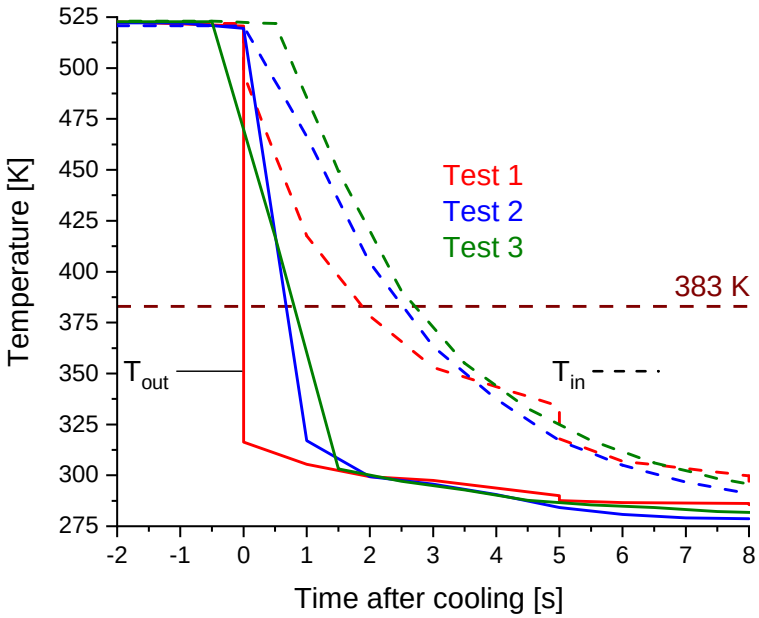

Fig. S1: Cooling of the catalyst with the ice water at the reaction conditions at t = 0 measured with two thermocouples placed inside at the top and outside at the bottom of the catalyst bed. Graphs from the inside thermocouple are shown as dashed profiles based on the outside thermocouple are solid. Data are from the three tests with the ice water. Lower sampling frequency for test 3 caused a less resolved cooling profile.

Temperature Programmed Desorption after quenching

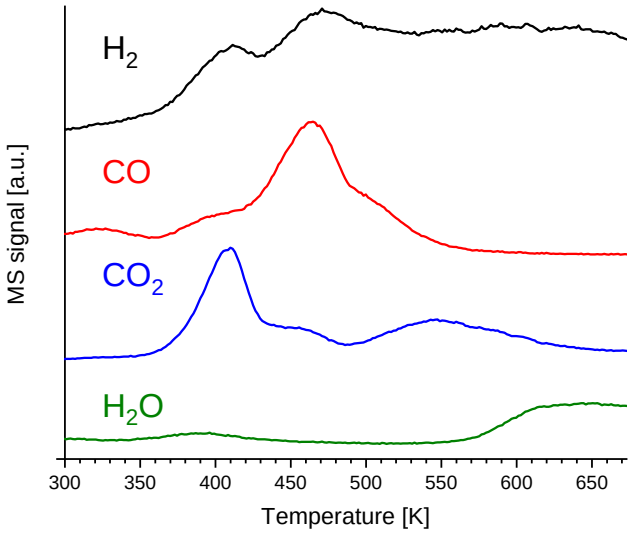

Fig. S2: Gas desorption during temperature programmed desorption (2 K/min as heating ramp and 42.7 Nml/min of He) after quenching at reaction conditions (T = 523 K, 50 bars of pressure in $CO_2/CO/H_2$ = 3/29/68). Gas signals were offset on the linear y-axis for clarity. Data were from test 2 using ice water to cool.

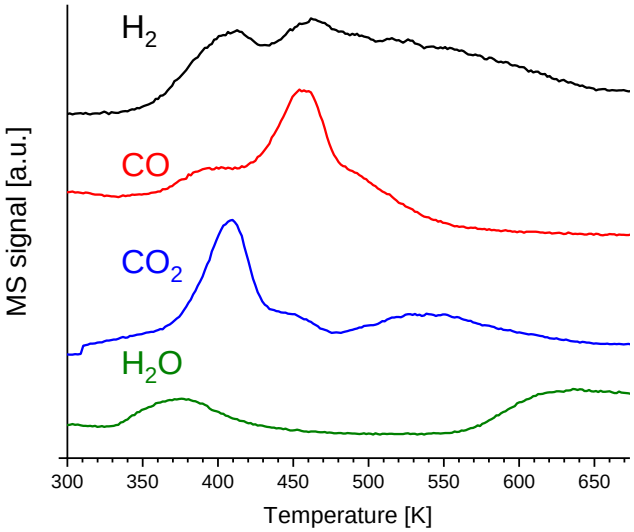

Fig. S3: Gas desorption during temperature programmed desorption (2 K/min as heating ramp and 42.8 Nml/min of He) after quenching at reaction conditions (T = 523 K, 50 bars of pressure in $CO_2/CO/H_2$ = 3/29/68). Gas signals were offset on the linear y-axis for clarity. Data were from test 3 using ice water to cool.

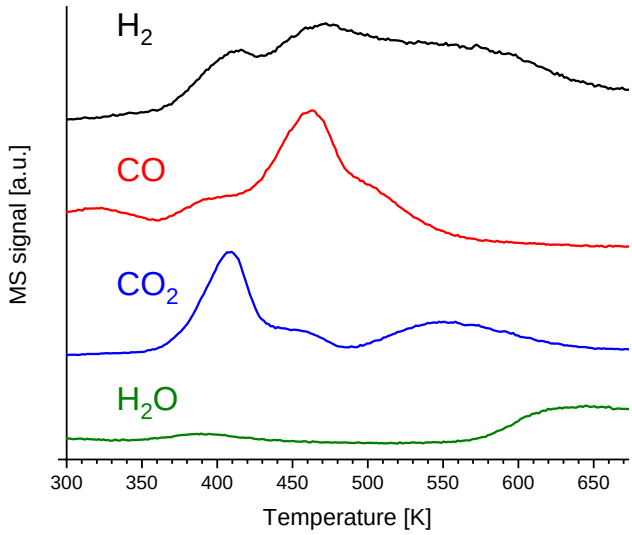

Fig. S4: Gas desorption during temperature programmed desorption (2 K/min as heating ramp and 42.2 Nml/min of He) after quenching at reaction conditions (T = 523 K, 50 bars of pressure in $CO_2/CO/H_2$ = 3/29/68). Gas signals were offset on the linear y-axis for clarity. Data were from test 4 using boiling water to cool.

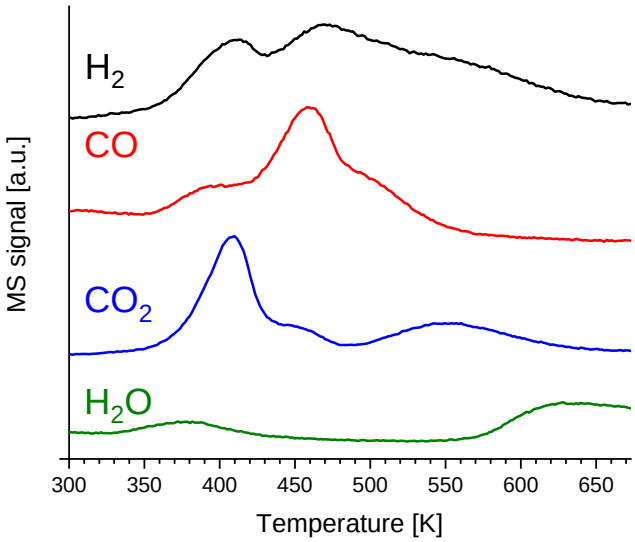

Fig. S5: Gas desorption during temperature programmed desorption (2 K/min as heating ramp and 44.7 Nml/min of He) after quenching at reaction conditions (T = 523 K, 50 bars of pressure in $CO_2/CO/H_2$ = 3/29/68). Gas signals were offset on the linear y-axis for clarity. Data were from the test using liquid N_2 to cool.

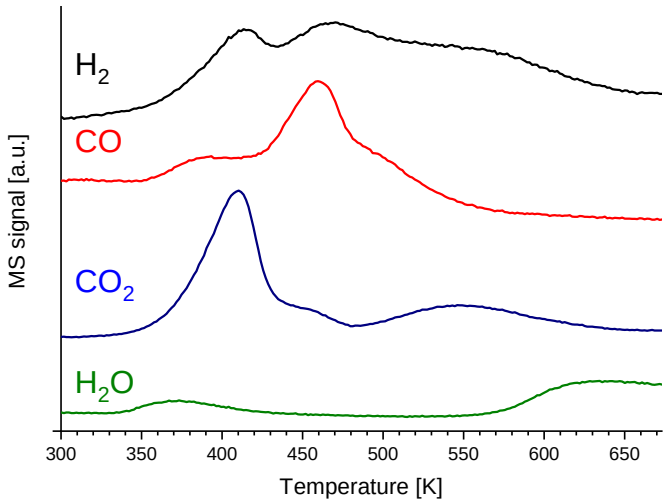

Fig. S6: Gas desorption during temperature programmed desorption (2 K/min as heating ramp and 44.3 Nml/min of He) after quenching at reaction conditions (T = 523 K, 50 bars of pressure in $CO_2/CO/H_2$ = 3/29/68). Gas signals were offset on the linear y-axis for clarity. Data were from the test using static air to cool.

Integration of desorbed CO_2

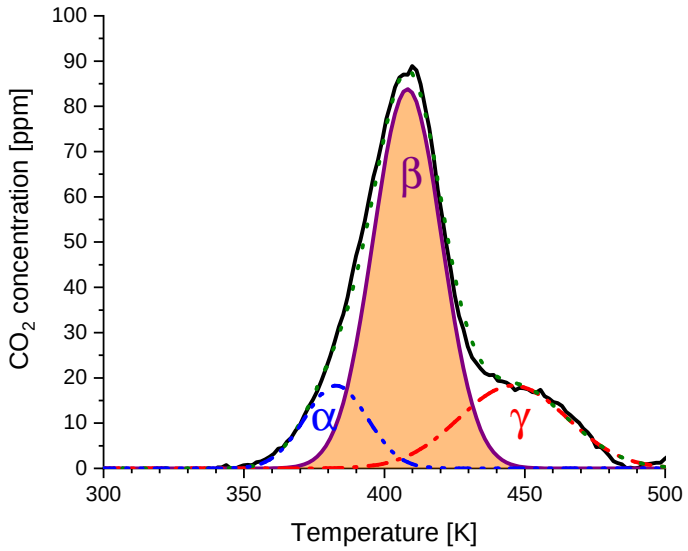

Fig. S7: Peak fitting to the measured black solid CO_2 desorption line using three Gaussian peaks (α, β, and γ), which sum up to dotted green profile. HCOO was quantified by the integrated area (orange) under the CO_2 β-peak. Heating ramp for the TPD on Raney Cu was 2 K/min. Data were from test 2 with ice water.

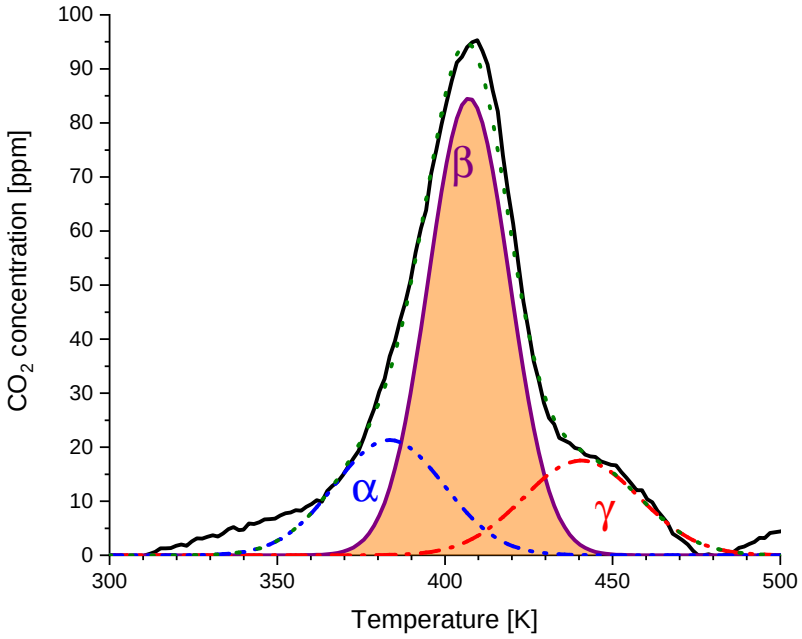

Fig. S8: Peak fitting to the measured black solid CO_2 desorption line using three Gaussian peaks (α, β, and γ), which sum up to dotted green profile. HCOO was quantified by the integrated area (orange) under the CO_2 β-peak. Heating ramp for the TPD on Raney Cuwas 2 K/min. Data were from test 3 with ice water.

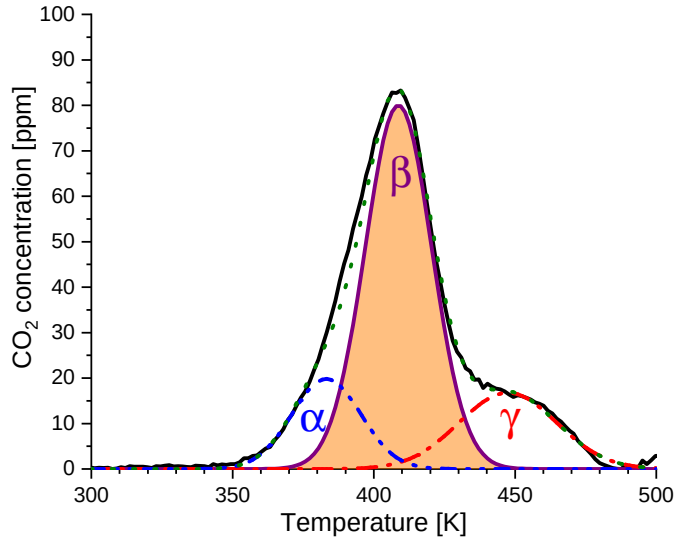

Fig. S9: Peak fitting to the measured black solid CO_2 desorption line using three Gaussian peaks (α, β, and γ), which sum up to dotted green profile. HCOO was quantified by the integrated area (orange) under the CO_2 β-peak. Heating ramp for the TPD on Raney Cuwas 2 K/min. Data were from the test with boiling water.

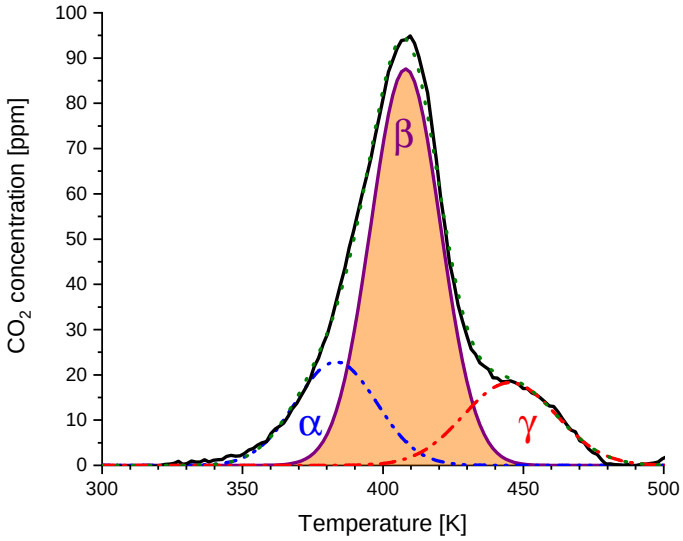

Fig. S10: Peak fitting to the measured black solid CO_2 desorption line using three Gaussian peaks (α, β, and γ), which sum up to dotted green profile. HCOO was quantified by the integrated area (orange) under the CO_2 β-peak. Heating ramp for the TPD on Raney Cu was 2 K/min. Data were from the test with liquid N_2.

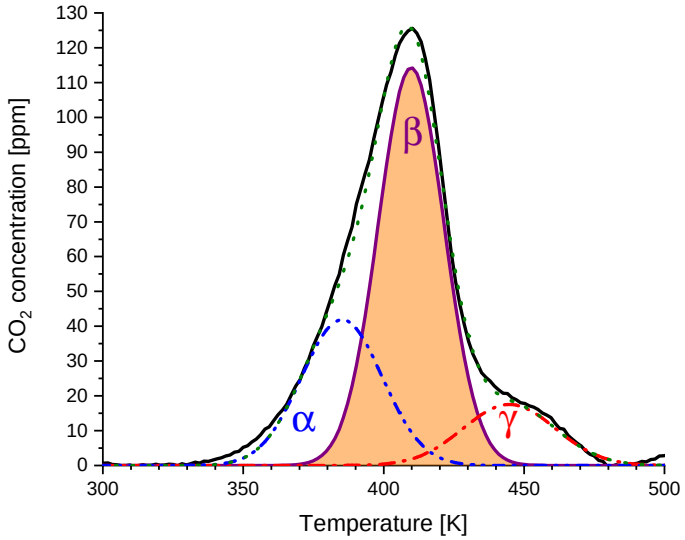

Fig. S11: Peak fitting to the measured black solid CO_2 desorption line using three Gaussian peaks (α, β, and γ), which sum up to dotted green profile. HCOO was quantified by the integrated area (orange) under the CO_2 β-peak. Heating ramp for the TPD on Raney Cuwas 2 K/min. Data were from the test with static air.

High pressure syngas switching between $CO_2/CO/H_2$ and $CO_2/N_2/H_2$ over Raney Cu

Fig. S12 compares the methanol turnover frequencies (TOF) over Raney Cu in $CO_2/CO/H_2$ (3/29/68) and $CO_2/N_2/H_2$ (3/29/68) after pre-reduction in 5 mol% H_2 and pressurization in He. The similar TOFs strongly indicate that CO does not contribute significantly to the methanol formation and that CO_2 is the main carbon source for methanol synthesis at the investigated reaction conditions over Raney Cu.

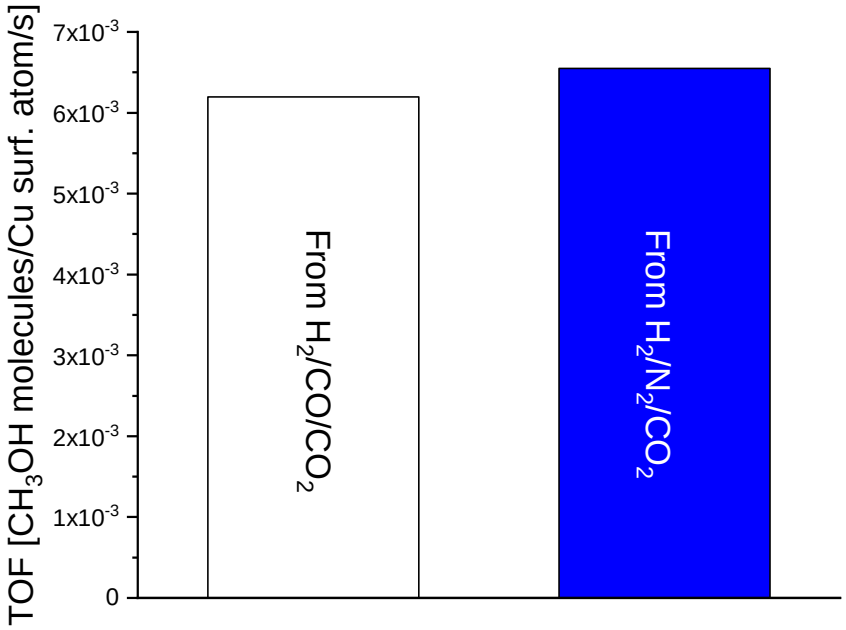

Fig. S12: Methanol turnover frequency in $CO_2/CO/H_2$ (3/29/68) and $CO_2/N_2/H_2$ (3/29/68) at 523 K, and 50 bar with a constant GHSV of 8.4 $\cdot 10^4$ $Nml/g_{cat.}/h$ over Raney Cu with Cu surface area of 5.18 $m^2/g_{cat.}$.

Temperature programmed hydrogenation of Cu nanopowder and blank experiment

In a TPH experiment after quenching during operation in syngas Raney Cu exhibited a low temperature (< 420 K) water formation (see Fig. 7 in the main text). To test if this water signal could be attributed to oxygen species (O or OH) on the Cu surface 2 verification experiments were conducted with unsupported Cu (from Sigma Aldrich CuO nanopowder). In one experimentunsupported Cu was quenched (using ice water) during operation at reaction conditions (448 K, 50 bar, $CO_2/CO/H_2$ = 3/29/68) and then subjected to a TPH. In another experiment the unsupported Cu was pre-reduced, cooled to ambient temperature in the reducing gas and then subjected to the TPH. Fig. S13 shows the water evolution in the TPH for these two experiments and for a blank run with only the quartz wool packing in the reactor. The figure shows that a similar water evolution occurs in the TPH for both the quenched catalyst and for the freshly reduced catalyst. For the freshly reduced sample there is no chance of oxygen deposition on the surface, and we therefore conclude that the water evolution is not due to reduction of oxygen species on the surface but rather due to water impurities in the H_2/N_2 mixture used for the TPH. These water impurities adsorb on the Cu at ambient temperature before the initiation of the TPH and then desorb during the initial stages of the TPH. Within the uncertainty we therefore cannot detect any deposition of oxygen species on the Cu surface from the syngas atmosphere at reaction conditions.

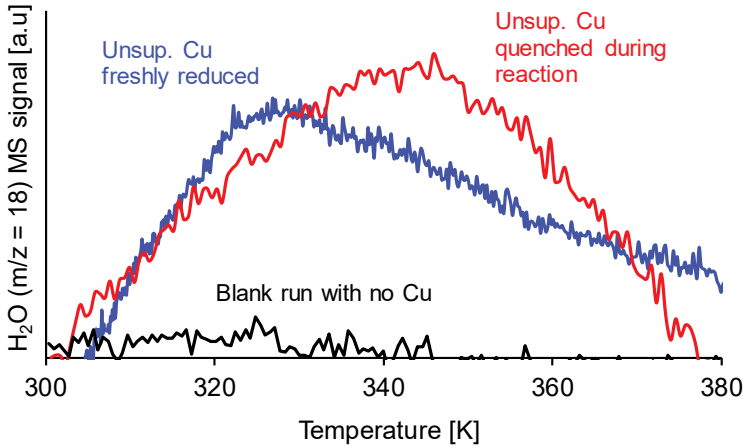

Fig. S13: Water evolution as a function of temperature during TPH (heat ramp is 2 K/min in 60 Nml/min 5% H_2/N_2) for unsupported Cu quenched during reaction (448 K, 50 bar, $CO_2/CO/H_2$ = 3/29/68) [red] and for unsupported Cu directly after pre-reduction [blue]. In both cases the unsupported Cu is obtained from Sigma-Aldrich CuO nanopowder. Also shown is a blank TPH for an empty reactor containing only the quartz wool packing [black].

X-ray photo-electron spectroscopy of Raney Cu and unsupported Cu

Surface area measurement on pre-reduced Raney Cu revealed a total BET surface area of 13.94 m^2/g of which 5.18 m^2/g was assigned to surface Cu. The remaining surface was suggested to be AlO_x as the second most predominant metal component in Raney Cu was Al with 0.81 wt% according to the manufacturer. Ex situ XPS analyses were applied to investigate the surface composition on Raney Cu after drying in a fume hood (predried Raney Cu), dried and reduced Raney Cu (reduced Raney Cu) and calcined but non-reduced unsupported CuO (fresh unsupported CuO) as a reference sample without Al species. Fig. S14 and Fig. S15 show the survey spectra collected for the Raney Cu samples including a small insertion figure with focus on the Cu $2p_{1/2}$ and Cu $2p_{3/2}$ regions. All peaks were accounted for and attributed to mainly Cu and O with minor C and Al concentrations. The detailed analysis of the Cu2p regions revealed that reduction of Raney Cu diminished the shake-up satellites attributed to CuO [1, 2] which verifies the reduction of the copper. In addition, the reduction of Raney Cu could facilitate alumina segregation to the surface due to lower surface energy of alumina compared to Cu [3, 4]. Fig. S16 and Fig. S17 displays the detailed spectra acquired in the characteristic energy regions for Al but these regions contained overlapping Cu peaks making the analysis more complex. Fig. S16 shows that the predried Raney Cu is very similar to CuO indicating that the dried sample is in an oxidized form. Perhaps the binding energy is shifted slightly for predried Raney Cu compared to CuO indicating a mixed $Cu_xAl_yO_z$ oxide phase. Fig. S16 shows that the pre-reduced Raney Cu exhibits a Cu3p peak at approximately 78 eV and an Al2p peak at 75 eV, as also seen in previous studies of Raney Cu [5], and the binding energy of the Al2p peak suggest that Al is in the oxidized form [5–8]. Further evidence for the presence of AlO_x in the surface of Raney Cu and the enhancement of AlO_x upon reduction of Raney Cu was seen by the small but distinct shoulder peak attributed to Al2s around 118 eV in accordance with [5, 8, 9] whereas the main peak corresponded to Cu3s at 122.4 eV [9]. In conclusion, XPS clearly showed presence of both metallic Cu and AlO_x in the surface of reduced Raney Cu.

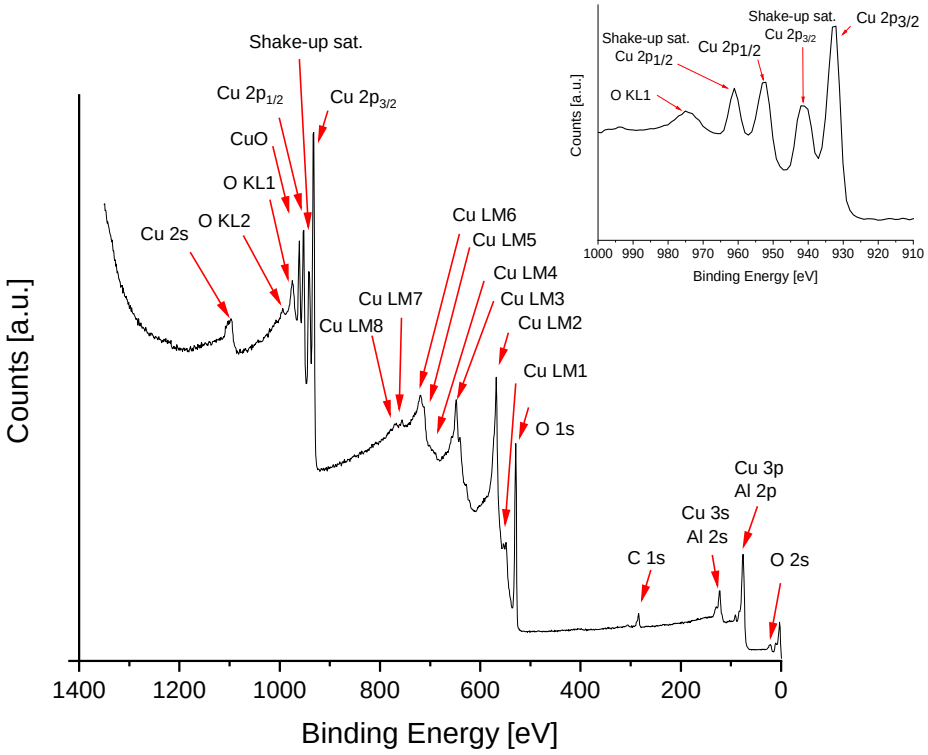

Fig. S14: Ex-situ survey XPS spectrum on predried Raney Cu with small insertion figure in the top right corner for detailed analysis of the Cu2p peak region.

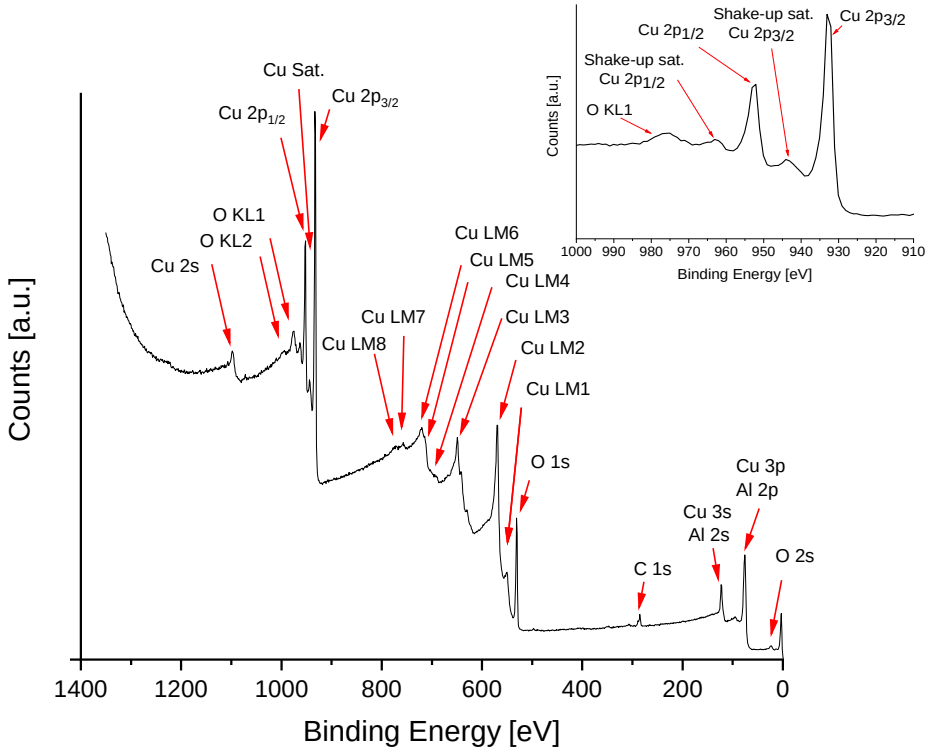

Fig. S15: Ex-situ survey XPS spectrum on reduced Raney Cu with small insertion figure in the top right corner for detailed analysis of the Cu2p peak region.

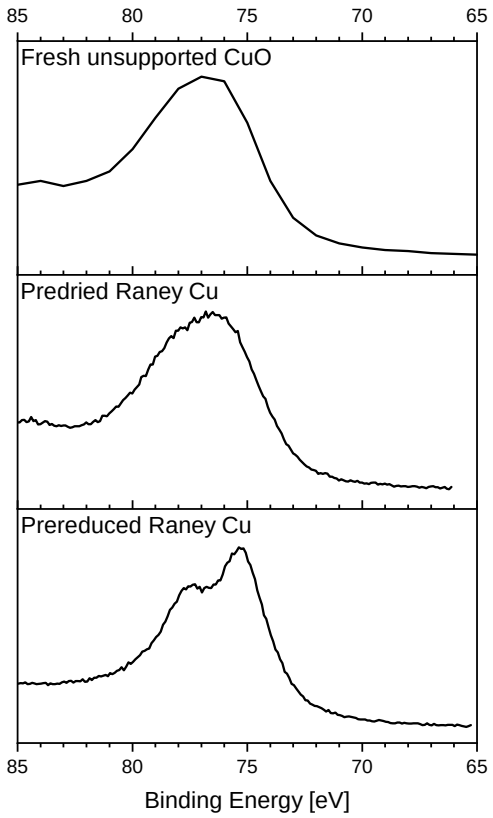

Fig. S16: Ex-situ XPS spectra in the region containing Al2p and Cu3p peaks.

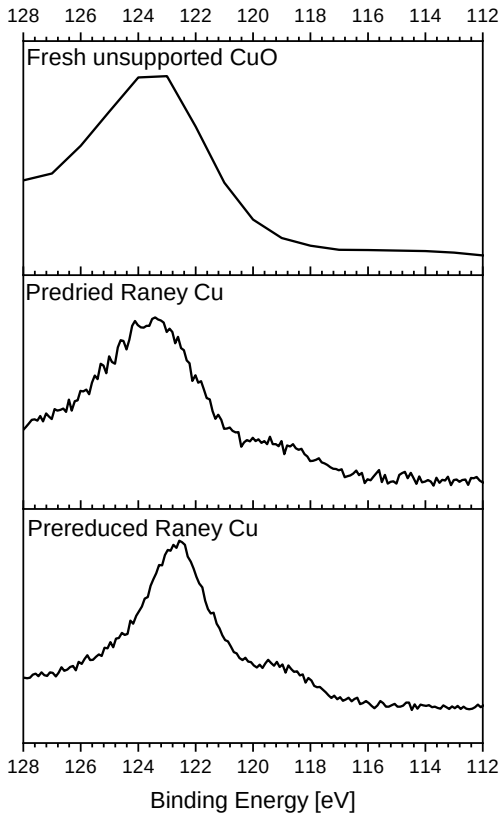

Fig. S17: Ex-situ XPS spectra in the region containing Al2s and Cu3s peaks.

References

[1] M. C. Biesinger, B. P. Payne, A. P. Grosvenor, L. W. M. Lau, A. R. Gerson, and R. St C. Smart. Resolving surface chemical states in XPS analysis of first row transition metals, oxides and hydroxides: Cr, Mn, Fe, Co and Ni. *Applied Surface Science*, 257(7):2717–2730, 2011. doi: 10.1016/j.apsusc.2010.10.051.

[2] A. I. Stadnichenko, A. M. Sorokin, and A. I. Boronin. XPS, UPS, and STM studies of nanostructured CuO films. *Journal of Structural Chemistry*, 49(2):341–347, 2008. doi: 10.1007/s10947-008-0133-1.

[3] L. Vitos, A. V. Ruban, H. L. Skriver, and J. Kollár. The surface energy of metals. *Surface Science*, 411:186–202, 1998. doi: https://doi.org/10.1016/S0039-6028(98)00363-X.

[4] A. Navrotsky, C. Ma, K. Lilova, and N. Birkner. Nanophase transition metal oxides show large thermodynamically driven shifts in oxidation-reduction equilibria. *Science*, 330(6001):199–201, 2010. doi: 10.1126/science.1195875.

[5] J. Laine, G. Ceballos, F. Severino, G. Castro, and C. Rojas. Structure and activity of a Raney copper film catalyst. *Catalysis Letters*, 10(1-2):11–17, 1991. doi: 10.1007/BF00764731.

[6] H. Li, A. Belkind, F. Jansen, and Z. Orban. An in situ XPS study of oxygen plasma cleaning of aluminum surfaces. *Surface and Coatings Technology*, 92(3):171–177, 1997. doi: 10.1016/S0257-8972(97)00079-0.

[7] E. Paparazzo. XPS and Auger Spectroscopy on mixtures of the oxides SiO_2, Al_2O_3, Fe_2O_3, and Cr_2O_3. *Journal of Electron Spectroscopy and Related Phenomena*, 43:97–112, 1987. doi: https://doi.org/10.1016/0368-2048(87)80022-1.

[8] J. A. Rotole and P. M. A. Sherwood. Gamma-Alumina (γ-Al_2O_3) by XPS. *Surface Science Spectra*, 5(1):18–24, 1998. doi: 10.1116/1.1247852.

[9] B. V. Crist. *Handbook of Monochromatic XPS Spectra: The Elements of Native Oxides - Vol 1*. XPS International (XI) LLC, 1999. doi: 10.1109/MEI.2003.1226740.

Appendix D

Supplementary information for *Characterization of oxide-supported Cu by infrared measurements on adsorbed CO* in chapter 6

Authors: Niels D. Nielsen[1], Thomas E. L. Smitshuysen[2], Christian D. Damsgaard[2,3], Anker D. Jensen[1], Jakob M. Christensen[1*]
[1] *Department of Chemical and Biochemical Engineering, Technical University of Denmark, Søltofts Plads Building 229, 2800 Kgs. Lyngby, Denmark*
[2] *Department of Physics, Technical University of Denmark*
Fysikvej, Building 311, 2800 Kgs. Lyngby, Denmark
[3] *National Centre fro Nano Fabrication and Characterization, Technical University of Denmark*
Fysikvej, Building 307, 2800 Kgs. Lyngby, Denmark
[*]**Correspondence to:** jmc@kt.dtu.dk

DOI:
https://doi.org/10.1016/j.susc.2020.121725

Journal specifications:
Surface Science, 2021, Volume 703, 121725

Date Accepted/Published:
27 August 2020 / 4 September 2020

S1 Supplementary Material

In situ XRD analyses of Cu crystallite and verification of activation procedure

Figs. S1 to S7 outline the recorded in situ XRD patterns applied to determine the Cu crystallite size. Inserted annotation are based on the ICSD database with the collection code written in parentheses with Cu (cc 64699), CuO (cc 87123), Cu_2O (cc 197686), SiO_2 (cc 89276) ZnO (cc. 197687), TiO_2-anatase (cc 154604), and Al_2O_3 (cc 85137) collection codes for the ICSD data base. All collection code data are obtained at ambient conditions.

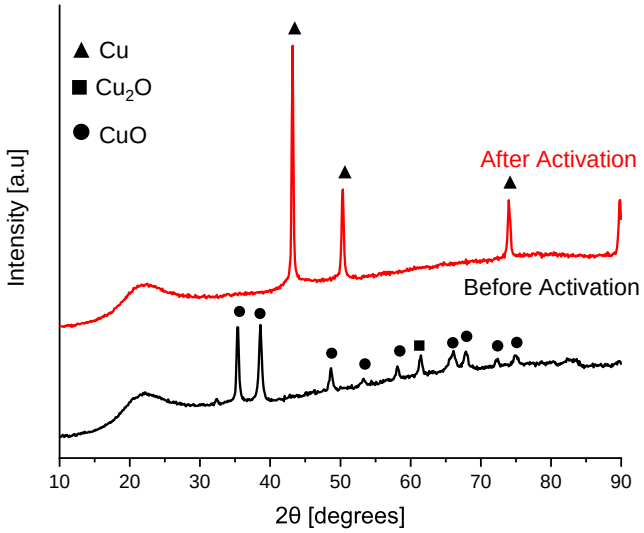

Fig. S1: In situ XRD at 298 K in 5% H_2/N_2 of Cu/SiO_2 before and after activation in 5% H_2/N_2 at 523 K.

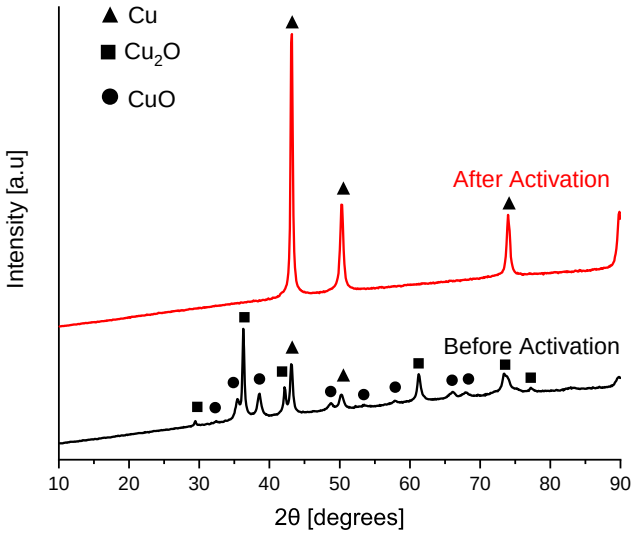

Fig. S2: In situ XRD at 298 K in 5% H_2/N_2 of Raney Cu before and after activation in 5% H_2/N_2 at 523 K.

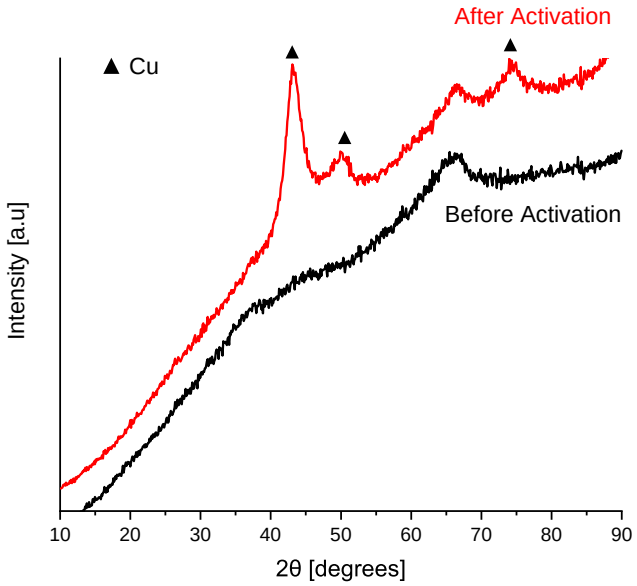

Fig. S3: In situ XRD at 298 K in 100% H_2 of Cu/Al_2O_3 before and after activation in first 5% H_2/N_2 and then 100% H_2 at 523 K.

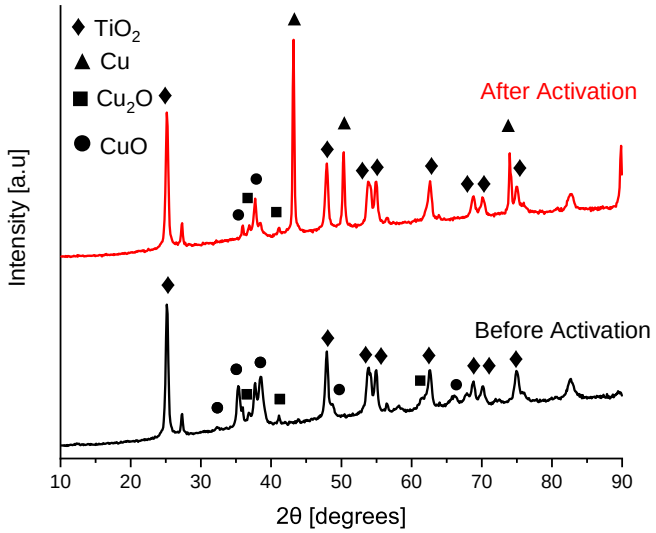

Fig. S4: In situ XRD at 298 K in 5% H_2/N_2 of Cu/TiO_2 before and after activation in 5% H_2/N_2 at 523 K.

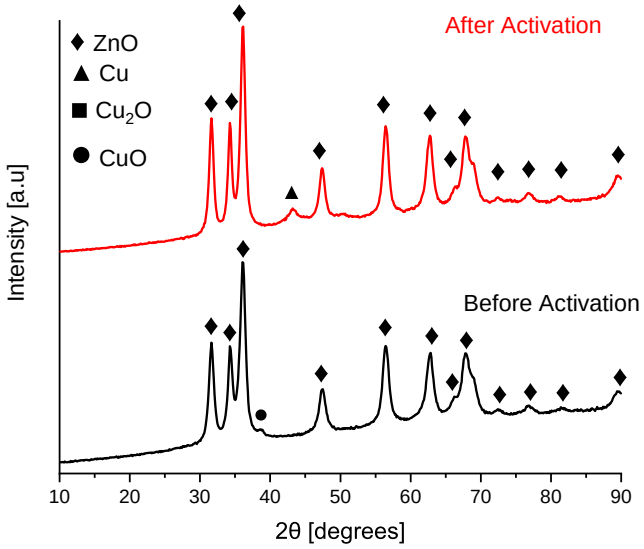

Fig. S5: In situ XRD at 298 K in 5% H_2/N_2 of Cu/ZnO before and after activation in 5% H_2/N_2 at 523 K.

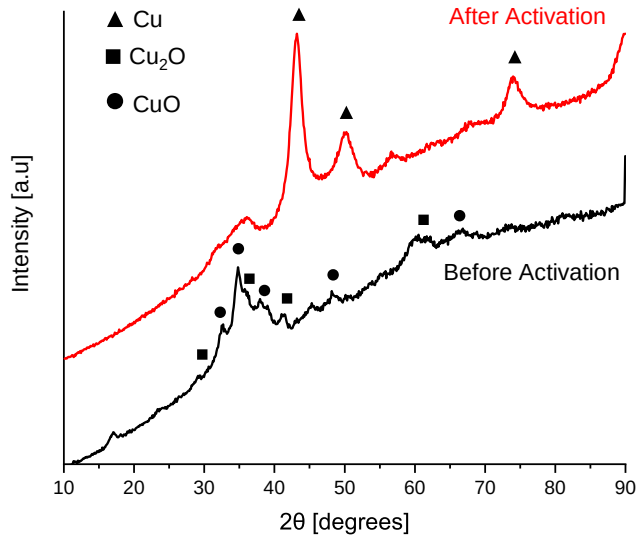

Fig. S6: In situ XRD at 298 K in 5% H_2/N_2 of Cu/ZnO/Al_2O_3 before and after activation in 5% H_2/N_2 at 523 K.

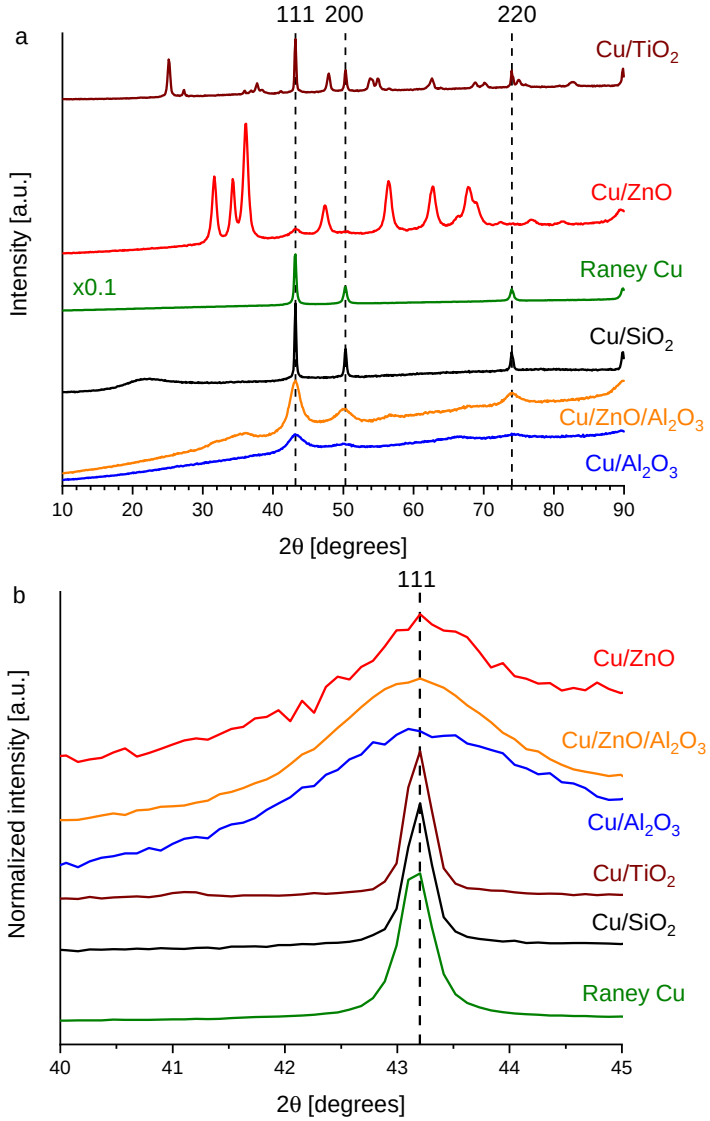

Fig. S7: a) In situ XRD at 298 K in reducing atmosphere of samples after activation with the high intensity of Raney Cu multiplied by 0.1 to fit the common intensity scale. b) Focused view of the 111 diffraction peak with peak heights normalized to facilitate comparison.

Additional tests for identification of IR bands

Fig. S8 shows the spectra in increasing concentrations of CO at 276 K for the Cu/Al_2O_3 sample that has been pre-reduced and then re-oxidized.

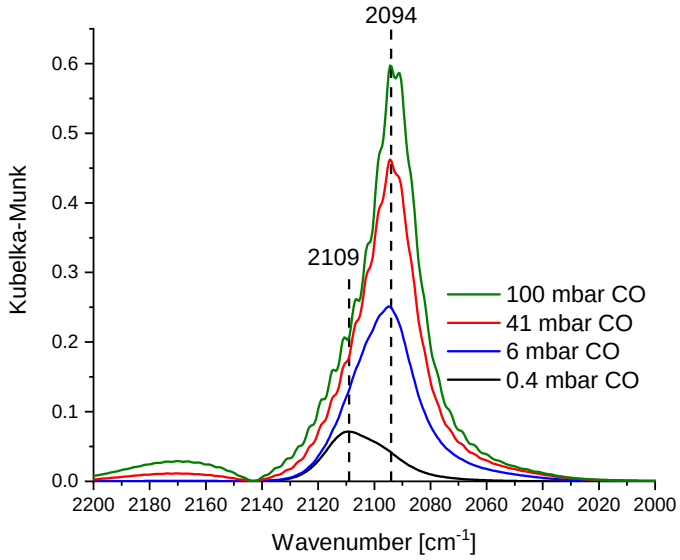

Fig. S8: IR spectra of pre-reduced and then re-oxidized (by 9% CO_2/N_2 at room temperature) Cu/Al_2O_3 in 0.4 mbar to 100 mbar CO and subsequent He flush at constant 276 K.

Fig. S9 shows the spectra during He flush of pre-reduced Cu/SiO_2 after prior exposure to CO. The collective drop in the bands makes it difficult to make clear conclusions about the stability of the different CO adsorption sites represented by the three bands.

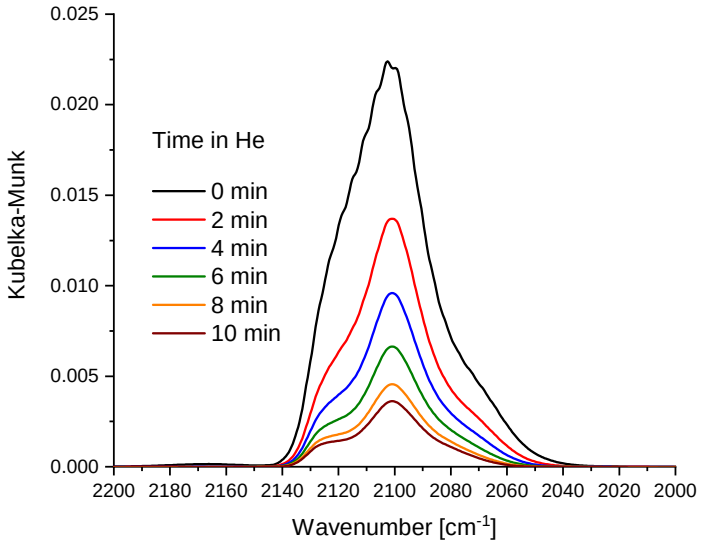

Fig. S9: IR spectra of pre-reduced Cu/SiO_2 during flushing in He at 276 K after prior exposure to 0.4 mbar CO.

Fig. S10 shows IR spectra of $Cu/ZnO/Al_2O_3$ in 0.4 mbar CO at 276 K after various stages of pre-reduction. Initially a single band at 2100 cm^{-1} characteristic of the oxidized sample is present. After treatment in 5% H_2 at 448 K the spectrum characteristic of the reduced phase is established. Further reductive treatment weakens and narrows the bands.

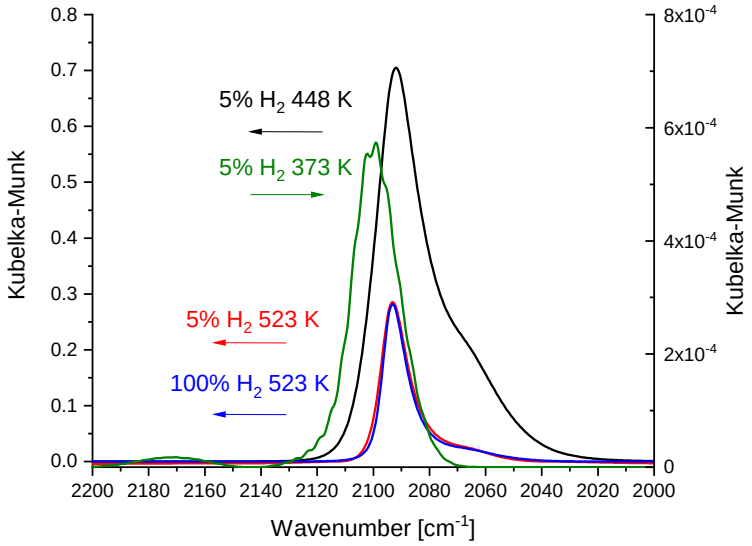

Fig. S10: IR spectra of pre-reduced Cu/SiO_2 during flushing in He at 276 K after prior exposure to 0.4 mbar CO.

Fig. S11 shows IR spectra during He flush of pre-reduced Cu/ZnO (Fig. S11a) and harshly pre-reduced $Cu/ZnO/Al_2O_3$ (Fig. S11b) after prior exposure to CO. The figure illustrates that the 2065-68 cm^{-1} band is eliminated more rapidly upon flushing than the 2093-2094 cm^{-1} band. This is especially evident in Fig. S11b where the low-frequency band is essentially eliminated when the high-frequency band maintains half of the original intensity.

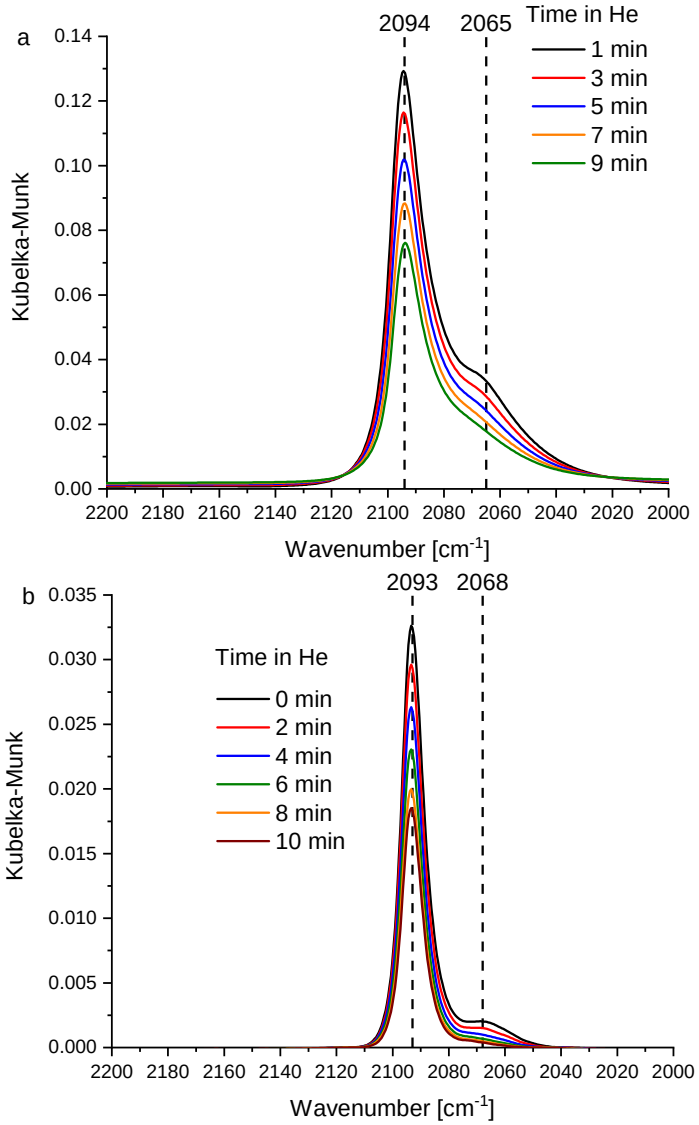

Fig. S11: a) IR spectra of pre-reduced Cu/ZnO as a function of time in He after prior CO adsorption (0.4 mbar) at 276 K. b) IR spectra of harshly pre-reduced (normal reduction and 9.5% CO at 573 K) $Cu/ZnO/Al_2O_3$ as a function of time in He after prior CO adsorption (0.4 mbar) at 276 K.

HCOO and CO co-adsorption experiment with cycles of CO adsorption and TPD for Cu/ZnO

Fig. S12 shows the IR spectrum of Cu/ZnO after exposure to $CO_2/N_2/H_2$ (3/29/68) exposure at 373 K and atmospheric pressure in the absorbance units. The figure shows the C-H features > 2700 cm^{-1} more clearly. The figure also shows the broad absorbance across the IR range indicative of free charge carriers in the ZnO conduction band.

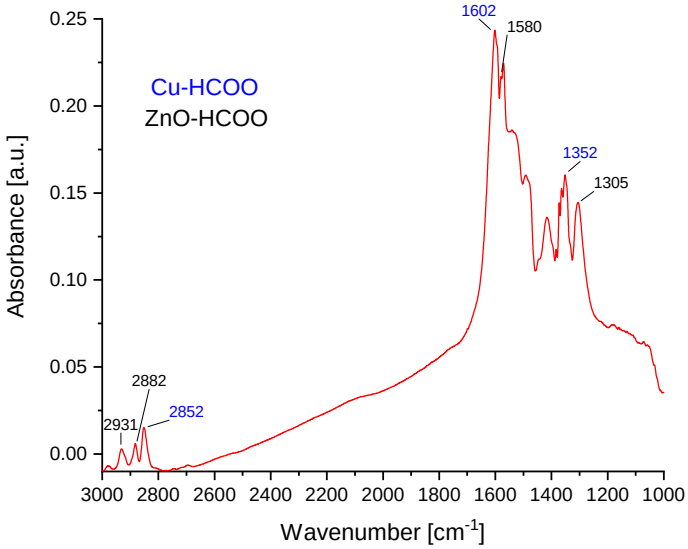

Fig. S12: IR spectrum in absorbance units of Cu/ZnO in He at 276 K HCOO bands after $CO_2/N_2/H_2$ (3/29/68) exposure at 373 K, atmospheric pressure. Cu and ZnO related species are marked in blue and black, respectively.

Figs. S13 and S14 display for Cu/ZnO the decline of the Cu-HCOO bands at 1352 cm^{-1} and 1602 cm^{-1} during the TPD to remove pre-deposited formate synthesized from CO_2/H_2, while the bands related to formate on ZnO (2882 cm^{-1} and 1580 cm^{-1}) remain relatively undisturbed as expected from their higher thermal stability compared to Cu-HCOO. Fig. S15 shows an overview of the TPD cycles including gas signals measured by a mass spectrometer (MS) for Cu/ZnO. Fig. S16 shows the same overview for Cu/SiO_2. Figs. S15 and S16 show that CO_2 desorbs during each TPD cycle indicating further decomposition of Cu-HCOO.

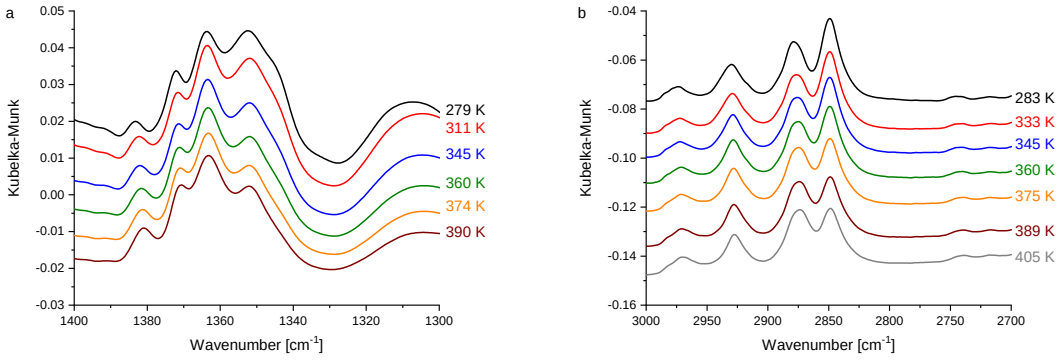

Fig. S13: Selected IR spectra of undiluted and pre-reduced Cu/ZnO during TPD to a) 393 K and b) 413 K in 45 Nml/min He with both 10 K/min to 323 K and then 2 K/min to a) 393 K and b) 413 K. Note primarily the decline in the Cu-HCOO feature around 1350 cm^{-1}. Spectra are linear offset for clarity.

Fig. S13: Selected IR spectra of undiluted and pre-reduced Cu/ZnO during TPD to a) 393 K and b)

413 K in 45 Nml/min He with both 10 K/min to 323 K and then 2 K/min to a) 393 K and b) 413 K. Note primarily the decline in the Cu-HCOO feature around 1350 cm^{-1}. Spectra are linear offset for clarity.

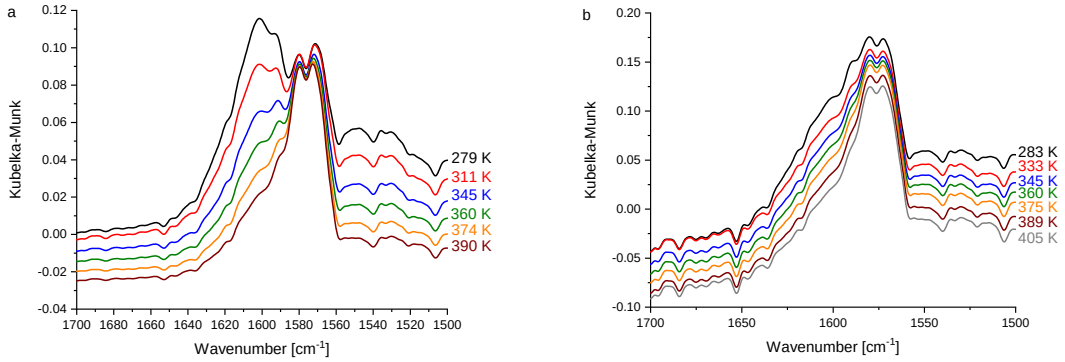

Fig. S14: Selected IR spectra of undiluted and pre-reduced Cu/ZnO during TPD to a) 393 K and b) 413 K in 45 Nml/min He with both 10 K/min to 323 K and then 2 K/min to a) 393 K and b) 413 K. Note primarily the decline in the Cu-HCOO feature around 1620 cm^{-1}. Spectra are linear offset for clarity.

Fig. S14: Selected IR spectra of undiluted and pre-reduced Cu/ZnO during TPD to a) 393 K and b) 413 K in 45 Nml/min He with both 10 K/min to 323 K and then 2 K/min to a) 393 K and b) 413 K. Note primarily the decline in the Cu-HCOO feature around 1620 cm^{-1}. Spectra are linear offset for clarity.

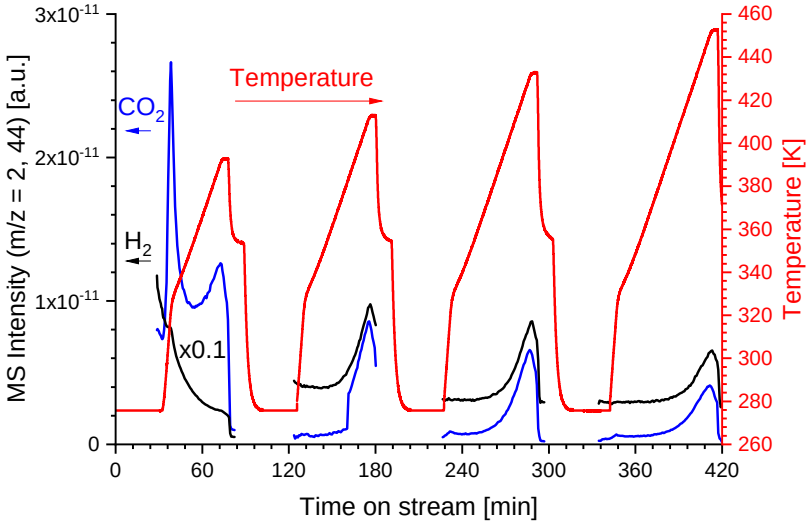

Fig. S15: Overview of temperature and MS intensities of CO_2 and H_2 during the TPD sequences to remove formate from Cu/ZnO with pre-adsorbed HCOO from exposure to $CO_2/N_2/H_2$ = 3/29/68, 373 K, 1 atm. In each period at 276 K a background spectrum is measured in He and then 0.4 mbar CO is adsorbed while sample spectra are recorded. Note the coincident desorption of H_2 and CO_2 related to Cu-HCOO desorption near the final TPD temperature of each sequence. The H_2 profile during the 393 K TPD is downscaled by a factor of 10 to fit the "MS Intensity" scale.

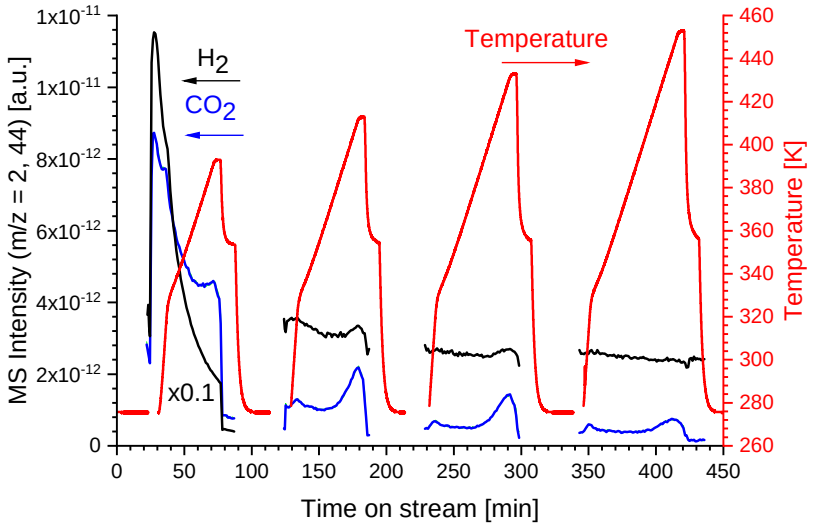

Fig. S16: Overview of temperature and MS intensities of CO_2 and H_2 during the TPD sequences to remove formate from Cu/SiO_2 with pre-adsorbed HCOO from exposure to $CO_2/N_2/H_2$ = 3/29/68, 373 K, 1 atm. In each period at 276 K a background spectrum is measured in He and then 0.4 mbar CO is adsorbed while sample spectra are recorded. Note the coincident desorption of H_2 and CO_2 related to Cu-HCOO desorption near the final TPD temperature of each sequence. The H_2 profile during the 393 K TPD is downscaled by a factor of 10 to fit the "MS Intensity" scale.

Further results from the formate decoration experiments

Fig. S17 shows the CO spectrum recorded on maximally covered Cu/ZnO directly after HCOO decoration with a distinct band at 2127 cm^{-1} and a broader feature centered around 2098 cm^{-1}. This spectrum corresponds to the "Post CO_2/H_2" spectrum in Fig. 11a in the main text.

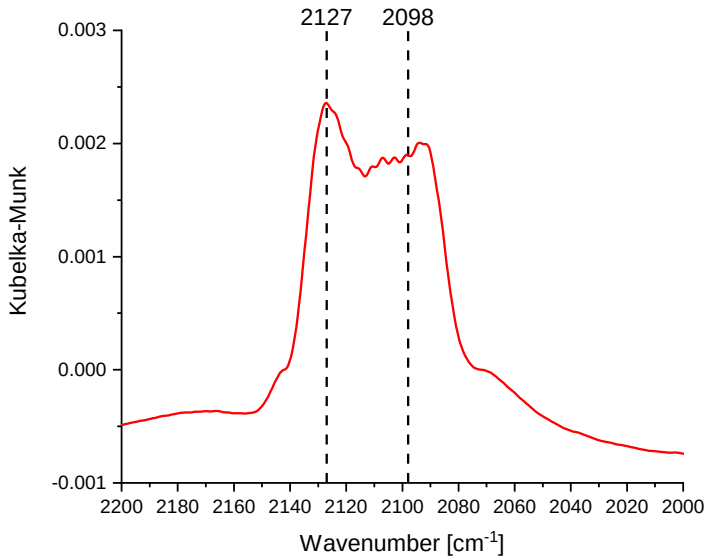

Fig. S17: IR spectra of pre-reduced and maximum HCOO decorated Cu/ZnO in 0.4 mbar CO at 276 K before TPDs.

Fig. S18 shows the IR spectra during CO dosage on the partly formate covered Cu/SiO_2 sample after TPD to 393 K. Fig. 11b in the main text shows that substantial formate still remains on the surface in this situation (i.e. the CO band intensity is not fully restored). If van der Waal interactions between CO and HCOO (i.e. CO$\cdots$H-COO complexes) are important then modifications should be visible seen in the formate regions (around $\nu_{OCO,sym} = 1350$ cm^{-1}, $\nu_{OCO,asym} = 1600$ cm^{-1} and $\nu_{C\text{-}H} = 2700$-3000 cm^{-1}) of the spectrum. However, Fig. S18 shows that for Cu/SiO_2 the CO band is the only observed band on an essentially featureless baseline. This indicates that the formate is not strongly perturbed and thus that such complexes between CO and HCOO are not the reason for the perturbation in the C-O frequency of adsorbed CO.
Fig. S19a shows the wider IR spectra for the CO adsorptions on partly HCOO decorated Cu/SiO_2. This is an extended version of Fig. 11b in the main text. It is evident that very little is seen in the spectral ranges associated with formate. Figs. S19b and S19c show detailed view of the formate ranges for the spectra recorded in CO after the TPD sequences. Figs. S19b and S19c show that there are no major frequency changes in the formate range even though the C-O frequency in chemisorbed CO is changed significantly with increasing TPD temperature (i.e. decreasing Cu-HCOO coverage). This invariance in the formate regions suggests that formation of CO$\cdots$ H-COO complexes is not the reason for the changing C-O frequency in the co-adsorbed CO.
Fig. S20a shows the entire IR spectrum during CO adsorption on the partially formate covered Cu/ZnO sample after TPD to increasing temperatures. The figure thus illustrates the wider spectrum for the data in Fig. 11a in the main text. The baseline contains small ripples in the formate regions. Figs. S20b and S20c show closer views of these ripples in the formate regions. These figures illustrate that there are no major frequency changes in these ripples in the baseline even though the C-O frequency in chemisorbed CO is changed significantly with increasing TPD temperature (i.e. decreasing Cu-HCOO coverage). This again suggests that formation of CO$\cdots$ H-COO complexes is not the reason for the changing C-O frequency in the co-adsorbed CO.

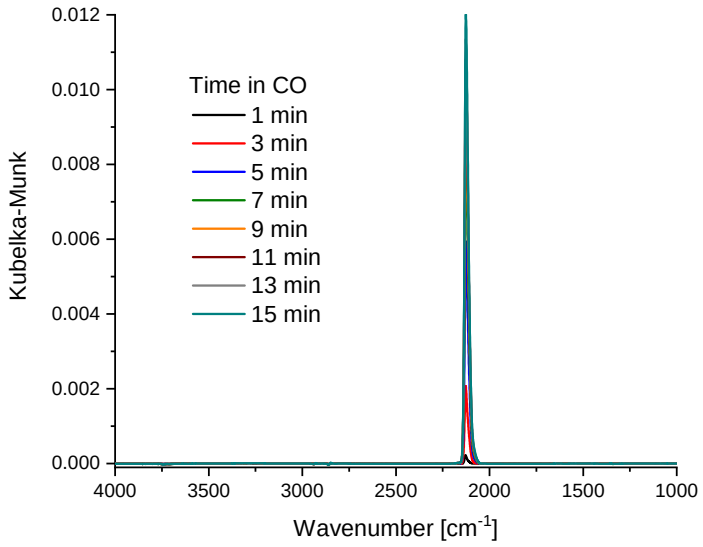

Fig. S18: IR spectra of pre-reduced and partly HCOO decorated Cu/SiO_2 after TPD to 393 K in 0.4 mbar CO at 276 K.

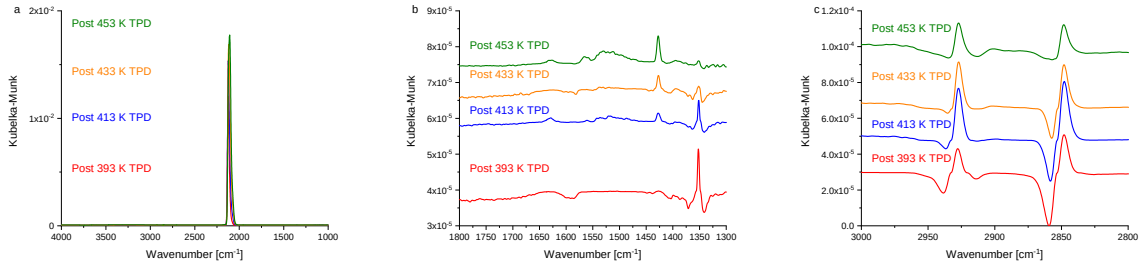

Fig. S19: IR spectra of pre-reduced and partially covered Cu/SiO_2 in 0.4 mbar CO at 276 K after TPDs to specific temperatures (393 K to 453 K) shown in a) full frequency range, b) low frequency range, and c) high frequency range. Spectra are offset for clarity.

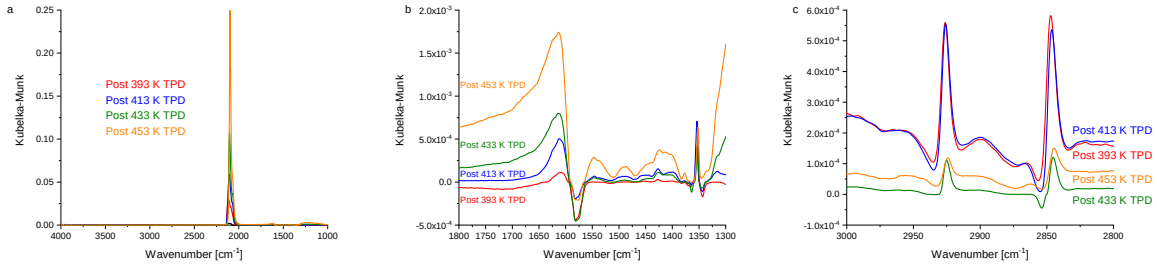

Fig. S20: IR spectra of pre-reduced and partially covered Cu/SiO_2 in 0.4 mbar CO at 276 K after TPDs to specific temperatures (393 K to 453 K) shown in a) full frequency range, b) low frequency range, and c) high frequency range. Spectra are offset for clarity.

Evaluation of a connection between particle/crystallite size and C-O frequency

Fig. S21 shows the Cu crystallite size and the Cu particle diameter determined from the Cu surface area as functions of the C-O frequency for the band assigned as the primary contribution from CO on the metallic surface for each sample. The results in Fig. S21 clearly shows that there is no correlation between either of the size estimates and the C-O frequency. This is in good agreement with the fact that the samples are generally expected to be in the size range without any effect of particle size.

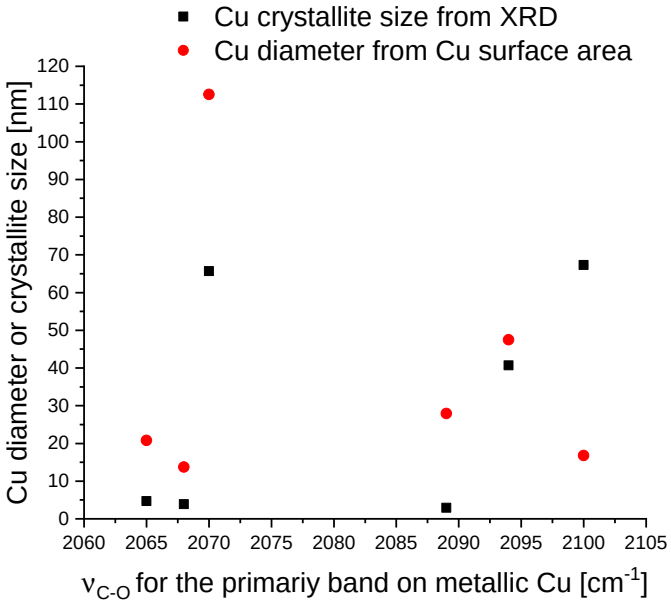

Fig. S21: Comparison between Cu diameter and crystallite size with the metallic C-O stretch across the investigated samples.

Appendix E

Supplementary information for *Support-dependent electron transfer to Cu explains the support effect for catalytic methanol synthesis over Cu* in chapter 7

Authors: Niels D. Nielsen[1], Anker D. Jensen[1], Jakob M. Christensen[1]

[1] *Department of Chemical and Biochemical Engineering, Technical University of Denmark, Søltofts Plads Building 229, 2800 Kgs. Lyngby, Denmark*

*__Correspondence to:__ jmc@kt.dtu.dk

Status:
In preparation

E1 Extended Data

Methods

Flow specifications

Flows are reported according to the normal conditions marked with "N" referring to 273.15 K and 1 atmosphere of pressure. Measurements involving methanol synthesis from syngas is performed in a previously described setup [1], which is modified for the DRIFTS dosage experiments by inserting a membrane port between the carbonyl trap and the gas entrance to the DRIFTS cell.

Synthesis of catalysts

Raney Cu was purchased from Strem Chemicals (Chemical Analysis from producer: 98.9 wt% Cu, 0.81 wt% Al, 0.1 wt% Fe, 0.05 wt% Ni) and received as an aqueous slurry, which was pre-dried in a fume-hood at ambient conditions before use. Unsupported Cu for spectroscopy studies was obtained from pure CuO (nanopowder < 50 nm, Sigma Aldrich), which was loaded without pre-treatments. Supported Cu catalysts (Cu/SiO_2, Cu/ZnO and $Cu/ZnO/Al_2O_3$) were synthesized from Cu(II) nitrate hemi(pentahydrate) (98.6%, Alfa Aesar) using co-precipitation ($Cu/ZnO/Al_2O_3$ with 56 wt% Cu, Cu/ZnO with 10 wt% Cu). Cu/SiO_2 was synthesized by incipient wetness impregnation of an aqueous nitrate ($Cu(NO_3)_2{\cdot}3H_2O \geq 99\%$ from Sigma Aldrich) solution onto pre-dried and crushed (150-300 µm) SiO_2 (SS61138, 250 m^2/g, from Saint Gobain) followed by drying overnight at 313 K. All dried precursors for supported Cu catalysts were calcined in 1 NL/min air flow with a heating ramp of 2 K/min to 573 K, which was maintained for 3 hours. Experiments on the bare SiO_2 were conducted on the crushed and sieve fractionated (150-300 µm) SiO_2 sample. Before any use Raney Cu, SiO_2, Cu/SiO_2 and ZnO-based samples were pre-reduced in a 60 Nml/min flow of 5% H_2/N_2 with a heating ramp of 1 K/min to 448 K and kept constant until water generation had terminated before heating further (1 K/min) to 523 K with again hold until no more MS detectable water. For unsupported Cu the pre-reduction terminated after the 2 h hold at 448 K, as this was found to be sufficient for complete CuO reduction.

Surface area measurement

The Cu surface area of pre-reduced catalysts were performed by applying the N_2O-Reactive Frontal Chromatography (RFC) method [2] conducted at 333 K using a 1% N_2O/He flow of 19 Nml/min. Determinations of the Cu surface areas were based on the N_2O uptake, a Cu:O stoichiometry [3] of 2:1 and an average Cu surface atom density of $1.47{\cdot}10^{19}$ atoms/(m^2 Cu) [4]. The N_2O-RFC experiments were performed in a Quantachrome IQ_2 setup with an attached Hiden Analytical QGA mass spectrometer.

Catalytic activity measurements

The high pressure activity tests were conducted in a flow reactor setup described in detail elsewhere [1]. The reactors were glass lined U-tubes (1/4" o.d., 4 mm i.d. from SGE Analytical Science). Effluent gas was analyzed by a Hiden HPR-20 EGA mass spectrometer and a Thermo Fisher Trace 1300 GC. After pre-reduction the reactor was pressurized in He to 50 bar at 448 K for unsupported Cu and 498 K for Raney Cu before switching to the reaction mixture ($CO_2/N_2/H_2 = 3/29/68$) with a total flow of 270-282 Nml/min. Unsupported Cu was in the pressurized feed gas heated with 1 K/min to 498 K. Gas chromatography was applied to quantify the produced methanol yielding maximum 0.07 mole% methanol in the effluent gas stream corresponding to 4.35% approach to equilibrium based on equilibrium calculations (T = 498 K, P = 50 bar, $CO_2/N_2/H_2 = 3/29/68$) using data from [5] with the assumption of ideality of the gas.

Quantification of formate coverage on Cu/SiO_2 at industrial reaction conditions

The coverage of formate on the Cu surface of Raney Cu, Cu/ZnO and Cu/SiO_2 under representative industrial methanol synthesis conditions was determined in the high pressure flow reactor (see section 2.3) using the method described in detail elsewhere [6]. After pre-reduction and pressurization in He the Cu/SiO_2 catalyst was exposed to reaction conditions (T = 523 K, $CO_2/CO/H_2$ = 3/29/68, P = 50 bar) using a syngas flow of 93-105 Nml/min, and the approach to steady state was followed using mass spectrometry (MS). Poor methanol activity over Cu/SiO_2 restricted the flow to around 100 Nml/min to improve the quantitative analyses of the methanol effluent. Pre-reduced Raney Cu and Cu/ZnO were pressurized in He before exposed to reaction conditions (T = 523 K, $CO_2/CO/H_2$ = 3/29/68, P = 50 bar) using a syngas flow of 280-282 Nml/min. In these experiments the maximal methanol effluent concentration was 0.22 mole% corresponding to 0.96% approach to equilibrium based on equilibrium calculations (523 K, 50 bar, $CO_2/CO/H_2$ = 3/29/68) using data from [5] with the assumption of ideality of the gas. Once steady state was reached the reaction was rapidly quenched (described in detail elsewhere [6]) by submerging the U-tube reactor in liquid N_2 or ice water, and the formate coverage was determined from integration of the CO_2 MS signal in a subsequent TPD in He. The CO_2 MS signal was calibrated beforehand from a certified 500 ppm CO_2 in He gas bottle from Air Liquide Denmark.

DRIFTS experiments

Infrared measurements were performed in a domed reactor cell and Praying Mantis DRIFTS unit from Harrick Scientific Products installed in a Nicolet iS50 FTIR spectrometer equipped with a liquid N_2 cooled MCT detector. Details of the setup is shown elsewhere [1]. Reported spectra constituted an average of 76 scans with a resolution of 4 cm^{-1}. Undiluted catalysts were used. Prior to adsorption experiments, the catalysts were activated according to the H_2 pre-reduction procedure outlined in section 2.1 and then thoroughly purged in He at 523 K.

Pre-reduced catalysts were flushed and cooled in He from 523 K (448 K for unsupported Cu) to 313 K, where a background spectrum in 310 Nml/min He was recorded. Acquisition of absorbance spectra started at 313 K, where 1 µl HCOOH ($\geq$ 98% Sigma Aldrich) was injected with a syringe into the 310 Nml/min He stream through a sealed polymer membrane on the gas line immediately before the DRIFTS cell. Continuous He flush was performed until the gas phase HCOOH signal (m/z = 46) measured by the mass spectrometer was undetectable. The HCOOH covered surface was heated by 2 K/min in 50 Nml/min H_2 (TPH) to 673 K with continuous recording of absorbance spectra based on the background spectrum recorded at 313 K before HCOOH dosage.

Silica was treated using the normal pre-reduction (see section 2.1) before being exposed to a methanol-water mixture inside the DRIFTS cell. After pre-reduction a background spectrum in He was measured at 523 K after thorough flushing at this temperature. Using the same syringe injection method as for the formic acid dosage, 1 µl of methanol-water (50/50 wt%) mixture was injected into the 310 Nml/min He stream at 523 K and ambient pressure. In this way silica was exposed to CH_3OH and H_2O at 523 K, while spectra were continuously collected during dosage and subsequent cooling in 310 Nml/min He to 313 K concurrent with gas analysis of the effluent stream using a MS. The methanol-water exposed Cu/SiO_2 surface was subsequently heated (TPD) in 45 Nml/min He with 2 K/min from 313 K to 673 K.

Reduced Raney Cu was flushed with He at 523 K before cooling to 448 K, where 1 µl methanol was injected into the 310 Nml/min He stream. Continuous He flow during subsequent cooling was applied before raising the temperature (TPH) by 2 K/min in 50 Nml/min H_2.

Cu/SiO_2 was pre-reduced (see section 2.1) and flushed with He at 523 K, where a background spectrum was recorded in He before pressurizing in He to 10 bar at constant temperature. He was replaced by $CO_2/CO/H_2$ (3/29/68) for 1 hour at 523 K before rapid cooling in the syngas mixture to room temperature. After pressure release and thorough He purge at room temperature, a TPD in 45 Nml/min He with 2 K/min as heating ramp was performed with continuous measurements of absorbance spectra based on the background spectrum recorded at 523 K before syngas exposure. Both supports (SiO_2, ZnO) and supported catalysts (Cu/SiO_2, Cu/ZnO, $Cu/ZnO/Al_2O_3$) were subjected to repeated cycles

consisting of heating by 1 K/min in diluted or undiluted H_2 to a final temperature before He flushing for 15 min at the final temperature and then cooling to room temperature in He, where a spectrum was recorded. This cycle was then repeated with medium and harsh reductive treatments. The samples were subjected to mild (60 Nml/min of 5% H_2 at 448 K for 1.5-4 h), medium (60 Nml/min of 5% H_2 at 523 K for 0.75-2.5 h) and harsh (50 Nml/min of 100% H_2 at 523 K for 1-3.5 h) reductions prior to spectrum acquisition. The spectrum recorded after mild reduction for each sample was used as the background for the spectra acquired after medium and harsh reductions.
Raney Cu, Cu/ZnO and Cu/ZnO/Al_2O_3 was heated in 60 Nml/min of 5% H_2 by 1 K/min to 448 K with constant temperature for 3 h before further heating to 523 K and constant temperature for 2 h. Next, the gas switched to 100% H_2 for 1.5-2 h at 523 K before 15 min He flush at 523 K and cooling. Finally, a TPD in 45 Nml/min He from room temperature to 673 K with 2 K/min as heating ramp was performed. The equivalent blank experiment involved heating in 100% H_2 to 523 K and 0.5 h hold before 15 min He flush, cooling and then 2 K/min TPD in 45 Nml/min He.

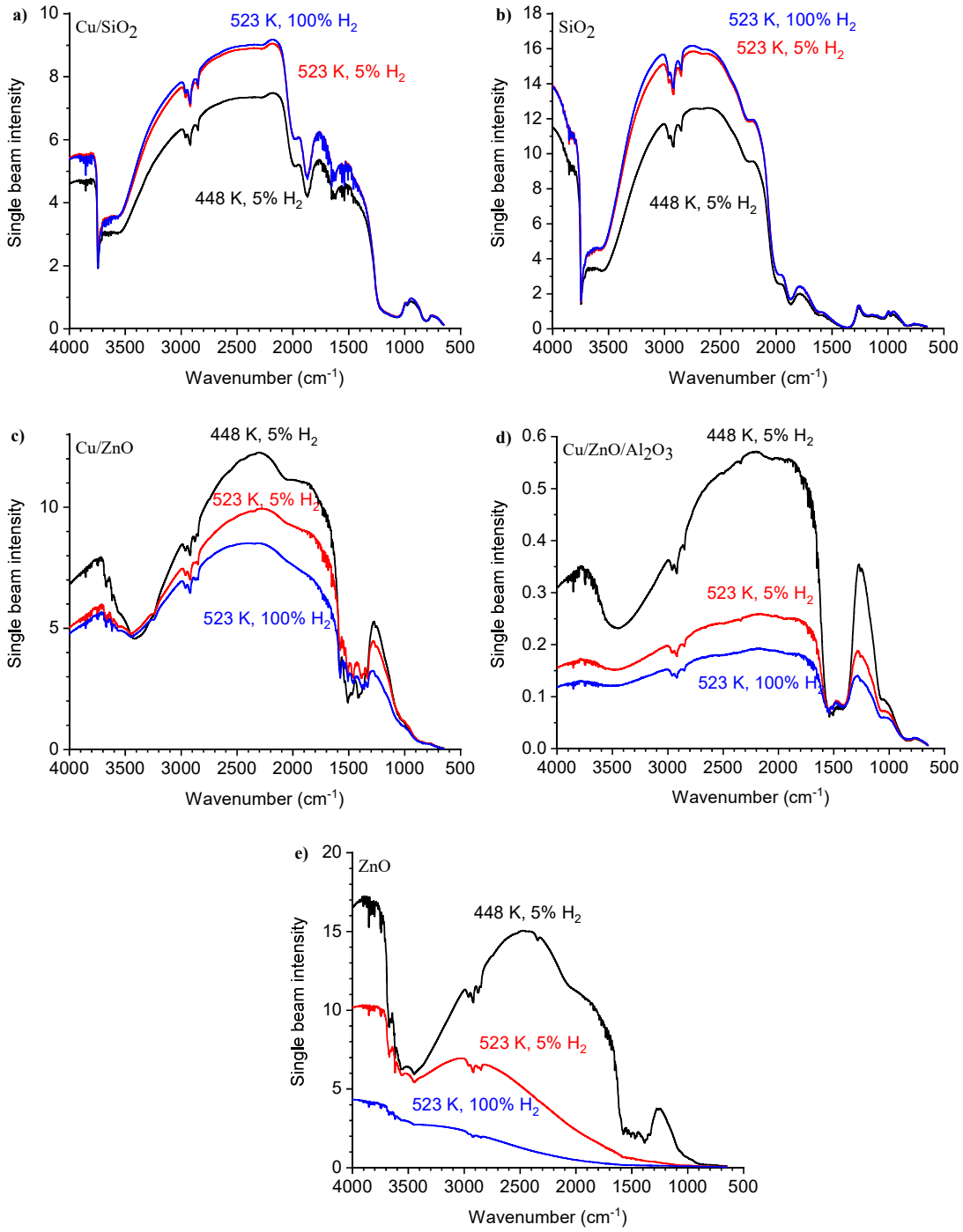

Extended Data Fig. 1| Raw single beam spectra collected in He at 313 K after H_2 treatment. The spectra are collected after mild (448 K in 5% H_2), intermediate (523 K in 5% H_2) and harsh (523 K in 100% H_2) reductions for **a** Cu/SiO_2, **b** SiO_2, **c** Cu/ZnO, **d** $Cu/ZnO/Al_2O_3$ and **e** ZnO.

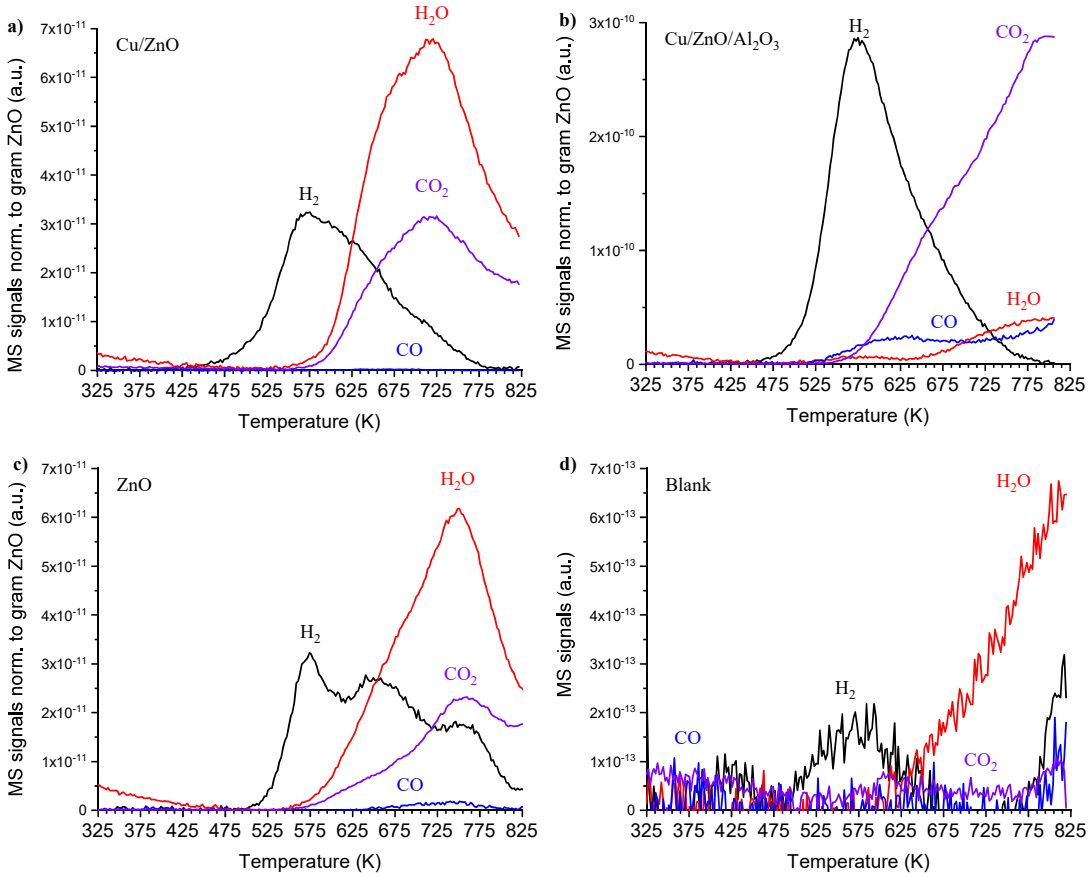

Extended Data Fig. 2| Evolution of gaseous species in temperature programmed desorption after H_2 pre-adsorption. MS signals for gaseous species desorbed during TPD with **a** Cu/ZnO, **b** Cu/ZnO/Al_2O_3, **c** ZnO and **d** a blank cell in 45 Nml/min He with 2 K/min as heating ramp. MS signals for the ZnO-based samples in **a** to **c** are normalized to the ZnO content (gram) for comparison. The blank experiment is not normalized. The results illustrate that the hydrogen desorption < 625 K occurs alone and is attributable to hydrogen desorbing from the ZnO structure. Above 625 K a multitude of gaseous species are evolved and any H_2 evolved at these temperatures is most likely the result of decomposing $H_xC_yO_z$ species on the ZnO surface.

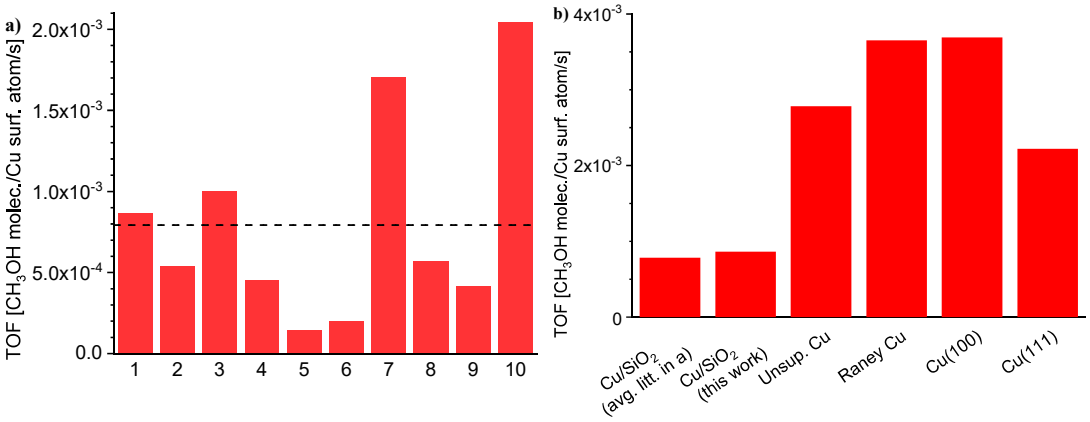

c

Entry no.	**T [K]**	**p_{H_2} [bar]**	**TOF reported [s^{-1}]**	**TOF extrapolated [s^{-1}]**	**Reference**
1	498	34	$8.61 \cdot 10^{-4}$	$8.61 \cdot 10^{-4}$	This work
2	533.15	24	$1.50 \cdot 10^{-3}$	$5.36 \cdot 10^{-4}$	Van den Berg et al. [7]
3	533.15	24	$2.80 \cdot 10^{-3}$	$1.00 \cdot 10^{-3}$	Van den Berg et al. [8]
4	523.15	8	$2.89 \cdot 10^{-4}$	$4.50 \cdot 10^{-4}$	Burch et al. [9]
5	533.15	6	$1.00 \cdot 10^{-4}$	$1.43 \cdot 10^{-4}$	Karelovic et al. [10]
6	500	4.48	$2.80 \cdot 10^{-5}$	$1.95 \cdot 10^{-4}$	Clarke et al. [11]
7	523	29.4	$4.00 \cdot 10^{-3}$	$1.70 \cdot 10^{-3}$	Robbins et al. [12]
8	523	37.5	$1.71 \cdot 10^{-3}$	$5.70 \cdot 10^{-4}$	Saito et al. [13]
9	523	37.5	$1.24 \cdot 10^{-3}$	$4.16 \cdot 10^{-4}$	Fujitani et al. [14]
10	413.15	4.5	$3.70 \cdot 10^{-6}$	$2.04 \cdot 10^{-3}$	Yang et al. [15]

d

Catalyst	**T [K]**	**p_{H_2} [bar]**	**E_{act} reported [kJ/mol]**	**TOF reported [s^{-1}]**	**TOF extrapolated [s^{-1}]**	**Reference**
Cu/SiO_2	498	34			$7.84 \cdot 10^{-4}$	Average of entries 2-10 in **c**
Cu/SiO_2	498	34		$8.61 \cdot 10^{-4}$	$8.61 \cdot 10^{-4}$	This work
Unsup. Cu	498	34		$2.78 \cdot 10^{-3}$	$2.78 \cdot 10^{-3}$	Nielsen et al. [6]
Raney Cu	498	34	55.3	$3.65 \cdot 10^{-3}$	$3.65 \cdot 10^{-3}$	Nielsen et al. [6]
Cu(100)	523	13.5	76.7	$3.55 \cdot 10^{-3}$	$3.69 \cdot 10^{-3}$	Nakamura et al. [16]
Cu(111)	523	13.5	73.6	$2.06 \cdot 10^{-3}$	$2.22 \cdot 10^{-3}$	Nakamura et al. [16]

Extended Data Fig. 3| Comparison of Cu/SiO_2 to the intrinsic properties of Cu. a The TOF for methanol synthesis by CO_2 hydrogenation with Cu/SiO_2 samples from this work and the literature corresponding to the entries in **c**. Here the present Cu/SiO_2 sample is investigated in CO_2 hydrogenation ($CO_2/N_2/H_2$ = 3/29/68, T = 498 K, P = 50 bar) and the literature values are extrapolated to the same conditions using a linear dependency on the hydrogen pressure as commonly [17] employed and an activation energy of 86.5 kJ/mole based on the average value from Karelovic et al. [10]. The dashed line is the average of all 10 reported TOFs (see details in **c**). **b** Comparison of the TOF for Cu/SiO_2 (both this work and the literature average) to unsupported Cu, Raney Cu and Cu single crystal surfaces measured or extrapolated to the same conditions (see details in **d**). The results verify that SiO_2 exerts a significant detrimental support effect corresponding to a factor of 3-4 on the TOF-value compared to Cu intrinsically.

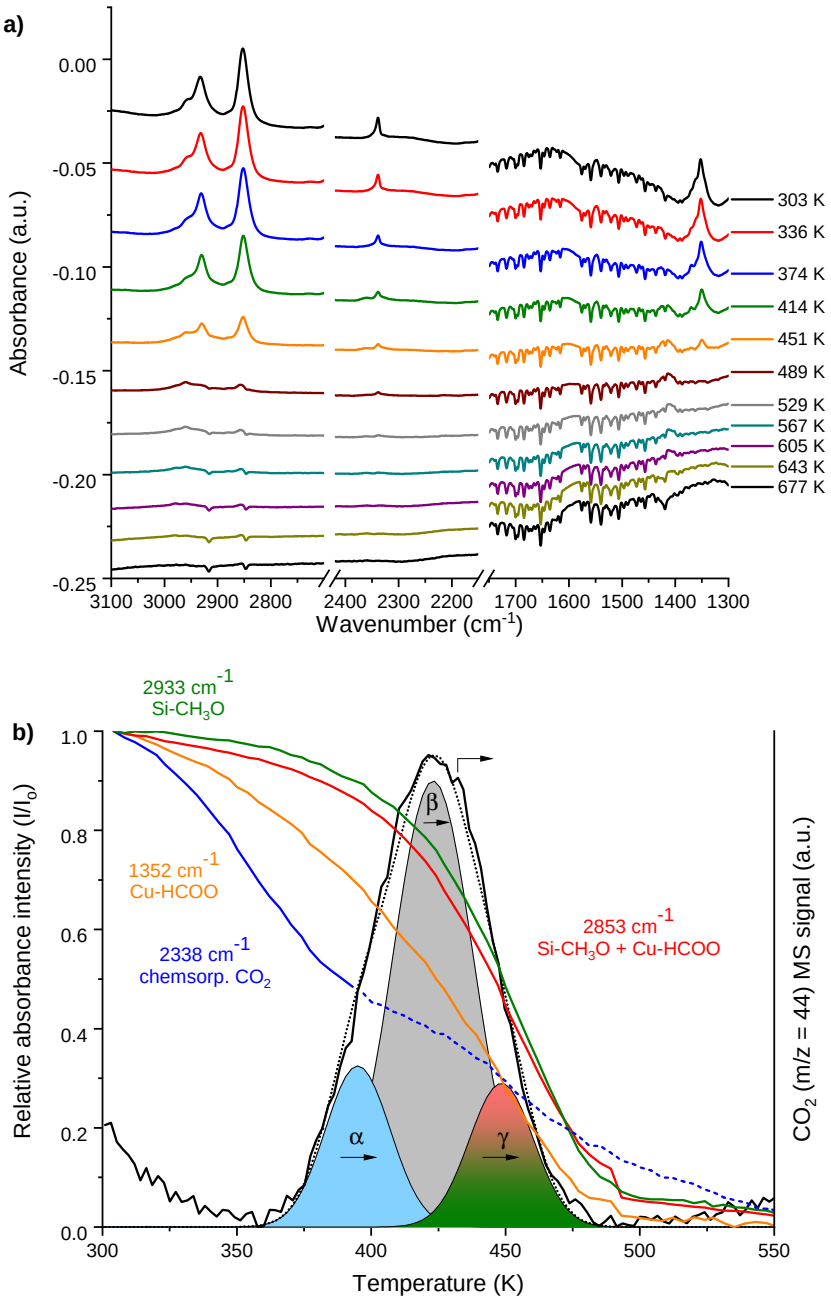
a)
Absorbance (a.u.)
0.00
-0.05
-0.10
-0.15
-0.20
-0.25
3100 3000 2900 2800
2400 2300 2200
1700 1600 1500 1400 1300
Wavenumber (cm-1)
303 K
336 K
374 K
414 K
451 K
489 K
529 K
567 K
605 K
643 K
677 K
b)
2933 cm-1
Si-CH3O
1352 cm-1
Cu-HCOO
2338 cm-1
chemsorp. CO2
2853 cm-1
Si-CH3O + Cu-HCOO
α
β
γ
Relative absorbance intensity (I/I0)
CO2 (m/z = 44) MS signal (a.u.)
1.0
0.8
0.6
0.4
0.2
0.0
300
350
400
450
500
550
Temperature (K)

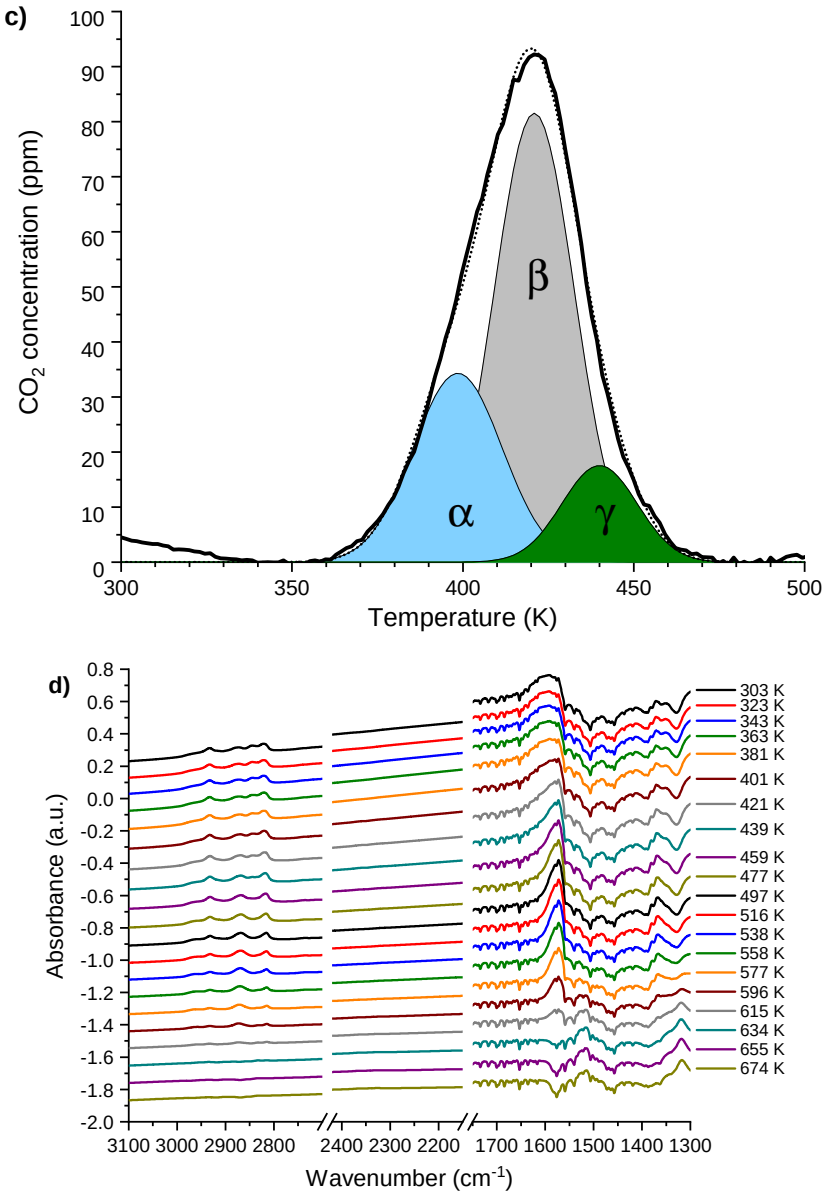
c)
CO2 concentration (ppm)
Temperature (K)
α
β
γ
d)
Absorbance (a.u.)
Wavenumber (cm-1)
303 K
323 K
343 K
363 K
381 K
401 K
421 K
439 K
459 K
477 K
497 K
516 K
538 K
558 K
577 K
596 K
615 K
634 K
655 K
674 K

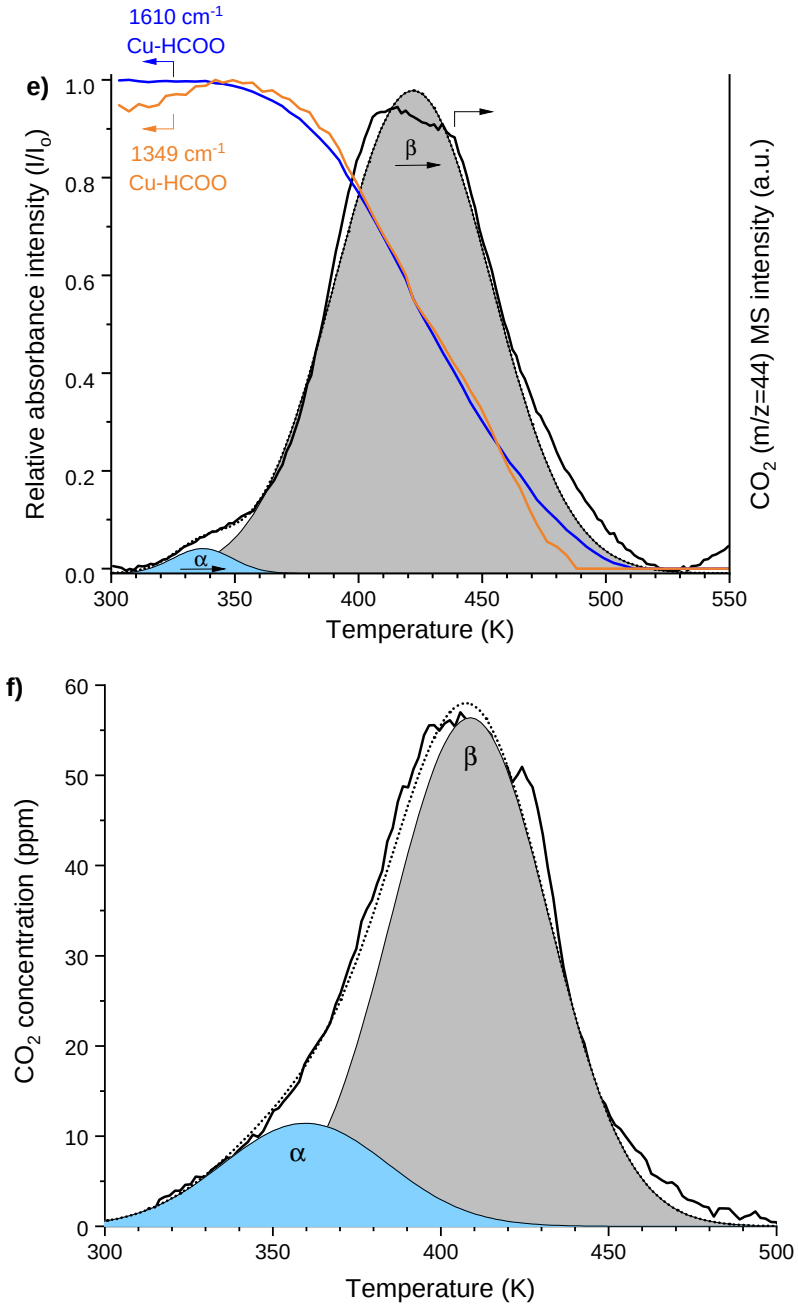
e)
1610 cm-1
Cu-HCOO
1349 cm-1
Cu-HCOO
β
α
Relative absorbance intensity (I/I0)
CO2 (m/z=44) MS intensity (a.u.)
Temperature (K)
f)
β
α
CO2 concentration (ppm)
Temperature (K)

g

Catalyst	**TOF [CH_3OH molecules (Cu surface atom)$^{-1}$ s^{-1}]**	**θ_{HCOO} [ML]**
Cu/SiO_2	$(1.48\pm0.11)\cdot10^{-3}$	0.0602±0.0389
Raney Cu	$(6.22\pm1.04)\cdot10^{-3}$	0.071±0.012
Cu/ZnO	$(3.61\pm0.54)\cdot10^{-2}$	0.267±0.087

Extended Data Fig. 4| Support dependence of the formate coverage on Cu during high pressure methanol synthesis and the associated methanol TOF. a IR absorbance spectra during TPD (2 K/min ramp in 45 Nml/min He) of Cu/SiO_2 after methanol synthesis (P = 10 bar, $CO_2/CO/H_2$ = 3/29/68, T = 523 K). Background spectrum is collected on the pre-reduced Cu/SiO_2 catalyst at 523 K in He before syngas exposure and IR spectra are offset for clarity. **b** Desorption of surface adsorbates and CO_2 during a TPD (identical experiment as in **a**) measured by their relative absorbance intensity progress with increased temperature. The surface adsorbates include Cu-HCOO at 1352 cm^{-1} and 2852 cm^{-1} [11, 18, 19], Si-CH_3O at 2933 cm^{-1} and at 2852 cm^{-1} [20] and chemisorbed CO_2 at 2338 cm^{-1} [21]. These desorption profiles provide guidance to deconvolution of the CO_2 TPD signal into its different contributions. The Cu-HCOO part of the deconvolution is used to estimate the HCOO coverage on Cu. **c** Desorbed CO_2 during a TPD (2 K/min in 42.4 Nml/min He) of Cu/SiO_2 (256.58 mg) after high pressure methanol synthesis (P = 50 bar, $CO_2/CO/H_2$ = 3/29/68, T = 523 K) is disentangled into chemisorbed CO_2 (α), Cu-HCOO (β) and Si-CH_3O (γ) based on the procedure outlined in **b**. Integration of β CO_2 is applied to quantify the formate coverage on Cu. **d** IR absorbance spectra during TPD (2 K/min in 45 Nml/min He) of Cu/ZnO after methanol synthesis (P = 10 bar, $CO_2/CO/H_2$ = 3/29/68, T = 523 K). Background spectrum is collected on the pre-reduced Cu/ZnO catalyst at 523 K in He before syngas exposure and IR spectra are offset for clarity. **e** Desorption of Cu-HCOO (at 1349 cm^{-1} and 1610 cm^{-1} [19]) and CO_2 during a TPD (identical experiment as in **d**) measured by their relative absorbance intensity progress with increased temperature. **f** Desorbed CO_2 during a TPD (2 K/min in 50.0 Nml/min He) of Cu/ZnO (104.36 mg) after high pressure methanol synthesis (P = 50 bar, $CO_2/CO/H_2$ = 3/29/68, T = 523 K) is deconvoluted into chemisorbed CO_2 (α) and Cu-HCOO (β) using the protocol presented in **e**. **g** Comparison of the formate coverage and methanol TOFs for Cu/SiO_2, Raney Cu and Cu/ZnO during methanol synthesis at high pressure (P = 50 bar, $CO_2/CO/H_2$ = 3/29/68, T = 523 K). Desorbed CO_2 disentanglement is based on [6] with characteristic Cu-HCOO desorption around 410 K. Cu/SiO_2 and Raney Cu yield relatively similar formate coverages, which implies that coverage differences cannot explain the four fold TOF difference between the catalysts.

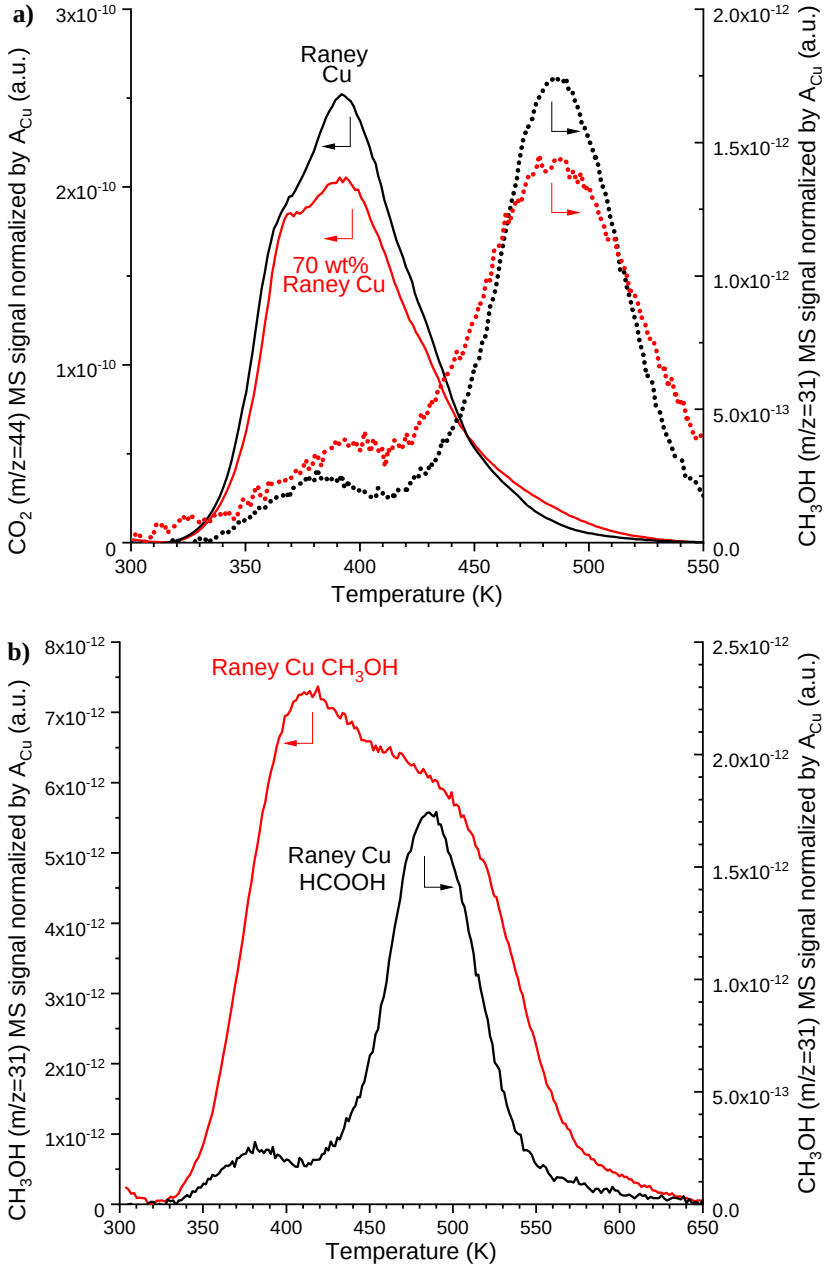

Extended Data Fig. 5| Roles of re-adsorption phenomena in temperature programmed hydrogenation with 2 K/min in 50 Nml/min H_2 on methanol or formate covered samples. **a** Gas desorption of CO_2 and CH_3OH normalized to the sample specific Cu surface area during TPH of Raney Cu and of a 70 wt% Raney Cu/30 wt% SiO_2 physical mixture after 1 µl formate adsorption at 313 K in 310 Nml/min He. Re-adsorption of methanol on SiO_2 is absent based on the similar CO_2 and CH_3OH profiles in presence (70 wt% Raney Cu and 30 wt% SiO_2) and absence (Raney Cu) of SiO_2. **b** TPH of formate (1 µl at 313 K in 310 Nml/min) and methanol (1 µl at 448 K in 310 Nml/min He) covered Raney Cu catalysts show that hydrogenation of formate to methanol initiates around 400 K but substantial re-adsorption on the catalyst surface delays the methanol signal towards higher temperatures.

References

[1] N. D. Nielsen, J. Thrane, A. D. Jensen, and J. M. Christensen. Bifunctional Synergy in CO Hydrogenation to Methanol with Supported Cu. *Catalysis Letters*, 150:1427–1433, 2020. doi: 10.1007/s10562-019-03036-7.

[2] G. C. Chinchen, C. M. Hay, H. D. Vandervell, and K. C. Waugh. The measurement of copper surface areas by reactive frontal chromatography. *Journal of Catalysis*, 103(1):79–86, 1987. doi: 10.1016/0021-9517(87)90094-7.

[3] R. Chatterjee, S. Kuld, R. V. D. Berg, A. Chen, and W. Shen. Mapping Support Interactions in Copper Catalysts. *Topics in Catalysis*, 62(7-11):649–659, 2019. doi: 10.1007/s11244-019-01150-9.

[4] O. Hinrichsen, T. Genger, and M. Muhler. Chemisorption of N_2O and H_2 for the Surface Determination of Copper Catalysts. *Chemical Engineering & Technology*, 23(11):956–959, 2000. doi: 10.1002/1521-4125(200011)23:11⟨956::AID-CEAT956⟩3.0.CO;2-L.

[5] G. H. Graaf and J. G.M. Winkelman. Chemical Equilibria in Methanol Synthesis Including the Water-Gas Shift Reaction: A Critical Reassessment. *Industrial and Engineering Chemistry Research*, 55(20):5854–5864, 2016. doi: 10.1021/acs.iecr.6b00815.

[6] N. D. Nielsen, A. D. Jensen, and J. M. Christensen. Quantification of Formate and Oxygen Coverages on Cu Under Industrial Methanol Synthesis Conditions. *Catalysis Letters*, 150(9): 2447–2456, 2020. doi: 10.1007/s10562-020-03162-7.

[7] V. D. Berg, Roy, G. Prieto, G. Korpershoek, L. I. Van Der Wal, A. J. Van Bunningen, S. Lægsgaard-Jørgensen, P. E. De Jongh, and K. P. De Jong. Structure sensitivity of Cu and CuZn catalysts relevant to industrial methanol synthesis. *Nature Communications*, 7(13057):1–7, 2016. doi: 10.1038/ncomms13057.

[8] R. Van Den Berg, J. Zečević, J. Sehested, S. Helveg, P. E. De Jongh, and K. P. De Jong. Impact of the synthesis route of supported copper catalysts on the performance in the methanol synthesis reaction. *Catalysis Today*, 272:87–93, 2016. doi: 10.1016/j.cattod.2015.08.052.

[9] R. Burch and R. J. Chappell. Support and additive effects in the synthesis of methanol over copper catalysts. *Applied Catalysis*, 45(1):131–150, 1988. doi: 10.1016/S0166-9834(00)82398-2.

[10] A. Karelovic, G. Galdames, J. C. Medina, C. Yévenes, Y. Barra, and R. Jiménez. Mechanism and structure sensitivity of methanol synthesis from CO_2 over SiO_2-supported Cu nanoparticles. *Journal of Catalysis*, 369:415–426, 2019. doi: 10.1016/j.jcat.2018.11.012.

[11] D. B. Clarke and A. T. Bell. An Infrared Study of Methanol Synthesis from CO_2 on Clean and Potassium-Promoted Cu/SiO_2. *Journal of Catalysis*, 154(2):314–328, 1995. doi: 10.1006/jcat.1995.1173.

[12] J. L. Robbins, E. Iglesia, C. P. Kelkar, and B. DeRites. Methanol synthesis over Cu/SiO_2 catalysts. *Catalysis Letters*, 10(1-2):1–10, 1991. doi: 10.1007/BF00764730.

[13] M. Saito, J. Wu, K. Tomoda, I. Takahara, and K. Murata. Effects of ZnO contained in supported Cu-based catalysts on their activities for several reactions. *Catalysis Letters*, 83(1-2):1–4, 2002. doi: 10.1023/A:1020693226903.

[14] T. Fujitani, M. Saito, Y. Kanai, T. Kakumoto, T. Watanabe, J. Nakamura, and T. Uchijima. The role of metal oxides in promoting a copper catalyst for methanol synthesis. *Catalysis Letters*, 25 (3-4):271–276, 1994. doi: 10.1007/BF00816307.

[15] Y. Yang, C. A. Mims, R. S. Disselkamp, C. H.F. Peden, and C. T. Campbell. Simultaneous MS-IR studies of surface formate reactivity under methanol synthesis conditions on Cu/SiO_2. *Topics in Catalysis*, 52(10):1440–1447, 2009. doi: 10.1007/s11244-009-9320-3.

[16] I. Nakamura, T. Fujitani, T. Uchijima, and J. Nakamura. A model catalyst for methanol synthesis: Zn-deposited and Zn-free Cu surfaces. *Journal of Vacuum Science & Technology*, 14(3):1464–1468, 1996. doi: 10.1116/1.579970.

[17] F. Studt, M. Behrens, R. Schlögl, E. L. Kunkes, N. Thomas, S. Zander, A. Tarasov, J. Schumann, E. Frei, J. B. Varley, F. Abild-Pedersen, and J. K. Nørskov. The Mechanism of CO and CO_2 Hydrogenation to Methanol over Cu-Based Catalysts. *ChemCatChem*, 7(7):1105–1111, 2015. doi: 10.1002/cctc.201500123.

[18] K. K. Bando, K. Sayama, H. Kusama, K. Okabe, and H. Arakawa. In-situ FT-IR study on CO_2 hydrogenation over Cu catalysts supported on SiO_2, Al_2O_3, and TiO_2. *Applied Catalysis*, 165 (1-2):391–409, 1997. doi: 10.1016/S0926-860X(97)00221-4.

[19] S. I. Fujita, M. Usui, and N. Takezawa. Mechanism of the reverse water gas shift reaction over Cu/ZnO catalyst. *Journal of Catalysis*, 134(1):220–225, 1992. doi: 10.1016/0021-9517(92)90223-5.

[20] D. B. Clarke, D. K. Lee, M. J. Sandoval, and A.T. Bell. Infrared studies of the mechanism of methanol decomposition on Cu/SiO_2. *Journal of Catalysis*, 150:81–93, 1994. doi: 10.1006/jcat.1994.1324.

[21] D. B. Clarke, I. Suzuki, and A.T. Bell. An Infrared Study of the Interactions of CO and CO_2 with Cu/SiO_2. *Journal of Catalysis*, 142:27–36, 1993. doi: 10.1006/jcat.1993.1186.

Appendix F

Supplementary information for *Bifunctional synergy in CO hydrogenation to methanol with supported Cu* described in chapter 8

Authors: Niels D. Nielsen[1], Joachim Thrane[1], Anker D. Jensen[1], Jakob M. Christensen[1*]

[1] *Department of Chemical and Biochemical Engineering, Technical University of Denmark, Søltofts Plads Building 229, 2800 Kgs. Lyngby, Denmark*

[*] **Correspondence to:** jmc@kt.dtu.dk

DOI:
https://doi.org/10.1016/10.1007/s10562-019-03036-7

Journal specifications:
Catalysis Letters, 2020, Volume 150, 1427-1433

Date Accepted/Published:
31 October 2019 / 14 November 2019

S1 Supplementary Material

Water inhibition of methanol synthesis

A number of studies have shown the inhibiting effect of water upon the methanol synthesis [1–4]. Figs S1 and S2 are given to illustrate the major low-temperature inhibition and possible contribution of competitive adsorption of water to the inhibition. Fig. S1 illustrates the inhibition by H_2O at lower temperatures by showing the relative methanol synthesis rate as a function of the H_2O partial pressure. Relative activities are calculated from the results of two studies [1, 2] investigating the addition of water to a CO_2/H_2 feed passed over a $Cu/ZnO/Al_2O_3$ catalyst. Fig. S1 shows that a few kPa of water partial pressure is sufficient to cause major inhibition of Cu-based catalysts at lower temperatures.

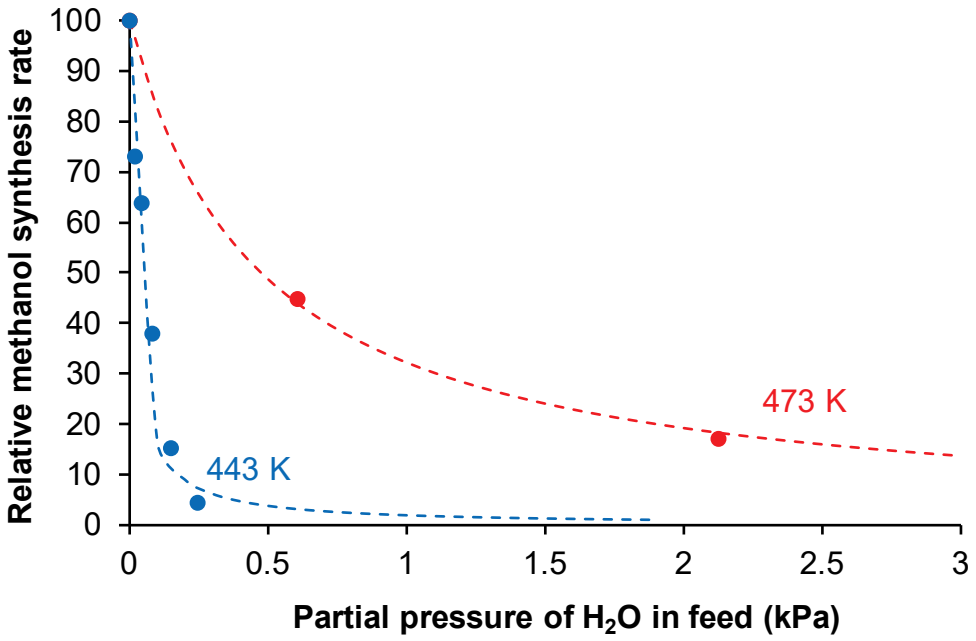

Fig. S1: Relative methanol synthesis rate as a function of the partial pressure of water in the $CO_2/H_2/H_2O$ feed passed over $Cu/ZnO/Al_2O_3$ at atmospheric pressure [1, 2].

Equilibrium calculations using the equilibrium data from Graaf and Winkelman [5] shows that the methanol concentrations at 443 K in fig. S1 are all below <10% of the equilibrium concentration, so equilibrium effects cannot be the main explanation for the strong water inhibition, which must instead be kinetic in nature. The water inhibition, which is reported to be reversible [2], is to be expected for all Cu catalysts from blocking of the active sites, as can be illustrated with a simple model based on water adsorption isotherm measurements by Słoczyński et al. [6, 7]. Fig. S2 shows the water coverage calculated from their [6, 7] data (defined as water uptake relative to a maximal water uptake of 270 µmol/$g_{cat.}$ for $Cu/ZnO/Al_2O_3$ and 19.7 µmol/$g_{cat.}$ for unsupported Cu) as a function of water partial pressure for $Cu/ZnO/Al_2O_3$ and unsupported Cu. This simple model suggests that at lower temperatures the water coverage and the resulting loss of free sites should become significant for Cu-based catalysts already at a few kPa of water pressure. It is therefore also reasonable to expect a significant loss of activity at such water pressures due to competitive adsorption of H_2O or its dissociation products.

The intrinsic properties of Cu

Unsupported Cu must be expected to represent the intrinsic properties of Cu, but a poor thermal stability means that only a low metal area can be achieved with this type of material. Two other Cu samples, namely Raney Cu and Cu/Al_2O_3 with a considerably higher Cu surface area, were therefore

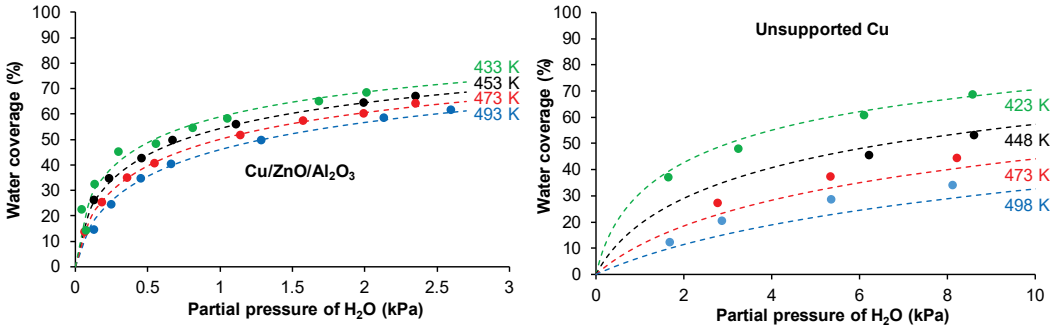

Fig. S2: Water coverage a function of H_2O partial pressure for both $Cu/ZnO/Al_2O_3$and unsupported Cu. Calculated coverages are based on adsorption isotherm measurements by Słoczyński et al. [6, 7]. The water coverage is obtained as the water uptake at a given H_2O partial pressure relative to a maximal water uptake of 270 µmol/g_{cat} for $Cu/ZnO/Al_2O_3$ and 19.7 µmol/g_{cat} for unsupported Cu [6, 7]. Dashed lines represent fitted Temkin isotherms.

also evaluated.
In assessing the behavior of unsupported Cu the low melting point of copper results in a poor thermal stability, and results are therefore expected to become increasingly uncertain with increasing temperature. When starting from 448 K and gradually raising the temperature, methanol formation from CO_2/H_2 was detectable at all temperatures, but 498 K was the first temperature where any methanol formation from CO/H_2 could be unambiguously identified by GC measurements. For this reason the assessment of unsupported Cu in fig. 1 in the main text was conducted at 498 K. Fig. S3 summarizes this evaluation of unsupported Cu.

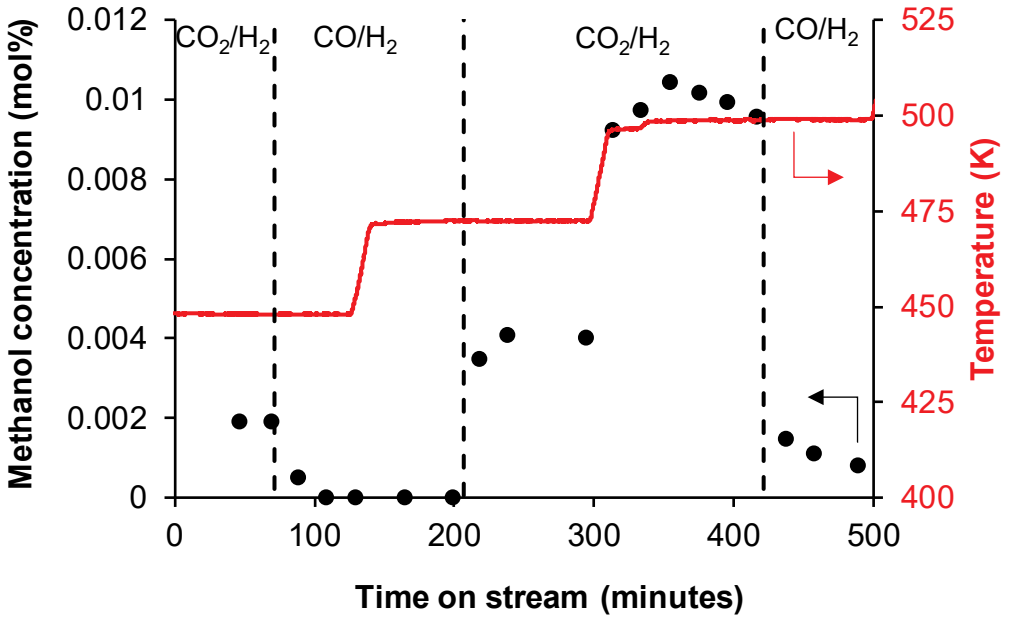

Fig. S3: Methanol effluent concentration with unsupported Cu as a function of time on stream. The feed is switched between CO_2/H_2 and CO/H_2 at varying temperatures. Reaction conditions: P = 5 MPa, H_2/CO_x/inert = 68/3/29, 280 NmL/min, 578 mg CuO. The Cu surface area of the sample is 0.49 m^2/g_{cat}.

Ex situ XPS analyses (described in the last section of this supplement) of the spent sample from the experiment in fig. S3 showed no signs of Ni or Fe, which indicates that results are without any influence of metal deposition from carbonyls. Figs. S4 and S5 show comparisons of methanol formation from

CO_2/H_2 and CO/H_2 with Cu/Al_2O_3 and Raney Cu, which were investigated at both 523 K and 498 K. Repeated investigations have shown the effects of the gas atmosphere to be reversible and independent of the order of the gas mixtures.

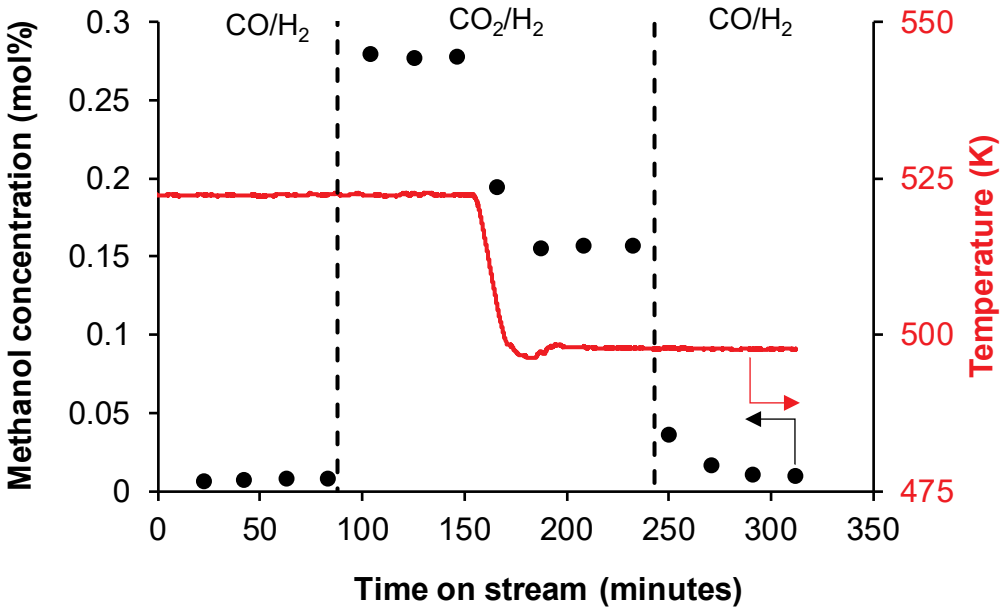

Fig. S4: Methanol effluent concentration with 50 wt% Cu/Al_2O_3 as a function of time on stream. The feed is switched between CO_2/H_2 and CO/H_2 at varying temperatures. Reaction conditions: P = 5 MPa, H_2/CO_x/inert = 68/3/29, 275 NmL/min, 148 mg catalyst. The Cu surface area of the sample is 7.16 $m^2/g_{cat.}$

Unsupported Cu, Raney Cu and the Cu-rich Cu/Al_2O_3 are expected to represent the intrinsic properties of Cu and are all consistent in showing the reaction to be much faster from CO_2. Fig. S6 shows that the conclusion is completely inverted when cycling between CO/H_2 and CO_2/H_2 for Cu/MgO at 523 K. Fig. S6 also illustrates that the increase in reaction rate in CO/H_2 is associated with a release of CO_2, which illustrates the inhibiting effect of CO_2 discussed in the main text and attributed to carbonate formation. Fig. S7 shows the results of a similar cycling experiment for the industry-type $Cu/ZnO/Al_2O_3$ catalyst.

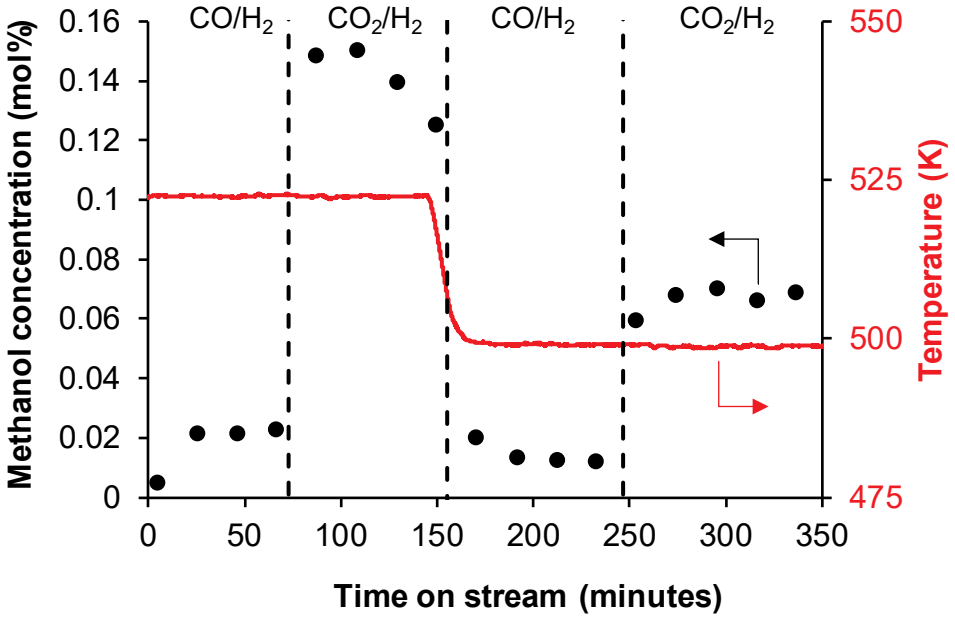

Fig. S5: Methanol effluent concentration with Raney Cu as a function of time on stream. The feed is switched between CO_2/H_2 and CO/H_2 at varying temperatures. Reaction conditions: P = 5 MPa, H_2/CO_x/inert = 68/3/29, 273 NmL/min, 296 mg catalyst. The Cu surface area of the sample is 5.18 $m^2/g_{cat.}$

.

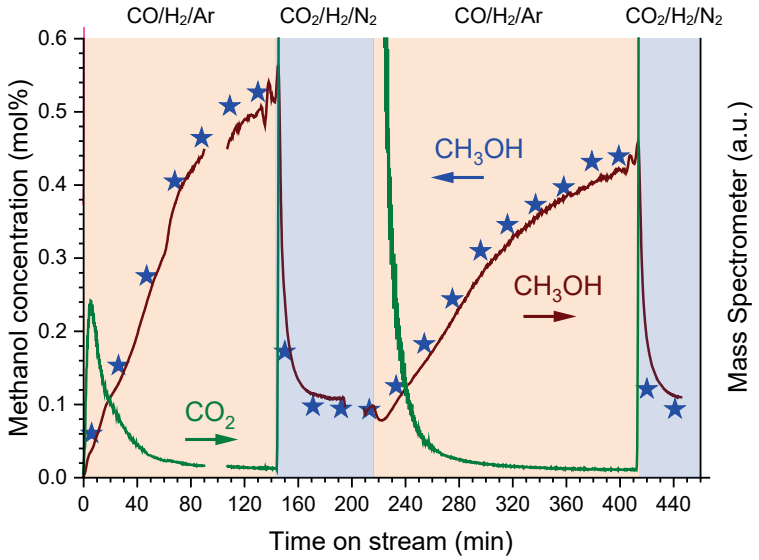

Fig. S6: Methanol effluent concentration (blue stars) with Cu/MgO as a function of time on stream. The feed is switched between CO_2/H_2 and CO/H_2 at 523 K. Reaction conditions: P = 5 MPa, T = 523 K H_2/CO_x/inert = 68/3/29, 280 NmL/min, 96.6 mg catalyst. The MS signals illustrate that the growth in methanol productivity is associated with a release of CO_2. The gaps in the MS signals are due to flow measurements where the flow is bypassing the MS. The Cu surface area of the sample is 6.00 $m^2/g_{cat.}$

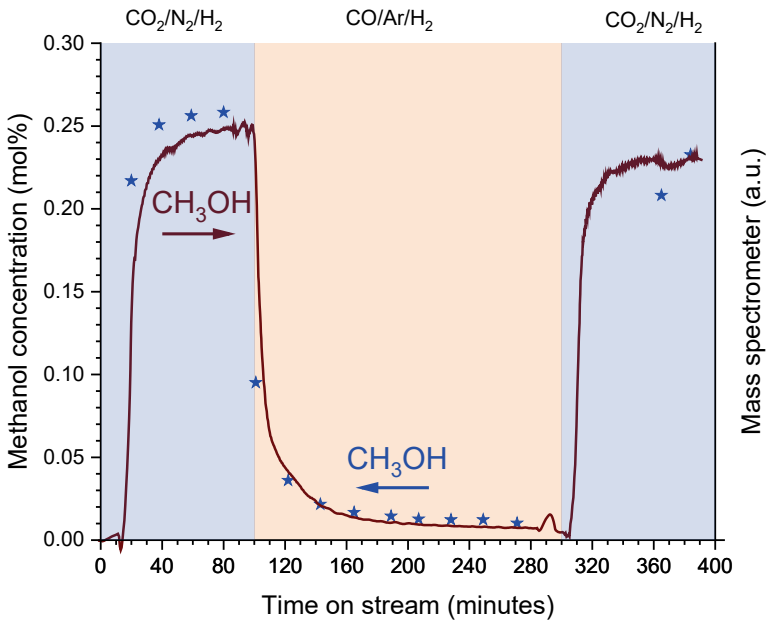

Fig. S7: Methanol effluent concentration (blue stars GC measurements, solid lines MS m/z = 31 signal) with $Cu/ZnO/Al_2O_3$ as a function of time on stream. The feed is switched between CO_2/H_2 and CO/H_2 at 523 K. Reaction conditions: P = 5 MPa, T = 523 K H_2/CO_x/inert = 68/3/29, 280 NmL/min, 13.1 mg catalyst. The Cu surface area of the sample is 20.25 $m^2/g_{cat.}$

CO hydrogenation results

A range of supported catalysts were tested for high pressure CO hydrogenation. Fig. S8 shows that the present results on CO hydrogenation indicate no clear correlation between methanol synthesis rate and copper surface area for the present catalysts on varying supports. Previous studies [8], [9] with varying Cu area on a fixed support material have similarly concluded that no correlation exists between Cu surface area and CO hydrogenation activity. Fig. 2 in the main text illustrates the methanol formation rates as a function of time on stream for the catalysts. Most catalysts are relatively stable in the CO/H_2 atmosphere. A clear exception is $Cu/ZnO/Al_2O_3$, which undergoes a pronounced gradual deactivation in the first hours on stream. This deactivation behavior of $Cu/ZnO/Al_2O_3$ may relate to further reduction of the catalyst, as CO_2 is evolved during the period of deactivation. The same deactivation of $Cu/ZnO/Al_2O_3$ in CO/H_2 is also observed by others [3, 10, 11]. Fig. 2 shows that both Cu/C and MgO/C (the latter from impregnation of $Mg(HCOO)_2$ onto carbon) are inactive, but the same impregnation of $Mg(HCOO)_2$ onto the inactive Cu/C catalyst creates an active MgO/Cu/C catalyst. The $Mg(HCOO)_2$ will decompose during the pre-reduction at 523 K (fig. S11 shows that formate decomposition is significant at 523 K), and additionally the integral methanol production of the MgO/Cu/C catalyst in fig. 2 far exceeds the amount of added formate, so the methanol production is due to a catalytic conversion of CO/H_2 and not due to the added formate acting as a sacrificial reactant. The activity of the Cu-MgO systems is thus due to a synergy of two materials with limited activity on their own. The negligible methanol production of Cu exchanged mordenite (Cu-MOR) is due to an absence of conversion, and no other products are observed (i.e. no DME or C_1-C_3 hydrocarbons) - i.e. not due to further conversion of formed methanol on acidic zeolite sites.

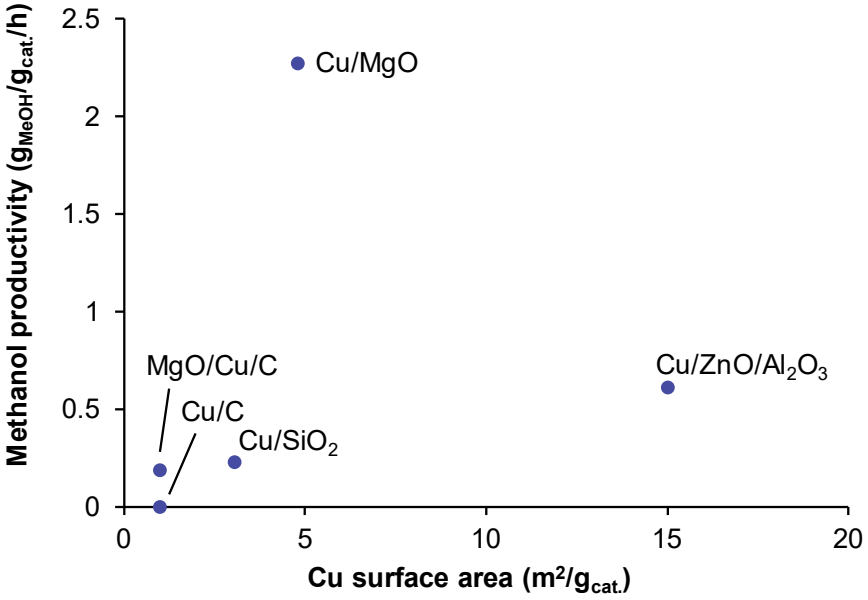

Fig. S8: Methanol synthesis rate in CO hydrogenation for a range of catalytic materials as a function of the Cu surface area estimated from titration with N_2O. Reaction conditions: T = 523 K, P = 5 MPa, flow = 300 NmL/min, H_2/CO = 67/33.

CO chemisorption and TPD

For the set of catalysts evaluated in figs. 2 and S8 the CO uptake was measured by pulse chemisorption at 303 K. The uptakes of the catalysts are summarized in table S1. After chemisorption the catalysts were subjected to a TPD and the results are summarized in S9. Fig. S9 shows that the catalysts typically have a major desorption around 323-337 K. The activation energy for CO desorption was estimated by a Redhead [12] analysis using eq. Eq. S1 [13].

$$E_{des} = RT_{\max} \ln\left(\frac{RT_{\max}^2 \nu}{E_{des}\beta}\right) \qquad \text{(Eq. S1)}$$

Here $T_{\max}$ is the temperature of maximal desorption rate, β is the heating rate of 2 K/min = 0.033 K/s and ν is the prefactor, assumed to be 10^{13} s^{-1}. This analysis gives an activation energy of desorption of 95-100 kJ/mol as summarized in table S1. This implies a binding strength too large to be on metallic Cu surface sites and is more representative of CO adsorbed on Cu^+ sites [14], [15].

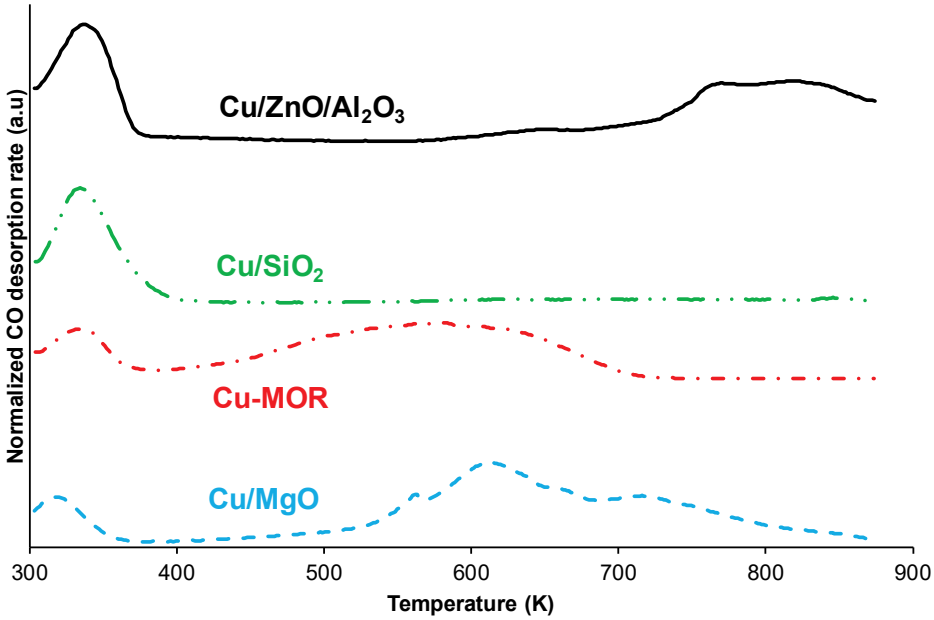

Fig. S9: The CO (m/z = 28) desorption rate as function of temperature during TPD after CO pulse chemisorption at 303 K. The signals are normalized by the intensity of the strongest desorption peak within each experiment. Heating rate: 2 K/min. Carbon supported samples are omitted due to major desorption assigned to species released from the activated carbon.

The metallic Cu surface area (and thus the number of metallic Cu^0 surface sites) has also been determined from titration with N_2O. For a Cu/SiO_2 catalyst, where only the 335 K CO desorption peak is seen the number of $Cu^{\delta+}$ species can be accurately determined from the CO chemisorption. With the number of Cu^0 sites from N_2O titration this gives a $Cu^{\delta+}/Cu^0$ ratio of 0.46 for Cu/SiO_2 illustrating that $Cu^{\delta+}$-O-Si linkages are quite prevalent in Cu/SiO_2. For the other samples there is also CO desorption at higher temperatures (attributable to e.g. formate species formed from the CO on the oxide), which means that not necessarily all CO chemisorption can be assigned to $Cu^{\delta+}$ species. This only allows us to conclude that the $Cu^{\delta+}/Cu^0$ is at least below 0.13 for $Cu/ZnO/Al_2O_3$. The fact that $Cu^{\delta+}$ sites are relatively plentiful for Cu/SiO_2, which only shows a moderate CO hydrogenation activity (see fig. S8), could indicate that it is not only $Cu^{\delta+}$ species that are important, but also the nature of the oxide. This does not necessarily imply that existing [16–18] correlations between $Cu^{\delta+}$ concentration and CO hydrogenation activity are invalid, but does imply that such correlation should only be expected, when the oxide component is kept fixed or relatively similar oxides are compared.

Table S1: CO chemisorption capacity, the primary CO desorption temperature and Redhead analysis for fig. S9.

Catalyst	**Cu/SiO_2**	**$Cu/ZnO/Al_2O_3$**	**Cu/MgO**	**Cu-MOR**	**Cu/C**	**MgO/Cu/C**
CO adsorption at 303 K ($\mu mol/g_{cat.}$)	34	49	143	361[a)]	6	25
Cu area [$m^2/g_{cat.}$]	3.1	15.0	4.8		1[b)]	1[b)]
$Cu^{\delta+}/Cu^0$ ratio	0.46	<0.13	[c)]		[c)]	[c)]
T_{max} (K)	335	337	323	336	-[e)]	-[e)]
E_{des} (kJ/mol)[d)]	99	100	95	99	-[e)]	-[e)]

[a] If the H_2 consumption during reduction is converted to a Cu^+ content assuming reduction from CuO to Cu_2O this corresponds to 365 µmol Cu^+/g_{cat} in good agreement with the CO uptake.
[b] Significant uncertainty due to the low area.
[c] As fig. S9 suggests that the 323-337 K peak assigned to $Cu^{\delta+}$ species is not the major desorption for MgO-based catalysts the number of $Cu^{\delta+}$ sites cannot be reliably determined from CO chemisorption.
[d] Determined from a Redhead analysis assuming a prefactor of 10^{13} s^{-1}.
[e] A broad desorption attributed to species from the carbon prevents conclusive TPD analysis.

Mechanistic investigations

To further elucidate the methanol formation during TPH fig. S10 shows IR spectra of the Cu/MgO catalyst during the TPH experiment (also partly shown in fig. 3 in the main text).
Fig. S10 shows that the methanol formation centered at 423 K is associated with the disappearance of the IR bands at 1360 cm^{-1} and 2834 cm^{-1} marked by arrows. These bands are attributed to a particular formate species, most likely a formate at the interface. Fig. S10 also shows that the higher temperature methanol formation centered at 523 K occurs in conjunction with the disappearance of formate on MgO (1625 cm^{-1} drops significantly from the black to the green to the gold spectra) and methoxide on MgO (1086 cm^{-1} drops significantly from the black to the green to the gold spectra). The 523 K methanol formation is therefore attributed to these species entirely on the oxide. Due to their higher conversion temperature the formates and methoxides entirely on the oxide are not likely to play a major role in the reaction – perhaps only that of complete spectators. These species on the MgO are also to a significant extent decomposing to CO during the TPH. This is illustrated in fig. S11, which shows the formation of methanol and CO during the TPH experiment.

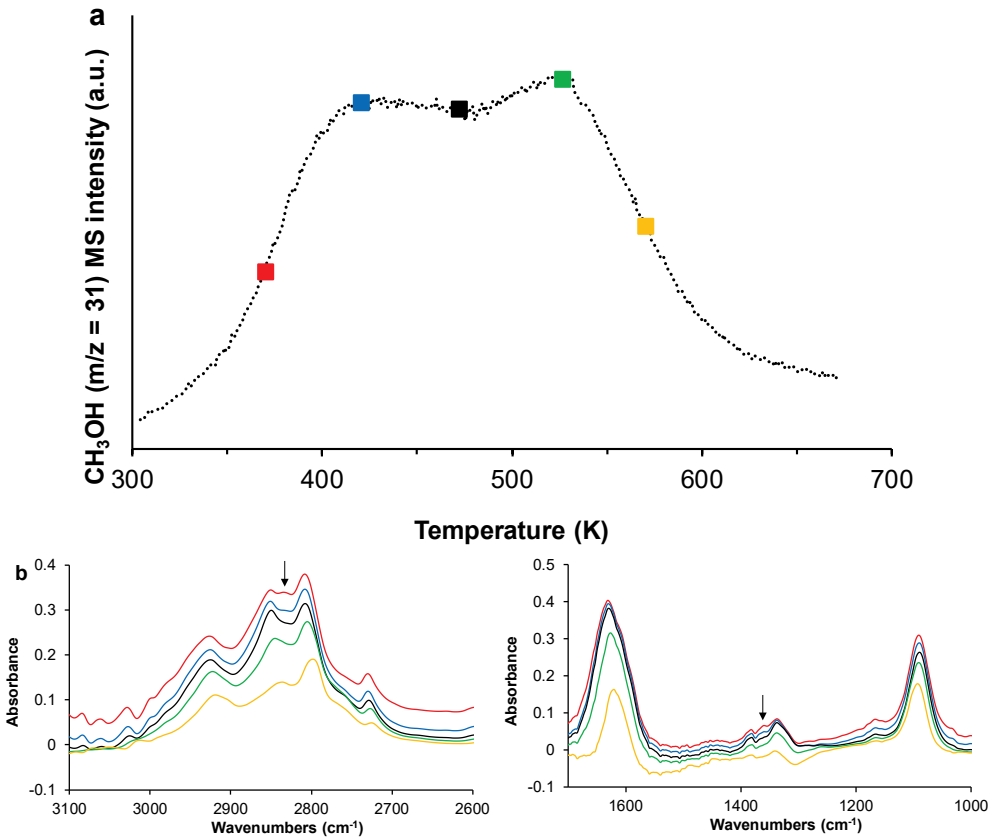

Fig. S10: a) The methanol formation during TPH of Cu/MgO previously exposed to CO/H_2 with colored markings indicating the location of the IR spectra. b) IR spectra taken during the TPH. The arrows indicate the IR bands changing during the first methanol formation peak (red→blue→-black), whereas the second methanol formation peak corresponds to a general decline in the formate (and methoxide) bands (black→green→gold).

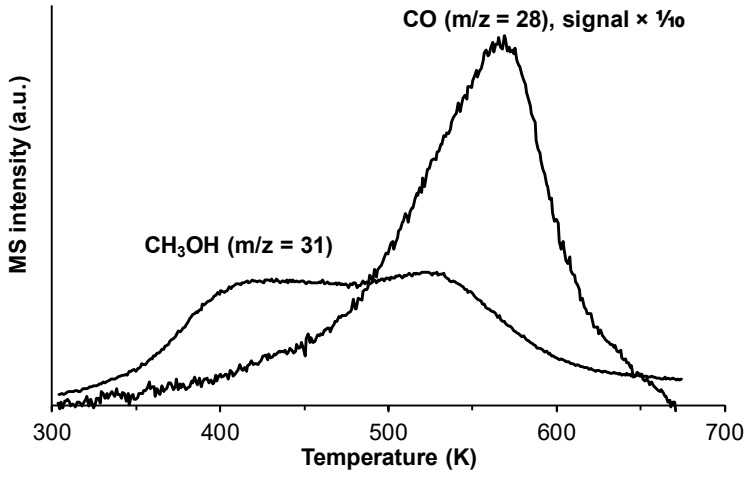

Fig. S11: MS intensities as a function of temperature during temperature programmed hydrogenation of the Cu/MgO catalyst after the exposure to $CO/H_2/Ar = 3/68/29$ at 523 K and atm pressure (and cooling in this gas). Conditions: 2 K/min, 50 NmL/min H_2 flow, 10 mg catalyst.

CO_2 deactivation of Cu/MgO

Fig. S12 shows the catalytic activity of Cu/MgO as a function of time on stream in either CO/H_2 or $CO_2/CO/H_2$. The figure illustrates that Cu/MgO contrary to the behavior of Cu itself is strongly inhibited (a factor of about 20) by CO_2.

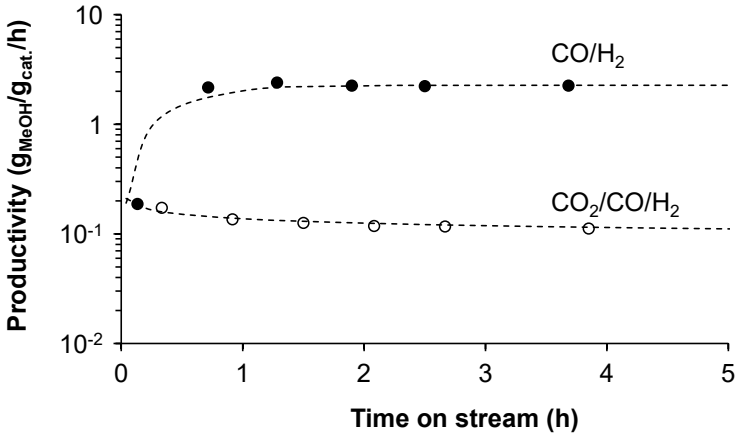

Fig. S12: The rate of methanol synthesis over Cu/MgO as a function of time on stream in CO/H_2 or $CO_2/CO/H_2$. Reaction conditions: T = 523 K, P = 5 MPa, flow = 300 NmL/min, H2/CO = 67/33, $H_2/CO/CO_2$ = 67/27/6. Cu surface area: 4.80 m^2/g.

The turnover frequency (TOF: the rate relative to the total number of Cu surface atoms) of the Cu/MgO catalyst operating in the presence of CO_2 in fig. S12 is $9{\cdot}10^{-3}$ s^{-1}. This estimate is based on the data point after 1.50 h on stream in S12, where an approximate steady state has been reached. Table S2 shows a comparison of this TOF to Cu single crystal results for the CO_2 hydrogenation to methanol extrapolated to the present conditions. Table S2 shows that within the uncertainty of extrapolation the TOF on Cu expected from single crystal studies is in the range of $5{\cdot}10^{-3} - 2 \cdot 10^{-2}$ s^{-1}. Since the Cu/MgO catalyst operating in CO_2 is in this interval, there is no reason to expect that the CO_2 hydrogenation on the Cu metal surface is strongly modified/inhibited under these conditions. The inhibition of Cu/MgO in the presence of CO_2 thus appears to be purely of the bifunctional CO-pathway, and the Cu metal surface continues to produce methanol from CO_2 in the normal fashion.
Fig. S13 shows a comparison between FTIR spectra in CO_2 (which should yield only carbonate bands) and $CO_2/CO/H_2$ to identify major carbonate contributions. The figure illustrates that carbonate has important contributions to the 858, 1078, 1340 and 1630 cm^{-1} bands. As discussed in the main text the band at 1254 cm^{-1} is most likely also a carbonate band but only one that can be formed in the atmosphere containing CO and H_2 in addition to CO_2.

Table S2: Comparison of the TOF for Cu/MgO operating in CO_2 in fig. S11 to single crystal studies in the literature. Notice that the TOF level of Cu/MgO corresponds reasonably to the expectation from single crystal data.

Catalyst	TOF (s^{-1}) at org. conditions†	Original Conditions		TOF (s^{-1}) at 3.35 MPa H_2 and 523 K⋆	Ref.
		T (K)	P_{H_2} (MPa)		
Cu/MgO	$9{\cdot}10^{-3}$	523	3.35	$9{\cdot}10^{-3}$	This work
Cu(111)	$2.06{\cdot}10^{-3}$	523	1.35	$5.11{\cdot}10^{-3}$	[19]
Polycryst. Cu	$2.98{\cdot}10^{-3}$	523	1.35	$7.39{\cdot}10^{-3}$	
Cu(100)	$3.55{\cdot}10^{-3}$	523	1.35	$8.81{\cdot}10^{-3}$	
Cu(311)	$5.23{\cdot}10^{-3}$	523	1.35	$1.30{\cdot}10^{-2}$	
Cu(110)	$8.27{\cdot}10^{-3}$	523	1.35	$2.05{\cdot}10^{-2}$	
Cu(111)	$8.42{\cdot}10^{-4}$	525	0.45	$5.86{\cdot}10^{-3}$	[20]
Polycryst. Cu	$1.2{\cdot}10^{-3}$	510	0.46	$1.36{\cdot}10^{-2}$	[21]

† TOF at the reaction conditions of the original study.

⋆ TOF extrapolated to the conditions of the current study. Rate expressions typically vary between reaction orders in H_2 from 0.5 to 2 and exhibit a lower order for other reactants [22–25], [26]. The activation energy is in the order of 75 kJ/mol for all Cu surfaces [19, 21, 25]. For simplicity conversion of reported TOFs to the presently used conditions is done using a linear extrapolation of the H_2 pressure and using an activation energy of 75 kJ/mol. Since most of the studies regarded here use temperatures close to 523 K, the temperature correction will not lead to great uncertainty, but the pressure correction is of significant impact.

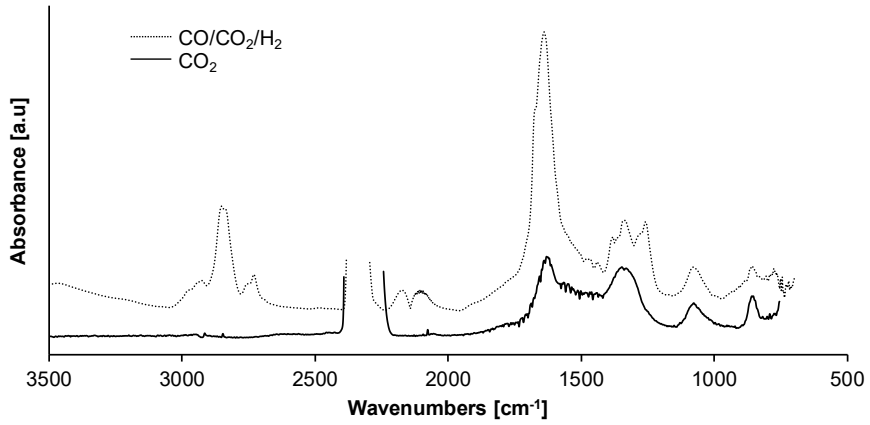

Fig. S13: FTIR spectra of Cu/MgO at 523 K and atmospheric pressure in flowing CO_2/N_2 (full line) or $CO_2/CO/H_2$ (dotted line). Conditions: CO_2/N_2 = 9/81, $CO_2/CO/H_2/N_2$ = 1.5/1.5/68/29.

Materials and methods

In all cases normal conditions, marked with an "N" on the flow refers to 273.15 K and 1 atm pressure and flow units (for example NmL/min) gives the flow corresponding to these reference conditions.

Catalyst preparation

The Cu/MgO, Cu/ZnO/Al_2O_3, Cu/Al_2O_3, unsupported Cu and Cu/C were all prepared by precipitation methods using metal nitrates ($Cu(NO_3)_2{\cdot}3H_2O$ ≥99%, $Zn(NO_3)_2{\cdot}6H_2O$ ≥98%, $Al(NO_3)3{\cdot}9H_2O$ ≥98%, $Mg(NO_3)_2{\cdot}6H_2O$ ≥98% from Sigma Aldrich or Alfa Aesar) and Na_2CO_3 (Sigma Aldrich, ≥99.8%). Conditions were typically taken from the optimal conditions found by Baltes et al. [27]. The Cu/MgO synthesis was inspired by Zander et al. [28] although a higher calcination temperature was selected to achieve a more complete decomposition of carbonates in order to avoid their disturbance of characterization results. For the unsupported Cu the precipitation method targeted the Gerhardtite structure observed by Behrens et al. [29] to precipitate around pH = 3-4. Table S3 gives an overview of the precipitation conditions. All precipitates were filtered and washed thoroughly in demineralized water and then dried at 313 K overnight before calcination. Samples were calcined in an alumina crucible within a tubular furnace in an air flow of 1 NL/min by ramping the temperature to the final temperature and holding this temperature for 3 hours. Details on the calcination are given in table S3. Two batches of Cu/MgO were prepared by identical methods, hence the slight variation in Cu area for Cu/MgO between figs. S6 and S8. Two batches of Cu/ZnO/Al_2O_3 were prepared and batch I (Cu area 20 m^2/gcat.) was used in fig. 1 (and fig. S7) while batch II (Cu area 15 m^2/gcat.) was used in 2 (and fig. S8).

Table S3: Overview of conditions used in preparations.

Catalyst	Nominal Cu content [wt%]	Temperature (K)	Ramp (K/min)	pH	Ageing[a)]	Calcination temperature (K)
Cu/MgO	20	338	1	9	1 h	723
Cu/ZnO/Al_2O_3 - I	56[b)]	338	1	6.5	1 h	573
Cu/ZnO/Al_2O_3 - II	56[b)]	338	1	6.5	1 h	603
Cu/Al_2O_3	50	338	2	6.5	1 h	573
Unsupported Cu	100	338	1	4[c)]	1 h	603
Cu/C[d)]	15	338	1	7	1 h	583[e)]

[a)] All ageing done at 338 K with unrestricted pH.
[b)] Cu:Zn:Al molar ratio: 6:3:1.
[c)] Dilute HNO_3 used to assist pH regulation.
[d)] Deposition precipitation on activated carbon (Norit Darco, 600 m^2/g).
[e)] Calcined in 1 NL/min flowing N_2 instead of air.

Cu ion-exchanged into mordenite was prepared from NH_4-MOR (Zeolyst CBV21A, SiO_2/Al_2O_3= 20) by ion-exchanging the initial NH_4-MOR twice in a 0.1 M $NaNO_3$ solution for 4 h at 353 K. The intermediate Na-MOR was then ion-exchanged twice in a 0.1 M $Cu(NO_3)_2$ solution (353 K, 4 h) to obtain Cu-MOR. In between all ion-exchange steps the slurry was filtered and the solid washed thoroughly with demineralized water. After drying overnight at 313 K it was calcined at 773 K (air, 1 NL/min, 1 K/min ramp) and kept at this temperature for 3 h. The hydrogen consumption during reduction (365 µmol Cu^+/g_{cat}) corresponds to 2.3 wt% Cu assuming reduction to Cu^+ only. This agrees well with the number of Cu^+ sites estimated from CO chemisorption. 20 wt% Cu on SiO_2 was prepared by impregnating SiO_2 (Saint Gobain SS61138, 250 m^2/g) with $Cu(NO_3)_2$. After drying overnight at 313 K the sample was calcined at 583 K (air, 1 NL/min, 1 K/min ramp) and kept at

this temperature for 3 h. MgO/Cu/C and MgO/C were prepared by impregnating either the calcined Cu/C catalyst (i.e. in the oxide form) or pure Norit Darco carbon with $Mg(HCOO)_2 \cdot 2H_2O$ (Sigma Aldrich, $\geq$ 98%) to 5 wt% Mg and drying in stagnant air at 313 K. The samples were loaded in the reactor, pre-reduced and tested without any calcination. All samples were pressed, crushed and sieved to 150-300 µm. Raney Cu (98.9 % Cu) was purchased from Strem Chemicals. Raney Cu was delivered as an aqueous slurry and was air-dried at room temperature in the fume hood to a substantially dried state (some oxidation by air may have occurred during this step) before loading into the reactor.

High pressure CO hydrogenation

Two different high-pressure reactor setups were used for the experiments presented in this paper. Conditions were chosen to give low conversions far from equilibrium. The highest CO conversion was 5% for Cu/MgO in fig. 2 and in all other cases conversion was considerably below this level. The CO hydrogenation experiments in fig. 2 (also represented in fig. S8) and fig. S12 were conducted in quartz reactor tubes in a high pressure flow reactor described in detail elsewhere [30] with the reactor effluent quantified by an Agilent Technologies 6890N GC-FID/TCD detection system. The catalyst was pre-reduced at atmospheric pressure by heating in a 100 NmL/min flow of 5 mol% H_2 in N_2 at 2 K/min to a temperature of 523 K and holding this temperature for 4 h. The CO hydrogenation experiments in fig. 1 (also represented in figs. S3-S7) were conducted in a reactor setup described in detail below. A diagram of the setup can be seen in fig. S14.

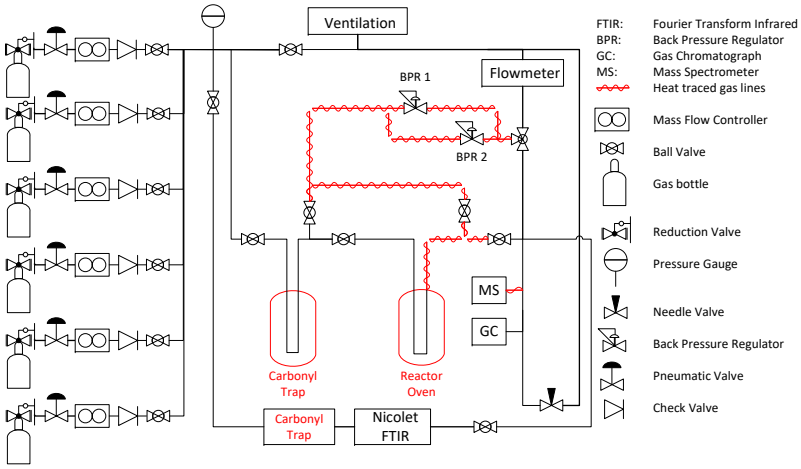

Fig. S14: PI diagram of the applied setup for high-pressure methanol synthesis experiments. Gasses were fed from left and passed first a carbonyl trap before either entering a) the reactor oven for high pressure experiments or b) the Nicolet FTIR for DRIFTS studies. For gas route a), the position of the three way valve controlled, whether the gas flowed to the GC and MS instruments or to the flowmeter. If gas was guided along route b), the effluent gas could similarly be analyzed by the GC and MS instruments.

Gasses were fed from pressurized cylinders, dosed by Brooks SLA5850 mass flow controllers and passed through a bed of activated carbon (Cabot Norit activated carbon with 1450 m^2/g as surface area) at ambient temperature, which acted as a carbonyl trap, before reaching the catalytic reactor. The reaction temperature was controlled by an Entech tubular oven (3 individually controlled heating zones) and monitored by two type-N thermocouples, one inside the reactor tube placed above the top quartz wool packing and one on the outside wall of the reactor tube placed at the position corresponding to the bottom of the catalyst bed. The reactor tubes were SGE Analytical Science glass lined tubes (1/4 in o.d., 4 mm i.d.) bent by a professional glass blower to a U-tube and connected to the setup by Swagelok fittings. The catalyst bed was placed in the reactor tube between wads of quartz wool (Quantachrome) in the inlet leg of the U-tube and held in place by the thermocouple on top of the quartz wool and a 28 mm quartz rod placed below the bottom quartz wool packing and resting on the

bottom of the U-tube. Reactor pressure was controlled by Baumann 51000 series pressure reduction valves and monitored by Yokogawa pressure transmitters measuring total pressure and reactor pressure drop. The gas flow rate was measured with a soap film flow meter downstream of the pressure reduction. Product analysis was made with a Thermo Fisher Trace 1300 GC fitted with one channel composed of a TG5 column leading to an FID detector and one channel composed of an OV-1 column followed by a Shincarbon column leading to a TCD detector. He was used as the carrier gas. A needle valve on a by-pass line to the purge system was adjusted to ensure that all GC measurements were made at the same pressure (identical to the pressure applied during gas calibration). Raney Cu was pre-reduced in a 50 Nml/min flow of 5% H_2/N_2 using a ramp of 1 K/min to first 448 K (holding for 2 hours) and secondly to 523 K (holding for 2 hours). For Cu/Al_2O_3 the same program was used, but then followed by a third holding step at 523 K in 100% H_2 (holding time 1 h) as previous N_2O-titration measurements had suggested that this step was required to reduce all Cu prior to syngas exposure. After pressurizing in He at 523 K the reactant flow was initiated. Unsupported Cu was pre-reduced in a 50 Nml/min flow of 5% H_2/N_2 using a ramp of 1 K/min to 448 K (holding for 3 hours). The system was then pressurized (at 448 K in He), and the unsupported Cu was tested with stepwise increasing temperature. A TPR on unsupported Cu showed that complete reduction is achieved with this reduction program. In all cases GC calibration was made with certified gas mixtures from AGA for normally gaseous species (H_2, CO, CO_2, DME, C_1-C_3 hydrocarbons) and by injecting a known volume of liquid into a known volume of gas in a Tedlar bag for normally liquid species (CH_3OH).

CO pulse chemisorption and CO-TPD

CO chemisorption and temperature programmed desorption (TPD) were conducted in a Quantachrome Autosorb iQ_2 setup with ≈0.5 g of sample in a quartz cell. The flow was 30 NmL/min in all stages of the experiments. After flushing with He for 25 min the sample was first pre-reduced in 5 mol% H_2 in N_2 by heating at 2 K/min to 523 K and holding this temperature for 4 h. The sample was then kept under vacuum for 2 h at 523 K to remove residual water. After cooling to 303 K the sample was at atmospheric pressure exposed to 270 µl pulses of CO in a He flow until no further uptake was observed. The CO uptake was quantified by the TCD detector in the Quantachrome Autosorb iQ_2 setup. At this stage the CO-TPD was conducted by heating the sample to 873 K at a rate of 2 K/min in He. The CO desorption profile was monitored by a Hiden Analytical QGA mass spectrometer.

Temperature programmed hydrogenation (TPH) of a model system

A model system was prepared by pre-reducing 5 g of Cu/SiO_2 in a flow reactor described elsewhere [30] and then passivating the sample by slowly letting air diffuse into the reactor tube. This sample was then impregnated with an aqueous solution of $Mg(HCOO)_2{\cdot}2H_2O$ to obtain 5 wt% $Mg(HCOO)_2$ on Cu/SiO_2 and drying in air at 323 K. Then 0.5 g of this sample was subjected to temperature programmed hydrogenation in a Quantachrome Autosorb iQ_2 setup. The H_2 flow was 30 NmL/min and the sample was heated at 2 K/min to 873 K. During the test effluent gasses were analyzed by a Hiden Analytical QGA mass spectrometer.

Cu area measurements by N_2O Frontal chromatography

The copper surface areas of the samples were measured using the frontal chromatography [31] technique in a Quantachrome Autosorb iQ_2 setup. The pre-reduction program was the same as in the respective tests described under "high pressure CO hydrogenation" above. After reduction the system was flushed in He at the final reduction temperature for at least 20 min, cooled to 333 K in He and flushed for an additional 30 min. The reduced sites were then titrated with a 20 NmL/min flow of 1 mol% N_2O in He, and the Cu area was calculated assuming N_2O:Cu = 1:2 [31, 32] and $1.47{\cdot}10^{19}$ Cu sites/m^2 [33].

DRIFTS measurements and associated TPH

In situ FTIR and subsequent TPH were conducted with a Harrick Scientific domed reaction chamber and Praying Mantis diffuse reflectance infrared fourier transform spectroscopy (DRIFTS) unit. This was done with a Nicolet iS50 FTIR Spectrometer with a liquid-N_2 cooled MCT detector using a 76 scan averaging and a 4 cm^{-1} resolution. Gas analysis was performed by a Hiden HPR-20 EGA mass spectrometer. The gas was fed to the DRIFTS reactor via a carbonyl trap from the setup also used to measure high pressure activity as illustrated in fig. S14. The catalyst samples (10 mg) were diluted to 10 wt% in KBr (Sigma Aldrich, FTIR grade). The temperature was measured by a thermocouple in the exhaust gas line of the Harrick reaction chamber directly below the metal screen supporting the sample. The catalysts were reduced in a 50 Nml/min flow of 5% H_2/N_2 using a heating ramp of 1 K/min to 448 K with 1 h dwell time before further heating with 1 K/min to 523 K and a 1 h dwell time, of which the last 30 min was in 100% H_2. Next, a 45 min He flush at 523 K was used to remove hydrogen before collecting the background spectrum at 523 K in He. This background was used for all subsequent spectra. At 523 K the He flow was replaced by a 200 Nml/min gas flow (CO/H_2/inert = 3/68/29 or $CO_2/CO/H_2$/inert = 1.5/1.5/68/29 or CO_2/N_2 = 9/81) with a duration of 1 h before cooling in the same syngas to 283 K. At this temperature the CO and CO_2 flows were removed, while the H_2 flow was increased to 200 Nml/min to flush away remaining CO, CO_2 and CH_3OH in the system (monitored by the MS). Around 30 minutes prior to the initiation of the TPH the hydrogen flow was lowered from 200 Nml/min to 50 Nml/min, which was the flow applied throughout the whole TPH. Using a 50 NmL/min flow of 100% H_2 the TPH was then performed as a 2 K/min ramping to 673 K with continuous collection of IR spectra and online gas analysis by the MS.

XPS measurements

X-ray photoelectron spectroscopy analyses on unsupported Cu were performed with a monochromatic and micro-focused Al K-Alpha source (1486.6 eV) equipped with a 180° double focusing hemispherical analyzer with a Thermo Scientific 128-channel detector and operating with an optimal base pressure of $6{\cdot}10^{-9}$ mbar. During experiment, the chamber pressure was $2{\cdot}10^{-8}$ mbar. The spectra were analyzed by the Avantage software and survey spectra were recorded on a fresh and spent catalyst post methanol synthesis as shown in fig. S15. The details on the methanol synthesis experiment are given in fig. S3. All peaks in the survey spectra were accounted for and assigned to expected Cu and O from the catalyst itself or N and C (due to exposure to the environment). Detailed analysis of characteristic regions for Fe and Ni showed no Fe or Ni associated XPS peaks, which substantiated the survey spectra results showing no indication of Ni or Fe impurities. Potential Ni and Fe impurities were therefore removed by the carbonyl trap (see fig. S16).

XPS measurement results

Fig. S3 shows survey spectra in the full energy range for both the fresh and spent unsupported Cu. Fig. S16 shows the absence of Ni in both fresh and spent unsupported Cu. The XPS binding energy range is chosen, because characteristic XPS Ni peaks would emerge here, if Ni were present. Therefore, the absence of XPS peaks in these regions substantiates absence of Ni contamination.

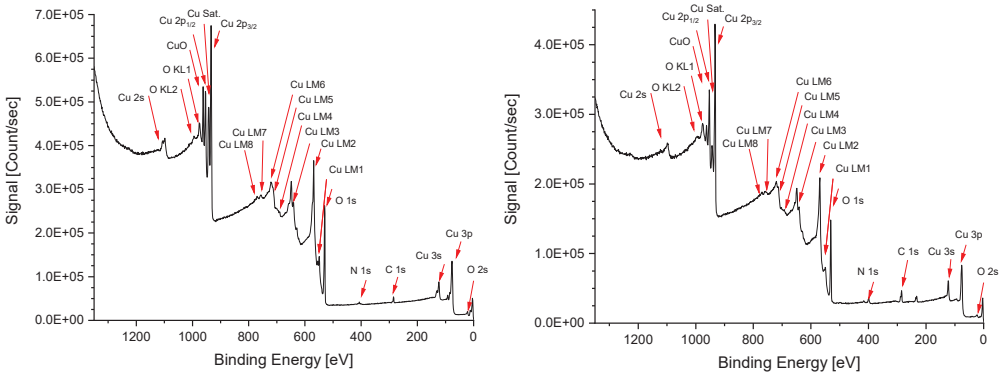

Fig. S15: Ex-situ XPS measurement of fresh and spent unsupported copper. Survey spectra after air exposure during transport to the XPS apparatus for unsupported Cu in a freshly calcined state (left) and after the reaction in fig. S3 (right).

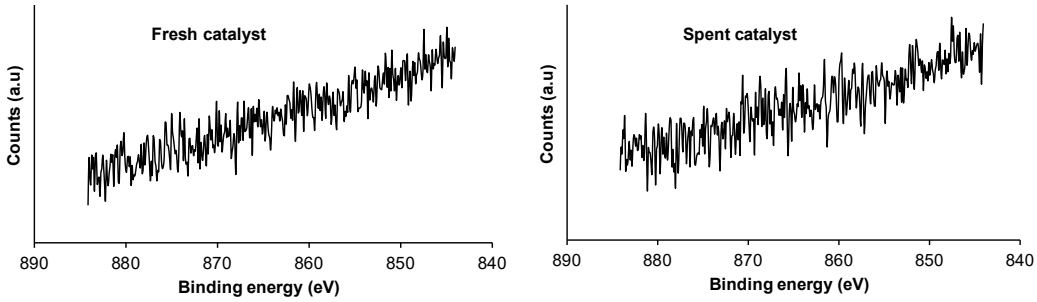

Fig. S16: XPS spectra of the Ni 2p region for the unsupported Cu sample before (left) and after (right) reaction. The reaction test can be seen in fig. S3.

References

[1] R. Bardet and J. Thivolle-Cazat. Hydrocondensation of carbon oxides, at atmospheric pressure on Cu-ZnO-Al_2O_3 catalysts. Influence of water on the formation of methanol. *Compt. Rend. Acad. Sci. Paris*, 299:423–425, 1984.

[2] O. Cherifi, S. Monteverdi, M. M. Bettahar, M. Foorissier, and V. Perrichon. Kinetics of CO_2 hydrogenation into methanol on a Cu-Zn-Al oxide catalyst. *Bull. Soc. Chim. Fr.*, pages 405–409, 1985.

[3] M. Sahibzada, I. S. Metcalfe, and D. Chadwick. Methanol Synthesis from $CO/CO_2/H_2$ over $Cu/ZnO/Al_2O_3$ at Differential and Finite Conversions. *Journal of Catalysis*, 174:111–118, 1998. doi: 10.1006/jcat.1998.1964.

[4] M. Saito, T. Fujitani, M. Takeuchi, and T. Watanabe. Development of copper/zinc oxide-based multicomponent catalysts for methanol synthesis from carbon dioxide and hydrogen. *Applied Catalysis A: General*, 138(2):311–318, 1996. doi: 10.1016/0926-860X(95)00305-3.

[5] G. H. Graaf and J. G.M. Winkelman. Chemical Equilibria in Methanol Synthesis Including the Water-Gas Shift Reaction: A Critical Reassessment. *Industrial and Engineering Chemistry Research*, 55(20):5854–5864, 2016. doi: 10.1021/acs.iecr.6b00815.

[6] J. Słoczyński, R. Grabowski, J. Janas, and J. Skrzypek. Adsorption model of methanol synthesis reactants on CuO-ZnO-Al_2O_3 catalyst-I. Adsorption on the catalyst. *Chemical Engineering Science*, 46(10):2599–2610, 1991. doi: 10.1016/0009-2509(91)80053-2.

[7] J. Słoczyński, R. Grabowski, and J. Janas. Adsorption Model of Methanol Synthesis Reactants on CuO-ZnO-Al_2O_3 Catalyst - II Adsorption on the individual components of the catalyst. *Chemical Engineering Science*, 46(10):2611–2623, 1991. doi: 10.1016/0009-2509(91)80054-3.

[8] J. L. Robbins, E. Iglesia, C. P. Kelkar, and B. DeRites. Methanol synthesis over Cu/SiO_2 catalysts. *Catalysis Letters*, 10(1-2):1–10, 1991. doi: 10.1007/BF00764730.

[9] W. R. A. M. Robinson and J. C. Mol. Characterization and catalytic activity of copper/alumina methanol synthesis catalysts. *Applied Catalysis*, 44(C):165–177, 1988. doi: 10.1016/S0166-9834(00)80051-2.

[10] J. Barbier, J. Fortin, P. Courty, and P. Chaumette. Rôle du dioxyde de carbone lors de la synthèse du méthanol sur catalyseurs à base de cuivre. *Bulletin de la Société chimque de france*, 6:925–929, 1987.

[11] J. S. Lee, K. H. Lee, S. Y. Lee, and Y. G. Kim. A Comparative Study of Methanol Synthesis from CO_2/H_2 and CO/H_2 over a $Cu/ZnO/Al_2O_3$ Catalyst, 1993. doi: 10.1006/jcat.1993.1342.

[12] P. A. Redhead. Chemisorption on polycrystalline tungsten. *Transaction of the Faraday Society*, 57:641–656, 1961. doi: 10.1039/TF9615700641.

[13] J. W. Niemantsverdriet and I. Chorkendorff. *Concepts of Modern Catalysis and Kinetics 2nd. edition*. Wiley-VCH, 2007. doi: 10.1002/3527602658.

[14] D. F. Cox and K. H. Schulz. Interaction of CO with Cu^+ cations: CO adsorption on $Cu_2O(100)$. *Surface Science*, 249(1-3):138–148, 1991. doi: 10.1016/0039-6028(91)90839-K.

[15] D.L. Roberts and G.L. Griffin. Adsorption behavior of Cu species in Cu/ZnO methanol synthesis catalysts. *Applications of Surface Science*, 19:298–306, 1984. doi: 10.1017/CBO9781107415324.004.

[16] J. R. Monnier, M. J. Hanrahan, and G. Apai. A study of the catalytically active copper species in the synthesis of methanol over Cu-Cr oxide. *Journal of Catalysis*, 92(1):119–126, 1985. doi: 10.1016/0021-9517(85)90241-6.

[17] G. R. Sheffer and T. S. King. Differences in the promotional effect of the group IA elements on unsupported copper catalysts for carbon monoxide hydrogenation. *Journal of Catalysis*, 116(2): 488–497, 1989. doi: 10.1016/0021-9517(89)90115-2.

[18] P. J. Chu, B. C. Gerstein, G. R. Sheffer, and T. S. King. NMR studies of ^{65}Cu and ^{133}Cs in alkali-metal-promoted copper catalysts. *Journal of Catalysis*, 115(1):194–204, 1989. doi: 10.1016/0021-9517(89)90018-3.

[19] I. Nakamura, T. Fujitani, T. Uchijima, and J. Nakamura. A model catalyst for methanol synthesis: Zn-deposited and Zn-free Cu surfaces. *Journal of Vacuum Science & Technology*, 14(3):1464–1468, 1996. doi: 10.1116/1.579970.

[20] J. Graciani, K. Mudiyanselage, F. Xu, A. E. Baber, and J. Evans. Highly active copper-ceria and copper-ceria-titania catalysts for methanol synthesis from CO_2. *Science*, 345(6196):546–550, 2014. doi: 10.1126/science.1253057.

[21] J. Yoshihara, S. C. Parker, A. Schafer, and C. T. Campbell. Methanol synthesis and reverse water-gas shift kinetics over clean polycrystalline copper. *Catalysis Letters*, 31(4):313–324, 1995. doi: 10.1007/BF00808595.

[22] G. C. Chinchen, P. J. Denny, J. R. Jennings, M. S. Spencer, and K. C. Waugh. Synthesis of Methanol - Part 1. Catalysts and Kinetics. *Applied Catalysis*, 36:1–65, 1988. doi: 10.1002/chin.198822352.

[23] G. H. Graaf. *The synthesis of methanol in gas-solid and gas-slurry reactors.* PhD thesis, Groningen, 1988.

[24] K. M. Vanden Bussche and G. F. Froment. A steady-state kinetic model for methanol synthesis and the water gas shift reaction on a commercial Cu/ZnO/Al2O3 catalyst. *Journal of Catalysis*, 161(1):1–10, 1996. doi: 10.1006/jcat.1996.0156.

[25] P. B. Rasmussen, P. M. Holmblad, T. Askgaard, C. V. Ovesen, P. Stoltze, J. K. Nørskov, and I. Chorkendorff. Methanol synthesis on Cu (100) from a binary gas mixture of CO_2 and H_2. *Catalysis letters*, 26(3-4):373–381, 1994. doi: 10.1007/BF00810611.

[26] N. Nomura, T. Tagawa, and S. Goto. Titania supported copper catalysts for methanol synthesis from carbon dioxide. *Reaction Kinetics and Catalysis Letters*, 63(1):9–13, 1998. doi: 10.1007/BF02475423.

[27] C. Baltes, S. Vukojević, and F. Schüth. Correlations between synthesis, precursor, and catalyst structure and activity of a large set of $CuO/ZnO/Al_2O_3$ catalysts for methanol synthesis. *Journal of Catalysis*, 258(2):334–344, 2008. doi: 10.1016/j.jcat.2008.07.004.

[28] S. Zander, E. L. Kunkes, M. E. Schuster, J. Schumann, G. Weinberg, D. Teschner, N. Jacobsen, R. Schlögl, and M. Behrens. The role of the oxide component in the development of copper composite catalysts for methanol synthesis. *Angewandte Chemie - International Edition*, 52(25): 6536–6540, 2013. doi: 10.1002/anie.201301419.

[29] M. Behrens, D. Brennecke, F. Girgsdies, S. Kißner, A. Trunschke, N. Nasrudin, S. Zakaria, N. F. Idris, S. B. A. Hamid, B. Kniep, R. Fischer, W. Busser, M. Muhler, and R. Schlögl. Understanding the complexity of a catalyst synthesis: Co-precipitation of mixed Cu,Zn,Al hydroxycarbonate precursors for $Cu/ZnO/Al_2O-3$ catalysts investigated by titration experiments. *Applied Catalysis A: General*, 392(1-2):93–102, 2011. doi: 10.1016/j.apcata.2010.10.031.

[30] J. M. Christensen, P. M. Mortensen, R. Trane, P. A. Jensen, and A. D. Jensen. Effects of H_2S and process conditions in the synthesis of mixed alcohols from syngas over alkali promoted cobalt-molybdenum sulfide. *Applied Catalysis A: General*, 366(1):29–43, 2009. doi: 10.1016/j.apcata.2009.06.034.

[31] G. C. Chinchen, C. M. Hay, H. D. Vandervell, and K. C. Waugh. The measurement of copper surface areas by reactive frontal chromatography. *Journal of Catalysis*, 103(1):79–86, 1987. doi: 10.1016/0021-9517(87)90094-7.

[32] J. W. Evans, M. S. Wainwright, A. J. Bridgewater, and D. J. Young. On the determination of copper surface area by reaction with nitrous oxide. *Applied Catalysis*, 7(1):75–83, 1983. doi: 10.1016/0166-9834(83)80239-5.

[33] O. Hinrichsen, T. Genger, and M. Muhler. Chemisorption of N_2O and H_2 for the Surface Determination of Copper Catalysts. *Chemical Engineering & Technology*, 23(11):956–959, 2000. doi: 10.1002/1521-4125(200011)23:11⟨956::AID-CEAT956⟩3.0.CO;2-L.

Appendix G

Catalyst Preparation

The catalyst preparation procedures including incipient wetness impregnation (IWI), co-precipitation (CP) and deposition precipitation (DP) applied for the synthesized catalysts are each followed by a subsequent calcination step. Details of the synthesized catalysts are summarized in this section. Copper(II) nitrate hemi(pentahydrate) ($Cu(NO_3)_2 \cdot 2.5\ H_2O$, abbreviated CN) is the Cu precursor for all the Cu supported catalysts. Metal nitrates are used as catalyst precursor materials because the alternative, easily accessible metal salts contain catalyst poisons such as sulfur and chloride [1]. Pure Cu catalysts include unsupported Cu either obtained by CP or bought as nanopowder from Sigma Aldrich or referring to Raney Cu, which is composed of 98.87 wt% Cu, 0.81 wt% Al, 0.10 wt% Al and 0.05 wt% Ni according to the analysis by the company (Strem Chemicals).

1 Incipient Wetness Impregnation

Catalyst preparation using the IWI method includes an aqueous impregnation solution, which is drawn into a (highly) porous support structure by capillary forces [2].
The Cu supported catalyst type prepared by IWI is Cu/SiO_2 (silica). A complete description of the procedure is shown in table S1. Crushed supports are fractionated to a sieve fraction of 150-300 µm before drying for minimum 12 hours at 383 K.

Table S1: Experimental steps for the IWI procedure with CN = copper(II) nitrate hemi(pentahydrate).

Step	***Task***	***Tools***	***Specifications***
1	Crushing	Mortar, crucible	Support is crushed
2	Fractionation	150 and 300 µm sieves	Support is fractionated
3	Drying	Oven	T = 383 K overnight
4	WPV	Water, 3 small sample beakers	WPV reached, when no support sticks to the beaker walls
5	Impregnation	CN (Cu precursor), water, support, beaker, spatula	Add first CN, second water, third support. Stir until the impregnated sample is homogeneous.
6	Drying	Oven	T = 313 KC overnight

The water pore volume (WPV) is expressed in equation Eq. S1 and designates the water content, which the porous support structure can adsorb before reaching water saturation.

$$WPV = \frac{m_{\text{wat}}}{m_{\text{sup}}} \qquad \text{(Eq. S1)}$$

Impregnation of CN into the porous structure occurs by dissolving CN in water, whereby CN is drawn into the porous support structure by capillary forces. WPV is applied to calculate the water content

in the aqueous CN solution to ensure that all of the impregnation solution gets incorporated into the porous structure. The average WPV of three measurements is used to prepare the CN impregnation solution with experimental values shown in tables S2.

Table S2: Water pore volume estimation for Cu/SiO_2 type catalyst before impregnation.

Catalyst : Exp. no.	$m_{\mathbf{sup}}$ [g]	$m_{\mathbf{wat}}$ [g]	$\boldsymbol{WPV} = m_{\mathbf{wat}}/m_{\mathbf{sup}}$ [%]
Cu/SiO_2 : 1	0.16059	0.20533	1.27860
Cu/SiO_2 : 2	0.16517	0.18357	1.11140
Cu/SiO_2 : 3	0.16507	0.19787	1.19870
Average			**1.1962**

After impregnation, the catalyst is dried overnight to evaporate the water from the porous structure. The variables for the IWI preparation method are shown below:

Copper weight percentage in final catalyst : $Cu_{wt\%}$ [%]
Mass of dried silica support : m_{sup} [g]
Mass of water : m_{wat} [g]
Water pore volume : WPV [%]
Mass of copper : m_{Cu} [g]
Molar amount of copper : n_{Cu} [mole]
Molar mass of copper : $M_{Cu} = 63.55\,\mathrm{g\,mole^{-1}}$
Molar mass of copper nitrate hemi(pentahydrate) : $M_{CN} = 235.89\,\mathrm{g\,mole^{-1}}$

with M_{Cu} given by [3] and M_{CN} provided by the manufacture (Sigma Aldrich).
The total weight of dried catalysts equals the weight of dried support and Cu ($m_{sup} + m_{Cu}$), which is related to Cu_{wt} as seen in equation Eq. S2. High $Cu_{wt\%}$ increases the risk of Cu particle sintering whereas low $Cu_{wt\%}$ reduces the area specific Cu surface area and the corresponding signal obtained for the Cu specific surface area measured by e.g. N_2O-RFC. Therefore 10-36 wt% Cu is employed.
Determination of the CN content in the CN solution is expressed together with the total catalyst weight (m_{tot}) after impregnation and subsequent reduction in equation Eq. S2. Combining these two equations yield an expression for m_{Cu} (see equation Eq. S3) that is used in equation Eq. S4 to determine the molar amount of Cu. From a stoichiometric 1:1 ratio between Cu and CN, it follows, that $n_{Cu} = n_{CN}$ as evident from equation Eq. S4. Estimation of m_{wat} is based on equation Eq. S5.

$$m_{tot} = m_{sup} + m_{Cu}\ ,\ Cu_{wt\%} = \frac{m_{Cu}}{m_{tot}} \quad \Updownarrow \tag{Eq. S2}$$

$$m_{Cu} = \frac{Cu_{wt\%}}{1 - Cu_{wt\%}} m_{sup} \tag{Eq. S3}$$

$$n_{Cu} = \frac{m_{Cu}}{M_{Cu}} = n_{CN} \tag{Eq. S4}$$

$$m_{wat} = m_{sup}\, WPV \tag{Eq. S5}$$

Provided with specific parameters for $Cu_{wt\%}$ (selected) and m_{sup} (measured), the CN and water amounts are determined based on the experimentally reported values shown in table S4. Following the impregnation is drying at 313 K for minimum 12 hours for a mildly and homogeneously drying of the catalyst, which is subsequently calcined.
A complete overview of the steps involved in the incipient wetness impregnation procedure is depicted in figure S1.

Table S3: Catalyst preparation parameters for incipient wetness impregnation with CN = copper(II) nitrate hemi(pentahydrate) - $Cu(NO)_3 \cdot 2.5H_2O$, (t) = theoretical value obtained from molar masses of compounds, m_{sup}, WPV and $Cu_{wt\%}$ and (m) = measured values.

Catalyst	$m_{\mathbf{sup}}$ [g]	***WPV*** [%]	$\mathbf{Cu_{wt\%}}$ [wt%]	$m_{\mathbf{CN}}$ [g]	$m_{\mathbf{wat}}$ [g]
$10Cu/SiO_2$	17.4935	1.1962	10	7.2149(t) 7.2151(m)	20.9263(t) 20.9448(m)

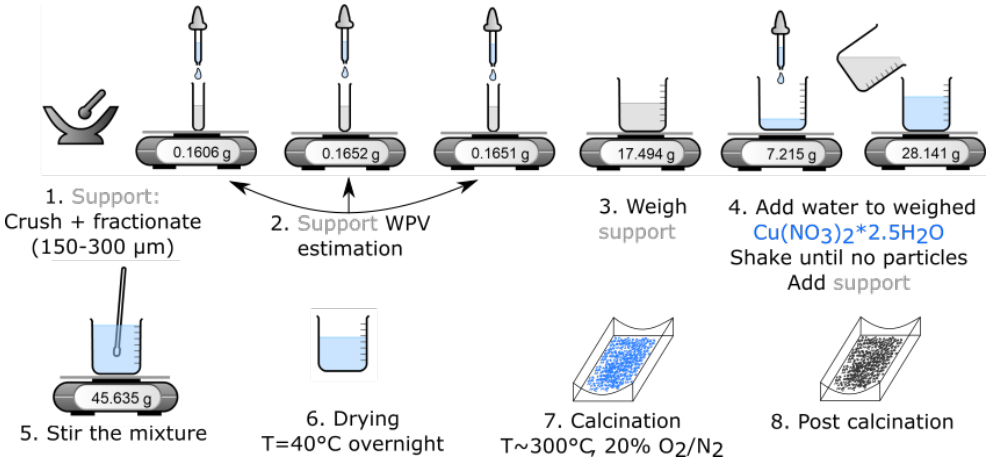

Fig. S1: Schematic for the IWI procedure shown with experimental parameters for catalyst preparation of $10Cu/SiO_2$ (see table S4).

Table S4: Catalyst preparation parameters for incipient wetness impregnation with CN = copper(II) nitrate hemi(pentahydrate) - $Cu(NO)_3 \cdot 2.5H_2O$, (t) = theoretical value obtained from molar masses of compounds, m_{sup}, WPV and $Cu_{wt\%}$ and (m) = measured values. The WPV for $36Cu/SiO_2$ catalyst is based on a single WPV determination, because the WPV of 1.233 was in good agreement with the WPV for the (same) SiO_2 previously estimated to be 1.1962. The 35.7 wt% and not 36 wt% Cu are due to an experimental error combined with limited amount of Cu nitrate solubility in water.

Catalyst	$m_{\mathbf{sup}}$ [g]	***WPV*** [%]	$\mathbf{Cu_{wt\%}}$ [wt%]	$m_{\mathbf{CN}}$ [g]	$m_{\mathbf{wat}}$ [g]
$10Cu/SiO_2$	17.4935	1.1962	10	7.2149(t) 7.2151(m)	20.9263(t) 20.9448(m)
$36Cu/SiO_2$	6.8507	1.233	35.7	14.1186(t) 14.1250(m)	8.44988(t) 8.4350(m)

2 Co-Precipitation

The following general description about the co-precipitation (CP) method is based on [4] unless otherwise stated and the synthesis parameters are based on the optimization work by Baltes et al. [5]. Heterogenous catalysts prepared by the CP method involve precipitation of one or more metals in conjunction with the support or its precursor. During precipitation a range of chemical reactions take place, which affects the dispersion, porous structure, particle size and shape etc. of the final catalyst,

hence good control of the preparation conditions are essential to obtain optimal catalyst properties. Advantageously, CP allows high metal loading of up to 60% generally, whereas IWI typically is restricted to maximum 30%. Moreover, CP prepared catalysts generally features high metal dispersion thus high volume activity.
On the other hand, the CP process generates significant amounts of salts, which must be washed away, and CP requires product separation obtained by typically filtration during catalyst preparation.
The major steps constituting the precipitation process are liquid mixing, nucleation and crystal growth creating primary particles and aggregation of these primary particles.
Liquid mixing concerns mixing of the typical aqueous solutions of catalyst and support precursors, which initiate a number of chemical reactions including nucleation. Before spontaneous (homogeneous) crystallization occurs, a certain level of supersaturation, s (defined as the actual concentration divided by the solubility for a specific compound) must be reached. The nucleation rate $\frac{\mathrm{d}N}{\mathrm{d}t}$ is described in equation Eq. S1 [6, 7].

$$\frac{\mathrm{d}N}{\mathrm{d}t} = \beta \exp\left[\frac{-16\pi\sigma^3\nu^2}{3(k_\mathrm{B}T)^3 \ln^2 s}\right] \qquad \text{(Eq. S1)}$$

with β a pre-exponential term, σ as the solid/fluid interfacial energy, ν as the solid molecular volume, T the temperature, k_B is Boltzmann's constant, and s is the supersaturation. Clearly, the nucleation rate depends strongly on T and s, and s must exceed a certain critical level to ensure simultaneous supersaturation of the metal and support precursors resulting in highly dispersed co-precipitates. Otherwise, precipitation of different components may undesirably take place at different times. Cooling of the precipitation solution (see equation Eq. S1) together with ion reactions in aqueous media, hydrolysis etc. constitute methods to facilitate supersaturation [4].
Crystal growth can be described by various mechanisms but a general expression for the crystal growth rate (k_g) is shown in equation Eq. S2 [6, 7].

$$k_\mathrm{g} = a(c - c_\mathrm{eq})^n \qquad \text{(Eq. S2)}$$

with a the growth rate constant, c the concentration, c_eq the equilibrium solubility concentration (for hydroxides and carbonates typically close to zero) and the kinetic exponent n (between 1-2 and normally close to 1).
Whereas the nucleation rate ($\frac{\mathrm{d}N}{\mathrm{d}t}$) depends exponentially on the supersaturation concentration (s), the crystal growth rate (k_g) depends more linearly on the concentration. Conclusively, high s favors nucleation rather than crystal growth with the result of highly dispersed precipitated products.
Mixing order of reactants and reaction conditions (e.g. temperature and pH) are highly important for the co-precipitated phases. Good process control is obtained by simultaneously and with good control adding reactants (e.g. catalyst precursor(s) and precipitation agent) under continuous stirring to ensure close to constant pH and minimum concentration gradients. Otherwise, mixed products with different and maybe undesired phases may be formed.
Hydrolysis between metal nitrate precursors employed in this project and water yields an acidic environment thus Na_2CO_3 is added as a so-called precipitating agent to keep a constant pH around 6.5 for optimal catalyst precursor synthesis.
The parameters for preparing the catalyst precursor and precipitation agent solutions are shown below (where the purity level of the catalyst precursors reported by the manufacture are taken into consideration):

Molar mass of aluminium nitrate nonahydrate : $M_\mathrm{AN} = 379.30\,\mathrm{g\,mole^{-1}}$

Molar mass of zinc nitrate hexahydrate : $M_\mathrm{ZN} = 302.61\,\mathrm{g\,mole^{-1}}$

Molar mass of sodium carbonate anhydrous : $M_\mathrm{SC} = 105.99\,\mathrm{g\,mole^{-1}}$

Target catalyst weight : $m_\mathrm{t.cat} = 15\,\mathrm{g}$

Volume precursor solution : $V_\mathrm{precur.} = 0.5\,\mathrm{l}$

Volume precipitating agent solution : $V_\mathrm{precip.} = 0.5\,\mathrm{l}$

with Na_2CO_3 as the precipitation agent. With a target catalyst amount of 15 g, the calcined and reduced catalyst should e.g. contain 1.5 g Cu for Cu/ZnO (10 wt% Cu).
For binary catalysts (Cu/ZnO, Cu/Al_2O_3), the amount of Cu, ZnO and Al_2O_3 precursor materials are determined by the molar masses of Cu, ZnO and Al_2O_3 and their specific molar ratio with each precursor material. The molarity of the precipitation agent solution is 0.75 M, which is determined based on the "acidity" strength for Cu^{2+}, Zn^{2+} and Al^{3+} w.r.t. CO_3^{2-}. A molarity of 0.75 M Na_2CO_3 is sufficient to balance the acidity strength caused by the catalyst precursors thus 0.75 M precipitation agent solution is used for all the CP catalysts.
The commercially type catalyst is prepared to yield a typical conventional catalyst molar ratio of 60:30:10 (Cu:Zn:Al) as discussed in section 4.

Table S1: Experimental steps for the co-precipitation procedure of Cu/ZnO. SC = sodium carbonate, cat. prec. sol = catalyst precursor solution, CN = copper(II) nitrate hemi(pentahydrate) and ZN = zinc nitrate hexahydrate.

Step	***Task***	***Tools***	***Specifications***
1	Heating	2 L beaker, 0.5 L water, thermometer, magnet, heat plate	Water heated to $T = 338$ K under continuous stirring
2	Injection	SC (precip. agent), cat. prec. sol. (here CN + ZN), 2 burets	Maintain pH $\approx$ 6.5 with SC while adding cat. prec., stirring, $T = 338$ K
3	Aging	Timer	Stirring, $T = 338$ K for 60 min.
4	Cooling	Stirring	$T \rightarrow 308$ K
5	Filtration and washing	Filter paper, funnel, 2.5 L water, pump, 1 L beaker, hose, bung	Wash cat. with $\sim$2.5 L water
6	Drying	Funnel, oven, 1 L beaker	Dry cat. (incl. funnel) overnight, $T = 313$ K

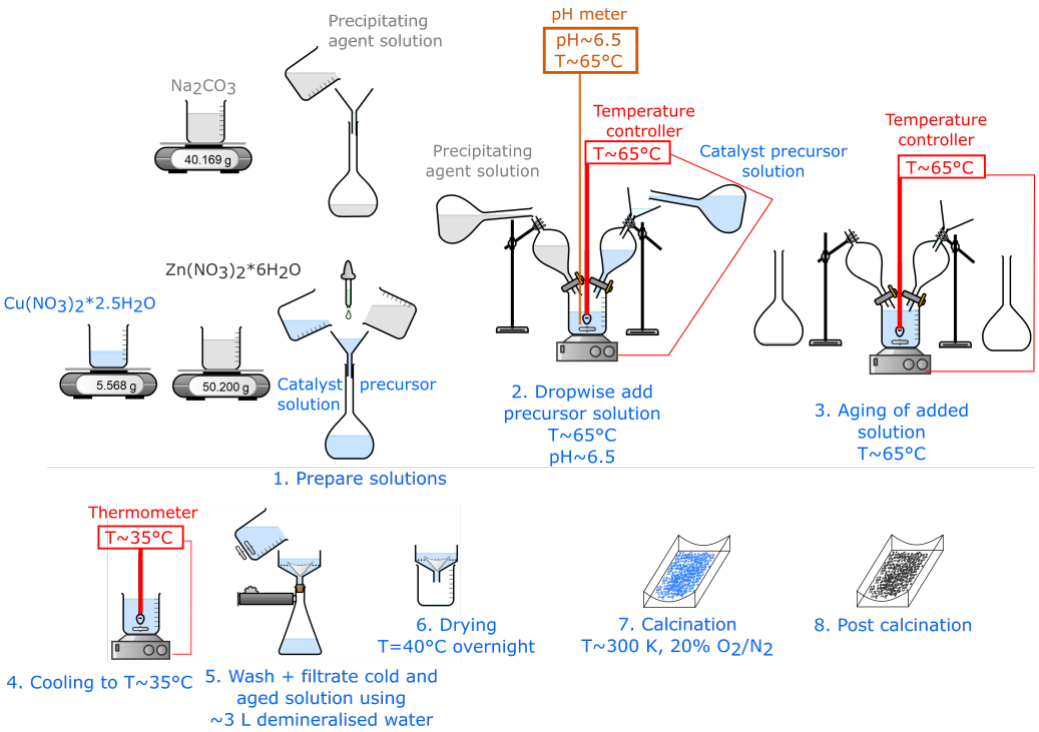

Fig. S2: Schematic for the co-precipitation procedure shown here with experimental values for preparation of the Cu/ZnO catalyst (see table S2).

Table S2 summarizes the parameters for the co-precipitation prepared catalysts synthesized in the project.

Table S2: Catalyst preparation parameters for co-precipitation with CN = copper(II) nitrate hemi(pentahydrate) - $Cu(NO_3)_2 \cdot 2.5\ H_2O$, ZN = zinc nitrate hexahydrate - $Zn(NO_3)_2 \cdot 6\ H_2O$, MN = magnesium nitrate hexahydrate - $Mg(NO_3)_2 \cdot 6\ H_2O$, AN = aluminium nitrate nonahydrate $Al(NO_3)_3 \cdot 9\ H_2O$, SC = sodium carbonate - Na_2CO_3, (t) = theoretical value obtained from molar masses of compounds, $m_{t.cat}$ and $Cu_{wt\%}$ and (m) = measured values. *Preparation of $Cu/ZnO/Al_2O_3$ is based on the metal molar ratio Cu:Zn:Al = 60:30:10 (equal to mass ratio: 56.4 wt% Cu, 36.1 wt% ZnO, 7.5 wt% Al_2O_3). Target catalyst loading was 7.5 to 15 g.

Catalyst	$\mathbf{Cu_{wt\%}}$ [**wt**%]	$m_{\mathbf{CN}}$ [**g**]	$m_{\mathbf{ZN}}$ **or** $m_{\mathbf{MN}}$ [**g**]	$m_{\mathbf{AN}}$ [**g**]	$m_{\mathbf{SC}}$ [**g**]
10Cu/ZnO	10	5.5679(t) 5.5671(m)	50.2002(t) 50.2022(m)	N.A.	40.1685(t) 40.1658(m)
67Cu/Al_2O_3	67	27.8394(t) 27.8397(m)	N.A.	27.9008(t) 27.9010(m)	40.1685(t) 40.1661(m)
56Cu/ZnO/Al_2O_3	60:30:10*	35.1251(t) 35.1249(m)	22.5301(t) 22.5308(m)	9.4132(t) 9.4137(m)	40.1685(t) 40.1699(m)
ZnO	N.A.	37.1854(t) 37.1847(m)	N.A.	N.A.	26.0481(t) 20(m)
20Cu/MgO	N.A.	5.568(t) 5.4924(m)	38.1705(t) 38.1610(m)	N.A.	45.700(t) 45.697(m)
20Cu/Al_2O_3	20	7.5948(m)	N.A.	58.8864(m)	33.3358(m)

*Molar ratio of 60:30:10 for Cu:Zn:Al.

The reactions occurring in the aqueous solution of metal precursors are listed in reactions R1, R2 and R3 in absence of Na_2CO_3:

$$Al(NO_3)_3 + 9\,H_2O \rightleftharpoons Al(OH)_3 + 3\,H^+ + 3\,{NO_3}^- + 6\,H_2O \quad \{R1\}$$

$$Cu(NO_3)_2 + 2\,H_2O \rightleftharpoons Cu(OH)_2 + 2\,H^+ + 2\,{NO_3}^- \quad \{R2\}$$

$$Zn(NO_3)_2 + 2\,H_2O \rightleftharpoons Zn(OH)_2 + 2\,H^+ + 2\,{NO_3}^- \quad \{R3\}$$

which demonstrates an overall acidic nature as a result of the metal precursor hydrolysis. Addition of Na_2CO_3 produces hydroxyl ions (OH^-) as seen in reaction R4, which reacts with H^+ causing a more neutral environment.

$${HCO_3}^- + H_2O \rightleftharpoons H_2CO_3 + OH^- \rightleftharpoons H_2O + CO_2 + OH^- \quad \{R4\}$$

3 Deposition Precipitation

DP prepared catalysts can have higher metal loading compared to catalysts prepared by the IWI method [8]. IWI prepared Cu/TiO_2 in this project featured low Cu surface area thus DP was the chosen method for synthesizing the Cu/TiO_2 catalysts. DP of Cu/TiO_2 catalysts containing 20 and 60 wt% Cu involved dissolving TiO_2 (anatase) in the beaker containing demineralized water (see step 1 in table S1) before continuing the synthesis protocol outlined in table S1.

Table S1: Catalyst preparation parameters for DP with CN = copper(II) nitrate hemi(pentahydrate) - $Cu(NO_3)_2 \cdot 2.5\ H_2O$, SC = sodium carbonate - Na_2CO_3, (t) = theoretical value obtained from molar masses of compounds, $m_{\mathrm{t.cat}}$ is the target mass and $Cu_{\mathrm{wt\%}}$ the obtained Cu wt% based on the measured (m) values.

Catalyst	$m_{\mathbf{t.cat}}$ [**g**]	$\mathbf{Cu_{wt\%}}$ [**wt**%]	$m_{\mathbf{CN}}$ [**g**]	$m_{\mathbf{TiO_2}}$ [**g**]	$m_{\mathbf{SC}}$ [**g**]
$20Cu/TiO_2$	10	20	7.4238(t) 7.4238(m)	8.00(t) 8.0072 (m)	6.6713(t) 6.6747(m)
$60Cu/TiO_2$	10	60	26.7258(t) 26.7240(m)	4.800(t) 4.800 (m)	24.0166(t) 24.00(m)

References

[1] J. B. Hansen and P. E. H. Nielsen. *Methanol Synthesis*, volume 2. Wiley-VCH Verlag GmbH, 2nd edition edition, 2008. doi: 10.1002/9783527610044.hetcat0148.

[2] A. V. Nelmark, L. I. Kheifez, and V. B. Fenelonov. Theory of Preparation of Supported Catalysts. *Industrial and Engineering Chemistry Product Research and Development*, 20(3):439–450, 1981. doi: 10.1021/i300003a006.

[3] J. W. Niemantsverdriet and I. Chorkendorff. *Concepts of Modern Catalysis and Kinetics 2nd. edition*. Wiley-VCH, 2007. doi: 10.1002/3527602658.

[4] M. Lok. Coprecipitation. In K. P. De Jong, editor, *Synthesis of Solid Catalysts*, chapter 7, pages 135–151. Wiley VCH, Weinheim, 2009.

[5] C. Baltes, S. Vukojević, and F. Schüth. Correlations between synthesis, precursor, and catalyst structure and activity of a large set of $CuO/ZnO/Al_2O_3$ catalysts for methanol synthesis. *Journal of Catalysis*, 258(2):334–344, 2008. doi: 10.1016/j.jcat.2008.07.004.

[6] J. Nyvlt. Precipitation of Catalyst Precursors Theoretical Fundamentals. *Crystal Research and Technology*, 30(6):737–745, 1995. doi: 10.1002/crat.2170300602.

[7] C. J. J. den Ouden and R. W. Thompson. Analysis of the formation of monodisperse populations by homogeneous nucleation. *Journal of Colloid And Interface Science*, 143(1):77–84, 1991. doi: 10.1016/0021-9797(91)90438-E.

[8] K. P. De Jong. Deposition Precipitation. pages 111–134, 2009. doi: 10.1002/9783527626854.ch6.

Appendix H

Flowreactor Calibrations

This chapter describes calibrations of the mass flow controllers (MFCs) and gas chromatograph (GC).

1 Mass Flow Controller Calibration

Harmful or toxic gasses including 100% H_2 and 9% CO_2/CO are calibrated using a 500 ml bubble flow meter, while less harmful gasses including 5% H_2/He, 100% He and 1% N_2O/He are calibrated using a Sensidyne flow meter. For quantitative experiments including TOF estimating, formate coverage quantification etc. the experiment specific flows are measured for improved quantitative accuracy. Figure S1 shows the MFC calibration for the standard different gas flasks with good linearity across the entire MFC set point range. Each data point is based on an average value of 5-10 measurements at each setpoint with "N" referring to normal conditions at 273.15 K and 1 atmosphere of pressure. Experiments involving CO adsorption using designated diluted CO in Ar, calibration tests with very diluted CO_2 in He, low temperature CO adsorption with N_2, CO_2/H_2 switching experiments with 9% CO_2/N_2 and CO_2 required changing the gas flasks followed by necessary gas flow calibration.

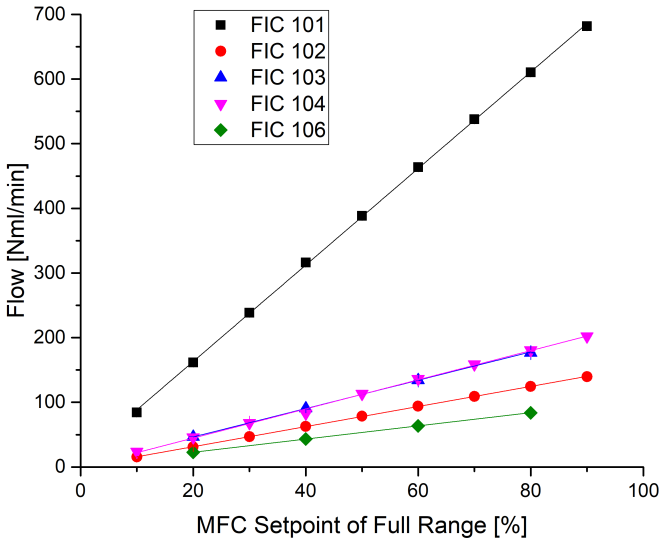

Fig. S1: MFC calibration for the different MFC's with the following configuration FIC 101 - He, FIC 102 - 1% N_2O/He, FIC 103 - 100 % H_2, FIC 104 - 5% H_2/He, FIC 105 - Limited use and experiment specific calibration, FIC 106 - 9%CO_2/CO. The maximum flow range is different for the various MFC's.

2 GC Calibration

GC calibration performed using gas flasks except for methanol calibration. The parameters included in the GC instrument method applied during calibration are optimized to detect and separate the interesting gas molecules, which includes CO, CO_2 (and N_2) monitored by the (back) Thermal Conductivity Detector (TCD), while DME, CH_3OH and CH_4 are measured by the (front) Flame Ionization Detector (FID).
The optimized method, which includes parameters for the auxiliary gas flows, oven temperatures etc., is also applied during methanol activity experiments to assign the detected gas molecules at specific retention times to the calibrated gas molecules. Gas flasks with different gas molecule concentrations for each specific gas molecule component are used to obtain linear calibration curves, which cover the gas concentrations expected for each specific gas molecule during experiments.
In the case of methanol, various liquid amounts of methanol are injected through a septum into 10 L tedlar sample bags, which after cleaning with ambient air are filled with 8 l of He.
Methanol concentrations corresponding to 0.5, 1 and 3 mole % methanol in He are prepared, before a membrane pump is applied together with an adjustable transformer to control the flow rate out of the sample bag and into the gas stream flowing through the GC. A final calibration point is collected using a gas flask with around 250 ppm methanol.

The GC calibrations for all the involved gas flasks are summarized in figs. S2 to S7, where the data points marked by a red cross are omitted, because these first injection data points are usually slightly distorted.
All calibrations exhibit linear behaviour except H_2, which as reported previously demonstrate non-linear behaviour, because the thermal conductivity of H_2, which is the signal detected by a TCD, varies with the molar concentration of H_2 [1]. Consequently, the gas calibration curve for H_2 is fitted to yield the best fit based on the collected data points. At around 70 mole % H_2, which is the region of interest for methanol synthesis in $H_2/CO/CO_2$ with molar ratio of 68/29/3, the calibration curve exhibits linear behaviour.

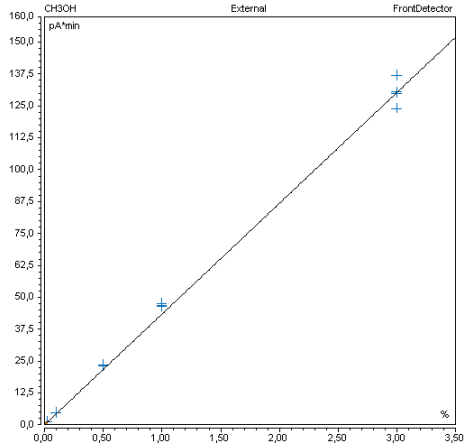

Fig. S2: CH_3OH calibration using a FID.

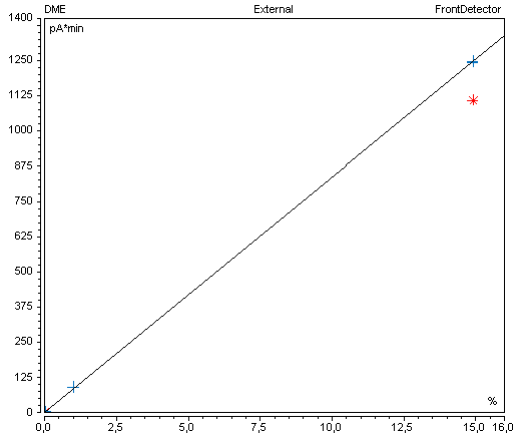

Fig. S3: C_2H_6O calibration using a FID.

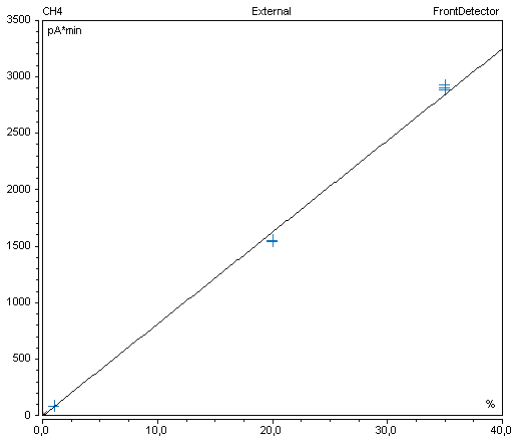

Fig. S4: CH_4 calibration using a FID.

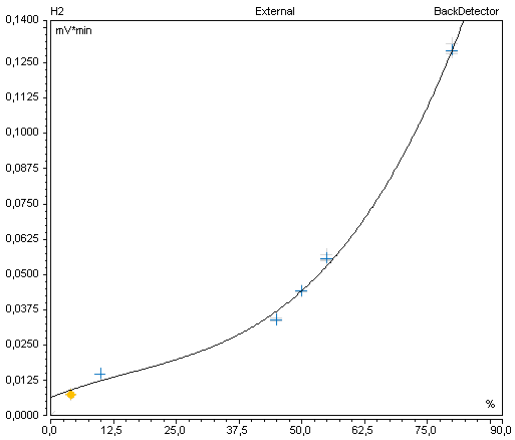

Fig. S5: H_2 calibration using a TCD.

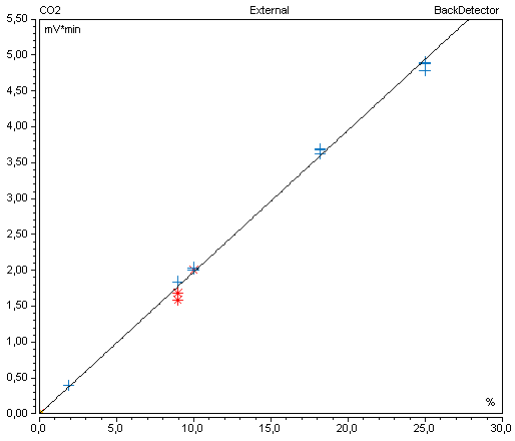

Fig. S6: CO_2 calibration using a TCD.

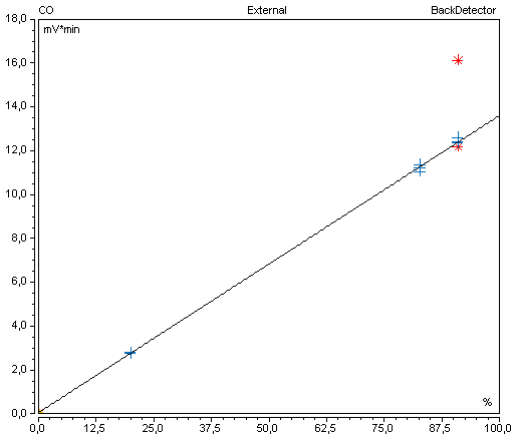

Fig. S7: CO calibration using a TCD.

References

[1] P. Mukhopadhyay and A. K. Barua. Thermal Conductivity of hydrogen-helium gas mixtures. *Brit. J. Appl. Phys.*, 18:635–640, 1967.